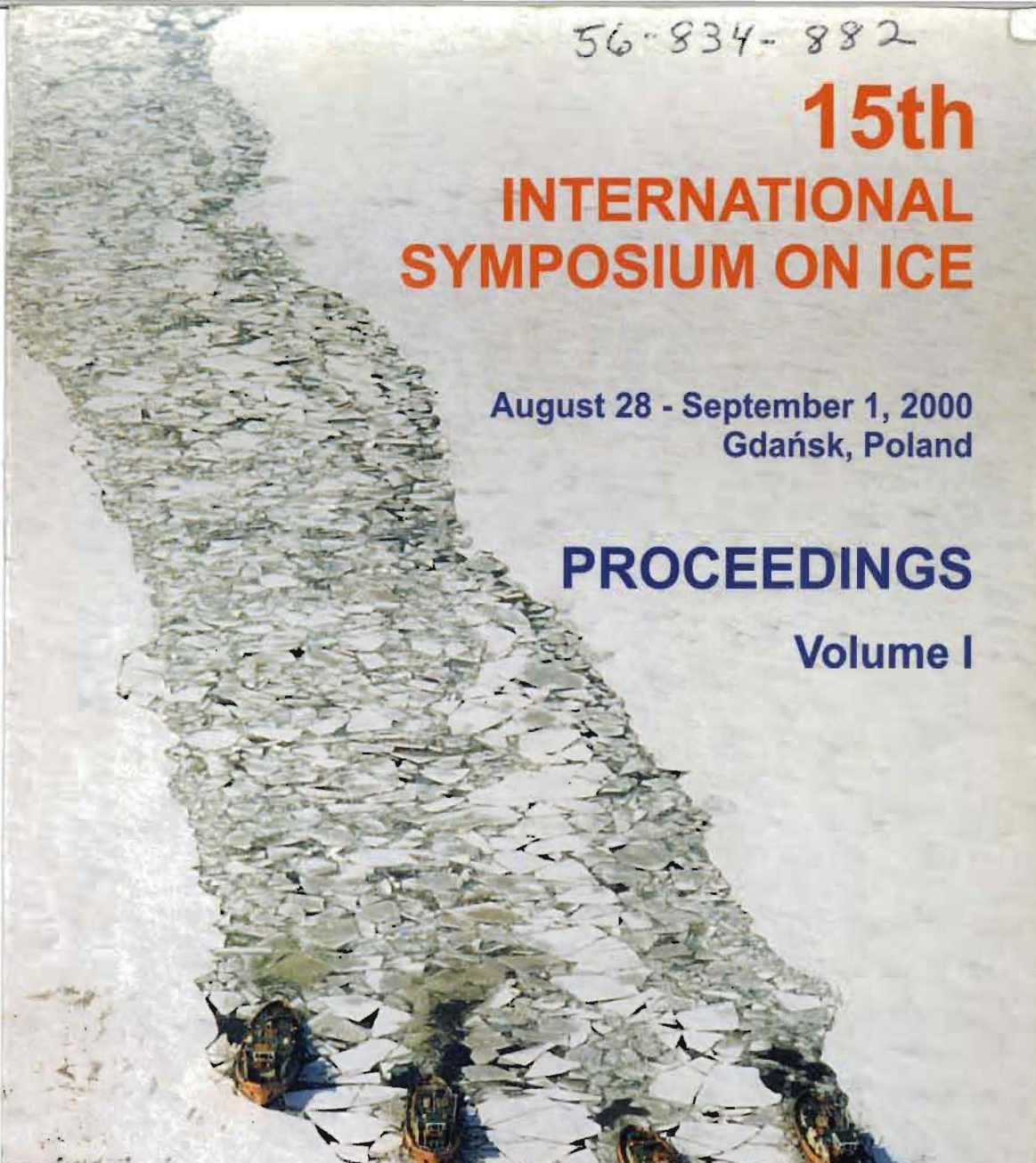


56-834-882

# 15th INTERNATIONAL SYMPOSIUM ON ICE

August 28 - September 1, 2000  
Gdańsk, Poland

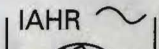
**PROCEEDINGS**  
Volume I



**IS** GDAŃSK  
2000



INSTITUTE OF HYDROENGINEERING  
POLISH ACADEMY OF SCIENCES



56000834-56000882  
MP 5756 MP 5757

SODHI  
157

# 15th INTERNATIONAL SYMPOSIUM ON ICE

August 28 – September 1, 2000  
Gdańsk, Poland

## PROCEEDINGS

Volume I



Editor: W. Majewski



INSTITUTE OF HYDROENGINEERING  
POLISH ACADEMY OF SCIENCES  
GDAŃSK, POLAND

INTERNATIONAL ASSOCIATION  
OF HYDRAULIC ENGINEERING AND RESEARCH



Gdańsk, 2000

Published by The Institute of Hydroengineering,  
Polish Academy of Sciences (IBW PAN), Gdańsk, Poland

Technical Editor: T. Jarzębińska

ISBN 83-85708-39-1

Copyright © by the Authors unless otherwise stated, 2000.

The materials and information contained herein are published in the exact form submitted by authors. No attempt has been made to alter the material except where obvious errors or discrepancies were detected. Any statements or view presented are totally those of the authors and should not necessarily be taken as having the support of the Symposium Organizing or Scientific Committee.

This book is published on the understanding that the authors are solely responsible for the statement made and opinions expressed in it and that its publication does not necessarily imply that such statements and/or opinions are or reflect the views or opinions of the organizers or publishers.

Copies of the proceedings may be obtained from:

Institute of Hydroengineering, Polish Academy of Sciences (IBW PAN)  
P.O.Box 61, 80-953 Gdańsk, Poland  
tel. +48 58 552 39 03  
fax: +48 58 552 42 11  
e-mail: sekr@ibwpan.gda.pl

Front cover designed by T. Jarzębińska

Photo on the cover: Icebreakers on Włocławek reservoir (Lower Vistula River). Author: B. Pawłowski

Printed and bound in Poland by GRAFIX

S-40074  
6/3/08

## PREFACE

15th International Symposium on Ice is being held in Gdańsk, Poland from 28 August to 1 September 2000. The first Ice Symposium was organised in 1970 in Reykjavik, Iceland. The present Symposium closes 30 years of Ice Symposia. Symposium is organised by the Institute of Hydroengineering of the Polish Academy of Sciences. The venue of the Symposium is the Centre of the Technical Society in Gdańsk (Dom Technika NOT).

Symposium is authorised by the Section on Ice Research and Engineering of the International Association of Hydraulic Engineering and Research. Patronage of the Symposium was kindly accepted by Paweł Adamowicz the Major of Gdańsk.

Symposium provides the opportunity for all specialists to exchange experience and challenges in ice research and engineering but also affords the possibility to visit beautiful city of Gdańsk and its surroundings. Gdańsk is an old hanseatic city with a 1000 - year history.

The program of the present Ice Symposium was developed in six main topics encompassing broad aspects of ice hydraulics, ice engineering, ice ecology and numerous engineering applications. The main topics are:

- A. River, lake, and sea ice processes,
- B. Ice mechanics and hydraulic structures in ice,
- C. Hydrological and meteorological influences on river, lake, and sea ice,
- D. Navigation and offshore activities in ice conditions,
- E. Environmental and ecological problems in lakes, rivers, and coastal zones in ice conditions,
- F. Ice forecasting and management of hydraulic and hydropower installations.

50 papers are included in this volume of Proceedings. Papers received from the general call for papers underwent review process in order to ensure technical quality and relevance to topics of the Symposium. This volume of Proceedings is published on the understanding that the authors are solely responsible for the statements and opinions expressed in it. Papers were technically edited without changing scientific or engineering contents.

Organisers of the Symposium hope that the papers published in the Proceedings of the Symposium represent a significant area of human endeavours and also reveal concerns and interests of ice engineers at the turn of millennium.

Gdańsk, August 2000

Wojciech Majewski  
Chairman of the Organising Committee

Conf. attend

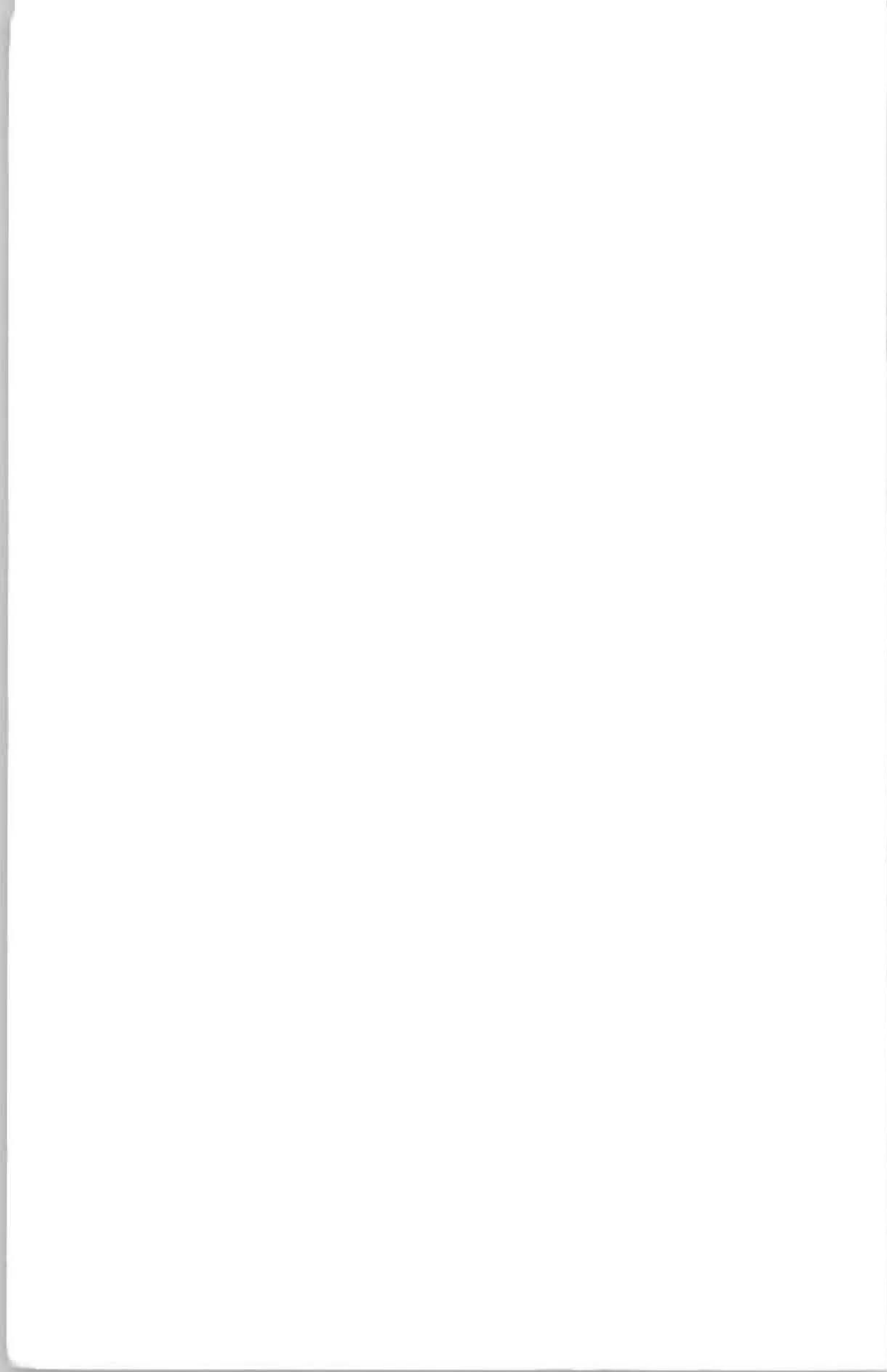


## TABLE OF CONTENTS

<b><u>A. RIVER, LAKE, AND SEA ICE PROCESSES</u></b>	1
M. Sztobryn, B. Kowalska <b>Reconstruction of sea-ice conditions in the Gulf of Gdańsk since XVI century</b>	3
Qianjin Yue, Shunying Ji, Xi Zhang <b>Sea ice observations on an offshore platform in Bohai Sea</b>	11
K.V. Høyland <b>Measurements of consolidation in three first-year ridges</b>	19
K.I. Gausland, O.T. Gudmestad, H.E. Krogstad, S. Løset <b>Detectability of ice ridges by synthetic aperture radar</b>	27
S. Løset, J.K. Økland <b>Ice drift speeds in the Pechora sea</b>	37
K.V. Høyland, G. Kjestveit, J. Heinonen, M. Määttänen <b>LOLEIF ridge experiments at Marjaniemi; the size and strength of the consolidated layer</b>	45
O. Smith <b>Formation and decay of stamukhas, Cook Inlet, Alaska</b>	53
G.A. Surkov, P.A. Truskov, S.V. Zemlyuk, V.N. Astafyev, A.M. Polomoshnov <b>Salinity of ice offshore Northeastern Sakhalin</b>	59
J. Heinonen, M. Määttänen <b>LOLEIF ridge-loading experiments-analysis of rubble strength in ridge keel punch test</b>	63
A. Dobrowolski, B. Głowacka, A. Kondzielski <b>Problems of slush ice formation and transport in the Middle Vistula River</b>	73
H.T. Shen, L. Liu, K. Hoshi, Y. Watanabe, K. Hirayama <b>Ice jam formation in the Shokotsu River</b>	81
E.P. Anisimova, E.N. Dolgoplova, A.A. Speranskaya <b>The comparison of roughness of the underneath of ice cover in river and in lake</b>	89
M. Grześ, W. Majewski <b>River ice problems on the Lower Vistula</b>	97
A. Jensen, K.V. Høyland, K.-U. Evers <b>Scaling and measurement of ice rubble properties in laboratory tests</b>	105
J. Meyssonier <b>Finite-element simulation of S2-columnar ice viscoplastic behaviour: sensibility analysis</b>	113
Ke Sujuan, Wang Ling, Chen Lanqin <b>Generation mechanism analysis of river underwater ice</b>	121

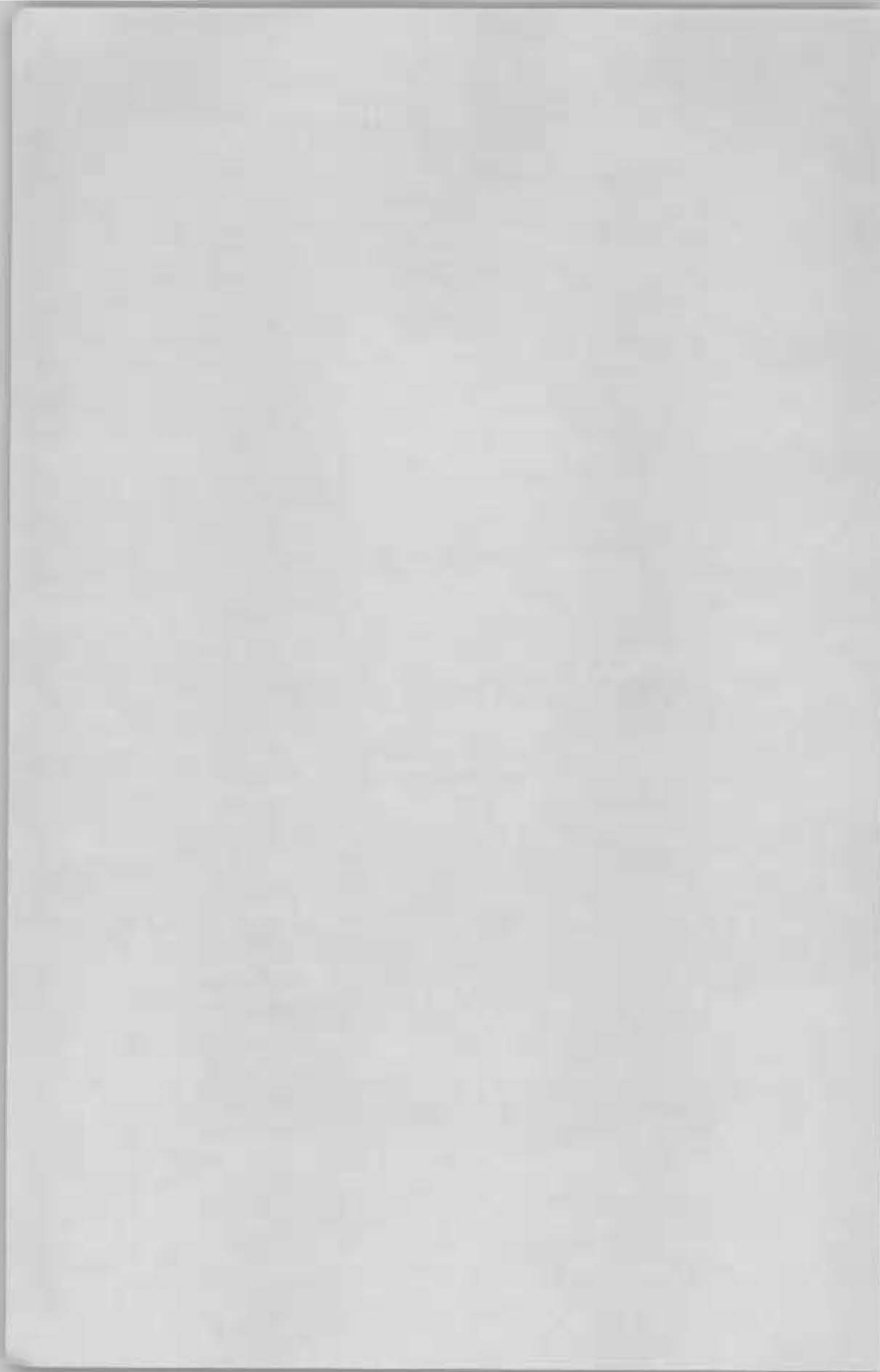
<b><u>B. ICE MECHANICS AND HYDRAULIC STRUCTURES IN ICE</u></b>	125
Q.J. Yue, X.J. Bi, X. Yu <b>Effect of ice-breaking cones for mitigating ice-induced vibrations</b>	127
G. Comfort, Y. Gong, S. Sing <b>Predicting static ice loads on dams</b>	135
G.W. Timco, R. Frederking, K. Smith, N. Billette <b>The Canadian PERD ice/structure interaction program</b>	145
M.G. Gladkov <b>Ice loads on multi-legged structures in arctic conditions</b>	153
D.S. Sodhi <b>Crushing failure during dynamic ice-structure interaction</b>	157
A. Barker, G. Timco, M. Sayed, B. Wright <b>Numerical simulation of the "Kulluk" in pack ice conditions</b>	165
J. Tuhkuri <b>Failure of the edge of an ice sheet against a vertical structure</b>	173
P. Liferov, O.T. Gudmestad, S. Løset, T. Mølmann <b>Design of arctic offshore pipelines to resist the forces from ice ridges</b>	181
G. Comfort, Y. Gong, S. Singh <b>The factors controlling static ice loads on dams</b>	189
T. Takeuchi, M. Sasaki, S. Kioka, N. Usami, H. Saeki, M. Kawamura <b>On the application of plane pressure panel to ice strength measurements</b>	199
S. Makita, K. Enoki, K. Izumiyama, F. Hara, H. Saeki <b>Modes of ice load acting on an ice boom for ice control</b>	207
T. Kitamura, M. Sato, M. Kato, Y. Watanabe, H. Saeki <b>The effect of drift ice on the stability of armor stones covering a doubly paced submerged breakwater in wave field</b>	215
T. Hayakawa, K. Kawai, M. Sato, M. Hanada, H. Saeki <b>Design of a facility for preventing overtopping of ice floes and estimation of ice load</b>	223
K. Shkhinek, T. Kärnä, S. Kapustiansky, A. Jilenkov <b>Numerical simulation of ice interaction with a vertical wall</b>	231
O. Kubit, R. Ettema <b>Ice-skimming booms for riverside diversions</b>	243
R. Ettema, L. Zabilansky, J. Wuebben <b>Observations on the winter performance of channel-stabilization structures</b>	251
Y. Yamauchi, K. Kamesaki <b>Unconsolidated rubble force of first year ridge acting on a vertical sided structure</b>	259

<b><u>C. HYDROLOGICAL AND METEOROLOGICAL INFLUENCES ON RIVER, LAKE, AND SEA ICE</u></b>	269
H. Baba, K. Hoshi, M. Yamazaki, H.T. Shen <b>Snowmelt runoff analysis for a breakup ice jam in the Shokotsu River basin</b>	271
D. Dybkowska-Stefek, M. Pluta <b>Ice jams on the Lower Odra</b>	279
N. Shatalina, G.A. Tregub, R.S. Frid <b>Calculation of water temperatures in a power plant reservoir with free-convection mixing considered</b>	287
X. Xia, H.T. Shen <b>Nonlinear interaction of shallow water wave with river ice covers</b>	295
Liu Cuijie, Yu Hong, Ma Xuemei <b>Ice flood in Northeast Region</b>	303
Duan Yuansheng, Liu Shubao, Li Yingshi <b>The causes of ice dam formation and its major contributing factors</b>	313
K. Szilder, E.P. Lozowski, T. Forest, G. Reuter, R. Gagnon <b>Modelling of wet ice accretions that result from spray</b>	323
Y. Hirai, M. Yamazaki, K. Hirayama, H. T. Shen <b>The March 1995 ice jamming in the Shokotsu River and Ashibetsu River</b>	331
<b><u>D. NAVIGATION AND OFFSHORE ACTIVITIES IN ICE CONDITIONS</u></b>	339
A. Jensen, S. Løset, J. Hellmann, O.T. Gudmestad, O. Ravndal <b>Model tests of an arctic tanker concept for loading oil Part I: Manoeuvring into loading position</b>	341
A. Jensen, S. Løset, K.V. Høyland, J. Hellmann, B.P. Vodahl <b>Model tests of an arctic tanker concept for loading oil Part II: Barge in a moored loading position</b>	353
K.-U. Evers, P. Jochmann, W. Kuehnlein <b>Ice model tests with an oil exploration barge in the North Caspian Sea</b>	363
<b><u>E. ENVIRONMENTAL AND ECOLOGICAL PROBLEMS IN LAKES, RIVERS, AND COASTAL ZONES IN ICE CONDITIONS</u></b>	371
Shen Xianchen <b>Effects of ice cover on the volatile phenol behavior and ecology in the northeast rivers of China</b>	373
E. Dolgopolowa, E. Tesaker <b>Turbulent structure of ice-covered flow and ice impact upon habitat in rivers</b>	381
S. Kioka, Y. Yasunaga, H. Saeki, H. Nishimaki <b>Evaluation of dominant parameters about the ice scour events</b>	391

<b><u>F. ICE FORECASTING AND MANAGEMENT OF HYDRAULIC AND HYDROPOWER INSTALLATIONS</u></b>	403
Shu-You Cao, Ran Li, Banjiuciren <b>Study of winter ice damage of Tanghe hydropower station in Tibet</b>	405
Guifen Li, Difang Xiao <b>A study of operation and control of Xigou hydropower plant during ice period</b>	411
<b><u>G. MISCELLANEOUS</u></b>	417
Jiang Du Hsin, Chen Hao Hua <b>Frozen ground from artificial ground freezing method for ice storage air conditioning system</b>	419

**TOPIC A**

**RIVER, LAKE, AND SEA ICE  
PROCESSES**





## RECONSTRUCTION OF SEA-ICE CONDITIONS IN THE GULF OF GDAŃSK SINCE XVI CENTURY

M.Sztobryn,<sup>1</sup> B. Kowalska<sup>1</sup>

### ABSTRACT

The authors aimed to reconstruct the ice conditions in the Gulf of Gdańsk from XVI to XIX century by Neural Network. Regular observations of sea-ice in this region reach as far back as the beginnings of XX century. For the time previous to XX century reliable information can be also derived from written sources, especially on the extremely cold or extremely warm winters. Reconstruction of ice conditions in the Gulf of Gdańsk was done in terms of three typical winter characteristics - mild, moderate and severe. The Neural Network was applied to two time series: the one consisting of the numbers estimating the maximum extent of ice cover in the Baltic Sea and the second one - the accumulated areal ice volume calculated for western Baltic Sea.

### INTRODUCTION

Long-time variation of the ice conditions in the Baltic Sea estimated for each winter by maximum ice extent, number of days with ice and other characteristics are one of the best indicators of the climatic changes in this part of Europe. This refers also to the region of Gulf of Gdańsk (Sztobryn and Krzysiński, 1999)

The Baltic Sea - due to its location and extension - remains under the climatic impact of nearly oceanic character in its western extremities and of the continental one in the north-east. These influences are additionally modified by the variety of particular basins - from deeper open waters, which easily remain free of ice even during strong winters to shallow indented gulfs, lagoons and narrow shoals which are the first to freeze, even if lying close to the North Sea.

Gulf of Gdańsk is lying a eastwards enough of the oceanic North Sea to painfully suffer the impacts of continental frost in winter. However adjoining the deeper waters of the Central Baltic Sea and being a comparatively deep and spacious basin itself , the Gulf of Gdańsk

---

<sup>1</sup> Instytut Meteorologii i Gospodarki Wodnej, Oddział Morski Gdynia, ul. Waszyngtona 42, 81-742 Gdynia, POLAND, Tel.: (48-58)-6205221, fax: (48-58)-6207101, e-mail: sztobryn@stratus.imgw.gdynia.pl

disposes over an adequate portion of accumulated summer heat and thus is able to resist against the ice formation longer, than other coastal basins.

During "normal" and mild winters there is no ice of "own origin" (the in-situ frozen surface waters) in the Gulf of Gdańsk, except of shallow, semi-closed bights and lagoons. Floating ice can be observed leaving the estuary of the river Wisła, also some coastal forms of ice are met. During severe winters ice cover is forming also by freezing of surface waters in the Gulf of Gdańsk. As a rule, in the Gulf of Gdansk ice is forming later (if any), than in the north-eastern parts of the sea. Usually, in normal winters, in Gulf of Gdansk ice is forming also later than in the shallow waters of the western parts of the Baltic Sea. These qualitative relation of Gulf of Gdansk to basins of earlier freezing time could help to complete the knowledge on the variation of winter severity in the region of Gulf of Gdansk in these spells in some few past centuries (prior to XIX century) for which the direct information is lacking. And this meant that suitable data sets were to be sought for and suitable method of data reconstruction had to be developed.

## **SOURCE MATERIALS AND DATA USED**

### **Baltic Sea**

The first paper based on quantitative data representing ice conditions of Baltic Sea winters was published by Seina and Palosuo (1993) and dealt with **maximum annual extent of ice cover (MAEIC)** on the Baltic Sea in the years 1720-1922. It was based on material collected by Jurva and Finnish Institute of Marine Research. In following years this series was successively completed. MAEIC is expressed either as the number of square km of the maximum (during the ice season) sea area covered by sea ice, or as the percent of the whole sea area (420 000 square km) covered by ice. Using their long time series the authors establish a 5 degree scale of winter severity for whole Baltic Sea: extremely mild (MAEIC < 19.3 %), mild (19.31-33.09 %), average (33.1-66.42 %), severe (66.43-91.19 %) and extremely severe (91.2-100 %).

Koslowski and others (1994, 1995, 1999) can derive another series of data from a study. However, the investigations by Koslowski, Loewe (1994) revealed that the severity of winter estimated by means of MAIEC parameter - does not always correspond with the severity in the western Baltic. They constructed a 7-degree scale on the basis of the calculation of the accumulated areal ice volume (expressed in meters) and it's numeral representation (**ice winter index numerals - V**) ranging from 0 to 3. Koslowski, Glaser (1995,1999) calculated the values of the AAIIV and V from 1501 to 1992 for western Baltic Sea.

The investigation by Schmelzer, Stanislawczyk, Sztobryn, performed in the nineties of the XX century proved that a parameter defined this way and calculated for particular basins is a very good indicator of the ice winter severity not only for the waters it was defined primarily.

### **Gulf of Gdańsk**

The earliest references on sea ice conditions in the Baltic Sea and Gulf of Gdańsk can be found already in some chronicles and other historical records (eg. Legal regulations in Hanseatic League; Matysik, 1958; Betin, 1962; Girguś, 1965; Namaczyńska, 1937; Walawender, 1932).

For these early years, however, the information on the severity of winters is scarce for this region and of weak reliable documentation. One can state that definite winter seasons were extremely severe, for instance 1496, 1546, 1568, when one could travel by sledges from Gdańsk to Hel; also the winters 1578, 1624, 1674, 1686, 1709, 1748 were very hard in this region. Regrettably, much more difficult would be to find the reliable ice data in the winters in-between.

Available is also ice information for the second half of nineteenth century. They are, regrettably, not very much regular and detailed, though reliable enough and are taken from the press, diaries and daily observations from some ports (eg. Baltijsk at the entrance to Zalew Wiślany).

Regular daily observations (which included information on the form of ice, ice extent and the obstructions to navigation due to ice) are available to the region of Gulf of Gdańsk since the end of nineteenth century. They begin in the winter season 1896/97 in the waters around Hel, since 1922/23 in the approaches and in the port of Gdańsk and since 1945/46 on the coastal in waters from Gdynia ( south-western part of the Gulf of Gdańsk) to Krynica Morska (south-eastern part).

Due to all diversity of data only a 3-degree scale of winter severity was used to reconstruct the character of ice conditions in previous ages in the Gulf of Gdańsk: 1 - very mild and mild winters, 2 - moderate winters and 3 - severe and very severe winters.

### **RECONSTRUCTION OF THE SEVERITY OF ICE CONDITIONS IN THE REGION OF GULF OF GDAŃSK BY NEURAL NETWORK**

#### **The neural network model**

To calculate the aimed reconstructed series of the 3-degree severity of ice conditions in the region of Gulf of Gdansk (SICGG) mathematical models were developed by the neural network and by method of regression on the basis of the XX century.

The comparison of actual (1922-1992) SICGG to 2 different classification methods (by MAEIC and by V) was done. Total conformability of SICGG with the ice conditions type calculated by means of index V (accumulated areal ice volume) for the areas of Western Baltic is as high as 66 % of winters. Similar comparison to the results gained by the MAEIC (for Baltic Sea as a whole) yield 57 % of conformable cases. Thus, actual ice conditions in the Gulf of Gdańsk were in 20 % of winters milder than gained using index V, and in 37 % of

winters milder than those calculated by MAEIC. These results remain in good agreement with experiences issuing from daily practice in the ice services.

### Description of the model

The neural network model was developed on the basis of optimum method of the network training which was checked using the training series, the testing and validating series, suitable option of the net structure (i.e. the number of layers and of neurons in particular layers). In order to find the optimum method of training following methods were tested: Multilayer Perceptron, Radial Basis Function and Probabilistic Neural Networks. From among the training methods the best agreement of the modelling results with the actual ones were gained using the Multilayer Perceptron -Back Propagation method.

Also several structures of neural network satisfying the theorem by Hecht-Nielsen were tested, beginning with the five-layer structure. The best projection of the actual conditions was gained for a four-layer structure of 5 neurons in the input layer, 3 neurons in the first hidden layer, 5 neurons in the second hidden layer and of one neuron in the output layer. The selection of such input data was decided due to the results of statistical analysis (precisely - cross correlation analysis, after the prior normalisation of data). For each neuron model a function of activation was calculated, in the form of a sigmoid function.

The comparison (Fig.1.) of the reconstructed series, calculated by means of the neural network and simple regression method was made for the data of the second half of nineteenth century from the writings and observational data referring to other basins of the southern Baltic Sea.

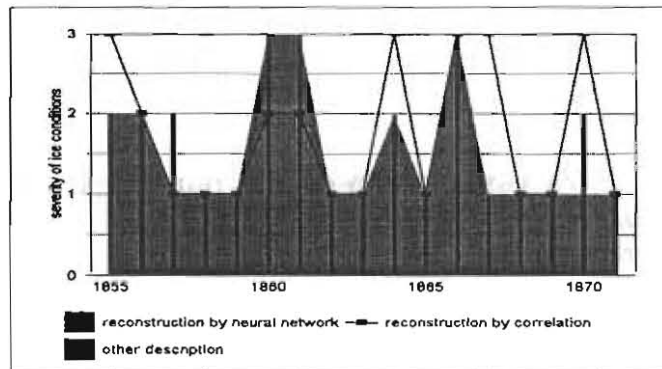


Fig.1. Comparison of the results of ice conditions gained by means of the neural network model and the regressive model and the region of the Gulf of Gdansk

In the majority of cases the reconstruction by means of neural network agreed with the data derived from the descriptive sources. Correlation coefficient was as high as 0.85 while for the regression model it reached scarcely 0,7 (0,68 precisely). For further calculations only the neural network model was applied.

The reconstruction for the years 1501-1900 -was made by means of the neural network model and on the basis of the variation of the index V in the same years, the variation of the parameter MAEIC in the years 1720-1900 and - due to the known quasi-8-annual periodicity of the ice conditions intensity (Sztobryn, 1994)- the values of the above mentioned parameters (after selection) of eight winters preceding.

#### Ice conditions in the Gulf of Gdańsk in the XVI to XIX centuries

The reconstruction SICGG in the centuries XVI to XVIII is shown in the Fig.2.-5. The results of reconstruction are in general in agreement with the scarce data from any documented sources.

The mild and average ice conditions in Gulf of Gdańsk were prevalent in XVI and in the first decade of XVII c.

The smallest number of severe and very severe winters was characteristic for the XVI century (Fig.2.), only 4 during the whole age, whereas the number of mild and average winters reached over 60 % with the longest warm period on the twenties of this century.

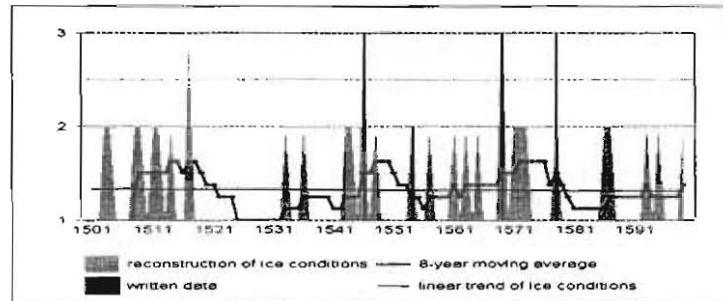


Fig.2. Reconstruction of ice conditions severity in the Gulf of Gdańsk during the XVI c.

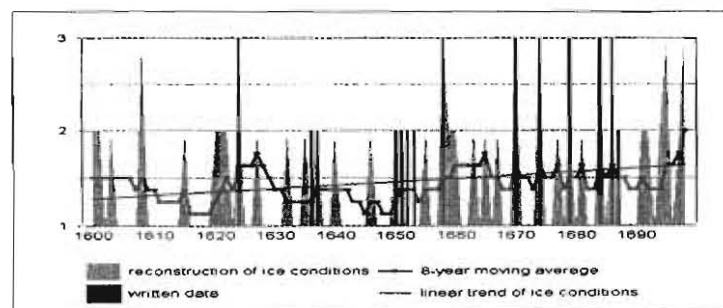


Fig.3. Reconstruction of ice conditions severity in the Gulf of Gdańsk during the XVII c.

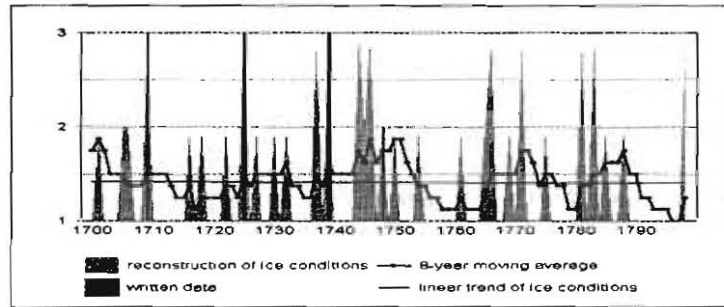


Fig.4. Reconstruction of ice conditions severity in the Gulf of Gdańsk during the XVIII c.

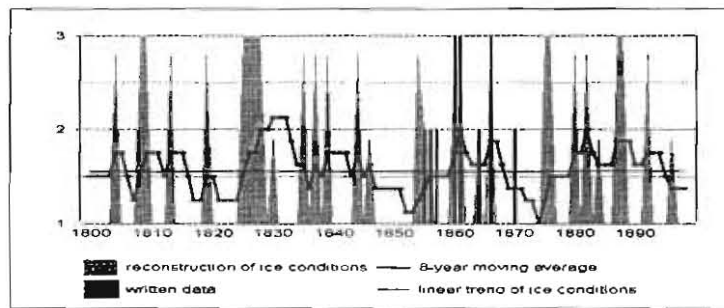


Fig.5. Reconstruction of ice conditions severity in the Gulf of Gdańsk during the XIX c.

XVII century (Fig.3.) brings an increasing number of severe and very severe winters, especially in the second half of century and decreasing number of mild winters.

The coolest spell fall on the XVIII (Fig.4.) and XIX centuries (Fig.5.), in which more than 30 % of winters were severe or average (severe: about 25 % in XIX c.). In XVIII century the coolest spells fall on the late forties, seventies and eighties of this century, where as only three comparatively warmer spells can be distinguished: in the second decade, about 1735 and in fifties. XIX century should be connected with the cold spell of the preceding, cold XVIII century the maximum number (in the investigated period) of the severe ice conditions appeared in this century.

The reconstruction shown that ice conditions as the indicator of winter climate were changed very significant during the investigated period from mild conditions in XVI century to rather severe in XIX.

## FINAL REMARKS

Good agreement of the results gained in reconstruction by neural network with the original data points on the possibilities of using this method in many climatological investigation of different time scale. It could be also used for spatial extrapolation onto the areas, where the data are sparse or irregular.

One should stress that the method used and the studies performed were applied for the first time to the problems investigated. The disposable information of real ice conditions in the Gulf of Gdańsk was scarce irregular, inhomogeneous and difficult to verify, it nevertheless proved sufficiently useful with the neural network method.

## REFERENCES

- GIRGUŚ R., STRUPCZEWSKI W. (1965): Wyjątki ze źródeł historycznych o nadzwyczajnych zjawiskach hydrologiczno-meteorologicznych na ziemiach polskich w wiekach od X do XVI, Warszawa, Wydawnictwa Komunikacji i Łączności.
- BETIN B., PREOBRAZENSKIJ J. (1962): Surowost zim w Ewropie i ledowost Baltiki, Leningrad.
- (1997): Project of IMGW, H-7, Gdynia.
- KOSŁOWSKI G., LOEWE P. (1994): The Western Baltic Sea Ice Season in Terms of a Mass-Related Severity Index 1879-1992, *Tellus* 46A, pp. 66-74.
- KOSŁOWSKI G., GLASER R. (1995): Reconstruction of the Ice Severity since 1701 in the Western Baltic, *Climatic Change* 31, pp. 79-98.
- KOSŁOWSKI G., GLASER R. (1999): Variations in Reconstructed Ice Winter Severity in The Western Baltic From 1501 To 1995, and their Implications for The North Atlantic oscillations, *Climatic Change* 41, pp. 175-191.
- MATYSIK S. (1958): Prawo morskie Gdańska, Warszawa, Wydawnictwo Prawnicze.
- NAMACZYŃSKA S. (1937): Kronika ksiąg elementarnych w Polsce i krajach sąsiednich w latach 1648-1696, Lwów.
- SCHMELZER N., SZTOBRYN M., STANISŁAWCZYK I. (1996 -1999): Ice Conditions in Zalew Szczeciński (Stettiner Haff) and in Zatoka Pomorska (Pommersche Bucht) During the Winter of 1995/96 - 1997/98, *Deutsche Hydrographie Zeitschrift*, Hamburg.
- SZTOBRYN M. (1994): Longterm Changes in Ice Conditions at the Polish Coast of the Baltic Sea. 12th International Symposium on Ice of the of the International Association for Hydraulic Research (IAHR), vol.1 pp. 345-354, Trondheim.
- SZTOBRYN M., KRZYMIŃSKI W. (1999): Extreme Sea Level Events, Sea-ice Conditions, Mean surface Temperature and Mean Salinity Changes During Last 45 Years - Gulf of Gdansk. *Publicationes Institutii Geographici Universitatis Tartuensis*, nr 84 Publications of Second Workshop on the Baltic Sea Ice Climate, Tartu, Estonia pp. 26-36.

SZTOBRYN M., STANISŁAWCZYK I., SCHMELZER N. (1999): Ice Conditions In the Szczecin Lagoon and Pomeranian Bay During the Normal Period 1961-1990, *Berichte des Bundesamtes für Seeschifffahrt und Hydrographie*, nr 20, pp. 1-37, Hamburg.

WALAWENDER A. (1932): *Kronika klęsk elementarnych w Polsce i w krajach sąsiednich w latach 1450-1586*, Lwów.



## SEA ICE OBSERVATIONS ON AN OFFSHORE PLATFORM IN BOHAI SEA

Qianjin Yue<sup>1</sup>, Shunying Ji<sup>1</sup>, Xi Zhang<sup>1</sup>

### ABSTRACT

In order to simulate the behaviors of the Bohai Sea ice more accurately, which is necessary to deal with the problem of ice-structure interaction, a field sea ice observation station was established on an offshore platform. The meteorological and oceanographic data and the sea ice conditions were recorded simultaneously and continuously. Based on the data, some thermodynamic and dynamic parameters, such as the solar radiation, the oceanic heat flux and the sea ice drag coefficients, were determined.

### INTRODUCTION

The numerical sea ice model was developed in the 1960s' and has been adopted to simulate the sea ice of the Arctic Pole and the Margin Ice Zone (Hibler, 1979; Parkinson et al., 1979; Lu, 1987). Wu (1991) used it to forecast the Bohai Sea ice of China. But owing to the offshore engineering activities, it is necessary to improve the model so as to satisfy the need of the problem of ice-structure interaction.

The sea ice in Bohai Sea is so strong dynamic under the action of tidal current and seasonal wind that it processes four characteristics: discontinuity of growth, non-stability of existence, rafting and heaping, and non-symmetry of distributions. For the purpose of obtaining sufficient data to determine the computational parameters in the sea ice numerical model, a sea ice observation station was established on the JZ20-2 platform in the Bohai Sea. Using the field data, the solar radiation, the oceanic heat flux and the drag coefficients of sea ice are determined respectively.

---

<sup>1</sup> State Key Laboratory of Structural Analysis of Industrial Equipment, Dalian University of Technology, Dalian, China, 116023, Tel.: +86-411-4708407, fax: +86-411-4708393, e-mail: yueqj@dlut.edu.cn

### SEA ICE OBSERVATION SYSTEM ON THE JZ20-2 PLATFORM

The sea ice observation station established on the Jz20-2 oil/gas platform in the Liaodong Bay mainly consists of four subsystems: weather station, current meter, marine radar system and video recorders. Its geographic coordinates are 40°30'N and 121°21'E as shown in Fig.1. Fig.2. gives the detail of the system. The layout of the equipment is shown in Fig.3.

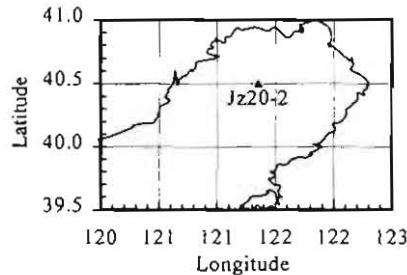


Fig.1. The position of sea ice observation station in the JZ20-2 area

#### Weather station

The weather station, 35m above the sea level, is installed on the top of the platform in order to avoid the influence of the platform. The air temperature, wind velocity, relative humidity, air pressure and solar radiation can all be recorded continuously, and a computer is connected to it to get the data per second during the whole winter.

#### Current meter

The current meter, 10m above the seabed, is laid down before the freezing period, and taken out in the next spring. Thus the oceanographic data, such as water temperature, salinity, current velocity and tide level, can be recorded per 15-minute during the whole winter.

#### Marine radar system

An improved marine radar system, RASCAR-3400M, has modern electron and computer technology with powerful transmitting power and lower receiving noise. It is applied to observe sea ice type and drifting tracks. The radar antenna is mounted on a tower set on the top of the platform. The total height is about 55m above the sea level.

#### Video camera

A video camera run by a computer automatically is fixed on a platform pile. It can analyze the digital images precisely. When the ice cover breaks and turns under the action of the cone plane, the sea ice thickness can be measured. At the same time, the sea ice type and velocity can also be obtained.

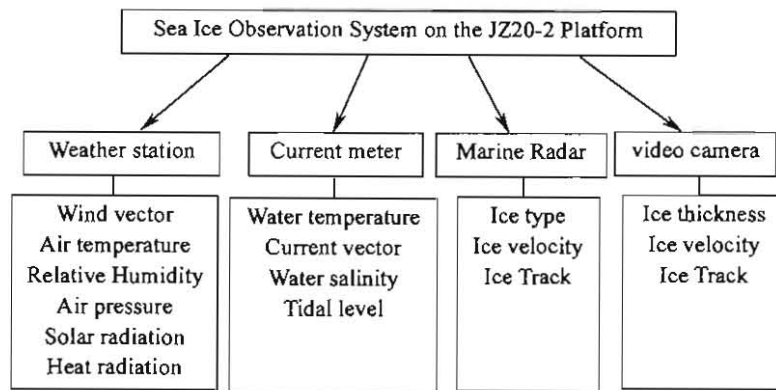


Fig.2. Sea ice observation system on the Jz20-2 platform

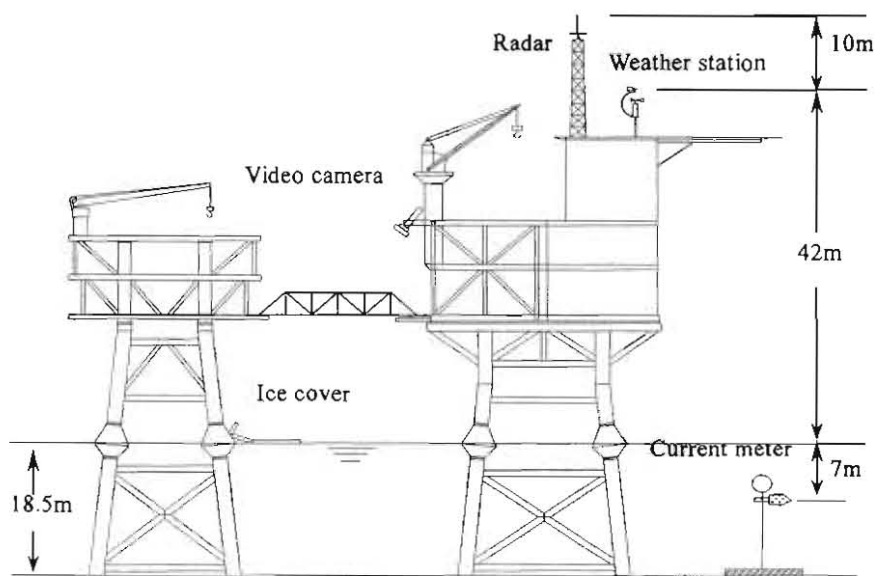


Fig.3. Layout of the sea ice observation station on the Jz20-2 platform

### COMPUTATIONAL PARAMETERS IN THE SEA ICE NUMERICAL MODEL

Based on the meteorological, oceanographic data and sea ice conditions measured on the JZ20-2 platform, solar radiation, oceanic heat flux and sea ice drag coefficients are analyzed.

#### Solar Radiation

Considering the effect of the atmosphere and cloud cover, the solar radiation can be calculated as follow:

$$Q_{se} = (1 - 0.0065C^2)Q_{s0}a^m \quad (1)$$

where  $Q_{se}$  and  $Q_{s0}$  are the intensity of solar radiation on a horizontal surface above the sea ice surface and above the atmosphere layer respectively,  $C$  is the cloud coefficient (in tenths),  $a$  and  $m$  are the transmittance of the atmosphere and the optical air mass respectively. As for the atmospheric transmittance, Glover et al. (1958) suggested the following relationship:

$$a^m = 0.99 - 0.17m \quad (2)$$

Based on the measured data on the JZ20-2 platform, we have  $m=0.83$ . The solar radiations observed and calculated are shown in Fig.4. We select the cloud coefficients as 10, 9, 8, 7, 3 and 0 according to different weather conditions of rain, snow, fog, heavy cloud, light cloud and clear sky. The calculated and measured results are both given in Fig.5.

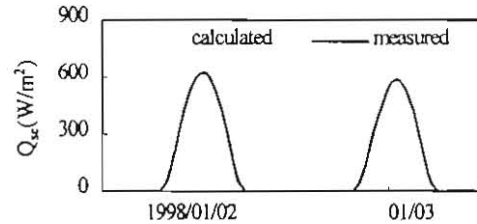


Fig.4. Measured and calculated results of solar radiation under clear sky

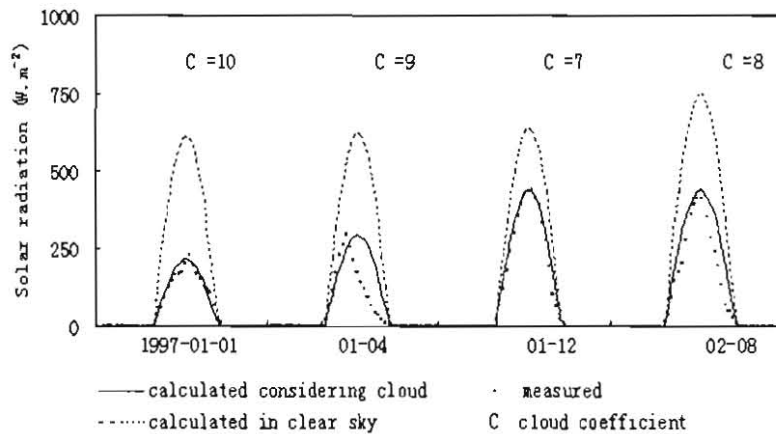


Fig.5. Measured and simulated solar radiation under different weather conditions

### Oceanic heat flux

The methods used to determine the ocean heat flux include eddy-correlate method (Mcphee, 1987), bulk model formulation (Josberger, 1987) and residual method (Shirasawa et al., 1997). In the residual method, the ocean heat flux is calculated as the difference between vertical heat flux within the growing sea ice and the latent heat released due to freezing at the ice-water interface.

At any location in the growing ice sheet, the energy balance at the ice-water interface can be given by:

$$F_w = -\rho_i L_i \left( \frac{dh_i}{dt} \right)_0 - F_c - Q_{sb} \quad (3)$$

where  $\rho_i$  is the sea ice density,  $L_i$  is the fusion heat of the sea ice,  $\left( \frac{dh_i}{dt} \right)_0$  is the sea ice growth rate at the ice-water surface,  $F_c$  is the molecular heat conduction,  $Q_{sb}$  is the solar radiation at the sea ice bottom. In the Bohai Sea, the ice thickness is very thin, (usually,  $h_i < 0.2$  m) the growing rate of sea ice at the bottom is affected by the solar radiation.

On the Jz20-2 platform, the ice thickness was measured four times per day at 8:00, 11:00, 14:00 and 17:00. Therefore, the oceanic heat flux can be obtained by integrating equation (3), we get

$$F_w = \left( \frac{h_{i(t_2)} - h_{i(t_1)}}{\rho_i L_i} - \int_{t_1}^{t_2} F_c(t) + Q_{sb}(t) dt \right) / (t_2 - t_1) \quad (4)$$

where  $h_{i(t_1)}$  and  $h_{i(t_2)}$  are the ice thickness at the time of  $t_1$  and  $t_2$ ,  $F_c(t)$  and  $Q_{sb}(t)$  are both the function of the time  $t$ . Using the thickness measured at 8:00 and 17:00 during the three days from 1998/1/14 to 1/16, the mean value of the calculated oceanic heat flux in the three days is  $179.65 \text{ Wm}^{-2}$ .

Using the method above, the oceanic heat flux is calculated during the winter of 1997-1998, and its trend and range are shown in Fig.6. We can see that, at the beginning of the ice period the oceanic heat flux has the maximum value, which is more than  $200 \text{ Wm}^{-2}$ , then decreases continuously, and finally in the melting period the value approaches zero.

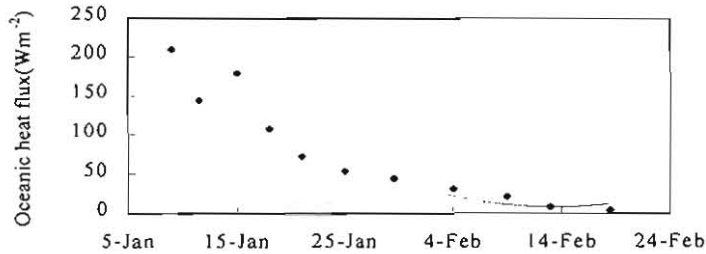


Fig.6. Oceanic heat flux during the winter of 1997-1998

### Drag coefficients

The momentum equation of the sea ice can be written as:

$$m \frac{dU_i}{dt} = \tau_a + \tau_w + m(a_k + g\delta + I) \quad (5)$$

where  $m$  is sea ice mass per unit area,  $\mathbf{U}_i$  is the horizontal ice velocity,  $\mathbf{a}_c = f\mathbf{K} \times \mathbf{U}_i$  is the acceleration caused by Coriolis' force, where  $f$  is the Coriolis parameter;  $\mathbf{k}$  is the unit vector in the  $x$  direction,  $g$  is the gravity acceleration,  $\delta$  is the non-dimensional sea-surface tilt vector, and  $I$  is the acceleration caused by internal ice stress.

Hibler (1979) found that the momentum equation is mainly controlled by the drag stresses of wind and current, and internal ice stress. In the sea zone of sub-polar or lower latitude, the sea ice is free drift, that is to say, the internal ice stress can also be ignored (Shen, 1994; Lu, 1987). So the equation (5) is simplified as:

$$\tau_a + \tau_w = \rho_i H_i \left( \frac{d\mathbf{U}_i}{dt} - \mathbf{a}_c \right) \quad (6)$$

Put  $\tau_a = \rho_a C_a |\mathbf{U}_a| \mathbf{U}_a$  and  $\tau_w = \rho_w C_w |\mathbf{U}_w| \mathbf{U}_w$  into equation (6), then decompose it into  $x$  (eastern) and  $y$  (northern) directions, we get:

$$\begin{cases} \alpha u_a + \beta u_w = \frac{du_i}{dt} - fv_i \\ \alpha v_a + \beta v_w = \frac{dv_i}{dt} + fu_i \end{cases} \quad (7)$$

where  $\alpha = \rho_a C_a (u_a^2 + v_a^2) / \rho_i h_i$ ,  $\beta = \rho_w C_w (u_w^2 + v_w^2) / \rho_i h_i$  and  $f = 2\omega \sin \phi$ ,  $u_a, v_a, u_w$  and  $v_w$  are the wind and current velocities in the eastern and northern directions respectively;  $\omega_e$  and  $\phi$  are the earth's angular frequency of rotation and local latitude.

From 11:45 on January 29 to 16:30 on 30, 1995, the wind, current and ice velocities measured are shown in Fig.7. With them, we obtain the mean drag coefficients:  $C_{a(42)} = 1.01 \times 10^{-3}$  ( $\sigma^2 = 0.37 \times 10^{-3}$ ) and  $C_{w(7)} = 0.61 \times 10^{-3}$  ( $\sigma^2 = 0.36 \times 10^{-3}$ ).

## CONCLUSIONS

A sea ice observation station was established on the Jz20-2 oil/gas platform in the Bohai Sea. It consists of four subsystems: the weather station, the current meter, the marine radar system and the video recorder. On the basis of the sea ice observation, some computational parameters in the sea ice numerical model, such as the solar radiation, the oceanic heat flux and the sea ice drag coefficients, were determined. In the solar radiation calculation, the cloud coefficients were classified into six groups according to different weather conditions. The oceanic heat flux during the winter of the 1997/1998 was calculated using the residual method, in which the solar radiation is considered. With the momentum balance of the sea ice drift movement, the sea ice drag coefficients of level ice were determined with the velocities of wind and current and sea ice measured at the same time.

For the difference of meteorological and oceanographic conditions in different sea areas, the computational parameters of the sea ice numerical model are not similar. Only with suitable

parameters adopted in the sea ice numerical model can the sea ice be simulated and forecasted successfully. Thus it is an important problem to determinate the parameters of different sea areas in the following work.

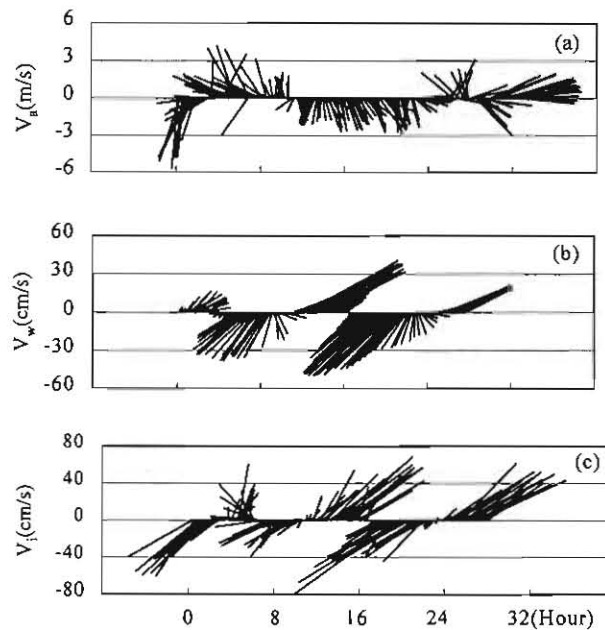


Fig.7. The wind (a), current (b) and sea ice (c) velocity vectors measured

#### ACKNOWLEDGEMENT

This paper was co-sponsored by the National Foundation of Natural Science, and in part by the Bohai Ocean Oil Corporation. We also thank the staff of the Jz20-2 platform for the great help in the field observation.

#### REFERENCES

- HIBLER W. D. (1979): A dynamic and Thermodynamic sea ice model. *J. phys. Oceanogr.*, 9, pp. 815-846.
- LU QIAN-MING (1987): On Mesoscale Modeling of the Dynamics and Thermodynamics of Sea Ice, Technical University of Denmark
- MCPHEE M.G., MAYKUT G.A., MORISON J. H. (1987): Dynamics and thermodynamics of the ice/upper ocean system in the marginal ice zone of the Greenland Sea. *J. of Geophysical Research*, 92(C7), pp. 7017-7031.

- PARKINSON C. L., WASHINGTON W. M. (1979): A large-scale numerical model of sea ice. *J. of Geophysical Research*, 84, pp. 311-337.
- SHEN H. H. (1994): Broken Ice Fields. *Proc. of the 12th Int. Symposium on Ice (IAHR)*, Trondheim, Norway, pp. 983-992.
- SHIRASAWA K. ET AL. (1997): Oceanic heat flux under thin sea ice in Saroma-ko Lagoon, Hokkaido, Japan. *J. Marine System*, 11, pp. 9-19.
- WETTLAUFER J.S. (1991): Heat flux at the ice-ocean interface. *J. of Geophysical Research*. 96(c4), pp. 7215-7236.
- JOSBERGER E.G. (1987): Bottom ablation and heat transfer coefficients from the 1983 Marginal Ice Zone Experiment. *J. of Geophysical Research*, 92(C7), pp. 7012-7016
- WU HUIDING (1991): Mathematical representations of sea ice dynamic-thermodynamic processes (in Chinese), *Oceanologia et limnologia sinca*, 22(4), pp. 321-327.



## MEASUREMENTS OF CONSOLIDATION IN THREE FIRST-YEAR RIDGES

K.V. Høyland<sup>1</sup>

### ABSTRACT

Results from examinations of consolidation in three first-year ice ridges are presented, discussed and compared with results from the literature. The relationship between the thickness of the consolidated layer and the level ice thickness varied from 1.39 to 1.85. The estimated thickness of the consolidated zone depended on the method of investigation, the drillings included a partly consolidated layer and gave a thicker consolidated zone than the temperature measurements did. The measured growth of the consolidated layer did however not depend on the method of investigation. The consistency of the unconsolidated rubble was clearly different at the two sites. It was soft and slushy at Spitsbergen, and harder in the Gulf of Bothnia. Three possible reasons are discussed: surrounding currents, different shapes and the difference in salinity.

### INTRODUCTION

Sea ice ridges are formed by compression or shear in the ice cover. They consist of ice blocks, slush, water, snow and air. The volume of non sea ice material to the total volume constitutes the macro porosity  $\eta$ . If a ridge is subjected to cold surface conditions the water pockets gradually freeze up and ice blocks adfreeze forming a frozen, or consolidated layer. Consolidation processes are governed by the meteorological conditions and continues throughout the cold season. The water underneath may add energy to the ice, and thus contribute to the deterioration of the (unconsolidated) rubble. There is probably seasonal variations in this flux and values between 0 and 18 W/m<sup>2</sup> has been measured for level ice (Heil et al., 1996). Ice ridges may represent the design load for structures in many arctic and sub-arctic marine areas. It is however not clear how these loads should be estimated. The prime lack of knowledge lies in information about the internal structure of the ridges. Increased knowledge about the size and the strength of the consolidated zone as well as the strength of the rubble is important. One problem is that the size of the consolidated layer is

---

<sup>1</sup> Department of Structural Engineering, Norwegian University of Science and Technology (NTNU), Trondheim, Norway /The University Studies at Svalbard (UNIS), Longyearbyen, Norway,  
e-mail: knut.hoyland@bygg.ntnu.no

not directly observable, it is thus important to relate it to easier accessible information such as the level ice thickness and the meteorological conditions. This paper focuses mainly on measurements of the thickness of the consolidated layer.

## EXPERIMENTAL

Measurements have been done on three different first-year ice ridges; Fig.1. shows the locations.

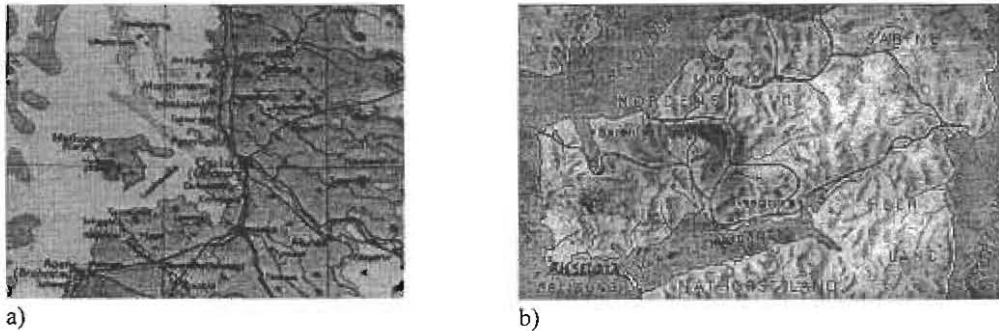


Fig.1. Maps over the areas, a) Marjaniemi outside Hailuoto in Finland. b) The Van Mijen fjord on Spitsbergen, \* the ridge outside Svartodden ridge, \*\* the ridge outside Camp Morten

The first ridge was instrumented in 1998 and was situated outside Svartodden in the Van Mijen fjord on Spitsbergen; the second was outside Camp Morten in the same fjord, whereas the third was outside the Marjaniemi weather station on Hailuoto outside Oulu in Finland. The general meteorological and oceanographical conditions differed significantly; the 1998 winter was very cold whereas the 1999 winter (at Spitsbergen) was very warm. In the Van Mijen fjord the ice usually forms in December, the melting begins from mid April (99) to mid May (98) and the ice leaves at the end of June. The ice thickness reaches normally around one metre in the end of April, and the sea water salinity is about 34 ppt. There are tidal currents in the fjord. At Marjaniemi the ice normally forms in December or January, the melting starts in late March or early April, and the ice is normally gone by May. The ice thickness normally reaches 0.6 m and the water salinity is from 0 to 6 ppt. There are practically no tide nor currents outside Hailuoto.

Table 1

Description of the three sites

	Svartodden 98 (Spitsbergen)	Camp Morten 99 (Spitsbergen)	Marjaniemi 99 (Finland)
Latitude	77.5° N	77.5° N	65° N
Instrumented period	2 March - 12 May	10 March - 5 May	25 Feb. - 25 March
Type of ridge	Short linear single ridge	Long curvilinear single ridge	Large rafted ridge-field

Measurements of temporal and spatial temperature development, geometry, block size and structure, salinity and porosity were done on all three ridges as well as on the level ice. The crystal structure of the consolidated layer was examined in the two 1999 cases, whereas density and uniaxial compression strength were only measured in the Finnish ridge. The compression tests were performed at the University of Oulu. Equipment and experimental procedures are given in Langeland (1998), Høyland and Løset (1999), Kyhring (1999) and Høyland et al. (2000).

## RESULTS

### Geometry and morphology

The two ridges in the Van Mijen fjord were singular ridges, whereas the one at Marjaniemi was part of a large ridged area with 3-5 layers of rafted ice. The Svartodden ridge had a sail height  $h_s$  of 1 m, the keel depth  $h_k$  was 4.4 m, the width 10 m and it was about 15 m long. The thickness of the blocks in the sail was between 0.2 and 0.25 m. The Camp Morten Ridge was long and curvilinear, had  $h_s$  of 1 m,  $h_k$  of 5 m, and a width of 15 m. The thickness of the blocks in the sail was 0.15 m. Visual inspection of the channels that were cut through the sail indicated that both of the Van Mijen ridges were formed in a similar way. It looked as if one side had been pressed up forcing the other sheet down. The ridge at Marjaniemi did not have the idealised triangular shape. The sail consisted of 0.2-0.3 m of rafted ice and was relatively flat. The keel depth was between 4 and 5 m, and the thickness of the blocks was 0.2 m.

### Porosity

Porosity measurements were done by drilling 2" holes and registering any drop of the drill as a pore. The keel consistence of Spitsbergen ridges made it difficult to get good data for the rubble porosity. It was difficult early in the season and impossible later. Table 2 sums up the results.

**Table 2**

The measured porosity in the three ridges

	Svartodden	Camp Morten	Marjaniemi
Sail	24% (93 holes)	-	21% (6 holes)**
Cons. + partly cons. layer	3.4% (93 holes)*	-	-
Rubble	33% (4 holes)	35% (uncertain)	38% (81 holes)

\*Most of these pores were found close to the rubble, probably in the partly consolidated layer.

\*\*The drilling was done in a nearby sail, less than 200 m from the thermistor-strings

### Meteorological conditions, snow cover and level ice thickness

The meteorological conditions and the snow cover basically govern the heat flux out from the ice. Tables 3 and 4 show the freezing degree-day index (FDD) and snow conditions. Some care should be taken in comparing FDD's for different latitudes. The influence of the solar radiation is not incorporated in the FDD-expression. And the solar radiation is more important

on Spitsbergen because the late part of the growth season takes place in the midnight sun. The thickness of the level ice was measured manually and with thermistor-strings (not for the Svartodden case). The initial thickness  $h_{i,0}$ , the final thickness  $h_{i,f}$  and the growth  $\Delta h_i = h_{i,f} - h_{i,0}$  are shown in Table 5.

**Table 3**

Some meteorological conditions

		Svartodden	Camp Morten	Marjaniemi
Instrumented period	Duration (weeks)	10	8	5
	FDD (°C days)	985	680	134
Growth period of the ridge	Duration (weeks)	10	7	3
	FDD (°C days)	985	624	126
Characterisation of winter		Cold	Warm	Normal

**Table 4**

The snow conditions (m)

	Svartodden	Camp Morten	Marjaniemi
Max. depth on level ice	0.4	0.3	0.05
Snow drift around the ridges	0-0.9	0-0.8	0-0.15

**Table 5**

The thickness of level ice (m)

Method	Svartodden	Camp Morten		Marjaniemi	
	Manual	Manual	Temperature	Manual	Temperature
$h_{i,0}$	0.95	0.70	0.6-0.7	0.47	0.4-0.5
$h_{i,f}$	1.16	0.85	0.7-0.8	0.60	0.5-0.6
$\Delta h_i$	0.21	0.15*	0.1	0.13	0.1

\*3-5 cm of superimposed ice

#### Keel consistence and oceanographical conditions

Measurements of water temperatures have been done by Kangas (2000). He found that the temperatures in the water masses were homogenous around freezing point in the fjord in late March '98, and that an intrusion of warm coastal water (up to  $T = -1.6^\circ\text{C}$ ) entered the fjord by late April '99. The ridge keel temperatures in an instrumented stamucha in the Van Mijen fjord in 1997 showed that it was heated from below as well as from above in late May and June. Temperatures up to  $-0.6^\circ\text{C}$  was recorded in the lower parts of the keel. The lowest temperatures could be found in the middle of the keel (Løset et al., 1998). Table 6 sums up some general keel conditions for the three ridges.

Table 6

## General keel conditions

	Svartodden	Camp Morten	Marjaniemi
Rubble consistence	Soft	Soft	Harder
Porosity measurements	Difficult / Impossible	Difficult / impossible	Relatively easy
Water salinity (ppt)	34	34	0-6
Assumed age at instrumentation	2 months	2 months	1 month
Surrounding currents	Strong tidal currents	Strong tidal currents	Little
Exposed area / keel volume ( $m^2/m^3$ )	0.65	0.67	0.25

**Consolidation**

Table 7 displays some key features from the measurements such as the growth of the consolidated layer  $\Delta h_{cons}$ , its relation to the growth of the level ice  $\Delta h_{cons}/\Delta h_i$ , the growth of the consolidated layer per day  $\Delta h_{cons}/day$ , the average final thickness of the consolidated layer  $h_{cons}$ , its relation to the final thickness of the level ice  $R_{avg}$ , the ratio of the maximum thickness of the consolidated layer to the final thickness of the level ice  $R_{max}$  and the duration of the growth.

**DISCUSSION****The thickness of the consolidated layer**

Examination of Table 7 reveals an important distinction. The three top rows comprise figures related to the growth of the consolidated layer  $\Delta h_{cons}$ , and in the three subsequent ones are values related to the total thickness of the consolidated layer  $h_{cons}$ . In the latter case it seems to be a systematic difference between the numbers derived from temperature measurements and the ones obtained from drillings. The temperature measurements predict a thinner consolidated zone. This difference cannot be found in the three top rows. Drilling results are generally more uncertain because they rely more on the person operating the drill. However, there is no reason to believe that this uncertainty should result in a systematic overestimation. Two reasons may be pointed out to explain this difference:

1. The given temperature derived data are minimum values
2. The drilling results include a partly consolidated layer. This layer probably exists below the fully consolidated one and has little mechanical strength and high temperature.

Explanation number one is not sufficient to explain the difference; even if the distance between the temperature sensors on the thermistor-strings (0.21 m) is added to  $h_{cons}^T$  it does not reach the value of  $h_{cons}^D$ . The warm winter of '99 resulted in thinner ice and shorter duration of growth than in '98. No difference can be seen in  $\Delta h_{cons}/\Delta h_i$  or  $\Delta h_c/day$ . If the ridges had been surveyed from their birth is it reasonable that a higher growth per day would

be found for the Svartodden case. The ridge at Marjaniemi had a higher growth per day; this is explained by it being less insulated because of a thinner snow cover.

**Table 7**

Key features of consolidation for the three ridges, number of drilled holes in brackets

	Svartodden*		Camp Morten		Marjaniemi	
	Temp.	Drillings (93)	Temp.	Drillings (43)	Temp.	Drillings (81)
$\Delta h_{cons}$ (m)	0.42	0.40	0.22	0.18	0.21	0.23
$\Delta h_{cons}/\Delta h_i$	2	1.90	2.2	1.88	2	1.75
$\Delta h_{cons}/day$ (cm/day)	0.75	0.77	0.79	0.84	1	1.02
$h_{cons}$ (m)	1.61	1.95	1.13	1.28	0.71	1.03
$R_{avg}=h_{cons}/h_i$	1.39	1.68	1.61	1.82	1.42	1.85
$R_{max}$	1.84	2.37	2.14	2.17		
Duration of growth	10 weeks		7 weeks		3 weeks	

\*At Svartodden did we not get data from the level ice string, so the values of level ice thickness are from drilling, this gives a higher value than a temperature string does, so the values for  $R_{avg}$  and  $R_{max}$  may be a little low. The central string failed in Svartodden and was not replaced until week 16. The estimated value for the thickness of the consolidated layer depends on weather this string is included or not. The growth of  $h_{cons}$  does an artificial jump between week 15 and 16 when string D is included. So to estimate the growth of  $h_{cons}$ , the temperatures in string D in week 10 are assumed based on the temperatures in the neighbouring strings. The growth of the consolidated layer then becomes 0.4 m - 0.43 m, a value of 0.42 m is chosen.  $R_{avg}$  and  $h_{cons}$  becomes 1.54 and 0.38 m when string D is excluded.

**Table 8**

Key features from some previous ridge experiments, <sup>T</sup> and <sup>D</sup> refers to weather temperature measurements or drillings have been used to examine the thickness

	$R_{avg}$	$\Delta h_{cons}/\Delta h_i$	Field / lab	Age (days)	Salinity (ppt)	$\eta$ (%)	Density (kg/l)
Coon et al. (1995)	1.24 <sup>D</sup>	1.87 <sup>D</sup>	Field	15	4.4-5.4	25-35	-
Croasdale et al. (1990)	1.6	-	Lab.	18	-	-	-
Frederking and Wriarth (1980)	1.75 <sup>D</sup>	-	Field, stamuc.	-	3-5	30	-
Kankaanpää (1997)	1.42 <sup>D</sup>	-	Field	-	0.3-0.8	30	0.8-0.9
Leppäranta et al. (1995)	1.75 <sup>D</sup>	1.85 <sup>D</sup>	Field	87	0.2-0.3	32	-
Timco and Goodrich (1980)*	1.39 <sup>T</sup>		Lab.	3.5		-	-
Veitch et al. (1991a and b)	1.25 <sup>T</sup>	1.54 <sup>T</sup> 1.35 <sup>D</sup>	Field	-	0.2-0.7	32	0.907

\*Only the experiment in which the initial phase is believed to have been exceeded

The presented results are comparable with other findings (Table 8).  $R_{avg}$  is reported to be less than two times the surrounding level ice thickness in all cases. Beketsky (1998) reports of average consolidated zone thickness of 3.5 m in the sea of Okhotsk, but the level ice thickness is not given so it is not clear what  $R_{avg}$  was.

#### **Deterioration of the keel and the oceanographical flux**

Three possible reasons for the striking difference in rubble consistence at Spitsbergen and in Finland can be identified. Firstly, the salinity is higher in the Van Mijen fjord, creating more porous ice that is more easily heated. Secondly, the shapes of the keels were different. The Van Mijen keels had inclined sides making the exposed area/keel volume bigger. This makes thermal and mechanical erosion created by surrounding currents more effective. Thirdly, there are strong tidal currents in the Van Mijen fjord, and there are almost none outside Hailuoto. It is also suggested that there are seasonal variations in the oceanographical flux in the Van Mijen fjord, and that it is zero in the cold season.

#### **CONCLUSIONS**

Three different ice ridges have been examined to gain increased insight in the effects of consolidation. The thickness of the consolidated layer has been examined in two ways, by temperature measurements and by drilling. The major findings of this paper are the following:

- The temperature measurements gave a ratio  $R_{avg} = 1.39-1.61$ , the drillings gave  $R_{avg} = 1.68-1.85$ . Thus the method of investigation seems to affect the result.
- The drillings probably include a partly consolidated layer in which the temperature is at the freezing point.
- The growth of the consolidated zone does not seem to be affected by the method of investigation.
- The consistence of the unconsolidated rubble was different in Van Mijen compared to at Marjaniemi. This may be due to differences in surrounding currents, shape of the keel and salinity of sea water.

#### **ACKNOWLEDGEMENT**

The author would like to thank civ. ings Arne Langeland, Morten Kyhring and Guro Kjestveit for their crucial assistance in the field work. Very important have also been dr. student Jaakko Heinonen and professor Mauri Määttänen from Helsinki University of Technology (HUT) who led the field program in Finland. The field work in Finland was a part of the LOLEIF project and the author is grateful for financial support and valuable discussion. Finally I would also like to thank my supervisor professor Sveinung Løset for encouragement and discussions.

#### **REFERENCES**

BEKETSKY S.P. (1998): Thickness distribution of consolidation hummock layer offshore Sakhalin. Proceedings of the 14th International Symposium on Ice (IAHR), Potsdam, New York, USA, July 27-31 1998, Vol. 1, pp. 357-359.

COON M.D., DOUGLAS C.E., GERALD S.K. (1995): Force displacement measurements of a first-year pressure ridge keel. ASME 1995, Ice mechanics, AMD-Vol. 207, pp. 239-254.

CROASDALE K.R., ALLEN N.F.B., MARCELLUS R.W. (1990): Thermal response of ice rubble: predictions and observations. Proceedings of the 10th International Symposium on Ice (IAHR), Espoo, Finland 20-24 Aug. 1990, Vol. 1, pp. 153-167.

FREDERKING R.M.W., WRIGHT B. (1982): Characteristics and stability of an ice-rubble field Issungnak, February-March 1980. NRC Technical memorandum, Jan 1982, No. 134, pp. 230-247.

HØYLAND K.V., KJESTVEIT G., HEINONEN J., MÄÄTTÄNEN M. (2000): LOLEIF ridge experiments at Marjaniemi. The size and strength of the consolidated layer. Submitted to IAHR 2000.

HØYLAND K.V., LØSET S. (1999): Measurements of temperature distribution, consolidation and morphology of a first-year sea ice ridge. Cold Regions Science and Technology 29 (1999) pp. 59-74.

KANGAS T-V. (2000): Cand Scient Thesis in Oceanography at Univ. of Bergen, in prep.

KANKAANPÄÄ P. (1997): Distribution, morphology and structure of sea ice pressure ridges in the Baltic Sea. Fennia 175:2, pp. 139-240. Helsinki ISSN 0015-0010.

KYHRING M. (1999): Thermo-mechanical properties of a first-year ice-ridge. Engineering diploma thesis at the University Studies on Svalbard (UNIS) / the Norwegian University of Science and Technology (NTNU), 40 p.

LANGELAND A. (1998): Measurements of geometry and temperature distribution of pressure ridges on Svalbard. Engineering diploma thesis at the University Studies on Svalbard (UNIS) / the Norwegian University of Science and Technology (NTNU), 40 p.

LEPPÄRANTA M., LENSU M., KOSLOFF P., VEITCH B. (1995): The life story of a first-year sea ice ridge. Cold Regions Science and Technology 23 (1995) pp. 279-290.

LØSET S., LANGELAND A., BERGHEIM B., HØYLAND, K.V. (1998): Geometry and physical properties of a stamucha found on Spitsbergen. Proceedings of the 14th International Symposium on Ice (IAHR), Potsdam, New York, USA, July 27-31 1998, Vol. 1, pp. 339-344.

TIMCO G.W., GOODRICH L.E. (1988): Ice rubble consolidation. Proceedings of the 9th International Symposium on Ice (IAHR), Sapporo, Japan, 1988, pp. 426-438.

VEITCH B., LENSU M., RISKÄ K., KOSLOFF P., KEILEY. P., KUJALA P. (1991a): Field observations of ridges in the northern Baltic Sea. Proceedings of the 11th International Conference on Port and Ocean Engineering under Arctic Conditions, St. John's, Canada, pp. 381-400.

VEITCH B., KUJALA P., KOSLOFF P., LEPPÄRANTA M. (1991b): Field measurements of the thermodynamics of an ice ridge. Report M-114, Laboratory of Naval Architecture and Marine Engineering, Helsinki University of Technology, Espoo, Suomi, 53 p.

## DETECTABILITY OF ICE RIDGES BY SYNTHETIC APERTURE RADAR

K.I. Gausland<sup>1</sup>, O.T. Gudmestad<sup>2</sup>, H.E. Krogstad<sup>3</sup>, S. Løset<sup>3</sup>

### ABSTRACT

Ice ridges are formed by compression or shear in the ice cover. They may pose a serious threat to shipping and offshore activities in these waters and it would therefore be a major asset to all these marine activities if synthetic aperture radar remote sensing could be used to identify ice ridges and estimate the ridge dimensions.

In order to make qualitative judgement of current SAR systems and establish demands for the future, established semi-empirical backscattering models for sea ice have been combined with mathematical ice ridge models in order to produce *simulated* SAR images of differently sized first-year ridges for various SAR resolutions and incident angles. The simulations show increased detectability for larger incident angles and greater small-scale surface roughness. Increased resolution appears to be less important for the detectability, but is needed for reliable ridge dimension estimates. In general, the simulations indicate that incident angles of about 35° or higher, with a resolution of 9×9 m or better, would give valuable information about the presence of ridges in level ice.

The validity of the simulations may however be questioned due to the uncertainty of small-scale surface roughness measurements of ice ridges. Further analysis is also necessary for investigating whether ice fractures may cause ambiguous signatures relative to ice ridges.

### INTRODUCTION

The large spatial extent of sea ice in arctic waters poses large difficulties for shipping, marine activities, and offshore operations. The Pechora Sea, containing substantial hydrocarbon resources, is among one of these areas. The ridges may represent the design loads on offshore platforms and may also hamper shipping and marine operations. Microwave remote sensing, independent of daylight and cloud cover, therefore provides a valuable asset to all marine

---

<sup>1</sup> TietoEnator Consulting AS, 0510 Oslo, Norway, e-mail: kjell-inge.gausland@tietoenator.com

<sup>2</sup> Statoil, 4035 Stavanger, Norway

<sup>3</sup> NTNU, 7491 Trondheim, Norway

activities in arctic waters, and represents the most promising technique for sea ice surveillance (Carsey, 1992).

This paper presents results from a study of the SAR's capability of detecting ice ridges (Gausland, 2000). Established semi-empirical backscattering models for sea ice have been combined with simplified mathematical models of ice ridges in level ice in order to produce simulated SAR images for a variety of input parameters.

During the analysis it became evident that there is actually a lack of small-scale surface roughness measurements of ice ridges. For surface scattering analysis the surface roughness is very important, and further measurements are required in order to support or possibly modify the currently developed backscattering models.

The paper is organised as follows: The first two sections briefly summarise the ice conditions of the Arctic seas and the physical basis for microwave remote sensing of ice. The following sections describe the SAR and the backscattering basis used in the SAR image simulations. The last two sections present and discuss results obtained by the simulation model.

### SOME CHARACTERISTICS OF ARCTIC SEA ICE

Sea ice in arctic waters constitutes of a number of different ice types. However, when simulating the SAR images used in this paper, only saline first-year ice is considered. For such ice, the surface *roughness* properties are very important for the backscattering of electromagnetic waves in the microwave domain. Based on Drinkwater (1989) and Onstott (1992), four different small-scale surface roughness types were chosen (Table 1).

**Table 1**

Surface roughness statistics for four first-year ice surfaces

Surface type	Roughness, $\sigma_{rms}$ (cm)	Correlation length, $l$ (cm)
A	0.108	0.538
B	0.493	2.778
C	0.766	7.75
D	1.74	12.8

The ice cover is a heterogeneous mixture of fresh ice, brine and air. The relative fraction of these constituents vary during wintertime mainly due to brine drainage. The surface layer may typically have a salinity of 7 ppt, which is slightly higher than in the middle layer of the ice. The middle layer has a lower salinity due to brine gravity drainage, wicking up of the brine, and the fact that the initial entrapment of salt is greater when the surface cover is created. Further down into the ice, the salinity again increases due to less time for brine drainage.

Deformation of first-year ice often results in the formation of ice ridges. The ridges may occur in a range of different shapes with a sail of 2 m, width of 10 m, and a keel depth of 10 m. The length may be several 100 metres. First-year ice ridges typically consist of ice blocks with arbitrary orientations (Løset et al., 1999).

It is also fairly common for first-year ice to be covered by snow, which is a mixture of ice and air. If the snow is wet, water droplets are also present in the mixture. Contrary to first-year ice, a typically 30 cm thick snow layer is normally not saline. It is also much less dense than the ice, ranging from 0.3 to 0.4 g/cm<sup>3</sup>, whereas first-year ice typically has a density of 0.915 g/cm<sup>3</sup>.

### THE PHYSICAL BASIS FOR SEA ICE REMOTE SENSING

The microwaves transmitted by radar are reflected and scattered by the target. Intuitively, an object may scatter an incident wave into all possible directions with varying strength, and this scattering pattern would vary with the incident direction. For a point scatterer the relationship between the incident power and the received power is referred to as the *radar cross section* is defined by:

$$\sigma = \frac{4\pi R^2 |E^s|}{|E^i|^2}, \quad (1)$$

where  $R$  is the range between the target and the radar receiver,  $E^i$  is the incident field and  $E^s$  is the scattered field along the direction under consideration.

The above equation is not formulated for area extensive targets and does not include polarisation effects. In practice, the radar cross section per unit area,  $\sigma^0$ , is the statistical average of the infinitely many point scatterers  $d\sigma$  occupying the illuminated area  $A$ :

$$\sigma_{ir}^0(\theta_i, \phi_i) = \frac{4\pi R^2 |E_r^s|^2}{A |E_i^i|^2}, \quad (2)$$

where the angles  $\theta_i$  and  $\phi_i$  define the incident angles, and the indices  $t$  and  $r$  signify the vertical or horizontal polarisation states of the transmitted and received waves, respectively.

The complex relative permittivity of the water-ice-snow system decides how electromagnetic waves propagate in the media according to Maxwell's equations. Many mathematical expressions for the permittivities have been proposed and a good overview is given by Hallikainen and Winebrenner (1992). An important effect of salinity, even as low as 4 ppt, is that microwave penetration into the medium is seriously diminished.

### THE SYNTHETIC APERTURE RADAR

For near real-time surveillance of sea ice, near polar orbiting satellites utilising synthetic aperture radars represent the most promising technique. The main reason for this is, although SARs have coarser resolution than comparable optical instruments, a radar may acquire images in all weather conditions and during complete darkness. It has already been

established that a SAR has the capability of detecting a variety of ice features (Johannessen, 1997).

Basically the SAR operates by radiating electromagnetic waves onto the ground and measuring the backscattered signals. In its simplest form, intensity images are formed on basis of the varying backscattering strength from different objects on the ground. During the image simulation process, a SAR satellite with properties given by Table 2 is modelled.

**Table 2**

Parameters of the SAR/satellite used in the simulations

Parameter	Value(s)
Altitude	785 km
Antenna	1 m by 10 m
Incident Angles	10-50°
Polarisation	VV
Resolution	3-25 m
Wavelength	0.057 m

A variety of techniques are used to form these images. The interested reader is referred to Ulaby et al. (1981, 1982, 1986).

### BACKSCATTER THEORY

Because ice and snow are physically and dialectically inhomogeneous, electromagnetic waves encountering these substances are not simply reflected and refracted. Rather, the illuminating radiation is scattered into a range of directions through surface and volume scattering and combinations of these depending on electromagnetic frequency, polarisation, direction of incidence, surface roughness, and dielectric properties of the scattering medium.

There are many ways of modelling backscatter from sea ice. Kim (1984) evaluated the solution of the radiative-transfer model against a simple semi-empirical model used by Ulaby et al. (1982) for describing backscattering from vegetation and snow. For the sea-ice case, Kim added a surface-scattering term resulting in the following equation for the backscattering coefficient of a one-layer model,

$$\sigma^0(\theta) = \sigma_s^0(\theta) + Y^2(\theta) \left( \sigma_v^0(\theta') + \frac{\sigma_g^0(\theta')}{L^2(\theta')} \right), \quad (3)$$

where:

$\sigma_s^0(\theta)$	is the backscattering from the surface,
$\sigma_v^0(\theta)$	is the volume scattering coefficient for the ice,
$\sigma_g^0(\theta)$	is the backscattering from the ice bottom interface,
$Y(\theta)$	is the transmission coefficient across the upper surface,
$L(\theta)$	is the one way loss factor through the layer, and
$\theta'$	is the refracted angle in the ice.

The surface and volume scattering terms are thus the most important, whereas the scatter from the ice bottom interface may be ignored because of absorption and scattering loss in the above medium. The refraction angle may be found simply by utilising Snell's law, while the transmission is the Fresnel power transmissivity.

Volume scattering is caused by varying dielectric constants throughout the medium. In sea ice, the volume scattering is caused by brine inclusion and air bubbles. For snow, volume scattering may be modelled as ice particles in air.

Surface scattering happens on the interface between two media with different dielectric constants. The amount of backscatter is largely a function of the surface roughness on a length scale comparable to the radar wavelength. The amount of backscatter increases with roughness from zero on a plane surface.

During the simulation of the radar images, a Kirchhoff model and a small-perturbation model are used to account for the varying surface properties in Table 1.

### **MODELLING RESULTS OF DIFFERENT ICE CASES**

In order to simulate SAR images from different ice fields, various mathematical models for calculating the backscatter were developed. One case considers a first-year ridge for each of the four different surfaces in Table 1. The ridges are assumed to be 500 metres long and with widths given in Table 3. The corresponding sail heights are adjusted to give a sail angle of approximately  $20^\circ$ .

Physically, an ice ridge is described on three length scales. On the macro scale, the ridge is assumed to possess a triangular shape. When incident radiation hits the ridge, the incident angles are adjusted to take into account the sail slopes when calculating the backscatter.

On the micro scale, the small-scale surface roughness is assumed to be similar to the surrounding ice. This is a first approximation model, as the breaking of the ice when the ridge is formed, may actually increase the roughness and thus the backscattered signal. Also, there is no reason to believe that the surface roughness of the ice bottom is similar to the roughness of the ice-air interface in case some of the blocks tip over.

The block structure of the first-year ridge is dominant on the meso scale. In the mathematical model the block structure is simulated by orienting the blocks as random facets superimposed on the triangular shape of the ridge. The facets are assumed to be 0.5 m by 0.5 m with a normal vector taking on a random angle in the upper hemisphere.

Using these extensions to the backscattering models for sea ice developed by other authors, SAR images have been simulated for varying ridge sizes on the surfaces mentioned for the different SAR/Satellite parameters as given in Table 2. Only the results for an incident angle of  $35^\circ$  are included in Table 3, see Gausland (2000) for further results. In the table the

possibility of detecting an ice ridge in a given simulated image is denoted by no, faint, or good. The small-scale surface roughness of Surfaces *A* and *B* is best given by a Gaussian correlation function while it is given by an exponential correlation function of Surfaces *C* and *D*. The specific Gaussian or exponential distribution parameters are given in the table.

**Table 3**

The table summarises the possibility of detecting an ice ridge on Surfaces *A* to *D* of Table 1 at an incident angle of 35° with varying SAR resolutions and ridge widths (or sizes)

Incident Angle 35°						
Surface A ( $\sigma_{rms} = 0.108$ cm, $l = 0.538$ cm)						
Resolution (m)	Ridge width (m)					
	1	4	7	11	15	20
25	No	No	No	No	No	No
15	No	No	No	No	No	No
9	No	No	No	No	No	No
3	No	No	No	No	No	No
Surface B ( $\sigma_{rms} = 0.493$ cm, $l = 2.778$ cm)						
25	No	No	No	No	Faint	Faint
15	No	No	No	Faint	Faint	Faint
9	No	Faint	Faint	Faint	Faint	Good
3	No	Faint	Good	Good	Good	Good
Surface C ( $\sigma_{rms} = 0.766$ cm, $l = 7.75$ cm)						
25	Faint	Faint	Faint	Good	Good	Good
15	Faint	Faint	Faint	Good	Good	Good
9	Faint	Faint	Faint	Good	Good	Good
3	Good	Good	Good	Good	Good	Good
Surface D ( $\sigma_{rms} = 1.74$ cm, $l = 12.8$ cm)						
25	Faint	Faint	Faint	Good	Good	Good
15	Faint	Faint	Faint	Good	Good	Good
9	Faint	Good	Good	Good	Good	Good
3	Good	Good	Good	Good	Good	Good

Another sea ice case that has been considered is the same ice fields and ice ridges as above, but now with a snow cover. The impact adding a snow cover to the previously mentioned ice fields are showed in Table 4 for an 11 m wide ridge.

Table 4

The table summarises the possibility of detecting a snow covered ice ridge on Surfaces *A* to *D* of Table 1 at an incident angle of 35° with varying *snow cover* properties

Incident angle 35°				
Surface A ( $\sigma_{rms} = 0.108$ cm, $l = 0.538$ cm)				
Resolution (m)	Snow Cover Properties			
	Thickness 20 cm		Thickness 50 cm	
	Radius 1 mm	Radius 2 mm	Radius 1 mm	Radius 2 mm
25	No	No	No	No
15	No	No	No	No
9	No	No	No	No
3	No	No	No	No
Surface B ( $\sigma_{rms} = 0.493$ cm, $l = 2.778$ cm)				
25	No	No	No	No
15	No	No	No	No
9	Faint	No	No	No
3	Faint	No	Faint	No
Surface C ( $\sigma_{rms} = 0.766$ cm, $l = 7.75$ cm)				
25	Good	No	Faint	No
15	Good	Faint	Faint	No
9	Good	Faint	Good	Faint
3	Good	Good	Good	Good
Surface D ( $\sigma_{rms} = 1.74$ cm, $l = 12.8$ cm)				
25	Faint	Faint	Faint	Faint
15	Faint	Faint	Faint	Faint
9	Good	Good	Good	Good
3	Good	Good	Good	Good

#### DISCUSSION AND CONCLUSIONS

From the simulations it is apparent that an increased incident angle greatly improves the possibility of detecting ice ridges. Increasing the resolution has in many cases not a significant impact on the ridge detectability. However, a fine resolution improves the ridge size estimates, which of course is very important for assessing the risks to the surface activities.

The surface roughness is also very important for the detectability. The simulations show increased detection capability when going from Surface *A* to *D*. Furthermore, it is likely that the backscatter from the ridges could be even stronger, since the small-scale surface roughness on the ridge is probably greater than on the surrounding ice. Unfortunately there is a scantiness of these roughness measurements as no references were found.

Depending on the frequency of encountering ice ridges with different surface roughness and the roughness of the surrounding ice, it may be beneficial to acquire satellite imagery at a shorter wavelength. By doing this, the surface will look more rough to the radar. Another idea is to image an area with different wavelengths if the area includes different ice surface roughness.

As expected, the simulated images indicate that the increased volume scatter from dry snow diffuse the ridge signatures and makes ridge detection more difficult. However, at a resolution of 9 m and better on the rougher surfaces, the detectability is still satisfying as compared to no snow cover.

None of the models that have been applied include the possibility of corner reflectors on the ice ridges. However, this possible shortcoming of the models were addressed by inspecting multi-look images produced from ERS-1 single look complex images. No corner reflectors could be identified on these 25-m resolution images.

The problem of signature ambiguities has not yet been discussed. If any sea ice feature has similar signatures as ice ridges, it must be fractures. Fractures are also long features with widths comparable to individual ridges or, if the fracture is wide, to ridge belts. In many cases it has been observed that fractures produce dark signatures in the ice due to young smooth ice in the fracture. However, at great wind speeds new fractures with open water may result in bright signatures. Brash ice in the fracture will also cause bright signatures.

In order to decrease the possibility of signature ambiguities, SAR images should not be obtained at low incident angles. Furthermore, it may be beneficial to analyse SAR images with knowledge of wind speeds in the area at the time of imaging so one may know in advance if the wind was sufficiently strong to cause signature ambiguities in open water fractures.

## REFERENCES

CARSEY F.D., editor (1992): *Microwave Remote Sensing of Sea Ice*, volume 68 of *Geophysical Monograph*. American Geophysical Union, 2000 Florida Avenue, NW, Washington, DC 20009, USA.

DRINKWATER M.R. (1989): LIMEX'87 ice surface characteristics; implications for C-band SAR backscattering signatures. *IEEE Transactions on Geoscience and Remote Sensing*, GE-27(5), pp. 501-513.

GAUSLAND K.I. (2000): *Modelling of Synthetic Aperture Radar Backscatter from Sea Ice and Ice Ridges*. MSc thesis (unpublished), Department of Industrial Mathematics, Norwegian University of Science and Technology, Trondheim.

HALLIKAINEN M., WINEBRENNER D.P. (1992): The physical basis for sea ice remote sensing. In: Carsey, F.D., editor, *Microwave Remote Sensing of Sea Ice*, volume 68 of

Geophysical Monograph, chapter 3, pp. 29-46. American Geophysical Union, 2000 Florida Avenue, NW, Washington, DC 20009, USA.

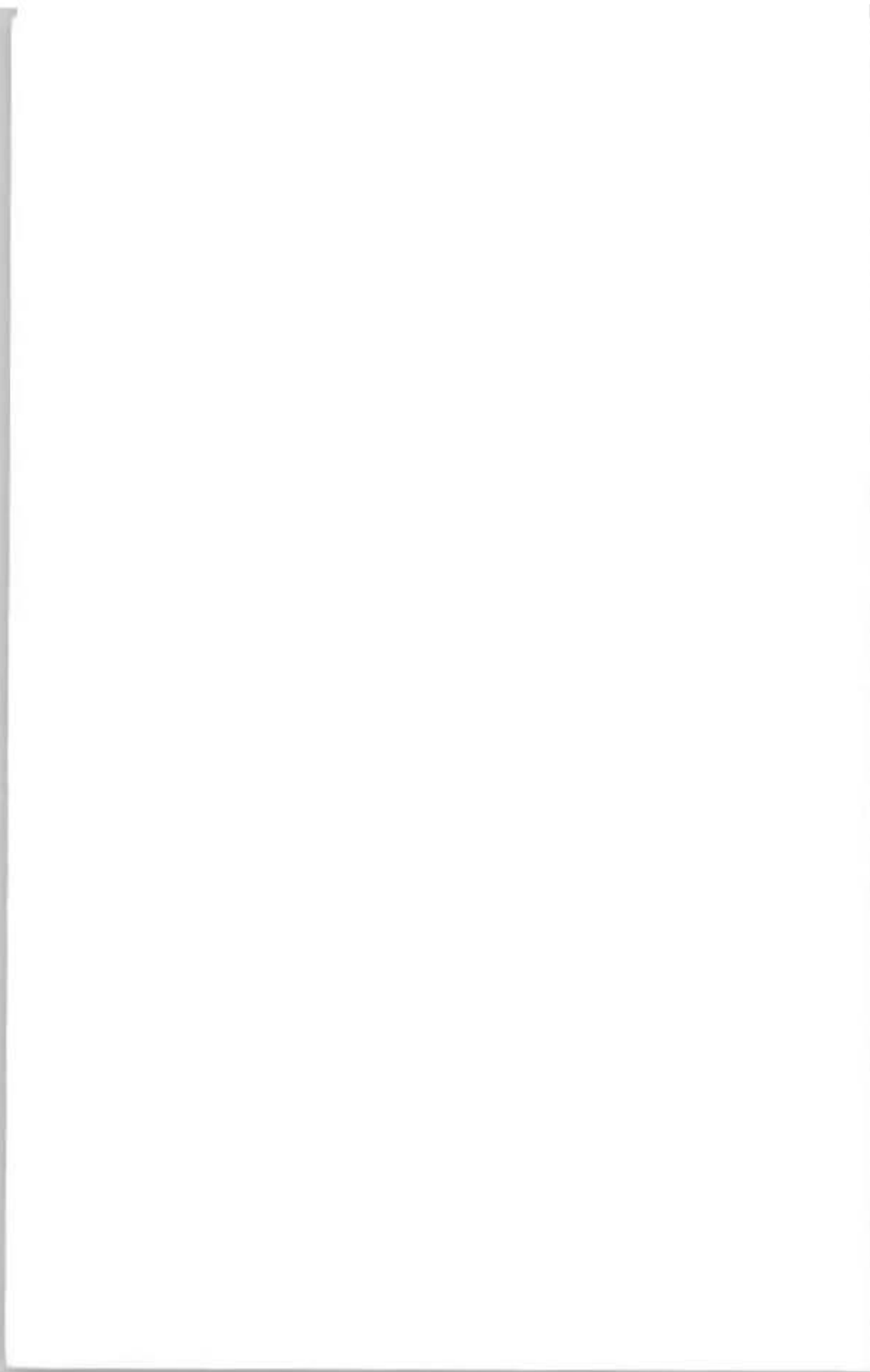
JOHANNESSEN O.M., SANDVEN S., DROTTHING Å., KLOSTER K., HAMRE T., MILES M. (1997): ERS-1 SAR Sea Ice Catalogue. ESA Publication Division, Noordwijk, The Netherlands.

KIM Y.S. (1984): Theoretical and Experimental Study of Radar Backscatter from Sea Ice. PhD thesis, University of Kansas, Lawrence, KS.

LØSET S., SHKHINEK K., GUDMESTAD O.T., STRASS P., MICHALENKO E., FREDERKING R., KÄRNÄ T. (1999): Comparison of the physical environment of some Arctic seas, *Cold Regions Science and Technology* (29)3, pp. 201-214.

ONSTOTT R.G. (1992): SAR and scatterometer signatures of sea ice. In: Carsey, F.D., editor, *Microwave Remote Sensing of Sea Ice*, volume 68 of Geophysical Monograph, chapter 5, pages 73-104. American Geophysical Union, 2000 Florida Avenue, NW, Washington, DC 20009, USA.

ULABY F.T., MOORE R.K., FUNG A.K. (1981, 1982, 1986): volume 1, 2, and 3 of *Microwave Remote Sensing: Active and Passive*. Addison-Wesley Publishing Company, Reading, Massachusetts.



## ICE DRIFT SPEEDS IN THE PECHORA SEA

S. Løset<sup>1</sup>, J.K. Økland<sup>1</sup>

### ABSTRACT

The paper analysis data collected from four Argos positioned buoys deployed on the drift ice mid-April 1998 in the Pechora Sea. The buoys transmitted their position for about 75 days. The collected position data are used to estimate the speed of the drift ice during this period. The distribution of speed fits a 2-parameter Weibull distribution with  $\theta = 0.212913$  and  $\gamma = 1.40610$ . Based on this distribution the one year and 10 years return period speed values are estimated to 1.16 m/s and 1.33 m/s, respectively. The validity of the data is discussed.

### INTRODUCTION

The ice conditions in the western Russian Arctic have been studied by a number of Russian scientists, for instance Zubov (1943) and Lebedev (1938). Later long-term observations are reported by Gorshkov and Faleev (1980) while in more recent years special reports are made for the most potential oil exploration waters (Mironov et al., 1994, 1997; Løset et al., 1997). However, the reporting is meagre on speed data for drifting sea ice.

The present paper starts by describing a data set of four buoys that were deployed on the drift ice in the Pechora Sea mid-April 1998. It continues with discussing the analysis of these data and how to provide statistics on drift speeds.

### CALCULATION PROCEDURE OF DISTANCES AND SPEEDS

Argos is a satellite-based location and data collection system. It consists of transmitters, receivers and a number of processing centres around the world. The receivers are carried on board NOAA polar-orbiting satellites. The location of the transmitter is at best (Class 3) within 150 m, while for Class 2 the accuracy is between 150 and 350 m. For Class 1 the accuracy is between 350 m and 1000 m (Argos, 1996).

In the present data the position of a buoy is given by five significant numbers. This introduces a kind of discretisation error. The uncertainty introduced by the round-off, or number of

---

<sup>1</sup> Department of Structural Engineering, Norwegian University of Science and Technology, Norway

digits, is then about  $\pm 55$  m in latitude, and  $\pm 20$  m in longitude. Thus, in worst case the buoy can be positioned  $(55^2+20^2)^{1/2}$  m  $\approx 60$  m away from the given position.

The four buoys (Buoys 06640, 22435, 24050 and 24051) were deployed on the drift ice in the Pechora Sea during mid-April 1998. The drift of the four buoys is shown in Fig. 1.

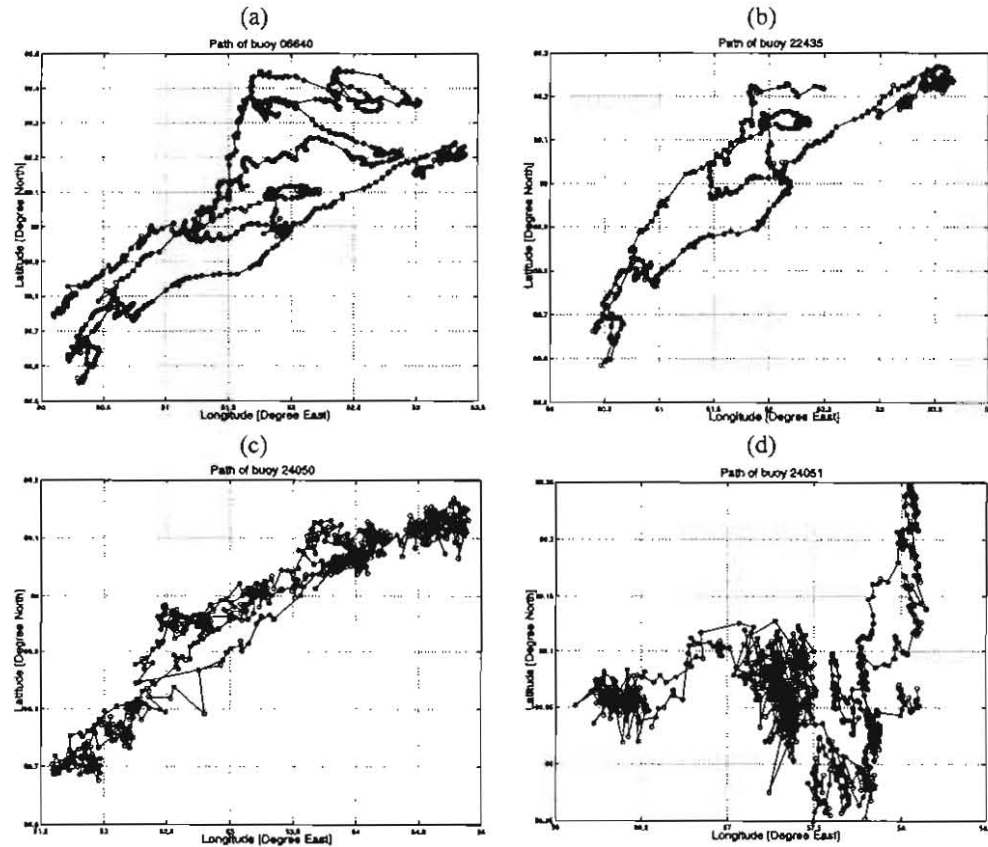


Fig.1. Drift of: (a) Buoy 06640, period 17.04-30.06.98; (b) Buoy 22435, 17.04-30.05.98; (c) Buoy 24050, period 17.04-10.06.98 and (d) Buoy 24051, period 20.04-23.06.98.

For each buoy the time spacing between two measurements varied widely with 1.5-2 hours as the most frequent interval. Assume that the total number of Argos observations for a buoy is  $N$ . Each observation is called  $\Omega_n$ , where  $n \in [1, N]$ . Further, assume that the observations are arranged according to time where  $\Omega_1$  is the first observation. Each observation contains the position,  $p_n$  and time  $t_n$ . Let  $\Delta p_n$  be the distance between  $p_{n+1}$  and  $p_n$ , and  $\Delta t_n = t_{n+1} - t_n$ . An estimate of the speed of a buoy is then given by:

$$v_n = \frac{\Delta p_n}{\Delta t_n} \quad (1)$$

There is some uncertainty in the measurements of positions. Assume that there is an error  $\epsilon_n$  in the observation. Then we may calculate an upper and lower bound for the speed by the following equations:

$$v_n^{\max} = \frac{\Delta p_n + \epsilon_n + \epsilon_{n+1}}{\Delta t_n} \quad (2)$$

$$v_n^{\min} = \left( \frac{\Delta p_n - \epsilon_n - \epsilon_{n+1}}{\Delta t_n}, 0 \right) \quad (3)$$

Let us study the buoy with most observations, Buoy 06640. This buoy provides 1368 observations of which 71 % is Class 3 data. If we use only Class 3 data ( $\epsilon_n = 150$  m), the values of  $v_n^{\min}$  will be as shown in Fig.2a. The figure shows a number of very high estimates of the speed – far beyond reasonable values. By inspections of the data it appears that for every speed  $v_n^{\min}$  higher than 1 m/s, the period  $\Delta t_n$  is very small. Therefore, we introduce the restriction that  $\Delta t_n$  should exceed 600 s. The results are shown in Fig.2b. Note that in both cases the lowest speed is calculated.

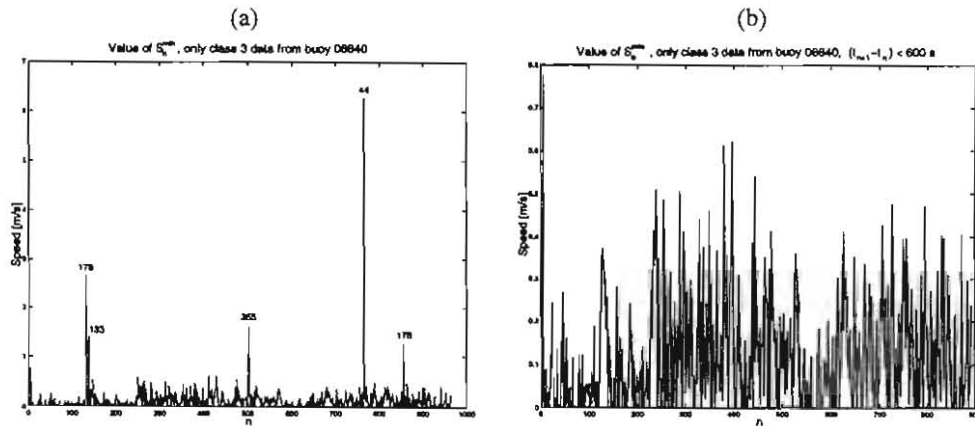
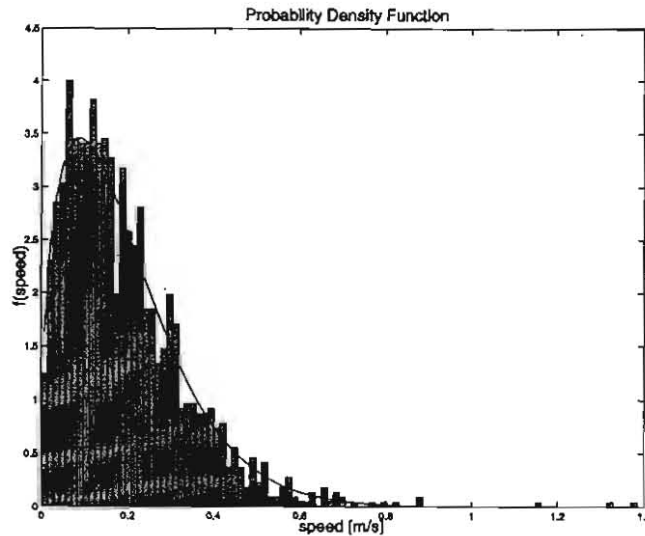


Fig.2. (a) Minimum speed  $v_n^{\min}$  for Buoy 06640. The x-axis displays the number of observations, and can be regarded as a time-scale.  $\Delta t_n$  (in seconds) is shown on each of the largest peaks; (b) minimum speed  $v_n^{\min}$  for Buoy 06640, with  $\Delta t_n > 600$  s.

### DISTRIBUTION OF SPEEDS

The upper, lower and mean speed for each of the four buoys are calculated. The mean speed is the speed calculated when using data without any correction for uncertainty.

When adding up estimates of speed that are calculated from only Class 3 values, we obtain a total of 1570 numbers for all the four buoys. With many observations we believe that the best possible estimate of the speed is the mean speed. A histogram of this speed is shown in Fig.3.



**Fig.3.** Histogram of the speed distribution from all four buoys (Class 3 data only, and  $\Delta t_n > 600$  s) and with a 2-parameter Weibull probability density distribution (*pdf*) fitted to the data ( $\theta = 0.212913$  and  $\gamma = 1.40610$ )

Based on the satellite observations during a period of 75 days, we suggest to represent the speed of the four buoys by a stationary stochastic process  $X(t)$ , having a cumulative 2-parameter Weibull distribution (Bury, 1975):

$$F_X(x) = 1 - \exp\left[-(x/\theta)^\gamma\right] \quad (4)$$

where the scale parameter  $\theta = 0.212913$  and the shape parameter  $\gamma = 1.40610$  in the present case. The fitting of the Weibull distribution is also shown in Fig.4.

Based on this statistics, we get the following estimates:

- The average drift speed is 0.19 m/s
- According to the proposed *pdf* of speed, the probability of exceeding a drift speed of 0.46 m/s is 5 %
- The probability of exceeding 0.63 m/s and 1.0 m/s is 1 % and 0.02 %, respectively.

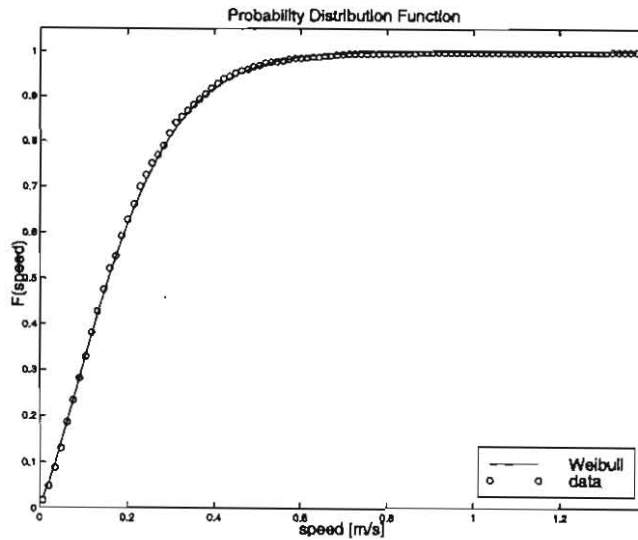


Fig.4. Cumulative probability distribution function plotted with the real data of the speed

#### RETURN PERIODS OF DRIFT ICE SPEEDS

Let  $X$  be a random variable with the cumulative probability density function  $F_X(x) = P(X \leq x)$ . If we make a series of independent observations of  $X$ , the expected number of observations until level  $A$  is exceeded equals:

$$N(A) = 1 / (1 - F_X(A)) \quad (5)$$

If the time step between independent observations equals  $\Delta t$ , the expected time until exceeding  $A$ , the *return period*, is

$$R(A) = \Delta t / (1 - F_X(A)) \quad (6)$$

For a continuous process  $X_t$ , the value of  $t$  is generally unknown, and knowledge of the stationary *pdf* is not sufficient to obtain it. Unless a more sophisticated mathematical description of  $X_t$  is available, this time step must be estimated, usually based on physical knowledge of the process. It must be sufficiently long to ensure independence, but not too long, as the process might then exceed level  $A$  between observations.

As seen from Eq. 6, the return period estimates are directly proportional to the time between independent observations. The satellite observations at hand are typically made every 1.5-2 hours, and the successive calculated speeds seem to be independent. However, the time between independent speed observations might well have been shorter, but due to lack of frequent observations, estimating this time falls into the category of educated guesswork. It follows from Eqs. 5 and 6 that the level  $A$  corresponding to a given return period  $R(A)$  equals:

$$A = \theta \left[ -\ln \left( \frac{\Delta t}{R(A)} \right) \right]^{1/\gamma} \quad (7)$$

If we assume that  $\Delta t$  is equal to 10 minutes, we get the return periods shown in Table 1.

Estimated return periods of speeds

Table 1

Return period	1 year	10 years	100 years
Level	1.16 m/s	1.33 m/s	1.49 m/s

## DISCUSSION

When calculating the speed we decided to use a threshold value for the time spacing of 600 s. In the following we will investigate the reasoning for this. Let us again use only Class 3 data from Buoy 06640, and we observe the following:

- If we do not use the threshold of 600 s, there must be an uncertainty of 280 m to have the lowest limit for the speed below 1.2 m/s
- According to Fig. 5 the high value for speed  $v_H$  occur every 8.5 to 9.5 day. We observe the same trend at the same time for the other three buoys.

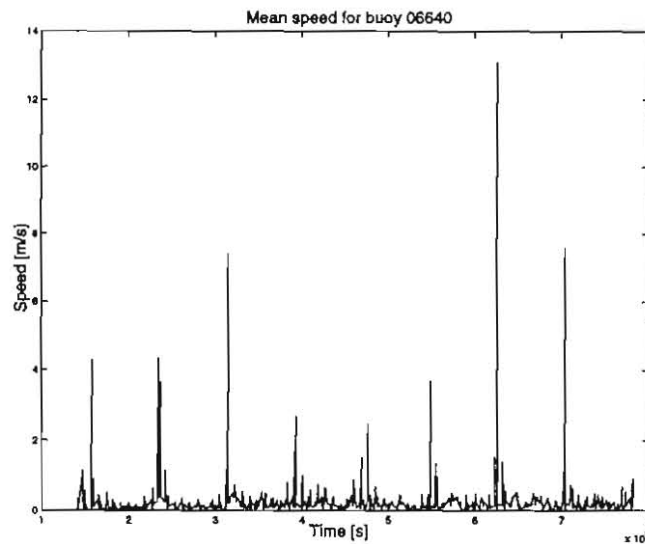


Fig.5. Mean speed for Buoy 06640 without threshold for time. The peaks occur with 8.5-9.5 days time spacing.

The satellites carrying the Argos system are travelling in polar orbits, and the polar plane are turning around the polar axis with the same rate as the Earth turns around the sun. There are at

least two satellites in service. The satellites are almost following the longitudes, but not completely. Due to the rotation of the Earth, the satellites are slowly changing longitudinal position. This means that observations at the poles will be more frequent than at Equator. We observe a peak in the speed when two observations are very close in time. This occurs when the two satellites are very close to each other, and there is an observation from each.

When the time spacing is small, the calculated speed will be very sensitive to uncertainty. This can clearly be seen from Eqs. 2 and 3. Thus it is possible to recognise that the accuracy of the data is not as good as we assumed and we have two possible explanations:

1. The uncertainty is considerably larger than assumed.
2. There is a systematic error in at least one of the receivers.

If the first explanation is the correct one, this would slightly change our results. The upper limit for speed would be somewhat higher, and the lower limit somewhat lower. Assume that the second theory is correct. We would then measure the path of the buoys to be longer than the real path. This would again lead to an overestimate of the speed. However, this means that our results are conservative.

The return period values shown in Table 1 should be used with care as they rely heavily on the accuracy of the probability function in Eq. 4. Making 100-year predictions based on data collected during 75 consecutive days is obviously speculative.

## CONCLUSIONS

The paper analysis data collected from four Argos positioned buoys deployed on the drift ice mid-April 1998 in the Pechora Sea. The buoys transmitted their position for about 75 days. The speed statistics provides the following estimates:

- The average drift speed is 0.19 m/s.
- According to the proposed *pdf* of speed, the probability of exceeding a drift speed of 0.46 m/s is 5 %.
- The probability of exceeding 0.63 m/s and 1.0 m/s is 1 % and 0.02 %, respectively.
- The levels of speed for return periods 1 year, 10 years and 100 years are 1.16 m/s, 1.33 m/s and 1.49 m/s, respectively.

The return period values should be used with care since e.g. making a 100-year prediction based on data collected during 75 consecutive days is obviously speculative.

## ACKNOWLEDGEMENT

The authors would like to thank Dag K. Onshuus (Norsk Hydro ASA) for advises in the project and the Northern Gateway Terminal Group for financial support.

## REFERENCES

- Argos (1996): Argos User's Manual. Toulouse, France, January.
- BURY K.V. (1975): Extremal models in applied science. Wiley, 625 p.
- GORSHKOV S.G., V.I. FALEEV Eds. (1980): Atlas of the Oceans. The Arctic Ocean. USSR Ministry of Defence.
- LEBEDEV V.V. (1938): Rost l'da v arkticheskikh rekakh i moriakh v zavisimosti ot otritsatel'nykh temperatur vozdukha. Problemy Arktiki, 5, pp. 9-25.
- LØSET S., SHKHINEK K., STRASS P., GUDMESTAD O.T., MICHALENKO E.B., KÄRNÄ T. (1997): Ice Conditions in the Barents and Kara Seas. In: Proceedings of the 16th International Conference on Offshore Mechanics and Arctic Engineering, Yokohama, 13-18 April 1997, Vol. IV, pp. 173-181.
- MIRONOV Y.U., SPICHKIN V.A., EGOROV A. (1994): Season variability and their variations in the region of mastering of the Barents and Kara Seas Offshore. Proceedings of the First International Conference on Development of the Russian Arctic Offshore (RAO-93), St. Petersburg, September 21-24, 1993, pp. 110-121.
- MIRONOV Y.U., LEBEDEV A.A., TYURYAKOW A.B. (1997): Estimate of the probability of Kara Ice occurrence in the vicinity of the Prirazlomnoye oil field in the Pechora Sea. Proceedings of the 16th International Conference on Offshore Mechanics and Arctic Engineering, Yokohama, 13-18 April 1997, Vol. IV, pp. 165-172.
- ZUBOV N.N. (1943): Arctic Ice. Izdatel'stvo Glavsermorpurti, Moscow (English translated by U.S. Naval Oceanographic Office, Washington D.C., 1955), 490 p.

## LOLEIF RIDGE EXPERIMENTS AT MARJANIEMI; THE SIZE AND STRENGTH OF THE CONSOLIDATED LAYER

K.V. Høyland<sup>1</sup>, G. Kjestveit<sup>1</sup>, J. Heinonen<sup>2</sup>, M. Määttänen<sup>2</sup>

### ABSTRACT

Measurements of spatial and temporal temperature development, geometry, porosity, salinity, density, crystal structure and uniaxial compression strength of a first-year ice ridge field have been performed. Thickness, salinity and density of the level ice were also measured. The test site was a large ridged area with 3-6 layers of rafted ice, the keel depth ranged from 4 to 9 m and the average porosity of the unconsolidated rubble was 38 %. The strength of the ice had a clear dependency of the depth below the water line from which it was taken: below and above 0.85 m. The strength of the consolidated layer was 5-7 MPa. The temperature measurements showed that the consolidated layer ended up being between 0.71 and 0.92 m, the drillings predicted a thicker layer, 1.05-1.11 m.

### INTRODUCTION

Sea ice ridges are formed by compression or shear in the ice cover. They are usually created by environmental forces such as winds and currents and especially in the shear zone between the landfast and drift ice. Ridges are porous features consisting of ice blocks, slush, water and in the sail also air and snow. The keel is often divided into an upper consolidated layer and a lower part of unconsolidated rubble. The consolidated zone grows throughout the cold seasons. Ridges may represent the design load for ships, coastal and offshore structures in many arctic and sub-arctic marine areas. It is however not clear what load a first-year ridge can exert on a given structure or how the ridge deforms. The loads are usually calculated by assuming that the load contributions from the sail, the consolidated layer and from the keel can be found independently and then added together (eg. Krankkala and Määttänen, 1984). Different ridge failure modes observed at the Molikpaq platform is reported by Timco et al. (1999). For a large number of the ridges the first failure occurred in the level ice behind the ridge. The ridge itself failed in different modes: shear, bending or spine failure. They reported that the measured loads were lower than those given by different load algorithms. Increased

---

<sup>1</sup> The Norwegian University of Science and Technology (NTNU), Trondheim, Norway,  
e-mail: knut.hoyland@bygg.ntnu.no

<sup>2</sup> The Helsinki University of Technology (HUT), Espoo, Finland

knowledge about the internal structure of first-year ridges is necessary to improve these load estimates. Crushing is the worst case scenario for the consolidated layer. Thus its size and compression strength are of special importance. We are in the following concerned with the consolidated zone, its size and the derivation of its material and physical properties. Several researchers (eg. Leppäranta et al., 1995; Croasdale et al., 1990; Frederking and Wright, 1980; Kankaanpää, 1997; Timco and Goodrich, 1988) have studied the vertical extension of the consolidated layer and it seems to be between 1.3 and 2 times the level ice thickness. It is however not clear how the consolidated layer should be defined, nor does it seem to exist a standardised method for examining the thickness of this layer. The water line is often used as an upper boundary as the blocks are loosely bound in the sail. The lower boundary is more difficult to define because it exists a partly consolidated layer beneath the fully refrozen one. This partly consolidated layer is a porous high temperature zone with less mechanical strength than the fully refrozen one, but the strength is probably higher than for the unconsolidated rubble. The determination of the lower boundary can be done either in a thermal-, or in a mechanical sense. If the thermal one is chosen, then the temperature becomes the prime indicator of consolidation. The temperatures in the consolidated layer are said to be below the freezing point. The measurements can be made by coring or by installing thermistor-strings. The thermal definition has the advantage that it is precise and that it is clearly related to measurements. The disadvantage is that it excludes the partly consolidated layer and that it takes more time and money than drilling. A mechanical definition will be related to a pronounced drop in some mechanical strength at a certain depth level. The best way to examine this is to take samples from different depths, and do eg. uniaxial compression tests. This is time and money consuming, so another popular way is by drilling. The major advantage of drilling is that it is quick to perform. It is however less precise as it depends to a larger degree on the driller. Another disadvantage is that it is more destructive so it becomes difficult to examine the temporal development. The thermal definition seems to estimate a thinner consolidated layer than what is found by drilling (Høyland, 2000).

## EXPERIMENTAL

The field-work was a part of the LOLEIF project and took place at Marjaniemi scientific station at the island Hailuoto outside Oulu in the north of Finland. The Helsinki University of Technology (HUT) organised and was responsible for the field-work. The work reported in this paper was a co-operation between HUT and the Norwegian University of Science and Technology (NTNU). The test site was located in an 8 km long chain of different shear - and pressure ridges off shore the western coast of Hailuoto. The ice formed in December and stayed until the first half of May. Six thermistor-strings were installed along a line in the rubble, and one in the level ice. Dataloggers were attached to all of the strings and logged the temperatures every sixth hour from 26 February to 25 March. The porosity and geometry was examined by drilling. The thermistor-strings, dataloggers, drilling equipment and procedures are described in Løset et al. (1998). Meteorological conditions were recorded at the scientific station at Marjaniemi. Ice was cut from the consolidated layer to make uniaxial compression tests and to measure salinity and density. The salinity and density measurements were done at location, whereas the horizontal uniaxial compression tests were done at the University of

Oulu. The density measurements were performed by mass divided by volume. The volume was measured by putting the samples into a plastic bag, submerging it in water and measuring the displaced volume. One set of the samples was left to drain for between 0.5 and 1 hour before measuring. The other set was taken directly from the water. The salinity, density and thickness of the level ice were also measured. The samples for the compression tests were cylindrical with length from 134.5 to 151.5 mm, and diameter varying from 67.5 to 69.5 mm. The tests were performed according to IAHR guidelines; the temperature of the ice was  $-10^{\circ}\text{C}$ , the velocity of the pushing plate was constant, ie almost constant strain rate of  $10^{-3}\text{ s}^{-1}$ . The force and the displacement were recorded, and some of the tests were recorded on video.

## RESULTS

### Geometry, morphology and porosity

The ridge was probably formed around 20 January 1999. The meteorological data show low pressure, low visibility and high wind-speed around this date. Simulations also show that the level ice thickness was about 0.2 m at that time (Høyland, in prep.). It was a large ridge area with 3-6 layers of rafted ice. The depth of the keel ranged from 4 to 9 metres, and was about 4.5 metres in the thermistor-area. The depth of the keel seemed to be independent of the visible sail. The thickness of the rafted layers was 0.2 m. The average porosity of the total keel in the thermistor-area was 0.34, whereas it was measured to be 0.38 in the unconsolidated part. A decreasing porosity was found in the three cross-sections that were drilled twice.

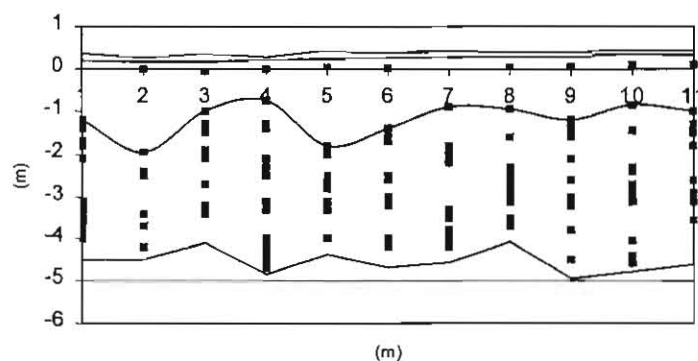


**Fig.1.** The thermistor cross-section 25.03.99. The black dots are pores, the grey area is the keel, the white area is the sail and the white dotted area is the snow layer. The solid lines represent the consolidated layer as being found by drillings.

### Salinity and density

Samples were taken from the consolidated layer and the level ice to measure salinity and density 23 and 24 March 1999. The results are displayed in Fig.2.

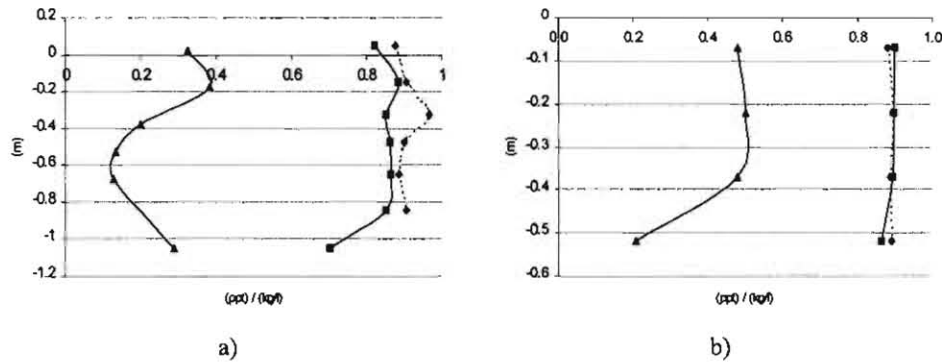


Fig.2. Vertical profile of salinity and density measurements. The solid line with triangles represents the salinity (ppt), the solid line with squares represents the drained density (kg/l) and the dotted line the undrained density (kg/l); a) the ridge and b) the level ice.

The standard deviation for density measurements of the consolidated layer was 0.03 kg/l for the undrained - and 0.06 kg/l for the drained samples. The corresponding values were 0.01 kg/l and 0.02 kg/l for the level ice.

#### Consolidation, level ice thickness and meteorological conditions

Thermistor-strings through an ice sheet can be used to measure its thickness. Table 1 displays the measured thickness of the level ice and the consolidated layer. It was a normal winter at Hailuoto; the freezing degree-day index for the growth period was 138°C days.

Table 1

The thickness of the level ice and the consolidated layer (m)

Date	Level ice thickness, $h_l$		Consolidated layer thickness, $h_{cons}$	
	26.02.99	25.03.99	26.02.99	25.03.99
Drilling	0.47	0.60	0.87*	1.11*
Temperatures	0.4 - 0.5	0.5 - 0.6	0.5 - 0.71	0.71 - 0.92

\*Average values from the neighbouring cross-sections gave 0.83 and 1.05.

#### Compression tests

The results from the compression tests are summarised in Fig.3. and Table 2.

The samples from the consolidated zone can be divided into two groups: samples without initial failures (undamaged ice), and those with initial failures (damaged ice). All the undamaged samples had similar stress-strain curves, an example is shown in Fig.4a.). The damaged ice did not have a typical pattern, and  $\sigma_{max}$  was less than for the transparent ice as shown in Fig.4b). No significant difference could be found for  $\sigma_{0.06}$  (the average stress at  $\epsilon =$

0.06) regardless of stress history or initial damage. It should also be noted that the average strain at peak stress was about the same for all depths above -85 cm.

**Table 2**

Results from the compression tests, average values and standard deviation

Depth (cm)	Number of tests	Av. Strain at Max. Comp. Stress - $\bar{\epsilon}$	Av. max. Comp. stress $\bar{\sigma}_{max}$ (MPa)	Av. stress at $\bar{\epsilon}=0.06$ $\bar{\sigma}_{0.06}$ (MPa)
15 to -5	6	$0.017 \pm 0.004$	$5.0 \pm 1.9$	$1.9 \pm 0.9$
-5 to -25	12	$0.016 \pm 0.006$	$5.2 \pm 1.8$	$2.1 \pm 0.7$
-25 to -45	10	$0.017 \pm 0.005$	$7.2 \pm 1.6$	$2.4 \pm 0.7$
-45 to -65	7	$0.017 \pm 0.006$	$6.2 \pm 1.1$	$2.5 \pm 0.5$
-65 to -85	4	$0.016 \pm 0.003$	$4.8 \pm 0.9$	$2.4 \pm 0.2$
-85 to -105	3	$0.044 \pm 0.020$	$1.5 \pm 0.4$	$1.3 \pm 0.6$
-105 to -125	4	$0.039 \pm 0.024$	$1.7 \pm 0.6$	$1.2 \pm 0.7$

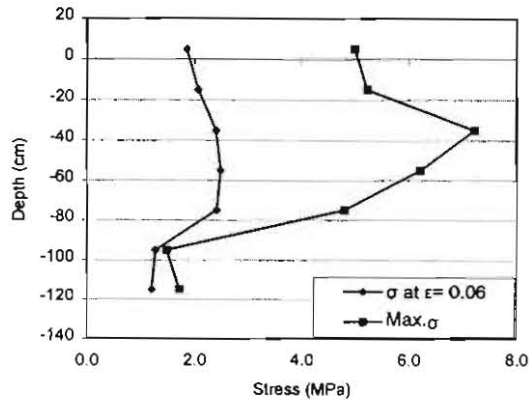


**Fig.3.** The average maximum stress  $\sigma_{max}$  and the average stress at strain equal to 0.06  $\sigma_{0.06}$  versus depth

## DISCUSSION

### Physical and mechanical properties

The salinity and density measurements are comparable to what has been found by others (Kankaanpää, 1997; Leppäranta et al., 1995; Veitch et al., 1991). The strength of the different depths seems to be related to the salinity and the density. The two highest compression strengths were found between 0.25 and 0.65 below the water-line, and this is where the two lowest salinity values were measured. The peak strength also corresponds with the maximum density. Though the numbers of samples were limited some comparison between the

consolidated layer and the level ice can be done. The density measurements show a bigger scatter for the consolidated layer than for the level ice, this is an indication that such a scatter may also yield for mechanical properties. This means that even if similar average values for some mechanical property of level ice and consolidated zone is measured, the strength of the total consolidated layer may still be less due to the weak points. Any use of tests such as these to predict real behaviour is phased with complicating factors such as scaling and the temperature dependence of ice strength. Table 3 presents some other results of compression tests of samples from the consolidated zone. Our values are a bit higher, but still comparable. An increasing strength with depth is also found by Veitch et al. (1991).

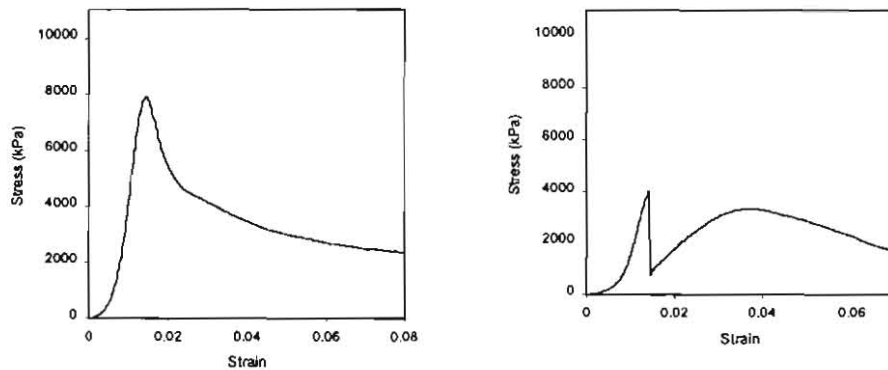


Fig.4. Stress-strain curves: a) An initially undamaged sample  
b) An initially damaged sample

Table 3

Compression test of the consolidated layer in ice ridges (MPa)

Testing temp.	Veitch et al., Lab. closed loop, horizontal, $\epsilon = 2 \cdot 10^{-3}$		Frederking and Wright, in field, vertical, $\epsilon = 10^{-4} - 4 \cdot 10^{-4}$
	depth (m) = 0 - 0.2	depth (m) = 0.2 - 0.4	
$T = -8^{\circ}\text{C}$	$3.8 \pm 1.2$	$5.2 \pm 1.4$	-
$T = -20^{\circ}\text{C}$	6.2	$6.8 \pm 2.6$	-
$T = -19^{\circ}\text{C}$	-	-	2.3 - 13.3

#### The thickness of the consolidated layer

The pronounced drop in mechanical strength of the samples taken from below 0.85 m is reasonable to interpret as a mechanical definition of the lower boundary of the consolidated layer. But note that the compression test were done at  $-10^{\circ}\text{C}$ , and that the in-situ temperature in the lower parts are close to  $T_f$ . Thus an artificial high strength may have been measured.

The values in Table 4 show that the thickness of the consolidated layer predicted by the uniaxial compression tests and the temperature measurements correspond well, and that the drillings predict a thicker layer. These data suggest that a thermal and a mechanical definition of the vertical extension of the consolidated layer correspond fairly well, and that the drillings include a partly consolidated layer and thereby overestimates the thickness of the consolidated zone. The growth of the consolidated layer during the measured period did not seem to be affected by the method of investigation. However any choice of definition or method of investigation should always be closely related to the purpose of the investigation.

**Table 4**

The final thickness of the consolidated layer by the different methods (m)

$h_{cons}$	Temperatures	Compression tests	Drillings
	0.71 - 0.92	0.85	1.05 - 1.11

### CONCLUSIONS

Measurements of spatial and temporal temperature development, physical and mechanical properties of a first-year ice ridge field have been done. Level ice conditions were also measured. The major findings are:

- The average uniaxial compression strength of the consolidated layer was 5-7 MPa
- The average strength of the partly consolidated layer was 1.5-1.7 MPa
- The porosity of the unconsolidated part of the keel was 38 %
- The final thickness of the consolidated layer was investigated in three ways:
  - Temperature measurements: 0.71-0.92 m
  - Compression tests: 0.85 m
  - Drillings: 1.05-1.11 m
- The growth of the consolidated zone did not seem to be affected by the method of examination.

### ACKNOWLEDGEMENT

This work has been undertaken within the LOLEIF-project in the framework of the EU-sponsored Marine Science and Technology (MAST-III). Programmed under contract no.MAS3-CT97-0078. We would also like to thank the crew from HUT, Dennis Tazov and the students from the University of Oulu who helped us during the testing.

### REFERENCES

CROASDALE K.R., ALLEN N.F.B., MARCELLUS R.W. (1990): Thermal response of ice rubble: predictions and observations. Proceedings of the 10th International Symposium on Ice (IAHR), Espoo, Finland 20-24 Aug. 1990, Vol. 1, pp. 153-167.

FREDERKING R.M.W., WRIGHT B. (1982): Characteristics and stability of an ice-rubble field Issungnak, February-March 1980. NRC Technical memorandum, Jan 1982, No. 134, pp. 230-247.

HØYLAND K.V. (in prep.): Simulations of the consolidation process in first-year ice ridges.

HØYLAND K.V. (2000): Measurements of consolidation in three first-year ridges. Submitted to IAHR in Gdansk 2000.

KANKAANPÄÄ P. (1997): Distribution, morphology and structure of sea ice pressure ridges in the Baltic Sea. *Fennia* 175:2, pp 139-240. Helsinki, ISSN 0015-0010.

KRANKKALA T., MÄÄTTÄNEN M. (1984): Methods for determining ice forces due to first- and multi-year ridges. Proceedings of the 7th International Symposium on Ice (IAHR), Hamburg, Germany 27-31 Aug. 1984, Vol. 4, pp. 263-287.

LEPPÄRANTA M., LENSU M., KOSLOFF P., VEITCH B. (1995): The life story of a first-year sea ice ridge. *Cold Regions Science and Technology* 23 (1995), pp. 279-290.

LØSET S., LANGELAND A., BERGHEIM B., HØYLAND K.V. (1998): Geometry and physical properties of a stamucha found on Spitsbergen. Proceedings of the 14th International Symposium on Ice (IAHR), Potsdam, New York, USA, 27-31 July 1998, Vol. 1, pp. 339-344.

TIMCO G.W., WRIGHT B., JOHNSTON M., FREDERKING R. (1999): First-year ice ridge loads on Molikpaq. Proceedings from Russian Conference on Arctic Offshore Engineering (RAO), St.Petersburg, Russia, 6-9 July 1999, Vol. 2, pp. 172-179.

TIMCO G.W., GOODRICH L.E. (1988): Ice rubble consolidation. Proceedings of the 9th International Symposium on Ice, Sapporo, Japan, 1988, pp. 426-438.

VEITCH B., LENSU M., RISKÄ K., KOSLOFF P., KEILEY P., KUJALA P. (1991): Field observations of ridges in the northern Baltic Sea. Proceedings of the 11th International Conference on Port and Ocean Engineering under Arctic Conditions, St. John's, Canada, pp. 381-400.



## FORMATION AND DECAY OF STAMUKHAS, COOK INLET, ALASKA

O. Smith<sup>1</sup>

### ABSTRACT

Ice that is grounded on tidelands and repeatedly covered by tidewater before floating free can be far more massive and dangerous to shipping than ambient level ice and offshore ridges. These ice blocks, or "stamukhas," carry heavy sediment loads and therefore are more massive than sea ice ridges of the same volume. Observations of stamukha formation in Cook Inlet, Alaska, indicate formation of these ice features can entrain and transport substantial mass of potentially contaminated tidelands sediment.

### INTRODUCTION

The Russian word "stamukha" has come into use by sea ice specialists with reference to a form of ice that was grounded on tidelands and repeatedly covered by tidewater or storm surge before floating free. The term "stamukha" is not defined in the WMO Sea-Ice Nomenclature (WMO, 1970). LaBelle et al. (1983) refer to "beach ice" as bottom-fast ice adhered to tidal flats, though winter mariners in Alaska call stamukhas beach ice, due to their tidelands origin. LaBelle et al. (1983) refer to "stamukhi" as resulting from "...beach ice which has broken free, been deposited higher on the mud flats, and frozen to the underlying mud...". An English plural convention, "stamukhas," is applied in this paper with regard to distinct blocks of ice originally formed as beach ice, whether or not they are regrounded or adhered to other ice pieces.

Stamukhas occur in the Arctic, but other forms of grounded ice are more commonly discussed in the literature, such as "ice pile-up" or "ice ride-up" (Kovacs and Sodhi, 1988), formed by compressive fracture of ice sheets. "Rubble piles" and "rubble fields" are composed of grounded ice features composed of broken sheet ice, frozen together to form a relatively continuous mass (API, 1988). "Rafted ice" and "ice ridges," features formed at sea by one sheet being pushed over another, may become grounded. These are all ice features associated

---

<sup>1</sup>University of Alaska Anchorage, Anchorage, Alaska, USA, 3211 Providence Drive, Anchorage, AK 99508;  
Tel.: 1-907-786-1910; fax: 1-907-786-1079, e-mail: afops@uaa.alaska.edu

with offshore processes, rather than repeatedly submerged fast ice. Nelson (1997) discussed stamukhas with other forms of Cook Inlet ice with reference to regional oil spill contingency planning.

Stamukhas are seen in both tabular and irregular shapes. Tabular stamukhas retain the original flat form of beach ice freshly separated from the bed. Irregular stamukhas are conglomerations of smaller pieces accumulated through repeated groundings and interaction with floating ice. Floating conglomerate stamukhas are readily distinguished by their higher, sometimes pinnacled sails, their dark sediment-laden appearance and, on close inspection, by the sediment striations of their component slabs. Their irregularity and higher freeboard usually cause stamukhas to stand out among level ice floes, but the entrained sediments' effect on buoyancy hides a deep submerged keel.

Recent observations of stamukhas discussed herein were made on the shore of Turnagain Arm near its junction with upper Cook Inlet and Knik Arm at Anchorage, Alaska, at 61° 3.5' N latitude. Cook Inlet is a large estuary in south-central Alaska that extends northward from 59° to 61° 30' north latitude (150 nautical miles). Level ice in Cook Inlet rarely exceeds the first-year-thin (up to 70 cm thickness) stage of development, but stamukhas of over 5 m depth are common in late winter. Sea ice first forms in upper Cook Inlet in October and disappears in April, except for larger stamukhas grounded high on the tidelands. Though stamukhas are interspersed with dark, solar energy-absorbing sediment grains, their large mass leaves them last of ice forms to melt. All ice of Inlet origin is usually gone by the end of May. Measurements by the author indicate Cook Inlet winter water in the vicinity of Anchorage is always well mixed with winter salinities ranging from 6-10 Practical Salinity Units (PSU, Fig.1.). Winter climate information for Anchorage is summarized in Table 1.

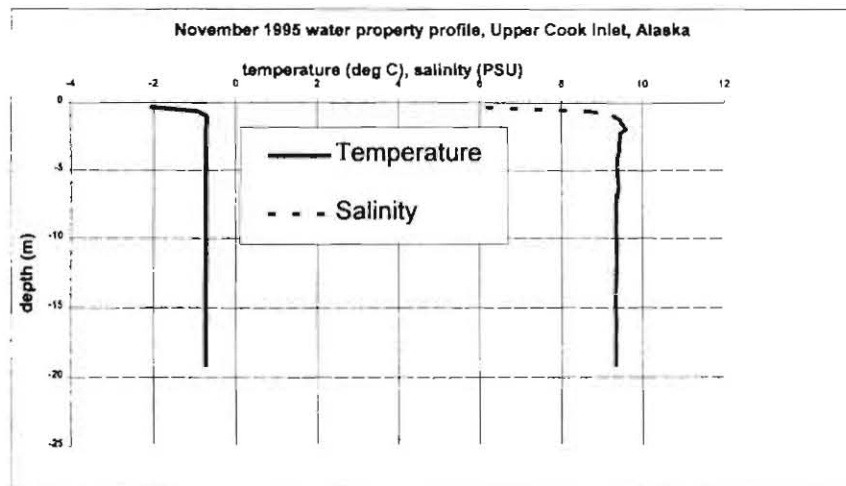


Fig.1. Representative winter water property profile, upper Cook Inlet, Alaska

Table 1

## Climate of Anchorage, Alaska

	Oct	Nov	Dec	Jan	Feb	Mar
Mean temperature (°C)	1.2	-5.7	-9.0	-9.6	-7.6	-3.9
Mean days below 0°C	20	28	30	30	27	28
Snowfall (m)	0.2	0.3	0.4	0.2	0.3	0.2

**FORMATION OF STAMUKHAS**

Stamukhas in Cook Inlet begin as fast ice frozen to the bed of tidelands. Cold air reduces the temperature of the tidelands and beach ice at low tide. Higher elevations on the tidelands have more air exposure, with surface temperatures cooling to ambient air temperature during low tide periods. Snow on the tidelands is melted by contact with incoming seawater at high tide, in turn cooling and freshening the seawater and accelerating freezing to beach ice below. Repeated direct exposure to cold air creates patterns vertical cracks in the coating of ice from thermal stress fractures. Buoyancy will float slabs free when the upward buoyant force on the slab exceeds the strength of the frozen sediment below. In general terms, the formation of stamukha conglomerates is summarized below:

1. Seawater freezes to cold tidal flats forming thin fast ice.
2. Fast ice is inundated by succeeding tides.
3. Fast ice becomes significantly colder than seawater from low tide air contact.
4. Fast ice grows upward during high tide submergence.
5. Extended buoyant forces during a spring tide dislodge pieces of fast ice.
6. Loose pieces, including brash and floes from offshore, settle on fast ice lower on the tidelands and adhere with tidewater "glue."
7. Increased buoyancy and longer submergence cause conglomerate pieces to break free.
8. Conglomerate pieces with increased draft are grounded lower on the tidelands, adhere to the fast ice on the bed, and eventually lift away additional ice and sediment on a succeeding high tide.

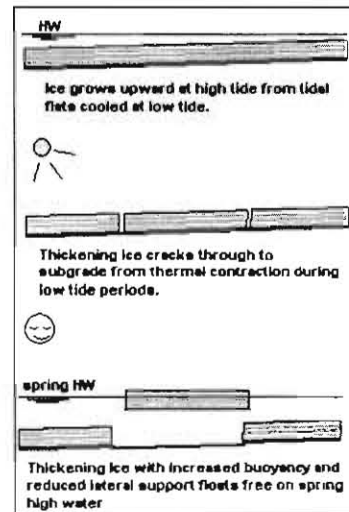


**Fig.2.** Formation sequence for tabular stamukhas

The extreme range and variability of Cook Inlet tides exaggerates this process. At Anchorage, the mean tide range is 7.9 m and the diurnal range is 8.8 m. Cook Inlet tides have a substantial diurnal inequality of ranges and extraordinary variability on all time scales, as indicated by recorded tide elevations in Fig.3. Predicted tides at Anchorage are based on computations with 114 tidal frequency constituents, more than any other tide station in the US. Extreme spring tide ranges at Anchorage exceed 12 m. Tidal currents in Cook Inlet regularly exceed 4 knots

in open areas and reach 6 knots near constrictions. These currents keep the water turbulent and well mixed throughout the year. Astronomical tides in the Arctic are much less. Diurnal tide ranges at Nome, Alaska ( $64^{\circ} 30' N$  latitude), Pt. Barrow, Alaska ( $71^{\circ} 22' N$  latitude), and Hershel Island, Canada ( $69^{\circ} 34' N$ ) are 0.5, 0.1, and 0.4 m, respectively. In these areas, wind-induced water level changes and spring runoff have greater influence on growth of stamukhas. Turbulence on the scale of Cook Inlet is only likely to occur in Arctic waters when winds on open water cause surface waves.

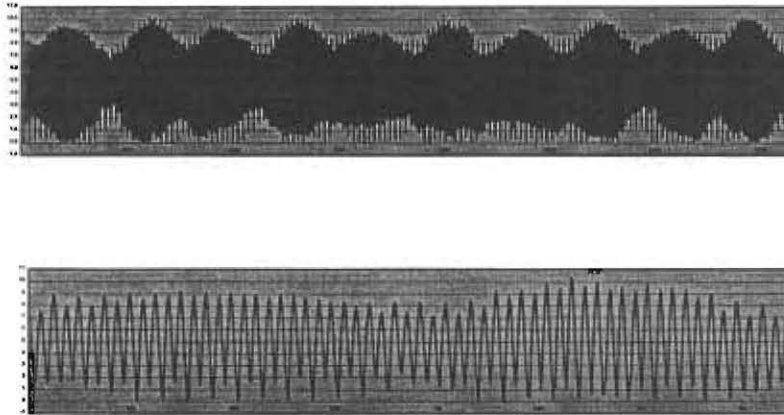


**Fig.3.** Tides measured at Anchorage, Alaska October 1999 - March 2000 (top) and December 1999 (bottom). The vertical grid is meters elevation.

#### **SALINITY AND ENTRAINED SEDIMENT CONCENTRATION IN STAMUKHAS**

Seven ice cores were collected from Turnagain Arm on upper Cook Inlet in February and March 1999. Cores were sawed into segments every 8 cm. Entrained sediment concentrations were determined by sieving and filtering melted segments. Bulk salinities were derived from concurrent conductivity and temperature measurements. The mean sediment concentration in stamukha segments was 24.938 g/l and the mean salinity was 1.07 PSU. Sand size particles with diameters greater than 63  $\mu$ m made up over 50 % of sediments filtered from grounded stamukhas. Fig.4. shows a profile of salinity and entrained sediment concentrations in a 1.6-m-long core extracted in March 1999 from a grounded stamukha.

The ice structure of the cores was granular with no evidence of columnar ice crystals. Fine particles were distributed in the ice between layers of coarser materials, probably associated with past direct contact with tidelands sediments. The water of upper Cook Inlet is highly turbid with suspended sediment of glacial origin in concentrations ranging from 1-2 grams per liter (Gatto, 1976; USACE, 1996). Irregularly spaced striations in tabular stamukhas may

relate to variations in duration of submergence (i.e., spring versus neap tides) and in concentration of suspended sediments at the site.

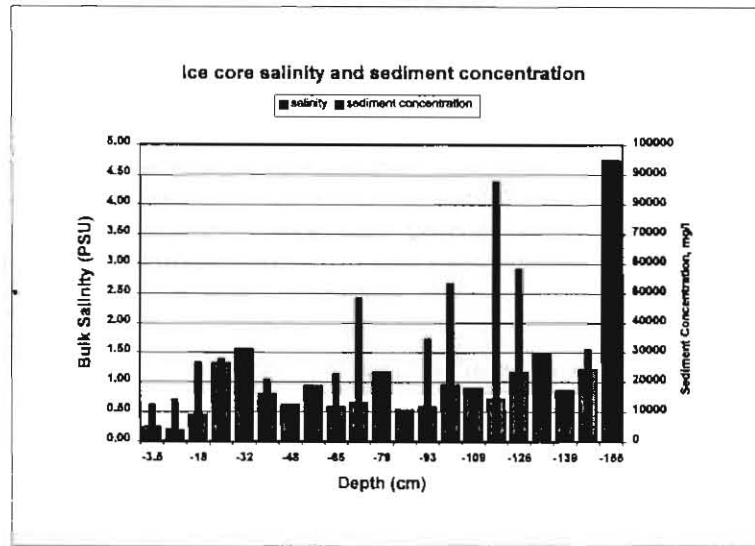


Fig.4. Salinity and entrained sediment concentrations in a 1.6 m core extracted from a stamukha grounded on upper Cook Inlet tidelands in March 1999

The formation of stamukhas promotes entrainment and transport of sediments by exposing unfrozen tidelands. The process of floating free a tabular stamukha appears to typically remove all the frozen sediment. "Mud lakes" were observed on the tidelands that seem to have been sites of recent removal of fast ice. Cold air eventually freezes these areas, but not before they are inundated at high tide and bed material is lifted into the water by tidal currents or contact with ice. Freeing of anchor ice to expose unfrozen bed sediments has been reported by others, eg., Reimnitz et al. (1987) as important to sediment dynamics in Arctic Seas. Sediments, some contaminated, have been found exposed on ice near the North Pole and in other areas across the Arctic Ocean (Tucker et al., 1999).

#### CONCLUSIONS

Cook Inlet, Alaska, is a sub-Arctic water body with extremes of tidal range, turbulence associated with tidal currents, and suspended sediment concentrations. These characteristics allow growth of extraordinary sediment-laden stamukhas. The extremes of Cook Inlet provide an opportunity for study of ice formation and sediment entrainment where these natural processes are strong and accessible. These processes will transport and disperse industrial contaminants in Cook Inlet, should winter spills occur. The Cook Inlet situation models the Arctic, where contamination is already being spread across international borders.

## REFERENCES

- API (1988): Recommended Practice for Planning, Designing, and Constructing Fixed Offshore Structures in Ice Environments. ANSI/API RP 2N-88, American Petroleum Institute, Washington, DC.
- GATTO L.W. (1976): Baseline Data on the Oceanography of Cook Inlet, Alaska. CRREL Report 76-25, Cold Regions Research and Engineering Laboratory, Hanover, New Hampshire, USA.
- KOVACS A., SODHI D. (1988): Onshore Ice Pile-up and Ride-up: Observations and Theoretical Assessment. In: Arctic Coastal Processes and Slope Protection Design, Technical Council on Cold Regions Engineering, American Society of Civil Engineers, New York.
- LABELLE J., WISE J., VOELKER R., SCHULZE R., WOHL G. (1983): Alaska Marine Ice Atlas. Environmental and Natural Resources Institute (ENRI, formerly Arctic Environmental Information and Data Center), University of Alaska Anchorage, Anchorage, Alaska.
- NELSON W. (1997): Cook Inlet Ice Formation and Oil Spill Clean-up Study. Cook Inlet Regional Citizens Advisory Council, Kenai, Alaska, USA.
- REIMNITZ E., KEMPEMA E., BARNES P. (1987): Anchor Ice, Seabed Freezing, and Sediment Dynamics in Shallow Arctic Seas. *J. Geophysical Research*, 92(C13), pp. 14,671-14,678, American Geophysical Union.
- TUCKER W., GOW A., MEESE D., BOSWORTH H. (1999): Physical Characteristics of Summer Sea Ice across the Arctic Ocean. *J. Geophysical Research*, 104(C1), pp. 1489-1504, American Geophysical Union.
- USACE (1996): Deep-Draft Navigation Interim Feasibility Report and Environmental Assessment, Cook Inlet, Alaska, Alaska District, US Army Corps of Engineers, Anchorage.
- WMO (1970): WMO Sea-Ice Nomenclature, WMO/OMM/BMO - No. 259.TP.145, World Meteorological Organization, Geneva.



## SALINITY OF ICE OFFSHORE NORTHEASTERN SAKHALIN

G.A. Surkov<sup>1</sup>, P.A. Truskov<sup>3</sup>, S.V. Zemlyuk<sup>2</sup>,  
V.N. Astafyev<sup>1</sup>, A.M. Polomoshnov<sup>1</sup>

### ABSTRACT

Sea ice salinity data obtained on the northeastern Sakhalin shelf from 1983 to 1995 is reported. Drift ice and fast ice reveal different salinity. The salinity values for drift ice are normally distributed and do not exhibit considerable seasonal variations from February to April. The average salinity of drift ice is within 4 ‰ to 6 ‰. The salinity of fast ice in Chaivo Bay is on average by 2 ‰ lower.

### INTRODUCTION

Salinity of sea ice, like its temperature and structure, is a main factor defining ice strength characteristics. Therefore, for over a decade (1983-1995), this parameter of ice was in the focus of the Laboratory of ice research at the SakhalinNIPImorneft Offshore Oil Institute.

Due to different conditions in which various types of ice have been formed, in salinity analysis, one should not confuse drift ice subjected to constant deformations and fast ice which is known for its relatively smooth growth of thickness. Fast ice salinity is also affected by fresh water of adjacent streams and rivers.

### EXPERIMENT

Salinity was measured with crushed ice specimens subjected to uniaxial compression tests. About 50 cm<sup>3</sup> of ice fragments was collected in a glass vessel with a sealed lid and conditioned in a warm place until full melting. The resultant liquid was stirred to a uniform mix before salinity measurements.

---

<sup>1</sup> Sakhalin Oil and Gas Institute, Okha, Sakhalin, Russia, 18, K.Marx St., Sakhalin Oil and Gas Institute, Okha, Sakhalin Region, Russia, 694490, Tel.: 7-(424-37)-254-95, fax: 7-(424-37)-249-17, e-mail: ice@smng.com

<sup>2</sup> Sakhalinmorneftegaz-Rosneft Co., Yuzhno-Sakhalinsk, Sakhalin, Russia

<sup>3</sup> Sakhalin Energy Investment Co., Moscow, Russia

Measurements were made with a salinity express meter Tigran-A, designed to determine the total concentration of water soluble salts in water. This instrument was engineered to measure salinity under field and laboratory conditions accurate to  $\pm 6\%$  at ambient temperatures from  $2^{\circ}\text{C}$  to  $40^{\circ}\text{C}$ .

#### Drift ice

Core samples were drilled in ice floes offshore northeastern Sakhalin in different locations from the Odoptu Bay to Chaivo Bay. From one ice field, we retrieved 17 core samples from holes spaced 20 m over an area of  $160 \times 160$  m.

#### Fast ice

Ice cores were cut from Chaivo Bay ice every two weeks from December till April.

### RESULTS AND DISCUSSION

#### Drift ice

The drift ice salinity histogram is well described by a normal distribution law. Fig.1. shows the recurrence probability of salinity measurements made in February, March and April. Seasonal variations in the salinity profile were insignificant. The average value of salinity from February to April remained stable at 4.9 ‰. The highest salinity value found was 13.2 ‰, the lowest value was 1.3 ‰.

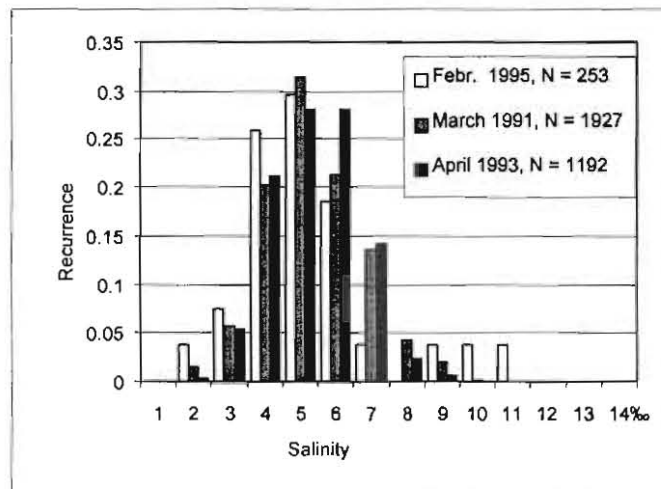


Fig.1. Relative frequency histogram of drift ice salinity measurements

A salinity versus ice-thickness analysis revealed that the average value was in a rather stable range of 4-6 ‰ with some trend to lower values for deeper ice sampling. Fig.2. shows the plots of ice salinity as functions of ice sampling depth for March. For February and April, the salinity behavior was exactly the same.

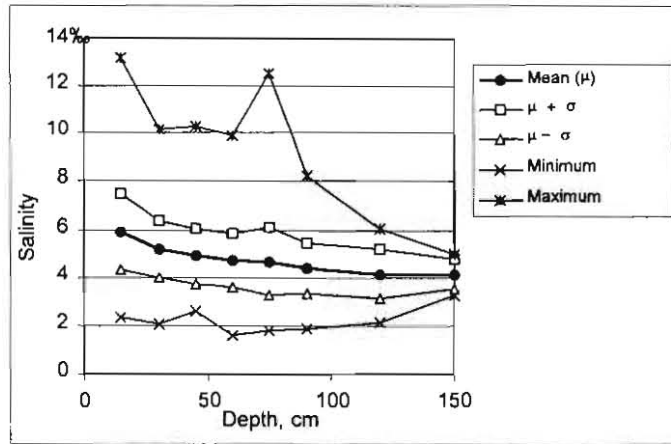


Fig.2. Salinity of sea ice as a function of sampling depth for March

We studied the salinity distribution profile for specimens sampled at different depths from the ice surface. Fig.3. shows the relative frequency histograms of salinity for ice sampled at three depths of 15, 60, and 90 cm. The histograms reveal an obvious trend to narrow profiles for samples from deeper ice layers.

Substantial scatter of salinity measurements noted in upper ice layers (around 11 ‰) becomes more condensed below a depth of 75 cm.

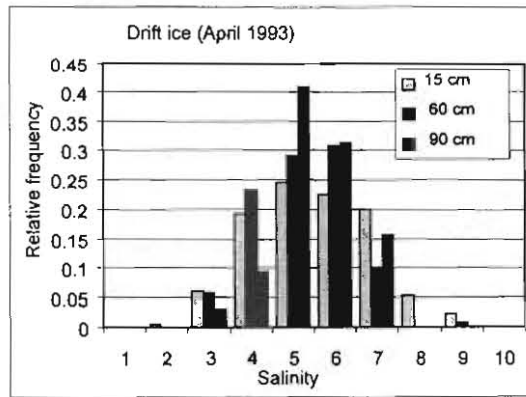


Fig.3. Salinity histograms of drift ice specimens sampled at different ice depths (April 1993)

### **Fast ice**

The fast-ice salinity distribution is also well described by a Gaussian curve. Ice studies in Chaivo Bay indicated that salinity substantially decreases with sampling depth. A seasonal salinity decline was also noted.

In January, the average salinity of the upper ice layer was found to be within 3 ‰ to 4 ‰; for the middle layer, it was 2.5-3.3 ‰; and for the bottom layer, 2.3-3.2 ‰. In February, the salinity of the upper and middle layers remained almost the same, whereas for the bottom layer it decreased to 2.0-3.0 ‰. In March, the average salinity of the middle layer decreases to 2.6-2.8 ‰, and that of the bottom layer to 1.6-2.5 ‰. The largest spread of salinity values was found in the upper layer (5 ‰), whereas in March, in the ice bottom layer it was 0.5-1.5 ‰.

### **CONCLUSIONS**

Studies of sea ice have indicated that the salinity of ice is generally distributed in a normal law and does not exhibit substantial seasonal variations in a period from February to April. Average salinity values are within 4 ‰ to 6 ‰ with a downward trend for specimens sampled from lower ice layers. The scatter of salinity measurements also decreases from 11 ‰ in the upper ice layer down to 2 ‰ in samples cut from 120-150 cm depths.

The salinity of fast ice from Chaivo Bay is on average by 2 ‰ below that of drift ice. Fast ice salinity exhibits trends similar to that of drift ice.



**LOLEIF RIDGE-LOADING EXPERIMENTS -  
ANALYSIS OF RUBBLE STRENGTH IN RIDGE KEEL PUNCH TEST**

**J. Heinonen,<sup>1</sup> M. Määttänen<sup>1</sup>**

**ABSTRACT**

Several punch tests for first-year ridge keels have been carried out for the EU-funded LOLEIF project. The tests have been performed in the Gulf of Bothnia, Finland, during winters from 1998 to 2000. In the punch test, a circular plate is pushed vertically downwards until the ridge keel collapses. An analytical limit load method is used for determining the strength parameters. The upper bound limit load is based on the balance between the external and the internal work rate. The internal work is defined by plastic dissipation describing the shear failure. Rubble strength is separated into two parts, cohesive and frictional strength by applying the Mohr-Coulomb yield criterion. The strength parameters cannot be defined by a single test. When geometrical quantities and the load capacity with knowledge about the failure mode are measured, the limits for cohesion and friction are solved. Approximative values or bounds for rubble strength are found by applying the analytical model for several test sets.

**INTRODUCTION**

Ice ridges are porous features consisting of ice blocks, slush, water and in the sail also air and snow. The keel is divided into an upper consolidated layer and a lower part of unconsolidated rubble. Because the internal structure of the keel is complicated, the mechanical behaviour of the keel and especially the ice rubble is poorly known. If ice rubble is treated like continuum material, the observations must be made on a scale large enough compared to the ice-block size to avoid the effects of individual ice blocks. Some approximative values for the continuum analysis do exist, but they are not generally accepted because rubble strength and stiffness depend on several variables. In the sense of continuum mechanics, the strength seems to be a combination of cohesion and internal friction. The latter is related to internal pressure. In this analysis, the other dependencies of the stress state are not studied.

---

<sup>1</sup> Helsinki University of Technology, Finland, Laboratory for Mechanics of Materials, Otakaari 4 P.O.Box 4100, FIN-02015 HUT, Tel.: +358-9-4513439, fax: +358-9-4513443, e-mail: Jaakko.Heinonen@hut.fi

The porosity of rubble depends on the ice-block shape and size, how the ice blocks are packed and connected together (if at all) as well as on the orientation of the blocks. The time history of the ridge has significant effects. The initial ice condition before the ridge was formed is an important indicator that determines firstly the ice-block thickness and the size in the other directions. Secondly, the snow thickness above the ice indicates how much slush is present in the pores. Environmental conditions around the ridge such as the ambient temperature and the wind as well as the snow situation play a major role in the heat transfer and consolidation by freezing. In the underwater part, the presence of currents causes shape modification of the ice blocks. In addition, the salinity has effects on the ice properties as well as block interaction.

Taking all these features into account, it is obvious that there are no individual values like cohesion or friction that describe the general features of ice rubble. These values are always connected to the internal structure of the keel and the time history beginning from the moment the ice started to form. It is important to conduct full-scale loading tests of the ridge keel in a real environment. If the internal structure is well studied, the results can be used for determining strength values and for relating them to other features of the ridge keel.

There are several studies of the mechanical properties of ice rubble. Experiments are mainly carried out in laboratories on a small scale. Weiss et al. (1981) measured unconsolidated rubble properties on a scale 1:10 for ice that was formed from high saline water (5-6 %). They reported the following values: cohesion from 1.7 to 4.1 kPa and friction angle from  $11^{\circ}$  to  $34^{\circ}$ . Cohesive strength was proportional to the ice rubble piece thickness giving the value of  $16 \pm 8$  kPa/m for cohesion divided by the thickness. Prodanovic (1979) measured saline unconsolidated ice rubble properties on a scale of 1:50. He reported values 0.25 and 0.56 kPa for cohesion as well as  $47^{\circ}$  and  $53^{\circ}$  for the friction angle corresponding to ice rubble piece thicknesses of 19 mm and 38 mm. The Mohr-Coulomb failure criterion is widely accepted for ice rubble according to the studies above. Ettema and Urroz-Aguirre (1989) and (1991) described the significance of internal friction consisting of contact friction between ice blocks and interlocking phenomena under rubble deformations. They studied why earlier reported values for internal friction are as high as, for example, Prodanovic (1979) reported. Their observation was that the internal stress state due to the buoyancy load causes confinement, which increases the frictional part of strength even if the external confinement force is zero. They also proposed that the cohesion of ice rubble is dependent on the stress state. Azarnejad and Brown (1998) performed small-scale punch tests, and concluded that better theories need to be developed for interpreting the results. In their small-scale punch tests, ice rubble was obtained from ice machines, and the tank was filled with fresh water. They also measured high values for the internal friction angle (most of the values were around  $50^{\circ}$ - $60^{\circ}$ ) and low values for cohesion (around 0.03-0.3 kPa).

There are some studies of in-situ field experiments: Leppäranta and Hakala, (1989) and (1992), Croasdale et al. (1997), Heinonen et al., (1998) and (2000). Leppäranta and Hakala (1992) reported similar values for cohesion (1.5 kPa to over 4.0 kPa) as did Weiss et al. (1981). It is known that properties in nature differ considerable from laboratory results

(Leppäranta and Hakala, 1989 and 1992; Croasdale et al., 1997) because the internal structure and time history are always different. In the laboratory, tests are always performed on a smaller scale, and ice rubble is artificially manufactured, which causes different ice fragment shapes and sizes. In addition, a different temperature history and salinity affect the freeze bonds and consolidation by freezing.

### TEST SET-UP

The principle of a punch test is shown in Fig.1. The sail was first removed and a circular plate of the consolidated layer was cut free from the surrounding solid ice field. The ridge keel was loaded by pushing the circular plate downwards. The purpose of the experiment was to load only the unconsolidated rubble of the ridge.

The force and the displacement of the pushing plate were measured. Movements inside the rubble as well as the evolution for the ridge keel fracturing were also monitored. A general description of the ice conditions at the test site in Marjaniemi, the Gulf of Bothnia, Finland, can be found in Høyland (2000) and Høyland et al. (2000).

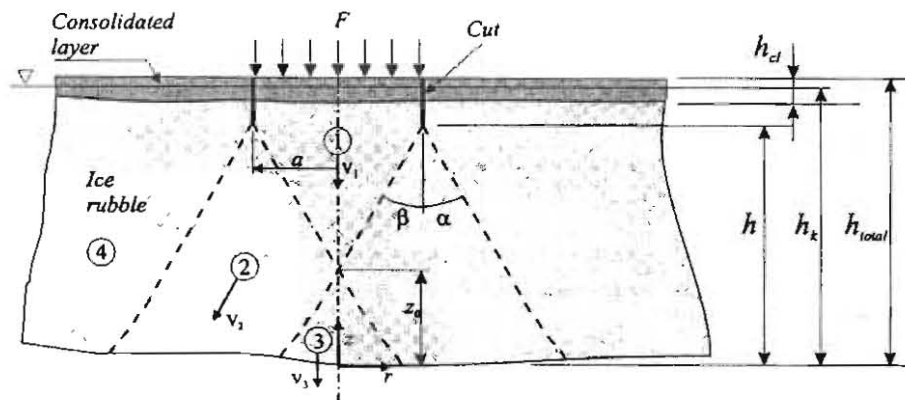


Fig.1. Ridge keel punch test. Cross-section of the keel with dimensions and failure mode.

### MATHEMATICAL MODEL

#### General

The assumptions made in the computational model were the following:

1. The material in the keel is homogenous through the thickness.
2. The load is distributed linearly inside the keel. Stress in the thickness direction is calculated directly from the external load.
3. Shearing determines the failure. The failure mode is conical and deformations in the shear lines are purely plastic. Deformations between the rigid blocks are kinematically admissible. The failure occurs through the keel simultaneously.
4. The failure criterion is defined by a Mohr-Coulomb yield function, which is a linear combination of the cohesive and the frictional strength.

5. The material inside the shear band is assumed to be incompressible. An elastic solution can then be applied for determining the horizontal stress components from the vertical one.

The major problem in this modified upper bound method is how to find the right mechanism (kinematic chain) for the fracture. The method is used to determine the limit load for the ridge keel. When the load is experimentally known, the solution is used for determining the material parameters.

### Upper bound solution

The limit load for pushing the ridge keel downwards is approximated by using the failure mechanism shown in Fig.1. Conical rigid blocks are moved downwards allowing plastic sliding at the boundaries. When the conical mechanism is used, two different cases are possible depending on the dimension  $z_0$ . If  $z_0$  is negative, the number of blocks is two, otherwise three. A cylindrical coordinate system ( $r$ ,  $\theta$  and  $z$ ) is used. The system is assumed to be axisymmetric, which reduces the problem to be only two dimensional ( $r$  and  $z$ ).

The limit load is defined from the balance for the internal and the external work rate.

$$\dot{W}^{ext} = \dot{W}^{int} \quad (1)$$

where  $\dot{W}^{ext}$  is the rate for the external work and  $\dot{W}^{int}$  is the rate for the internal work. The external work is defined by

$$\dot{W}^{ext} = \mathbf{F} \cdot \mathbf{v} + \mathbf{B} \cdot \mathbf{v} = \mathbf{F}_1 \cdot \mathbf{v}_1 + \sum_{k=1}^{k_{max}} \mathbf{B}_k \cdot \mathbf{v}_k \quad (2)$$

where  $\mathbf{F}$  is the external force pushing the platen downwards and  $\mathbf{v}$  is the velocity of the platen.  $\mathbf{B}$  is a buoyancy force.  $\mathbf{v}_k$  is the velocity where the subscript refers to the block  $k$ .  $k_{max}$  is the number of moving blocks (two or three) and it depends on the failure kinematics.

$$B_i = \int_V \gamma_i dV \quad (3)$$

where the buoyant volume force  $\gamma$  is defined as

$$\gamma_r = 0 \quad ; \quad \gamma_z = (\rho_w - \rho_i) (1 - \eta) g \quad (4)$$

where  $\rho_w$  is the water density and  $\rho_i$  is the ice density,  $\eta$  is the porosity of the rubble, and  $g$  is the gravitational acceleration ( $g = 9.81 \text{ ms}^{-2}$ ).

The internal work is defined as plastic work, which occurs in the shear lines between each block.

$$\dot{W}^{int} = \int_{A_1} \tau v_{12} dA + \int_{A_2} \tau v_{24} dA + \int_{A_3} \tau v_{23} dA \quad (5)$$

where  $A$  is the area of the sliding surface.  $v_{ij}$  is a magnitude of the velocity jump over the sliding surface between the blocks  $i$  and  $j$ , and  $\tau$  is a shear strength affecting the shear plane.

The shear stress on the shear plane is modelled using the Mohr-Coulomb criterion

$$|\tau| = c - \sigma_n \tan \phi \quad (6)$$

in which  $c$  is the cohesion and  $\phi$  is the angle of internal friction, both of which are material constants that are determined by an experiment.  $\sigma_n$  is the normal stress affecting the surface.

Due to the buoyance force, there is an initial stress state in the keel. These stresses are small compared to those caused by the external load. Therefore, it is assumed (assumption 2) that the internal stress state is linear through the thickness and it is determined according to the external load. The stress distribution is defined in Eq. 7 and it is visually shown in Fig.2.

$$\sigma_z = -\frac{F}{\pi a^2} \frac{z}{h} \quad (7)$$

which partially fulfils the stress boundary conditions.

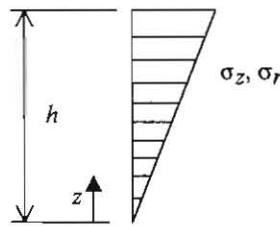


Fig.2. Stress distribution in z-direction

Because the stress dependence on a radius is not taken into account, the stress state does not satisfy the stress boundary conditions at the upper boundary of the keel completely. It is assumed (assumption 5) that in the failure surface the rubble behaves like incompressible plastic material and the Poisson value is chosen 0.5. Therefore, the horizontal stress components can be written according to Timoshenko et al. (1987).

$$\sigma_r = \sigma_\theta = \sigma_z \quad (8)$$

The normal stress affecting the shear plane is a combination of the stress components.

$$\sigma_n = \sigma_z \sin \alpha + \sigma_r \cos \alpha \quad (9)$$

#### Failure kinematics

For the rate equations 1 and 2, we have to define the velocities of the blocks and the velocity jumps over the sliding surfaces. The movements of the rigid blocks 1, 2 and 3 are determined according to continuity, which means that the velocity field is kinematically admissible (Chen and Han, 1988).

The rigid blocks 1 and 3 move vertically. Thus, the velocities are

$$\mathbf{v}_1 = \mathbf{v}_3 = \begin{Bmatrix} v_r \\ v_t \end{Bmatrix} = \begin{Bmatrix} 0 \\ v \end{Bmatrix} \quad (10)$$

The other velocities and velocity jumps can be written as

$$|v_2| = \frac{v}{\cos \alpha + \cos \beta} ; \quad v_{12} = v_{23} = \frac{v}{\frac{\sin \beta}{\tan \alpha} + \cos \beta} \quad (11)$$

For simplicity, we approximate that the angles  $\alpha$  and  $\beta$  are equal. Thus, the velocities and the velocity jumps are

$$v_2 = v_{12} = v_{23} = v_{24} = \frac{v}{2 \cos \alpha} \quad (12)$$

### Geometrical quantities

$$\frac{z - z_0}{h - z_0} a \quad ; \text{ when } z = (z_0, h)$$

The surface differential for a cone is

$$dA = 2 \pi r dz \quad (13)$$

The radius for the outer cone surface is

$$r = (h - z) \tan \alpha + a \quad (14)$$

For the inner cone surface the radius is

$$r = \begin{cases} \frac{z_0 - z}{h - z_0} a & ; \text{ when } z = (0, z_0) \\ \frac{z - z_0}{h - z_0} a & ; \text{ when } z = (z_0, h) \end{cases} \quad (15)$$

where the dimension  $z_0$  is defined as

$$z_0 = h - \frac{a}{\tan \alpha} \quad (16)$$

If  $z_0 < 0$ , the number of the blocks is two, otherwise three.

### Solution for limit load

By using Eqs. 5 and 6 we find the internal work rate

$$\dot{W}^{\text{int}} = \int_{A_1} [c - \sigma_n(z) \tan \phi] dA v_{12} + \int_{A_2} [c - \sigma_n(z) \tan \phi] dA v_{24} + \int_{A_3} [c - \sigma_n(z) \tan \phi] dA v_{23} \quad (17)$$

In case  $z_0 < 0$ , block 3 does not exist and the third part of the internal work rate drops out. Finally, by applying the energy balance, Eq. 1, the limit load is determined as a function of the geometry, the strength values and the fracture mode like

$$F = f(a, h, c, \phi, \alpha) \quad (18)$$

The closed form solution is too long to be presented here.

## ANALYSIS

### Concepts for determining strength values

Several tests have been performed with different values for  $a$  and  $h$ , also with a different  $a/h$  ratio. The angle  $\alpha$  for the shear band is measured. Values for the strength parameters, i.e. cohesion and friction, have to be determined experimentally, but they cannot be defined by a single test. However, a connection between the cohesion and friction angle is found for every test.

If several results with different test set-ups are applied, representative values for cohesion and friction can be introduced presuming similar ice rubble behaviour in different test places. However, it is well known that the ridge keel is not homogenous. In the same ridged area, the ice-block size is approximately the same, but the porosity varies. The porosity affects the strength and its variation has to be taken into account. The first approximation is that it mainly affects the cohesive strength not frictional. By using a linear connection between porosity and cohesion, we find

$$c(\eta) = \frac{1-\eta}{1-\bar{\eta}} \bar{c} \quad (19)$$

where  $\bar{\eta}$  is the average porosity of the ridge field, whereas  $\eta$  is the local porosity value at the individual test site. Correspondingly,  $\bar{c}$  is the average value for cohesion in the ridge field and  $c$  is the local cohesion value at the test site.

### Results

The experimental results are presented in Table 1. Maximum values for the load  $F_{max}$  and the main dimensions, the keel depth  $h_k$ , the effective keel depth  $h$ , the diameter of the platen  $d$  and the ratio  $d/h$ , as well as the average porosity of the rubble  $\eta$  are shown. In addition, the values for the angle  $\alpha$  are given.

Table 1

Main values describing the punch tests

Test #	$F_{max}$ (kN)	$\alpha$ (°)	$d$ (m)	$h_k$ (m)	$h$ (m)	$d/h$	$\eta$ (%)
2	765	20.6	3.32	4.55	3.95	0.84	39
6	936	45.4	3.35	4.02	2.78	1.21	31
9	695	20.8	3.40	5.63	4.03	0.84	35
10	758	48.4	4.50	4.47	3.13	1.44	46
11	1120	20.0	4.05	6.36	4.96	0.82	41*

\*) Porosity measurements were not performed at Test Site 11. It is assumed to be the average of Test Sites 9 and 10, because Test Site 11 is situated between these sites.

By applying the limit load prediction, the dependency between cohesion  $\bar{c}$  and the friction angle  $\varphi$  is found, as shown in Fig.3. In addition, the result from the data analysis based on the least squares method is shown by a circular area. The values are presented in Table 2.

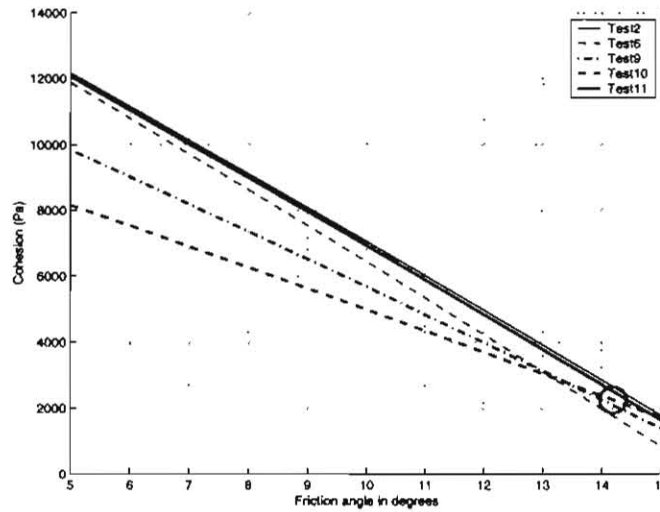


Fig.3. Dependency between cohesion and the internal friction angle. The result from the data analysis based on the least squares method is shown by circular area.

Table 2  
Best-fit results from experiments in 1999 for ice rubble strength parameters according to Mohr-Coulomb failure criterion

Cohesion	Friction angle
2.3 kPa	14°

The representative strength values are found from Fig.3. visually by looking for the cross-point of the curves. It is quite difficult to say exactly what the values for the strength parameters are, because two of the curves are parallel and they do not cross at the same point as the others. Nevertheless, the class of magnitude is quite easily observed. The slope of the curves depends on many factors such as the  $d/h$  ratio and the failure angle  $\alpha$ . Field tests should therefore be performed with a wide range of  $d/h$  to obtain nonparallel curves.

## DISCUSSION

The upper bound method is based on the simultaneous shear failure assumption through the keel. In reality, due to the uneven stress distribution, a progressive failure occurs. Thus, the strength parameters analyzed above are the minimum values. The stress state assumption inside the keel is comparable to the solution for axisymmetric semi-infinite solid (Timoshenko et al., 1987). The assumed pressure against the failure surface, however, is higher in the middle part of the keel, which causes higher frictional load capacity. This is one important reason for the low value of the friction angle reported in Table 2. An improved solution for the stress state inside the keel can be found numerically using the finite element method. Our results are comparable to the lower values in the small-scale tests found in Weiss et al. (1981). In addition, cohesion divided by the ice-block thickness is inside the range of  $16 \pm 8$  kPa/m. Furthermore, the cohesive strength is within the range that Leppäranta and Hakala (1989) and (1992) found in field tests. If a different analysis method is used, like the finite element method, the results might differ considerably (Kjesteit, 1999).

## ACKNOWLEDGMENT

This work has been undertaken within the LOLEIF Project in the framework of the EU-sponsored Marine Science and Technology (MAST-III) Programme under contract no. MAS3-CT97-0078.

## REFERENCES

- AZARNEJAD A., BROWN T.G. (1998): Observations of ice rubble behaviour in punch tests. Proc. of the 14th International Symposium on Ice (IAHR), Clarkson University, Potsdam, New York, USA, Vol. 1, pp. 589-596.
- CHEN W.F., HAN D.J. (1988): Plasticity for Structural Engineers. Springer-Verlag, New York, 606 p., ISBN 0-387-96711-7.
- CROASDALE & ASSOCIATES Ltd. (1998): In Situ Ridge Strength Measurements Local & Global.
- (1997): Proposal for a Joint Industry-Government Project, 24 p.
- ETTEMA R., URROZ-AGUIRRE G.E. (1989): On Internal Friction and Cohesion in Unconsolidated Ice Rubble. Cold Regions Science and Technology, 16, pp. 237-247.
- ETTEMA R., URROZ-AGUIRRE G.E. (1991): Friction and Cohesion in Ice Rubble Reviewed. Proc. 6th Int. Speciality Conf., Cold Regions Engineering, pp. 316-325.
- HEINONEN J. (1998): Ridge Loading Experiments. Field Experiments in Winter 1998, Unpublished report for the LOLEIF Project, 25 p.
- HEINONEN J., MÄÄTTÄNEN M., HØYLAND K.V., KJESTEIT G. (2000): Ridge Loading Experiments, Field Experiments in Winter 1999. Unpublished report for the LOLEIF Project, 73 p.

HØYLAND K.V. (2000): Measurements of Consolidation in Three First-Year Ridges. Proc. of the 15th International Symposium on Ice (IAHR), Gdansk, Poland, in press.

HØYLAND K.V., KJESTVEIT G., HEINONEN J., MÄÄTTÄNEN M. (2000): LOLEIF Ridge Experiments at Marjaniemi, The Size and Strength of the Consolidated layer. Proc. of the 15th International Symposium on Ice (IAHR), Gdansk, Poland, in press.

KJESTVEIT G. (1999): Investigation of Mechanical Properties of Ice Ridges. Norwegian University of Science and Technology, Department of Structural Engineering, Master Thesis, 46 p.

LEPPÄRANTA M., HAKALA R. (1989): Field Measurements of the Structure and Strength of First-year Ice Ridges in the Baltic Sea. 8th International Conference on Offshore Mechanics and Arctic Engineering, Vol 4., pp. 169-174.

LEPPÄRANTA M., HAKALA R. (1992): The Structure and Strength of First-year Ice Ridges in the Baltic Sea. Cold Regions Science and Technology, 20, pp. 295-311.

PRODANOVIC A. (1979): Model Tests of Ice Rubble Strength. Proc. of the Fifth International Conference on Port Ocean Engineering Under Arctic Conditions (POAC), Trondheim, Norway, Vol 1., pp. 89-105.

TIMOSHENKO S.P., GOODIER J.N. (1987): Theory of elasticity - 3. Ed., McGraw-Hill, Singapore, 567 p., ISBN 0-07-Y85805-5.

WEISS R.T., PRODANOVIC A., WOOD K.N. (1981): Determination of Ice Rubble Shear Properties. Proc. of the International Symposium on Ice (IAHR), Quebec, Canada, vol 2, pp. 860-872.



## PROBLEMS OF SLUSH ICE FORMATION AND TRANSPORT IN THE MIDDLE VISTULA RIVER

A. Dobrowolski<sup>1</sup>, B. Głowacka<sup>1</sup>, A. Kondzielski<sup>1</sup>

### ABSTRACT

The slush ice (mainly frazil ice) formation and transportation in the Middle Vistula River has been considered.

The Middle Vistula River shows complex combinations of various morphological elements. On braiding river reaches with many bed forms (e.g. Puławy Region) the turbulent mixing and water overcooling has gone up. These two phenomena have caused intensive slush ice formation.

Aircraft video imagery has shown river morphology effect on slush ice transport condition and ice cover formation on regulated as well as unregulated reaches, and in Włocławek reservoir backwater.

Heated water discharges have caused slush ice transport condition changes and have formed ice phenomena free zones. For example, during winter time, heated water discharge from Koźnice Power Station to Vistula River has activated the side channel near Pilica tributary. This has caused morphological processes changes in Vistula River.

Critical value of water stream slush ice saturation has been observed. Over this value ice formation has caused border ice mass increase due to slush ice settling. This phenomenon has been recorded using video camera and confirmed by intensity of slush transport measurements in Vistula River cross-sections near Warsaw and Zakroczym.

### ICE PHENOMENA ON THE MIDDLE VISTULA

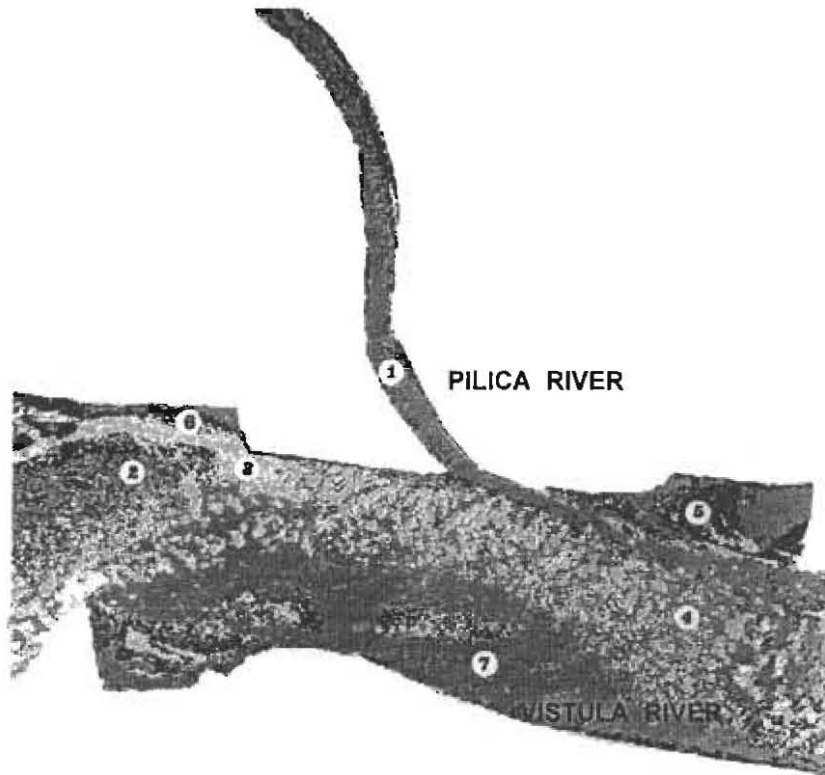
Ice phenomena in some Polish rivers are characterized by long time of slush ice formation and its run at the beginning and at the end of concerning occurrence (Kupczyk et al., 1986).

---

<sup>1</sup> Institute of Meteorology and Water Management, Warsaw, Poland, 61, Podleśna, 01-673 Warsaw,  
Tel./fax: (48-22)8640605, e-mail: Andrzej\_Dobrowolski@imgw.pl

The main component of slush ice in the Vistula River is frazil ice, which is formed in overcooled river water. In the beginning the single frazil crystals aggregate. As the water overcooling - the volume and crystallization ratio of aggregations grow up. Slush ice content in river water also grows up. The pancake ice is formed and together with broken parts of ice cover, bottom and border ice run downstream in upper layer of water.

The picture of winter airborne Vistula image made near Pilica River tributary shows the course of this phenomenon (Fig.1.).



1. loose slush
2. dense slush
3. compact slush
4. ice floe
5. border ice with smooth surface
6. border ice with rough surface
7. free water surface

**Fig.1.** Slush ice transport and transformation

In the Middle Vistula River, about 250 km upstream Włocławek Reservoir, the complex river bed morphology is favorable for frazil formation. In the meandering and braiding river with many different bars which divide up the river bed into arms, hydraulic parameters are changed significantly along the river course (Fig.2.).

Hydraulic parameters values calculated for research reach of Vistula River near Swider tributary: for mean flow the cross-section area, its mean depth and mean flow velocity vary about 1,5 times, and the Froude number varies in range of 0,170 to 0,405.



**Fig.2.** River bed morphological conditions for ice jam formation

Hydraulic parameters variability of the river bed causes intensive mixing in the water stream. They can be expressed in numbers (Donczenko, 1980) by turbulent mixing coefficient changes (about 3 times). Turbulent mixing speeds up water overcooling and frazil formation. Slush ice sticks over river bed forms quite quickly and the effective cross-section becomes smaller. The slush ice stream flows among river bed forms. Airborne video images allow to document this stream and, as a consequence main river stream configuration. Slush ice flows into braiding part of river and freezes - faster in more shallow river arms (Fig.3.).

Airborne video images of frozen slush ice in Vistula River near Dęblin allow to mark out the main stream among bed river forms (Fig.4.).

River regulation makes slush ice run easier (Fig.5.). Fast freezing of area among water structures as a result of water flow decrease has been observed.



**Fig.3.** Slush ice transport in branched Vistula River bed

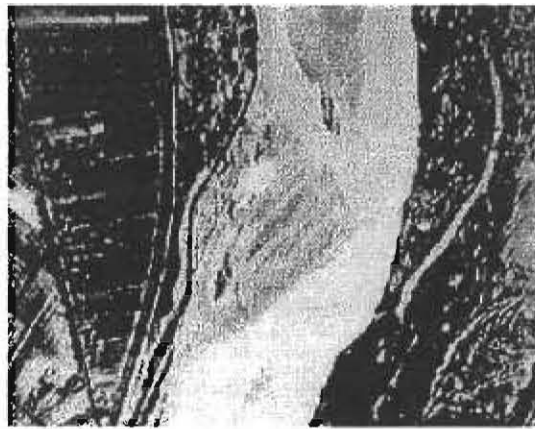


**Fig.4.** Frozen slush ice

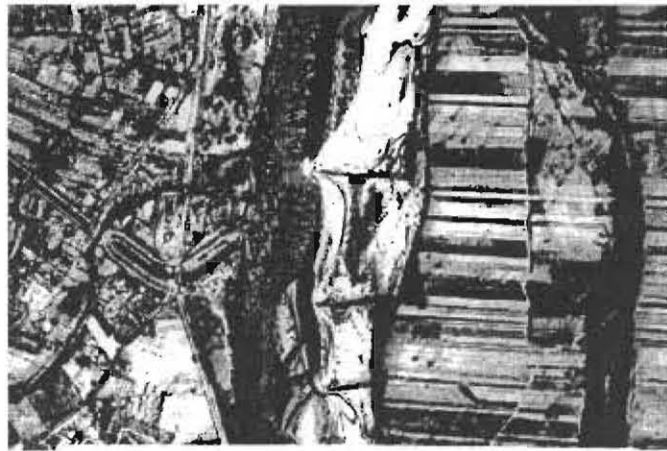


**Fig.5.** Ice run on the regulated river reach

River flow decrease in Włocławek Reservoir backwater causes sediment deposition. In winter time, the backwater is also fast freezing zone (Fig.6.). The ice cover formation in this reservoir begins about 20 days earlier than in Middle Vistula River (Grześ, 1989). Freezing progress begins at the water dam and follows upstream. In case of sufficiently high water velocity (Froude number exceeds the critical value), slush ice carried by river can flow under the ice cover (Mayer, 1989).

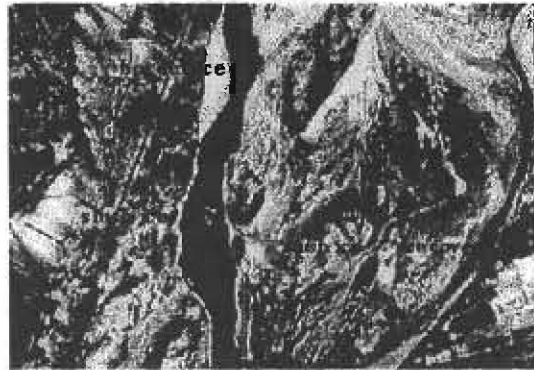


Fig.6. Freezing of Włocławek Reservoir backwater

The ice run in Vistula River, its influx to Włocławek Reservoir, and freezing on to ice cover, can cause the ice filling of the reservoir, and, as a consequence ice jam flood. The disastrous ice jam flood took place in 1982. Floating dams to stop ice inflow from Middle Vistula River to reservoir have been installed. However, when water level is high, the ice can flow over floating dam. But for mean water level, flow velocity over dam is enough high, and the ice can be drawn under the dam. Then, a lot of slush ice in reservoir backwater are observed (Dobrowolski & Żelaziński, 1994). Ice transfer to reservoir is confirmed by airborne video images of reservoir ice cover with visible zones of frozen pancake ice (Fig.7.).

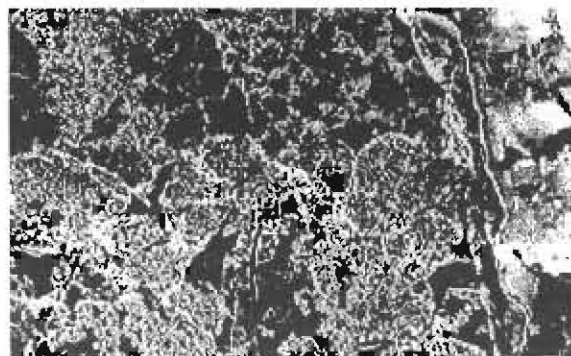
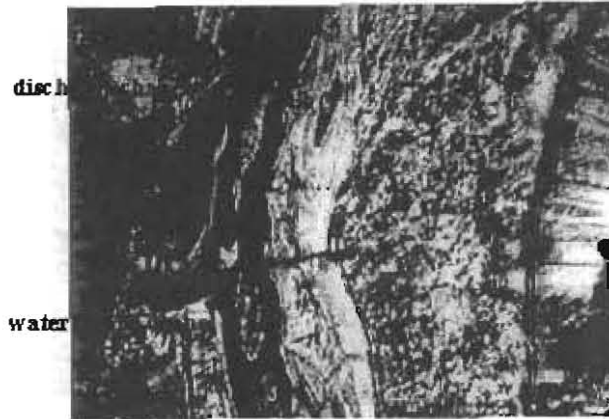


Fig.7. Pancake ice freezing in Włocławek Reservoir

Frazil ice transport in Middle Vistula River and other ice phenomena are affected by raised temperature water inflows.

Heated water discharges (water temperature gradient is about 10 to 12 deg) from thermal power station create heated water flux in river and ice phenomena free zone, eg. Koziencice Power Plant (Fig.8.).



**Fig.8.** Effect of heated water discharge from Koziencice Power Plant on Vistula River ice phenomena

Down the discharge, river water mean temperature increases, causing shortening of slush ice run-off duration and its intensity. Heated water flux remaining near left river bank has caused unfreezing of Vistula River lateral arm near Radomka tributary. An intensive water flow through this arm has caused change in time the fixed change of main river stream location, and as a consequence, the change of this lateral arm to main river channel in this region. The effect of heated water from Siekierki Power Plant, Powisle PP, and Zeran PP, on Vistula River near Warsaw, but in smaller range, has been observed.

Ice phenomena diversity also appears in Vistula River near Narew tributary. On airborne video image, Narew River is free of slush ice (water temperature is about 4°C), and only small border ice zones have been observed. In the same time in Vistula River, when water temperature is about 0°C, slush ice flow has been observed. The effect of Narew River on Vistula River ice cover is limited because of small water temperature difference.

Frazil formation and transport has been observed also in Vistula River downstream Warsaw. Significant river channel contraction in Warsaw causes bed erosion in city limits, and eroded sediments deposition grows up downstream Warsaw. River bed morphology in Warsaw - Zakroczym reach, becomes braided again, so it is favorable for water overcooling and frazil formation. For similar flows in this reach, and for similar hydrodynamic condition, the diversity of frazil formation intensity is caused by different heat exchange intensity between

water and atmosphere. In observed cases, for low water level in Vistula River, frazil has been formed at sudden air temperature drop. Ice transport has taken place in upper water zone.

In two analyzed time period, an interesting phenomenon has taken place: at air temperature drop to  $-16^{\circ}\text{C}$ , ice volume was only 5 % of water volume at cross-section, whereas at air temperature drop to  $-9^{\circ}\text{C}$ , ice volume was about 8 % of water volume (Dobrowolski & Kondzielski, 1992). Video recording of river surface has shown that frazil volume increase as river water cooled, and the „saturation” level has been achieved. Then, part of floating frazil has linked to border ice (Fig.9.).



Fig.9. Slush ice linking to border ice

In spite of further water overcooling, the frazil volume transported by river has not grown up. But ice border zone has widened. It has to be added that frazil saturation limit level in water about 10% has been observed in specialized laboratory in Zielonogorsk, in Science Academy, former Soviet Union (Gołek verbal information).

#### CONCLUSIONS

River bed morphology of Middle Vistula River has a significant effect on slush ice (including frazil) formation and transport, and on other ice phenomena courses. Also the effect of human activities as river regulation, heated water discharges has been observed.

Along regulated to some extent and unregulated Vistula River bed, there are reaches conducive to ice jam formation. Morphology of these reaches is typical for meandering and braiding river, which runs wild as an effect of significant sediment inflow from the basin to the river.

Possibility of slush ice inflow to Włocławek Reservoir with unfavorable meteorological and hydrological conditions like in 1982, threatens with ice jam flood as before.

In research of analyzed processes, video techniques, especially airborne, with computer processing of video images are very useful.

#### REFERENCES

DOBROWOLSKI A., GOŁEK J. (1989): Changes of the ice thermal regime in the river caused by heated water discharges. Proc. of Ice Seminar, Warsaw 1989, pp. 55-65.

DOBROWOLSKI A., KONDZIELSKI A. (1992): Ocena natężenia przepływu lodu prądowego w rzece nizinnej. Wiadomości IMGW, tom XV (XXXVI), z.4, pp. 47-56 (in Polish).

DOBROWOLSKI A., ŻELAZIŃSKI J. (1994): Operacyjna prognoza dopływu lodu do zbiornika Włocławek na Wiśle. Wiadomości IMGW, tom XVII (XXXVIII), pp. 75-82 (in Polish).

DONCZENKO R.W. (1980): Model of freeze-up process in river. Trudy GGI, vyp. 270, Gidrometeoizdat (in Russian).

GRZEŚ M. (1985): Problem zatorów i powodzi zatorowych na dolnej Wiśle. Przegląd Geograficzny, vol. LVII, No.4. (in Polish).

KUPCZYK E., IWIŃSKI J., NOWICKA M., GOŁEK J. (1986): Charakterystyka zjawisk lodowych na głównych rzekach polskich i związane z tym metody pomiarów i obserwacji. Inf.Proj. CBSiPW Hydroprojekt, nr 1 (in Polish).

MAYER I.(1989): Hydraulics of ice jam development. Proc. of Ice Seminar, Warsaw, pp. 179-188.



## ICE JAM FORMATION IN THE SHOKOTSU RIVER

H.T. Shen<sup>1</sup>, L. Liu<sup>1</sup>, K. Hoshi<sup>2</sup>, Y. Watanabe<sup>3</sup>, K. Hirayama<sup>4</sup>

### ABSTRACT

A study on the breakup ice jam occurred in the Shokotsu River in 1995 is presented. This study investigated the reason for the occurrence of the ice jam by analyzing the available hydro-meteorological data as well as hydraulic and geometric characteristics of the River. This analysis showed that the breakup of the ice cover was triggered by a sudden increase in basin runoff produced by rainfall during a warm spell. The jam was initiated at a section where there are rapid reductions in channel slope, flow velocity and top width. Numerical simulation was carried out to analyze the dynamics of the ice jam formation and evolution to supplement the limited information obtained from field observations.

### INTRODUCTION

Rivers in northern Japan are usually ice-covered for several months in the winter. Most of these rivers originate from mountainous areas, and flow through coastal plains before discharging into the ocean. Because of the steep channel slope in the mountainous reach, and the rapid reduction of slope when approaching the coastal zone, severe ice runs and ice jams can occur in these rivers if premature breakups occur before the melt out of the ice cover. In this paper, the March 1995 ice jam in the upper Shokotsu River is used as an example for analyzing breakup ice jam formation in rivers in northern Japan (Shen, 1999).

### THE SHOKOTSU RIVER ICE JAM

The Shokotsu River is located in the northeastern part of Hokkaido. Its main stem is 84 km long. The river flows from its upstream mountainous area to the narrow coastal plain near

---

<sup>1</sup> Department Of Civil & Environmental Engineering, Clarkson University, Potsdam, Ny 13699-5710 USA  
e-mail: htshen@clarkson.edu

<sup>2</sup> Hokkaido River Disaster Prevention Research Center, 9f, 2<sup>nd</sup> Yuuraku Building, South 1 West 1, Chuo-Ku Sapporo, Japan 060-0061

<sup>3</sup> Civil Engineering Research Institute, Hokkaido Development Bureau, Hiragishi 1-3, Toyohira-Ku, Sapporo, Japan 062-8602

<sup>4</sup> Engineering Department, Iwate University, 4-3-5 Ueda, Morioka, Iwate, Japan 020-8551

Monbetsu before discharging into the Okhotsk Sea. The drainage area of the River is 1,240 km<sup>2</sup>, which includes 1,141 km<sup>2</sup> mountainous area and 83 km<sup>2</sup> flat land. The design discharge capacity of the river is 1,300 m<sup>3</sup>/s. The channel is very steep. The channel slope in the upper reach is typically in the order of 1/300. During the winter months the river is covered by ice with heavy snow cover, and the discharge is typically in the order of 10 m<sup>3</sup>/s or less. On March 18, 1995, an ice jam of 3.4 km long formed in the River between kp 6/16 and kp 0/20, near the Town of Upper-Shokotsu (Fig.1.). This was the only ice jam occurred on the river during the ten year period between 1989 and 1998. The jam thickness was over 80 cm. Ice rubble and the floodwater spilled into the snowfield of the floodplains threatened the Town of Upper-Shokotsu and National Highway No. 273. The flood level remained above the 37.40 m design water level for three days. The revetment of the inner bank of the main channel was damaged along the bend around kp 2/18 to 8/18 due to the shear force of the ice run (Hokkaido Development Bureau 1998).

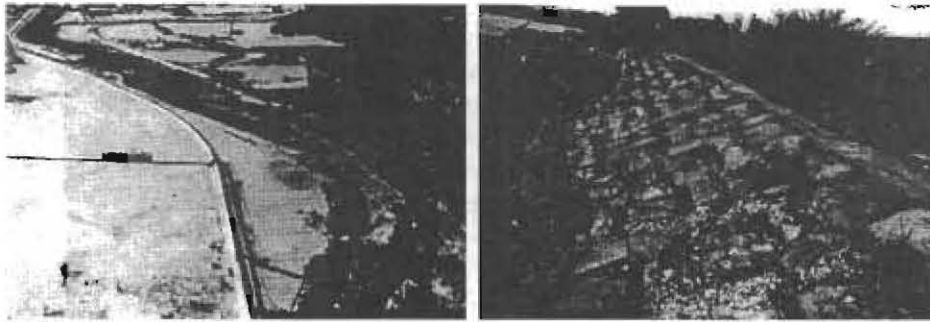


Fig.1. a. Ice Jam in the Shokotsu River between kp 6/16 and kp0/20, March 1995:  
b. Damages to the concrete mats on the convex bank of the bend

#### DATA ANALYSIS

Field observations of the flow and ice conditions were made periodically during the winter at several cross sections along the River.

#### Ice cover breakup

Fig.3. compares the water level at Upper Shokotsu with the precipitation record at Mombetsu during the six day period between March 16 and March 21, 1995. This figure shows a gradual rise of water level starting from March 16, 1995, due to the above freezing air temperature since March 14. The ice cover breakup occurred between Hours 22:00 and 23:00 of March 17. The 5.5 mm rainfall along with the accelerated snowmelt triggered the breakup on that day. The peak rainfall occurred at Hour 18:10 at a rate of 2 mm/hr. Due to the steep basin slope, this surface runoff can reach the river within a short time to produce the discharge increase that caused the breakup (Baba et al., 2000). Fig.2. shows the air temperature record for warm mid-March winters. This confirmed that the rainfall on March 17, 1995 was the key factor in the initiation of the breakup. The warm temperature alone could not cause a rapid increase in

snowmelt runoff enough to trigger the breakup. Shortly after the breakup, an ice jam was initiated between Hours 23:00 and 24:00. The jam caused the water level to rise at a rate of about 0.45 m/h. The peak level of 39.54 m was reached within six hours. This peak level was above the critical water level of 39.40 m.

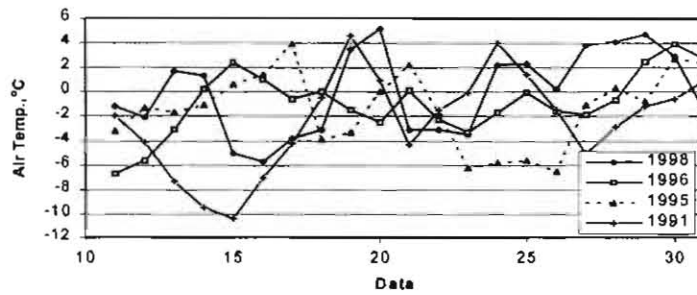


Fig.2. Air Temperature Variations from March 10 to March 31 during Several Warm Winters at Takinoue

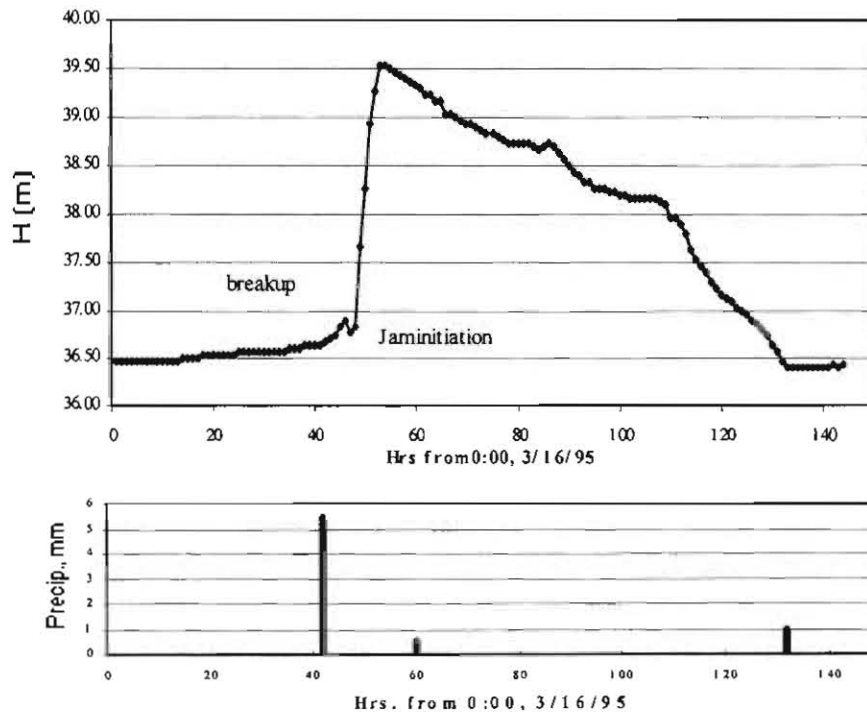


Fig.3. Comparison of Water Level and Precipitation at Upper Shokotsu

### Ice jam location

Field records as shown in Fig.1. indicated that the ice jam was initiated between kp 6/16 and kp 0/17. Fig.4. shows the daily discharge at Utsutsu Bridge in March 1995.

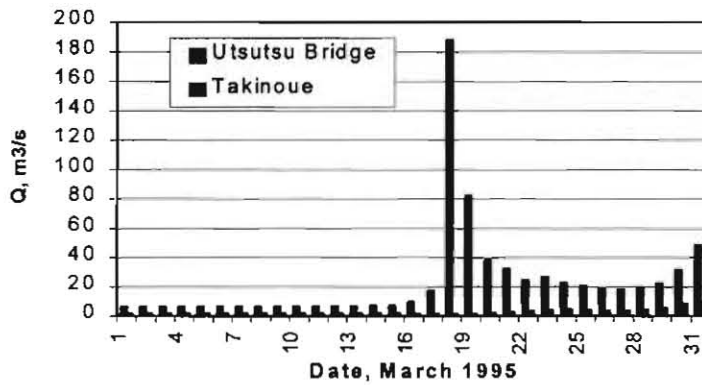


Fig.4. Daily Discharge at Utsutsu Bridge, March 1995

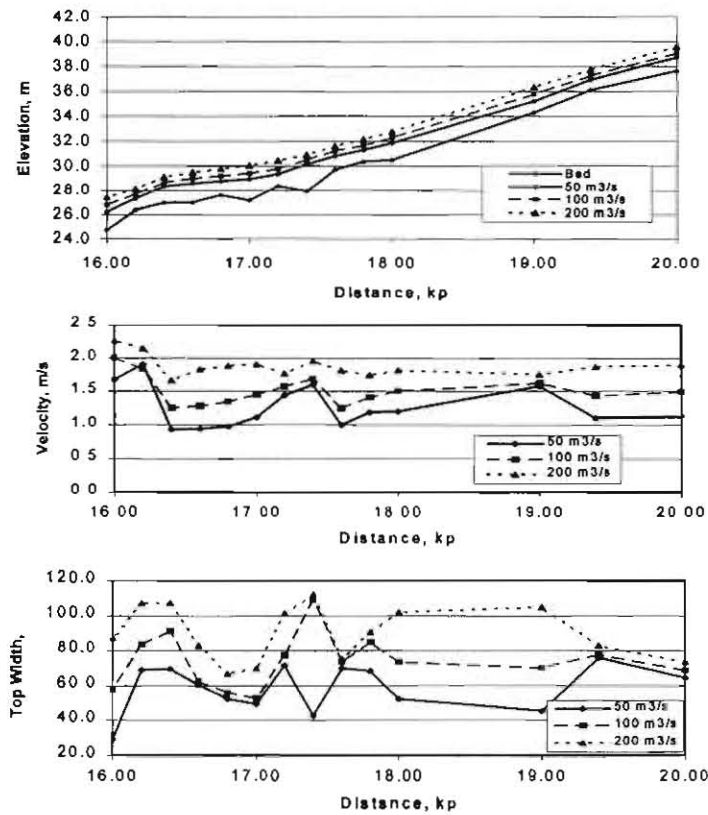


Fig.5. Variations of channel profiles, velocity, and top width between kp 16 and 20

Fig.5. shows plots of the channel bed profile and simulated variations of water surface profile, surface width, and flow velocity along the river reach. It clearly showed that there are rapid reductions in channel slope, flow velocity, and top width as the flow approaching kp 0/17. All of these contributed to the convergence of the ice run and the initiation of ice jam near this location.

#### NUMERICAL SIMULATION

Numerical simulation using the computer model DynaRICE (Liu et al., 1998; Lu et al., 1999) was made to provide more insights to the jam formation process. The model domain covers the reach between kp 0/15 and kp 0/20. The simulation starts from Hour 22:00, March 17. The bed elevation for the reach is shown in Fig.6. Values of the bed Manning's coefficients used were 0.03~0.035 for the main channel, and 0.05 for flood plains. Ice model parameters were the same as those used in Liu et al. (1998). Fig.7. shows the comparison of observed and simulated water levels at Upper Shokotsu. The simulation showed that the ice jam initiated immediately after the break up (Fig.8.). At the jamming time, the water discharge was about 30 m<sup>3</sup>/s or less. The water velocity near kp 8/16 was between 0.5 and 0.6 m/s. The premature breakup provided a large amount of ice supply to initiate the ice jam, especially when it was occurred before a significant increase in water discharge and water level. After it was initiated, the jam extended to upstream within 2 to 3 hours while there was no significant water discharge increase. The significant water discharge increase after this shoved more ice into the jammed reach and thickened the jam. By Hour 6:00, March 18, the water level reached the maximum value of 39.54 m. The simulated ice jam covered the reach between kp 6/16 and kp 7/19 as shown in Fig.8. This result compared well with the field condition.

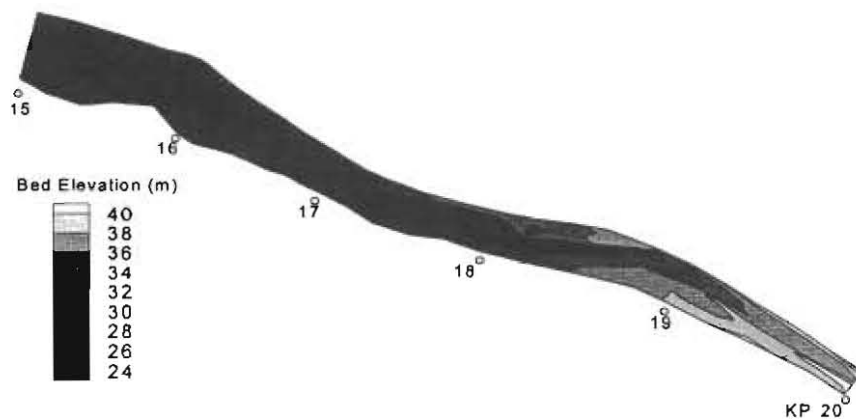


Fig.6. River Bed Elevation between kp 0/15 and kp0/20

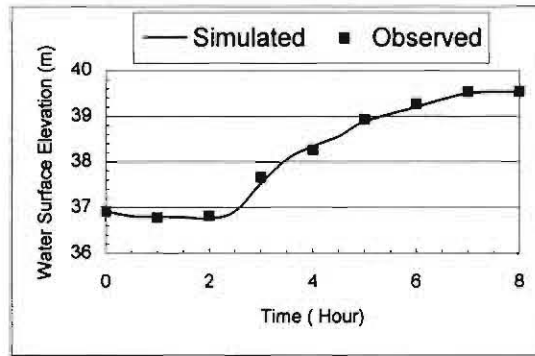


Fig.7. Observed and Simulated Water Levels at kp 4.1/19

### SUMMARY

In this paper a study on the 1995 ice jam in the Shokotsu River is presented. The jam was produced by the premature breakup of the ice cover in the river during the night of March 17. This breakup was triggered by a sudden increase of runoff caused by the rainfall around Hour 18:10, March 17. Due to the steep channel slope, the breakup was followed immediately by an ice run. This quickly resulted into the formation of the jam in the vicinity of kp 8/16. Analysis of river hydraulic characteristics and channel geometry, showed that the initiation of the jam was caused by the reduction of channel slope and flow velocity near kp 8/16. The narrow top width at this section and the bend immediately downstream enhanced the jamming potential. Numerical simulation of the ice jam dynamics confirmed these analysis and reproduced the ice jam processes and related flow conditions. This study serves as an example for analyzing breakup jam in steep rivers in a snowy region.

### ACKNOWLEDGEMENTS

This study was performed during H.T. Shen's sabbatical leave at the Hokkaido River Disaster Prevention Research Center, Japan.

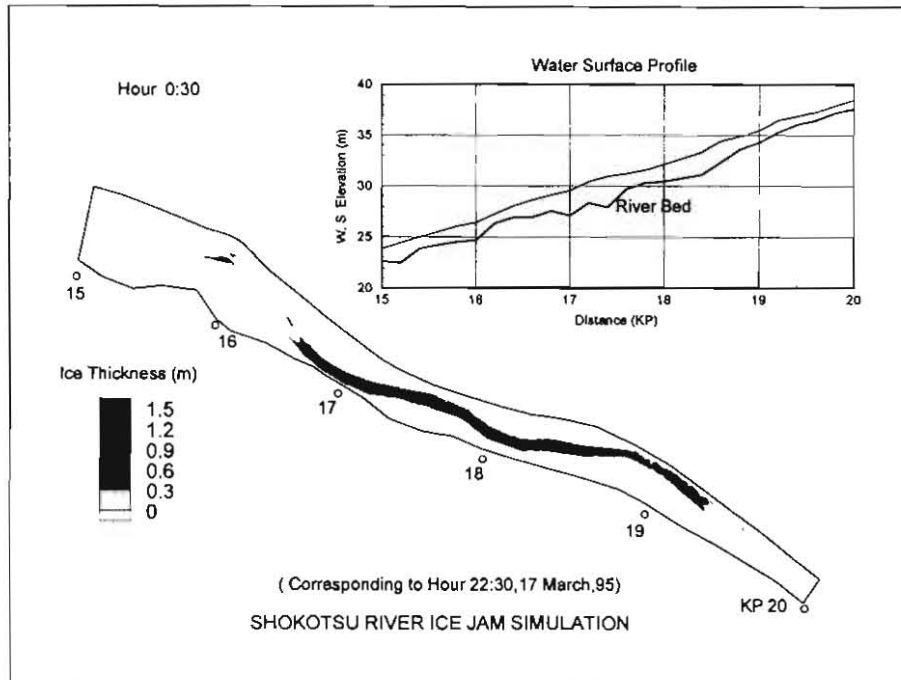


**Fig.8a.** Initial Ice Jam Thickness and Water Surface Profile at Hour 0:30

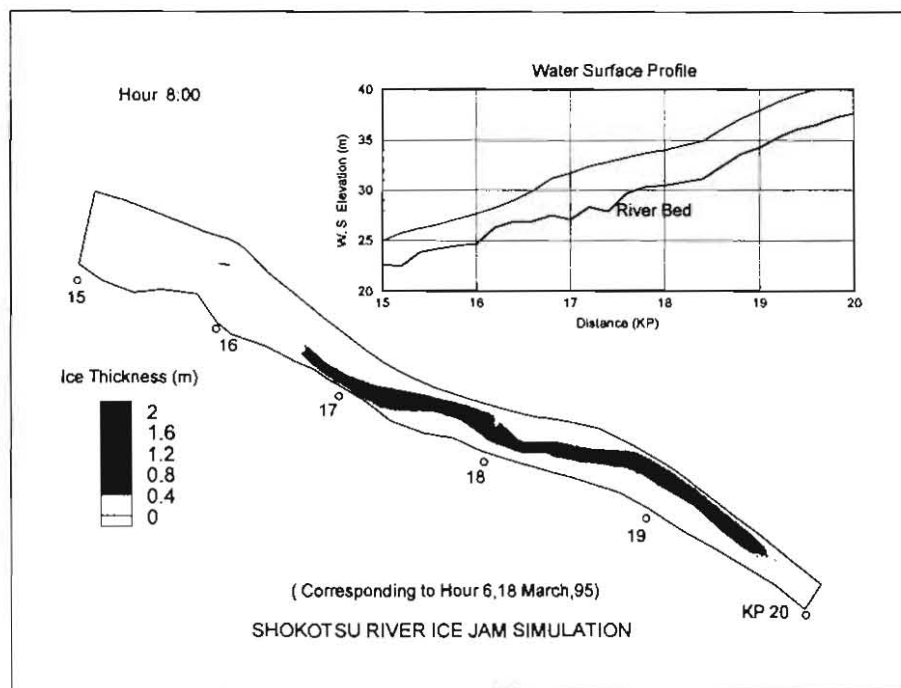


**Fig.8b.** Initial Ice Jam Thickness and Water Surface Profile at Hour 8:00

## REFERENCES

BABA H., HOSHI K., YAMAZAKI M., SHEN H.T. (2000):. Snowmelt analysis in the Shokotsu River basin for a breakup jam. Proc., 15th IAHR Ice Symp., Gdansk.

Hokkaido Development Bureau (1998): Shokotsu River Ice Jam. Internal Report, Abashiri Development Department, Abashiri, Hokkaido.

LIU L., SHEN H.T., TUTHILL A. (1998): A numerical model for river ice jam evolution. Proceedings, International Symposium on Ice, IAHR, V. 2, Potsdam, N.Y.

LU S., SHEN H.T., CRISSMAN R.D. (1999): Numerical study of ice jam dynamics in upper Niagara River. *Journal of Cold Regions Engineering, ASCE*, 13(2), pp. 78-102.

SHEN H.T. (1999): Shokotsu River ice jam formation. Report, Hokkaido River Disaster Prevention Research Center, Foundation, Sapporo, 23p.

SHEN H.T., CHEN Y.C., WAKE A., CRISSMAN R.D. (1993): Lagrangian discrete parcel simulation of river ice dynamics. *International Journal of Offshore and Polar Engineering*, 3(4), pp. 328-332.



## THE COMPARISON OF ROUGHNESS OF THE UNDERNEATH OF ICE COVER IN RIVER AND IN LAKE

E.P. Anisimova<sup>1</sup>, E.N. Dolgoplova<sup>2</sup>, A.A. Speranskaya<sup>1</sup>

### ABSTRACT

The roughness of the underneath of ice cover in two natural streams is investigated. Comparison of Rossby numbers for these streams shows considerably different regimes of interaction of these flows with the ice cover. The estimate of the thickness of the boundary layers is presented.

### INTRODUCTION

It is well recognized that the ice cover on reservoirs and rivers is formed differently because velocity of a stream results in stirring of water all over the depth of the river. The roughness of the undersurface of ice strongly depends on conditions of ice formation and varies over a wide range throughout the winter. When the heat exchange coefficient is small, the basic part of the cooling heat is released in the water surface layer. This case corresponds to a quiet and quick freezing by forming the ice crust on the surface of the reservoir. In case of big coefficient of heat exchange (active turbulent mixing in rivers) the distribution of crystallization heat is nearly uniform along the depth, that induces production of frazil and anchor ice. As a consequence, the freezing of the stream delays and the roughness of the underside of ice can be high at the moment of freeze-up.

The roughness of the undersurface of ice is one of the dominant factors of forming the boundary layer at the ice cover and the structure of ice-covered flow in the whole. It is very useful to know the parameter of ice roughness for both mathematical simulation and fundamental study of ice-covered flow.

The paper presents the results of comparison of experimental examination of ice-covered streams in the River Moskva and in the Lake Baykal.

---

<sup>1</sup> Physical Department, Moscow State University, Russia

<sup>2</sup> Water Problems Institute, Russian Academy of Sciences, Russia, 117735 Moscow, ul. Gubkina, 3, Russia  
Tel.: 7 (095) 135 72 01, fax: 7 (095) 135 54 15, e-mail: endol@iwapr.msk.su

## INVESTIGATION OF THE FLOW IN THE LAKE BAYKAL

The ice-covered flow in the Lake Baykal is induced by the outflowing Angara River. Big velocity of the river (~6 m/s) causes water opening at the river head which exists throughout the winter. The characteristic features of this flow are stable density stratification and the mixing layer at the boundary between the flow and the bulk of water. Two types of vertical distributions of the flow velocity were observed: (i) near the water opening, where the local velocity maximum near the lower surface of ice was seen (~1 m from the ice cover), and (ii) at the distance of ~0.3 km and more from the edge of ice which were formed by integral influence of the outflowing Angara River (Anisimova et al., 1998). The local maximum (i) which was formed by difference between the velocity of the flow and that of the river becomes smaller as we move away from the river head, and the velocity profile becomes typical for an ice-covered flow.

### Viscous sublayer

Let us consider the structure of the boundary layer at the ice cover near the open water (velocity profile (i)). Analysis of the structure of this layer shows that it is almost the same as that developing above the glass bottom of the flume, and the velocity distribution in it can be described by the Pouaseille equation (Anisimova et al., 1998):

$$u = \frac{1}{2\mu} \frac{dp}{dx} y^2 + ay + b, \quad (1)$$

where  $p$ -pressure,  $\mu$ -dynamic viscosity,  $\mu/\rho = \nu$ ,  $\nu$ -kinematic viscosity of water,  $\rho$ -density of water.

Using dimensionless variables  $u^* = u/u_{\max}$ ,  $y^* = y/H$ ,  $x^* = x/H$ ,  $p^* = pH/\mu u_{\max}$  and taking into account the boundary conditions for Eq. 1, we obtain instead of 1:

$$u^* = y^*(2 - y^*). \quad (2)$$

Comparison of measured velocity distributions for the ice-covered flow in the Lake Baykal with Eq. 2 shows good correspondence (Anisimova et al., 1998).

To estimate the thickness of the boundary layer  $\delta$  we use the expression for unbounded plate (Schlichting, 1968)  $\delta = 5\sqrt{\nu x/U_{\infty}}$ , where  $x$  is the distance from the open water, and  $U_{\infty}$  is the maximum velocity of the profile (i). The calculated magnitudes of  $\delta$  increase as we move away from the river head into the lake and change over the range 13-62 cm, which is approximately the location of local maximum of velocity.

### Defect velocity law

To investigate vertical distribution of velocity of the flow in the Lake Baykal far from the head of the River Angara (profiles of velocity (ii)), the analysis of 60 velocity profiles was performed. It shows that the logarithmic region extends down to the depth  $H$ , where

$u(y) = u_{\max}$ . It was found that shear velocity  $u_*$  increases with the increase of  $Re$ . This dependence can be presented as:

$$u_* = a Re^{7/11}, \quad (3)$$

where  $a$  is an empirical coefficient.

Introducing dimensionless coordinates  $u^+ = u/u_*$ ,  $y^+ = yu_*/\nu$ , and using the logarithmic law for experimental velocity profiles, we obtain

$$u^+ = A \ln(y^+) + B, \quad (4)$$

where  $A=1/\kappa$  is the same for all measured profiles ( $\kappa$  is the Karman's constant) and  $B$  depends on a particular profile and varies in a wide range. The dependence  $u_*(Re)$  and the range of variation of  $B$  in Eq. 4 show that the flow does not reach fully developed turbulent regime (although there are several profiles, which are near to the profile of turbulent flow). Since it was shown that mean velocity profile in ice-covered flow fits defect velocity law sufficiently well (Schlichting, 1968; Cebeci & Bradshaw, 1984; Tsai & Ettema, 1996), we use it to describe the distribution of velocity of the ice-covered flow:

$$\frac{u_{\max} - u(y)}{u_*} = 2.5 \ln\left(\frac{H}{y}\right). \quad (5)$$

Expression 5 was obtained under the assumption that the Prandtl mixing length is  $l = \kappa y$ . This leads to  $du/dy \rightarrow \infty$  as  $y \rightarrow \infty$ , i.e. the condition of adhesion at the lower surface of ice is violated. Following Rossby we introduce parameter of roughness of the lower surface of ice  $y_0$ , and instead of Eq. 5 we obtain:

$$\frac{u_{\max} - u(y)}{u_*} = 2.5 \ln \frac{H}{y + y_0}. \quad (6)$$

#### Parameter of roughness

The values of roughness  $y_0$  were found from the measured velocity profiles at the places with large depth, where the condition  $y_0 \ll y$  was valid. Calculated values of the roughness  $y_0$  were used to obtain the velocity defect law profiles. Comparison of Eq. 6 with the measured flow velocity distributions shows good correspondence (the mean square error is 0.027) (Anisimova et al., 1998). Since there is practically no scattering of the data, one can identify Eq. 6 as a selfsimilarity profile for the flow under consideration.

The parameter of roughness of the lower surface of ice varied over the wide range  $\sim 5\div 35$  cm. The dependence of  $y_0$  on the shear velocity (Fig. 1.) shows that on the lower surface of ice in the Lake Baykal the hydraulically smooth flow is formed. At the lower surface of ice, turbulent shear stress was defined from the data as:  $\tau_0 = \rho u_*^2$ . As the measurements were

performed from January till May, the roughness of the lower surface of ice varied considerably, and as a consequence  $\tau_0$  changed from 0.05 to 1.6 g/cm<sup>2</sup>.

### **INVESTIGATION OF THE ICE COVER IN THE RIVER**

The appearance of the ice cover on a river results in considerable changes in structure of the flow, for instance, in transport of sediments and admixtures and also in increase of hydraulic friction. The roughness of the ice cover is one of the main parameters defining the structure of ice-covered stream. We consider the ice-covered flow in the river using the flat-stream approximation, because for most of plane rivers the width-to-depth ratio is a big number.

The usual description of an ice-covered flow is that of a stream composed of two currents, one of which is formed near bottom and another under the ice cover. Measurements of velocity profiles of the ice-covered flows show that the roughness of the lower surface of ice and bottom are different. The existing data indicate also that the models in which velocity profile is supposed to have a maximum on a single horizon can be considered only as approximate schemes. Usually, the measurements of velocity profiles in nature and in flume streams show the existence of a layer of considerable dimension in which the gradient of velocity is practically zero (Smith & Ettema, 1994; Dolgoplova, 1996).

#### **The reach of experiment**

The investigation of ice-covered flow was performed in the River Moskva in winter. The fundamental characteristics of the river are: Reynolds number  $Re=10^6$ , Froude number  $Fr=2 \cdot 10^{-2}$ , the mean width  $B=70$  m, mean depth  $H=2$  m, mean velocity reaches 0.6 m/s, the thickness of ice varies from 13 cm to 40 cm. The bottom consists of sand.

Two practically rectilinear study reaches were chosen (the distance between reaches was 600 m), each of them was about 400 m, and 20 measuring sections were laid out with 40 m between neighboring sections. There were up to 9 verticals in the measuring section. To choose suitable cross-sections for measurements of mean velocity profiles, we measured depth and thickness of ice on each vertical.

Three cross-sections were chosen in the upper reach and two - in the lower. Mean velocity profiles measured at five verticals in each cross-section are presented in (Dolgoplova, 1998). The river bed of chosen cross-sections had nearly trapezoidal shape. There was warm water discharge at the right bank of the river in the second cross-section at the upper reach. The spreading of warm water could be traced by measuring the thickness of ice across and along the river.

#### **Mean velocity distributions**

Following the classical representation of an ice-covered flow mentioned above, we will divide it into two streams, assuming that distribution of mean velocity of each of them is described by the power law (Dolgoplova, 1996). This description enables us to find the location of the maximum velocity and to calculate analytically the mean velocity profile for the whole stream

which is in good correspondence with the measured one. The position of the level of the maximum velocity was used to define the thickness of the current formed by the ice cover. The distribution of velocity of this current was described by velocity defect law (Dolgoplova, 1998). In this case the Rossby parameter of roughness was found by the same method as for the flow in the lake.

#### **Roughness of ice in river**

Near the place of warm water discharge a block of ice was cut out (dimensions 0.9 m × 0.6 m). The lower surface of ice of this block consisted of alternating sequences of funnels (depth about 6 cm, diameter 2-3 cm), and water galls of mean dimension 6-8 cm. Near this place the thickness of ice had its minimum - 13 cm and the calculated parameter of roughness had the maximum value -2.6 cm. The results of calculation of  $\gamma_0$  are presented in Fig.2. as a function of shear velocity. Although the magnitudes of Rossby parameter in the Moskva River are by several orders smaller than those in the lake, a hydraulically rough flow is formed at the underneath of ice in the river.

Analysis of thickness of ice along the study reach shows that it strongly depends on the warm water, which was discharged near the right bank at the beginning of the reach. We did not observe the increase of the thickness of ice near the banks as it was noted in (Larsen, 1973; Engmann & Kellerhals, 1974). This can be explained not only by the warm water discharge, but also by the small depth of the river as compared with the rivers investigated in above mentioned works ( $H=5-12$  m).

Along all the reach of study, beginning with the second cross-section, the thickness of ice near the right bank was about 20-25 cm, which is considerably smaller than the mean magnitude, and shows the influence of warm water discharge through about 1 km down the river. This fact confirms the distribution of the transfer coefficient through the depth of the ice-covered flow which is presented in (Shen & Harden, 1978), where it is shown that the transfer coefficient has two maxima (corresponding to division of the flow into two flows) in the bottom flow and in the flow formed by the ice cover. Between these currents the transfer coefficient has its minimum, which prevents warm water mixing all over the depth.

The approximate estimate of the thickness of the boundary layer at the lower surface of ice was made by using the expression (Nikitin, 1963):

$$u_\delta = 5.6 u_* \quad (7)$$

where  $u_\delta$  is the velocity at the boundary of the layer. Analysis of the numerous results obtained in various experimental settings in laboratories and in nature made possible to argue (Nikitin, 1963) that relation 7 is valid for smooth and rough riverbeds at different regimes of turbulent streams.

Using the measured velocity nearest to the ice, we calculate the ratio  $u_s/u_*$ . In most cases this ratio is much larger than 5.6, that is our probe worked outside of the boundary layer. At three verticals at the right bank of the cross-section II and at the two verticals in the middle of the river in the cross-section III the ratio  $u_s/u_* < 5.6$ . In these cases the propeller was at the distance 10 cm from the ice cover. The distance between cross-sections II and III was 40 m. Thus we may suppose that there is a turbulent boundary layer at the underneath of the ice cover of thickness about 10 cm which is spreading from the right bank to the middle of the river for 40 m.

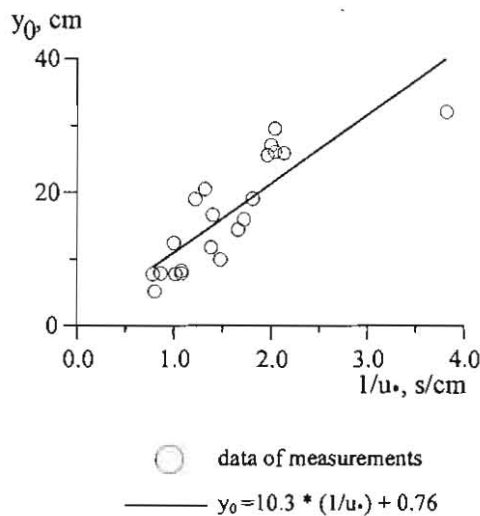


**Fig.1.** The dependence of the roughness parameter on the shear velocity in the Lake Baykal

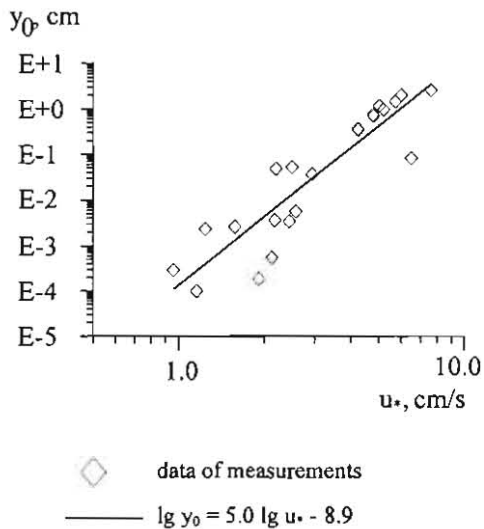


**Fig.2.** The dependence of the roughness parameter on the shear velocity in the River Moskva

### CONCLUSIONS

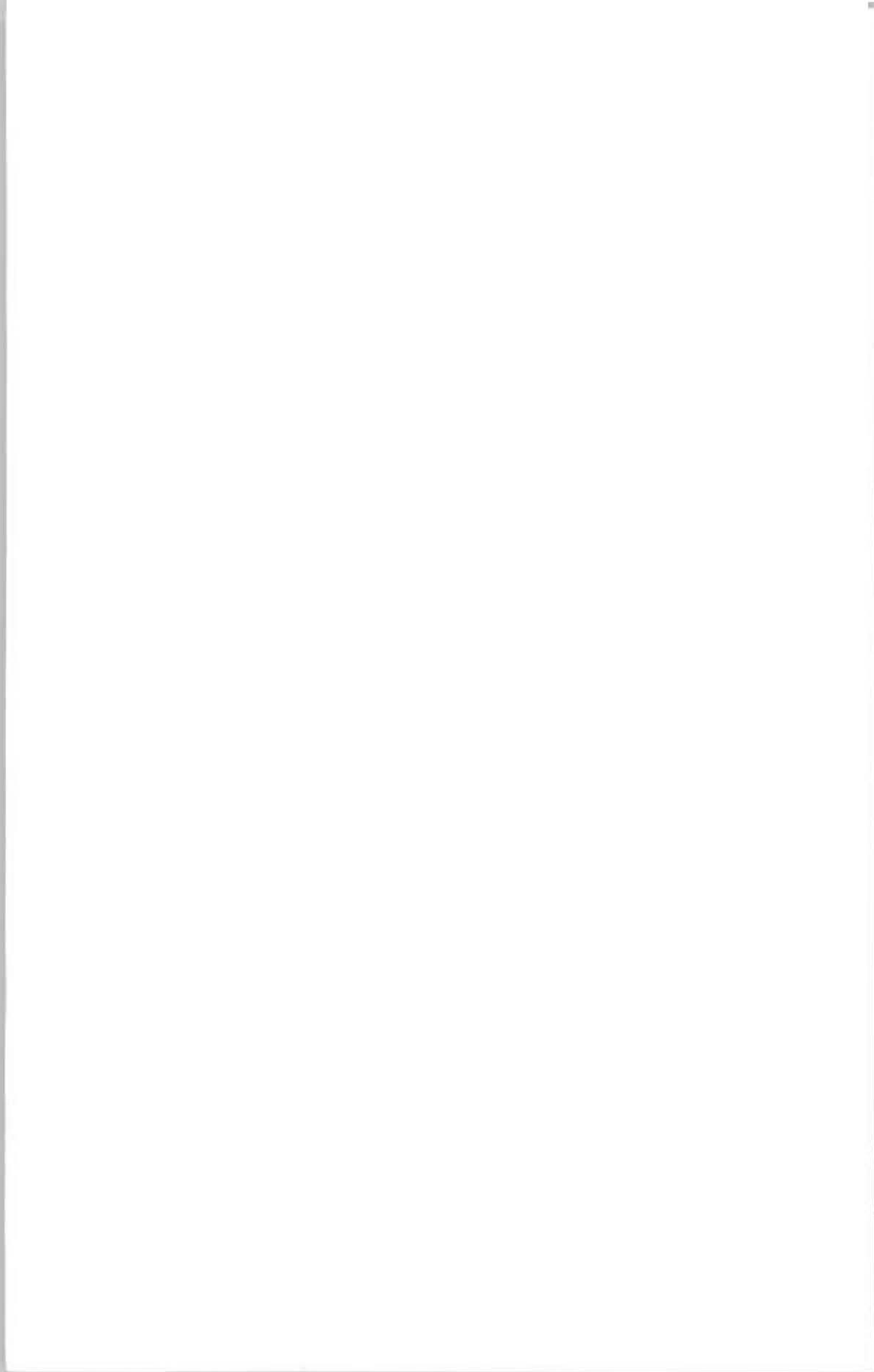
Although the ice-covered flows in the lake and river both have large Reynolds numbers, the characters of these flows are very different. In the Lake Baykal, near the open water there is formed a boundary layer with velocity distribution described by the Pouaseille equation and which thickness is increasing as one moves away from the opening. At the large distances from the opening, the flow is transitional from the laminar to the turbulent one and is nicely described by the defect velocity law which takes into account the roughness parameter of the under-ice surface. The roughness parameter varied in a wide range and its dependence on  $u_*$  shows that in the Lake Baykal the hydraulically smooth flow is formed. The dependence  $y_0(u_*)$  for the River Moskva indicates the hydraulically rough regime of the stream.

## ACKNOWLEDGMENT

This work was partially supported by RFBR (Grant No. 97-05-65528)

## REFERENCES

- ANISIMOVA E.P., DOLGOPOLOVA E.N., SPERANSKAYA A.A. (1998): Flow in ice-covered low flowage water body. Proc. of the 14th Symp. on Ice, Potsdam, New York, USA, pp.49-52.
- CEBECI, T., BRADSHAW P. (1984): Physical and computational aspects of convective heat transfer. New York: Springer-Verlag.
- DOLGOPOLOVA E.N. (1996): Resistance of ice-covered nature flows. Proc. 13th Int. Symp. on Ice, IAHR, Beijing, pp. 497- 504.
- DOLGOPOLOVA E.N. (1998): Velocity distribution in ice-covered flow. Proc. of the 14th Symp. on Ice, IAHR, Potsdam, New York, USA, pp. 123-129.
- ENGMANN J.E.O., KELLERHALS R. (1974): Transverse mixing in an ice-covered river. J. Water Resources Res. v.10. No. 4. pp. 775-784.
- LARSEN P.(1973): Hydraulic roughness of ice covers. J. Hydr. Div. v.99. No. 1. pp. 111-119.
- NIKITIN I.K. (1963): Turbulent riverbed stream and processes in the region near bottom. (Rus),Kiev, Acad. of Sciences of Ukraine.
- SCHLICHTING H. (1968): Boundary-layer theory. Sixth ed., McGraw-Hill, New York.
- SHEN H.T., HARDEN T.O. (1978): The effect of ice cover on vertical transfer in stream channels. Water Resources Bull. V.14, No. 6, pp. 1429-1439.
- SMITH B.T., ETTEMA R. (1994): Flow over dunes in ice-covered channels. Proc. 12th Int. Symp. on Ice, IAHR, Trondheim, Norway, pp. 84-92.
- TSAI W.F., ETTEMA R. (1996): A study of ice-covered flow in an alluvial bend. IAHR Technical report No. 376, Iowa Institute of Hydraulic Research.



## RIVER ICE PROBLEMS ON THE LOWER VISTULA

M. Grześ<sup>1</sup>, W. Majewski<sup>2</sup>

### ABSTRACT

Vistula is the largest Polish River. The river flows from south in the north direction which has an essential influence on thermal and ice regime. From hydrographic point of view Vistula river can be divided into three sections: upper, middle and lower. Lower Vistula is the river section 391 km long and has very high ice jam potential. Numerous floods occurred in the past during winter time. They appeared either in the beginning of winter during ice formation or in spring during ice run. This river section is very important from economic and engineering point of view. The paper presents studies of ice phenomena along Lower Vistula and engineering solutions which were assumed to limit the negative consequences of ice jam formation and floods.

### VISTULA RIVER

Vistula River is the largest Polish river and one of the largest in Europe. It is the second largest river (after Neva) of the Baltic Sea Basin. The total length of Vistula River is 1068 km. The source of Vistula is in the south of Poland in Carpathians at the altitude 1100 m above sea level. The average discharge at the river mouth is 1080 m<sup>3</sup>/s, which gives the average annual outflow of 34 km<sup>3</sup>. The maximum and minimum observed discharges (1951-1990) are 7840 and 253 m<sup>3</sup>/s respectively. The total Vistula River catchment is 194 000 km<sup>2</sup> of which 169 000 km<sup>2</sup> is within Polish boundaries i.e. 87 %. The Vistula catchment which is in Poland constitutes 54% of the total Polish surface area. From hydrographic point of view Vistula can be divided into three distinctly different sections: Upper Vistula, Middle Vistula and Lower Vistula. These three river sections constitute three river catchments. They represent different geographic and climatic conditions. High rocky mountains in the south and flat plains in the north. Severe winters with much snow in the mountains and milder winters in the north due to the influence of the sea. The average precipitation for Vistula catchment is 600 mm, similar to the whole Poland. Maximum average yearly precipitation occurs in the mountain region

---

<sup>1</sup> Toruń University, Institute of Geography, Fredry 6/8, 87-100 Toruń, Poland, Tel.: +48 -56-622 7307, fax: +48-56-622 7308, e-mail: gmark@geo.uni.torun.pl

<sup>2</sup> Institute of Hydroengineering of the Polish Academy of Sciences in Gdańsk, Kościarska 7, 80-953 Gdańsk, Poland, Tel.: +48 -58-552 3903, fax: +48 -58 -552 4211, e-mail: wmaj@ibwpan.gda.pl

(1700 mm) and the lowest in the region of Lower Vistula (450 mm). Vistula has one of the highest flood potential in Europe with nonuniform flow distribution in time. Vistula is characterised by significant sediment transport (suspended and bed load). At present water pollution in Vistula is still very high, and results mainly from industrial and domestic sewage discharges. The total volume of water stored in retention reservoirs over Vistula catchment does not exceed 6 % of the annual average outflow.

### **LOWER VISTULA**

Lower Vistula is 391 km long river section with very diversified character of the channel. Upstream part is a braided channel close to the natural. Between Plock and Włocławek there is the run-off-river reservoir Włocławek and downstream from it Vistula is trained river with limited meandering and finally estuarine section. Lower Vistula can be divided into four sections. Lower. First - the most upstream section 68 km long is only partly trained with braided channel, sand bars and islands. Average widths of river channel extends from 360 to 800 m. The width of flood channel is from 700 to 1700 m. About 100 km<sup>2</sup> of flood plains along the river is protected by flood embankments which were designed for the discharge of 1% probability. This river section usually produces significant amount of frazil ice in the beginning of winter. Second section of the Lower Vistula extends along 57 km and includes run-of-river reservoir formed by low head barrage. Surface area of the reservoir is 70 km<sup>2</sup> and the volume 400 mln m<sup>3</sup>. Włocławek project was completed in 1970 as one of the projects of the Lower Vistula Cascade. Up till now it operates as a single project with all consequences of such situation (local erosion, sedimentation, ice regime). Third section, just downstream from the dam - 43 km long is partly trained with damaged channel by the picking operation of hydraulic powerplant. Discharge along this section is very nonstationary, changing considerably several times during day due to the operation of hydraulic powerplant. Fourth section - 223 km long, extends to the river mouth. It has been trained for navigation in the XIX century. Protection against flood waters is by means of embankments and high banks of the river valley. The last 30 km of this section is under influence of the sea which often causes ice blockade or high water elevation.

#### **Ice jams along Lower Vistula**

Studies of ice jam phenomena on the Lower Vistula were initiated already in XIX century. These were one of the first in Europe. The best known and described in detail was ice jam in 1840 in the Pleniewo region close to Gdańsk. The dammed waters of Vistula broke through the sand dunes along sea coast over the length of 1.5 km and formed a new river outlet to the Bay of Gdańsk called Wisła Śmiała (Bold Vistula). The largest known ice jam appeared in the region of Tczew in 1885. At this time approximately 440 km<sup>2</sup> of the valley were flooded. 126 villages were under water (Grześ, 1991).

Every two or three years in the delta region of Vistula significant ice jams with floods occurred. The reason for many ice jams in the estuarine section of Vistula was the complicated layout of river channels. They branched approximately 10 km from the sea to the West (Gdańsk Vistula) and to the east (Elbląg Vistula). Upstream from this point was another

east branch Nogat. In 1895 it has been decided to make radical change in river channel layout. The straight new Vistula channel was constructed leading Vistula waters and floating ice directly to the sea. Since that time there was no winter or summer flood in this region. Nogat, Gdańsk Vistula and Elbląg Vistula were cut off from the main channel by means of navigation locks. Problems of icebreaking and the influence of sea ice, however, remained till today. Now ice problems moved downstream to the location of sedimentation cone, which formed at the mouth of Vistula main channel, due to shortening of Vistula channel. Deposits of Vistula sediments are moved into the Bay of Gdańsk by means of extended wavebreakers on both sides of river channel. These wavebreakers are now more than 2 km long. Estuarine section of Vistula is shown in Fig.1.

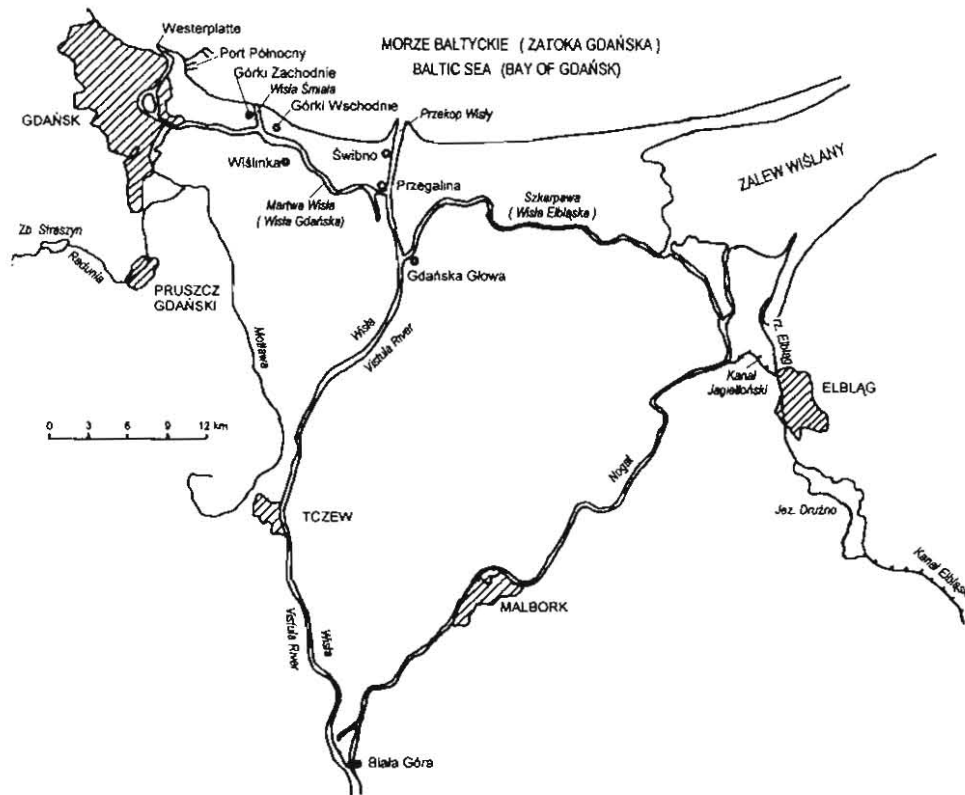


Fig.1. Estuarine section of Vistula

The first, unfortunately not successful attempts to control ice formation on the Lower Vistula started already at the end of XVIII century. They were based on directing ice floes into River Nogat (branch of Vistula). Specially constructed heavy sledges were used for ice breaking. This was kind of prototype of icebreaker. The first icebreaker mechanically propelled by

steam engine was introduced in 1881. Since that time river icebreaking has been the most effective active method for controlling ice break-up and elimination of ice jams. The main difficulty in the use of icebreakers on Vistula River was their draught (1.5 to 2.0 m) which remains till today. When training of the Vistula River channel (downstream from km 718) was completed at the end of XIX and beginning of the XX century the possibilities of icebreaking increased considerably. The drop of ice jam frequency occurrence was quite significant. However upstream from this point (km 718) where the river channel remained in natural state one or even several ice jams were observed each winter. It was interesting that ice jams usually formed approximately in the same locations along the river channel, which were well known to the river exploitation service. This situation changed significantly after the completion of Włocławek project in 1970. Run-of-river reservoir divided the Lower Vistula Section into 3 parts (upstream from reservoir, reservoir, and downstream from reservoir).

### **WŁOCLÁWEK PROJECT**

Włocławek Project consists of earth dam 20 m high and 650 m long with 10 bay spillway section equipped with steel vertical gates for discharging water and ice, hydraulic powerplant of the capacity 162 MW operating in picking power mode, and navigation lock (115 m long and 12 m wide). Layout of the Włocławek project is shown in Fig.2. The barrage forms run-of-river reservoir of the volume 400 mln. m<sup>3</sup> and the length about 50 km. Reservoir is situated between two large cities Włocławek and Płock. Maximum discharge which was observed during the operation of the project was 6900 m<sup>3</sup>/s. Maximum design discharge through the powerplant is 2200 m<sup>3</sup>/s. Steel vertical gates can be lowered by 2.20 m and thus provide the discharge of 1300 m<sup>3</sup>/s. When discharge is higher it is necessary to raise the gates. With fully opened gates the discharge through the spillway is 7500 m<sup>3</sup>/s. The main aim of the project was the production of electric energy, improvement of navigation, and to provide possibilities of water supply for various purposes. Formation of the reservoir initiated significant sedimentation in the upstream part of the reservoir (about 1.5 mln m<sup>3</sup> per year). Sedimentation caused erosion downstream from the reservoir. The main problems which appeared on the reservoir and the barrage during winter operation were:

- formation of hanging dams due to the inflow of large amounts of frazil ice thus causing increased water elevations,
- operation of spillway gates and navigation lock due to freezing,
- ice breaking on the reservoir and ice discharge downstream.

Włocławek project caused important changes in hydraulic and ice regime in the reservoir. Comparison of ice regimes before and after dam construction indicates that total duration of ice phenomena did not change and lasts on the average about 80 days per year. Considerable changes are, however, in the duration of particular forms of ice regime. Frazil ice movement was shortened from 48 to 8 days. Floating ice changed from 9 to 6 days. Duration of solid ice cover on the reservoir increased from 25 to 64 days.

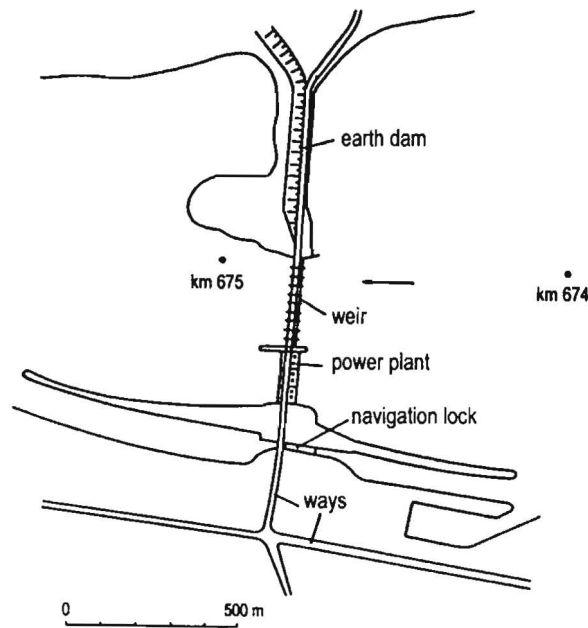


Fig.2. Layout of Włocławek project

#### EXAMPLES OF EXTREME ICE SITUATIONS ON WŁOCŁAWEK RESERVOIR

Włocławek reservoir extends along Vistula River over 50 km. However, its essential part 42 km long is between two important cities Włocławek and Płock each of the population more than 100 thousand inhabitants. With constant water elevation at the Włocławek dam required for hydraulic powerplant, depending on the character of ice cover on the reservoir water elevations at Płock cross-section (42 km upstream) may vary considerably from water elevation at free water surface. In some cases the increase reached 200 to 250 cm.

In winter 1978/9 ice cover formed during low discharge ( $1000 \text{ m}^3/\text{s}$ ). Rapid formation of ice cover on the reservoir was accompanied by the formation of numerous hanging dams and frazil deposits under solid ice cover. When in the beginning of March river discharge increased to about  $3000 \text{ m}^3/\text{s}$  rapid increase in water elevation in Płock was observed. River discharge is denoted by  $Q$ , free surface water elevation (calculated) -  $H'$ , and water surface elevation with ice cover (measured) -  $H$ . During some days water surface elevation with ice cover was higher than 170 cm. In January 1981 despite low discharge ( $1200 \text{ m}^3/\text{s}$ ) water surface elevation in Płock was nearly 200 cm higher than for free surface flow with the same discharge. This was caused by very nonuniform ice cover with numerous hanging dams thus creating high flow resistance. The sequence of changing discharge and water elevation is shown in Fig.3.

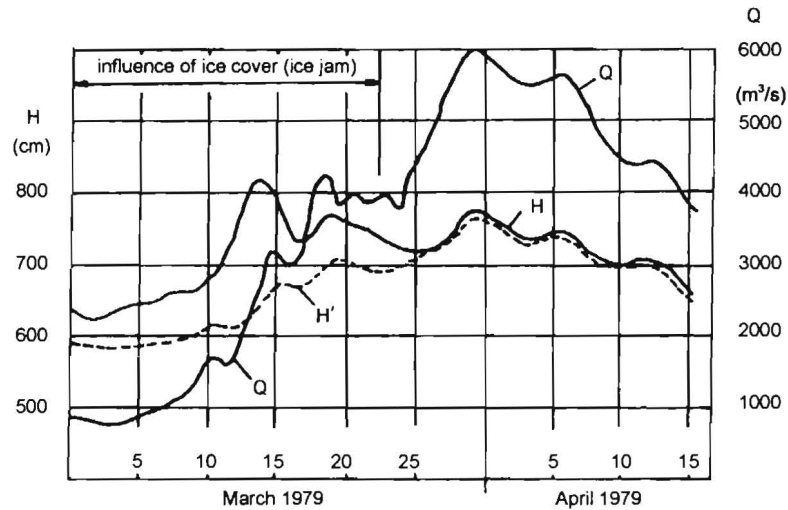


Fig.3. Discharge and water elevations in Płock during winter 1978/9

Due to very unfavourable hydrological and meteorological conditions (drop of air temperature during one day of nearly 30 °C, strong wind blowing in the upstream direction, and high discharge) very high water elevations occurred in Płock. They exceeded the crest of flood dykes which resulted in inundation of 10 000 ha of land and 2230 farms (Majewski, 1996). The changes of water elevations and discharge for Płock gauge are shown in Fig.4.

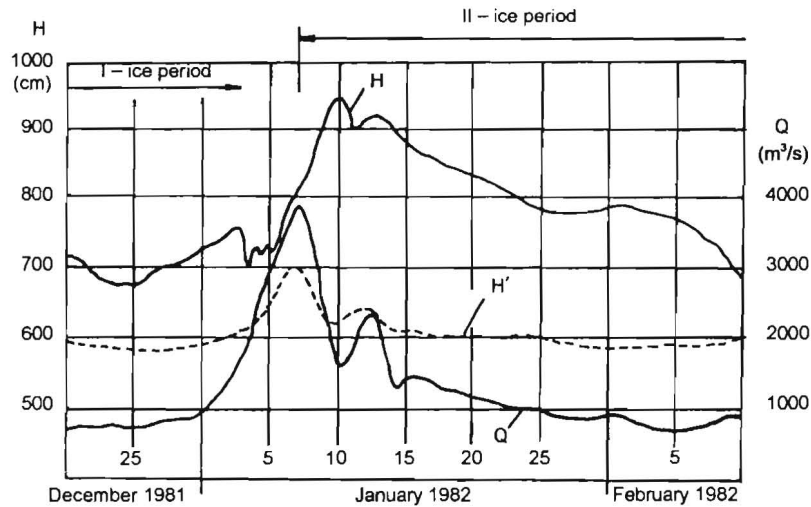


Fig.4. Discharge and water elevations in Płock during winter 1982

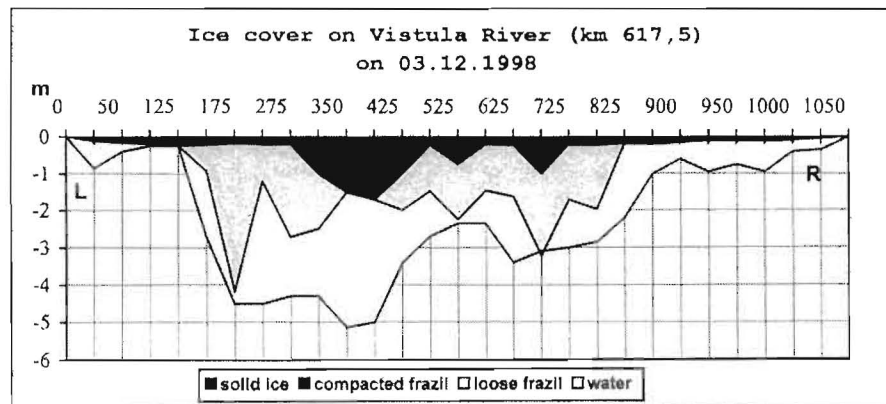
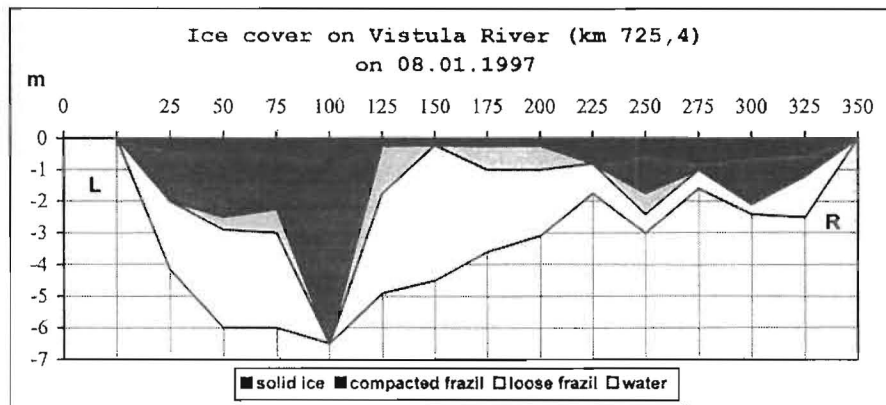
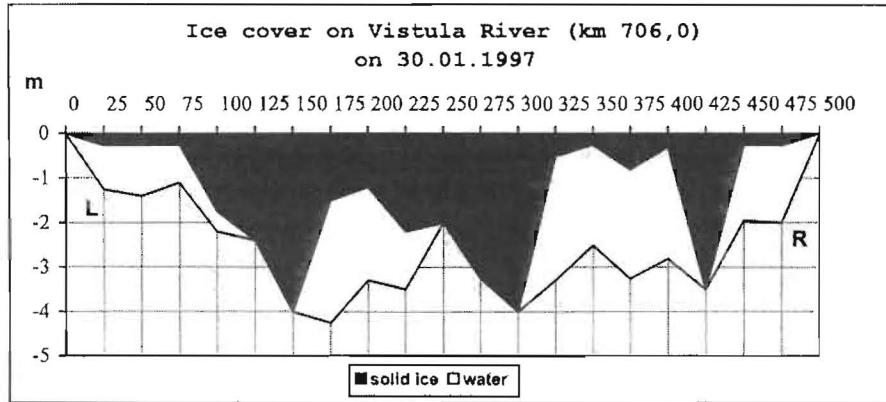


Fig.5. Examples of ice cover on Vistula River

### **ICE COVER FORMATION ON VISTULA RIVER**

The dominant form of ice formation on the Vistula is a run of frazil ice and frazil pans. This period usually takes about 50-60 % of ice phenomena in general. During mild winters the phase of freeze-up is the only phase of the full cycle of ice phenomena. A characteristic feature of the winter season on the Vistula is the occurrence of two or even more cycles of ice phenomena. In some situations this overlapping of ice phases leads to dangerous phenomena in ice cover formation. The mixture of frazil slush deposits and ice floes very often leads to dangerous ice jams (Majewski & Grześ, 1986). Some cross-sections of Vistula with ice cover are shown in Fig.5. One of the very important and efficient forms of mitigating the influence of ice phenomena on flow characteristics in the Lower Vistula is ice breaking. It depends on the accuracy of meteorological and hydrological forecasts as well as progress of ice breaking. This can be from few hundred meters to 20 km per day. It depends on water depth and the thickness and composition of ice cover.

### **CONCLUSIONS**

Ice phenomena have been always a very important feature of the Lower Vistula. Most floods which occurred here resulted from severe ice jams. During last 30 years since Włocławek Reservoir was put into operation about 30 severe ice jams of various type and location occurred. One of them caused severe flood in 1982. A lot of experience in operating hydraulic project Włocławek during winter conditions was gained. One of the most efficient means was and still is ice-breaking.

### **REFERENCES**

- GRZEŚ M. (1991): Ice jams and ice-jam floods on the Lower Vistula, Mechanism and processes. Institute of Geography and Spatial Management, Polish Academy of Sciences, Warsaw (in Polish).
- MAJEWSKI W., GRZEŚ M. (1986): Formation of ice cover on impounding reservoir and its influence on roughness coefficients and flow conditions. Proceedings of the IAHR Symposium on Ice, Iowa City, Vol. 1.
- MAJEWSKI W. (1996): Ice problems during 25 years of the operation of hydraulic project Włocławek on Vistula River. Proceedings of the 13th IAHR International Symposium on Ice, Beijing vol. 1.



## SCALING AND MEASUREMENT OF ICE RUBBLE PROPERTIES IN LABORATORY TESTS

A. Jensen<sup>1,3</sup>, K.V. Høyland<sup>1</sup>, K.-U. Evers<sup>2</sup>

### ABSTRACT

Physical and mechanical properties of level ice and ice ridges have been scaled and determined in laboratory tests. Tempering the ice surface scales the strength of the level ice, the unconsolidated ice rubble is as in nature already at the freezing point and this makes a temperature scaling impossible. Small-scale mechanical tests showed that the ice blocks from the ridge were stronger than the level ice. Salinity and ice temperature profiles were measured. Ice rubble properties in three trapezoidally shaped ridges were investigated. The consolidated layer was cut along the perimeter of a circular plate ( $d=0.7$  m), and the plate was loaded vertically in order to penetrate through the ice ridge. The force and displacement of the plate were recorded simultaneously. Results from the tests are reported together with material properties derived from a simplified analytical model.

### INTRODUCTION

Sea ice ridges are formed by compression or shear in the ice cover. They consist of an overwater part (the sail) which is a mixture of ice blocks, air and snow, and an underwater part (the keel) in which there are ice blocks and water. The keel is divided into a consolidated - and an unconsolidated part. First-year sea ice ridges are major obstacles to transport and operations in waters where first-year ice prevails, such as the Pechora Sea, the Barents Sea and the Baltic Sea. The load these ridges may exert on a ship or a structure is not well known and the present load algorithms seem to overestimate the real loads (Timco et al., 1999). Laboratory work is a vital part of the strive to gain insight into the ridge-structure interaction process and, thereby improve the load estimates. One of the major problems with laboratory testing is scaling. Scaling is done according to which effects that dominate the problem, gravity, inertia, velocity etc. Gravity forces dominate our problem thus Froude scaling is used. The basic idea here is that the gravity field is not scaled and that the basic scaling unit is the length  $\lambda$ . Some work has been done on ridge-structure interaction in the laboratory (Keinonen

---

<sup>1</sup> The Norwegian University of Science and Technology (NTNU), Norway

<sup>2</sup> Hamburgische Schiffbau-Versuchsanstalt (HSVA), Germany

<sup>3</sup> Barlindhaug Consult as, Norway

and Nyman, 1989; Eranti et al., 1992; Løset et al., 1998; Kamesaki and Yamauchi, 1999). However, no standardised method for ridge production in ice facilities seems to exist. The ridges are usually made by cutting the ice manually and making a pile. More advanced and realistic ridge formation has been done in the laboratory by Tuhkuri et al. (1998), but they have not made any mechanical testing of their ridges. Laboratory tests of ice rubble have been done by several authors with different equipment, see Ettema and Urroz-Aguirre (1991) and Timco and Cornet (1999) for an overview of results and methods. The rubble is often considered to be almost cohesionless, and small values of the cohesion  $c$  is often found, but a wide scatter of values for the angle of internal friction  $\phi$  have been reported. A plug, or a push down test where the consolidated layer is pre-cut and the rubble is loaded vertically was originally done in-situ by Leppäranta and Hakala (1992), and has been done in the laboratory by Azarnejad and Brown (1998). One problem is the derivation of material properties from the recorded force and displacement, as the stresses on the failure plane are not known.

## **EXPERIMENTS, RESULTS AND ANALYSIS**

### **Procedure for production and consolidation of the ridges**

The experiments carried out in the Large Ice Tank of the Hamburg Ship Model Basin (HSVA), were designed to simulate the most severe ice conditions in the Pechora Sea. Løset et al. (1997) gives an overview of the ice conditions in the area. The design level ice thickness was 1.2 m and the design keel depth was 18 m in the testing. The maximum block thickness in such a ridge is about 1.1 m (Tucker and Govoni, 1981; Sayed and Frederking, 1988). The block size distribution in ridge sails has been examined by eg Veitch et al. (1991) and Kaankanpää (1997). They report that the length and the width of the blocks were between 1.5 and 5 times the thickness. However, it is possible that larger blocks exist in the lower part of the keel (Mauri Määttä, personal communication).

The model ice sheets were produced according to the procedure described by Evers and Jochmann (1993). The characteristic parameter of the level ice was the flexural strength, because the predominant ice failure mode in ice-ship interaction is bending. The proper flexural strength was obtained by heating the ice so that the target strength and thickness was reached. The scaling factor  $\lambda$  was equal to 25. The other parameters were scaled according to Froude scaling (see eg. Løset et al., 1998).

The ridge production procedure is explained in Jensen et al (2000). Three different level ice sheets were produced with embedded ridges (3000, 4000 and 5000), and three different ridges were tested: 4000, 5001 and 5002. Fig.1. shows a longitudinal cross-section of ridge 5002.

After the ridge formation the freezing continued until the target level ice thickness was reached (48 mm). The level ice growth during the consolidation period was about 10 mm. The ridge was examined after each test by cutting it into pieces and inspecting it visually. The thickness of the consolidated layer was between 10 and 15 cm. The results are comparable to what Timco and Goodrich (1988) found in their laboratory work.

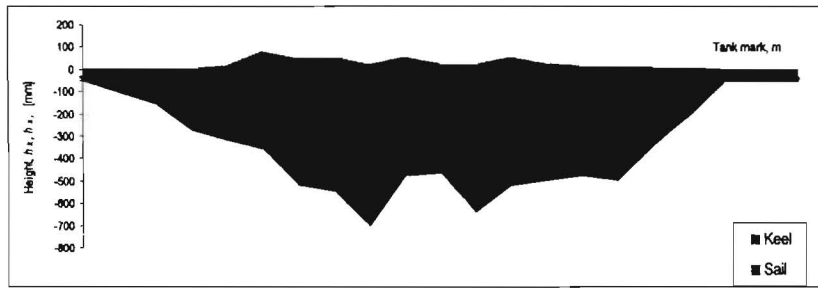


Fig.1. Longitudinal profile of ridge 5002

**Testing of physical properties; salinity, density and temperature**

Measurements were done on salinity, density and temperature development in the level ice and in the ridge. The temperature development in the ridges is shown in Fig.2. During the consolidation phase the cold front ( $T < T_f$ ) advanced less than 5 cm below the water line, ie the internal redistribution of heat was essential to explain the observed consolidation thickness of 10-15 cm. The temperature at the ice/water interface was constantly at the freezing point ( $T_f = -0.5^\circ\text{C}$ ). Warming-up of the ice is necessary to obtain the correct scaled flexural strength. The temperature profile shows that the consolidated layer and the keel was colder than the surface of the level ice, ie at the freezing point or below.

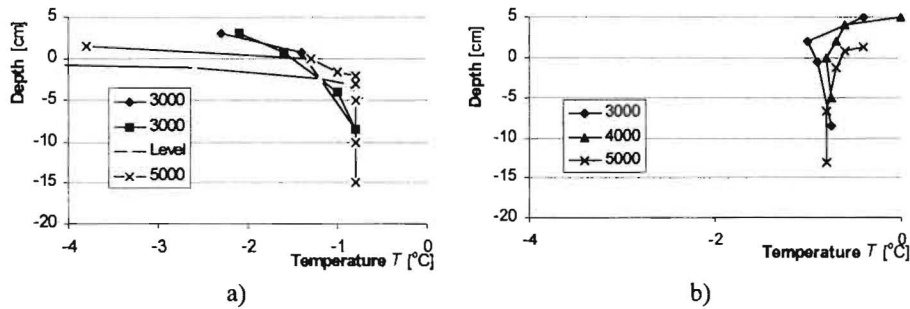


Fig.2. Temperature profiles a) during consolidation process and b) prior to testing

Table 1

Salinity and density

	Density (kg/m <sup>3</sup> )	Salinity (ppt)		
		Sail	Keel	Level ice
Average value	867	3.18	3.35	3.46
Standard deviation	49	0.84	0.64	0.36
Number of samples	10	14	5	18

Table 1 displays the salinity and density measurements. 38 samples of the level ice and the ridges were taken for salinity measurements. Little difference was found between the level ice (3.46 ppt) and the keel (3.35 ppt), but the salinity in the sail (3.18 ppt) was a bit lower. It was a clear trend of decreasing salinity with time; it decreased about 0.8 ppt per day. The salinity of the water in the basin was 8.5 ppt. Ten measurements of density were done (8 by the mass divided by volume method, 1 with mass and buoyancy and 1 with volume and buoyancy).

#### Testing of mechanical properties of the level ice and individual ridge blocks

Two tests were carried out to examine the mechanical properties: beam bending and a hardness test. In the hardness test two different steel balls were used. They were dropped from a certain height  $h_{ba}$  (20 or 25 cm) and the indentation diameter,  $d_{sn}$ , and the penetration depth,  $h_{sn}$ , were measured by a slide gauge. The mass of the steel balls,  $m_{ba}$ , were 90 and 150 g, and the diameter,  $d_{ba}$ , 28.3 and 33 mm respectively. This kind of testing is described by Moldestad (1999). The energy balance in Eq. 1 defines an average material resistance  $\bar{F}_{sn}$ :

$$m_{ba} \cdot g(h_{ba} + h_{sn}) = \int_0^{h_{sn}} F_{sn} dh = \bar{F}_{sn} \cdot h_{sn} \quad (1)$$

where  $h_{sn}$  is the penetration depth.

The hardness,  $H$ , is defined as the material resistance divided by the contact area between the ice and the steel ball ( $S_{bs}$ ):

$$H = \frac{\bar{F}_{sn}}{S_{bs}} \quad (2)$$

The test results showed a significant scatter, however a general trend was seen and average values are summarised in Table 2

The strength decreased with increasing temperature.

**Table 2**  
Mechanical properties from sheet 5000 (number of drop tests in brackets)

Testing time (h)	15:00	16:00	20:00	22:00
Approx. bending strength, $\sigma_b$ (kPa)	55-60	45-55	20-30	15-20
Hardness of level ice, $H$ (kPa)	65 (18)	58 (3)	13 (2)	22 (2)
Hardness of cons. layer, $H$ (kPa)			94 (6)	252 (8)
Hardness of sail, $H$ (kPa)			69 (2)	
Hardness of refrozen pocket, $H$ (T-ice) (kPa)			76 (2)	

#### Ridge penetration test

The sail was removed and the consolidated layer was cut. Fig.4. shows the set-up. The circular ballasted plate was hanging in a crane and lowered carefully down so that it smoothly touched the ice. Zero of the load cell was taken and the plate was lowered further down until it was obvious that the ridge had failed. After failure, the plate was lifted up, re-lowered and finally

lifted up again. The velocity of the crane was constant and force and displacement versus time were recorded. Fig.3. shows a typical force and displacement curve versus time for the testing and Table 4 shows the key values calculated from the tests. The angle  $\alpha$  is found by adjusting the calculated buoyancy force to the measured one.

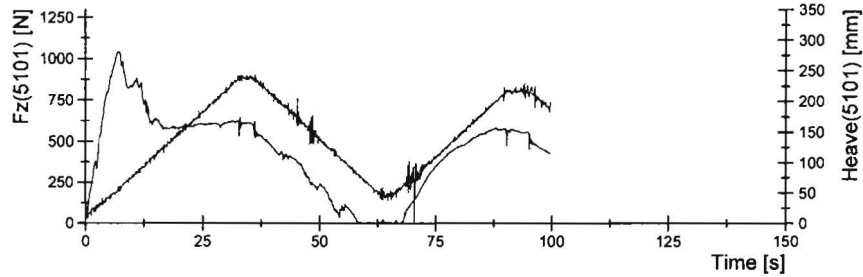


Fig.3. Force and displacement curve during testing

Table 3

Key values from the measurements

Test	$F_{max}$	$F_b(\text{max load})$	$F_b(\text{max displ.})$	$h_k$	$h_{eff}$	radius	$\alpha$
4000	1274 N	324 N	677 N	0.550 m	0.450 m	0.35 m	33.5°
5001	1043 N	259 N	612 N	0.559 m	0.499 m	0.35 m	22°
5002	818 N	276 N	629 N	0.559 m	0.499 m	0.35 m	25°
5003	758 N	97 N	124 N	0.559 m	0.499 m	0.10 m	31°

A simple analytical analysis of the plug test is done as follows. A failure plane with stresses  $\tau_\alpha$  and  $\sigma_\alpha$  as shown in Fig.4a, is assumed. The vertical distribution of stresses is assumed to be linear as shown in Fig.4b., where  $\tau_\alpha = 2 \cdot \bar{\tau}$  and  $\sigma_\alpha = 2 \cdot \bar{\sigma}$ .

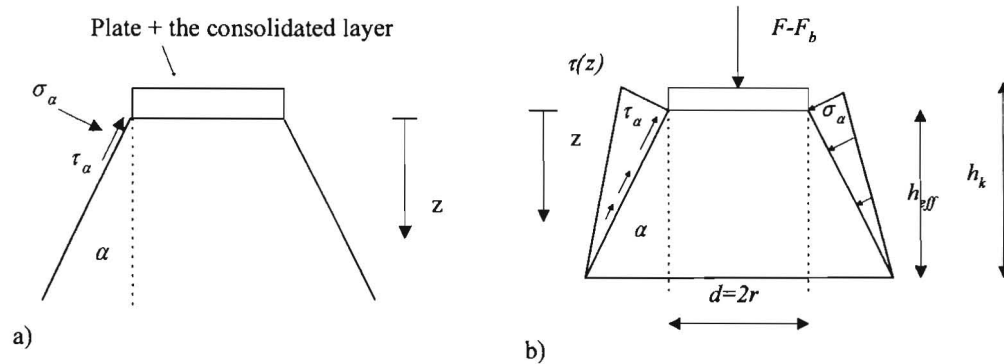


Fig.4. Simple analytic model for shear punch analyses

Vertical equilibrium of the cone in Fig.4b. and the Colomb-Mohr yield criterion give the following two equations:

$$\bar{\tau} = \frac{F - F_b}{\cos \alpha \cdot S} + \bar{\sigma} \cdot \tan \alpha \quad (3)$$

$$\tau_\alpha = c + \sigma_\alpha \cdot \tan \varphi \quad (4)$$

where  $F$  is the applied force,  $F_b$  the buoyancy force and  $S$  the surface on which the stresses act.  $c$  is the cohesion and  $\varphi$  the angle of internal friction.

This gives us two equations and four unknowns. When the normal stress on the failure plane is between the limits given in (5), the extreme values for the material parameters presented in Table 5 can be calculated.

$$\frac{F}{3 \cdot \pi \cdot r^2} < \sigma_\alpha < \frac{F}{\pi \cdot r^2} \quad (5)$$

where  $r$  is the radius of the plate.

**Table 4**

Extreme values for  $c$  and  $\varphi$  if  $\sigma_\alpha$  is between the limits given in Eq.5

Test			
	4000	5001	5002
$c_{max}$ (Pa)	3338 – 1915	2423 – 1622	1895 – 1174
$\varphi_{max}$ (-)	45 – 61	42 – 61	44 – 61

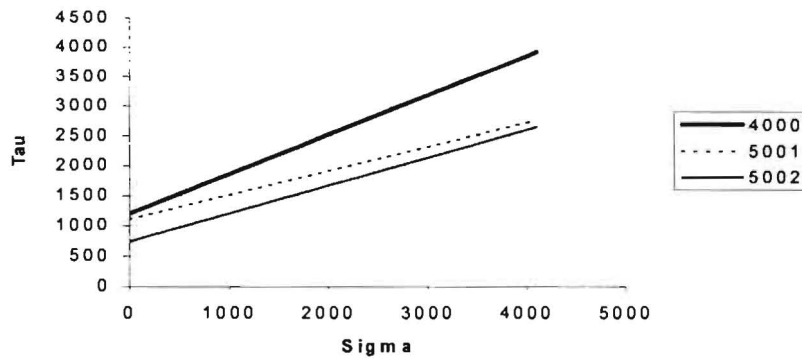


**Fig.5.** The equilibrium equation for the three plug tests

In Fig.5. the equilibrium equations for the three tests are shown. If we assume that the same material properties yield for the two ridges and that the normal stress on the failure plane is the bigger in test 4000 and the smaller in the 5002 test, then the following range of the material parameters  $c$  and  $\varphi$  can be estimated:  $c < 500$  Pa and  $25^\circ < \varphi < 40^\circ$ .

## DISCUSSION AND CONCLUSIONS

The ratio of the thickness of the consolidated layer to the thickness of the model level ice was 2-3, this is higher than what has been found in the real world (see eg. Frederking and Wright, 1982; Kaankanpää, 1997; Leppäranta and Hakala, 1992). 3-4 layers of refrozen rafted ice were also observed in the unconsolidated part of the keel, this may be more than what exists in a real ridge.

The hardness,  $H$ , found from the drop test is not a well-defined material parameter in relation to the flexural strength, thus it can only be used as an index value. Measurements of the flexural strength and the hardness show that the ice in the ridge was too strong compared to the level ice. It is well known that the ice strength decreases with increasing temperature, and the temperature difference between the level ice and the ridge keel explains the difference in strength. In nature the temperatures in the unconsolidated rubble are at the freezing point, whereas the average temperature of the level ice is normally below  $T_f$ .

The analytical solution does not give exact material properties as the stresses on the failure plane are unknown, but we suggest  $c < 500$  Pa and  $25^\circ < \varphi < 40^\circ$ . The cohesion has the dimension Pa and should thus be scaled with a factor 25, this gives a full-scale cohesion of  $c < 12$  kPa. The material properties of unconsolidated ice rubble are not yet well established, but our suggested values are comparable to what others have found (Ettema and Urroz-Aguirre, 1991).

## ACKNOWLEDGEMENT

The authors would like to thank the Hamburg Ship Model Basin (HSVA), especially the ice tank crew, for the hospitality, technical support and professional execution of the test programme in the ARCTECLAB. The research activities carried out at the Large Scale Facility ARCTECLAB were granted by the TMR Programme from the European Commission through contract N°ERBFMGECT950081. We would also like to thank the initiator of the project professor Sveinung Løset for practical support and interesting discussions, Denis Tazov for helping us during testing and for being a magician with computer graphics and apples. Navion and Statoil provided additional financial support without which the tests would not have become what they did.

## REFERENCES

- AZARNEJAD A., BROWN T.G. (1998): Observations of ice rubble behaviour in punch tests. Proceedings of the 14th International Symposium on Ice (IAHR), Potsdam, New York, USA, July 27-31 1998, Vol. 1, pp. 589-596.
- ERANTI E., LEHMUS E, NORTALA-HOIKKANEN A. (1992): First-year ice ridge characteristics and loads on offshore structures. San Francisco, USA, 14-19 June, 1992, pp. 681-687.
- ETTEMA R., URROZ-AGUIRRE G.E. (1991): Friction and cohesion in ice rubble revisited. Proc. Cold Regions Engineering, West Lebanon, New Hampshire, USA, pp. 316-325.

- EVERS K.-U., JOCHMANN P. (1993): An Advanced Technique to Improve the Mechanical Properties of Model Ice Developed at the HSVA Ice Tank. Proceedings of the 12th International Conference on Port and Ocean Engineering under Arctic Conditions (POAC), 17- 20 Aug. 1993, Hamburg , Vol. 2, pp. 877-888.
- KANKAANPÄÄ P. (1997): Distribution, morphology and structure of sea ice pressure ridges in the Baltic Sea. *Fennia* 175:2, pp 139-240. Helsinki. ISSN 0015-0010.
- KAMESAKI K., YAMAUCHI Y. (1999): Experimental study for first-year ridge load. Proceedings of the 9th International Offshore and Polar Engineering Conference (ISOPE), Brest, France, 30 May-4 June 1999, Vol. 2, pp. 518-522.
- KEINONEN A., NYMAN T. (1978): An experimental model scale study on the compressible, frictional and cohesive behaviour of broken ice mass. Proceedings of the 10th International Conference on Ice (IAHR), Luleå, Sweden, 12-16 June 1989, Vol. 2, pp. 335-353.
- LEPPÄRANTA M., HAKALA R. (1992): The structure and strength of first-year ridges in the Baltic Sea. *Cold Regions Science and Technology*, 20 (1992), pp. 295-311.
- LØSET S., KANESTRØM Ø., PYTTE T. (1998): Model tests of a submerged turret loading concept in level ice, broken ice and pressure ridges. *Cold Regions Science and Technology* 27 (1998), pp. 57-73.
- MOLDESTAD D. A. (1999): Some aspects of ski base sliding friction and ski base structure. Dr Thesis Dep. of Structural Engineering-NTNU Trondheim, Norway, 197 pages.
- SAYED M., FREDERKING R.M.W. (1988): Measurements of ridge sails in the Beaufort Sea. *Canadian journal of Civil Engineering* 16, pp. 16-21.
- TIMCO G.W., CORNET A.M. (1999): Is  $\phi$  a constant for broken ice rubble?. Proc. 10th workshop on river ice management with a changing climate, J.C.Doering Ed., Winnipeg, Mantioba, Canada, 8-11 June 1999, pp. 318-331.
- TIMCO G.W., WRIGHT B., JOHNSTON M., FREDERKING R. (1999): First-year ice ridge loads on Molikpaq. Proceedings from the 4th International Conference on Development of Russian Arctic Offshore (RAO), St. Petersburg, Russia, 6 -9 July 1999, Vol. 2, pp. 172-179.
- TIMCO G.W., GOODRICH L.E. (1988): Ice rubble consolidation. Proceedings of the 9th International Symposium on Ice (IAHR), Sapporo, Japan, pp. 426-438.
- TUCKER III W.B., GOVONI J.W. (1981): Morphological investigations of first-year sea ice pressure ridge sails. *Cold Regions Science and Technology*, 5, pp. 1-12.
- TUHKURI J., LENSU M., HOPKINS M.A. (1998): Laboratory and field studies on ridging of an ice sheet. Proceedings of the 14th International Symposium on Ice (IAHR), Potsdam, New York, USA, July 27-31 1998, Vol. 1, pp. 397-404.
- VEITCH B., LENSU M., RISKA K., KOSLOFF P., KEILEY P., KUJALA P. (1991): Field observations of ridges in the northern Baltic Sea. Proceedings of the 11th International Conference on Port and Ocean Engineering under Arctic Conditions, St. John's, Canada, pp. 381-400.



**FINITE-ELEMENT SIMULATION OF S2-COLUMNAR ICE  
VISCOPLASTIC BEHAVIOUR: SENSIBILITY ANALYSIS**

**J. Meyssonier<sup>1</sup>**

**ABSTRACT**

Finite-element simulations of compressive creep of a polycrystal of S2-columnar ice loaded in the plane perpendicular to the long direction of the columns are presented. The computations are done by modelling each grain as a transversely isotropic incompressible continuous viscoplastic medium whose symmetry axis is the c-axis of the crystal. The results show that, due to the very strong anisotropy of ice, the number of grains required to homogenize the viscoplastic properties is large, at least 500 for linear behaviour and 1000 for non-linear behaviour, and that the influence on the homogenized properties of the nature of the boundary conditions applied to the polycrystal cannot be neglected.

**INTRODUCTION**

Many models are currently developed to account for the strain induced evolving anisotropy of polar ice, in order to improve polar ice-sheet flow models. Most are based on micro-macro homogenization schemes which aim at deriving the mechanical properties of a polycrystal from the known behaviour of its grains. Considering the exceptionally strong anisotropy of ice in the viscoplastic regime, assessing these models is mandatory. This can be done by comparison with finite-element simulations. Such numerical studies of ice were done by McKenna (1992) on the transitory creep of S2-ice, and by Elvin (1996) on its elastic properties. The present paper is a limited study of the influence on the results of finite-element simulations of compressive creep of S2-columnar ice, of the number of grains used to describe the polycrystal, of the distribution of the grains crystallographic orientations, of the nature of the applied boundary conditions, and of the parameter which controls the anisotropic behaviour of the ice single crystal.

---

<sup>1</sup>Laboratoire de Glaciologie et Géophysique de l'Environnement, CNRS et Université Joseph Fourier, (UJF-Grenoble I), France. BP 96, F-38402 Saint-Martin d'Hères Cedex, France, Tel.: 33 4 76 82 42 70, fax: 33 4 76 82 42 01, e-mail: jacques@glaciog.ujf-grenoble.fr

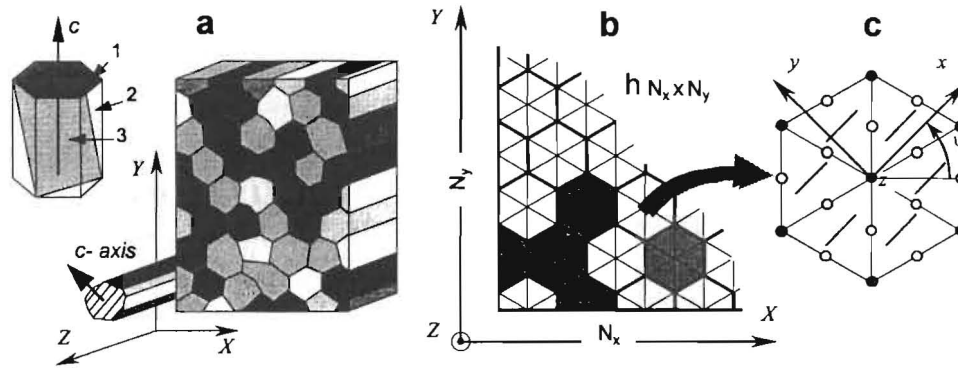


**Fig.1.** a) hexagonal structure of ice (1: basal, 2: prismatic, 3: pyramidal planes) and structure of S2-ice: the long axes of the grains are parallel to the same direction Z and the grains c-axes are distributed at random in the (X,Y) plane;  
 b) structure of the finite-element meshes used in the study;  
 c) each basic hexagonal grain is made of six-nodes triangular elements: the basal planes of the 6 triangles (parallel to the x axis) are at angle  $\psi$  from the X-axis.

#### GRAIN AND S2-ICE BEHAVIOUR

Each grain is modelled as a transversely isotropic incompressible continuous medium whose symmetry axis is the c-axis. For linear behaviour this is equivalent to the approach involving the basal prismatic and pyramidal slip systems (Meyssonnier and Philip, 1999a). In the non-linear case this simplification is justified by Kamb (1961). Since the c-axes of the grains are randomly distributed in the plane perpendicular to their long direction, S2-ice can also be considered as a macroscopically transversely isotropic incompressible medium (Fig.1a.).

For such a linear medium, the constitutive relation, expressed in the material-symmetry-reference frame with rotational symmetry axis along  $x_3$ , links the deviatoric stress tensor  $\mathbf{s}$  and the strain-rate tensor  $\mathbf{d}$  by

$$s_{11} - s_{22} = 2\eta (d_{11} - d_{22}), \quad s_{33} = 2\eta \frac{4\alpha - 1}{3} d_{33}, \quad s_{12} = 2\eta d_{12}, \quad s_{23} = 2\eta\beta d_{23}, \quad s_{31} = 2\eta\beta d_{31} \quad (1)$$

where  $\eta$  is the viscosity for shear in the plane of isotropy ( $x_1, x_2$ ),  $\alpha$  is the ratio of the viscosity in uniaxial compression along  $x_3$  to that in the plane ( $x_1, x_2$ ), and  $\beta$  is the ratio of the viscosity for shear parallel to the plane ( $x_1, x_2$ ) to  $\eta$ . Relation 1 models the grain behaviour, with  $x_3$  along the c-axis, as well as S2-ice behaviour, with  $x_3$  along the long direction of the columns. Following Meyssonnier and Philip (1999b) the simplest generalisation of Eq. 1 is adopted for the non-linear behaviour. It results in replacing  $\eta$  in Eq. 1 by the apparent viscosity  $\eta^*$  given by

$$\eta^* = A^{-1/n} \dot{\gamma}_0^{(1-n)/n} = A^{-1/n} \dot{\epsilon}_0^{1-n} \quad (2)$$

where A is a fluidity parameter ( $A=1/\eta$  in the linear case  $n=1$ ) and the invariants given by

$$\gamma_0^2 = (4\alpha-1)d_{33}^2 + (d_{11}-d_{22})^2 + 4d_{12}^2 + 4\beta(d_{23}^2 + d_{31}^2), \quad \tau_0^2 = \frac{9}{4(4\alpha-1)}s_{33}^2 + \frac{1}{4}(s_{11}-s_{22})^2 + s_{12}^2 + \frac{1}{\beta}(s_{23}^2 + s_{31}^2) \quad (3)$$

in the material symmetry axes, are linked by

$$\tau_0 = \eta \dot{\gamma}_0, \quad \dot{\gamma}_0 = A\tau_0^n \quad (4)$$

(note that when the medium is isotropic,  $\alpha=\beta=1$ , relations 1-4 reduce to Glen's flow law).

#### FINITE ELEMENT MODELLING

Since the viscoplastic behaviour of the ice single crystal is extremely anisotropic, the deformation of a grain loaded in a plane containing its c-axis can be considered as two-dimensional. This plane strain assumption was then adopted to model the creep flow of S2-ice loaded in its plane of isotropy (perpendicular to the long direction of the columns). The two-dimensional problem was solved in the S2-polycrystal reference frame  $\{X,Y,Z\}$  shown in Figure 1a, with the Z axis perpendicular to the plane of flow. The finite-element solution was obtained by using a mixed velocity-pressure formulation, with the pressure p acting as a Lagrange multiplier to enforce the incompressibility condition (Meyssonnier, 1989).

The S2-ice polycrystal was modelled by a regular array of hexagonal grains with the same dimensions, and each hexagonal grain was modelled by six triangular elements (see Fig.1b. and c.). In each basic triangle a quadratic interpolation of the velocities and a linear interpolation of p were adopted. The c-axes of the grains were in the (X,Y) plane. The local reference frame  $\{x,y,z\}$  of a grain was such that its y axis coincided with the c-axis, and the z axis was taken along the Z axis of the global reference frame. The trace of the basal plane (i.e. x axis) was at angle  $\psi$  with respect to the X axis of the global reference frame (see Fig.1c.). The orientation of the basal plane of a hexagonal grain was fixed by assigning the same value  $\psi$  to the orientations of its six constituent triangular elements. To ensure a homogeneous distribution of the grains orientations, each grain was assigned an orientation  $(2n-1)\pi/2N_T$ , with n integer in the range  $1 \leq n < N_T$ ,  $N_T$  denoting the total number of hexagonal grains in the finite-element mesh, the value of n being drawn at random (only once).

The grain behaviour was modelled by relations (1)-(3) with indices  $\{1,2,3\}$  corresponding to  $\{z,x,y\}$ , respectively. The finite-element system was obtained by computing the viscosity matrix in the local reference frame of each grain before expressing it in  $\{X,Y,Z\}$ .

#### NUMERICAL SIMULATIONS

The value of parameter  $\beta$  in relation (1), which characterizes the relative resistance to shear parallel to the basal plane, was varied from  $\beta=1$  (isotropy) to  $\beta=0.0001$ , the relevant range for ice being  $0.01 \leq \beta \leq 0.0001$  (Mansuy and others, 1999). Since  $\beta$  represents the essential feature of the grain behaviour, the finite element simulations were performed with a unique

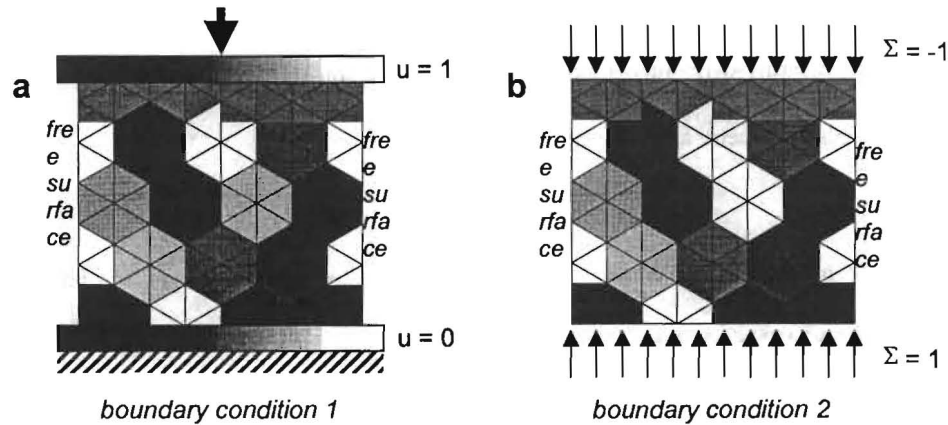


**Fig.2.** The two types of boundary conditions applied to simulate uniaxial compression of ice: a) prescribed velocity (with perfect sliding at the ice /platen interface), b) prescribed stress

value of  $\alpha = 1$ . The non-linear behaviour of S2 ice was accounted for by adopting the value  $n=3$  for exponent  $n$  in relation 2. However the sensibility analysis was also done with  $n=1$ .

The aim of the study being to derive the bulk properties of the polycrystalline aggregate from the knowledge of the grain behaviour, two types of boundary conditions were applied to simulate a uniaxial compression of S2-ice. The first type (Fig.2a.) simulated a conventional test in which the compression is applied through rigid platens with perfect sliding between platens and ice: a constant vertical velocity was prescribed on the upper horizontal side of the finite element mesh. The second type (Fig.2b.) consisted in applying a constant vertical stress vector on each horizontal side (doing so the deformation of the outer grains is not constrained). A condition of free surface on the two vertical sides was assumed for both types.

Different meshes consisting of  $N$  horizontal layers of  $N$  grains were studied. The total number of grains,  $N_T=N^2$ , was varied between 16 and 1024.

The influence of the distribution of the grains c-axes orientations was assessed by performing each simulation (i.e. for given values of  $\beta$ ,  $N$ , and a given boundary condition type) with five different random distributions.

## RESULTS

The macroscopic (bulk) fluidity  $A_M$  of the polycrystal was obtained by comparing the power dissipated when considering the polycrystal as a homogeneous medium,  $P_M$ , to that computed in the finite-element simulations,  $P_{EF}$ . With type-1 boundary condition, and for plane strain, the non zero components of the strain-rate experienced by the homogeneous medium are  $d_{YY}=U/H$  and  $d_{XX}=-d_{YY}$ , where  $U$  is the prescribed velocity and  $H$  is the polycrystal height. Taking into account relations (2),(3) and (4) leads to  $P_M=A_\mu^{-1/n} (2U/H)^{(n+1)/n}$ . On the other

hand, a straightforward dimensional analysis shows that the power dissipated per unit volume is  $P_{EF} = P_{T1} A_{\mu}^{-1/n} U^{(n+1)/n} / HL$ , where  $L$  is the polycrystal width,  $A_{\mu}$  is the microscopic fluidity which characterizes the grain behaviour, and  $P_{T1}$  is the total dissipated power derived from the finite-element computation with dimensionless values of  $A_{\mu}=1$  and  $U=1$ . Expressing that  $P_M = P_{EF}$  provides the following expression of  $A_M$  for type-1 boundary condition

$$A_M / A_{\mu} = 2(2L/P_{T1})^n / H \quad (5)$$

For type-2 boundary condition (and plane strain), the non zero components of the deviatoric stress in the homogeneous medium are  $s_{YY} = \sigma/2$  and  $s_{XX} = -s_{YY}$ , where  $\sigma$  is the applied stress. From relations (2)-(4), the macroscopic power  $P_M = A_M \tau_0^{n+1}$  is obtained as  $P_M = A_M (\sigma/2)^{n+1}$ , and the power dissipated by the finite element model is  $P_{EF} = P_{T1} A_{\mu} \sigma^{n+1} / HL$ , where  $P_{T1}$  is the total power computed with  $A_{\mu}=1$  and  $\sigma=1$ . The macroscopic fluidity corresponding to type-2 boundary condition is then given by

$$A_M / A_{\mu} = 2^{n+1} P_{T1} / HL \quad (6)$$

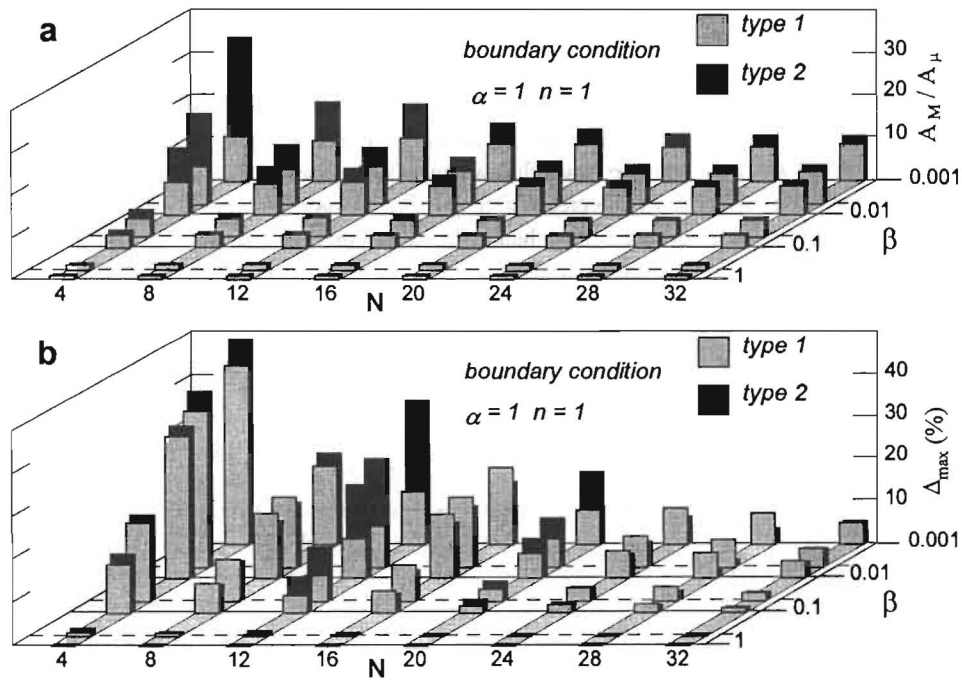


**Fig.3.** a) average of the macroscopic to microscopic fluidity parameters ratios  $A_M/A_{\mu}$ ,  
b) maximum deviation from the average of five computed values of  $A_M/A_{\mu}$ ,  
as functions of the grain anisotropy parameter  $\beta$  and of  $N = N_T^{1/2}$  (linear behaviour).

Fig.3a, 4a. and c. show the variation of  $A_M/A_\mu$  with respect to  $N$  (the number of grains is  $N_T=N^2$ ), the boundary condition type and  $\beta$ . Each point represents the average of 5 values of  $A_M/A_\mu$ , obtained by using relations 5 and 6 and the values of  $P_{TI}$  from 5 finite-element computations for 5 different distributions of the grains orientations. The relative maximum deviation  $\Delta_{max}$  of these 5 values of  $A_M/A_\mu$  from the average is shown in Fig.3b., 4b. and d.

## DISCUSSION

As expected, Fig.3a. and 4c. show that  $A_M/A_\mu$  tends towards 1 when  $\beta$  tends towards 1 (since the computations were done with  $\alpha=1$ ,  $\beta=1$  corresponds to isotropic grains, then to a homogeneous isotropic polycrystal). Also, for all the meshes and  $\beta$  tested, in the linear case  $n=1$  as well as for  $n=3$ , the values of  $A_M/A_\mu$  obtained with type-2 boundary condition are higher than with type-1 boundary condition. The differences increase with decreasing  $\beta$  and decreasing number of grains  $N_T$ . For  $\beta=0.001$  (a reasonable value for ice), this difference is about 20% for  $n=1$ , and up to 200% for  $n=3$ , with the larger number of grains (1024) used. This is the consequence of the less constraining effect of type-2 boundary condition which allows the outer grains to deform freely. On the other hand, the end effect provoked by type-1 boundary condition is all the more pronounced that the number of grains is lower and the degree of anisotropy is higher. For  $n=1$  and  $n=3$ , type-1 boundary condition leads to a  $A_M/A_\mu$  ratios almost independent of  $N_T$  (see Fig.3a. and 4a.). For  $n=1$ , the  $A_M/A_\mu$  ratios obtained with type-2 boundary condition seem to reach a stable level when  $N_T$  increases (Fig.3a.), whereas for  $n=3$  there is no tendency to stabilisation for the largest numbers of grains (Fig.4a.). The maximum deviation  $\Delta_{max}$  of  $A_M/A_\mu$  from its mean value exhibits the same trend that the difference in  $A_M/A_\mu$  ratios obtained with the two types of boundary conditions (Fig.3b., 4b., 4d.). The increase of  $\Delta_{max}$  with decreasing  $\beta$  and  $N_T$  shows the influence of the spatial distribution of the grains orientations, enhanced by an increasing degree of anisotropy. For  $n=1$  and  $\beta=0.001$ ,  $\Delta_{max}$  becomes less than 10% for  $N_T \geq 576$ , and is less than 5% for  $N_T = 1024$ . For  $n=3$  and the same  $\beta$ , the  $\Delta_{max} = 10\%$  level is reached only for  $N_T = 1024$  and type-1 boundary condition (Fig.4b.).

## CONCLUSION

The macroscopic fluidity parameter  $A_M$  characterizing the viscoplastic behaviour of S2-ice has been derived from the total dissipated power computed with finite-element simulations of a uniaxial compression in the plane of isotropy of a two-dimensional polycrystal. The results for linear behaviour show that a good estimate of  $A_M$  can be obtained with a number of hexagonal grains greater than 500. Since the viscoplastic anisotropy of ice is much stronger than its elastic anisotropy, this does not disagree with Elvin's (1996) recommendation of 230 grains for homogenizing the elastic properties of S2-ice. Taking into account the non-linear behaviour of ice leads to consider a larger number of grains, at least in the order of 1000, in order to homogenize the viscoplastic properties (McKenna, 1992, used only 256 grains). In the range of parameter  $\beta$  which characterizes the anisotropy of the grain ( $0.01 \leq \beta \leq 0.0001$ ),  $A_M$  appears to be very dependent on the type of boundary condition applied to the polycrystal. In this respect, some improvement is needed before using the present model as a reference for assessing other homogenisation schemes.

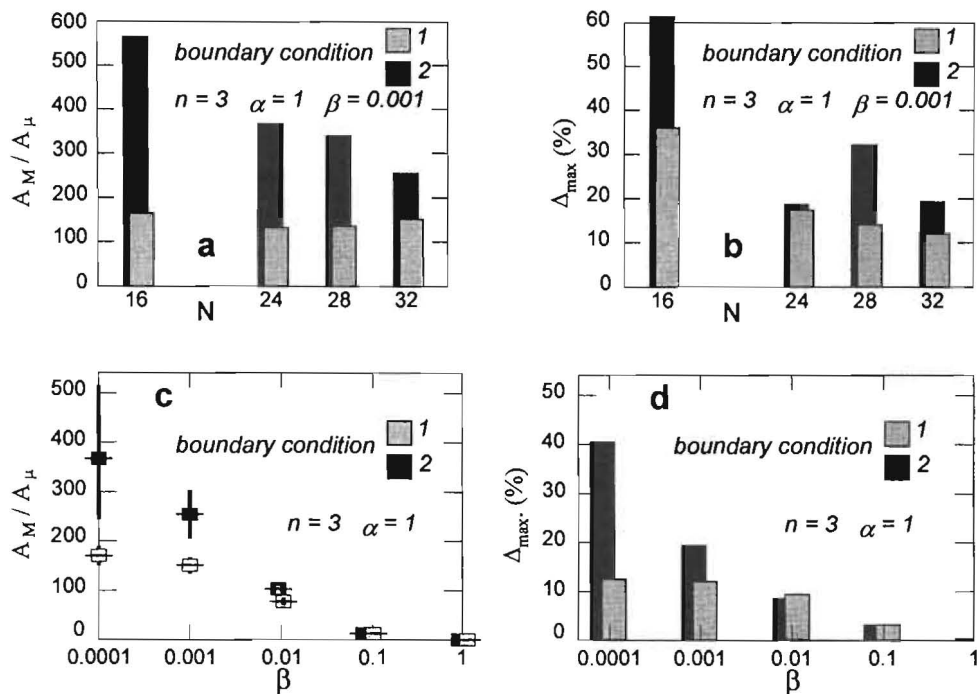


**Fig.4.** a) average of  $A_M/A_\mu$  ratios; b) maximum deviation  $\Delta_{max}$  from average of five computed values of  $A_M/A_\mu$  as function of  $N = N_T^{1/2}$  for  $\beta=0.001$  ( $\alpha=1$ ,  $n=3$ ); c) average of  $A_M/A_\mu$ ; d)  $\Delta_{max}$  as function of  $\beta$  for  $N_T=1024$  grains ( $N=32$ ,  $n=3$ ).

## REFERENCES

- ELVIN A.A. (1996): Number of grains required to homogenize elastic properties of polycrystalline ice. *Mech. Mater.* 22, pp. 51-64.
- KAMB W.B. (1961): The glide direction in ice. *J. Glaciol.*, 3(30), pp. 1097-1106.
- MANSUY P., MEYSSONNIER J., PHILIP A. (1999): Modelling the ice single-crystal viscoplastic behaviour. In Hutter, K., Y.Wang and H. Beer, eds. *Advances in cold-regions thermal engineering and sciences: technological, environmental and climatological impact*. Berlin, etc. Springer-Verlag, (Lecture Notes in Physics 533), pp. 215-224.
- MCKENNA R.F. (1992): Discrete modelling of grain scale deformation mechanisms for ice in compression. *Proc. IAHR Ice Symposium 1992, Banff, Alberta*, pp. 152-163.
- MEYSSONNIER J. (1989): Ice flow over a bump: experiment and numerical simulations. *J. Glaciol.*, 35(119), pp.85-97.

MEYSSONNIER J., PHILIP A. (1999a): Comparison of Finite-Element and homogenization methods for modelling the viscoplastic behaviour of a S2-columnar ice polycrystal. *Ann. Glaciol.*, 30, (In Press).

MEYSSONNIER J., PHILIP A. (1999b): Remarks on self-consistent modelling of polycrystalline ice. In: Hutter, K., Y. Wang and H. Beer, eds.. *Advances in cold-regions thermal engineering and sciences: technological, environmental and climatological impact*. Berlin, etc. Springer-Verlag, (Lecture Notes in Physics 533), pp. 225-236.



## GENERATION MECHANISM ANALYSIS OF RIVER UNDERWATER ICE

Ke Sujuan<sup>1</sup>, Wang Ling<sup>1</sup>, Chen Lanqin<sup>2</sup>

### ABSTRACT

Based on observed data on the Zhaojunfen reach in the upper Yellow River from 1979 to 1982, the time taking place underwater ice, the condition taking place underwater ice and the distribution of underwater ice have been analyzed in this paper. The generation mechanism of ice in water has been analyzed too.

### TIME OF PRODUCING UNDERWATER ICE

After autumn, water surface ice can be created firstly in river channel due to air temperature drops. Then water body colder and underwater ice can be appeared due to turbulent flow. Thus underwater ice appears later than water surface ice while ice drift appears on river. But if temperature drop intensity is strong, underwater ice can appears earlier or the same time with water surface ice. Table 1 shows that the observed date of underwater ice generation. It shows that the time is short from appearing ice flower to underwater if air temperature is low and long if air temperature is high during ice drift appearing early period. For example, in 1954, the time appearing water surface ice was the same as appearing underwater ice because the daily average air temperature was  $-11.2^{\circ}\text{C}$ ; in 1980, the time appearing underwater ice was 5 days later than appearing water surface ice because the daily average air temperature was above  $-5^{\circ}\text{C}$ .

### THE CONDITION OF UNDERWATER ICE GENERATION

Underwater ice generates mainly during ice flow period. This time, heat exchange takes place directly from water body to air, then underwater ice can create due to turbulent flow. Its volume depends on factors such as water flow velocity, air temperature etc.

After river is frozen up, ice cover can prevent the relation between water body and air. At the same time, heat exchange between air and water body becomes solid heat transmit form and water body release heat flux is little than open water surface. So ice cover thickness can

---

<sup>1</sup> Bureau of Hydrology, YRCC, Zhengzhou 450004, China

<sup>2</sup> Bureau of Conservancy, An Hui Province, He Fei, China

increase due to colder water becomes ice at ice cover bottom. But underwater ice can not appear again due to release heat flux from water body to air by colder air temperature and under ice cover heat exchange balance between release and accumulate state by thicker ice cover. This can be testified by observed result. For example, we could not find underwater ice at web as a tool observing underwater ice placed under ice cover.

**Table 1**

Date Appearing Underwater Ice at Zhaojunfen reach

years	1954	1955	1956	1980	1981
Date appearing ice flower	24 <sup>th</sup> ,Nov.	17 <sup>th</sup> , Nov.	11 <sup>th</sup> , Nov.	27 <sup>th</sup> , Nov.	7 <sup>th</sup> ,Nov.
Date of appearing underwater ice	24 <sup>th</sup> ,Nov.	18 <sup>th</sup> ,Nov.	12 <sup>th</sup> ,Nov.	2 <sup>nd</sup> ,Dec.	9 <sup>th</sup> ,Nov.
Air temperature during the period of appearing ice flower to appearing underwater ice (°C)	-12.2	-8.0,-7.5	-9.9,-10.2	-3.3,-3.3, -2.2,-4.9, -4.7,-9.9	-8.7, -2.6, -2.1

#### THE UNDERWATER ICE EVALUATION INSIDE ONE DAY

The generation quantity of underwater ice will vary continuously according to air temperature variety inside one day. From 12 to 15, Jan. in 1981, We place 8 webs along river cross section at 17 o'clock each day. It was 3 m between each web. These webs were used to observe underwater ice weight. We observed one time per 3 hours. The observed results were shown in Table 2.

**Table 2**

The underwater ice observed results

Date	Items	17	20	23	2	5	8	1	14	Y
12 <sup>th</sup>	Ta	-2.0	-5.4	-7.8	-12.4	-15.4	-12.5	-2.5	1.8	-15.4
	Wu		1400	6400	7400	7400	4800	1150	0	7400
13 <sup>th</sup>	Ta	-0.6	-2.2	-4.0	-6.0	-7.0	-6.2	-6.0	-3.0	-7.0
	Wu		350	4700	3700	3000	7900	5400	0	7900
14 <sup>th</sup>	Ta	-0.2	-10.0	-13.0	-15.0	-16.5	-12.2	-9.0	-4.0	-16.5
	Wu		8200	16400	6400	3750	5400	550	0	16400
15 <sup>th</sup>	Ta	4.8	-4.0	-14.0	-15.0	-17.0	-14.6	-9.4	-8.0	-17.0
	Wu		1500	6400	7900	4800	12900	1150	0	12900

Note: Ta indicates air temperature(°C), Wu indicates underwater ice weight(g), Y indicates the maximum value or the minimum value.

From Table 2, we knew that underwater ice appeared mainly from 20 o'clock to 8 o'clock. The time appearing the maximum value was 0~3 hours later than the time appearing the minimum air temperature. This was due to heat exchange between air and water body took

place inside this time. And the magnitude of wind velocity could affect underwater ice too. For example, the maximum value of underwater ice weight occurred between 20 o'clock and 23 o'clock on 17<sup>th</sup> Jan. because strong temperature dropped by great wind. And the underwater ice generation volume was very little between 8 o'clock and 17 o'clock because air temperature was high relatively during this time.

### THE LONGITUDINAL AND VERTICAL DISTRIBUTION OF UNDERWATER ICE

The longitudinal distribution of underwater ice intensity is mainly affected by water depth, flow velocity and riverbed etc. For example, underwater ice intensity distribution result on 16<sup>th</sup>~18<sup>th</sup> Jan. 1981 was showed in Table 3. From Table 3, we knew that different underwater ice was occurred on different webs. It showed that the longitudinal distribution of underwater ice being different in despite of water depth was 3.5~4.5 m and flow velocity was 0.57~0.72 m/s. It explained that the longitudinal distribution of underwater ice being affected mainly by water depth and flow velocity.

**Table 3**

Longitudinal Distribution of Underwater Ice on Different Webs

Date		16		17		18	
		<i>Wu</i>	Ratio(%)	<i>Wu</i>	Ratio(%)	<i>Wu</i>	Ratio(%)
Max	Value	29.4	54	39.9	70	23.1	66
	Place	2 <sup>#</sup>		8 <sup>#</sup>		5 <sup>#</sup>	
Min	Value	16.0		27.8		15.2	
	Place	1 <sup>#</sup>		5 <sup>#</sup>		2 <sup>#</sup>	

Note: *Wu* indicates underwater ice weight(g).

Beside, the vertical distribution of underwater ice condensed volume is affected by factors such as water depth, flow velocity and riverbed etc. For example, the observed data of underwater ice on Zhaojunfen reach at Feb. 1981 showed the maximum volume took place on river bed 13 times in 16 times on the same vertical point. At Jan. 1982, it took place 312 times on site down near water surface, then the maximum value were dropped to riverbed according to reducing water depth. Thus underwater ice condensed volume would be small if water depth was deep and would be big if water depth was shallow and water velocity was slow. From observed data, we knew that underwater ice could be appeared if water depth was bigger than 6 m.

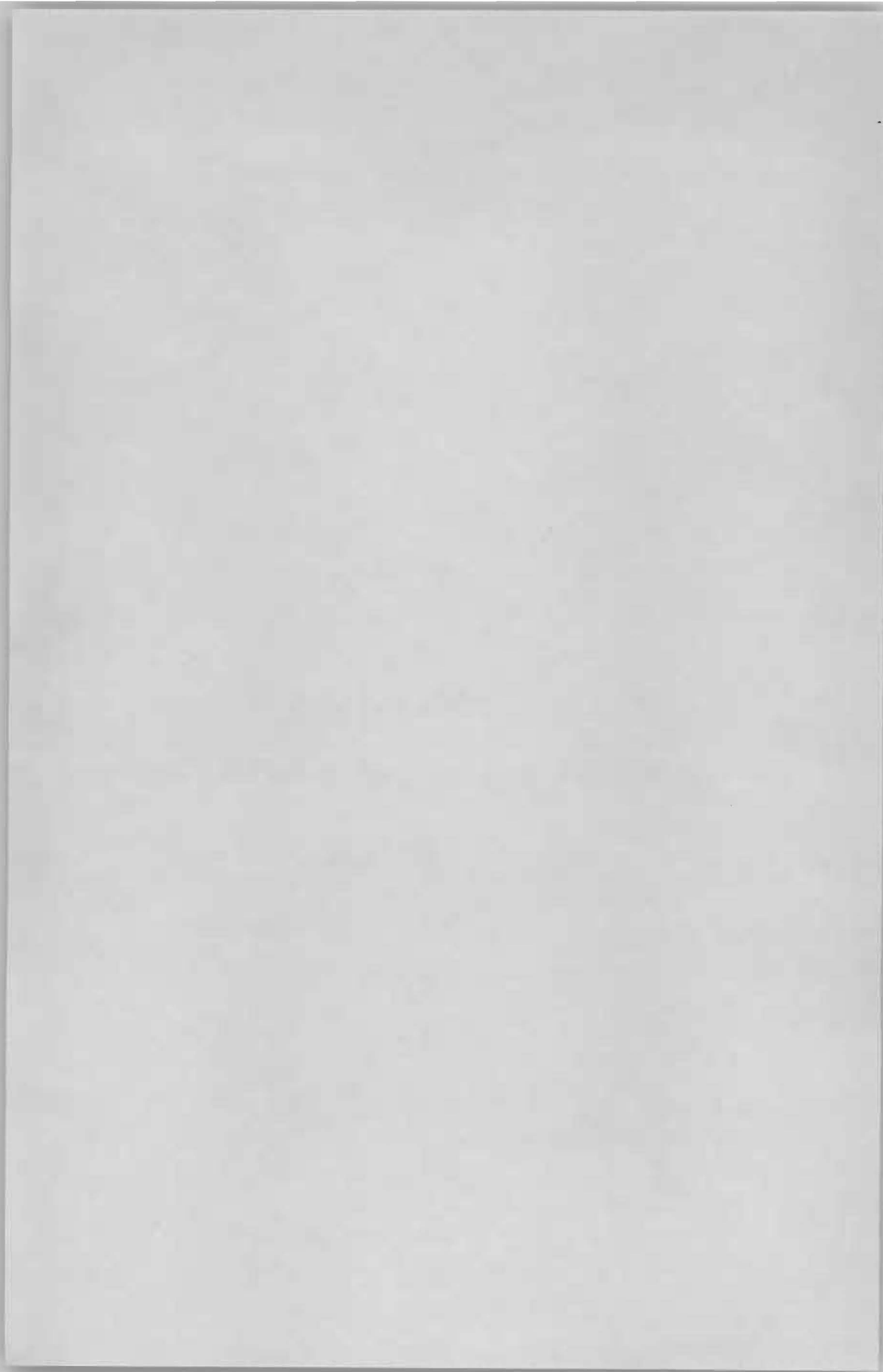
From above analysis, we know that the generation mechanism is very complex and there are many affected factors. In general, the magnitude of underwater ice condensed volume depends on water depth and flow velocity.

## **CONCLUSION**

At present, the generation mechanism of river underwater ice has not been recognized clearly by scientists. The primary generation mechanism of underwater ice based observed data in 3 years is analyzed in this paper. It shows that the main factors affecting underwater ice are water depth and flow velocity. We believe that the great achievement about underwater ice generation research will be gained if we can develop some experiments about underwater ice under the possible conditions.

**TOPIC B**

**ICE MECHANICS  
AND HYDRAULIC STRUCTURES  
IN ICE**





## EFFECT OF ICE-BREAKING CONES FOR MITIGATING ICE-INDUCED VIBRATIONS

Q.J. Yue<sup>1</sup>, X.J. Bi<sup>1</sup>, X. Yu<sup>1</sup>

### ABSTRACT

The effect of mitigating ice-induced vibrations by adding ice-breaking cone is approximately evaluated based on full-scale tests. The tests were conducted on vertical and conical structures at the same time. The displacement responses of the structures are recorded simultaneously and continuously. The failure processes of ice sheet acting on the two kinds of structure were also monitored by video camera. The dynamic behaviours of ice induced vibrations of vertical structure and conical structure are discussed. The test results reveal that more comprehensive work should be done in the subject of using ice-breaking cone to mitigate ice-induced vibrations on platform.

### INTRODUCTION

As we know, offshore structures in ice-covered area need to resist static and dynamic ice forces and many engineering problems could be involved if strong vibrations was induced. It will decrease the fatigue life of the structure, harm the health of the staff or damage the facilities on the deck especially for the natural gas production platform.

Normally, the offshore jacket structure is constructed with cylindrical pipes. It is originally designed to withstand ice force with vertical face. In addition, it is often very compliant as huge mass it has to support on its top. A lot of literatures discussed the ice induced vertical compliant structure vibrations. It has been demonstrated that strong vibrations could be induced by ice. The main objective of studying ice-structure interaction is to evaluate the ice force accurately, but it is also required to find ways to mitigate ice force or the ice-induced vibration.

One of promising approaches to reduce ice force is to install ice-breaking cone, which could transform ice failure from crushing into bending. Croasdale (1980), Wessels and Kato (1988)

---

<sup>1</sup> State Key Laboratory of Structural Analysis of Industrial Equipment, Dalian University of Technology, Dalian University of Technology, Dalian, 116023, China, Tel.: +86-411-4708407, fax: +86-411-4708393, e-mail: yueqj@dlut.edu.cn

reviewed early theoretical and experimental studies of ice force on conical structure. Chao (1992) summarised the formulae of predicting ice force on declined or conical structure. All these researches gave the conclusion that static ice force could be reduced significantly if an ice-breaking cone was installed on a narrow vertical structure despite more full-scale test data need to support this idea. But we lack the test data to evaluate if the ice-breaking cone could mitigate ice-induced vibration.

Yue et al. (1998) have measured the ice-induced vibrations of structures installed with ice-breaking cone. They found that dynamic response of the structure increases with ice speed and for the compliant conical structure the breaking frequency of ice sheet could be near or equal to the predominant frequency of the structure at a special ice speed. Later on, Yue et al. (2000) conducted tests of ice-induced vibrations on both the conical and vertical structures and discussed the mechanism of ice interacting with the two kind structures. In this paper, we try to discuss the effect of mitigating ice-induced vibrations of vertical structure with ice-breaking cone.

### TEST ARRANGEMENTS

The JZ20-2 gas field, consisting of several jacket platforms, is located in the north part of Bohai Bay of China, with about two months ice covered period. The MUQ is the central platform for reprocessing natural gas and living apartment. The MNW is the production platform near the MUQ. In order to reduce ice force and mitigate ice-induced vibration, they were installed with ice-breaking cones on each leg since 1992. Full-scale tests had conducted on MUQ and MNW to investigate the ice force and ice induced vibrations since then. Yue et al. (1998) reported the tests conducted on MUQ and MNW. Fig.1. is the test deployment of MUQ and MNW.

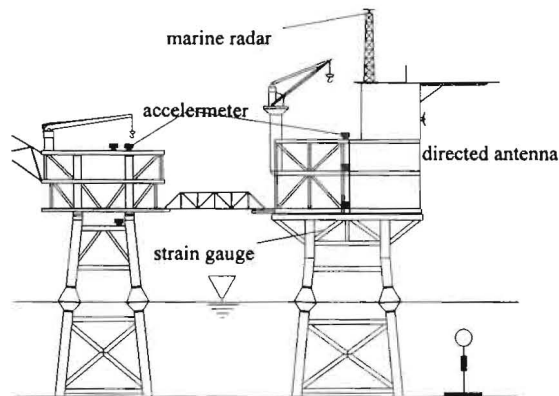
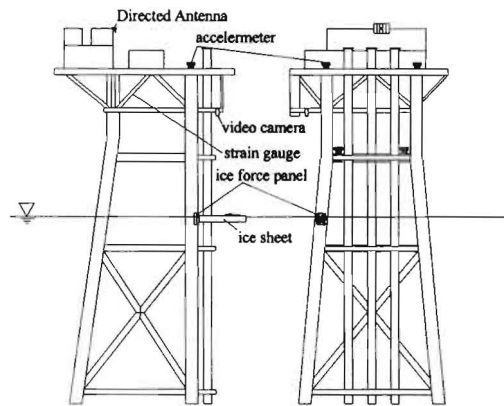


Fig.1. Sketch of test arrangement in MUQ & MNW platform



**Fig.2.** Sketch of test arrangement in MS platform

The MS platform, 3 km away from MUQ, is a new platform without ice-breaking cone. We set 6 accelerometers on two levels of the platform, stick several strain gauges on the frame. The rate of data sampling for response is 64 Hz. We also fixed several load panels on a leg for trying to measure the ice force directly, but unfortunately, they were damage by an ice-breaker when it docked to the platform before the tests. This work will be continued next year. A video camera was set over the interface of ice and the structure so that the failure process could be monitored. Fig.2. is the sketch of test arrangement in MS platform.

As MS is an automatic platform, a wireless local network system was adopted. Test data are stored in hard disk and send to MUQ platform where a center computer manages the test data from MUQ, MNW and MS platforms. Fig.3. is the diagram of test system.

#### **ICE-INDUCED VIBRATIONS OF CONICAL STRUCTURE**

As tide level is about 4 m, the ice-breaking cones of MUQ and MNQ are designed as double side. It is observed that ice always fails in bending no matter acting on up-ward or downward cone. That means the static ice forces could be reduced after the ice-breaking cones added. In order to evaluate the effect of mitigating vibrations, failure frequencies of ice sheet acting on the cones were investigated. Detail measurements show that the average breaking lengths are about 7 times of the ice thickness when ice acts on up-ward cone. Fig.4. shows the relationship of measured the breaking length and thickness. For the breaking lengths are scattered in a small range, the ice force frequency is in a narrow band, which means the energy of exciting forces concentrates in a narrow frequency zone. Since the breaking frequency of ice sheet depends on ice thickness and ice speed, the combination of ice speed and thickness when breaking frequency equals to the natural frequency of the structure could be determined as shown in Fig.5. So that, strong vibrations could still be induced at special condition.

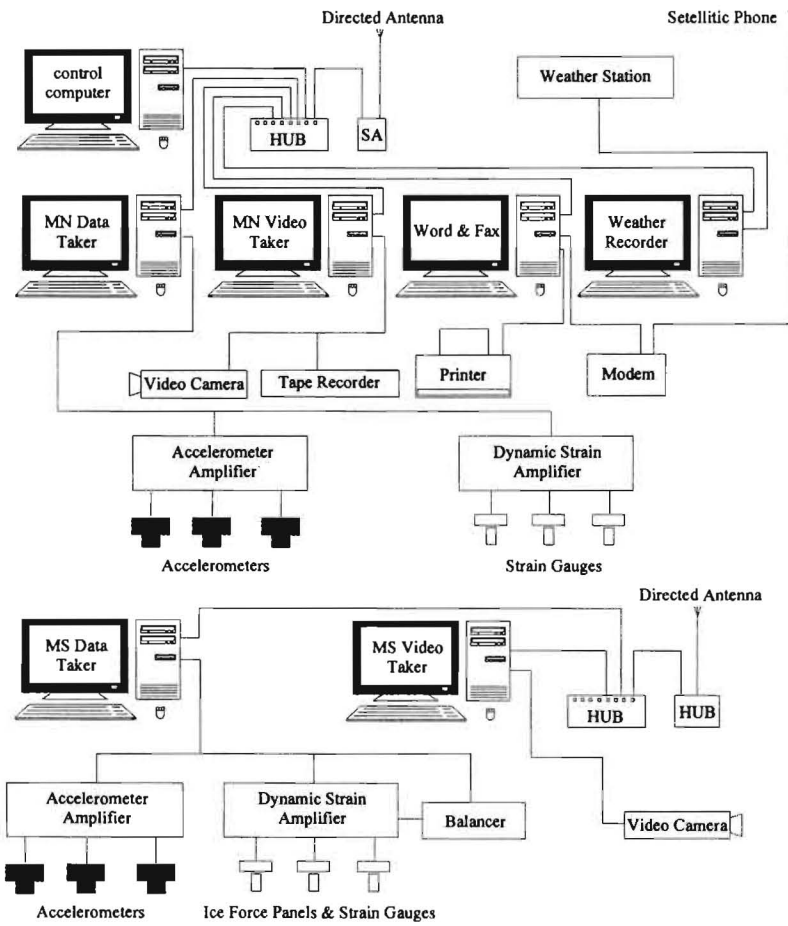


Fig.3. Diagram of test system

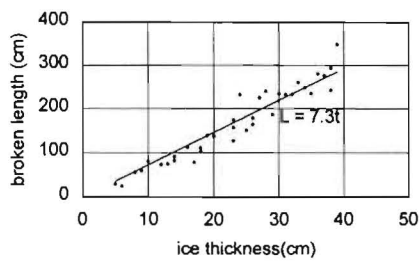


Fig.4. The relationship of the breaking length and thickness of ice sheet

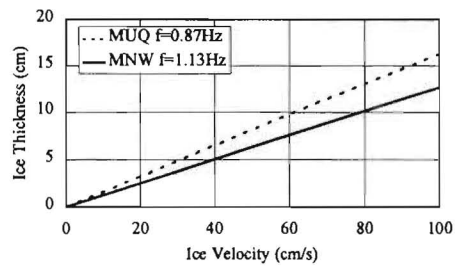


Fig.5. The combination of ice speed and thickness when breaking frequencies equal to the structure natural frequencies

## ICE INDUCED VIBRATIONS OF VERTICAL STRUCTURE

The interaction between ice and vertical structure is so complicated that it has not been well understood. It has been found that in a special condition steady-state vibrations could be occurred (Engelbrekston, 1983; Määttänen, 1977) and many efforts have been made to explain and simulate this phenomenon (Kärnä, 1989; Sodhi, 1994).

We also found the phenomenon of ice-induced steady-state vibrations on MS platform. The typical displacement response is shown in Fig.6. It took place at ice speed of 2-4 cm/s. And it appeared in very short period because the ice speed is very fast at most time. The displacement amplitude at steady-state vibrations is much bigger than that at high ice speed. We also noticed the structure did not unloaded thoroughly when the structure swung back. The vibrations would be much stronger if the structure unloaded completely. The residual force will play as additional damping.

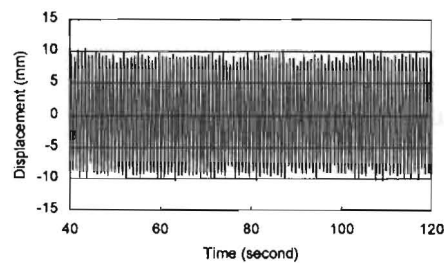


Fig.6. Steady-state vibrations in MS platform

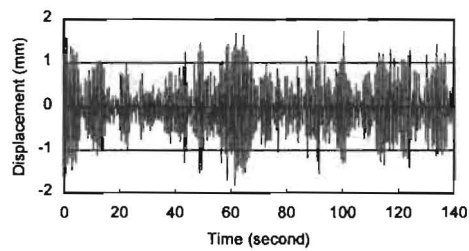


Fig.7. Random-state vibrations in MS platform at high ice speed

The mechanism of unloading process during steady-state vibrations has not been well understood but it seems to link with the behaviour of ice within ductile-brittle transition. During loading stage, the ice moves in the same direction as the structure. The loading rate of ice sheet near the structure is just in ductile range as the relative speed of ice and structure is lower than the absolute ice speed. And the damage zone, which includes dense micro-cracks, is formed. When the structure swings back, the loading rate of ice sheet is just in the brittle range as the relative speed is higher and make the damage ice fails more easily so that the structure unloaded. But for the compliant structure, the distance of swinging back at the ice acting area will be bigger than the damaged length formed in loading stage. So that the ice could not easily cleared up. The damaged field around the structure is the key to describe unloading process. Sodhi (1991) measured the residual force during structure moving back. As ice load panels were damaged, we could not determine the residual force during stage of unloading. This work will be continued next year.

When the ice moves faster, the response of the structure is much smaller than that in steady-state vibration. The ice fails rather irregular, some times in crushing and some times in

buckling. The typical displacement response of the structure at high ice speed is shown in Fig.7.

#### THE DISCUSSION OF EFFECT OF ICE BREAKING CONE

We could approximately evaluate the effect of mitigating vibrations with ice-breaking cone by the test results of MS and MUQ platforms. Fig.8. shows the displacements of MS and MUQ platform, in which each point represents the maximum displacement within ten minutes.

As the predominant frequencies, the stiffnesses, and the positions of the accelerometer are different, we could not compare them directly. We know that the response will depend on the stiffness and frequency of structure if a load function is determined.

Supposing the ice-breaking cones of MUQ were added on the MS platform, and subjected to the same load conditions as that of MUQ, the displacements of MS could be evaluated approximately. Having considered the differences between the two structures, such as the stiffness, natural frequency of the structure, the response of the MS platform with ice breaking cones will bigger than that of MUQ, but it is still smaller than the present maximum value of the MS platform. There is no phenomenon of steady-state vibrations in the response of MUQ, we can expect that the maximum vibrations is reduced and the steady-state vibrations will be avoided by adding ice-breaking cone, but at high ice speed the effect of adding cone is not so apparent.

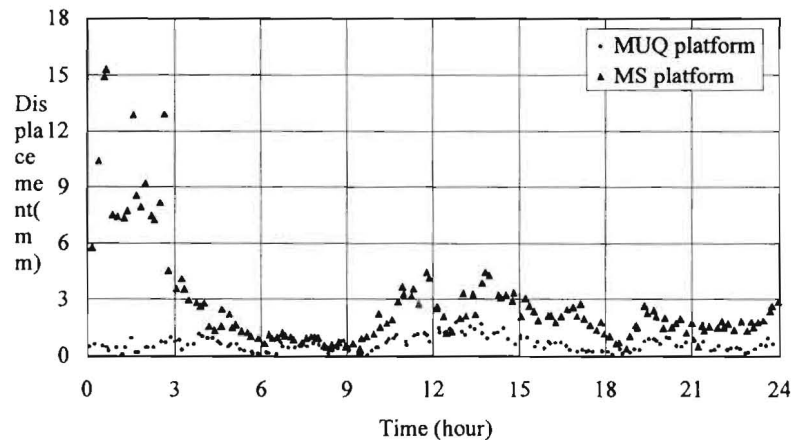


Fig.8. Displacements of MS and MUQ platforms

#### THE CONCLUSION AND DISCUSSION

The effect of mitigating ice-induced vibrations with ice-breaking cone is evaluated by primary analyzing the tests conducted on vertical and conical structure at same time. For the structure without ice-breaking cone, the steady-state vibrations can be induced and the strongest vibrations will appear in this stage. But we also find the vibrations have not reached its

maximum value because the structure is not thoroughly unloaded. The unloading process need more studies in detail. For the structure with ice-breaking cones, the vibrations will increase with the increase of ice speed. At a special condition the breaking frequency of ice sheet can equal to the predominant frequency of the structure, strong vibrations will be induced.

After adding ice-breaking cone, the steady state vibrations can be avoided because the failure type of ice sheet changes from crushing to bending, but the effect of ice-breaking cone is not so apparent at high ice speed.

For the fatigue analysis of structures, both the amplitude and numbers of vibrations need to be considered. So the more comprehensive studies should be carried out for using ice breaking cone to mitigate vibration.

## REFERENCES

CHAO, J.C. (1992): . Comparison of sheet ice load prediction methods and experimental data for conical structures. Proc. of OMAE conference, Vol. IV, pp. 183-193.

CROASDALE K.R. (1980): Ice forces on fixed rigid structures. CRREL Report 80-26, A state-of-the-art report by the IAHR working group on ice forces (Carstons, T. ed.), USA Cold Regions Research and Engineering Laboratory, pp. 34-106.

ENGELBREKSTON A. (1983): Observations of resonant vibrating lighthouse structure in moving ice. Proc. 7th Int. Conference on Port and Ocean Engineering under Arctic Conditions (POAC), Helsinki, Vol. II, pp. 855-864.

KÄRNÄ M.G., WRIGHT W.H. (1989): Dynamic response of narrow structures to ice crushing. Cold Regions Science and Technology, 17, pp. 173-187.

MÄÄTTÄNEN M. (1977): Stability of self-excited ice-induced structural vibrations. Proceedings of 4th International Conference on Port and Ocean Engineering under Arctic conditions (POAC), St. John's Newfoundland, Canada, Vol. II, pp. 684-694.

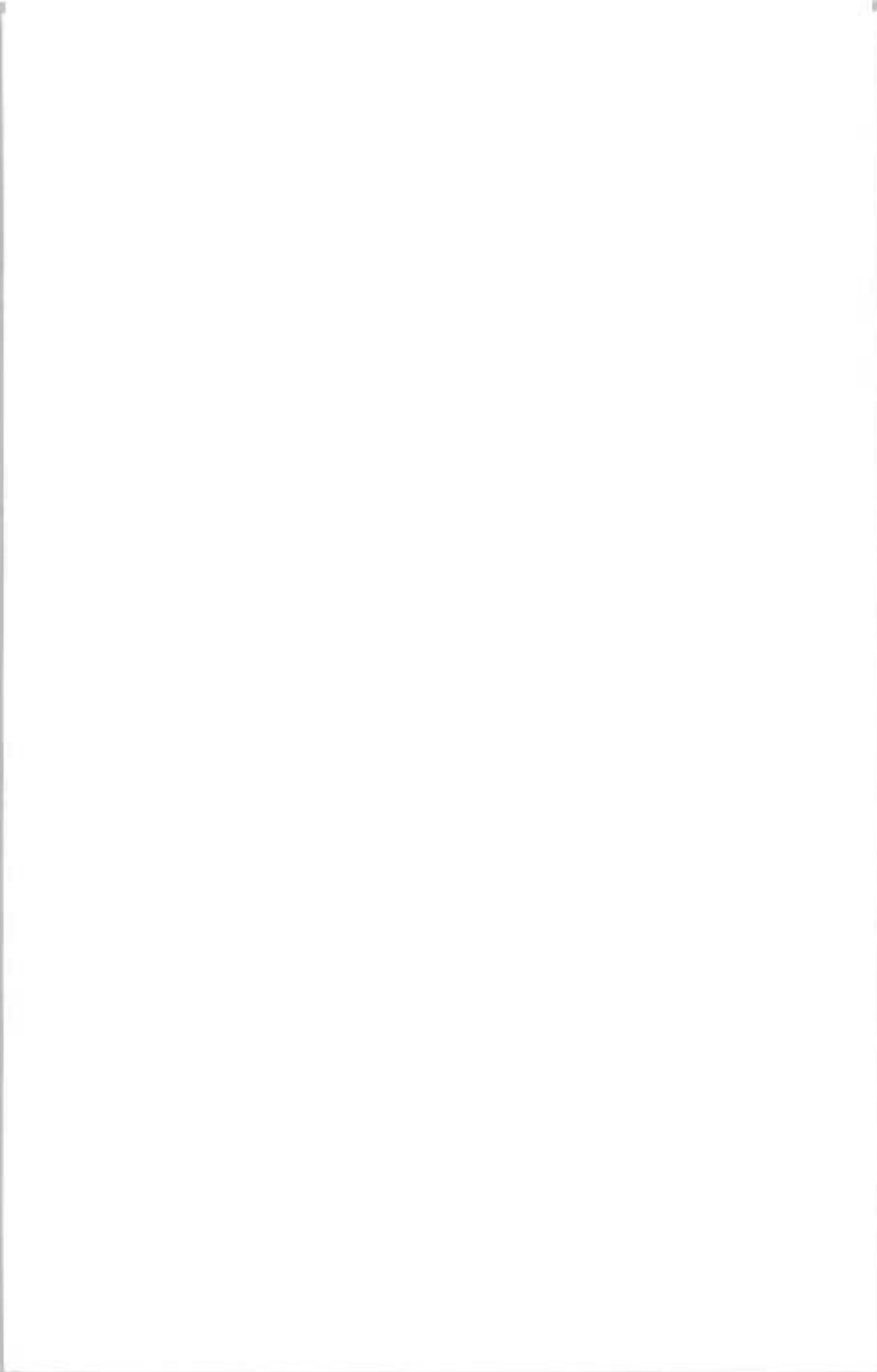
SODHI D.S. (1991): Ice-structure interaction during indentation tests, Ice-structure interaction: Proceeding of IUTAM-IAHR (S. Jones et al. Eds.) Spring-Verlag, pp. 619-640.

SODHI D.S. (1994): A theoretical model for ice-structure interaction., Proc. of 12th International Association for Hydraulic Research (IAHR) Symposium on Ice, Trondheim, Vol. II, pp. 807-815.

WESSELS E., KATO K. (1988): Ice forces on fixed and floating conical structures. Proc. of the 9th International IAHR Symposium on Ice. Sapporo, Japan, Vol. II, pp. 666-707.

YUE Q.J., BI X.J. (1998): Full-scale tests and analysis of dynamic interaction between ice sheet and conical structures. Proc. of 14<sup>th</sup> International Association for Hydraulic Research (IAHR) Symposium on Ice, Vol. II, Potsdam.

YUE Q.J., BI X.J. (2000): Ice-Induced Jacket Structure Vibrations in Bohai Sea. J. of Cold Regions Engineering (ASCE) (will be pressed).





## PREDICTING STATIC ICE LOADS ON DAMS

G. Comfort<sup>1</sup>, Y. Gong<sup>1</sup>, S. Singh<sup>2</sup>

### ABSTRACT

An eight-year field program was undertaken from 1991-92 to 1998-99 to: (a) measure the loads in the ice sheet near the dam; (b) measure the load distribution between a gate and pier, and: (c) compare the loads on wooden and steel stoplogs. The most significant finding has been to show the importance of water level changes on ice loads. Ice loads are much higher and more variable (compared to purely thermal loads) when significant, but not excessive, water level changes occur. Ice load predictors have been developed, and they predict thermal loads well. They are less accurate for loads produced by a combination of water level and ice temperature changes.

### INTRODUCTION AND SCOPE OF PAPER

Ice loads exerted on hydro-electric dams are not well understood although dams have been built and operated for many years in northern climates. A field program was undertaken from 1991-92 to 1998-99 to: (a) measure the loads in the ice sheet near the dam; (b) measure the load sharing between a gate and pier, and: (c) compare the loads on wooden and steel stoplogs. Results are presented and analyzed in detail in Comfort et al. (1996; 1998a; 1999). The 1991-92 to 1995-96 results are summarized in Comfort et al. (1997 and 1998b) among other papers as well as in the annual field reports, which are available from the Canadian Electricity Association (CEA). This paper describes methods that have been developed for predicting ice loads. A companion paper describes the factors controlling ice loads in more detail (Comfort et al., 2000). In view of the significance of water level changes, the following cases were analyzed separately:

- Case 1: Water Level Changes are Negligible - in this case, ice loads are generated thermally.
- Case 2: Combined Thermal/Water Level Regime - water level changes affect the ice loads significantly here. See Comfort et al, 2000 for further information.

---

<sup>1</sup> Fleet Technology Ltd., Kanata, Canada, 311 Legget Drive, Kanata, Ont., Canada, K2K 1Z8,  
Tel.: 613-592-2830; fax: 613-592-4950; email: gcomfort@fleetech.com

<sup>2</sup> Newbridge Networks, Kanata, Canada

Fr 226

## PREDICTING THERMAL ICE LOADS (NEGLIGIBLE WATER LEVEL CHANGES)

### General Approach

These ice loads are comprised of two parts: (a) residual loads, which are loads that were present before the start of the loading event, and; (b) line load increases produced by ice temperature rises – these result from air temperature rises; and/or from precipitation, particularly snowfalls. The most rational analysis approach (which also provided the best fit to the data) was to predict these two load components separately (Eq. 1). The analyses were based on events producing line loads greater than 30 kN/m (2 kips/ft) because they are of greater interest for design. Also, these data are more reliable because larger loads can be resolved more accurately.

$$LL_{total} = \Delta LL_{ther} + LL_{Residual} + LL_{contingency} \quad (1)$$

where :  $LL_{total}$  = the total line load

$\Delta LL_{ther}$  = the line load increase produced by ice temperature changes

$LL_{Residual}$  = the residual load in the ice sheet before the thermal event occurred

$LL_{contingency}$  = a load contingency that was added to ensure that the predicted line loads provide an upper bound to the measured line loads.

### Predicting Residual Loads

Lower residual loads are to be expected for events starting in cold ice than for warm ice, because the previous stresses are less likely to be fully decayed in warm ice. The data support this (Fig.1. and Eq. 2), although there is scatter due to variations in the time elapsed between events.

$$LL_{Residual} \text{ (in kN/m)} = -0.0528 * A_i + 21.37 \quad (2)$$

where :  $A_i$  = the ice temperature profile area, in °C\*cm, at the start of the event. (see Comfort et al., 1998b for a definition of the ice temperature profile area).

### Predicting Line Load Increases Due to Ice Temperature Rises

The best-fit equation for  $\Delta LL_{ther}$  in Eq. 1 was determined as given below.

$$LL_{ther} \text{ (in kN/m)} = 0.064 * \Delta A^{0.6} * h^{0.88} * Dur^{(\text{Min}(\log 160/\Delta A, 0))} \quad (3)$$

where:  $\Delta A$  = the change in ice temperature profile area, in °C\*cm

$h$  = the ice thickness, in cm

$Dur$  = the event duration, in days.

### Measured vs Predicted Thermal Loads and the Load Contingency Required

The predicted loads (obtained by summing  $\Delta LL_{ther}$  and  $LL_{Residual}$ ) were compared with the measured total loads to evaluate the load contingency ( $LL_{contingency}$ ) required. See Fig.2. The predictive error (defined as the measured load minus the predicted load) can be approximated by a normal distribution with a mean of -7 kN/m (0.5 kips/ft), and a standard

deviation of 13 kN/m (0.9 kips/ft). The overall range between the predicted and measured values is  $\pm 23$  kN/m. A value of 25 kN/m for  $LL_{contingency}$  would ensure that the predicted loads bound the measured loads for all events. A value of 13 kN/m (0.9 kips/ft) for  $LL_{contingency}$  would ensure that the predicted loads exceed the measured loads for 90 % of the events analyzed.

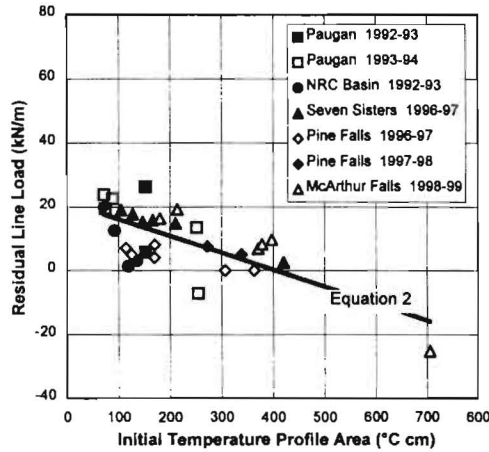


Fig.1. Residual Loads

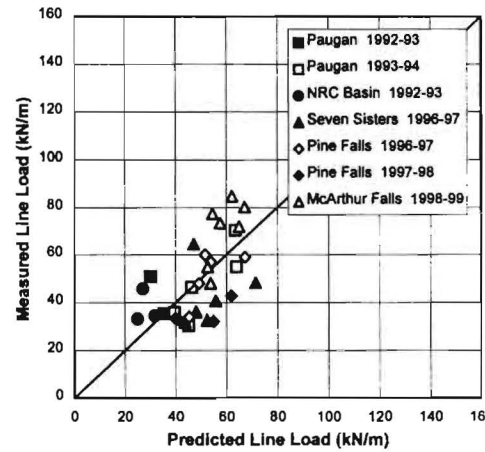


Fig.2. Measured vs Predicted Total Loads

### Range of Applicability for the Thermal Load Predictors

Table 1

Ranges of Variation in the Thermal Load Database for the Key Parameters

Parameter	Max. Value	Min. Value
Total Load, $LL_{total}$ , (kN/m)	85	6
Residual Load, $LL_{Residual}$ , (kN/m)	26	-25
Line Load Increase due to Thermal Effects, $\Delta LL_{ther}$ , (kN/m)	110	8
Ice Thickness, $h$ , (cm)	80	15
Change in Ice Temperature Profile Area, $\Delta A$ , ( $^{\circ}C \cdot cm$ )	418	17
Event Duration, $Dur$ , (days)	9.2	0.2
Ice Temperature Profile Area at the Start of Event, $A_i$ , ( $^{\circ}C \cdot cm$ )	705	56

### PREDICTING LOADS AT SITES WITH SIGNIFICANT WATER LEVEL CHANGES

#### Introduction and Review of Loading Events

This is the most important case because it has generated the highest loads (Comfort et al., 2000). Unfortunately, it is difficult to analyze because many parameters affect the loads produced. A review of the loading events (Fig.3.) indicated the following:

- **Water Level Changes:** Although events typically lasted several days, water level changes had the most significant effect in the last 2-3 days leading up to the peak load when they produced large load “spikes”. The early part of the event was dominated by thermal effects.
- **Interaction Between Ice Temperature and Water Level Changes:** Although some events occurred in which no ice temperature rises took place, the largest loads were produced by a combination of ice temperature and water level changes. The highest loads were produced after ice temperature changes had “pre-stressed” the ice initially.
- **Effect of Ice Temperature Magnitudes:** Higher loads were produced when the ice was colder at the start of the event, as this affected the “interaction” loads described above.
- **Effect of Ice Temperature Changes Before the Event:** Lower loads were produced when the ice temperature had been decreasing prior to the event start compared to the case where the ice temperature had been stable for some time before the event occurred.

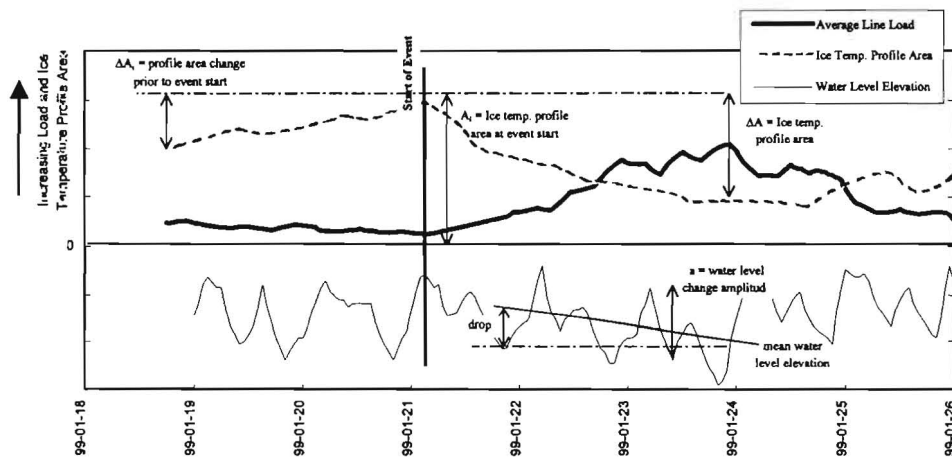


Fig.3. Schematic for a Combined Water Level Change/Thermal Loading Event

### Overview of Analysis Approach

The following form was adopted for modelling the total load,  $LL_{total}$ :

$$LL_{total} = LL_{Residual} + \Delta LL_{Thermal} + LL_{Water Level} + LL_{Contingency} \quad (4)$$

- where :
- $\Delta LL_{Thermal}$  = the “pure thermal” load, as defined by Eq. 3.
  - $LL_{Water Level}$  = the “water level change” load, which is produced by water level changes
  - $LL_{Residual}$  = the load in the ice prior to the loading event, termed the residual load
  - $LL_{Contingency}$  = an additional line load that was added to the predicted load to ensure that the measured load did not exceed the predicted load .

### Predicting "Water Level Change" Loads: Trend Analysis

Key parameters were identified by comparing them to the "water level change" load ( $LL_{water\ level\ change\ w/o\ contingency}$  - Eq. 5). This is related to several factors as listed below:

$$LL_{water\ level\ change\ w/o\ contingency} = LL_{total} - LL_{Residual} - \Delta LL_{Thermal} \quad (5)$$

where:  $LL_{total}$  = the total line load measured during the event  
 $LL_{Residual}$  = the residual line load measured during the event  
 $\Delta LL_{Thermal}$  = the thermal line load predicted using equation 3;

- (a) water level change amplitude and ice thickness - these had the most significant effect. For all dam sites, the ice load reduced greatly as the ratio between the water level change amplitude,  $a$ , and the ice thickness,  $h$ , increased (Fig.4.). The  $a/h$  ratio was defined based on the average water level change amplitude for the 2-3 day period prior to the peak load (Fig.3.).

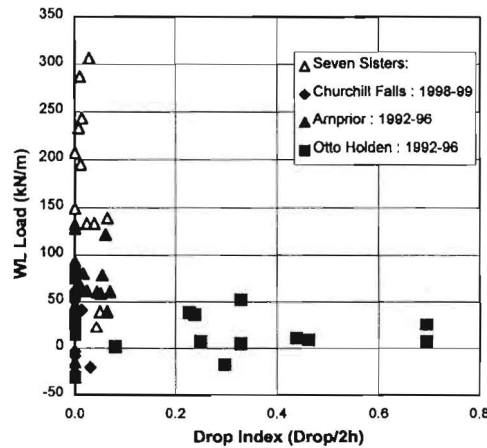
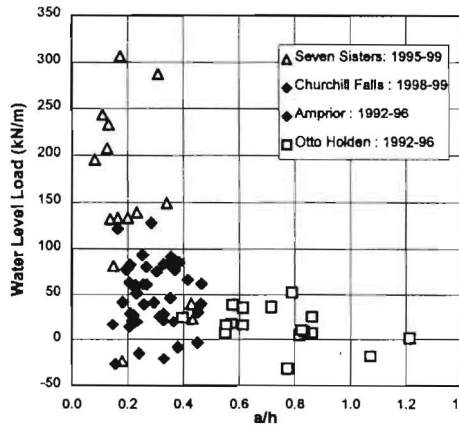


Fig.4. Water Level Change Load vs  $a/h$       Fig.5. Water Level Change Load vs Drop Index

- (b) water level change frequency (defined as the number of cycles per day) - this was not included in the ice load equations because water level change loads were not dependent on it.
- (c) a drop or rise in mean water level - higher loads are expected when the water level is cycled about the same mean level, versus cases where drops or rises in mean water level occur. This effect is related to the ice thickness as well. Water level drops or rises of more than two ice thicknesses would cause the water level change loads to decrease to nil or to a very low value because the ice sheet would lose contact with the dam. The water level change load decreased with the *Drop Index* (defined in Fig.3. and Eq. 6 below). See Fig.5.

$$\text{Drop Index} = | \text{drop or rise} | / (2 * h) \quad (6)$$

where :  $| \text{drop or rise} |$  = the absolute value of the drop or rise in mean water level over the 2-3 days preceding the peak load, in cm

$h$  = the ice sheet thickness, in cm.

- (d) change in ice temperature profile area - higher loads were produced when large ice temperature changes occurred in combination with water level changes (Fig.6.).
- (e) duration of loading - long duration events produced lower water level change loads, which is similar to the trend observed for purely thermal loads.
- (f) ice temperature at the start of an event - This had a significant effect as larger water level loads were produced by colder ice than warmer ice.
- (g) ice temperature profile area change before the start of an event - higher loads tended to be produced if the ice temperature had been stable for several days before the event. Reduced loads occurred if the loading event was immediately preceded by a drop in ice temperature.

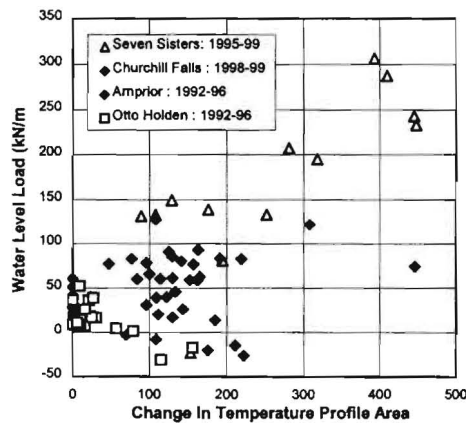


Fig.6. Effect of Profile Area Change

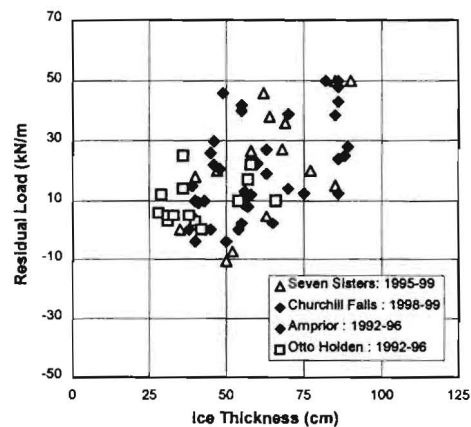


Fig.7. Residual Load vs Ice Thickness

### Predicting “Water Level Change” Loads: Equations Developed

The following equations were developed based on the observed trends and an error minimization analysis.  $LL_{Water Level}$  contains the two components below, in keeping with the trends observed.

- (a) the “pure water level change” load - this is the load produced solely by a water level change.
- (b) the “interaction” load - this is the second term. It models the observed interaction effects with higher loads being produced when water level and ice temperature changes both took place.

$$LL_{Water Level} = f(\text{temp \& water level changes}) * (5 + 7.5 \times 10^{-8} * \Delta A^2 * A_i^{1.2} / Dur^{0.4}) \quad (7)$$

where:  $f(\text{temp \& water level changes}) = f(\Delta A_i) * f(drop) * f(a/h)$  (8)

$$f(\Delta A_i) = \text{the maximum of: } 0 \text{ or } 1 - 4(\Delta A_i / A_m)^{1.4} \quad (9)$$

$$f(drop) = \text{the maximum of: } 0 \text{ or } 1 - 20 * (drop / 2h)^2 \quad (10)$$

$$f(a/h) = 0.22 \text{ for } a/h < 0.22, \text{ and; } 1 / (a/h)^2 \text{ for } a/h \geq 0.22 \quad (11)$$

$Dur$  = Duration of the event, in days

$a$  = the average water level change amplitude (absolute value), in cm, over the 2-3 days leading up to the peak load (Fig.3.)

$h$  = reservoir ice thickness, in cm

$\Delta A$  = profile area change (absolute value), in °C\*cm

$\Delta A_i$  = initial profile area change (absolute value) prior to the start of the event, in °C\*cm

$A_i$  = ice temperature profile area (absolute value) at the start of the event, in °C\*cm

$drop$  = drop or rise (absolute value) in mean water level during the event, in cm

$A_m$  = the maximum ice temperature profile area, in °C\*cm, (defined as  $20 * h$ , in cm) (12))

### Predicting Residual Loads: Trend Analysis and Equations Developed

Although residual loads are affected by several parameters, the ice thickness and the  $a/h$  ratio were found to have the greatest effect (Fig.7. and 8., respectively).

The best-fit equation for the residual loads with respect to these parameters is shown below.

Eq. 13 predicted the measured residual loads within 29 kN/m (2 kips/ft). See Fig.9.

$$LL_{Residual} \text{ (in kN/m)} = 0.37 * f(h) + 1.47 / (a/h) \quad (13)$$

Where:  $f(h) = h - 25$ , for  $h > 25$  cm. For  $h \leq 25$  cm, Eq. 13 is not applicable. (14)

### Predicted vs Measured Loads and the Load Contingency Required

The required contingency load, (i.e.,  $LL_{Contingency}$ ) was evaluated by comparing the predicted loads (which were calculated by summing  $LL_{Residual}$ ,  $\Delta LL_{ther}$ , and  $LL_{Water Level}$ ), with the measured loads (Fig.10.). The required load contingency is a measure of the prediction error. It is normally distributed with a mean of zero, and a standard deviation of 45 kN/m. The probability that the required contingency load will be less than 60 kN/m (4 kips/ft) is 90 % (Fig.11.).

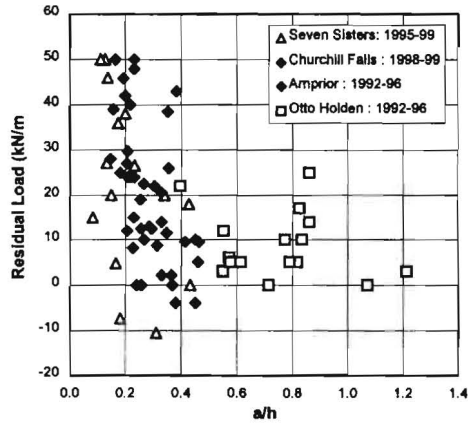


Fig.8. Residual Load vs  $a/h$

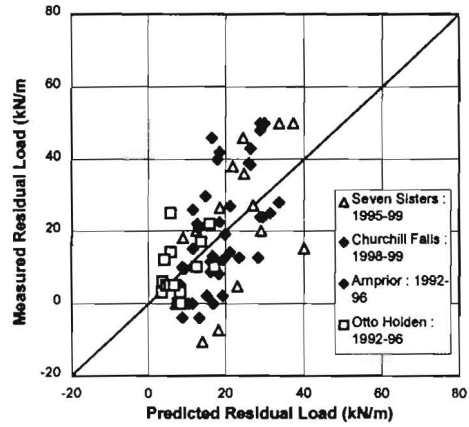


Fig.9. Predicted vs Measured Residual Loads

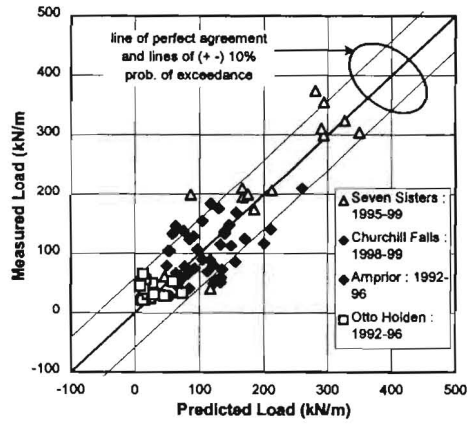


Fig.10. Predicted vs Measured Loads

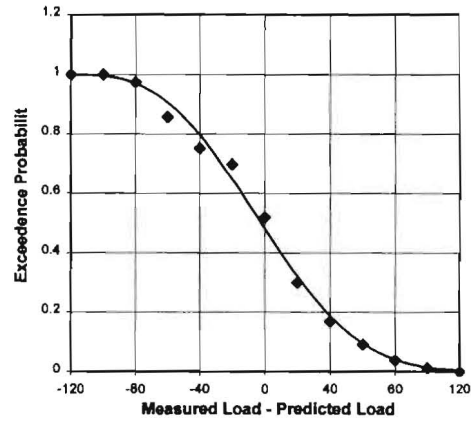


Fig.11. Load Contingency Distribution

## Range of Applicability for the Combined Water Level Change/Thermal Load Predictor

**Table 2**

Ranges of Variation for the Events in the Combined Water Level Change/Thermal Load Database

Parameter	Max.	Min.
Total Line Load, $LL_{total}$ , (kN/m)	374	21
Residual Line Load, $LL_{Residual}$ , (kN/m)	50	-10
Reservoir Ice Sheet Thickness, $h$ , (cm)	90	28
Water Level Change Amplitude $a$ , (cm)	51	7
Water Level Change Amplitude/Ice Thickness, $a/h$	1.21	0.08
Forebay Mean Level drop, $drop$ , (cm)	50	-50
Forebay Level Drop Index, $ drop /2h$ – Eq. 6	0.69	0
Water Level Change Frequency (cycles/day)	2.25	0.25
Event Duration, $Dur$ , (days)	14.2	0.15
Ice Temperature Profile Area Change During the Event, $\Delta A$ , ( $^{\circ}C \cdot cm$ )	448	0
Ice Temperature Profile Area Change Before the Event, $\Delta A_i$ , ( $^{\circ}C \cdot cm$ )	530	0
Ice Temperature Profile Area at the Start of the Event, $A_i$ , ( $^{\circ}C \cdot cm$ )	608	0

### CONCLUSIONS

Much progress has been made towards understanding static ice loads on hydro-electric structures, and the mechanisms generating them. Methods have been developed to predict the ice load. The algorithms predict thermal loads well as a load contingency of 13 kN/m (0.9 kips/ft) would be adequate for 90 % of the loading events. Loads produced by a combination of water level and ice temperature changes can not be predicted as well, as the required load contingency to cover 90 % of the events is 60 kN/m (4 kips/ft). Further work in this area would be useful.

### ACKNOWLEDGEMENTS

The work was sponsored by the Canadian Electricity Association (CEA-R&D projects 9038 G 815; 9502 G 2015, EG 910012, T992700-0203 and T992700-0204), with partial funding from Manitoba Hydro, Hydro-Quebec, Ontario Hydro, Nfld. Light and Power Co. Ltd., Nfld. and Labrador Hydro, and the Canadian Dam Safety Ass'n. (CDSA). The project was administered by T. Glavicic-Theberge of the CEA. The project monitors were G. Schellenberg of Manitoba Hydro, R. Lupien and Tai Mai Phat of Hydro-Quebec, G. Smith and P. Bhat of Ontario Hydro, A. Kumar of B.C. Hydro, P. Halliday of Nfld. Light & Power Co. Ltd., R. Barnes and E.G. Piercy of Nfld. and Labrador Hydro, and W. Pawlikewitch of Manitoba Hydro (who represented the CDSA). Assistance was provided by operations personnel at Hydro-Quebec (S. Robert, A. Pednault, R. Brazeau and A. Bond); Ontario Hydro (J. Whyte, G. James, G. McLeod, C. Stevens and J. Tremblay); Manitoba Hydro (T. Armstrong, P. Roach and G. Ferguson); and Nfld. & Lab. Hydro (D. Hodder, and G. Tucker).

## REFERENCES

COMFORT G., GONG Y., SINGH S. (2000): The Factors Controlling Static Ice Loads on Dams. Proc. IAHR Symposium on Ice Problems, Gdansk, Poland.

COMFORT G., ABDELNOUR R., GONG Y., SINGH S., DINOVIETZER A. (1999): Update No. 2 to Static Ice Loads On Hydro-Electric Structures. Ice Loads Monograph No. 2, CEA projects EG 910012 and T992700-0204.

COMFORT G., ABDELNOUR R., GONG Y., SINGH S., DINOVIETZER A (1998a): Static Ice Loads On Hydro-Electric Structures. Ice Loads Monograph No. 2, CEA proj. EG 910012.

COMFORT G., SINGH S., GONG Y. (1998b): Static Ice Loads On Dams: Loads on the Dam Face, and on Wooden vs Steel Stoplogs. CDA Conference, Halifax.

COMFORT G., GONG Y., SINGH S., ABDELNOUR R. (1997): Static Ice Loads On Hydro-Electric Structures: Loads Exerted Along A Dam Face; And A Comparison Of The Loads Exerted On Wooden And Steel Stoplogs. CDSA Conference, Montreal.

COMFORT G., ABDELNOUR R., GONG Y., DINOVIETZER A. (1996): Static Ice Loads On Hydro-Electric Structures. Ice Loads Monograph, CEA project 9038 G 815.



## THE CANADIAN PERD ICE/STRUCTURE INTERACTION PROGRAM

G.W. Timco<sup>1</sup>, R. Frederking<sup>1</sup>, K. Smith<sup>2</sup>, N. Billette<sup>2</sup>

### ABSTRACT

The Canadian Government, through its Program of Energy Research and Development (PERD) has sponsored research in the area of ice/structure interaction for several years. This work is related to the safe and economic development of Canada's offshore oil & gas resources. For the past 3 years, the National Research Council (NRC) of Canada in Ottawa has managed 4 major projects within the program, with a total annual budget of \$600k (Can). This paper describes each of these projects and provides information on the availability of the research results that can be accessed by the international community.

### INTRODUCTION

The Program of Energy Research and Development (PERD) is a Canadian federal government program that has the objective of providing the science and technology necessary for Canada to move towards a sustainable energy future. The program is divided into 6 Strategic Intents, which cover a range of energy research and development (R&D) issues. The expansion and diversification of Canada's oil and gas production is one of the Strategic Intents. As part of this Intent, funding is supplied to federal government departments to perform R&D related to the development of offshore oil & gas resources. In Canada, ice is the major impediment to offshore development. Therefore, as part of the PERD initiative, funding is supplied to investigate, and try to minimize, the influence of floating ice for offshore development. This research has been managed over the years by the Canada Oil & Gas Lands Administration (COGLA), Public Works Canada (PWGSC) and the National Energy Board (NEB). For the past 3 years, the Canadian Hydraulics Centre (CHC) of the National Research Council (NRC) of Canada in Ottawa has managed the Ice/Structure Interaction program for PERD. It has done this with the advice of an Advisory Committee. At the present time, this committee, which is chaired by G. Timco of the NRC, is comprised of 8 industry members (K. Kennedy, BP Amoco; G. Lever, Petro-Canada; W. Smink, Husky Oil; K. Roberts, Chevron; W. Spring,

---

<sup>1</sup> National Research Council, Ottawa, Ont., Canada, Tel.: 613.993.6673, fax: 613.952.7679,  
e-mail: [garry.timco@nrc.ca](mailto:garry.timco@nrc.ca)

<sup>2</sup> Office of Energy R&D, NRCan, Ottawa, Ont., Canada

*garry.timco@nrc.ca*

*www.chc.nrc.ca*  
*Cold regions technology*  
*PERD Ice/Structure Interaction Program*

*Mobil; J. Weaver, Exxon; S. Bruneau, North Atlantic Pipeline Partners; D. Seidlitz, Gulf Canada*) and 9 government members (B. Dixit, *National Energy Board*; W. Bobby, *Canada-Newfoundland Offshore Petroleum Board*; P. Timonin & J. Reid, *Transport Canada*; M. Cheung, *Public Works & Government Services Canada*; T. Carrieres, *Environment Canada*; S. Prinsenber, *Fisheries and Oceans*; and R. Frederking & G. Timco, *National Research Council*). The Committee meets twice a year to provide guidance on research directions.

The NRC has managed 4 major projects within the program, with a total annual budget of \$600k (Can). These projects are:

1. Operational experience from the Beaufort Sea
2. Ice-related problems hindering the Grand Banks development
3. Ice problems related to East Coast activities
4. Ice loads on actual offshore structures

Part of this research is carried out directly by the NRC, but the majority of the work is contracted to the private sector using Government of Canada contracting rules in response to Request for Proposals issued by the NRC. In addition, several university researchers carry out related research of more fundamental nature. This paper will describe the overall objective of each project, and provide information on obtaining the results of the research.

#### **OPERATIONAL EXPERIENCE FROM THE BEAUFORT SEA**

The objective of this project is the orderly acquisition and documentation of Industry and Government reports and data, which were obtained during the intense exploration activity in the Canadian Beaufort Sea frontier region.

During the 1970's and 1980's, an enormous effort was spent in the exploration of hydrocarbons in the Beaufort Sea region of Canada. Several major Oil Companies were involved in this offshore exploration. In total, 88 wells were drilled between 1972 and 1989, during which time most of the current knowledge of operating in ice-infested waters was developed. This technology includes bottom-founded, ice-resistant structures, floating drillship systems, and various icebreakers. The information on Beaufort Sea design work, the field experience and operating expertise developed, the data that was acquired, and the supporting research effort is extremely valuable and irreplaceable. Oil companies and the Canadian government spent many tens-of-millions of dollars in collecting information in this frontier region. The work focuses on collecting, cataloguing, archiving and analyzing the engineering reports and ice load data from the Beaufort Sea development.

The archiving and cataloguing of the reports have been carried out at 2 different locations. The general engineering and environmental reports have been catalogued by the Arctic Institute of North America (AINA, 1999) and stored at the University of Calgary library (Tull, 1999). The reports and data related to ice forces on structures have been catalogued and stored at the Canadian Hydraulics Centre of the NRC (Timco, 1998). The data analysis has

successfully analyzed a number of the ice loading events in the Beaufort Sea on the Molikpaq (Rogers et al., 1998) as well as other Arctic structures (Timco et al., 1999).

This project is now complete. It should be noted, however, that significant oil and gas discoveries were made in the Beaufort Sea, including the Amauligak oil reservoir. Current discovered reserves for this region are 12 trillion cubic feet of gas and 1.6 billion barrels of oil, with an estimated value of over \$30B. To date, these reserves have not been developed. In spite of these large reserves, there is currently no activity in the Canadian Beaufort region. In future years, it is anticipated that activity will again commence there. The results of this project will be extremely valuable for this development.

#### **ICE-RELATED PROBLEMS HINDERING THE GRAND BANKS DEVELOPMENT**

The objective of this work is to identify and address the ice-related problems that interfere with the development of the Grand Banks petroleum resources, off the East Coast of Canada.

The Grand Banks region off the East Coast of Canada has proven oil and gas resources with an estimated 1.6 billion barrels of oil, 4 trillion cubic feet of gas and 237 million barrels of natural gas liquids. If there were no ice present in this region, conventional drilling technology could be used for oil and gas production. However, the presence of icebergs and occasional pack ice intrusions significantly affects the manner in which the exploration, production and transportation of the oil and gas take place.

The production of these reserves commenced in 1997 with the Hibernia development using a large gravity-based structure (GBS) as a drilling and production platform. The Terra Nova field is scheduled to begin production in early 2001. This field will be developed using a floating production, storage and offloading (FPSO) system. This vessel will be moored on-site, with the capability of disconnecting and moving off location to avoid an intruding iceberg. Plans are well underway for other sites on the Grand Banks including the development of the Whiterose and Ben Nevis fields. These, and other smaller fields, are in different ice conditions and innovative technology will be required to produce cost-effective solutions to deal with icebergs and sea ice. Wright (1998a) identified iceberg impact loads and downtime due to pack ice incursion as 2 key problem areas. This PERD project takes a proactive approach to identifying and addressing these, and other, ice-related problems.

Work on the *iceberg* problem has focused on several fronts:

*Iceberg Population Density* - It is necessary to understand the iceberg population density as a function of both location and date, to provide correct risk assessment of iceberg collisions at each of the sites on the Grand Banks. Since there was no comprehensive, single-source of information on this, NRC contracted Fleet Technology and Agra/Seaborne (Fleet & Agra/Seaborne, 1998) to collect this information. They developed a comprehensive database from computer-stored records that provides full information on the historic iceberg population in the Grand Banks region off the East Coast of Canada. The initial work was completed in March 1998 with small annual updates. Professor Jordaan of Memorial University of

Newfoundland (MUN) critically reviewed this database and compared it to the database developed by MUN using aerial photographs as the sources of data (Jordaan et al., 1999). He discusses the differences and the implications with regard to risk analysis.

*Iceberg Shape and Size Analysis* - The shape and size of icebergs play a key role in several different aspects of ice engineering in the Grand Banks region. For example, the detailed shape of an iceberg will define the local pressures and pressure distribution during an impact process. Also, deep draft icebergs pose a threat to any sub-sea facilities and/or pipeline. Thus, considerable effort has been placed in developing the details of iceberg shape and size. Canatec Consultants, in collaboration with ICL Isometrics, Coretec and Westmar produced a report (Canatec et al., 1999) and an accompanying database that documents all of the available information on the shapes of profiled Grand Banks icebergs. The Canadian Hydraulics Centre of the NRC (Barker et al., 1999) used this information to develop a program to visualize the 3-dimensional shape of those icebergs that had 3-D profiling. This analysis presents a means of quickly and easily seeing the shape and complexity of actual icebergs.

Fleet Technology (Comfort, 1998) evaluated different approaches that could be used to provide a detailed profile of the shape of an iceberg. This information is important for understanding the collision mechanics with a structure or seabed facility. In many cases, it is necessary to know only the maximum draft of an iceberg so that iceberg management procedures can be implemented if there is possibility of contact with seabed facilities. Canadian Seabed Research (CSR, 2000) looked at methods for quickly and accurately determining the maximum draft of floating icebergs. Croasdale et al. (2000a) prepared an overview of iceberg scour and the risk of interaction with sub-sea facilities.

*Iceberg Management* - Physical management of icebergs has been done for several years on the Grand Banks with varying degrees of success. However, a reliable iceberg management scheme will allow more safety and less disconnect for floating vessels. To address current approaches, PERD funded C-CORE and Wright (C-CORE, 1998) to review the state-of-the-art of iceberg towing, and produce an overview plan to improve iceberg management for protecting offshore structures. More recently, PERD has been a member of a Joint Industry Project headed by C-CORE to improve iceberg management and detection techniques.

Work on the issue of pack ice incursion relates to *stationkeeping in pack ice*. This has been addressed using various approaches including laboratory impact tests (Frederking et al., 1999), reviewing past physical model tests in ice (Fleet & Marineering, 1999), collecting available full-scale information on moored vessels in ice (Wright, 1998b & 1999), and through the development of sophisticated numerical models which allow a wide range of scenarios to be addressed (Sayed et al., 1999). This work has provided a significant increase in the understanding of the conditions in which a moored vessel can stationkeep in moving pack ice. The analysis indicates that concentrations of pack ice higher than 0.7 are required before there is a significant increase in mooring line loads. This result has implications for both moored drillships and tankers loading in pack ice conditions. Fleet and SMS (2000)

investigated different methods for retrofitting the FPSO to measure mooring line loads during its deployment in pack ice conditions.

#### **ICE PROBLEMS RELATED TO EAST COAST ACTIVITIES**

The objective of this work is to assess the ice environment and identify the key ice issues that would interfere with the development of the frontier regions off the West Coast of Newfoundland.

The development of the oil and gas reserves off the West Coast of Newfoundland would require offshore platforms that would be subjected to moving ice during the winter months. The current knowledge of the ice regime in this area is not well detailed. This project focused on practical problems related to the ice regime and the development of this region.

Canatec (Pilkington et al., 1997) undertook a detailed study of all of the environmental conditions in this region, including the ice regime, iceberg population, wave climate, etc. Sandwell (Spencer et al., 1998) used this information to look at possible offshore platforms that could be used for development in this region. This work determined that first-year ridges would be the likely design-load limiting environmental factor. Since little detailed information about the ridges from this region was known, a dedicated field trip was carried out in 1999 to measure the ridge characteristics at a number of different sites off the West Coast of Newfoundland (Johnston, 1999; Croasdale et al., 2000b).

#### **ICE LOADS ON ACTUAL OFFSHORE STRUCTURES**

The objective of this program is to carry out, obtain, and analyze large-scale measurements of ice loads on structures. In addition, results from past programs of ice-load measurements are compiled and analyzed to develop a comprehensive understanding of ice loads, and the factors that affect ice loads.

Work in this project covers a wide range of activities, all focused at full-scale ice loads and developing an understanding of the loads, and factors affecting the loads. This project has funded full-scale measurements on the Confederation Bridge (Brown et al., 1999; Kubat et al., 2000), and the development of a comprehensive collection of all available measurements of ice loads on offshore and coastal structures. This was done as part of a Joint Industry Project, which led to the development of the NRC Ice Load Catalogue (Timco et al., 1999). The Regulatory Codes used for structural design have been reviewed with an emphasis on the ice loading aspects through a comparison of different international codes (Tseng et al., 1998) and a focused review of the application of codes for Grand Banks development (Allyn et al., 2000). Also, a number of University Professors have been funded to investigate more fundamental aspects of ice loads and their origins.

#### **SUMMARY AND CONCLUSIONS**

This paper has presented a very brief overview of the work carried out for the Canadian PERD Program and managed by the CHC/NRC. The majority of the research is publicly available

and can be obtained by interested parties by downloading the files and datasets from the Cold Regions Technology Section of the CHC web site ([www.chc.nrc.ca](http://www.chc.nrc.ca)). The reports are formatted in Adobe Portable Document Format *pdf* and the databases are based on Microsoft Access platform (*mdb* or *mde*). The available reports and databases are indicated in the references. The web site is kept up-to-date with new reports, as they become available.

The work funded by PERD in the area of ice/structure interaction has led to significant advances in the understanding of ice load levels, and the factors affecting these loads. The research has been very focused and balanced between the needs of Industry and Government Regulators. It has had a significant impact in the development of the Canadian offshore petroleum resources.

## REFERENCES

AINA (1999): Arctic Technology Preservation Project Bibliographic Database. PERD/CHC Report 35-54. [AINA99.pdf](#)

ALLYN N. ET AL. (2000): The Use of Codes for Ice Loads on Structures on the Grand Banks. PERD/CHC Report , [GB\\_codes00.pdf](#)

BARKER A., SKABOVA I., TIMCO G. (1999): Iceberg Shape Visualization. PERD/CHC Report 20-44. [Iceberg\\_visual99.pdf](#); various [.avi files](#).

BROWN T. ET AL. (1999): Year Two of the Confederation Bridge Ice Monitoring Program. Proceedings OMAE99, Paper OMAE99-1171, St. John's, Nfld., Canada.

CANATEC ET AL. (1999): Compilation of Iceberg Shape and Geometry Data for the Grand Banks Region. PERD/CHC Report 20-43, [Berg\\_shapes99.pdf](#); [3diceberg1.mde](#)

C-CORE (1998): An Assessment of Current Iceberg Management Capabilities. PERD/CHC Report 20-33. [Manage98.pdf](#)

COMFORT G. (1998): Investigation of Techniques for Continuously Profiling Ice Features. PERD/CHC Report 5-91. [Profiler98.pdf](#).

CROASDALE ET AL. (2000a): Iceberg Scour and Risk in the Grand Banks Region. PERD/CHC Report, [Scour00.pdf](#)

CROASDALE ET AL. (2000b): Field Study of the Ice Characteristics off the West Coast of Newfoundland. PERD/CHC Report 2-70. [WNFLD\\_00.pdf](#)

CSR (2000): Techniques for Determining the Maximum Draft of Icebergs. PERD/CHC Report, [Max\\_Draft00.pdf](#)

FLEET & AGRA/SEABORNE (1998): PERD Iceberg Database for the Grand Banks Region, PERD/CHC Reports 20-36 and 20-40. [Iceberg98.pdf](#), [Iceberg99.pdf](#), [PERD\\_Iceberg99.mdb](#)

FLEET & MARINEERING (1999): Evaluation of Ice Model Test Data for Moored Structures. PERD/CHC Report 26-195. [Model\\_stat99.pdf](#)

- FLEET & SMS (2000): Techniques for Measuring Global Loads on the Terra Nova FPSO. PERD/CHC Report, [FPSO\\_moor00.pdf](#)
- FREDERKING R., TIMCO G., REID S. (1999): Sea Ice Floe Impact Experiments. PERD/CHC Report 8-96. [Impact99.pdf](#)
- JOHNSTON M. (1999): Field Study of Ice Characteristics off the Western Coast of Newfoundland. PERD/CHC Report 2-67. [WNfld\\_field99.pdf](#)
- JORDAAN I., PRESS D., MILFORD P. (1999): Iceberg Databases and Verification, PERD/CHC Report 20-41, [MUNverif99.pdf](#); [municebergs.mdb](#)
- KUBAT I., FREDERKING R., HAYAKAWA T. (2000): Response of the Confederation Bridge to Ice Action. Proceedings CSCE Conference (in press), London, Ont., Canada. [Tilt\\_M00.pdf](#)
- PILKINGTON R., HILL C., LANGFORD C. (1997): A Review of the Environmental Conditions on the West Coast of Newfoundland. PERD/CHC Report 20-34. [WN\\_can97.pdf](#)
- ROGERS B. ET AL. (1998): DynaMAC: Molikpaq Ice Loading Experience. PERD/CHC Report 14-62. [Dynamac98.pdf](#)
- SAYED M., FREDERKING R., BARKER A. (1999): Numerical Simulation of Pack Ice Forces on Structures: A Parametric Study. PERD/CHC Report 9-80. [Num\\_sim99.pdf](#)
- SPENCER P. ET AL. (1998): Ice Regimes off the West Coast of Newfoundland. PERD/CHC Report 20-35. [WN\\_Sand98.pdf](#)
- TIMCO G. (1998): NRC Centre for Ice Loads on Offshore Structures. PERD/CHC Report 35-51. [NRC\\_Centre98.pdf](#)
- TIMCO G., JOHNSTON M., FREDERKING R. (1999): The NRC Ice Load Catalogue. Proceedings POAC'99, Vol. 1, pp 444-453, Helsinki, Finland. [NRC\\_ILC99.pdf](#)
- TSENG J. ET AL. (1998): Comparison of International Codes for Ice Loads on Offshore Structures. PERD/CHC Report 11-20. [codes98.pdf](#)
- TULL E. (1999): Cataloguing of Northern Petroleum Industry Reports. PERD/CHC Report 35-55. [UCreport99.pdf](#)
- WRIGHT B. (1998a): Ice Problems Related to Grand Banks Petroleum Fields. PERD/CHC Report 20-6. [Problems98.pdf](#)
- WRIGHT B. (1998b): Moored Vessel Stationkeeping in Grand Banks Pack Ice Conditions. PERD/CHC Report 26-189. [WR\\_stat98.pdf](#)
- WRIGHT B. (1999): Evaluation of Full-scale Data for Moored Vessel Stationkeeping in Pack Ice. PERD/CHC Report 26-200. [Full\\_stat99.pdf](#)



## ICE LOADS ON MULTI-LEGGED STRUCTURES IN ARCTIC CONDITIONS

M.G. Gladkov<sup>1</sup>

### ABSTRACT

Home and foreign recommendations on determining ice loads imposed on multi-legged structures are considered, a refined method of calculating the loads mentioned is suggested. Proceeding from calculations of ice loads acting on a four-legged platform typical for the oil production field in Cook Inlet, prospects of the construction of multi-legged platforms in Russian arctic regions, in particular on the North-eastern shelf of Kolguev Island are estimated.

### INTRODUCTION

In the light of the task raised for the Russian science and industry in the field of constructing ice-resistant structures to develop oil and gas discoveries on the arctic shelf, the long-term experience of successful operation of oil-process multi-legged steel platforms in Cook Inlet (Alaska) cannot be disregarded. The present research objective has been estimating feasibility of multi-legged platforms construction in arctic regions on the basis of the analyses of ice conditions within the oil field on the North-eastern shelf of Kolguev Island and calculations of ice forces acting on a platform typical for Cook Inlet used as the analog. The region to the North - eastern from Kolguev Island is chosen as being nearest to Cook Inlet in its rather moderate ice regimes.

The support block of one of three similar oil platforms in operation in Cook Inlet since 1966 is shown in Fig.1. All the platforms are designed with extreme (of 1 to 100 years' probability) total load of 21.2 MN (Bhat & Cox, 1996). The value is obtained from multiplying a load due to crumpling warm even ice (of thickness 0.65 m and surface temperature - 3°C) with one leg by the multiple of  $K_p=2.83$  and coefficient of  $K_s=2$  (Blenkarn, 1970).

---

<sup>1</sup> B.E.Vedeneev VNIIG, St. Petersburg, Russia, fax: 535-67-20, e-mail: uugidro@gidro.odusz.electra.ru

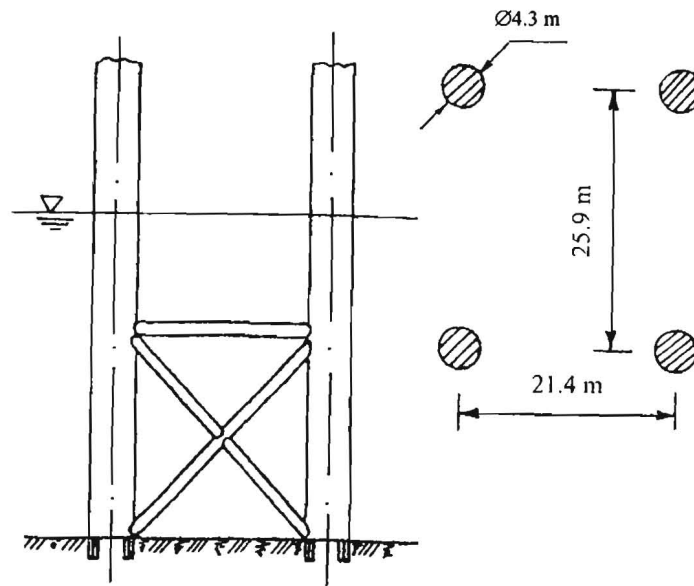


Fig.1. Support block of the oil platform (Anna) typical for Cook Inlet

#### METHOD FOR TOTAL LOAD ESTIMATION

Total ice load exerted on a platform is calculated by the equation

$$F_p = K_p K_s F_{b,p}. \quad (1)$$

The multiple  $K_p$ , showing by how many times the total ice load on a multi-legged platform exceeds the ice load from one leg is written as

$$K_p = n_i K_1 K_2. \quad (2)$$

where  $n_i$  denotes the quantity of legs in contact with ice;  $K_1$  is the factor of non-uniformity of ice (considering very low probability of equal ice strength near all the legs) established by equation

$$K_1 = \frac{1 + k_1 n_i^{-1/2}}{1 + k_1}, \quad (3)$$

Here  $k_1$  is the strength variation coefficient of ice under uniaxial compression accepted to be equal to 0.2;  $K_2$  is the factor considering the interference of neighbouring supports, it is calculated by the linear interpolation between values of 1 at  $d/a_p \leq 0.3$  and  $k_1/k$  at  $d/a_p = 1$ ,

where  $d$  is the width (diameter) of a support at the level of ice action,  $a_p$  is the projection of the distance between axes of any pair of neighbouring supports on the frontal plane of an ice field acting on the structure,  $k_n$  is the coefficient to consider non-full contact between ice and platform supports,  $k$  is the same but between ice and one support.

As concerns  $K_S = 2$  which is used in today's foreign practice (API RP 2N, 1992) to take account of probable increase in the maximum force of even ice at the expense of the formation of consolidated hummocks and stamukhas, and besides due to load dynamics (Blenkarn, 1970), it seems to be well-founded and the home Code of practice (SNiP, 1995) recommends the same coefficient  $k_r = 1,5$  to 2 for an arctic sea. So our calculations involve  $K_S = 2$ .

The load on a leg due to ice crumpling  $F_{b,p}$  is calculated by the improved Korzhavin formula (Gladkov, 1994) included into the Code of practice (SNiP, 1995):

$$F_{b,p} = mk_b k_v R_c b h, \quad (4)$$

where  $m$  is the shape coefficient of a platform support in plan;  $k_b$  is the coefficient of ice crushing;  $k_v$  is coefficient of ice deformation velocity;  $R_c$  is the strength characteristic of ice under compression;  $h$  is the design thickness of ice.

## RESULTS

Let the total ice load imposed on a four-legged platform in an oil production field on the North-eastern shelf of Kolguev Island be calculated with a structure assumed to occur under the most unfavourable (diagonal) action of extreme (from the viewpoint of its thickness and strength) even ice. The increase in ice load due to the formation of hummocks and dynamic effects will also be taken into consideration.

According to the existing Code of practice (SNiP, 1995) initial data are as follows:

- Maximum thickness of ice of 1% probability  $h = 1.2$  m.
- Speed of ice motion  $V = 0.2$  m/s.
- Mean temperature of ambient air in the period of largest ice loads (April)  $t_a = 7.1^\circ\text{C}$ .
- Temperature on the air (or snow) /ice interface  $t_u = -7.1^\circ\text{C}$ .
- Temperature on the water/ice interface  $t_b = -1.93^\circ\text{C}$ .
- Ice salinity  $s_i = 5.1\%$ .
- Quantity of supports interacting with ice  $n_i = 3$ .

Values of parameters involved into Eqs. 1 through 4 are the following:

- Coefficient of special non-uniformity of ice  $K_1$  calculated by Eq. 3 is equal to 0.93.
- Coefficient of interaction  $K_2$  of neighbouring supports of dimensions shown in Fig.1. is equal to 1.
- Coefficient of shape of a support in plan  $m$  is equal to 0.83 (as for a cylindrical leg).
- Coefficient of ice crushing  $k_b$  equals 2.9 at  $b/h = 3.6$ .

- Coefficient of ice deformation velocity  $k_v$  equals 0.3 when ice deformation velocity within the zone of ice-support interaction  $\dot{\epsilon}_e = 1.2 \cdot 10^{-2} \text{ s}^{-1}$ .

Strength characteristic of ice under compression  $R_C$  determined by the method (Gladkov, 1994) included into the Code of practice (SNIIP, 1995) as the value of ice strength under uniaxial compression averaged over ten layers of ice field at linear distribution of temperatures from  $t_u$  to  $t_b$ , given salinity  $s_i$  and trustworthy probability  $\alpha = 0.99$  is (0.67-1.08) MPa.

Eq. 4 yields the load on a leg of  $F_{b,p} = (2.4-4.0)$  MN. Total ice load on a platform as determined by equation 1 is  $F_p = (13.4-22.4)$  MN.

### CONCLUSION

The total ice load on the Anna type platform in the oil production field on the Northeastern shelf of Kolguev Island appeared to equal from  $F_p^d = 13.4$  MN to  $F_p^u = 22.4$  MN at trustworthy probability  $\alpha = 0.99$ . So calculated extreme load of ice  $F_p^u$  is in favourable agreement with the design value of 21.2 MN used for the platforms of the type indicated. Proceeding from these results we consider that from the point of view of their ice resistance the multi-legged platforms in operation in Cook Inlet are fully suited for the use in arctic seas with moderate ice regimes.

### REFERENCES

- BHAT SH.U., COX G.F. (1995): Ice loads on multi-legged structures in Cook Inlet. Proc. of the 13th Intern. Conference POAC-95, Murmansk, Russia, Vol. 4, pp. 51-61.
- BLENKARN K.A. (1970): Measurements and analysis of ice forces on Cook Inlet structures. Annu. Offshore Technol. Conference, Ind., Houston, Texas, Rep. No. OTS 1261, pp. 365-368.
- GLADKOV M.G. (1994): On determination of load from moving ice fields on vertical piles of hydraulic structures. Izvestia VNIIG B.E.Vedeneev, Vol. 228, pp. 21-25.
- Draft API RP 2N (1992): Planning, designing and constructing fixed offshore structures in ice environments. Official Publication of American Petroleum Institute, Washington.
- SNIIP 2.06.04-82\* (1995): Loads and Actions on Hydraulic Structures due to Wave, Ice and Ship Effects/ Minstroy Rossii - GP TsPP.



## CRUSHING FAILURE DURING DYNAMIC ICE-STRUCTURE INTERACTION

D.S. Sodhi<sup>1</sup>

### ABSTRACT

We discuss the results of medium-scale and small-scale indentation tests, which were conducted by pushing flat indentors against the edges of freshwater ice sheets. In these tests, we installed grid-based tactile pressure sensors at the ice-structure interface to measure the pressure generated during an interaction. The experimental data show that there is ductile deformation of ice at low indentation speeds and continuous brittle crushing at high indentation speeds. During a typical cycle of the dynamic ice-structure interaction at intermediate speeds, the tactile sensor data indicate that the ice deforms in a ductile manner during the loading phase, and fails in a brittle manner during extrusion phase. For continuous brittle crushing, theoretical estimates of global force are derived in terms of the average and the standard deviation of non-simultaneous local force per unit width. For high rates of indentation, we find the effective pressure measured during small-scale indentation tests to be close to those measured on full-scale structures.

### INTRODUCTION

Structures placed in an ice environment need to be designed and built strong enough to resist any ice action. The force required to fail an ice feature against a structure generally limits the interaction force resulting from a relative motion between them. An ice sheet may fail against a structure in bending, buckling, crushing, or a combination of these failure modes. During the full-scale ice force measurement program on the 110 m wide Molikpaq structure (Wright et al., 1986; Wright and Timco, 1994; Hardy et al., 1998), the observers recorded the modes in which the moving ice cover failed against the structure. They found that, although the ice crushing occurred during only 1 % of the observations, it caused some of the highest forces on the structure, which at times vibrated because of the interaction (Jefferies and Wright, 1988). In this paper, we restrict our discussion to the ice forces generated between a moving floating ice sheet and a structure. The objectives of this paper are to discuss the results of indentation

---

<sup>1</sup>U.S. Army Cold Regions Research and Engineering Laboratory, Hanover, NH, USA, 72 Lyme Road, Hanover, NH 03755, Tel.: +1-603-646-4267, e-mail: dsodhi@crrel.usace.army.mil

tests and to compare the effective pressure measured during those tests with the measured values of effective pressure on full-scale structures during brittle crushing.

#### **INDENTATION TESTS WITH TACTILE SENSORS**

As part of a five-year program involving laboratory and field tests in Japan, medium-scale indentation tests were conducted on sea ice in the harbor of Lake Noto, Hokkaido, by pushing a segmented indenter against the edges of floating ice sheets (Sodhi et al., 1998). Measurements on each 10 cm wide segment included forces in three directions and the moment about a horizontal line parallel to the indenter face. During the tests conducted from 1998 to 2000, grid-based tactile sensors were installed on the face of the segmented indenter to measure interfacial pressure during indentations at three speeds. The load cells and the tactile sensors provided data on the total interaction force, the actual contact area, and the magnitude of interfacial pressures. The tactile sensor data indicated both a "line-like" contact during high-speed (3 and 30 mm s<sup>-1</sup>) indentation tests, and a gradually enlarging contact area attributable to creep deformation of the ice during low-speed (0.3 mm s<sup>-1</sup>) indentation tests. The ductile-to-brittle-transition speed was between 0.3 and 3 mm s<sup>-1</sup> during these indentation tests. Masterson et al. (1999) report that the ductile-to-brittle transition took place at approximately 3 mm s<sup>-1</sup> during tests in which a feedback control hydraulic system was used to force spherical indentors into an ice wall. From these results, it appears that the transition takes place over a very narrow range of indentation speeds during interactions with rigid structures.

Sodhi (in review) recently conducted indentation tests by pushing flat plate indentors against the edges of freshwater ice sheets. The structure supporting the indenter plate was compliant, thus inducing dynamic ice-structure interaction during tests at a range of indentation speeds. The testing apparatus was the same as that used in earlier tests (Sodhi, 1991a), except that grid-based tactile sensors were installed at the ice-structure interface to measure the pressure generated as a result of the interaction. Besides obtaining magnitudes of the actual contact area and the ice-structure interfacial pressure, the tactile sensor data provide insights into the processes taking place during ice crushing at various indentation speeds. As in previous studies, there is ductile deformation of ice during low-speed indentation and brittle crushing during high-speed indentation tests. During intermittent crushing at intermediate indentation speeds, the results of this study confirm previous speculations (Sodhi, 1991b) that there is ductile deformation of ice during the loading phase and non-simultaneous brittle crushing during the extrusion phase of a dynamic ice-structure interaction cycle. This results in a saw-tooth pattern in the time-history plots of ice forces, and an intermittent advance of the structure into the ice at highly variable speeds that differ by one to two orders of magnitude. Sodhi (in review) provides more details on the test procedure and the results of this study.

#### **LOCAL AND GLOBAL ICE FORCES DURING BRITTLE CRUSHING**

It is evident from the indentation tests data (Joensuu and Riska, 1989; Sodhi et al., 1998; Sodhi in review) that the areas of high pressure during continuous brittle crushing events are narrow regions in the middle of an ice sheet, and that the ice fails non-simultaneously across

the width of a structure or an indenter. To include the correlation of non-simultaneous local forces with the forces generated in neighboring points, Dunwoody (1991) presented a model for non-simultaneous failure of ice across the width of a structure to estimate the global force from the local force per unit width. He considered the global force to be given by:

$$g(t) = \int_w f(x, t) dx, \quad (1)$$

where  $f(x, t)$  is the local force per unit width of a structure,  $x$  is the position of a point across the width of the structure,  $t$  is the time, and  $w$  is the width of the structure. The local force varies with respect to both time  $t$  at a point and position  $x$  at an instant in time. The variation of local force across the width as well as with respect to time depends on the number of contacts, the size of crushing zones, and the duration of the high-pressure zone at a point. Under the assumption that the ice failure process is the same across the width of the structure, the average local force per unit width  $\mu_{f(t)}$  is independent of the position of a point on the structure, implying the average global force  $\mu_{g(t)} = E[g(t)] = wE[f(t)] = w\mu_{f(t)}$ . Dunwoody (1991) assumed a spatial correlation function in terms of a negative exponential function:

$$R_{f(t)}(x_2 - x_1) - (E[f(t)])^2 = \sigma_{f(t)}^2 \exp\left(-\frac{|x|}{L}\right), \quad (2)$$

where  $R_{f(t)}(x_2 - x_1)$  is the auto-covariance function of the local force  $f(t)$ ,  $x$  is the distance between two points at  $x_2$  and  $x_1$  on the structure,  $\sigma_{f(t)}$  is the standard deviation of the local force  $f(t)$ , and  $L$  is a length parameter in the above equation to express correlation of forces over a distance and may be related to the size and density of the crushing zones. The variance of the global force (Dunwoody, 1991; Sodhi, 1998) is given by:

$$\sigma_{g(t)}^2 = 2L\sigma_{f(t)}^2 \left[ w - L \left\{ 1 - \exp\left(-\frac{w}{L}\right) \right\} \right]. \quad (3)$$

Assuming a Gaussian distribution for the global force  $g(t)$ , we can obtain an estimate of the maximum global force on the structure:

$$F_{\max} = \mu_{g(t)} + 3\sigma_{g(t)}, \quad (4)$$

where the factor 3 relates to a probability of exceedance equal to 0.0013 for a Gaussian distribution. Dividing both sides of Eq. 4 by the structure width  $w$  and the ice thickness  $h$ , we get the following expression for the relative pressure ratio  $A_r$  of maximum effective pressure to average local pressure:

$$A_r = \frac{P_{\max}}{\mu_{f(t)}/h} = 1 + 3 \frac{\sigma_{f(t)}}{\mu_{f(t)}} \sqrt{2 \frac{L}{h} \frac{h}{w} \left[ 1 - \frac{L}{h} \frac{h}{w} \left( 1 - e^{-\frac{w}{L}} \right) \right]}, \quad (5)$$

where  $\mu_{f(t)}/h$  is the average local effective pressure, and  $\sigma_{f(t)}/\mu_{f(t)}$  is the coefficient of variation of the local load per unit width.

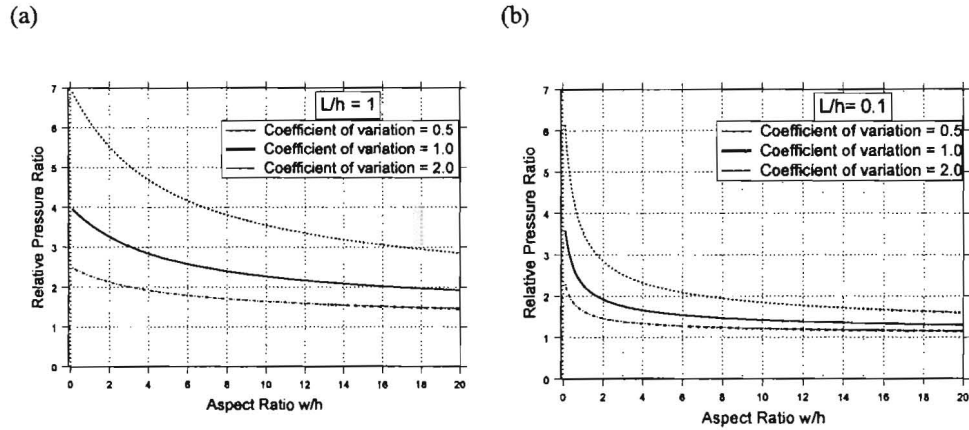


Fig.1. Plots of relative pressure ratio  $p_{max}h/\mu_{f(t)}$  versus aspect ratio  $w/h$  for three values of coefficients of variation and for: a)  $L/h = 1$  and b)  $L/h = 0.1$

Fig.1. shows plots of the relative pressure ratio  $A_r$  with respect to aspect ratio  $w/h$  for three values of the coefficient of variation ( $\sigma_{f(t)}/\mu_{f(t)} = 2.0, 1.0,$  and  $0.5$ ) and for two values of the ratio of correlation length to ice thickness ( $L/h = 1$  and  $0.1$ ). The plots in Fig.1. show a trend of decreasing relative pressure ratio with increasing aspect ratio. It is important to account for this effect when comparing the effective pressure from small-scale tests with those measured on full-scale structures, because of the higher effective pressure measured on narrow structures.

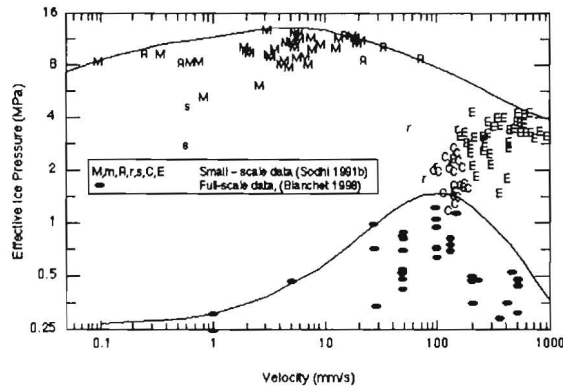


Fig.2. Plots of effective pressure measured on full-scale structures and during small-scale indentation tests with respect to ice drift velocity (from Blanchet, 1998 and Sodhi, 1991b).

### COMPARISON OF ICE FORCES MEASURED AT DIFFERENT SCALES

Fig.2. shows plots of effective pressure from small-scale indentation tests and full-scale measurements with respect to indentation rate, as presented by Blanchet (1998). Most of the small-scale data are from tests with a 50-mm-wide indenter, and some are from tests with a 100-mm-wide indenter (Sodhi, 1991a). The symbols in the plots of data in Fig.2. refer to the maximum and average effective pressure measured at particular times during small-scale indentation tests (Sodhi, 1991b). The small-scale data are in two groups: a high-pressure range from 8 to 14 MPa for low-speed indentation, and a low-pressure range from 1 to 4 MPa for high-speed indentation. Among the high-speed ( $>100 \text{ mm s}^{-1}$ ) indentation test data, the symbol 'C' in Fig.2. denotes the average pressure measured during continuous brittle crushing of ice, and these data can, therefore, be directly compared with full-scale data after taking into account the effect of aspect ratio. The aspect ratio during those indentation tests (Sodhi, 1991a) was in the range of 1.5 and 5.3, with an average value of 2.6. Assuming a ratio of  $L/h$  equal to 10, we find that the aspect ratio effect  $A_r = 1.82$  for a value of  $w/h$  equal to 2.6. If the effective pressures from small-scale tests are divided by a factor of  $A_r$  ( $=1.82$ ), we get the maximum effective pressure on a wide structure, and this results in a good agreement between the two sets of data shown in Fig.2.

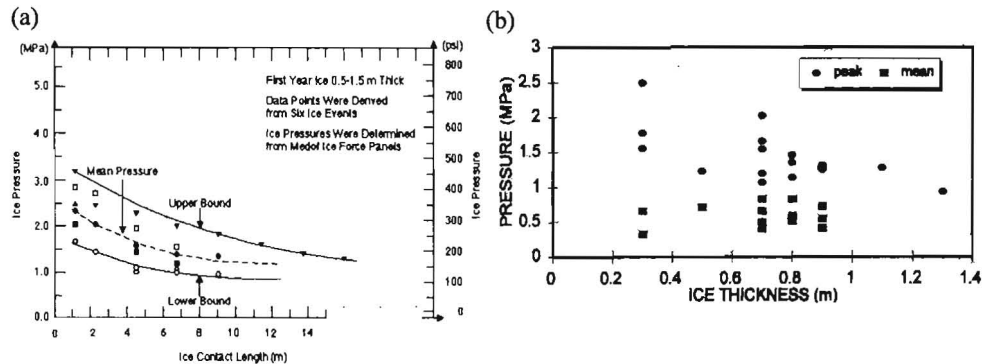


Fig.3. Plots of effective pressure measured at a) Tarsuit P-45 (from Wright et al. 1986), and b) Tarsuit P-45 and Amauligak I-65 (from Wright and Timco, 1994) locations

As shown in Fig.3., Wright et al. (1986) and Wright and Timco (1994) presented data on effective pressure measured at the Molikpaq structure during interactions with first-year level ice. Though the details of these measurements are not readily available, most of the data on crushing failure of first-year ice were obtained during ice drift speeds greater than  $100 \text{ mm s}^{-1}$  (Hardy et al., 1998). Because no severe structural vibrations were reported during those interactions, it appears that the ice failed in continuous brittle crushing. Thus, the comparison of full-scale data on effective pressure should only be made with small-scale data when ice fails in the brittle crushing mode, which is active during high-speed indentation tests.

Fig.4. shows plots of maximum effective pressure vs. aspect ratio from small-scale indentation tests at speeds greater than  $100 \text{ mm s}^{-1}$ . The data shown in this figure are from the recent indentation tests (Sodhi, in review), as well as from previous indentation tests conducted at CRREL during 1991-92 with segmented indentors (Sodhi, 1992 and 1998). In Fig.4., the effective pressure decreases with increasing aspect ratio, but it remains constant for aspect ratios greater than about 8. To relate effective pressure from small-scale tests to full-scale situations, we choose the data from tests with aspect ratios greater than 8. The effective pressure, measured during small-scale tests at high speeds and having high aspect ratio, is between 1.5 and 2.5 MPa. The range of pressure obtained during full-scale measurement and shown in Fig.3. is between 1 and 3 MPa. The ranges of the two sets of data being close to each other validates the idea of similarity of brittle crushing processes in small-scale and full-scale situations. This means that any scale or size effect on effective pressure during brittle crushing is absent.

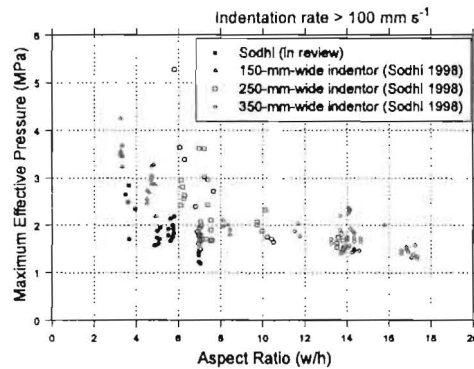


Fig.4. Plots of maximum effective pressure measured during indentation tests at indentation rates greater than  $100 \text{ mm s}^{-1}$  with respect to aspect ratio  $w/h$

## CONCLUSION

We review the results of small-scale and medium-scale indentation tests, in which grid-based tactile sensors were installed to measure interfacial pressure. The data indicate that there is ductile deformation of ice, resulting in the simultaneous generation of pressure across the indenter width during low rates of indentation, and brittle failure, leading to non-simultaneous generation of forces across the indenter width during high rates of indentation. At intermediate rates of indentation, the data show that there is ductile deformation of ice during the loading phase and brittle failure of ice during the extrusion phase of a dynamic ice-structure interaction cycle, resulting in a 'saw tooth' pattern in the time-history plots of the ice forces. Based on measurements of interfacial pressure with tactile sensors, we present a statistical method to estimate the global ice force on a structure in terms of the average, the standard deviation, and correlation length of the local force per unit width. Using this methodology, we derive the aspect ratio effect, which has been observed by many researchers from their indentation test results. Lastly, we compare the effective pressure measured during

small-scale indentation tests for brittle crushing with those measured on Molikpaq and other full-scale structures. We find a good agreement between full-scale data on brittle crushing and those from small-scale tests having high aspect ratios and the same indentation speed as in full-scale. This means that any scale or size effect on effective pressure during brittle crushing is absent.

## REFERENCES

BLANCHET D. (1998): Ice loads from first-year ice ridges and rubble fields. *Canadian Journal of Civil Engineering*, 25: pp. 206-219.

DUNWOODY A.B. (1991): Non-simultaneous ice failure. A report to Amoco Production Company, Tulsa, Oklahoma.

HARDY M.D., JEFFERIES M.G., ROGERS B.T., WRIGHT B.D. (1998): DynaMAC: Molikpaq ice loading experience. PERD/CHC Report 14-62, Kohn-Crippen, Calgary, Alberta, Canada.

JEFFERIES M.G., WRIGHT W.H. (1988): Dynamic response of Molikpaq to ice-structure interaction. In: *Proceedings, 7th International Conference on Offshore Mechanics and Arctic Engineering (OMAE)*, Houston, Texas, vol. IV, pp. 201-220.

JOENSUU A., RISKI K. (1989): Contact between ice and structure (in Finnish). Laboratory of Naval Architecture and Marine Engineering, Helsinki University of Technology, Espoo, Finland, Report M-88.

MASTERSON D.M., SPENCER P.A., NEVEL D.E., NORDGREN R.P. (1999): Velocity effects from multi-year ice tests. In: *Proceedings, 18th International Offshore Mechanics and Arctic Engineering Conference*, St. John's, Newfoundland, Canada, OMAE99/P&A1127.

SODHI D.S. (1991a): Ice-structure interaction during indentation tests. In: *Ice-Structure Interaction: Proceedings of IUTAM-IAHR Symposium*, Edited by S. Jones et al. Springer-Verlag, Berlin, pp. 619-640.

SODHI D.S. (1991b): Effective pressures measured during indentation tests in freshwater ice. In: *Proceedings, 6th International Cold Regions Engineering Specialty Conference*, Hanover, N.H., February 26-28, Edited by D.S. Sodhi. American Society of Civil Engineers Publications, New York, pp. 619-627.

SODHI D.S. (1992): Ice-structure interaction with segmented indentors. In: *Proceedings, 11th IAHR Symposium on Ice 1992*, Banff, Alberta, Canada, vol. 2, pp. 909-929.

SODHI D.S. (1998): Non-simultaneous crushing during edge indentation of freshwater ice sheets. *Cold Regions Science and Technology*, 27: pp. 179-195.

SODHI D.S., TAKEUCHI T., NAKAZAWA N., AKAGAWA S., SAEKI S. (1998): Medium-scale indentation tests on sea ice at various speeds. *Cold Regions Science and Technology*, 28: pp. 161-182.

SODHI D. S. (in review): Crushing failure during ice-structure interaction. *Engineering Fracture Mechanics*.

WRIGHT B., PIKINGTON G.R., WOOLNER K.S., WRIGHT W.H. (1986): Winter ice interactions with an arctic offshore structure. In: Proceedings, 8th IAHR Symposium on Ice, Iowa City, Iowa, vol. III, pp. 49-73.

WRIGHT B.D., TIMCO G.W. (1994): A review of ice forces and failure modes on the Molikpaq. In: Proceedings, 12th IAHR Symposium on Ice, Trondheim, Norway, vol. 2, pp. 816-825.



## NUMERICAL SIMULATION OF THE “KULLUK” IN PACK ICE CONDITIONS

A. Barker<sup>1</sup>, G. Timco<sup>1</sup>, M. Sayed<sup>1</sup>, B. Wright<sup>2</sup>

### ABSTRACT

Vessel stationkeeping in moving pack ice is an important issue for floating production systems that are being considered for use in ice-covered waters. In order to be effective, it is important that the loads generated by moving pack ice are within the range of the capabilities of their mooring systems. To better understand loads on moored vessels in ice, the full-scale data from the Kulluk, which was a floating drilling unit used in the Beaufort Sea, were analyzed and summarized for different conditions. A new two-dimensional model of ice-structure interaction was applied and compared to the full-scale Kulluk data. One base case was selected and a good correlation was obtained by adjusting the mechanical properties of the pack ice in the numerical model. The analysis shows that this model, with suitable calibration, can be used to predict loads on a moored vessel over a wide range of pack ice conditions, such as those found in the Grand Banks of Canada, the Pechora Sea or offshore Sakhalin in Russia.

### INTRODUCTION

The “Kulluk” was a conical drilling unit that was used for exploratory drilling in the intermediate to deeper waters (20-50 m) of the Beaufort Sea during the 1980’s and early 1990’s. It was designed as a “second generation” drilling system to significantly extend the open water season, by beginning drilling operations in the spring break-up period and continuing until early winter. It drilled twelve wells at a variety of locations.

During its deployment in the Beaufort Sea, it was exposed to a wide range of moving pack ice conditions. This is the only moored vessel, on a worldwide basis, that has stationkept in a “near full spectrum” of pack ice, from low concentrations of thin ice to high concentrations of rough first-year and multi-year ice. The loads on the mooring lines were monitored and this

---

<sup>1</sup> Canadian Hydraulics Centre, National Research Council, Ottawa, Canada, Building M-32, Montreal Road, Ottawa, Ontario, K1A 0R6, Tel.: (613) 990-2511, fax: (613) 952-7679, e-mail: anne.barker@nrc.ca

<sup>2</sup> B. Wright & Associates, Calgary, Canada

information provides a unique data set of the forces of a moored vessel in pack ice conditions (Wright, 1999).

Stationkeeping in moving pack ice is an important area of ice engineering in many different applications. For example, on the East Coast of Canada, the Terra Nova development will soon begin using a Floating Production Storage and Offloading (FPSO) system that will have to stationkeep, on occasion, in moving pack ice conditions. In other ice-covered regions such as the Beaufort Sea, the Pechora Sea and offshore Sakhalin, proposals have been considered to load tankers in moving pack ice conditions from offshore terminals. Thus, this topic has important implications in ice engineering for many ice-infested offshore regions.

The data from the Kulluk in the Beaufort Sea are extremely valuable and cover a wide range of ice conditions. However, the results are vessel specific and they do not cover the full range of situations that could be encountered in a moving pack ice scenario. A two-dimensional numerical model, which is based on a "Particle in Cell" approach, has been developed that can extend the range for predicting loads to other vessel shapes. In this paper, the loads on the Kulluk are briefly described. Then, the numerical model is briefly presented, and the results of different full-scale situations are presented.

#### FULL-SCALE KULLUK DATA

The Kulluk had deck and waterline diameters of 100 m and 70 m respectively, an operating draft of 11.5 m, and a displacement of 28,000 tonnes. It had a unique downward sloping circular hull which failed the oncoming ice in flexure at relatively low force levels, and an outward flare near its bottom, to ensure that broken ice pieces cleared around it and did not enter the moonpool or become entangled in the mooring lines (see Fig.1.). The vessel had a strong radially symmetric mooring that, in combination with its circular shape, provided an omni-directional capability to resist ice and storm wave forces. The mooring system was comprised of twelve 0.09 m wire lines and was capable of resisting relatively high ice forces. Ice management was a very important factor in enhancing the Kulluk's stationkeeping performance in ice. Typically, the Kulluk was supported by several CAC 2 icebreakers during its Beaufort Sea operations in heavy pack ice conditions. These icebreaking vessels broke the ice updrift of the Kulluk into small fragments, which were typically 10 to 30 m in diameter.

The loads on the mooring lines were measured during the Kulluk's deployment. Wright (1999) has summarized the loads and categorized them according to the ice conditions. Fig.2. shows a plot of the measured full-scale loads as a function of the ice thickness, for ice concentrations of 0.9 (i.e. 9/10<sup>th</sup> coverage) and higher. For this sub-set of the data, there was good ice management but relatively poor clearance around the Kulluk. In these situations, there was a "tightness" in the pack ice, which resulted in the formation of an updrift rubble wedge at the structure (see Fig.3.). Note that, although there is scatter, there is a definite trend of increasing load with increasing thickness. Wright has characterized the upper bound load  $L_p$  as a linear relationship with thickness  $h$  as (see Fig.2.):

$$L_p \text{ (MN)} = 0.86h \text{ (m)} + 0.91 \quad (1)$$

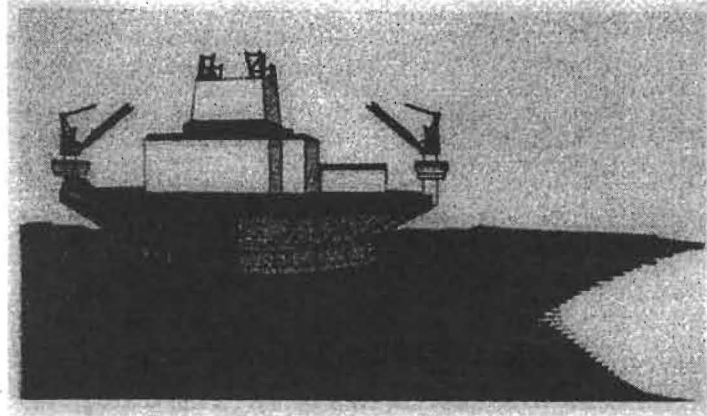


Fig.1. Illustration of the Kulluk showing its key design features

### NUMERICAL MODEL

The two-dimensional numerical model used in the present study was developed by Sayed et al. (2000). The model captures the salient features of several scenarios of ice-structure interaction. For example, ice thickness build-up and moving ice edges as well as the formation and evolution of leads can be simulated. The model also has the flexibility to include appropriate formulations of ice rheology such as the Mohr-Coulomb yield criterion. An overview of the main approach is given here. Details of the formulation of the model, however, cannot be adequately covered because of space limitations. For those details, see Sayed et al. (2000) and Barker et al. (2000).

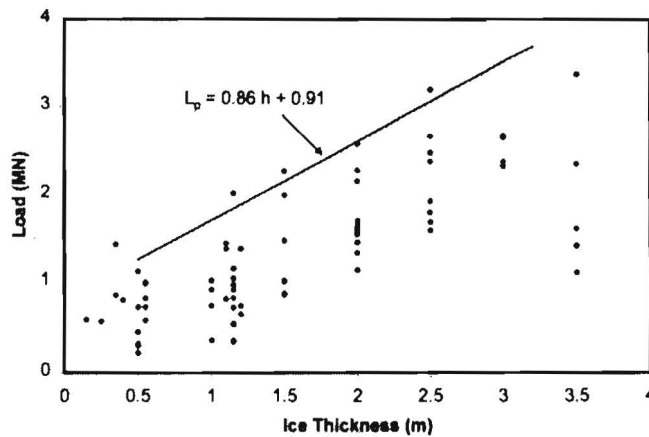
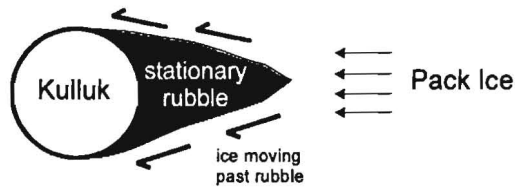


Fig.2. Measured loads on the Kulluk in tight managed ice with poor clearance and updrift rubble wedge (after Wright, 1999)



**Fig.3.** Schematic of updrift rubble wedge at Kulluk in tight pack ice  
(after Wright, 1999)

The main features of the model include a plastic yield rheology, a Particle-In-Cell (PIC) approach for ice advection, and an implicit solution of the governing equations. The behaviour of broken ice covers has always been considered to follow a cohesionless Mohr-Coulomb yield criterion. This intuitive assumption is based on the discrete nature of the ice cover and observations of deformation modes that resemble those of coarse granular materials. The idealized rigid-plastic rheology is implemented in the numerical model using a viscous plastic formulation (Hibler, 1979). For the cohesionless Mohr-Coulomb yield condition, material properties are expressed in terms of an angle of internal friction,  $\phi$ , which accounts for the frictional *strength* of the material. The numerical implementation of the viscous plastic model also includes a compressibility formula. That formula relates the mean normal stress (or pressure) to ice concentration (or aerial coverage). A parameter,  $P^*$ , is used to express the compressibility of the ice cover (see Sayed et al., 2000).

In the present model, according to the PIC approach, an ensemble of discrete particles represents the ice cover. Each particle has a volume, which remains constant. The area of each particle may be reduced, and the thickness accordingly increases, as pressure increases. This situation would correspond to increasing ice thickness. Thus, ice pile-up and ridging can be accounted for. Note that ice growth and decay are not a concern for the present problem.

The linear momentum and rheology equations govern the movement and deformation of the ice cover. Particles are individually advected in a Lagrangian manner. Therefore, a continuity equation is not needed. The linear momentum equations include the inertial terms, water drag, and gradient of the internal ice stress. The momentum and rheology equations are solved using an Eulerian (fixed) grid. The semi-implicit finite difference method of Zhang and Hibler (1997) is used.

#### **TEST CASE**

For the test case, records in tight, managed ice were extracted from the original Kulluk database into an Excel spreadsheet. For these cases, there was good ice management but poor clearance around the structure with the formation of a rubble wedge upstream of the structure (see Fig.3.). A base case was selected that had the following properties: mean ice thickness  $h$  of 1.5m, ambient ice drift speed  $v$  of 0.2m/s and local ice concentration  $c$  of 0.95.

Although several laboratory studies examined the properties of ice rubble, the results cannot be extrapolated to the larger scale of the present ice cover. Therefore, the values of material properties had to be determined by matching the numerical predictions and field observations of a well-documented case. Model performance is subsequently tested by comparing predicted peak loads, using those material properties under a range of conditions, to observations. Preliminary runs examined a range of values of the two parameters that determine material properties. From those runs, and previous results (Sayed et al., 2000), a value of 25 kPa for the compressibility parameter,  $P^*$ , was found to produce the appropriate behaviour. The runs also examined the influence of the angle of internal friction,  $\phi$ , on the predicted load. The resulting load on the vessel is plotted versus time for different values of  $\phi$  in Fig.4. The runs show that a  $\phi$  of  $27^\circ$  results in a good agreement between the predicted and measured peak loads (predicted peak load = 2.27 MN, and measured peak load = 2.20 MN).

Four other representative runs were performed, varying the velocity and thickness parameters, creating a small parametric study. The  $\phi$ ,  $P^*$  and concentration values remained the same throughout these runs. These test runs and their resulting peak loads may be found in Table 1.

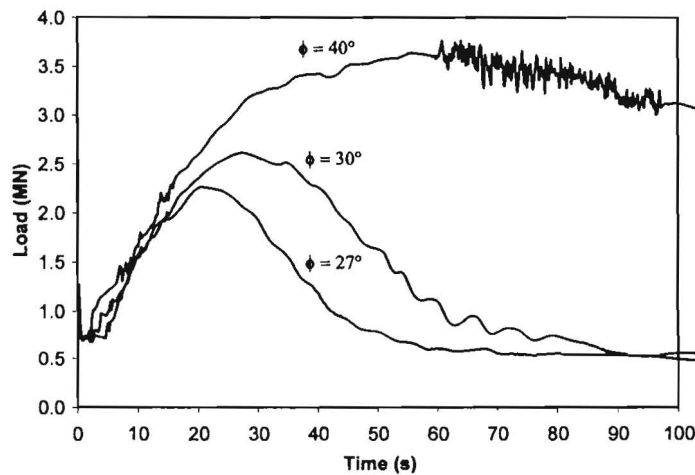


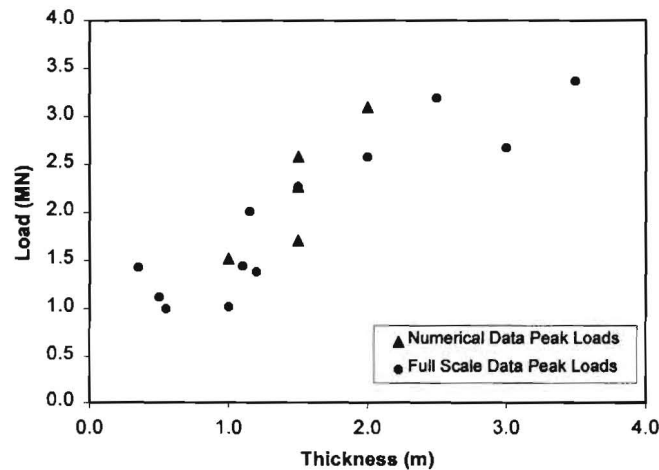
Fig.4. The effect of  $\phi$  on numerical peak load

Fig.5. shows the effects of ice thickness and velocity on the peak numerical load. Also plotted in Fig.5. are the full-scale peak loads for various ice thickness. There is a linear dependency of load upon thickness, similar to Fig.2. Also, the three data points at  $h = 1.5$  m represent three different velocities. In this case, the model shows a linear dependency upon velocity. This dependency is not observed in the full-scale data over the range of full-scale velocities and due to the scatter in the full-scale data. The model dependency occurs as a result of the momentum of the pack ice and produces a relationship where load increases with increasing velocity, as one would expect

**Table 1**

Numerical program input data and peak loads

	Velocity (m/s)	Thickness (m)	$\phi$ (°)	Concentration	Full-Scale Peak Load (MN)	Numerical Peak Load (MN)
Base case	0.2	1.5	27	0.95	2.20	2.27
Run1	0.2	1.0	27	0.95	1.77	1.52
Run2	0.2	2.0	27	0.95	2.63	3.10
Run3	0.1	1.5	27	0.95	2.20	1.71
Run4	0.3	1.5	27	0.95	2.20	2.58



**Fig.5.** Numerical load versus initial ice thickness, for  $\phi = 27^\circ$ ,  $c = 0.95$

The output from the numerical program simulations produces force-time data as well as ice thickness, concentration, pressure and velocity data at specific time steps. For example, Fig.6. shows a “snapshot” of the ice concentration around the Kulluk for the base case, 300 s after the start of the run. This can be compared to the schematic of the rubble wedge build-up around the Kulluk that was experienced in the field (Fig.3.), after Wright (1999).

**CONCLUSIONS**

The full-scale data that was examined was obtained from conditions involving tight, managed ice. The upper bound to the peak loads observed at the Kulluk in these conditions is defined by the equation  $L_p = 0.86h + 0.91$ , as developed by Wright (1999). The numerical model used for this study showed good agreement with the full-scale data. Using  $\phi = 27^\circ$ , a linear relationship was observed between thickness and peak load. A linear relationship with ice

velocity was found, but not indicated by full-scale data. Future analysis using this technique can be used to obtain information on loads on moored vessels for a wide range of conditions.

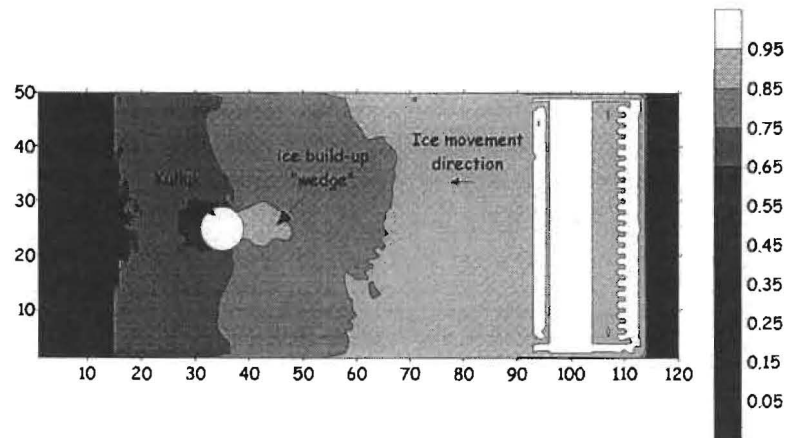


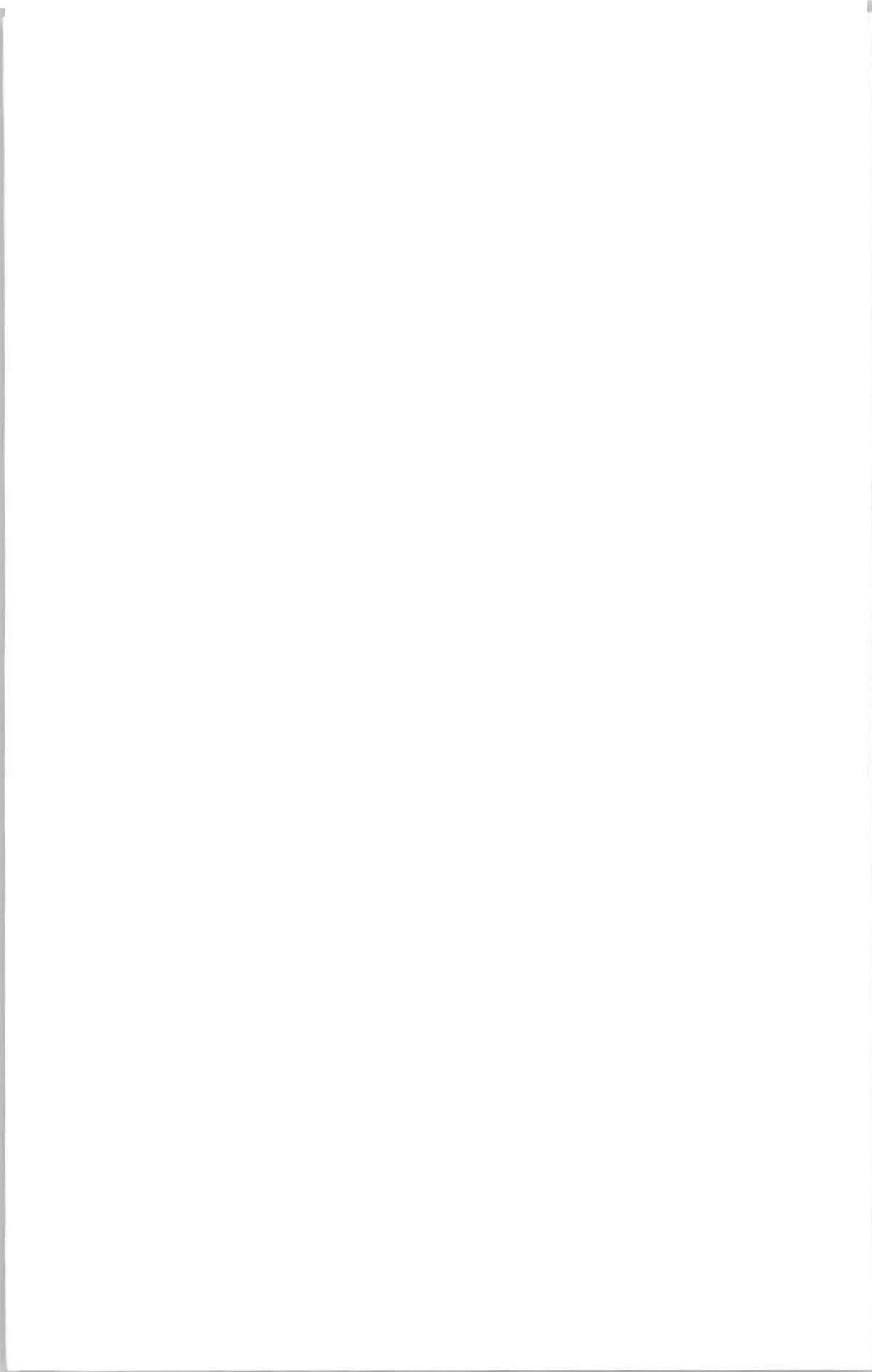
Fig.6. Ice concentration profile around Kulluk generated from a numerical simulation showing the ice build-up in front of the Kulluk

#### ACKNOWLEDGEMENTS

The authors would like to gratefully acknowledge the support of the Program on Energy Research and Development (PERD) in the funding of this project.

#### REFERENCES

- BARKER A., SAYED M., TIMCO G. (2000): Numerical simulation of the "Kulluk" in pack ice conditions. PERD/CHC Report HYD-TR-050, Ottawa, Canada.
- HIBLER W.D.III (1979): A dynamic thermodynamic sea ice model. *J. Physical Oceanography*, Vol. 9, No. 4, pp. 815-846.
- LU S., SHEN H.T. (1998): Constitutive laws for river ice dynamics. 14th International Symposium on Ice, ed. H-T. Shen, Potsdam, USA, Vol. 1, pp. 109-116.
- SAYED M., FREDERKING R.M.W., BARKER A. (2000): Numerical simulation of pack ice forces on structures: a parametric study. To appear in Proceedings of the 10th International Offshore and Polar Engineering Conference (ISOPE '2000), Seattle, USA, May 28-June 2.
- WRIGHT B. (1999): Evaluation of Full Scale Data for Moored Vessel Stationkeeping in Pack Ice. PERD/CHC Report 26-200, Ottawa, Canada.
- ZHANG J., HIBLER W.D.III (1997): On an efficient numerical method for modelling sea ice dynamics. *J. Geophysical Research*, Vol. 102, No. C4, pp. 8691-87.





## FAILURE OF THE EDGE OF AN ICE SHEET AGAINST A VERTICAL STRUCTURE

J. Tuhkuri<sup>1</sup>

### ABSTRACT

Characteristic to the brittle failure process of an ice sheet against a vertical structure is formation of discrete ice pieces and a line-like ice-structure contact. It is suggested that such a brittle ice edge failure is dominated by propagation of macrocracks, and should be analysed by using fracture mechanics. This approach is used to analyse field test data from a field program, where a 1.5 m wide structure was indented into a floating ice sheet.

### INTRODUCTION

Local ice loads are caused by failure of ice against a structure. Many different failure modes have been observed. In the microcracking mode, microcracks grow under applied load. If the load reaches a high enough level, the ice fails through coalescence of the microcracks to form pulverised ice. In this mechanism, the contact area between the structure and ice is large; of the order of ice thickness. The flaking mode, on the other hand, is characterised by absence of microcracks and transmission of the contact force through small areas of high pressure. In general, the microcracking mode dominates at low indentation velocities or at high temperatures when ice creeps, while at high velocities or at low temperatures ice responds in a brittle manner and fails through the flaking mechanism. However, it should be recognised that boundary conditions like confinement, also have a strong effect on the failure mechanism, as will be discussed below. (For a review, see eg. Daley et al., 1998.)

The scope of this paper is the brittle ice failure process. Joensuu and Riska (1989) were the first to observe that during brittle failure the ice-structure contact was a thin wavering line. This line-like contact was confirmed by attaching a window into an icebreaker (Riska, 1991). Similar observations have also been made by Gagnon (1991), Frederking et al. (1990), and Tuhkuri (1995). The search for explanation of the small contact area has led to different models (Daley, 1991; Gagnon, 1999; Jordaan and Xiao, 1998; Tuhkuri, 1996a). In the following, a set of results from the Medium Scale Field Indentation Tests (MSFIT) performed

---

<sup>1</sup>Helsinki University of Technology, Ship Laboratory, Espoo, Finland, P.O.Box 5300, FIN-02015 HUT,  
Finland, Tel.: +358-9-451-3509; fax: +358-9-451-3493, e-mail: jukka.tuhkuri@hut.fi

in Japan is analysed. More information of the tests and earlier analyses have been given by Takeuchi et al. (1997), Nakazawa et al. (1999), and Sodhi et al. (1998). This paper will concentrate on brittle ice failure. In lower indentation velocities, other failure modes were observed in the MSFI tests, but these are not discussed here.

#### FIELD DATA

The purpose of the MSFI tests was to investigate ice pressure and failure characteristics during indentation of a vertical structure into level ice. The test site was in northern Hokkaido in Notoro Lake, which is connected to the Sea of Okhotsk. The test analysed here was performed in February 4, 1999. During the test, a 1500 mm wide and 700 mm high indenter was pushed into a 168 mm thick ice sheet at a velocity of 3 mm/s. A novel feature of the tests was the use of thin pressure sensing panels which were attached to the indenter surface and they covered an area of 1440 mm by 440 mm. On that area there were 44 rows and 144 columns of pressure sensors, so the grid size of the sensors was 10 mm x 10 mm.

Fig.1. shows the measured total load. During the initial stage of the test, the load reached a value of 750 kN. After this peak, the load settled into a more or less constant level at about 100 kN. Fig.2a. and 2b. show examples of the pressure distribution during the initial stage and during the steady state failure, respectively. The high initial force is related with a wide contact area, while the steady state failure is characterised by a narrow contact area. After the test, the ice edge was cut into six vertical sections and lifted on the ice. Fig.3. shows sketches of the ice edge and shows a general wedge shape, but also that the edge had a step-like profile and that the ice sheet had several horizontal cracks.

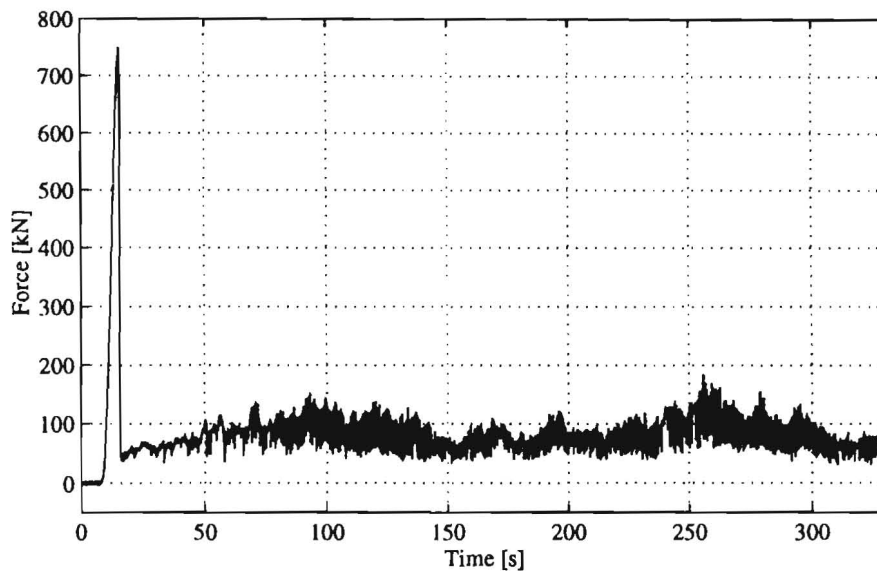


Fig.1. The load-time record during an MSFI test

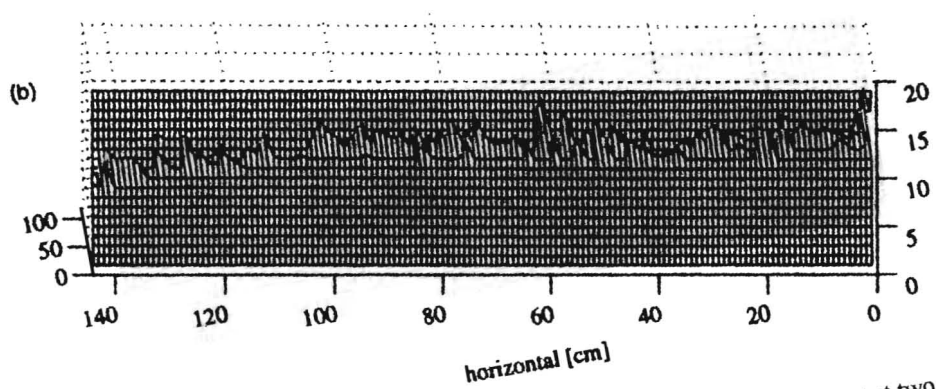
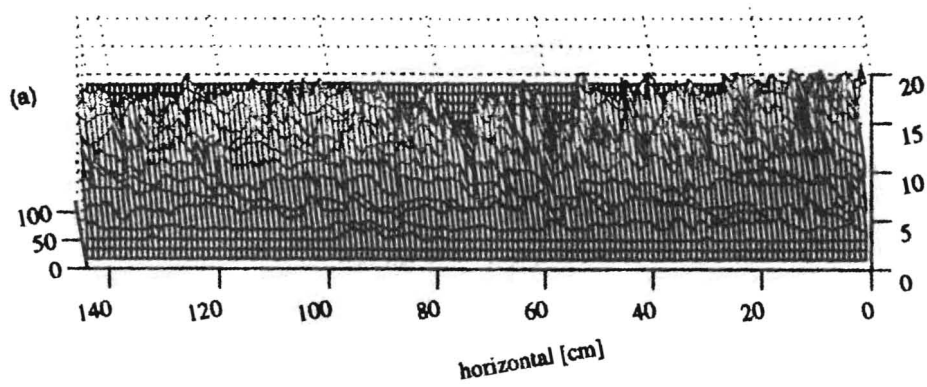


Fig.2. The pressure distribution at the ice-indentor interface during an MSFI test at two time instants: a)  $t = 14$  s, b)  $t = 150$  s. Results from a 200 mm high section of the pressure sensors is shown. Ice thickness was 168 mm. The pressure values are arbitrary.

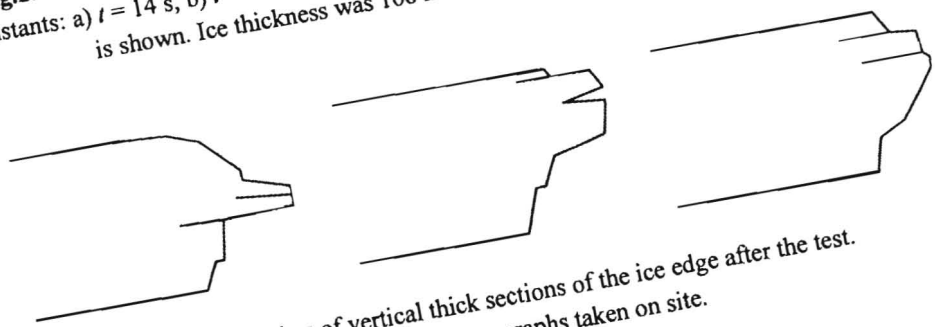


Fig.3. Sketches of vertical thick sections of the ice edge after the test. Drawn after photographs taken on site.

### MODELLING OF BRITTLE ICE EDGE FAILURE

During the indentation process described above, the ice failed into fragments. Two main models have been used to describe this process. It can be assumed that the ice fails through formation of cracks *within* the material. An alternative approach is to assume that the ice fails through formation of cracks at the ice-structure *interface*. Flaking belongs to the latter group and it has three stages: (i) initiation of a crack, (ii) propagation of the crack, and (iii) deflection of the crack to a free surface resulting into a flake. The crack initiation is not analysed here. It is simply assumed, following Cotterell et al. (1985) and Thouless et al. (1987), that surface cracks exist. Cotterell et al. considered a tool indenting a brittle body and assumed a Hertzian contact producing a partial cone crack that then extends and forms a flake. This is analogous to the assumption that ice is loaded only on a small area, i.e. that the ice-structure interface has some roughness.

The second stage of flaking, crack propagation, can be studied by using Linear Elastic Fracture Mechanics and the Boundary Element Method (BEM). Tuhkuri (1996a) has developed a model where a crack is assumed to propagate to the direction that minimises  $|K_I|$ . Fig.4. shows a model of an ice edge loaded with an indenter. A population of surface cracks is assumed. If Cracks 1 and 9 are inclined outwards they are open at their tips and have thus non-zero  $K_I$ . The other cracks will remain closed irrespective of their inclination. Therefore, for this crack population the one closest to a free edge will advance first. By simulating the growth of Crack 1 and reconfiguring the BE mesh, Tuhkuri (1996a) showed that Crack 2 will propagate rapidly after the first one, a third crack will follow the second one, and so on. Such a cascade of cracks will remove material from the ice edge and produce an irregular surface. The analysis showed further, that for a non-symmetric wedge, it is more probable that a crack propagates close the less steep side. In other words, a blunt wedge will get sharper.

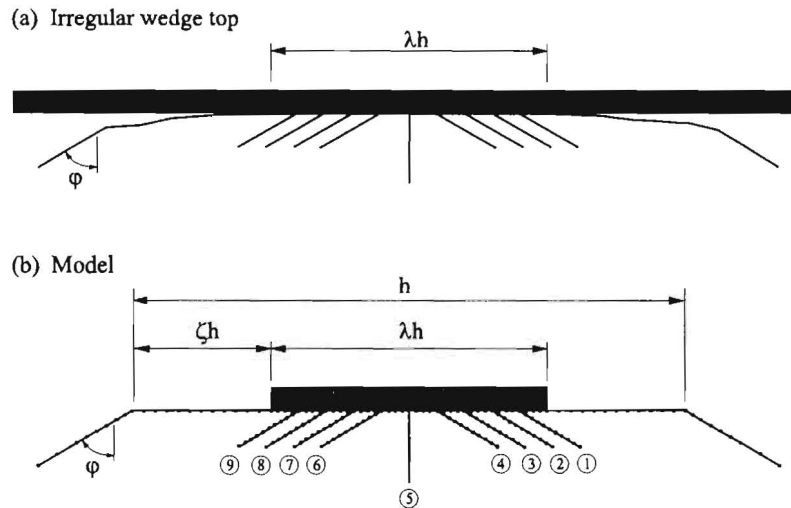


Fig.4. a) An irregular wedge top loaded by an indenter.  
b) An idealised model of the loaded wedge top.

The calculations proved also that the basic behavior of one crack can be captured by modelling that crack only. One of the key results then obtained was that a propagating crack does not deflect to the free surface to form a flake, unless there is a force component directed towards the free surface. Fig.5. shows results from BE analysis (Tuhkuri, 1996b). Similar results have been obtained experimentally by Cotterell et al. (1985) and Thouless et al. (1987). Thus, the third stage of a flaking process, deflection of the crack to a free surface to form a sharp flake, requires a force component directed towards the free edge. Such a force component may arise if the crack path is undulating. But even if the outward force component is zero, the partially formed flake can fail through buckling (Thouless et al., 1987).

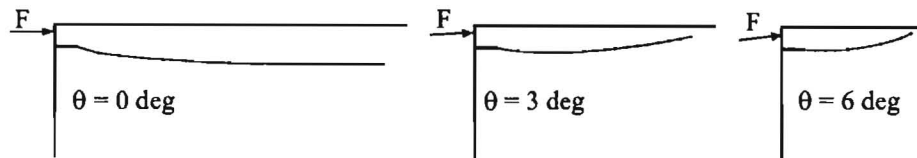


Fig.5. Calculated edge crack paths for three different inclinations of the force.

### COMPARISON OF EXPERIMENTS AND CALCULATIONS WITH DISCUSSION

The field test results introduced above can be summarised as follows:

1. The first load peak was connected with high loads and a wide pressure area (Fig.2a.).
2. The subsequent steady-state failure process was characterised with a lower load level and a narrow line-like contact area (Fig.2b.).
3. The ice edge, as studied after the test, had a step-like profile forming a wedge shape. Also horizontal cracks within the ice sheet were observed. (Fig.3.)

These results are in line with those obtained from the calculations and are discussed below.

The first assumption in the calculation model is formation of surface cracks at the ice-indentor interface. If such surface cracks do not form or they do not propagate, high loads are obtained. Tuhkuri (1995) has studied this problem in tests where ice blocks were broken against a structure. When the ice edge was flat, a similar load-time record than in Fig.1. was obtained with an initial peak followed by a steady-state process. During the initial loading microcracks formed within the ice and the load peak was connected with pulverisation of the ice. After that the ice edge was rough and the subsequent failure was a sequence of events reshaping the ice edge. But when the ice edge was initially wedge shaped with a  $90^\circ$  opening angle, the first load peak did not occur, and the steady-state fragmentation process initiated at the first contact. Importantly, the force level during the steady-state process was not affected by the initial ice edge shape.

It is probable that a similar chain of events occurred also during the MSFI test. At first the indentor hit a smooth ice edge and cracks formed within the ice until the crack density was so high that the ice pulverised and created a rough ice edge. Then the contact was through small irregularities in the ice. This contact type favors formation and propagation of surface cracks

and the failure can be analysed with the model shown in Fig.4. Characteristic to the process is that the flakes form in cascade and that for a non-symmetric wedge the flakes form from a less steep side. Therefore, the process can sustain itself, and that is reflected in the force-time record, in the wedge shaped ice edge, and in the contact pressure distribution during the steady-state failure process. The calculation model and the field observations also suggest that horizontal cracks will grow in the ice. Their existence is a sign that the load has been mostly horizontal. In addition, the step-like form of the ice edge is a natural result from the crack growth process. It is suggested that each step was formed when a partially formed flake broke off from the parent material.

A note on terminology can also be given. Above the flaking process was defined to have three stages: (i) initiation and (ii) propagation of a crack, and (iii) deflection of the crack to a free surface. It is usually presumed that a flake is sharp, and thus the deflection should be gradual. On the other hand, horizontal cracks in an ice sheet are often called cleavage cracks, and a flaking process and formation of cleavage cracks are considered as different processes. However, when ice failure is analysed as growth of cracks, these two processes are not very different: If the stage (iii) of a flaking process does not occur, a cleavage crack is obtained.

### CONCLUSIONS

This paper has discussed the results from MSFI tests in the context of brittle edge failure. This approach is different than the microcracking approach as it is assumed that the failure initiates from surface cracks. It was shown that the observed failure process can be modelled and analysed by considering the growth of one or a few cracks originating from the ice-structure interface. It is important to recognise, that crack propagation is a load releasing mechanism. This means that high loads are obtained when surface cracks either do not initiate or do not propagate. Further work should concentrate on studying the load required to drive the cracks and thus break the ice in different crack growth scenarios.

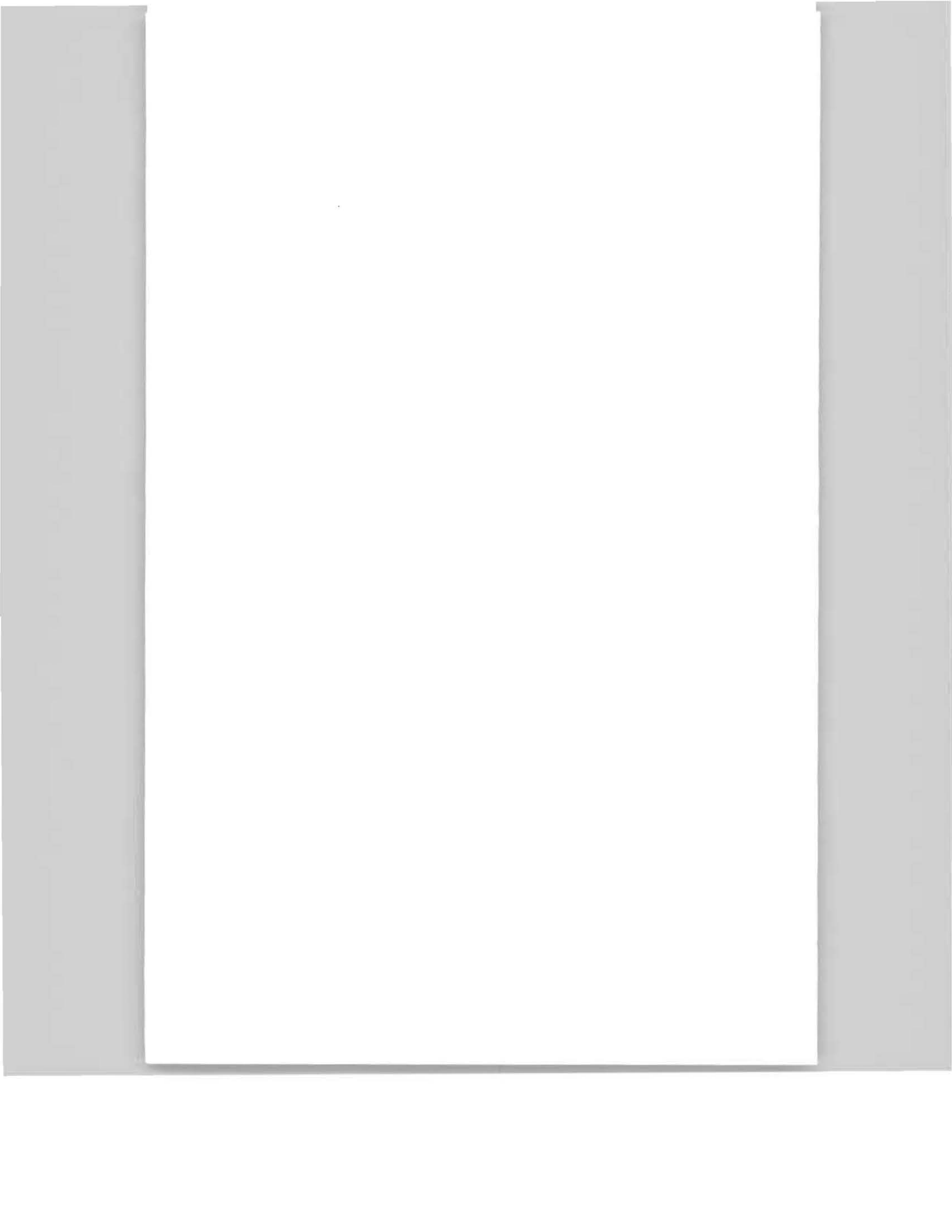
### ACKNOWLEDGEMENTS

I am grateful to Japan Ocean Industries Association (JOIA) for the opportunity to analyse the data from the MSFI tests. I am also grateful to Dr. Kaz Kato and Dr. Dev Sodhi for their help in dealing with the data. This work has been funded by the Academy of Finland.

### REFERENCES

- COTTERELL B., KAMMINGA J., DICKSON F.P. (1985): The essential mechanics of conchoidal flaking. *Int. Journal of Fracture*, 29: pp. 205-221.
- DALEY C. (1991): Ice edge contact, a brittle failure process model. *Acta Polytechnica Scandinavica, Me 100*, Helsinki, 92 p.
- DALEY C., TUHKURI J., RISKKA K. (1998): The role of discrete failures in local ice loads. *Cold Regions Science and Technology*, 27: pp. 197-211.

- FREDERKING R., JORDAAN I.J., MCCALLUM J.S. (1990): Field tests of ice indentation at medium scale. Hobson's Choice ice island, 1989. IAHR 90, Vol. 2, Espoo, pp. 931-944.
- GAGNON R.E. (1991): Heat generation during crushing experiments on freshwater ice. Physics and Chemistry of Ice, Hokkaido University Press, pp. 447-455.
- GAGNON R.E. (1999): Consistent observations of ice crushing in laboratory tests and field experiments covering three orders of magnitude in scale. POAC'99, Vol 2, Helsinki, pp. 858-869.
- JOENSUU A., RISKKA K. (1989): Contact between ice and a structure. Helsinki University of Technology, Ship Laboratory, Report M-88, 57 p. + App. (In Finnish).
- JORDAAN I.J., XIAO J. (1998): Compressive ice failure. IAHR'98, Vol 2, Potsdam, New York, pp. 1025-1031.
- NAKAZAWA N. ET AL. (1999): Medium scale field indentation test (MFIT). Rational evaluation of ice forces on structures, Ship Research Institute, Japan, pp. 264-279.
- RISKKA K. (1991): Observations of the line-like nature of ship-ice contact. POAC'91, Vol. 2, St. John's, pp. 785-811.
- SODHI D.S. ET AL. (1998): Medium-scale indentation tests on sea ice at various speeds. Cold Regions Science and Technology, 28: pp. 161-182.
- THOULESS M.D. ET AL. (1987): The edge cracking and spalling of brittle plates. Acta metall. mater., 35: pp. 1333-1341.
- TUHKURI J. (1995): Experimental observations of brittle failure process of ice and ice-structure contact. Cold Regions Science and Technology, 23: pp. 265-278.
- TUHKURI J. (1996a): Experimental investigations and computational fracture mechanics modelling of brittle ice fragmentation. Acta Polytechnica Scandinavica, Me 120, Helsinki, 105p.
- TUHKURI J. (1996b): Computational fracture mechanics analysis of flake formation in brittle ice. IAHR '96, Vol. I, Beijing. pp. 54-61.
- TAKEUCHI T. ET AL. (1997): Medium-scale field indentation tests: ice failure characteristics in ice-structure interactions. ISOPE'97, Vol II, Honolulu, pp. 376-382.





## DESIGN OF ARCTIC OFFSHORE PIPELINES TO RESIST THE FORCES FROM ICE RIDGES

P. Liferov<sup>1</sup>, O.T. Gudmestad<sup>2</sup>, S. Løset<sup>3</sup>, T. Mølmann<sup>4</sup>

### ABSTRACT

For design of offshore pipelines in the Arctic, problems related to ice scouring caused by moving ice ridges pose a design challenge in nearshore and shallow water areas. This paper discusses the major challenges and a new solution is presented, implying that the pipelines will be trenched to the depth of the keel of the ridges only, while the pipeline wall thickness will be increased to resist the forces caused by the soil deformation below the keels. This solution represents a large cost saving compared to deep trenching. Numerical examples are given that document that a 25 % increase in pipeline wall thickness will be sufficient for the Pechora Sea conditions.

### INTRODUCTION

Ice scouring of the seabed is among the main challenges for pipeline engineers in the Arctic. This is a widespread feature of most of the coastal regions of the northern continents and it poses a significant threat to offshore pipelines associated with offshore oil production facilities in the Arctic. Ice scouring is a phenomenon that occurs when an ice body (ice ridge or iceberg) moves while in contact with the seabed. Ice scouring is of great economic significance due to the possibility of damage to submarine pipelines. The main method of pipeline protection from drifting pressure ridge impact is its trenching or burial. The design of a marine pipeline in a shallow sea in the Arctic has therefore to define a trenching depth that will minimise the risk of pipeline damage by drifting ice. A hazard model for selecting the optimal trenching depth, which is based on long-term field observations, is likely to be coupled with a mechanical model in order to account for possible types of interaction between the ice ridge and the pipeline. Thus, for a well-founded choice of the optimum pipeline

---

<sup>1</sup> Barlindhaug Consult AS, Tromsø, Norway and St. Petersburg State Technical University, Russia  
N-9291 Tromsø, Norway; Tel.: +47 77 62 26 36; fax: +47 77 62 26 99; e-mail: pavel.liferov@barlindhaug.no

<sup>2</sup> Statoil, Stavanger, Norway

<sup>3</sup> Norwegian University of Science and Technology, Trondheim, Norway

<sup>4</sup> Barlindhaug Consult AS, Tromsø, Norway

trenching depth, it is necessary to know parameters associated with pressure ridges and soil interaction that is caused by stressing and deformation of the soil beneath the moving ice body.

## **SOME SPECIFICS OF THE PECHORA SEA**

### **Possible Pechora Sea field development scenarios**

Several fields in the Pechora Sea, offshore Northwest Russia, have the potential of being developed. The Prirazlomnoye field in water depths of 15-20 m is at present under development while the Dolginskaya field further north in 30-40 m water depth is being explored. Due to heavy ice cover up to 8 months a year, the fields in the area are likely to be developed by steel caissons resting on the sea floor (Gudmestad et al., 1999). Pipelines will bring the oil from wellhead platforms to processing platforms, and the developments may also be linked to onshore fields with pipelines. It should be noted that the water depth contour line of 20 m stretches north about 50 km from the shoreline.

### **Ice conditions in the Pechora Sea**

The Pechora Sea is characterised by its severe ice conditions. The area where oil production and loading facilities are planning to be installed is ice covered from 175 to 295 days a year (Løset et al., 1999). The maximum distance of landfast ice extension is about 15 km. The drifting ice is generally a medium thick first-year ice by the end of the winter season, or in extremely cold years, the ice may reach a thickness of 1.6 m. Second-year ice or multi-year ice has never been observed in this area. In the drift ice zone, the amount of ridges decreases away from the shear zone. Most sources report an upper limit of about 20 metres for the maximum possible keel depth of ice ridges (Løset et al., 1999). This is a limiting value determining the maximum water depth where pipelines have to be trenched. In the Pechora Sea this water depth corresponds to a distance of about 80 km from shore.

## **ICE SCOURING AND PIPELINE TRENCHING DEPTHS**

When considering the pipeline required trenching depth, the following two key questions should be answered:

1. What is the maximum expected scour depth?
2. What effects may possible subgouge deformations have on pipelines?

The depth and length of ice scour tracks can be estimated either by conducting detailed bottom surveys of the sea floor or by developing a theoretical model based on the mechanics of iceberg scour.

However, a pipeline trenched below the maximum gouge depth is not necessarily safe. Substantial subgouge deformations may in some instances extend to more than twice the gouge depth (Woodworth-Lynas et al., 1996). On the other hand, their effect on a pipeline may not be substantial enough to cause any serious problems for pipeline integrity. The task is therefore to estimate the influence of subgouge soil deformations and stressing on a pipeline and to evaluate its response. Another item that has to be considered is direct interaction between the ice ridge keel and the pipeline. Although straightforward calculations (Palmer et

al., 1990) indicates that the force required to cut one of the large gouges frequently seen in the Beaufort Sea is more than 10 MN, it is not a cause to exclude pipeline – keel interaction from the preliminary analysis. The requirement of safe interaction between ridge keel and pipeline may always be considered based on a quite low strength of the lower part of the keel compared to the strength of the pipeline.

## ICE RIDGE - SOIL - PIPELINE INTERACTION

### General idea

The effect of the gouging ice on a pipeline depends on the level of the pipeline with respect to the gouge, and on the deformation of the soil as the ice cuts the gouge (Palmer et al., 1990). Contact between the ice and the pipeline only occurs if the bottom of the free-floating ice is below the top of the pipe. If the pipeline located lower than that, damage is unlikely to occur, as it will be shown below.

### Pipeline - displaced soil interaction scenario

From the pipe point of view, the most important question is not how far down the gouging deformation extends, but whether their magnitude and type are dangerous for the pipeline.

In the process of scouring, the ice body scoops out a series of soil wedges in front of it. Below the bottom of the keel the ice passing over it drags the soil forward. When the keel passes the pipeline below, it is not absolutely obvious that the displaced soil below the keel carries the pipeline with it. Besides, the displaced soil may rather be fully compacted as it interacts with the pipeline and/or (depending on the level of soil deformations) passes over and/or below the pipeline. The interaction can be schematically represented as a fluid flow around the circular structure. This suggestion is based on the fact that the components of the system, i.e. the gouging ice ridge, the upper (active/displaced) layer of the seabed, and the buried pipeline have dimensions that are of the same order of magnitude approximately but with quite different mechanical characteristics. It is therefore reasonable to assume that the pipeline will not be displaced as much as soil does. Due to its large stiffness compared to that of the surrounding soil, the pipeline may only be stressed as a result of the soil displacement around (or partly around) it. This type of pipeline - soil interaction is schematically shown in Fig. 1.

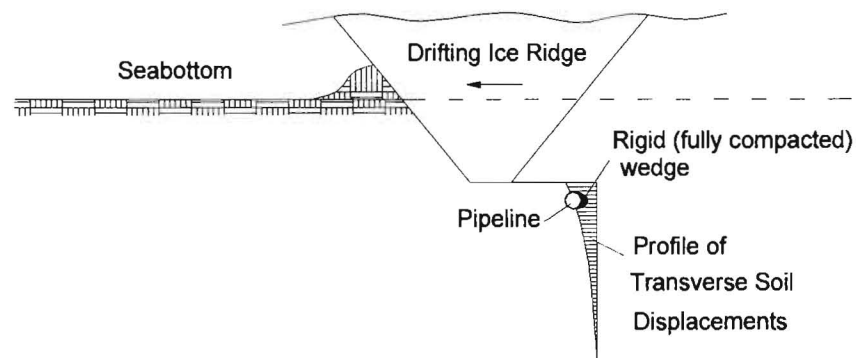


Fig. 1. Pipeline displaced soil interaction

A theoretical approach to confirm the current assumption can be based on a comparison of the energy required to displace the pipeline from its original position with the energy required to displace the soil in shear around the pipeline. It is likely that the system will tend to do as little work as possible while producing soil or pipeline displacement. In other words, the system will tend to follow by the way of the least resistance before it gets to a new static equilibrium. The work that has to be done in order to deform the pipeline elastically equals the work ( $W$ ) done by internal forces in the pipeline during its deformation. It may be expressed as:

$$W = -\int_0^l \frac{M^2 dl}{2EJ} - \int_0^l \frac{N^2 dl}{2EF} - k \int_0^l \frac{Q^2 dl}{2GF} \quad (1)$$

where  $M$ ,  $N$ , and  $Q$  are internal forces in the element of length  $l$ , and where  $E$  is the modulus of elasticity,  $F$  the cross sectional area,  $J$  the moment of inertia and  $G$  the modulus of elasticity in shear. It must also be mentioned, that the work of internal forces is always negative. For the case of pipeline bending we may neglect (in the first approximation) the effect of longitudinal and shear deformations and express the work of internal forces done on the displacement of a pipeline as:

$$W = -\int_0^l \frac{M^2 dl}{2EJ} \quad (2)$$

Based on the known characteristics of the pipeline and the soil, this work may be estimated. From the preliminary calculations it may be seen that the work to displace the soil around the pipeline is much less than the work required for pipeline bending. Therefore, the present problem may now be treated as a problem of additional pipeline stressing due to the soil displacements around it but not as a problem of significant pipeline displacement.

The pipeline has to withstand the stresses imposed by the ice crossing above it. Whether or not the pipeline will collapse under the stresses applied through the soil can be determined by the application of the lower bound theorem of plasticity (Prager, 1959). Fig.2. shows the pipeline trenched in a soil medium, in which the principal axes of stresses are in a plane perpendicular to the pipe axis, and the state of stress is described by the principal stresses  $q$  and  $r$ , (where compressive forces are positive);  $q$  is larger than  $r$ , and the third principal stress is intermediate. The stresses may be idealised to be uniform over a distance large compared with the diameter of the pipeline.

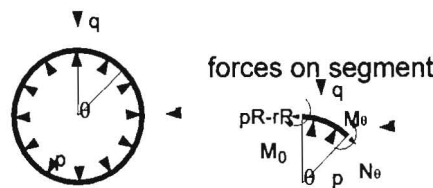


Fig.2. Stressed condition of a trenched pipeline

The limiting condition of the pipeline is (Palmer et al., 1990):

$$\frac{(q-r)R^2}{Yt^2} = 1 - \frac{1}{2}[(p-r)^2 + (q-r)^2] \cdot \left(\frac{R}{Yt}\right)^2 \quad (3)$$

which describes the combinations of  $p$ ,  $q$  and  $r$  which a pipe with wall thickness  $t$ , outer radius  $R$  and yield strength  $Y$  can withstand.

#### Direct impact interaction scenario

This type of interaction may conveniently be divided into three stages: pre-stressing, impact, and pull-over. It is also reasonable to suggest that maximum pull-over force on the pipeline will be limited by the ridge keel shear strength, as the ridge keel may split in shear while in contact with a pipeline. Whether a pipeline will remain static throughout the whole contact time or not, is not easy to predict. On one hand, the pipeline may bend in a similar way as it will behave under the pressure from a body with higher strength properties. However, the ice strength is much lower than that of steel and therefore the ice keel has to absorb more impact energy than the pipeline. The overall force  $T$  on a pipeline may not be larger than the mobilised shear resistance along the failure surface in the lower part of the ice keel, which can be expressed as:

$$T = \int_A \tau dA \quad (4)$$

where  $\tau$  is a maximum shear strength of the lower part of the ridge, and  $A$  is the area where shear resistance has been mobilised. The contact force  $T$  can be presented as a uniformly distributed linear load. The pipeline will, however, also be pre-stressed by the surrounding soil. The limit condition at which circumferential yield can occur may now be written as:

$$\frac{M_\theta + M'_\theta}{1/4Yt^2} = 1 - \left(\frac{N_\theta + N'_\theta}{Yt}\right)^2 \quad (5)$$

where  $N_\theta$ ,  $N'_\theta$  and  $M_\theta$ ,  $M'_\theta$  are circumferential membrane and bending stress resultants caused by soil stressing and ice pressure respectively.

#### NUMERICAL RESULTS AND DISCUSSION

Numerical calculations have been carried for some specific conditions of the Pechora Sea. Soil stresses are estimated based on the ice scour model (Chari, 1979) and the required pipeline wall thickness has then been estimated. An evaluated ratio between the pipeline wall thickness  $t$  and the soil stress differences  $q-r$  is presented in Fig.3. (the internal pressure is kept to a value of 15 MPa).

Stress differences exceeding 0.3 MPa are unlikely to occur under gouges in the Pechora Sea. It is therefore seen from Fig.3. that the pipeline wall thickness may have to be increased from about 16 mm (to resist the internal pressure) up to 20 mm for a 36 inch (914.4 mm) pipeline in

order to resist the forces caused by the soil deformation below the ice keels. In practice, a number of safety factors must be applied to this preliminary estimation and finally the pipeline wall thickness for the case given above may have to be increased up to 30 mm. The analysis can also be extended to show that under certain conditions the pipeline can theoretically withstand forces applied directly by the lower part of the ice keel to the area near the top of the trenched pipeline. The pipeline wall thickness for a 36 inch pipeline has then to be of about 25 mm (safety factors not accounted for).

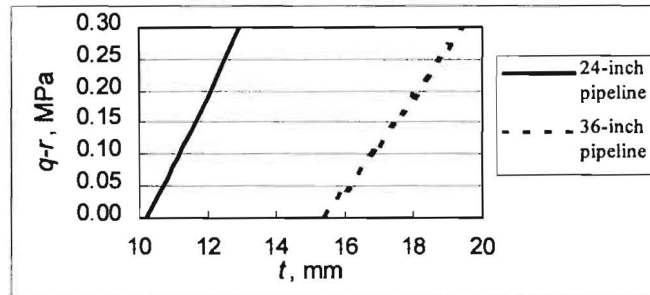


Fig.3. Ratio between the pipeline wall thickness and stress differences in the soil

### CONCLUSIONS

Submarine pipelines normally represent the most efficient way to transport hydrocarbons from offshore fields to onshore terminals or to onshore trunklines which can transport the hydrocarbons further to the market. The design of offshore pipelines has been given much attention and such pipelines can be laid and operated down to about 2000 m water depth. The major findings are as follow:

- Stress differences exceeding 0.3 MPa are unlikely to occur under gouges in the Pechora Sea.
- A pipeline with wall thickness increased from about 16 mm up to 20 mm for a 36 inch pipeline will resist the forces caused by the soil deformation below the ice keels.

The evaluation presented has only a preliminary character and has to be reviewed in more detail as well as being confirmed experimentally in a realistic project situation. The concept of increased wall thickness to resist soil deformations under gouges should be further analysed as the costs of increased steel thickness can be considerable less than the costs of extended trenching.

## REFERENCES

CHARI T.R. (1979): Geotechnical aspects of iceberg scours on ocean floors. Canadian Geotechnical Journal, v.16, N2, 1979. pp. 379-390.

GUDMESTAD O.T., ZOLOTUKHIN A.B., ERMAKOV A.I., JAKOBSEN R.A., MICHTECHENKO I.T., VOVK V.S., LØSET S., SHKHINEK K.N. (1999): Basics of Offshore Petroleum Engineering and Development of Marine Facilities - With Emphasis on the Arctic Offshore. Stavanger, Moscow, St. Petersburg, Trondheim, April 1999, 344 p.

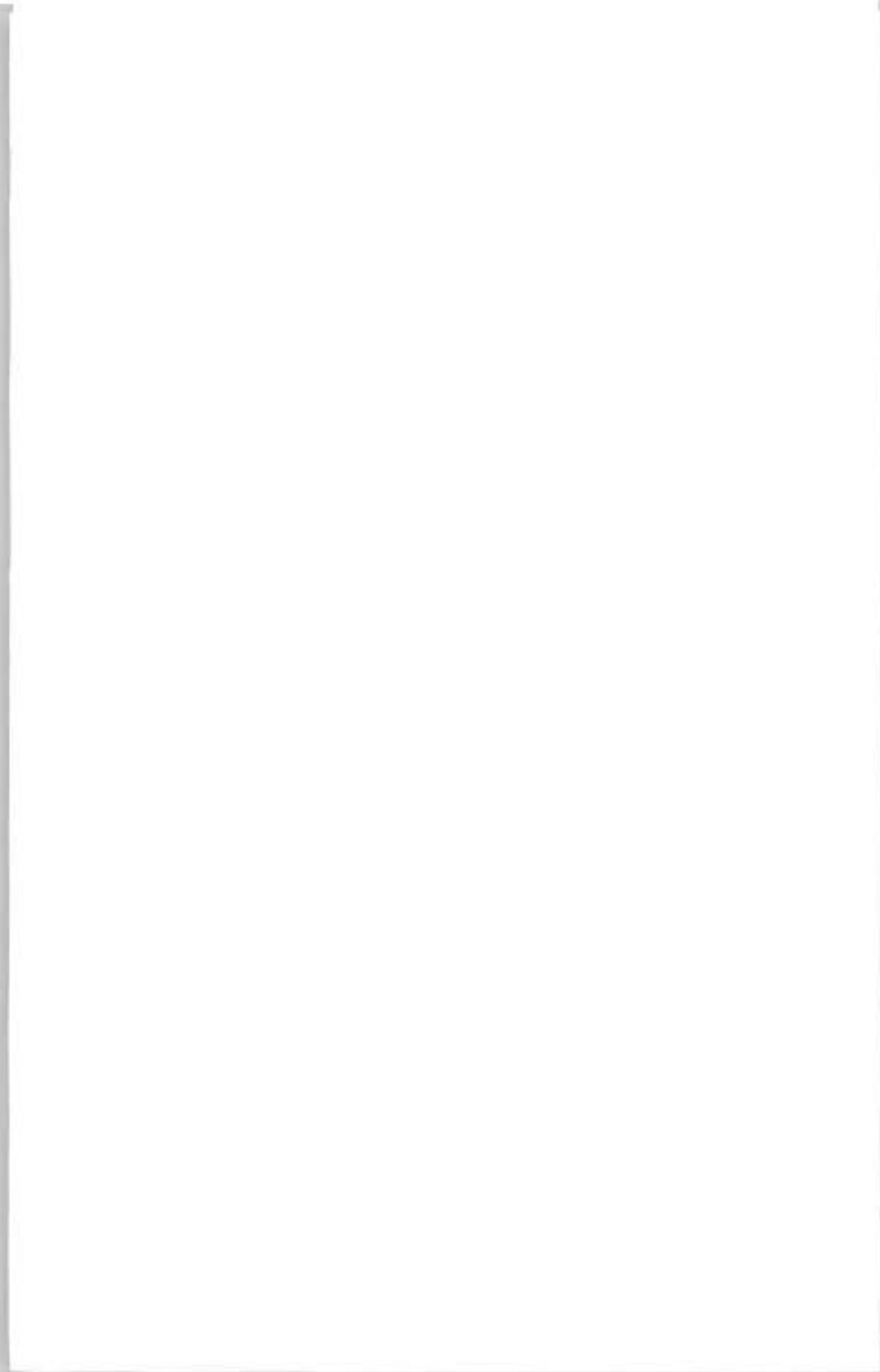
GUDMESTAD O.T., VOLDEN A., SKAER J. (1999): Fabrication issues for platforms to be installed in the Pechora Sea of the Russian Arctic Offshore. Proceedings of the Fourth International Conference on Development of the Russian Arctic Offshore (RAO-99), pp. 139-146.

LØSET S., SHKHINEK K.N., GUDMESTAD O.T., STRASS P., MICHALENKO E., FREDERKING R., KÄRNÄ T. (1999): Comparison of the physical environment of some Arctic seas, Cold Regions Science and Technology (29)3, pp. 201-214.

PALMER A.C., KONUK I., COMFORT G., BEEN K. (1990): Ice gouging and safety of marine pipelines. Proceedings of the 22th (1990) Annual Offshore Technology Conference, pp. 235-244.

PRAGER W. (1959): Introduction to plasticity. Addison-Wesley, 1959.

WOODWORTH-LYNAS C.M.L., NIXON J.D., PHILLIPS R., PALMER A.C. (1996): Subgouge deformations and the safety of Arctic marine pipelines. Proceedings of the 28th (1996) Annual Offshore Technology Conference, pp. 235-244.





## THE FACTORS CONTROLLING STATIC ICE LOADS ON DAMS

G. Comfort<sup>1</sup>, Y. Gong<sup>1</sup>, S. Singh<sup>2</sup>

### ABSTRACT

An eight-year field program was undertaken from 1991-92 to 1998-99 to: (a) measure the loads in the ice sheet near the dam ; (b) measure the load distribution between a gate and pier, and : (c) compare the loads on wooden and steel stoplogs. The most significant finding has been to identify the importance of water level changes on the resulting ice loads. Ice loads are much higher and more variable compared to purely thermal loads when significant, but not excessive, water level changes occur. The maximum measured line loads for these two cases are 85 kN/m and 374 kN/m, respectively. Preliminary analyses have shown that ice loads can be affected significantly by the reservoir shape when the reservoir sides are significantly softer than the dam.

### INTRODUCTION AND SCOPE OF PAPER

Ice loads exerted on hydro-electric dams are not well understood although dams have been built and operated for many years in northern climates. A field program was undertaken from 1991-92 to 1998-99 to: (a) measure the loads in the ice sheet near the dam; (b) measure the load distribution between a gate and pier, and : (c) compare the loads on wooden and steel stoplogs. Results are presented and analyzed in detail in Comfort et al. (1998a & 1999). The 1991-92 to 1995-96 results are summarized in Comfort et al. (1997 and 1998b) among other papers as well as in the annual field reports, which are available from the Canadian Electricity Association (CEA).

This paper is focussed on ice loads for dam safety analyses. The ice loads measured in the reservoir ice sheet are most applicable for this case. A companion paper describes methods that have been developed to predict the ice load (Comfort et al., 2000).

---

<sup>1</sup> Fleet Technology Ltd., Kanata, Canada, 311 Legget Drive, Kanata, Ont., Canada, K2K 1Z8  
Tel.: 613-592-2830; fax: 613-592-4950 ; e-mail: gcomfort@fleetech.com

<sup>2</sup> Newbridge Networks, Kanata, Canada

### ICE LOADS IN THE RESERVOIR ICE SHEET: MAXIMUM MEASURED LOADS

Probably, the most significant finding of the work to date has been to identify the importance of water level fluctuations on the ice loads produced. Ice loads are much higher and more variable compared to purely thermal loads when significant, but not excessive, water level changes occur (Tables 1 and 2 - see also Fig.1.).

**Table 1**

Thermal Load Database Summary (Negligible Water Level Changes Occur)

Site & Owner	Winter	Total No. of Events	No. of Events: Loads > 30 kN/m	Max Line Load (kN/m)
Paugan Dam (Hydro-Quebec)	1992-93	12	2	51
	1993-94	9	5	70
120 m by 60 m basin (Nat. Res. Council)	1992-93	10	3	46
Seven Sisters (Manitoba Hydro)	1996-97	9	6	64
Pine Falls Dam (Manitoba Hydro)	1996-97	8	6	60
	1997-98	7	3	43
McArthur Falls (Manitoba Hydro)	1998-99	7	7	85

**Table 2**

Combined Water Level Change/ Thermal Load Database  
(Significant Water Level Changes Occur)

Dam & Owner	Monitoring Period		No. of Events	Peak Load, kN/m (kips/ft)
	Winters	No. of Yrs.		
Arnprior (Ont. Hydro)	1992-93 to 1995-96	4	30	210 (14.3)
Otto Holden (Ont. Hydro)	1993-94 to 1995-96	3	17	65 (4.4)
Seven Sisters (Man. Hydro)	1995-96, 1997-98, 1998-99	3 <sup>1</sup>	15	374 (25.4)
Churchill Falls (Nfld. & Lab Hydro)	1998-99	1	15	80 (5.4)

<sup>1</sup> The 1996-97 data were not included in this database because water level changes were "small and slow" in 1996-97 (Fig.1.). The 1996-97 events at Seven Sisters were included in the thermal load database (Table 1).

### DEFINING SIGNIFICANT WATER LEVEL CHANGES

Although forebay level fluctuations follow a complex pattern, they can be divided as follows. It should be noted that the information presented here applies to ice that is about 0.3 to 0.7 m thick.

- steady reservoir drawdown - this breaks the ice away from the dam, producing low ice loads;

- a large one-time drop or rise (i.e., more than the ice thickness) - This will reduce ice loads if the ice does not refreeze strongly to the shore or dam. Large one-time drops reduced loads at:
  - (a) the Otto Holden dam – no more ice loading events occurred each year after the water level was lowered by 2 to 3 m in late February.
  - (b) the Seven Sisters dam - a large water level drop in early January, 1997 contributed significantly to the much lower ice loads measured there during the 1996-97 winter.
- cyclical water level changes – Their effect is related to the average water level frequency and amplitude, and they can be generally classified as follows (Fig.1. and 2.):
  - (a) “Small and Slow” – water level changes have a negligible effect, and the loads are primarily thermally-induced. This produces relatively low, quite uniform loads (Figure 1 and Table 1).
  - (b) “Large and Frequent” – This case produces low ice loads (Fig.1.) because these water level changes inhibit the formation of a strong bond between the ice and the dam. Hinge-shaped cracks are produced which prevent high ice loads from being developed at the dam.
  - (c) “Intermediate” – This causes the highest ice loads because these water level changes produce ice crack and ice cover conditions that greatly resist ice sheet movements (Fig.1.). The ice cracks produced are vertical, or near-vertical, with a great deal of new ice growth in them.

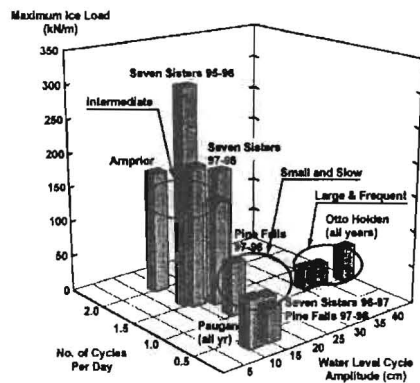


Fig.1. Ice Load Vs Water Level Changes

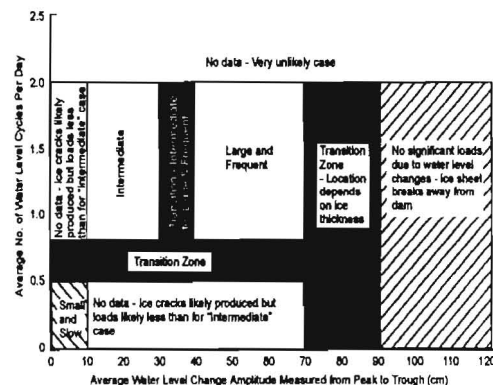


Fig.2. Water Level Change Regime Map

In view of the significance of water level changes, the following cases were analyzed separately.

- Case 1: Water Level Changes are Negligible – in this case, ice loads are generated thermally.
- Case 2: Combined Thermal/Water Level Regime – water level changes affect the ice loads significantly here. This case covers all other parts than “Small and Slow” (Fig.1. and 2.).

## REVIEW: THE ICE LOADING EVENTS AT THE SEVEN SISTERS DAM

These field data are of great interest because the highest loads have been measured here. As well, the loads have varied significantly from year to year, due to various factors (Table 3).

- 1995-96 and 1998-99-High loads (of 324 and 374 kN/m, respectively) were measured due to:
  - (a) Large ice temperature changes - 1998-99 and 1995-96 were the two coldest winters and they produced the largest maximum ice temperature profile area changes (Table 3).
  - (b) Forebay level changes – Water level changes were in the “intermediate” range which causes high ice loads. As well, the forebay was cycled within a narrow range over the whole winter.
- 1996-97 - The maximum line load (i.e., 62 kN/m) was much less than those for 1995-96 and 1998-99, despite the fact that 1996-97 was a relatively cold winter as well. The much lower loads in 1996-97 can be traced to two differences in water level fluctuation patterns:
  - (a) a large one-time drop occurred near the start of the winter which broke the ice free from the dam. This may have created a “hinge” mechanism that would relieve ice loads (Fig.3.).
  - (b) water level fluctuations were in the “Small and Slow” category which does not produce significant ice loads due to water level fluctuations (Fig.1.).

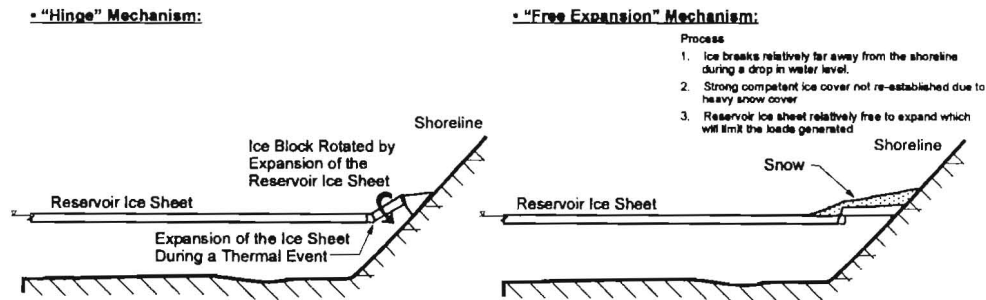


Fig.3. Hinge Mechanism Created by a Large One-Time Drop in Water Level

- 1997-98 - the maximum line load (i.e., 199 kN/m) was also much less than those for 1995-96 and 1998-99. This is mainly due to the fact that 1997-98 was a mild winter, as water level fluctuation patterns in 1997-98 were generally similar to those in 1995-96 and 1998-99.

Table 3

## Summary Of Results At The Seven Sisters Dam

Ice Loads	Air & Ice Temp.	Water Level Changes	
<b>1995-96 winter</b>			
Very high loads measured Max. Load = 324 kN/m	Cold winter - Large ice temperature changes Max profile area change = 445 °C*cm	Drop in early winter ? Fluctuation amplitude Fluctuation frequency Fluctuation pattern	No +/- 5 to +/- 7.5 cm Peaked every 12 to 24 hours Quite regular
<b>1996-97 winter</b>			
Low loads measured: Max. load = 62 kN/m	Cold winter - Large ice temperature changes Max. profile area change = 351 °C*cm	Drop in early winter ? Fluctuation amplitude Fluctuation frequency Fluctuation pattern	Yes - 45 cm over Jan. 3-6, 1997 +/- 5 to +/- 10 cm Peaked roughly every 4 days Irregular
<b>1997-98 winter</b>			
Lower loads measured Max load = 199 kN/m	Warm winter - small ice temperature changes Max. profile area change = 92 °C*cm	Drop in early winter ? Fluctuation amplitude Fluctuation frequency Fluctuation pattern	No +/- 7.5 to +/- 12.5 cm Peaked every 12 to 24 hours Sometimes irregular
<b>1998-99 winter</b>			
Very high loads measured: Max load = 374 kN/m	Cold winter - Large ice temperature changes Max. profile area change = 448 °C*cm	Drop in early winter ? Fluctuation amplitude Fluctuation frequency Fluctuation pattern	No +/- 7.5 to +/- 10 cm Peaked every 12 to 24 hours Sometimes irregular

This comparison shows that:

- (a) very high ice loads will develop if large ice temperature changes occur in combination with "Intermediate" forebay level changes. This occurred twice (in 1995-96 and 1998-99) with the same result (regarding the loads produced) which adds reliability to the measured results.
- (b) effect of ice temperature vs water level changes - in 1997-98, significant ice loads (i.e., >150 kN/m (10 kips/ft)) occurred due to the effects of "intermediate" water level change patterns despite the much smaller ice temperature changes in that winter (than 1995-96 and 1998-99).
- (c) the ice loads will be greatly reduced if forebay level fluctuations follow the pattern that took place in 1996-97. Although large ice temperature changes also occurred in 1996-97, the water level change pattern below more than "compensated" for this, which produced low loads.
  - (i) the water level was dropped significantly, and held there for the rest of the winter, and
  - (ii) subsequent water level fluctuations were in the "small and slow" range.

## EFFECT OF RESERVOIR SHAPE

### Introduction and Purpose of Analyses

The Arnprior and the Seven Sisters dams are the only ones where ice loads exceeding 150 kN/m (10 kips/ft) have been measured in the eight years of monitoring done to date. Higher maximum loads have been measured at Seven Sisters by about 2 (Table 2) despite relatively similar ice temperature and water level changes at each dam. The reservoirs at the Seven Sisters and Arnprior dams are "lake-shaped" and "river-shaped", respectively (Fig.4. and 5.). Preliminary finite element analyses were used to assess whether this difference may have contributed to the observed variation. To make the analyses more general, basic cases were analyzed (Fig.6.).



Fig.4. Seven Sisters Dam and Reservoir



Fig.5. Arnprior Dam and Reservoir

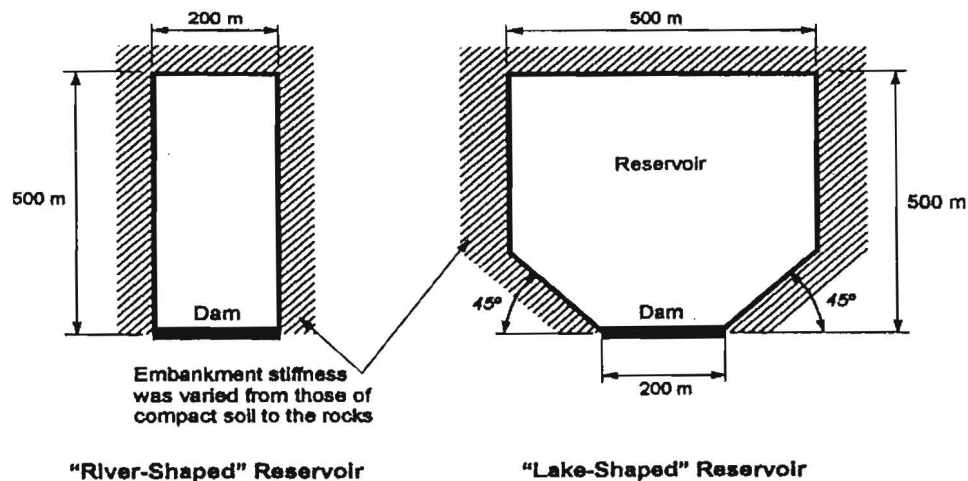


Fig.6. Reservoir Geometries Selected for Analysis

### Approach

Plane stress conditions were assumed, as well as linear-elastic deformations in the ice sheet, the dam, and the reservoir sides. See Table 4 for material properties. The reservoir was assumed to be frozen over with a uniform 1 m thick ice sheet that underwent a uniform temperature rise of 10°C. The dam stiffness was taken to be uniform along its length. Local variations, such as those produced by stoplogs and piers, were not included. The reservoir embankment around was assumed to have uniform stiffness throughout its perimeter. The boundary conditions were selected to represent those for an ice sheet that is not bonded at the reservoir edges (due to cracks that normally form at the reservoir edges), but is in contact with it. In plane ice sheet displacements perpendicular to the boundary (due to thermal expansion) were resisted by springs, whereas any movement parallel to the boundary was unrestricted.

**Table 4**

Material Properties Used for the Dam, the Ice and the Embankment

Material	Properties
Dam	Stiffness: 2000 MN/m
Ice	Young's Modulus $E$ : 4 Gpa Poisson's Ratio: 0.3
Embankment	Ranged as follows to cover range of materials: <ul style="list-style-type: none"> <li>• Compacted soil to loosely packed rock: Stiffness = 20 to 200 MN/m/m - see text below</li> <li>• Rock face: Stiffness = 10.000 MN/m/m - see text below</li> </ul>

The reservoir stiffness was estimated by assuming that the ice stresses were dissipated in a length equal to two times the loading width, and that the applied ice stresses were applied uniformly through the ice thickness. Hence, the stiffness per unit length of reservoir,  $K$ , is:

$$K = (area_{loaded} * E) / active\ length \quad (1)$$

where:  $area_{loaded}$  = the area loaded by the ice sheet

$E$  = the elastic modulus

$active\ length$  = the length over which stresses are dissipated in the material (assumed to be two times the loading width)

For a 1 m ice thick ice sheet, and a 2 m  $active\ length$ , Eq. 1 produces a reservoir side stiffness per unit length equal to half of the Young's modulus for the reservoir material.

### Results: Effect of Reservoir Shape

The results (Fig.7. and 8.) show that reservoir shape is an important factor influencing the ice loads when the reservoir sides are significantly softer than the dam. In this case, differences in

ice loads of up to a factor of about 2 could possibly be expected due to variations in reservoir shape.

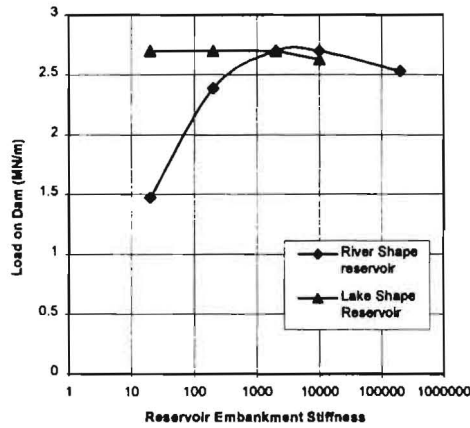


Fig.7. Results in Engineering Units

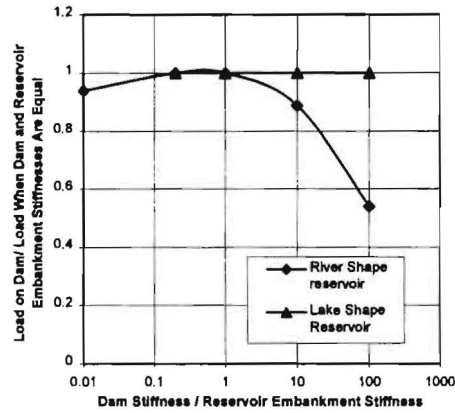


Fig.8. Non-Dimensional Results

Unfortunately, direct conclusions (comparing the expected loads at Seven Sisters and Arnprior) are not possible because the reservoir and dam stiffnesses at these sites are not known. However, because the reservoir sides at each of these dams are berms, it is likely that they are significantly softer than the dams at these sites. These calculations suggest that part of the observed ice load variations between these two sites (Table 2) may be attributable to variations in reservoir shape although further analyses are required to verify this. The work should also be followed up with more detailed analyses that take ice creep into account.

### CONCLUSIONS

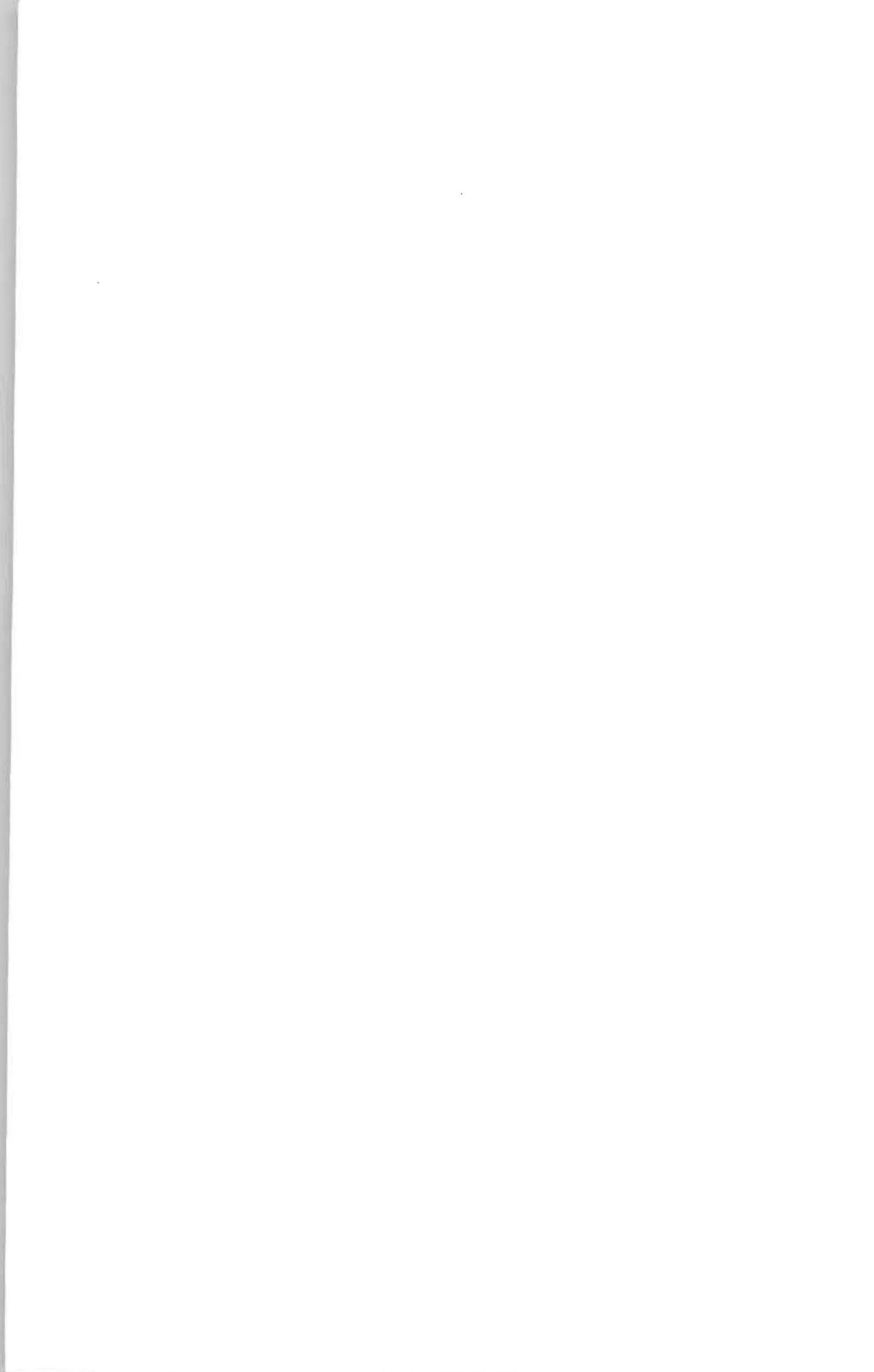
The ice load database has been expanded, and now contains 8 years of measurements. Progress has been made towards understanding static ice loads on hydro-electric structures, and the mechanisms generating them. The most significant finding of the work has been to identify the importance of water level changes on the resulting ice loads. Ice loads are much higher and more variable compared to purely thermal loads when significant, but not excessive, water level changes occur. The water level fluctuation patterns that induce relatively high, and low, ice loads have been identified. Preliminary analyses have shown that loads in a lake-shaped reservoir may higher than those for a river-shaped reservoir by a factor of up to about 2 when the reservoir sides are significantly softer than the dam. It would be useful to investigate the effect of reservoir shape further with field data collection and more detailed analyses.

## ACKNOWLEDGEMENTS

The work was sponsored by the Canadian Electricity Association (CEA-R&D projects 9038 G 815; 9502 G 2015, EG 910012, T992700-0203 and T992700-0204), with partial funding from Manitoba Hydro, Hydro-Quebec, Ontario Hydro, Nfld. Light and Power Co. Ltd., Nfld. and Labrador Hydro, and the Canadian Dam Safety Ass'n. (CDSA). The project was administered by T. Glavicic-Theberge of the CEA. The project monitors were G. Schellenberg of Manitoba Hydro, R. Lupien and Tai Mai Phat of Hydro-Quebec, G. Smith and P. Bhat of Ontario Hydro, A. Kumar of B.C. Hydro, P. Halliday of Nfld. Light & Power Co. Ltd., R. Barnes and E.G. Piercy of Nfld. and Labrador Hydro, and W. Pawlikewitch of Manitoba Hydro (who represented the CDSA). Assistance was provided by operations personnel at Hydro-Quebec (S. Robert, A. Pednault, R. Brazeau and A. Bond); Ontario Hydro (J. Whyte, G. James, G. McLeod, C. Stevens and J. Tremblay ); Manitoba Hydro (T. Armstrong, P. Roach and G. Ferguson) ; and Nfld. & Lab. Hydro (D. Hodder, and G. Tucker).

## REFERENCES

- COMFORT G., GONG Y., SINGH S. (2000): Predicting Static Ice Loads On Dams. Proc. IAHR Symposium on Ice Problems, Gdansk, Poland.
- COMFORT G., ABDELNOUR R., GONG Y., SINGH S., DINOVIETZ A. (1999): Update No. 2 to Static Ice Loads On Hydro-Electric Structures : Ice Loads Monograph No. 2, CEA projects EG 910012 and T992700-0204.
- COMFORT G., ABDELNOUR R., GONG Y., SINGH S., DINOVIETZ A (1998a): Static Ice Loads On Hydro-Electric Structures. Ice Loads Monograph No. 2, CEA proj. EG 910012.
- COMFORT G., SINGH S., GONG Y. (1998b): Static Ice Loads On Dams: Loads on the Dam Face, and on Wooden vs Steel Stoplogs. CDA Conference, Halifax.
- COMFORT G., GONG Y., SINGH S., ABDELNOUR R. (1997): Static Ice Loads On Hydro-Electric Structures: Loads Exerted Along A Dam Face; And A Comparison Of The Loads Exerted On Wooden And Steel Stoplogs. CDSA conference, Montreal.
- COMFORT G., ABDELNOUR R., GONG Y., DINOVIETZ A. (1996): Static Ice Loads On Hydro-Electric Structures. Ice Loads Monograph, CEA project 9038 G 815.





## ON THE APPLICATION OF PLANE PRESSURE PANEL TO ICE STRENGTH MEASUREMENTS

T. Takeuchi<sup>1</sup>, M. Sasaki<sup>1</sup>, S. Kioka<sup>2</sup>, N. Usami<sup>2</sup>, H. Saeki<sup>2</sup>,  
M. Kawamura<sup>3</sup>

### ABSTRACT

The plane pressure panel sensor has the capability of measuring many pressures inside a small area, and has recently been applied to evaluation of ice pressure in ice/structure interaction. However, it is not clear how the sensor responds to various test conditions. The purpose of the paper is to examine the characteristics of the plane pressure panel sensor under various test conditions through loading tests, and evaluate its applicability to ice strength measurements.

### INTRODUCTION

The plane pressure panel sensor is a powerful tool that enables real time display of a pressure distribution on 1936-grid points inside a 238mm\*238mm area. It was first used for ice pressure measurements by Wako and Izumiyama (1997) and also for measurements of local ice pressure in medium-scale field indentation tests in the JOIA project (Sodhi et al., 1998; Takeuchi et al., 1998; Nakazawa et al., 1999). It yielded new findings for ice failure patterns depending on indentation speed  $V$  through change in ice pressure distribution with time. However, an integral value (total ice force) of measured ice pressure data does not correspond to total ice force measured by a load cell, following the direct way for the converted factor against output data. Therefore, in order to examine the sensor's response under various test conditions, two types of loading tests of more than 170 cases, based on ice failure pattern in ice/structure interaction, were conducted using specimen made of artificial rubber with an elastic modulus similar to that of natural sea ice. The paper examines the applicability of plane pressure panel to ice strength measurements.

---

<sup>1</sup> Hachinohe Institute of Technology No.88-1, Oobiraki, Myo, Hachinohe, Aomori, Japan,  
Tel.:+81-178-25-8196, fax:+81-178-25-0722, e-mail:take@hi-tech.ac.jp

<sup>2</sup> Hokkaido University,

<sup>3</sup> Shimizu Corporation

## TESTS

The plane pressure panel sensor (Tekscan Inc., Fig.1.) used in the test can measure pressures at 1936-grid points (44-rows\*44-columns) inside a 238 mm\*238 mm area 0.1 mm thick. The sensor is made of impact ink and an electrode painted on a synthetic resin film, and can measure the pressure from voltage change, using the characteristic that the electrical resistance of impact ink varies with applied pressure. The change in interfacial pressure distribution is measured over a time period, and the total force can be evaluated by integrating all the pressures. Two types of loading tests, shown in Fig.2. (TYPE-1) and Fig.3. (TYPE-2), are conducted in order to consider the behaviour of ice in ice/structure interaction (Fig.4.). (TYPE-1) is a compressive strength test, which is related to an ice sheet crushing failure, as shown in Fig.4. (TYPE-2) is a sliding test under compressive loading, which is related to an ice sheet flaking failure, as shown in Fig.4. Artificial cylindrical rubber specimens 3 cm high by 10 cm diameter, having an elastic modulus similar to that of sea ice (Saeki, 1983), were used. Three types of homogeneous elastic moduli (90°, 70°, and 50°), combined elastic moduli of circumferential part of (90°) with core parts of (70°, 50°, and 30°), and combined elastic moduli of circumferential part of (70°) with core parts of (50° and 30°) were prepared. As shown in Figs.2. and 3., Teflon sheets of various thicknesses (0.05 mm, 0.1 mm, and 0.3 mm) were also used. In the paper, the effects of sheet thickness  $S$ , specimen elastic modulus  $E$ , atmospheric temperature  $T$ , vertical  $V_v$  and horizontal  $V_h$  loading speed, fluctuating load, and test type on accuracy by plane pressure panel sensor measurements were investigated.

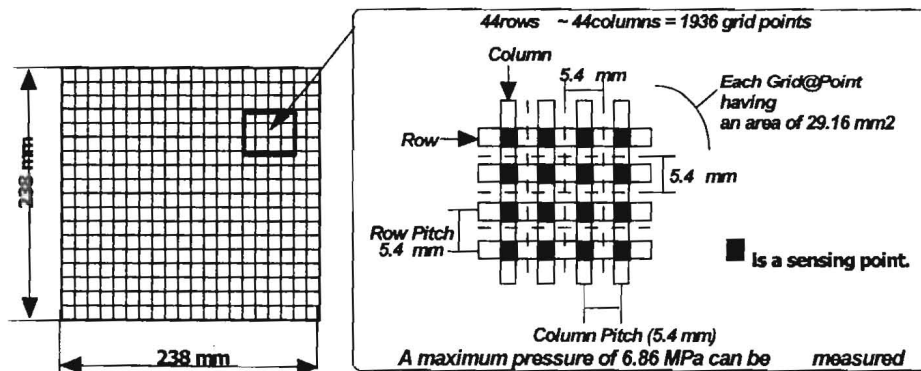


Fig.1. Plane Pressure Panel Sensor

## RESULTS

### Calibration of Output data

A bilinear calibration curve as shown in Fig.5. which expresses the relationship between output value and converted pressure, was utilized to obtain an actual interfacial pressure occurring in loading process at each grid. Although linearly converted pressures against output values are guaranteed only from 55 to 255 by the manufacturer, total force  $F_p$  integrated by  $K$  (Calibration Factor)=1 does not correspond to total force  $FL$  by the load cell,

as shown in Fig.6. Therefore,  $K$  is determined from the comparison of maximum  $F_p$  with maximum  $F_l$ .

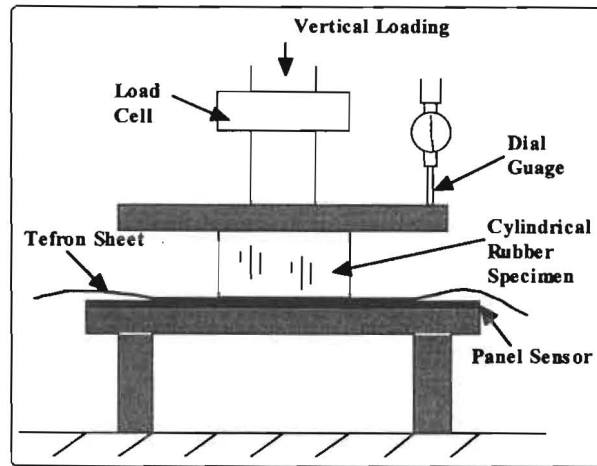


Fig.2. Compressive Test (Type-1)

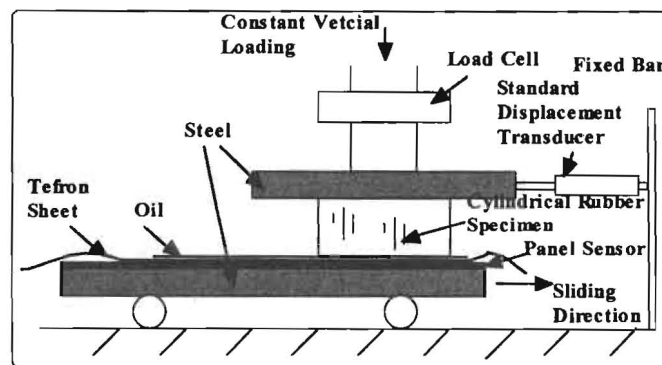


Fig.3. Sliding Test (Type-2)

### Type-1 Test

#### Recurrence

The total force  $F_p$  obtained by the panel sensor under the same test conditions is plotted versus loading time as shown in Fig.7a., 7b., and 7c. Although the maximum applied loading  $F_p$  is different, the curve of  $F_p$  against time is almost the same. This in turn shows the recurrence of measurements.

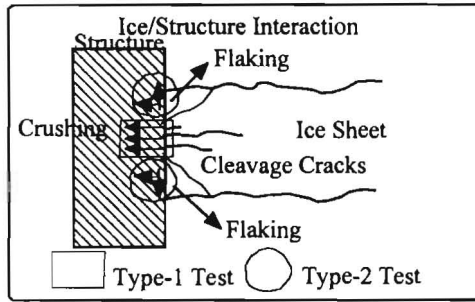


Fig.4. Ice/Structure Interaction

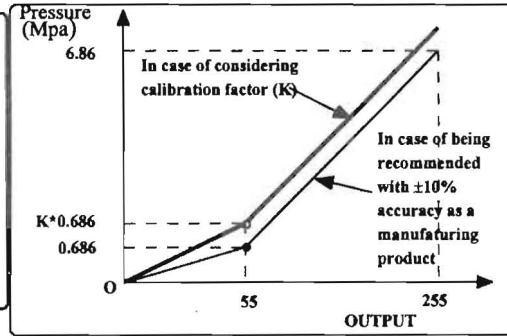


Fig.5. Calibration curve in bi-linear form

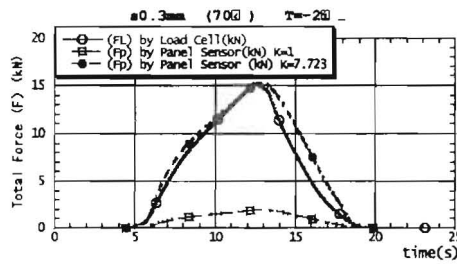


Fig.6. Total Force versus time

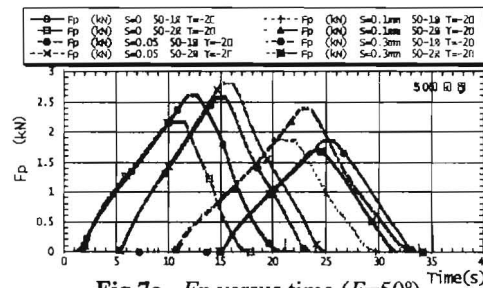


Fig.7a.  $F_p$  versus time ( $E=50^\circ$ )

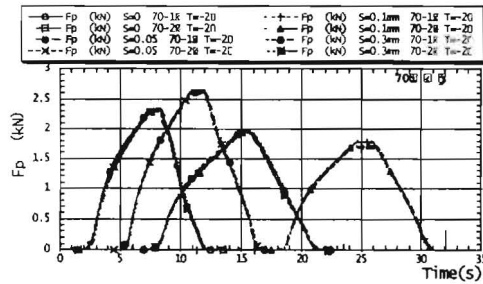


Fig.7b.  $F_p$  versus time ( $E=70^\circ$ )

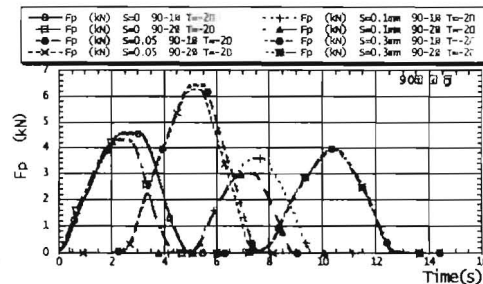


Fig.7c.  $F_p$  versus time ( $E=90^\circ$ )

### Effect of Sheet Thickness

It is better to use a panel sensor repeatedly for several tests. Therefore, for the purpose of durability, the effects on calibration accuracy of Teflon sheets with various thicknesses (0, 0.05, 0.1 and 0.3mm) is examined from the ratio  $E_p/EL$  of elastic moduli estimated by both panel sensor and load cell measurements. Fig.8. shows the sheet thickness  $S$  versus the ratio  $E_p/EL$ , which is approximately constant for ratios smaller than 1.

Effect of Specimen Elastic Modulus

The effect of specimen elastic modulus on calibration accuracy is examined from the ratio  $Ep/EL$  of elastic modulus estimated by both panel sensor and load cell measurements. Fig.9a., 9b. show hardness  $H_d$  ( $^{\circ}$ ) (in place of elastic modulus) versus the ratio  $Ep/EL$ , which is approximately constant for ratios smaller than 1.

Effect of Atmospheric Temperature

Fig.10. shows atmospheric temperature  $T$  versus the ratio  $Ep/EL$ . Lower temperatures make the specimen harder, so that the tendency is similar to that of the hardness of specimen.  $Ep/EL$  is approximately constant with smaller than 1.

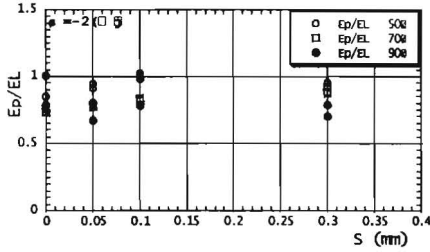


**Fig.8.**  $S$  versus the ratio  $Ep/EL$

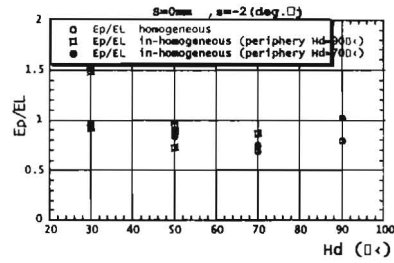


**Fig.9a.**  $H_d(^{\circ})$  versus  $Ep/EL$

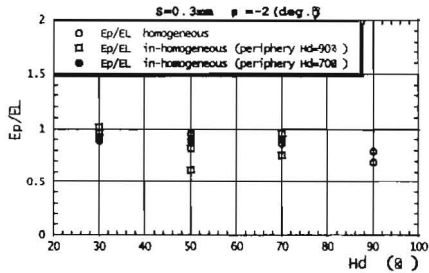


**Fig.9b.**  $H_d(^{\circ})$  versus  $Ep/EL$

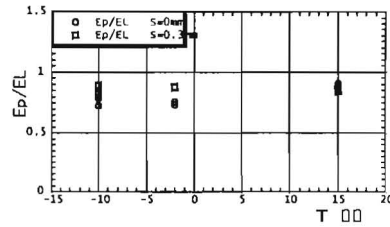


**Fig.10.**  $T$  versus the ratio  $Ep/EL$

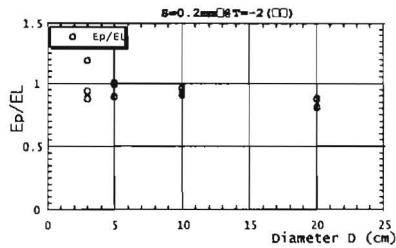


**Fig.11.**  $D$  versus  $Ep/EL$

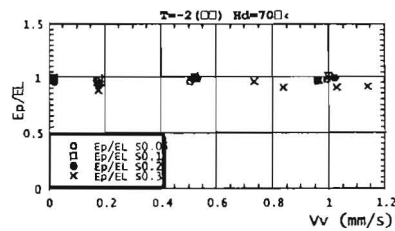


**Fig.12.**  $V_v$  versus  $Ep/EL$

### Effect of Specimen Diameter

Fig.11. shows specimen diameter  $D$  versus the ratio  $Ep/EL$ .  $Ep/EL$  is approximately constant, but larger  $D$  gives  $Ep/EL$  smaller than 1. This may reflect the value of output data ranging from 0 to 55, which yields smaller accuracy.

### Effect of vertical loading speed

Fig.12. shows vertical loading speed  $V_v$  versus the ratio  $Ep/EL$ .  $Ep/EL$  is constant, thus having little influence on vertical loading speed  $V_v$ .  $Ep/EL$  is slightly smaller than 1.

### Effect of loading fluctuation

Since loading fluctuation occurs in ice/structure interaction, loading tests were conducted as shown in Fig.13a. and b. Fig.14. shows the ratio  $Fp/FL$  for loads estimated by both panel sensor and load cell measurements. The ratio  $Fp/FL$  at the convex peak gave higher accuracy than that at the concave peak. This also reflects the value of output data ranging from 0 to 55, which yields smaller accuracy.

### **Type-2 Test**

The effect on calibration accuracy of horizontal loading speed  $V_h$  under constant vertical loading is examined. Time series of force  $Fp$  and  $FL$  measured by both panel sensor and load cell measurements are shown in Fig.15a., b. and c. Smaller  $V_h$  gives higher accuracy of measured force, while higher  $V_h$  gives the differences between  $Fp$  and  $FL$ . Pressure distributions for higher  $V_h$  are shown in Fig.16a. and b., and non-uniform distribution under output data ranging from 0 to 55 and change of contact area due to deformed specimen may give smaller accuracy. Therefore, the relation between  $Fp/FL$  and  $V_h$  becomes as shown in Fig-17.

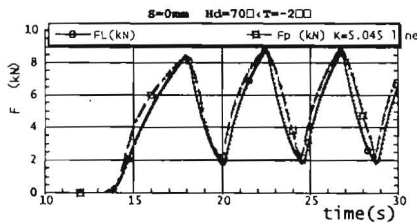


**Fig.13a.** Time series of applied force

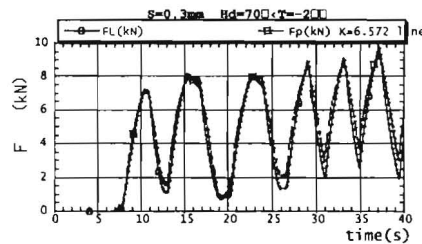


**Fig.13b.** Time series of applied force

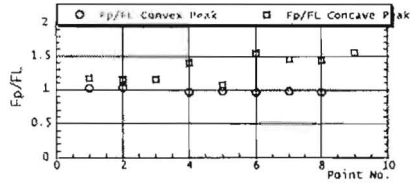


Fig.14.  $F_p/FL$  at each peak

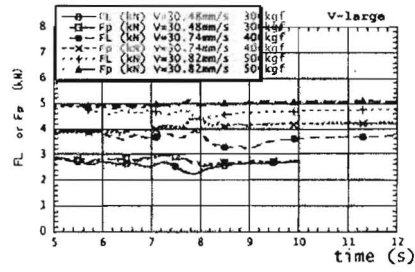


Fig.15a. Time series of Force large  $V_h$

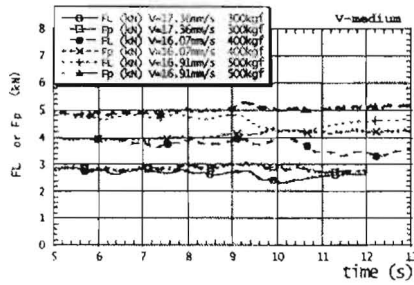


Fig.15b. Time series of Force medium  $V_h$

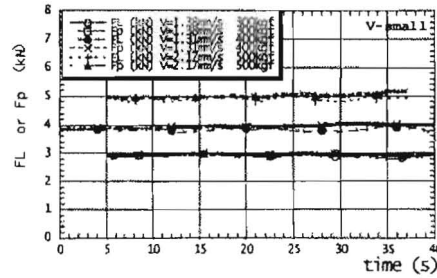


Fig.15c. Time series of Force small  $V_h$

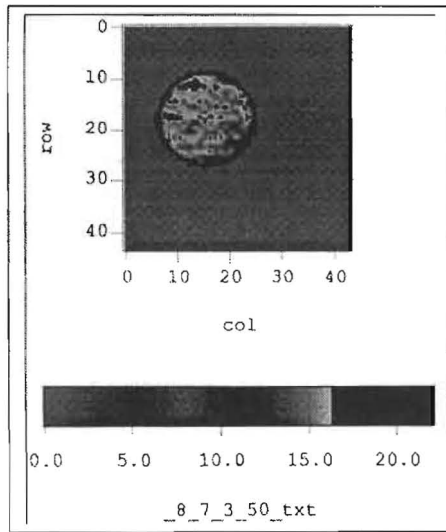


Fig.16a. Pressure distributions for higher  $V_h$  at time=5.4 s

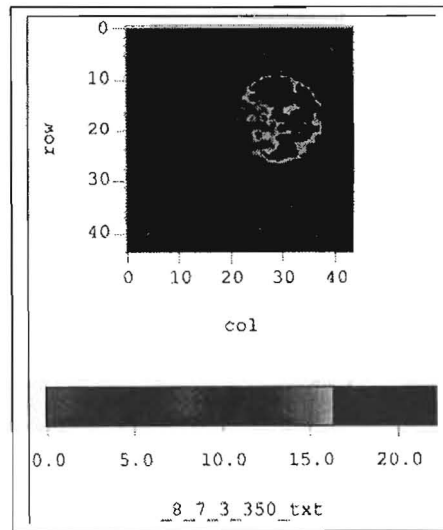


Fig.16b. Pressure distributions for higher  $V_h$  at time=8.5 s

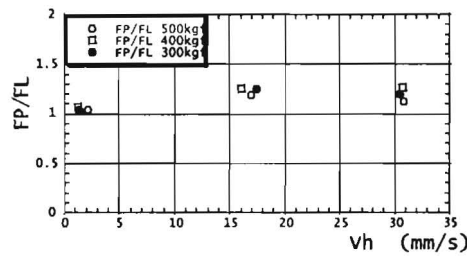


Fig.17.  $F_p/FL$  versus  $V_h$

### CONCLUDING REMARKS

From two types of loading tests under various test conditions, the characteristics of a plane pressure panel sensor were investigated through comparison with load cell measurements.

Through the use of a bi-linear conversion curve, it is found that the effects of Teflon sheet thickness  $S$ , atmospheric temperature  $T$ , specimen hardness ( $^{\circ}$ ) and vertical loading speed  $V_v$  on the difference evaluated by both panel sensor and load cell measurements are small, and panel sensor measurements recur. However, the conditions of larger specimen size, larger horizontal speed  $V_h$  under vertical loading, and concave peaks under loading fluctuation reduce the accuracy. Thus, a more accurate method is required to convert output data ranging from 0 to 55.

### REFERENCES

- NAKAZAWA N., AKAGAWA S., KAWAMURA M., SAKAI M., MATSUSHITA H., TERASHIMA T., TAKEUCHI T., SAEKI H., HIRAYAMA K. (1999): MEDIUM SCALE FIELD INDENTATION TESTS (MSFIT) -Results of 1998 winter Tests. Proc. of 9th Int. Offshore and Polar Eng.(ISOPE99), Vol.2., pp. 498-504.
- SAEKI H. (1983): Kaigan-Kaiyoukouzoubutsu-no-Taihyousekkeihou (in Japanese). Doctor of Engineering Thesis, pp.1-336.
- SODHI D., TAKEUCHI T., AKAGAWA S., NAKAZAWA N., SAEKI H. (1998): Medium-scale indentation tests on sea ice at various speeds. Journal of Cold Regions Science & Technology 28, pp. 161-182.
- TAKEUCHI T., AKAGAWA S., KAWAMURA M., SAKAI M., MATSUSHITA H., TERASHIMA T., NAKAZAWA N., HIRAYAMA K., SAEKI H. (1998): On the ice/structure in medium scale field indentation tests (part3). Proc. of Civil Engineering in the Ocean, Vol.14, pp. 423-428,
- WAKO D., IZUMIYAMA K. (1997): Ice Load Distribution on a Flat Indentor (in Japanese). Proc. of 97' Cold Region Technology Conference, Vol.13, pp. 412-417.



## MODES OF ICE LOAD ACTING ON AN ICE BOOM FOR ICE CONTROL

S. Makita<sup>1</sup>, K. Enoki<sup>2</sup>, K. Izumiyama<sup>3</sup>, F. Hara<sup>4</sup>, H. Saeki<sup>5</sup>

### ABSTRACT

Lake Saroma, which has two waterways connecting to the Okhotsk Sea, is a relatively deep and a tranquil lake with salinity similar to that of the Okhotsk Sea. The lake is therefore an ideal place for aquaculture of scallops, oysters and other marine products. However, from January to February the ice floes that move down along the coast of the Okhotsk Sea drift into the lake through its two waterways, causing serious damage to the aquacultural facilities. In order to prevent such damage, a dike for control of ice floes consisting of 13 ice booms was constructed at the No.1 waterway. Tensile forces acting on the main wire of the ice boom at Lake Saroma were measured by the Hokkaido Development Bureau in 1996 and 1997. The data showed that the tensile force did not always depend on the flow speed and surface area of ice field.

### INTRODUCTION

Ice floes trapped in the ice boom gains fluid force. This fluid force acts as an ice load via ice floes on the main wire of the ice boom. Since both ends of the main wire are fixed by structures, tensile force acts on the main wire. The fluid force acting on ice floes changes depending on the flow velocity and area of ice field, so generally the tensile force changes depending on the flow velocity and area of ice field.

### TENSILE FORCE ACTING ON AN ICE BOOM

Data of tensile forces, flow velocities and lengths of the ice field measured in Feb. 21, 1996, Feb.22, 1996 and Feb. 9, 1997 are shown in Fig.1., 2. and 3., respectively. In these days, some phenomena suggesting that the tensile force acting on the main wire of the ice boom did not depend only on these factors were observed.

---

<sup>1</sup> Dept. of Engineering Hokkaido University, Hokkaido, Japan, North 13, West 8, Sapporo, Hokkaido, Japan, Tel.: +81-11-706-6183, fax: +81-11-726-2296, e-mail: makita@kowanws1.hyd.eng.hokudai.ac.jp

<sup>2</sup> Akita National College of Technology, Akita, Japan

<sup>3</sup> Hokkaido Tokai University, Hokkaido, Japan

<sup>4</sup> Hokkaido Development Engineering Center, Hokkaido, Japan

<sup>5</sup> Hokkaido University, Sapporo, Japan

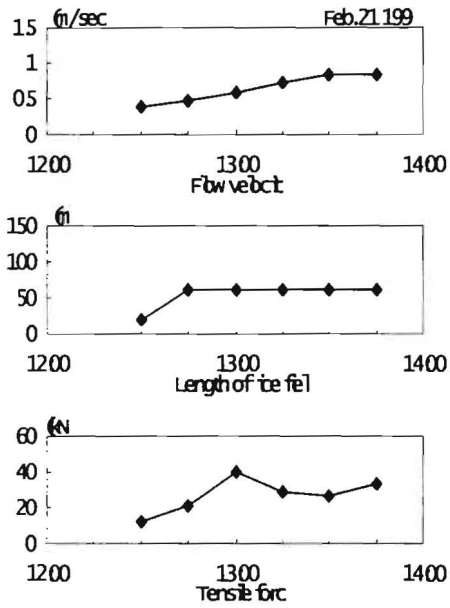


Fig.1. Feb. 21, 1996

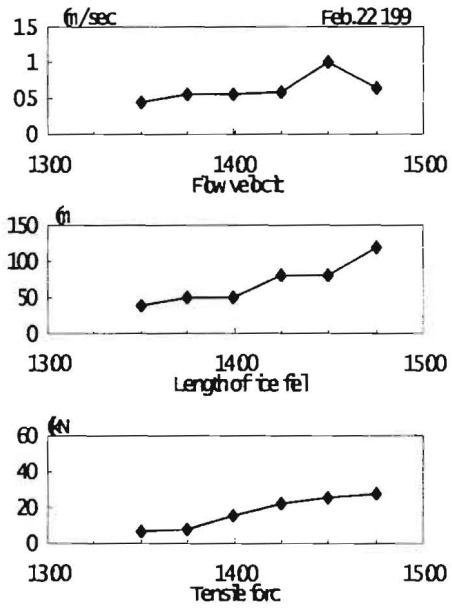


Fig.2. Feb. 22, 1996

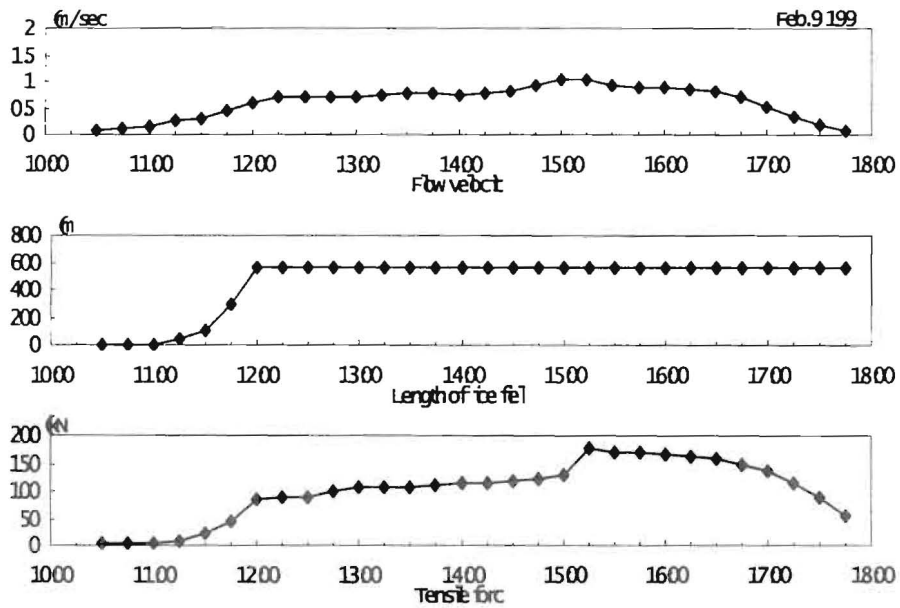
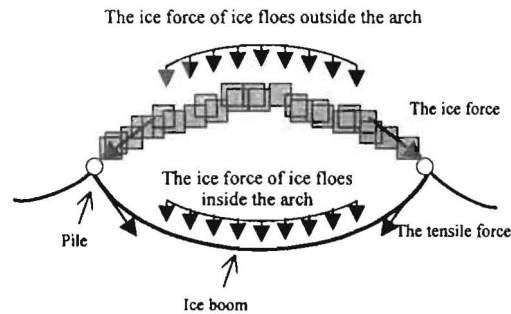


Fig.3. Feb. 9, 1997

As can be seen in the figures, the temporal change in tensile force on Feb. 22, 1996 is typical example of the change depending on the flow velocity and length of the ice field. The tensile force increased with increases in both the flow velocity and length of the ice field. However, on February 21, 1996, the change in tensile force has the peak at 13:00, despite the fact that there was only a gradual increase in flow velocity and almost no change in length of the ice field. At this time, videos taken by CCD cameras showed a large ice sheet had collided with ice floes trapped in the ice boom, indicating that the large transient tensile force was probably caused by the transmission of the load from the collision to the ice boom. A different pattern of changes was observed during the period from 12:00 to 15:00 on February 9, 1997. During this period, the flow velocity doubled from 0.6 m/s to 1.2 m/s, the length of the ice field only changed slightly. The tensile force increased very gradually from 12:00 to 15:00 but showed a sudden large increase at 15:00. The following phenomena were responsible for this change in tensile force. At 12:00 noon, the ice floes trapped in the ice boom had formed an arch extending between the two pile of the ice boom, and at 15:00, the arch broke up. From 12:00 to 15:00, only the fluid force acting on ice floes located inside the arch acted as ice force on the ice boom. The fluid force acting on the ice floes located outside the arch was transmitted through the formed arch and acted as a horizontal ice force on piles directly. The ice forces acting on the ice boom and piles are illustrated in Fig.4.



**Fig.4.** Mode of ice force during arching

The ice forces from the trapped ice floes acting on the ice boom can be categorized into the following three modes:

1. All of the fluid force acting on the trapped ice floes acts as ice force on the ice boom, and the degree of tensile force therefore depends on the flow velocity and the influence length of the ice field.
2. A large ice sheet collides with the ice floes trapped in the ice boom, and the load from the collision acts as ice force on the ice boom, causing a temporary rise in tensile force.
3. The ice floes trapped in the ice boom form an arch between the two fixed structures, and only the fluid force acting on the ice floes in the arch act as ice force on the ice boom. In this case, the degree of tensile force depends only on the flow velocity under the ice floes forming an arch; the influence length of the ice field has no effect on tensile force.

#### **EXPERIMENTAL METHOD**

A channel of 2 m in width and 10 m in length was used for the experiments (Fig.5.). In the midstream part of the channel, two piles were set, and an ice boom was attached to the two piles. Experiments were conducted to see whether model ice floes that had been floated in the channel from the upstream direction and had been trapped in the ice boom would form an arch when the ice boom was removed.

In the experiments, the distance between the piles  $b$  was varied within the range of 30~100 cm, and the flow velocity was set at 5, 10 or 15 cm/s. The model ice floes were blocks made from polypropylene, each measuring 3 cm in side length  $a$  and 0.3 cm in height  $h$  ( $h/a=0.1$ ). It is reported by Kunimatsu et al. (1993) that the most-frequently observed ice floes near the coast in the Sea of Okhotsk has a area corresponded to a area of 3~4 m square and a height 30~40 cm. Also, the distance between the piles used in the dike for the control of ice floes at Saroma Lagoon is 110 m. Accordingly, the scale of this experiment corresponds to a scale of 1/100~1/150 in Fluid similitude.

### EXPERIMENTAL RESULTS AND DISCUSSION

The results of experiments on arching with changes in the length of the ice field are shown in Fig.6. Where the vertical axis in each figure is the ratio of the length of the ice field  $R$  to the distance between piles  $b$  and the horizontal axis in each figure is the ratio of the side length of ice floes  $a$  to the distance between piles  $b$ .

As can be seen in the figures, when the ratio of the side length of ice floes to the distance between piles  $a/b$  increases, the ratio of the length of the ice field to the distance between piles  $R/b$ , which is necessary for arching, also increases. These results indicate that arching occurs more easily when the ratio of the side length of the ice floes to the distance between piles increases, and that arching will occur even if there is a large distance between piles as long as the length of the ice field is sufficiently large.

The necessary conditions for arching of moving ice floes caused by piers of a bridge was investigated by Hara et al. They showed the condition for arching using the rate of the area covered by the ice floes  $Q$  and the ratio of the side length of ice floes and the distance between piers  $a/b$  in Fig.7. In the experiment on condition for arching of trapped ice floes, the rate of the area covered by the ice floes is considered to be 100%. In order to compare the results of Hara et al.

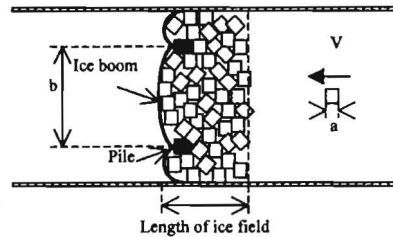


Fig.5. Experimental device

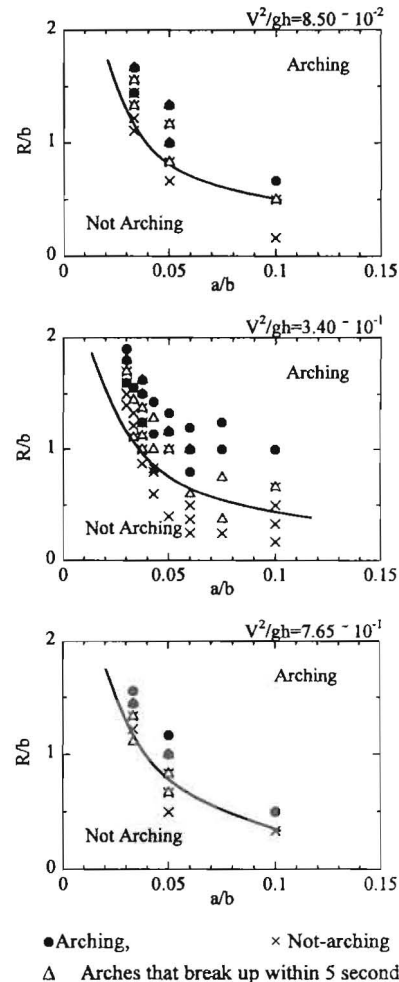


Fig.6. Condition for arching

with our results, we calculated the relationship between the value of square on the fluid number  $V^2/gh$  and the value of  $a/b$ , the necessary conditions for arching at the area covered by the ice floes is 100%. The relationship is shown in Fig.8.

When  $V^2/gh = 8.50 \times 10^{-2}$ , the necessary value  $a/b$  is  $1.47 \times 10^{-1}$ . Since the ice floes in the experiment conducted by Hara et al. were drifting downstream, we compared their results with our results assuming the length of ice field in their experiment to be zero. A comparison of the results is shown in Fig.9.

Assuming that the distance between piles is constant, as the length of the ice field increases, the side length of ice floes, which is a necessary condition for the formation of an arch, becomes smaller. It was clarified that arching occurs much more easily in the case where ice floes trapped in an ice boom, than in the case where the ice floes drift downstream, as occurs between piers of a bridge. Actually the ice boom span is 110 m. Assuming that the side length of ice floes is 3~4 m, the ratio of the side length of ice floes to distance between the fixed structures  $a/b$  would be about 0.03, and in the present experiments, it was confirmed that arching occurs under the conditions of flow velocity of 5 cm/s, the side length of model ice floes  $a$  of 3 cm, and distance between piles  $b$  of 90 cm ( $a/b = 0.03$ ). If these experimental-scale values of flow velocity and the length of the ice field are converted into true-scale values, they become 0.61 m/s and 160 m, respectively. On-site measurements of flow velocity and the length of the ice field were greater than these values, confirming that arching occurs in the dike for control of ice floes at Saroma Lagoon. In the present experiments, cases in which the arch formed by ice floes broke up in less than 5 seconds after the ice boom had been removed

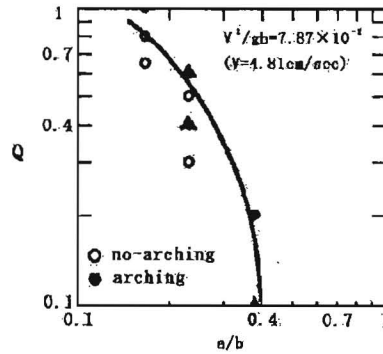


Fig.7. Condition for arching proposed by Hara et al.

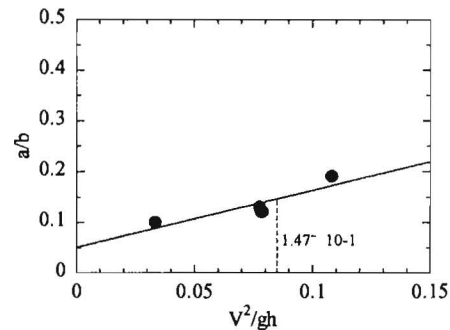


Fig.8. Relationship between  $a/b$  and  $V^2/gh$

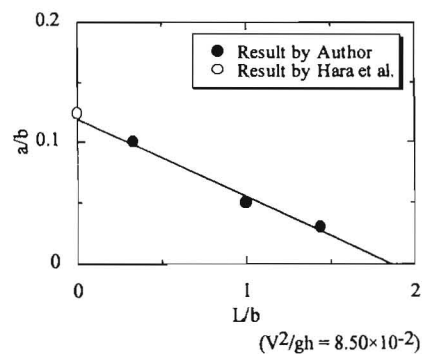


Fig.9. Comparison of the experimental results

were considered to be non-arching cases. However, the ice floes had formed an arch before the ice boom was removed, and it is thought that the ice force of the ice floes outside the formed arch acted directly on the fixed structures. Thus, in the case of a real ice boom, it is possible that a decrease in tensile force of the main wire occurs even under the condition that the arch broke up in less than 5 seconds in this experiment.

#### ANALYSIS OF TENSILE FORCE ON FEBRUARY 9, 1997

The changes in the tensile force on Feb. 9, 1997 calculated from the flow velocity and the length of the ice field are shown in Fig.10.

Since the shapes of the bottom surfaces of ice floes are complex and can easily change, the shearing force coefficient changes variously. Thus, before 12:00, the tensile force is calculated using the shearing force coefficient  $C_{SW} = 0.015$ , which was back calculated assuming that there was no arching. It is reported that in the case that the ratio of the height to the side length of the ice floe is 0.1, ice floes submerge under the ice field and form ice jam when the flow velocity exceeds about 0.6 m/s. Thus, after 12:15, the tensile force is calculated using the shearing force coefficient  $C_{SW} = 0.15$ , which was obtained for a group of ice floes that makes ice jam by Kawai et al.. The measured value is much greater than the calculated value. This result testifies that an arch was formed.

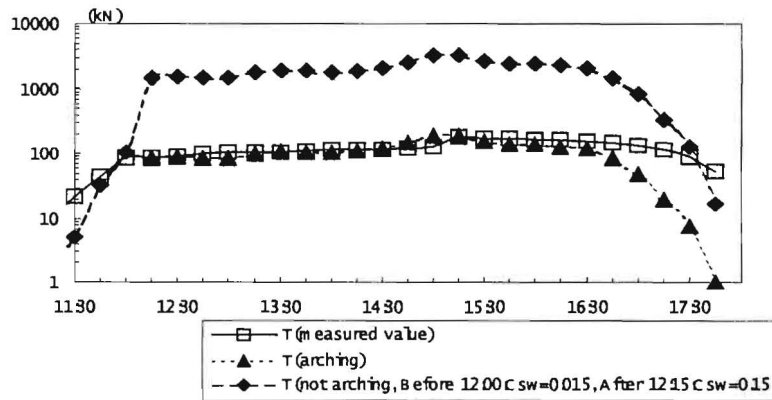


Fig.10. Calculated shearing forces on Feb. 9, 1997

In the ice boom at Saroma lagoon, the arching occurs when the flow velocity exceeds 0.61 m/s. The area of the ice field inside the arch is calculated from the tensile force measured at the ice boom on the basis of the assumption that an arch had formed at 12:15, the time when the flow velocity exceeded 0.6 m/s. The area is 1673 m<sup>2</sup> and if the shape of the arch is approximated as a parabola, the ratio of the rise of the arch to the span of piles is 0.19. The shape of the arch is shown in Fig.11. Change in the tensile force acting on main wire of the ice boom was calculated from mean value of the area of the ice field inside the arch (1673 m<sup>2</sup>).

After 14:45, calculated value of tensile force decreased sharply depending on the flow velocity. However, the measured value of the tensile force decreased very gradually and became greater than the calculated value.

It is supposed that the arch became loose gradually caused by the decrease of the flow velocity and the fluid force acting on the ice floes located outside the arch began to act on the ice floes located inside the arch.

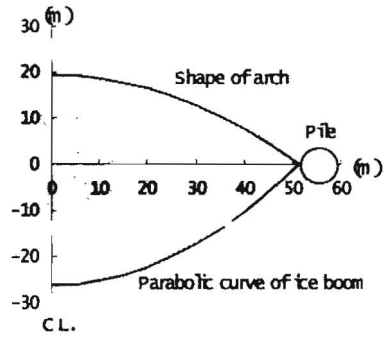


Fig.11. Shape of arch

### ARCH SHAPE

Arch shapes can be divided into those with a large and a small rise. The rise tends to be small when there is a relatively slow flow velocity and long influence length, and it tends to be large when there is a relatively fast velocity flow and long influence length. As the length of the ice field increases, the arch tends to extend in a direction normal to a straight line joining the two piles. In the present experiments, the square-shape arch and triangle arch were observed. The arches observed in the experiments are shown in Fig.12., 13., 14. and 15.



Fig.12. An arch with a small rise

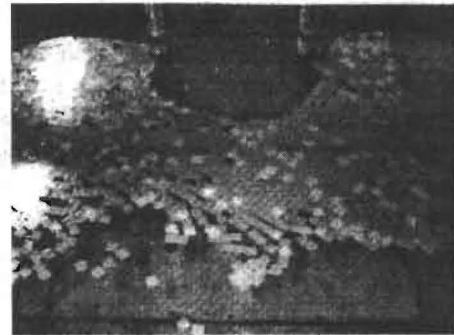


Fig.13. An arch with a large rise



Fig.14. A square-shape arch

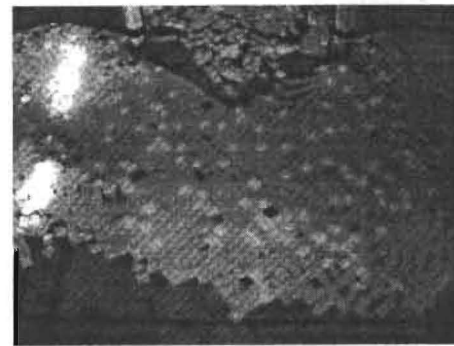


Fig.15. A triangle-shape arch

## CONCLUSIONS

1. The ice force acting on an ice boom at Saroma Lagoon could be classified into three modes on the basis of measurements of tensile force acting on the ice boom and the pattern of trapped ice floes.
2. The results indicated the possibility that when ice floes are completely trapped in the ice boom, a part of the fluid force acting on the ice floes is transmitted via the ice floes to the ice boom, and the remainder of the fluid force, due to arching of the ice floes, acts on the fixed structures. In this case, the tensile force acting on the main wire would decrease.
3. If the side length of ice floes becomes larger with respect to the distance between the piles, arching occurs more easily. If the distance between the piles is large, a long length of ice field is needed for arching to occur.
4. It is much easier for ice floes that have stopped drifting to form an arch than it is for ice floes that are drifting, such as those drifting downstream in a river.
5. The results of the experiments showed that arching occurs if the ratio of the side length of ice floes to the distance between piles is 0.03, indicating the possibility of arching occurring at the ice boom set in Saroma Lagoon.
6. Changes in tensile force acting on the main wire of the ice boom in Saroma Lagoon on February 9, 1997 were analyzed assuming that arching occurred at 12:15. and assuming that the ice force of ice floes outside the arch act on the fixed structures, a force greater than the tensile force would act on the main wire of the ice boom.
7. The arches of ice floes formed at an ice boom can be divided into two types: those with a large rise and those with a small rise. An arch with a small rise has a tendency to be formed when there is a relatively slow flow velocity and short influence length of the ice field, and an arch with a large rise has a tendency to be formed when there is a relatively fast flow velocity and long influence length of the ice field.

## REFERENCES

- HARA F. (1994): Condition of arch formation by ice floes at bridge piles. Proceedings of the 12th international symposium on ice, Vol.2, pp. 867-873.
- ENOKI K. (1992): Control of ice floes movement by using ice boom. Proceedings of civil engineering in ocean, Vol.8, pp. 153-158.
- KUNIMATSU S. (1993): Study on size of drift ice at the Okhotsk sea of Hokkaido. Proceedings of civil engineering in ocean, Vol.9, pp.95-100.



**THE EFFECT OF DRIFT ICE ON THE STABILITY OF ARMOR  
STONES COVERING A DOUBLY PLACED SUBMERGED  
BREAKWATER IN A WAVE FIELD**

**T. Kitamura<sup>1</sup>, M. Sato<sup>2</sup>, M. Kato<sup>3</sup>, Y. Watanabe<sup>4</sup>, H. Saeki<sup>4</sup>**

**ABSTRACT**

An artificial reef or a combination of an artificial reef and a gentle slope-type sea wall is now thought to be desirable as a coastal protection facility in terms of appearance, amenity and durability. However, the construction of an artificial reef is costly and takes a long time.

Moreover, since an artificial reef occupies a large area of water, there is often opposition from local fishermen to the construction of such a facility. To overcome these problems in the construction of an artificial reef, the authors proposed the construction of a doubly placed submerged breakwater as a coastal protection facility. In this study, we carried out experiments to four determines.

**FOUR DETERMINES**

1. the dynamic behavior of drift ice near a doubly placed submerged breakwater
2. the dynamic behavior of drift ice near a doubly placed submerged breakwater in an area where there are both waves and drift ice
3. the stability of material covering the submerged breakwater in an area where there are both waves and drift ice
4. the effect on sea life in the area between the two submerged breakwaters.

**EXPERIMENTAL METHOD**

A doubly placed submerged breakwater must be effective in preventing the generation of waves if it is to be accepted as a useful facility for coastal protection and for increasing marine resources. The results of experiments carried out on model doubly placed submerged

---

<sup>1</sup>Hokuo consultant, Hokkaido, Japan, 11-chome, West-7 North-1, Obihiro-si, Hokkaido, Japan

Tel.: +81-155-26-3775, fax: +81-155-22-5961

<sup>2</sup>Nisimura Gumi co. Ltd., Hokkaido, Japan

<sup>3</sup>Nihon data service co., Hokkaido, Japan

<sup>4</sup>Dept. of Engineering Hokkaido University, Hokkaido, Japan

breakwaters built at scale ratios of 1:30 to 1:40 have shown that a large distance between the two submerged breakwaters and a crown water depth of 4 cm are desirable. In the present study, experiments were carried out using a two-dimensional wave flume of 24.0 m in length, 1.0 m in width and 1.0 m in height (Fig.1).

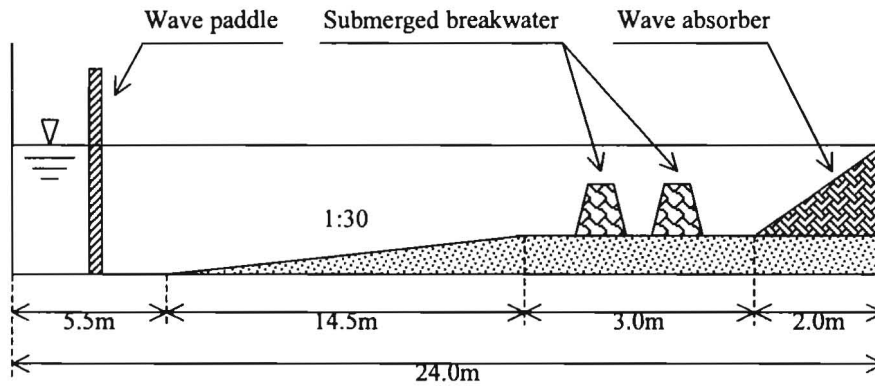


Fig.1. Experimental apparatus

Fig.2. shows a cross-sectional view of the model of a doubly placed submerged breakwater used in the experiments.

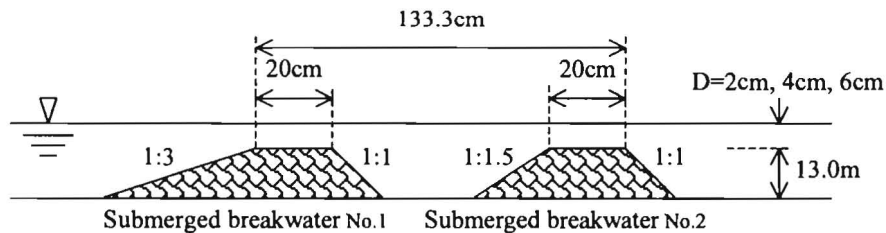


Fig.2. Conceptual illustration of a doubly placed submerged breakwater

The widths of both crowns were 20 cm. The slopes of the breakwater further from the shore (breakwater 1) on the seaward side were made 1:3 and 1:1.5 for block stability, and the slope of the breakwater nearer the shore on the shoreward side was made 1:1. Rubble stones, each weighing 140 g on average, were used to cover the breakwaters, and the amount of stones used for the covering on a 1/30 scale corresponds to 3.8 t for a breakwater of actual size. Tests were conducted at each water depth setting, each wave height setting, and each period setting in the experiments to ensure that the stones would not be dispersed by the waves. The crown water depths tested in the experiments were 0, 2 and 4 cm, with corresponding water depths of 13, 15 and 17 cm, respectively. Based on wave conditions in the Japan Sea and Okhotsk Sea,

wave periods of 1.10 and 1.83 seconds were used in the experiments. On a scale of 1/30 based on Froude similitude, these wave periods correspond to actual wave periods of 6 and 10 seconds, respectively. Considering the fact that the wave height in the Okhotsk Sea in winter decreases when the surface of the sea becomes covered with ice floes and the fact that submerged breakwaters are set in relatively shallow water, the wave height was set in the range of 2~9 cm in the experiments. This range corresponds to an actual range of 60~270 cm. The dimensions of the model ice floes used in the experiments were based on the results of surveys carried out by Kunimatsu et al. (1993) on the sizes and thicknesses of ice floes drifting along the coast of Utoro and along the Hokkaido coast of the Sea of Okhotsk.

The side lengths of the rectangular model ice floes were 3, 7, 10, 13, 16 and 21.7 cm (Fig.3.), and the thicknesses were 1.6, 3.2 and 4.8 cm for the model ice floes with a side length of 21.7 cm and 1, 2, 3, 4, 5, 6, 7 and 9 cm for the other model ice floes. The first experiment (experiment 1) was designed to determine the effects of the size and thickness of the ice floes on the two breakwaters. In this experiment, a single model ice floe of each of the above sizes and thicknesses was placed in the water on the seaward side of breakwater 1, and overtopping as well as destruction or dispersion of the rubble stones used for construction of the breakwater were examined over a 3-minute period. It should be noted that since the model ice floes were made from polypropylene with a specific gravity of 0.9 and they had a greater modulus of elasticity than that of sea water, the experimental results would be more on the safer side compared to results using real ice floes. The second experiment (experiment 2) was designed to determine the pattern of piling-up of multiple ice floes near the breakwater and the effect of multiple ice floes on destruction or dispersion of the rubble stones. A total of 182 model ice floes were used in this experiment. The side lengths of the ice floes were the same as those used in experiment 1, and the thicknesses were 1 cm for ice floes with a side length of 3 cm and 2 cm for the other ice floes. The ratios of the numbers of ice floes with side lengths of 3, 7, 10, 13, 16 and 21.7 cm were 3, 25, 27, 23, 15 and 7 %, respectively.

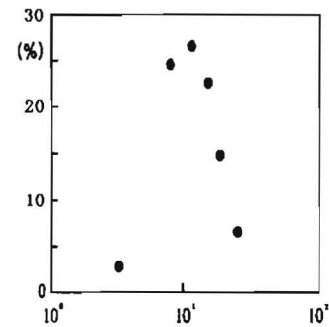


Fig.3. Frequency distribution of model ice floes

## RESULTS AND DISCUSSION

### Effects of individual ice floes

Fig.4. shows representative results of overtopping when the side length and thickness of the ice floes were changed. The experiment was carried out 5 times under the same conditions. In the figure, cases where the ice floes did not overtop breakwater 1, piled up on the top of breakwater 1, and overtopped breakwater 1 are indicated by the symbols  $\times$ ,  $\Delta$  and  $\circ$ , respectively. Cases where the ice floes piled up on the top of breakwater No.2 are indicated by the symbol  $\blacktriangle$ , and cases where the ice floes overtopped both breakwaters are indicated by the symbol  $\bullet$ . The definitions of the symbols used for labeling the  $x$  and  $y$  axes are as follows:

$D$  is the crown water depth of the breakwater,  $H_0$  is the wave height,  $t$  is the ice thickness,  $S_0$  is the side length of a rectangular-shaped ice floe, and  $L_0$  is the wave length. In Fig.4., the area above the broken line indicates cases in which the ice floes overtopped both breakwaters, and the area below the solid line indicates cases in which the ice floes did not overtop breakwater No.1. As mentioned above, the experiment was carried out 5 times under the same conditions, and the reproducibility was very high.

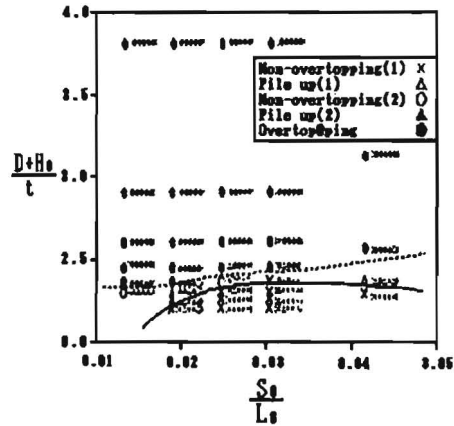


Fig.4. Properties of the ice floes

Fig.5. shows typical movements of the ice floes, suppression of overtopping, and the range of dispersion of rubble stones. In each of the graphs, the horizontal axis is the sum of the crown water depth  $D$  and the wave height  $H_0$  divided by the ice thickness  $t$ , and the vertical axis is the weight of the ice  $W_i$  divided by the weight of the stones  $W_s$ . In each graph, symbols are applying to representative value obtained from fig.4., the mean numbers of dispersion of rubble stones are shown above symbols.

#### Effect of wave period ( $T = 1.83$ s and 1.10 sec)

Fig.5a. and 5b. show a comparison of the effects of wave periods of 1.83 s and 1.10 s. In both cases, the slope of breakwater No.1 on the seaward side was 1:3 and the crown water depth  $D$  was 0 cm. In both figures, the area under the solid line is the range in which ice floes do not overtop breakwater No.1, and the area above the broken line is the range in which the ice floes overtop both breakwaters. As can be clearly seen in the figures, the shorter wave period had a greater effect on the suppression of ice floe movement, and the area of suppression of ice floe movement in the case of the longer wave period was small. The shorter wave period caused greater damage to the rubble stones, probably because the ice floes were carried by standing waves due to the large reflectivity of the longer wave period. Moreover, the area of damage to the stones almost coincided with the area in which the breakwater control the intrusion of ice floes. This is because when the ice floes move along the surface of the breakwater, especially when they are swept back in a backwash, they drag over the stones, causing some of the stones to come loose.

#### Effect of slope of the breakwater (1:1.5 and 1:3)

A comparison of the results shown in Fig.5a. and 5c. when the slopes of the breakwater were 1:1.5 and 1:3, respectively, show that there was almost no difference in the areas of suppression of ice floe movement but that there was a slightly greater suppressive effect in the case of the 1:1.5 slope. Moreover, within the area in which ice floe movement was completely suppressed, some dispersion of rubble stones was seen, and the dispersion of stones was more pronounced the smaller  $(D+H_0)/t$  was and the larger  $W_i/W_s$  was.

### Effect of crown water depth

( $D = 0, 2$  and  $4$  cm; non-dimensional crown water depth  $D/H_0 = 0, 0.22$  and  $0.44$ )

- In the case of  $T=1.83$  s and  $H_0/L_0=0.048$   
A comparison of the results of experiments shown in Fig.5a., 5e. and 5f., in which the wave period  $T$  was 1.83 s and the slope of the breakwater was 1:3 in each case, shows that the area of ice floe movement suppression was large but the damage was great when  $D/H_0$  was 0.22 or less ( $D \leq 2.0$  cm). On the other hand, when  $D/H_0=0.44$  ( $D=4$  cm), the suppression of ice floe movement was greater the larger the value of  $(D+H_0)/t$  was. This is because the ice floes were carried by the standing waves that form at the front surface of breakwater No.1 and could not approach the breakwater. There was almost no damage to the rubble stones when  $D/H_0$  was 0.22 or greater, but the damage increased suddenly when  $D/H_0$  was 0. Thus, these results indicate that although there is a greater effect on suppression of ice floe movement the smaller the crown depth is, a smaller crown depth also causes greater damage to the blocks and thus reduces the stability of the blocks.
- In the case of  $T=1.10$  s and  $H_0/L_0=0.0086$   
A comparison of Fig.5b., 5j. and 5k. shows that when  $D/H_0$  was 0, movement of the ice floes was suppressed when the value of  $(D+H_0)/t$  was small, but the stability of the blocks was poor. When  $(D+H_0)/t$  was 0.22 or greater, the movement of ice floes was also suppressed when  $(D+H_0)/t$  was large.
- In the case of  $T=1.83$  s and  $H_0/L_0=0.0086$   
A comparison of Fig.5g., 5h. and 5i. shows that when  $D/H_0$  was 0.44 or greater, the effect on suppression of ice floe movement was greater the larger was the value of  $(D+H_0)/t$ , suggesting an effect of standing waves. When  $D/H_0$  was 0, the area of suppression of ice floe movement was large. Thus, the blocks covering a breakwater will be stable if  $D/H_0$  is 0.44 or greater, and the damage will be great when  $D/H_0$  is 0.

The above results that a smaller crown depth causes reduces the stability of the blocks agree with the results considering the influence of only wavelength.

### **Piling-up of ice floes near the breakwaters and overtopping**

In this section, we will discuss the results of experiments on the piling-up and overtopping of multiple ice floes. As mentioned previously, the sizes and thickness of the model ice floes used in these experiments were based on the results of surveys on the actual sizes and thicknesses of ice floes. Fig.6. shows representative examples of the results of the experiments in which the wave period was 1.83 s, crown water depth was 0 cm, slope of the breakwater was 1:3, and wave heights  $H_0$  were 2.5, 3.5, 6.5 and 7.5 cm. When  $H_0$  was 2.5 cm (Fig.6a.), none of the model ice floes (having side lengths of 3.0, 7.5, 10.0, 13.0, 16.0 and 21.7 cm) overtopped breakwater 1. This is because the larger ice floes pile up on the top of the breakwater, stopping the movement of other ice floes.

When  $H_0$  was 3.5 cm (Fig.6b.), the ice floes with a side length of less than 13 cm overtopped breakwater 1 and some of them drifted toward the shore, while the medium-sized ice floes

(with side lengths of 7.5, 10.0 or 16.0 cm) piled up on breakwater 1 and stopped the movement of the other ice floes.

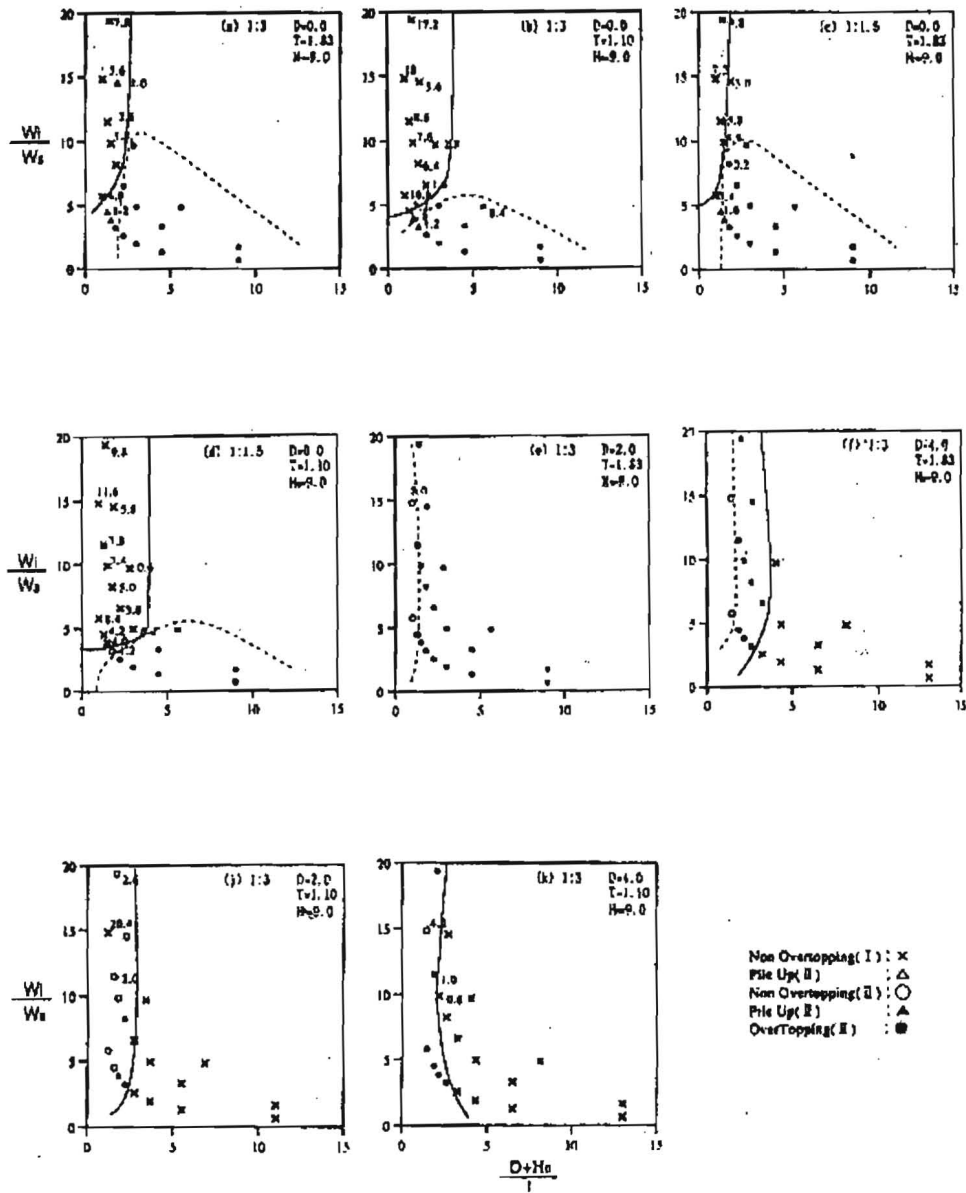
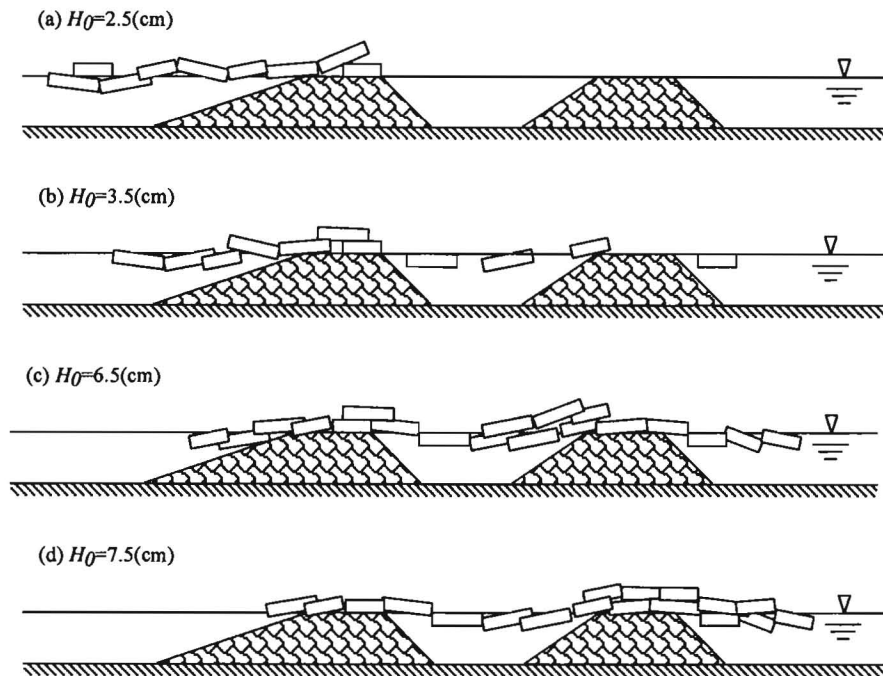


Fig.5. Areas of overtopping and suppression of movement of the ice floes



**Fig.6.** Conceptual illustrations of ice floes overtopping a doubly placed submerged breakwater

When  $H_0$  was 6.5 cm (Fig.6c.), the model ice floes of all side lengths overtopped breakwater 1 and piled up on the shoreward side of breakwater 2 and between the two breakwaters. The same result was obtained when the wave period was set at 7.5 cm (Fig.6d.). Thus, when the wave height was 6.5 cm or larger, the drift force acting on the ice floes pushed them in the shoreward direction until they piled up between the breakwaters and on the shoreward side of breakwater 2. However, it was found that since the ice floes between the two breakwaters and on the shoreward side of breakwater 2 were being pushed in the shoreward direction by drift force due to waves, the vertical and horizontal movements of the ice floes that piled up on the shoreward side of breakwater 1 were very small. Thus, the ice floes would not have a great effect on marine resources.

### CONCLUSIONS

1. In the experiments using individual model ice floes in which the slope of the breakwater and the crown water depth were kept constant, a shorter wave period produced a greater effect on the suppression of ice floe movement but also caused greater damage to the rubble stones.
2. In experiment 1, at the same wave periods and crown water depths, the suppressive effect on ice floe movement was greater when the slope of the breakwater was 1:5 than when it was 1:3.

3. In experiment 1, at the same wave periods and breakwater slopes, the suppressive effect on ice floe movement was greater, but the damage to the stones was also greater, when the crown water depth was smaller.
4. In experiment 2, in which multiple model ice floes were used, all of the ice floes overtopped breakwater 1 when the wave height was 6.5 cm or larger. Moreover, the vertical and horizontal movements of the ice floes that had overtopped the breakwater were very small.

One of the purposes for the development of doubly placed submerged breakwater is utilize the area between the two breakwaters for raising marine products such as kelp and sea urchins. Most of the damage to marine products such as kelp and sea urchins in coastal areas of the Sea of Okhotsk is caused by the movement of ice floes due to waves. The moving ice floes scrape off kelp from the rocks and crush sea urchins.

The results of this study showed that there is almost no movement of ice floes between and behind two submerged breakwaters and that the ice floes do not come into contact with the sea floor. Thus, the doubly placed submerged breakwater that the authors have developed is able to provide the same degree of coastal protection as that provided by an artificial reef in the case of a coastal area in which the difference between tide levels is small. Moreover, by laying rocks on the seabed between the two breakwaters, the area between the two breakwaters would provide an ideal area, unaffected by ice floes, for raising marine products.

#### **REFERENCES**

- ENOKI K. (1992): Control of ice floes movement by using ice boom. Proceedings of civil engineering in ocean, Vol. 8, pp. 153-158.
- MIZUNO Y. (1992): Interaction between sea ice floes and artificial reef. Proceedings of civil engineering in ocean, Vol. 8, pp. 165-169.
- SATO M. (1993): Hydraulic properties of dubbly-placed submerged rubble mount. Proceedings of civil engineering in ocean, Vol. 9, pp. 273-278.



## DESIGN OF A FACILITY FOR PREVENTING OVERTOPPING OF ICE FLOES AND ESTIMATION OF ICE LOAD

T. Hayakawa<sup>1</sup>, K. Kawai<sup>2</sup>, M. Sato<sup>2</sup>, M. Hanada<sup>3</sup>, H. Saeki<sup>4</sup>

### ABSTRACT

In 1992, when ice floes drifted to the shore, sea ice from the Okhotsk Sea crashed over the South Breakwater of Abashiri Harbor which faces the Okhotsk Sea by over topping, destroying pipelines and dolphins behind the parapet as well as causing significant damage to boats moored behind the sea wall. The possibility of such a huge overtopping of ice is a serious problem in light of the fact that the ice floes off Abashiri have recently become a popular tourist attraction and the breakwater is increasingly being used as a esplanade by tourists viewing the ice floes. Thus, the construction of an amenity-oriented breakwater that can prevent damage caused by overtopping of ice floes and provide a safe esplanade for tourists is needed.

### METHOD FOR PREVENTING ORVERTOPPONG OF ICE FLOE

Four methods for preventing overtopping of ice floes are 1) increasing the crown height of the breakwater, 2) increasing the crown height and covering the front surface of the breakwater with armor concrete blocks, 3) constructing another detached or submerged breakwater further offshore, 4) constructing a pack ice barrier in front of the breakwater, and 5) constructing an ice overtopping barrier on top of the breakwater.

In this study, we calculated the impact load of overtopping ice floes acting on top of the breakwater, which is the cheapest of the above four methods, and we designed a prototype model. We also carried out experiments to determine the speed of ice floes overtopping the breakwater and the impact ice load acting on a steel pipe with a circular cross section.

---

<sup>1</sup> Hokkaido Development Bureau Civil Engineering Research Institute, Hokkaido, Japan, Hiragisi 1-jo 3-tyome, Toyohira-ku, Sapporo, Hokkaido, Japan, Tel.: +81-11-841-1111, fax: +81-11-824-1226

<sup>2</sup> Nisimura Gumi co. Ltd., Hokkaido, Japan

<sup>3</sup> Kajima Corporation, Hokkaido, Japan

<sup>4</sup> Dept. of Engineering Hokkaido University, Hokkaido, Japan

## DESIGN METHOD

The sizes of model ice floes used in calculations to test the effectiveness of a prototype design of an ice overtopping barrier were based on the results of surveys of ice floe sizes and thickness conducted by Kunimatsu et al. The side lengths of the ice floes used in the calculations (2, 3, 4, 6, 8 and 10 meters) were based on the results of a survey conducted in 1992 at Utoro Beach facing the Okhotsk Sea, and the thickness (0.6, 0.7, 0.8, 0.8, 0.8 and 0.8) were based on the results of surveys conducted in 1993 at Omusaro Beach, beaches near Monbetsu Airport, and Sanri Beach in Lake Saroma. The cross-sectional dimensions of the breakwater used in the calculations are shown in Fig.1. The crown height of the breakwater,  $h_c$ , was 4.2 m and the foot depth of breakwater,  $h_b$ , was 6.6 m. The distance between the top of the crown and the lower surface of an ice floe overtopping the breakwater  $z$  indicates the height of the overtopping ice floe, and  $U_i$  represents the velocity of ice floe when it is overtopping the breakwater. Wave periods of  $T = 6, 8, 10$  and  $12$  sec, based on typical wave periods observed in the Okhotsk Sea, were used in the calculations, and the deepwater wavelength  $L_0$ , deepwater wave height  $H_0$  and wave height in front of the breakwater  $H$  for each wave period were calculated.

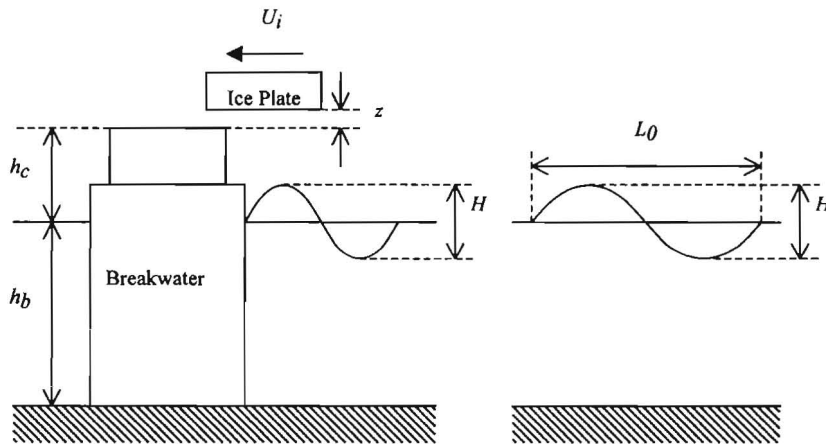


Fig.1. Cross-sectional view of the design of an ice overtopping barrier

$U_i$  was calculated from the velocity of horizontal movement of water particles  $U$ , side length of an ice floe  $a$  and wavelength  $L_0$  based on the experimental results of Sakai et al., and the range of momentum of an ice floe was examined.  $U$  was calculated by

$$U = \frac{\pi H \cosh 2\pi(h_b + z)/L}{T \sin 2\pi h/L} \sin\left(\frac{2\pi}{L}x - \frac{2\pi}{T}t\right) \quad (1)$$

and the maximum value of  $U$  at  $z = 0$  (in calm water) was used as the reference value.

Fig.2. shows the relationship between  $(H_0-h_c)/z$  and  $H_0/L_0$ , and the point at which the collision force of the ice floe acted on the ice overtopping barrier was calculated by obtaining the height of the overtopping ice floe from the graph.

Fig.3. shows the relationship between the collision force of an overtopping ice floe when it collides with an upright pile with a circular cross section and the momentum of the ice floe based on the results obtained by the authors. The vertical axis is the non-dimensional collision force of the ice floe obtained by dividing the maximum collision force of the ice floe by the ice force  $F$ . Here,  $F$  is calculated by the Eq. 2. proposed by Saeki et al. for estimating the maximum ice force acting on a structure with a circular cross section when the strain rate at indentation is  $10^3 \text{ s}^{-1}$ :

$$F = 5.0\sqrt{D} \cdot h \cdot \sigma_c \quad (2)$$

where 5.0 is the form factor of a structure with a circular cross section,  $D$  is the diameter of the structure (cm),  $h$  is the ice thickness (cm), and  $\sigma_c$  is the unconfined compressive strength ( $\text{kgf/cm}^2$ ). The force from the

collision of ice floe acting on the ice-overtopping barrier in the prototype design was calculated from the relationship between the force from the collision of an ice floe and the momentum of the ice floe.

The prototype design was calculated using stainless steel piles with a circular cross section that had a diameter of 10 cm and steel thickness of 32 mm. The value of compressive strength of the ice floe  $\sigma_c$  used in the calculations was  $20 \text{ kgf/cm}^2$  which was based on the results of past experiments.

### DISCUSSION

Fig.4. shows the relationship between the time  $t$  from the collision of the ice floe with the pile until maximum collision force is exerted and the momentum  $M$  of the ice floe. When the momentum is small,  $t$  is around 5 m·s, but  $t$  remains constant at 1 m·s when the momentum exceeds 300 kg·m/s. Based on these results, since it is difficult to consider that a single overtopping ice floe drifting in Okhotsk Sea would collide simultaneously with several upright piles, it is necessary to design a structure for the ice

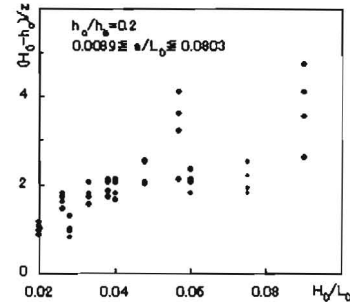


Fig.2a. Relationship between  $(H_0-h_c)/z$  and  $H_0/L_0$

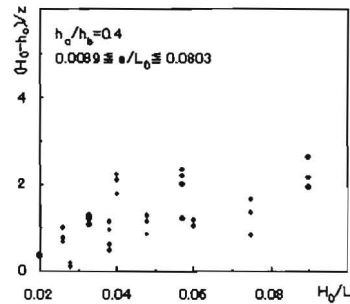


Fig.2b. Relationship between  $(H_0-h_c)/z$  and  $H_0/L_0$

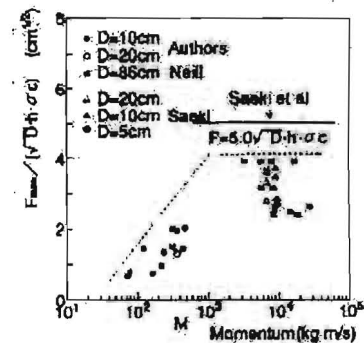


Fig.3. Relationship between the collision force and the momentum

overtopping barrier that can withstand the collision force of an ice floe acting on a single pile. Moreover, since the results of experiments carried out in Monbetsu in 1996 showed that the collision force acting on horizontal components of an ice overtopping barrier is greater than that acting on vertical components, it is important to place the horizontal components of the ice overtopping barrier behind the vertical components so that overtopping ice floes will first collide with the vertical components.

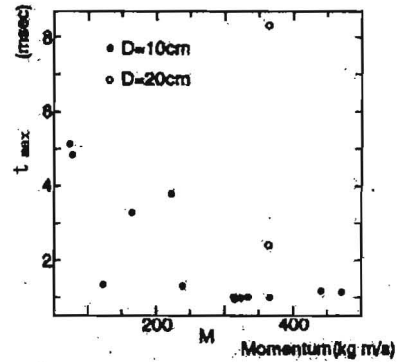


Table 1 shows the movement velocities and momentum of ice floes according to the ice floe size wave conditions.

Fig.4. Relationship between the time until maximum collision force is exerted and the momentum

Table 1

Properties of an overtopping ice floe according to wave conditions

T (s)	L <sub>0</sub> (m)	H (m)	size of the ice floe			U <sub>i</sub> (m/s)	M (kg m/s)	z (m)
			a (m)	h (m)	m (kg)			
6	56.16	4.356	2.0	0.6	220	3.45	759	0.6
			3.0	0.7	579	3.27	1893	
			4.0	0.8	1176	2.72	3199	
			6.0	0.8	2645	2.00	5290	
			8.0	0.8	4702	1.09	5125	
			10.0	0.8	7347	0.36	2645	
8	99.84	4.686	2.0	0.6	220	11.23	2471	1.0
			3.0	0.7	579	9.83	5692	
			4.0	0.8	1176	8.42	9902	
			6.0	0.8	2645	5.62	14865	
			8.0	0.8	4702	1.40	6583	
			10.0	0.8	7347	0.74	5437	
10	156.00	4.818	2.0	0.6	220	4.47	983	non-overtopping
			3.0	0.7	579	3.79	2194	
			4.0	0.8	1176	3.21	3775	
			6.0	0.8	2645	2.33	6163	
			8.0	0.8	4702	1.46	6865	
			10.0	0.8	7347	0.58	4261	
12	224.64	4.884	2.0	0.6	220	1.40	308	non-overtopping
			3.0	0.7	579	1.26	730	
			4.0	0.8	1176	1.12	1317	
			6.0	0.8	2645	0.98	2592	
			8.0	0.8	4702	0.84	3950	
			10.0	0.8	7347	0.7	5143	

As can be seen in the table, the momentum is greatest when the wave period is 8 s and the side length of the ice floe is 6 m. Moreover,  $M > 10^3$  kg·m/s in almost all cases. Fig.3. showed that the collision force increases with increases in momentum when the momentum is less than  $10^3$  kg·m/s, but the envelope shows an almost constant value at momentum greater than  $10^3$  kg·m/s, and the collision force of an ice floe is about 80 % of the ice force at indentation when the equation for estimating the maximum ice force at indentation is applied to calculation of the collision force. In other words, the collision force of the ice  $F_i$  is:

$$F_i = 0.8 \cdot 5.0 \sqrt{D} \cdot h \cdot \sigma_c \quad (3)$$

When the collision forces of ice were calculated for ice floe thicknesses of 60, 70 and 80 cm, the ice forces acting on an upright pile with a circular cross section were found to be 15.2, 17.7 and 20.2 tf, respectively. When the collision force of the ice acts perpendicularly on a pile, calculation shows that an ice-overtopping barrier with piles of about 10 cm in cross-sectional diameter will not be able to resist the force. When the collision force of ice acts on an upright pile with a circular cross section, the structure of the barrier must have a large cross section, which would increase construction costs.

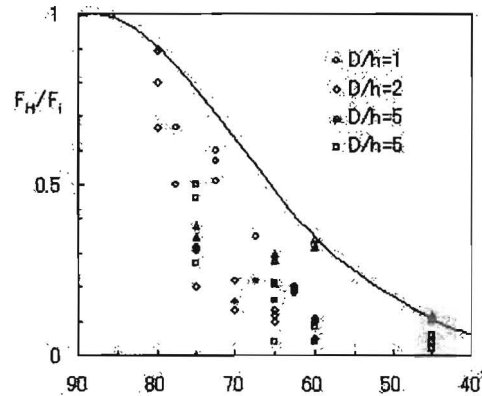


Fig.5. Relationship between the angle of inclination of a pile and force from the collision of an ice floe with the pile

Fig.5. shows the relationship between the angle of inclined piles and collision force based on the results of past experiments carried out by Saeki et al. If the collision force when the piles are inclined is represented by  $F_H$  and the angle between the horizontal plane and the pile with a circular cross section is represented by  $\theta$  ( $^\circ$ ), then

$$\frac{F_H}{F_i} = 0.425 \cdot \cos 4\left(\frac{\pi}{2} - \theta\right) + 0.575 \quad (4)$$

For example, if a pile is inclined at an angle of  $60^\circ$ , the ice force acting on the pile is only about 36 % of that acting on an upright pile. Thus, inclining the piles is an effective method for reducing the force from collision of an ice floe, and a smaller cross-sectional area of the ice-overtopping barrier would mean a reduction in construction costs.

Fig.6. shows the method for calculation of stress acting on each part of an ice-overtopping barrier when force from collision of an ice floe acts on the ice-overtopping barrier. In Fig.6a., the barrier consists of two piles with a circular cross section joined at the top by a hinge. This type of barrier is named *type A*. In Fig.6b., a pile with a circular cross section is joined at the

midpoint of the pile on the seaward side of the breakwater and set an angle parallel to the pile on the shoreward side. This type of barrier is named *type B*. The results of calculations of stresses acting on each part of the barrier when the shape of the barrier (both *types A* and *B*) is changed showed that a metal pipe with a diameter of about 10 cm will have sufficient strength to withstand the force from an ice floe colliding perpendicularly with the barrier. From the point of view of ensuring sufficient space behind the ice overtopping barrier and reducing the force from collision of an ice floe, an angle of  $60^\circ$  is thought to be the most appropriate. If the piles are set at an angle of  $60^\circ$ , the type A structure has sufficient strength to withstand the axial force but not the bending force, while the degree of stress acting on each part of the type B structure is within the range of allowable stress for the cross section. Since both types A and B are not so strong in terms of stress due to bending force, a barrier with sufficient resistance against bending should be designed by making the distance between the vertical components of the barrier short.

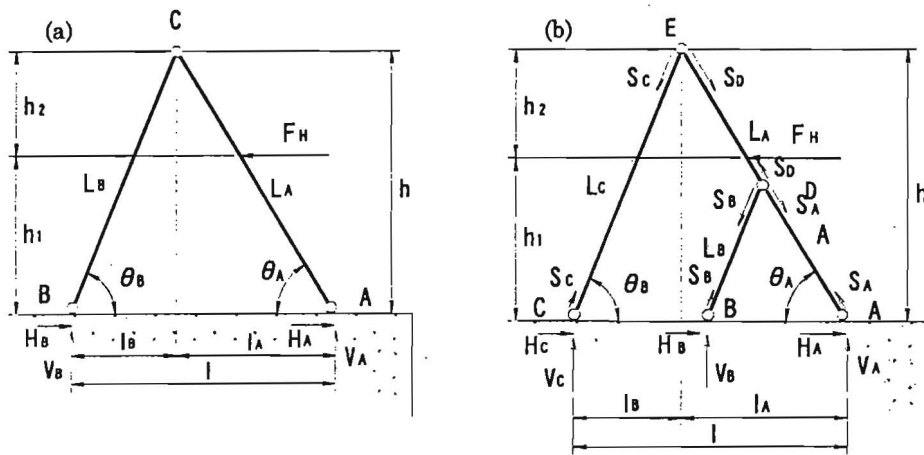


Fig. 6. Structures of ice overtopping barriers

Table 2

The cross-sectional properties of the steel pipes used in the prototype design are shown in Table 2.

Cross-sectional properties of the steel pipes used in the prototype design

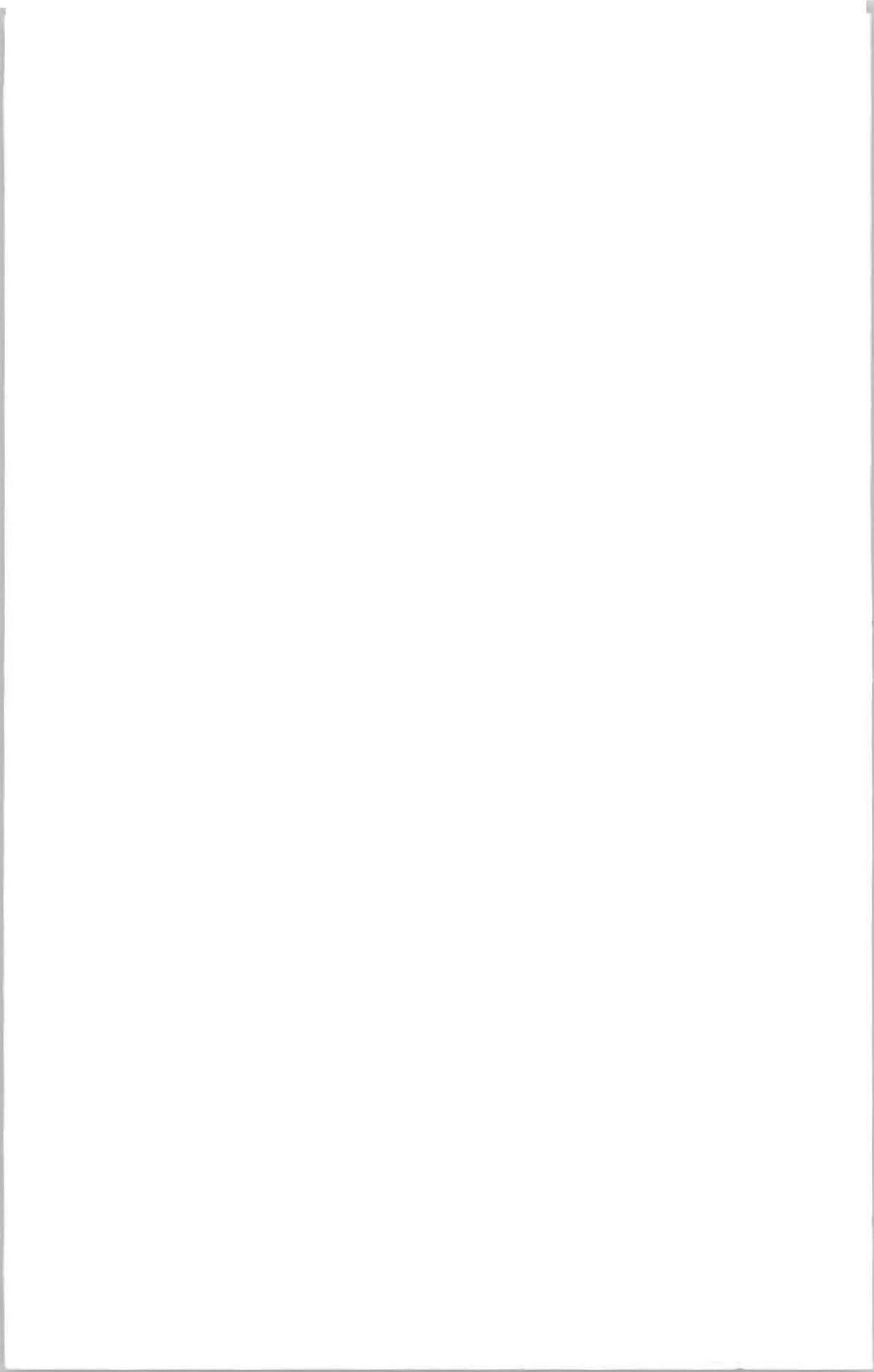
Area of cross section ⊙	68.36 cm <sup>2</sup>
Area of cross section of pile ○	96.53 cm <sup>2</sup>
Moment of inertia area	482.63 cm <sup>2</sup>
Allowable bending stress	1600 kgf/cm <sup>2</sup>
Allowable tensile stress	1600 kgf/cm <sup>2</sup>
Allowable shearing stress	915 kgf/cm <sup>2</sup>

## CONCLUSIONS

1. If the force from collision of an ice floe  $F_i$  acting on a pile with a circular cross section is expressed as the momentum  $M$  of the ice floe,  $F_i \propto \log M$  when  $M < 10^3$  and  $F_i = 0.8 \cdot 5.0 \sqrt{D} \cdot h \cdot \sigma_c$ , when  $M > 10^3$ .
2. Since the relationship between the time from the collision of an ice floe with a pile until maximum collision force is exerted and the momentum of the ice floe indicates the unlikelihood of a single overtopping ice floe colliding simultaneously with several upright piles, it is necessary to consider the collision force of an ice floe acting on a single pile in the design of the ice overtopping barrier.
3. Since the force from collision of ice floe acting on horizontal components of the barrier is greater than that acting on vertical components, the horizontal components should be placed behind the vertical components.
4. Setting the piles of the ice overtopping barrier at an inclined angle is effective because the force from collision of an ice floe acting on a pile set at an inclined angle is much smaller than the ice force acting on upright pile.
5. Since stress due to bending moment is the weakest point of the structure of an ice overtopping barrier, the distance between piles that an overtopping ice floe will directly collide with should be made as short as possible.

## REFERENCES

- KUNIMATSU S. (1993): Study on size of drift ice at the Okhotsk sea of Hokkaido. Proceedings of civil engineering in ocean, Vol. 9, pp. 95-100.
- SAKAI Y. (1994): Overtopping velocity of ice floe on the breakwater due to wave action. Proceedings of civil engineering in ocean, Vol. 10, pp. 247-252.





## NUMERICAL SIMULATION OF ICE INTERACTION WITH A VERTICAL WALL

K. Shkhinek<sup>1</sup>, T. Kärnä<sup>2</sup>, S. Kapustiansky<sup>1</sup>, A. Jilencov<sup>1</sup>

### ABSTRACT

Several methods are available for the prediction of global ice loads acting on offshore structures. A further development of these models is retarded by problems in understanding details of the ice fracture mechanisms and contact phenomena. This paper presents results of a numerical study of the ice fracturing process in a condition where a sheet of level ice drifts against a vertical faced structure. A 2D process in a vertical section of the ice sheet is modelled. The ice is considered as brittle or quasibrittle material using a modified Mohr-Coulomb failure criterion. The frictional forces on the ice-structure interface are assumed to be rate dependent at a range of low sliding velocities. A finite-difference computer programme is used to investigate the propagation of tensile and shear cracks. The results of a parametric study show that the basic features of the ice fracture process depend mainly on the ratio between the uniaxial tensile and compressive strengths of the material.

### INTRODUCTION AND OBJECTIVES

This paper addresses problems that arise in modelling dynamic ice loads acting on vertical faced offshore structures. The highest dynamic loads occur if the ice at different cross sections in front of the structure fails almost simultaneously in a failure mode known as crushing with spalling (Timco, 1986). In this failure mode, the peak global load is controlled by brittle ice failure and an extrusion process that occurs in the vicinity of the ice edge.

Morgenstern & Nuttall (1971) and Assur (1972) assumed that the failure of the ice edge is caused by shear stresses. This view was supported by Croasdale et al. (1977) who proposed a shear failure mode across the ice sheet as depicted in Fig.1a,b. The symmetric failure mode (Fig.1a.) was considered relevant for the first impact between flat surfaces of the ice edge and the structure. The asymmetric failure (Fig.1b.) was assumed to take place while the structure continues penetrating into the ice sheet. Pure crushing (Tsuprik, 1992; Kamesaki, et al 1997)

---

<sup>1</sup> St. Petersburg State Technical University, Russia

\* Polytechnicheskaya 29, 195251 St. Petersburg, Russia, Tel.: +7-812-247 5953, e-mail: shkhinek@cef.spbstu.ru

<sup>2</sup> VTT Building Technology, Espoo, Finland

and pressure melting (Gagnon, 1999) have also been seen at the ice edge as depicted in Fig.1b. After a failure due to crushing with spalling, the ice edge has often a stepwise wedge shape. To study the failure process on this kind of ice edge, Joensuu & Riska (1989) and Fransson et al. (1991) conducted laboratory tests on wedge shaped ice samples. They found that the ice pressure concentrated in a narrow line-like area and the failure process was modelled as sequential asymmetric flaking (spalling) due to shear failure (Daley, 1991).

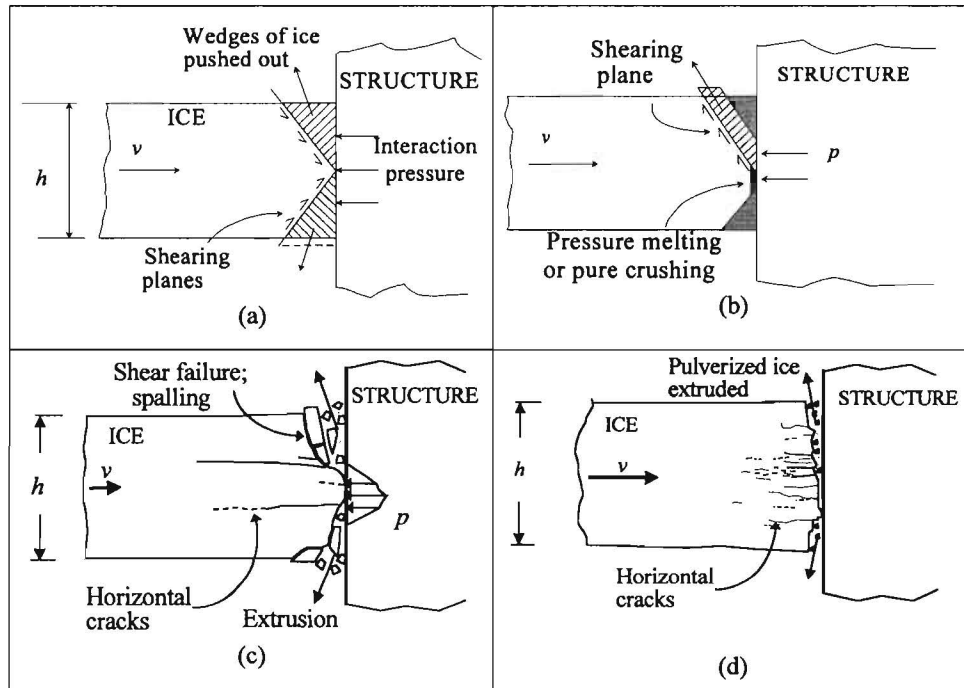


**Fig.1.** Observed/assumed variants of the ice failure mode titled "crushing with spalling".

- a) Symmetric shear failure; b) Asymmetric shear failure,
- c) Fracture with a combination of horizontal and shear cracks;  
compliant structure,  $v = 30 \text{ mm/s}$ ,
- d) Fracture with horizontal cracks; compliant structure,  $v = 80 \text{ mm/s}$ .

Hirayama et al. (1975) used strain gauges to measure the strains in the ice sheet in front of a pile that was penetrating into the ice sheet. They concluded that the maximum ice force occurs concurrently with the development of horizontal cleavage cracks that emanate from the ice edge due to the vertical strains in the ice sheet. Similar horizontal cracks have been reported from indentation tests made both in-situ (Zabilansky et al., 1975; Tsuprik, 1992; Fransson & Nyström, 1994; Kawamura et al., 1996; Takeuchi et al., 1999) and in laboratory (Fransson et al., 1991; Muhonen et al., 1992/Fig.52; Kärnä, 1994/Fig. 6; Tuhkuri, 1996). Taylor (1981) reported about indentation tests, where the crushing failure mode incorporated a combination

of horizontal tensile cracks and inclined shear cracks. Fig.1c. depicts this phenomenon as observed in thin sections taken after the indentation test No 54 reported by Muhonen et al. (1992). A high speed video record taken in similar tests showed that after each major failure event, fractured ice was extruded simultaneously up and down from the ice-structure interface. Fig.1d. depicts how the ice failure mode was changed when the nominal indentation velocity was increased from 30 mm/s (in Fig.1c.) to 80 mm/s. It is evident that the indentation velocity influences the length of the horizontal cracks as well as the wedge shaped form of the ice edge.

Details of the ice failure in crushing and spalling are not fully understood as discussed by Daley et al. (1998). In particular, the interplay between the horizontal and shear cracks needs more clarification. Therefore, the main objective of this paper is to elucidate the roles of the horizontal tensile cracks and the shear cracks in brittle ice failure.

## METHOD OF SIMULATION

### The main assumptions

This paper addresses a situation, where a semi-infinite ice sheet with thickness  $h$  is drifting at a constant velocity  $v_x = v_{ice}$  against a rigid and vertical wall. We will consider a 2D problem in a vertical plane and assume that the ice failure is brittle. The geometry of the ice edge is simplified as shown in Fig.2. The natural roughness and edge shaped geometry of the ice edge is modelled by a protrusion element with a length  $l$  and width  $w$ . This part of the intact ice is assumed to be in direct contact with the wall. In the upper and lower part of the interface, the contact forces between the intact ice and the wall are transmitted through a layer of crushed ice.

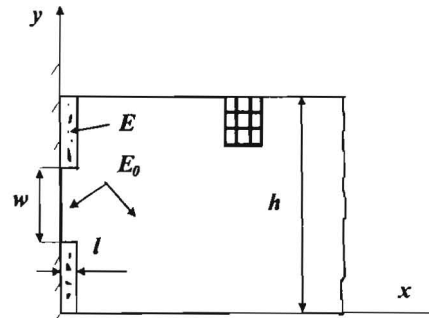


Fig.2. Ice edge geometry used in the present numerical study

The fragmented material is characterised by a compression modulus  $E$  and the parameters of the Mohr-Coulomb failure law; the cohesion  $c_r$  and the angle  $\phi_r$  of the internal friction. The intact ice is considered as brittle or quasibrittle. The material is elastic with modulus  $E_0$  until ice failure. The strength of the ice is modelled using a modified Mohr-Coulomb or Tresca failure criterions in some ranges as depicted in Fig.3. The ice sheet is assumed to be

homogenous and isotropic. Furthermore, we assume that the stress distribution and the ice failure process is symmetric about the middle level of the ice sheet.

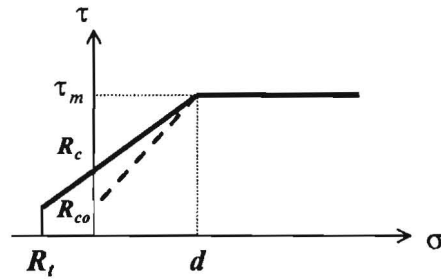


Fig.3. The modified Coulomb-Mohr failure criterion for ice strength ( $R_{CO} \equiv R_{res}$ )

#### Model for computation

The momentum equilibrium equations and the constitutive equations of the ice sheet are written as:

$$\rho \frac{\partial v_i}{\partial t} = \frac{\partial \sigma_{ij}}{\partial x_j} + g_i \quad (1)$$

$$\frac{\partial \sigma_{ij}}{\partial t} = 2G(\dot{\epsilon}_{ij} - \frac{1}{3}\dot{\epsilon}H_{ij} - rS_{ij}) \quad (2)$$

$$\frac{\partial P}{\partial t} = -K(\dot{\epsilon} - 2r\Lambda\tau) \quad (3)$$

where:

$$\tau^2 = \frac{3}{8}S_{ij}S_{ij} \quad (4)$$

$$\dot{\epsilon} = \dot{\epsilon}_{kk}, \quad (k=1,2) \quad (5)$$

Here  $x_1, x_2$  ( $x_1 \equiv x, x_2 \equiv y$ ) refer to the axis of the Cartesian system. Summation over a repetitive index ( $i, j=1,2$ ) as well as a plane strain condition is assumed. A dot above a symbol represents time derivative and the parameter  $v_i$  is the velocity in direction  $i$  ( $i=1,2$ ). Further mechanical parameters needed are the ice density  $\rho$ , shear modulus  $G$ , bulk modulus  $K$ , coefficient of dilatancy  $\Lambda$  and the acceleration  $g_2$  due to gravity.  $H_{ij}$  is the Kroneker's function ( $H=0$  if  $i \neq j$ , otherwise  $H=1$ ). The parameter  $r$  is a scalar factor used to control a condition where the stress condition achieves the level of the failure envelope (Kärnä et al., 2000).

The stress tensor is written in two parts as:

$$S_{ij} = \sigma_{ij} + P \quad (6)$$

$$P = -\frac{1}{3}\sigma_{kk} \quad (k=1,2,3) \quad (7)$$

As it was mentioned above, the Mohr-Coulomb failure criterion is used to describe the brittle failure behaviour of the intact ice. Hence, it is assumed that shear failure will occur if:

$$\sigma_2^f = -R_c + \sigma_1 N \quad (8)$$

or

$$S_2^f = -R_c + NS_1 + (1 - N)P \quad (9)$$

where:

$$S_1 = \sigma_1 + P \quad (10)$$

$$N = \frac{1 + \sin \varphi}{1 - \sin \varphi} \quad (11)$$

and  $\sigma_1, \sigma_2$  are the maximal and minimal principle stresses (compressive stresses are negative),  $R_c$  is the unconfined uniaxial strength,  $\varphi$  is the angle of internal friction of the intact ice. The upper index  $f$  refers to parameters on the failure surface. As illustrated in Fig.3., tensile failure takes place if  $\sigma_1 = R_t$ , where  $R_t$  is the tensile strength. If both shear and tensile failure can occur simultaneously, then the Fridman's (1952) criterion

$$\left| \frac{\sigma_2}{\sigma_2^f} \right| > \frac{\sigma_1}{R_t} \quad (12)$$

is used. If Eq. 12 is true, then shear failure is assumed instead of tensile failure.

After a fracture within a cell of the discretised model, the fractured ice inside the intact ice can still resist stresses (Doris, 1989). An unconfined residual strength parameter  $R_{CO} \equiv R_{res}$  together with an angle  $\varphi_0$  of friction are used in the Mohr-Coulomb law to characterise the strength of the fractured ice. The brittle or quasibrittle behaviour of the ice material is considered by assuming that there is an immediate reduction in the ice strength when the stress trajectories within a cell reach the peak yield surface of the intact ice defined by  $(R_c, \varphi)$ . The stress path in the cell concerned is then moved from the peak yield surface to the residual yield surface defined by  $(R_{res}, \varphi_0)$ .

The initial conditions in the ice sheet are given by  $v_x = v_{ice}$  and  $v_y = 0$ . The boundary conditions for the rigid and immovable structure are assumed as:

$$\sigma_{xy} = \sigma_{yy} = 0 \text{ if } y = 0 \text{ or } y = h \quad (13a)$$

$$\sigma_{xy} = f \sigma_{xx} \text{ and } v_x = 0 \text{ for } x = 0, 0 \leq y \leq h \quad (13b)$$

where  $f$  is a friction coefficient. Saeki et al. (1984) showed that the kinetic friction between ice and structure depends on the sliding velocity. Kärnä and Järvinen (1999) proposed that the rate dependant friction should be considered in the analysis of dynamic ice-structure interaction. Therefore, we approximated the kinetic friction coefficient in most simulations using the formula

$$f = \begin{cases} f_{\max} & \text{for } v_{oy} < v_{y\min} \\ a - b \ln v_{oy} & \text{for } v_{y\min} \leq v_{oy} \leq v_{y\max} \\ f_{\min} & \text{for } v_{oy} > v_{y\max} \end{cases} \quad (14)$$

where  $v_{oy}$  is the relative sliding velocity at the ice-structure boundary. Using the data of Saeki et al. (1984) for ice/concrete contact, the coefficients of this formula were taken as  $v_{y\min} = 20$  mm/s,  $v_{y\max} = 300$  mm/s,  $f_{\max} = 0.25$ ,  $f_{\min} = 0.045$ ,  $a = 0.14$  and  $b = 0.0645$ .

In the numerical solution, the ice sheet was discretised with 21 cells in the vertical direction and 80 cells in horizontal direction. A non-reflecting boundary condition was used at the end section of the model to avoid the reflection of longitudinal and shear waves from this boundary. Further details of the numerical method are given by Shkhinek et al. (1999) and Kärnä et al. (2000).

### TENSILE AND SHEAR CRACKS

A series of numerical simulations was carried out to study how various parameters influence the ice failure mode. The present paper studies the growth of horizontal and shear cracks during the ice fracture process. The main parameters of the model were varied as follows:

- $h = 1$  m;  $w/h = 0.15; 0.25; 0.35; 0.45, 0.80$  m;  $l/h = 0.06$
- $v_{ice} = 0.03 - 0.04$  m/s
- $E_0 = 5$  GPa;  $E/E_0 = 0.005$
- $R_C = 2$  MPa;  $R_t/R_C = 0.1$  or  $0.3$ ;  $R_{res}/R_C = 0.05$ .

Preliminary analysis indicated that the ice failure mode depends mainly on the ratio  $R_t/R_C$  between the tensile and compressive strengths. A review of existing data indicates that this ratio varies mostly in the range 0.15-0.30. Fig.4. and 5. show the simulated fracture patterns of the ice edge for  $R_t/R_C = 0.1$  and  $R_t/R_C = 0.3$  respectively. The white cells of the model net show the horizontal tensile cracks whereas the black cells failed according to the shear failure criterion.

Fig.4. and 5. illustrate that the ice failure mode considered involves two failure processes; shear failure and tensile failure. Shear failure develops first when the protrusion at the ice edge is destroyed. The stress concentration in the area of the protrusion induces local shear failure in a small part of the sheet nearby the protrusion. Subsequently, both  $\sigma_x$  and  $\sigma_y$  increase due to the ice motion towards the structure. At some instant the tensile stress  $\sigma_y$  induces one or several horizontal cleavage cracks, which divide the sheet in two or several layers. The layers are subjected both to bending and compressive forces. As the tensile strength is less than the compressive strength, the cleavage cracks continue to grow. They can propagate from the ice edge to a distance of about 2-2.5 times the sheet thickness.

In the case of  $R_t/R_C = 0.1$ , bending of the layers occur concurrently with shear crack formation at the edge of the ice sheet (Fig.4.). This process leads to a development of vertical tensile

cracks. These cracks arise at the tip of the horizontal cracks and lead to failure due to bending of the layers.

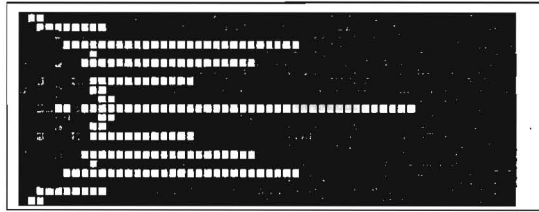


**Fig.4.** The fracture pattern of the ice edge after 20.61 ms after the initial contact. A flat ice surface was assumed. Interaction parameters were  $v_x = 0.03$  m/s,  $R_C = 2$  Mpa,  $R_t/R_C = 0.1$ ,  $R_{res}/R_C = 0.3$ . White and black colours indicate correspondingly tensile and shear failure within a cell.

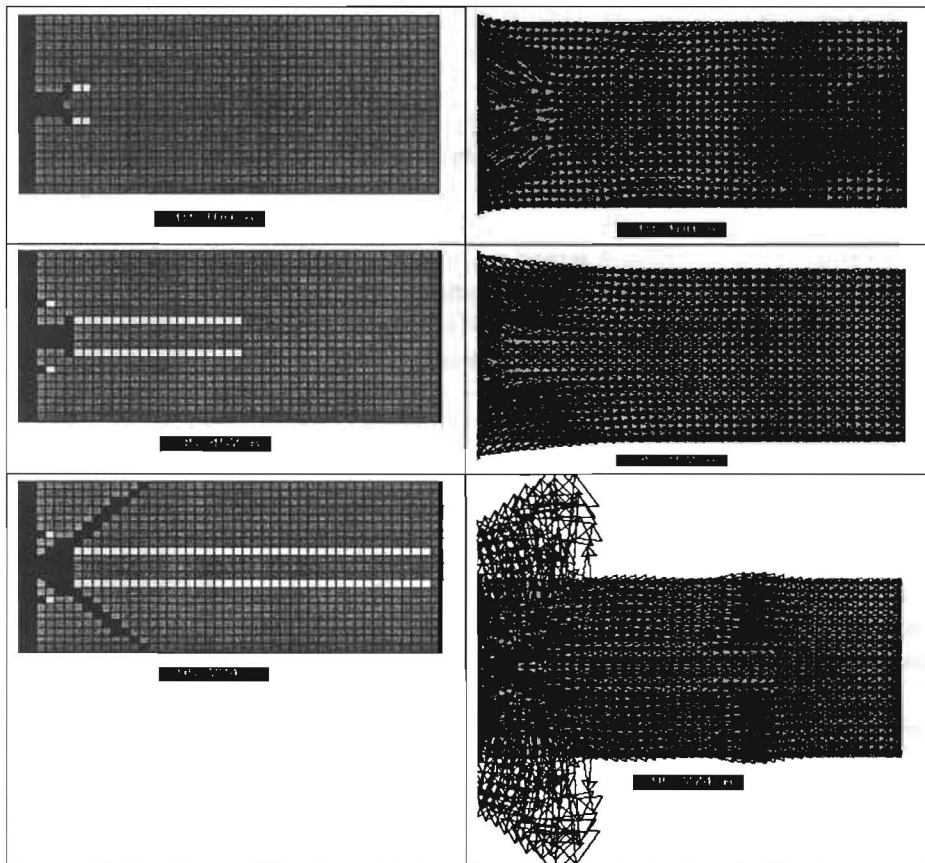


**Fig.5.** A failure mode where shear cracks dominate the failure pattern.  $v_x = 0.04$  m/s,  $R_C = 2$  Mpa,  $R_t/R_C = 0.3$ ,  $R_{res}/R_C = 0.05$ ,  $w/h = 0.15$ .

In the case of  $R_f/R = 0.3$  shear cracks that are inclined to the horizontal axis emanate from the structure surface concurrently with the horizontal cracks. The ice force and the stresses reach their peak values at the time instant when the shear cracks reach the free surface (Figs.5. and 6.). Two triangles between the structure surface and the inclined cracks form at this time and they begin to extrude from the ice-structure contact area. The arrows on the right sided figures indicate velocity vectors of the material deformation.

Our simulations indicate that under some conditions longitudinal cleavage cracks form at the tip of an inclined shear crack before the shear crack reaches the free surface. This phenomenon (indicated in Fig.1c.) has been observed in several field and laboratory tests. Hence, it seems that tensile cracks can sometimes restrict the development of shear cracks. The time record of the load has a complicated pattern in this case. After a significant drop, the force continues to increase because of an unbroken layer that transmits the load.

### LOCAL PRESSURES

Experiments show that local stresses within the ice sheet can significantly exceed the average contact pressure and the unconfined ice strength (Frederking et al., 1990). The same feature was obtained in the present simulation.

Fig.6. shows the global load as well as the local stresses in the centre of the protrusion element. The simulation depicted in Fig.5. is considered. Maximal local stress occurred in this simulation in the beginning of interaction (at 10-20 ms) while the bearing capacity of the protrusion element was exceeded. A second major peak occurred concurrently with the peak of the global load at 95.7 ms. Fig.6. shows that the maximal stresses exceed the unconfined uniaxial strength by a factor of 2 or more. At a lower indentation velocity this factor attained a value of 5.5 due to an increased effect of the velocity dependent friction. The second peak of stresses is associated with a significant confinement ( $\sigma_y \approx \sigma_x$ ) in the central part of the contact area. The abrupt drops in local stresses correspond to events of instant energy discharge due to ice extrusion.

Fig.7. shows the ice fracture pattern and the distribution of the stress component  $\sigma_y$  on three cross sections close to the ice edge about five milliseconds before the drop in the global load. A comparison with Fig.5. shows that the shear cracks develop very rapidly just before the peak load. It can also be seen that the local stress concentration at the ice edge is attenuated to an almost constant level at a distance of  $x = 0.5h$  from the ice edge.

The influence of the frictional forces at the ice-structure interface were studied in three simulations. First, the friction coefficient was assumed as  $f = 0.0$  or  $f = 0.25$ . Then, the friction was assumed to be rate dependent using Eq. 14. The results (Fig.8.) show that the local contact pressure at the ice edge increases about 70 % when the confining effect due to the friction is considered.

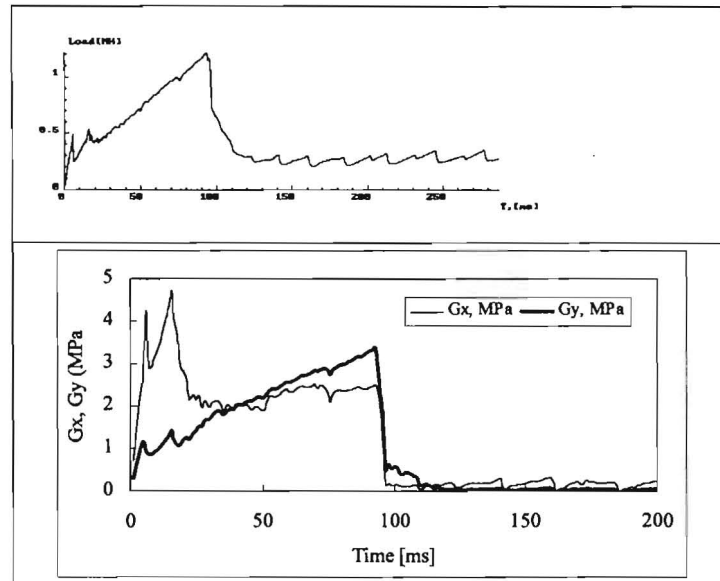


Fig.6. Time signals of the global load as well as the nondimensional normal stresses  $\sigma_x$  and  $\sigma_y$  in the centre of the protrusion in the conditions considered in Fig.5.

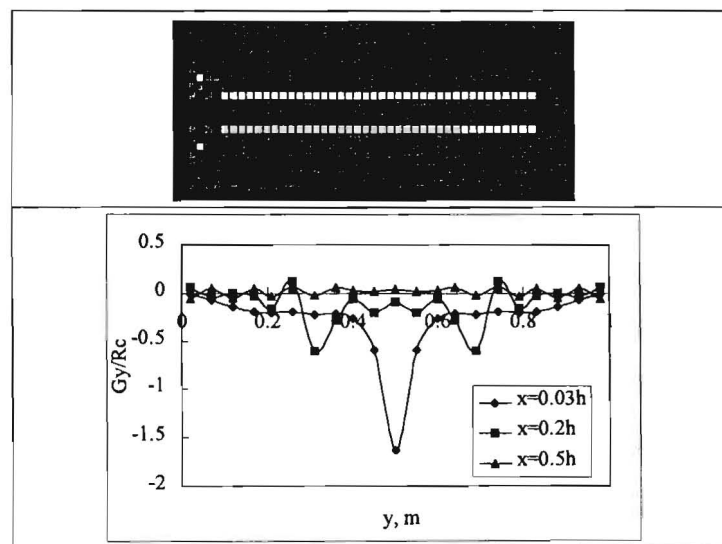


Fig.7. Distribution of the stress component  $\sigma_y$  on three cross sections of the ice edge at the time instant 90.191 ms of the simulation shown in Fig. 5.

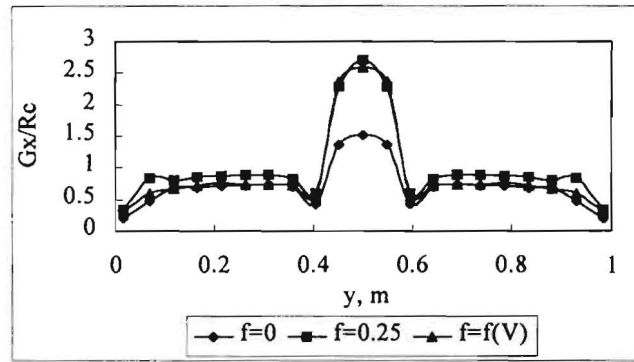


Fig.8. Distribution of the contact pressure along the contact area for different friction coefficients.  $v_x = 0.03$  m/s.

### CONCLUSIONS

This paper addresses the interaction of a vertical faced structure with a drifting level ice. Attention is drawn to a compressive ice failure mode known as crushing with spalling. Our numerical results show that both horizontal tensile and inclined shear cracks develop at the ice edge if this kind of ice fracture occurs. The tensile cleavage cracks divide the ice sheet in horizontal layers that are subjected to compressive and bending stresses in the subsequent interaction process.

The main conclusions of the present analysis are the following:

1. The ratio between the uniaxial tensile and compressive strengths of natural ice is usually in the the range of  $R_t/R_c = 0.15-0.30$ . Under these circumstances the compressive failure begins by the formation of horizontal cleavage cracks. These cracks appear to trigger the macroscopic compression failure but they do not control to peak load. The peak ice load occurs concurrently with a rapid propagation of inclined shear cracks within the ice volume at the ice edge. Bazant and Xiang (1997) have found the same result in studies of the brittle failure of a column
2. Horizontal tensile cracks do not develop if  $R_t/R_c \approx 0.5$ . Our analysis indicates that the influence of these cracks increases when this ratio decreases. In particular, the appearance of the tensile cracks appears to increase the global load because they may restrict the propagation of the shear cracks.
3. The local contact pressures can exceed the unconfined compressive strength by a factor of 2.5 to 5.5.
4. One of the main reasons of the increase in local contact pressures is the confinement that arises due to formation of the stagnation zone in the central part of the ice sheet. This zone forms at any friction coefficient and the confinement effect increases with the friction coefficient.

## ACKNOWLEDGEMENTS

The work reported here was supported by INTAS, the International Association for the promotion of cooperation with scientists from the New Independent States of the former Soviet Union and the cooperation agreement INTAS 97-1665

## REFERENCES

- ASSUR A. (1972): Structures in ice infested waters. Proc. 2nd Symposium on Ice (IAHR'72). Leningrad.
- BAZANT Z.P., XIANG Y. (1997): Size effect in compression fracture: splitting crack band propagation. *J. Eng. Mech.*, Vol. 123, No 2, pp. 162-172.
- CROASDALE K.P., MORGENSTERN N.R., NUTTAL I.B. (1977): Indentation tests to investigate ice pressure on vertical piers. *J. Glaciology*, Vol. 19, No 81, pp. 301-312.
- DALEY C. (1991): Ice edge contact, a brittle failure process model. *Acta Polytechnica Scandinavica, Mechanical Engineering, Series N 100*, 92 p.
- DALEY C., TUHKURI J., RISKKA K. (1998): The role of discrete failures in local ice loads. *Cold Reg. Sci. Techn.* 2(1998), pp. 197-211.
- DORIS J.F. (1989): The use of residual strength in the calculation of crushing loads on wide structures. Proc. 10th Int. Conf. Port Ocean Eng. Arctic Cond., Luleå, June 12-16, 1989, Vol. 1, pp. 467-480.
- FRANSSON L., OLOFSSON T., SANDKVIST J. (1991): Observation of the failure process in ice blocks crushed by a flat indenter. Proc. 11th Conf. Port Ocean Eng. Arctic Cond. Memorial University of Newfoundland, St. John's, Vol. 1, pp. 501 - 514.
- FRANSSON L., NYSTRÖM M. (1994): Non-simultaneous ice failure on wide and narrow off-shore structures. Proc. 12th IAHR Ice Symp., Trondheim, Norway, August 33-26. 1994. Vol. 2, pp. 774-783.
- FREDERKING R., JORDAAN I., MCCALLUM J. (1990): Field tests of ice indentation of medium scale Hobson's Choice Island, 1989. Proc. 10th Ice Symp., Vol. II, pp. 931-944.
- FRIDMAN J.B. (1952): *Mechanical Properties of Metals*. Moscow, 350 p. (in Russian).
- GAGNON R.E. (1999): Consistent Observations of Ice Crushing in Laboratory Tests and Field Experiments Covering Three Orders of Magnitude in Scale. Proc. 15th Int. Conf. Port Ocean Eng. Arctic Cond. Helsinki, Aug. 23-27, 1999. Vol. 2, pp. 858-870.
- HIRAYAMA K., SCWARZ J., WU H.C. (1975): Ice forces on vertical piles: indentation and penetration. Proc. 3rd IAHR Ice Symp., Hanover New Hampshire, pp. 429-445.
- JOENSUU A., RISKKA K. (1989): Contact Between Ice and a Structure. ESPOO, Helsinki University of Technology, Ship Laboratory, Report M-88, 57 p. (In Finnish).
- KAMESAKI K., TSUKUDA H., YAMAUCHI Y. (1997): Indentation tests with vertically placed ice sheets. Proc. 14th Int. Conf. Port Ocean Eng. Arctic Cond. Yokohama. pp. 245-250.

KAWAMURA M., TAKEUCHI T., AKAGAWA S., TERASHIMA T., NAKAZAWA N., MATSUSHITA H. AOSHIMA M., KATSUI H., SAKAI M. (1996): Ice-structure interactions in medium scale field indentation tests. Proc 13th IAHR Ice Symp., Beijing, Vol. 1, pp. 228-236.

KÄRNÄ T. (1994): Finite ice failure depth in penetration of a vertical indenter into an ice edge. *Annals of Glaciology* 19 1994, pp. 114-120.

KÄRNÄ T., JÄRVINEN (1999): Symmetric and asymmetric flaking process. Proc.15th Int. Conf. Port Ocean Eng. Arctic Cond. Helsinki, Aug. 23-27, 1999. Vol. 3, pp. 988-1000.

KÄRNÄ T., SHKHINEK K., KAPUSTIANSKY S., JILENKOV A. (2000): Numerical simulation of dynamic ice-structure interaction. VTT Research Notes. Technical Research Centre of Finland. Espoo. 2000 (in preparation).

MORGENSTERN N.R., NUTALL J.B. (1971): The interpretation of ice strength from in-situ indentation tests. (Report to Imperial Oil Ltd., March).

MUHONEN A., KÄRNÄ T., ERANTI E., RISKÄ K., JÄRVINEN E., LEHMUS E. (1992): Laboratory Indentation Tests with Thick Freshwater ice. Vol. I, VTT Research Notes 1370, Technical Research Centre of Finland, Espoo, 92 p.

SAEKI H., ONO T., NAKAZAWA N., SAKAI M., TANAKA S. (1984): The Coefficient of Friction Between Sea Ice and Various Materials Used in Offshore Structures. Proceedings of OTC Conference, Vol. 1, OTC 4689.

SHKHINEK K., KAPUSTIANSKY S., JILENKOV A., KÄRNÄ T. (1999): Proc. 15th Int. Conf. Port Ocean Eng. Arctic Cond. Helsinki, Aug. 23-27. Vol. 2, pp. 877-886.

TAKEUCHI T., SASAKI M., AKAYAWA S., KAWAMURA M., SAKAI M., HAMAN Y., KUROKAWA A., SAEKI H. (1999): Contact Ratio in Ice/Structure Interaction Based on Statistical Generation of Ice Failure Surface. Proc. 9th ISOPE Conference, Vol. II, pp. 505-511.

TAYLOR T.P. (1981): An experimental investigation of the crushing strength of ice. Proc. 6th Int. Conf. Port Ocean Eng. Arctic Cond. Québec, July 27-31, 1981. Vol. 1, pp. 332-345.

TIMCO G.W. (1986): Indentation and penetration of edge-loaded freshwater ice sheets in the brittle range. Proc. 5th Int. Offshore Mechanics and Arctic Eng. Symp., Vol. IV, ASME, New York, pp. 444-452.

TSUPRIK V.G. (1992): Consideration of the mode of contact ice failure in determining ice forces acting on offshore structures. Proc. 2nd ISOPE Conf., San Francisco, Vol. II, pp. 790-794.

TUHKURI J. (1996): Experimental Investigations and Computational Fracture Mechanics Modelling of Brittle Ice Fragmentation. *Acta Polytechnica Scandinavica, Mech.Eng.Series*, 120: 105 p.

ZABILANSKY L.J., NEVEL D.E., HAYNES F.D. (1975): Ice forces on simulated structures. Proc. 3rd IAHR Ice Symp., Hanover, NH. USA. pp. 387-395.



## ICE-SKIMMING BOOMS FOR RIVERSIDE DIVERSIONS

O.Kubit<sup>1</sup>, R. Ettema<sup>2</sup>

### ABSTRACT

Skimming booms guide, or “skim”, ice away from an undesired area. They usually are placed at acute angles to river currents; so as to have a flow velocity acting along the boom face. Ice, consequently, is flushed along the boom face. Ice-skimming booms usually are a first line of defense in an ice-control system at diversions. As this paper shows, they are an attractive alternative, since, for relatively low concentrations of ice flow, they can effectively eliminate ice blockage of diversions, at least for situations entailing low concentrations of drifting ice.

### INTRODUCTION

Most water-resource projects involving water diversions (e.g., for thermal plants, hydroelectric plants, pumping stations, and navigation locks) require some form of control to prevent drifting ice from clogging intakes, adversely affecting flow patterns, and requiring awkward ice removal and disposal systems. Skimming booms are a potentially useful ice-control option for deflecting or skimming drifting ice away from a diversion. Ice-skimming booms have many similarities to ice-retention booms, and commonly serve secondary functions as debris and safety booms.

Numerous variables may influence the performance of skimming booms. Kubit (2000) provides a fairly detailed discussion on about 30 non-dimensional parameters that influence boom performance. A definition sketch of variables for a general bent boom is shown in Fig.1., which illustrates how a bent boom is placed riverward to diminish the influence of flow diversion on ice drift. The most important design variables for skimming booms are orientation, depth, and the relative magnitudes of flow currents in the river and diversion. Fairly numerous articles describe retention-boom performance; eg. Kennedy and Lazier (1965), Perham (1988), Foltyn et al. (1996), and Abdelnour et al. (1998).

---

<sup>1</sup> Iowa Institute of Hydraulic Research, Department of Civil and Environmental Engineering, University of Iowa, Iowa City, Iowa, 52246; PH (650) 593-5063; e-mail: owenkubit@hotmail.com

<sup>2</sup> Iowa Institute of Hydraulic Research, Department of Civil and Environmental Engineering, University of Iowa, Iowa City, Iowa, 52246; PH (319) 335-5224; FAX (319) 335-5238; e-mail: robert-ettema@uiowa.edu

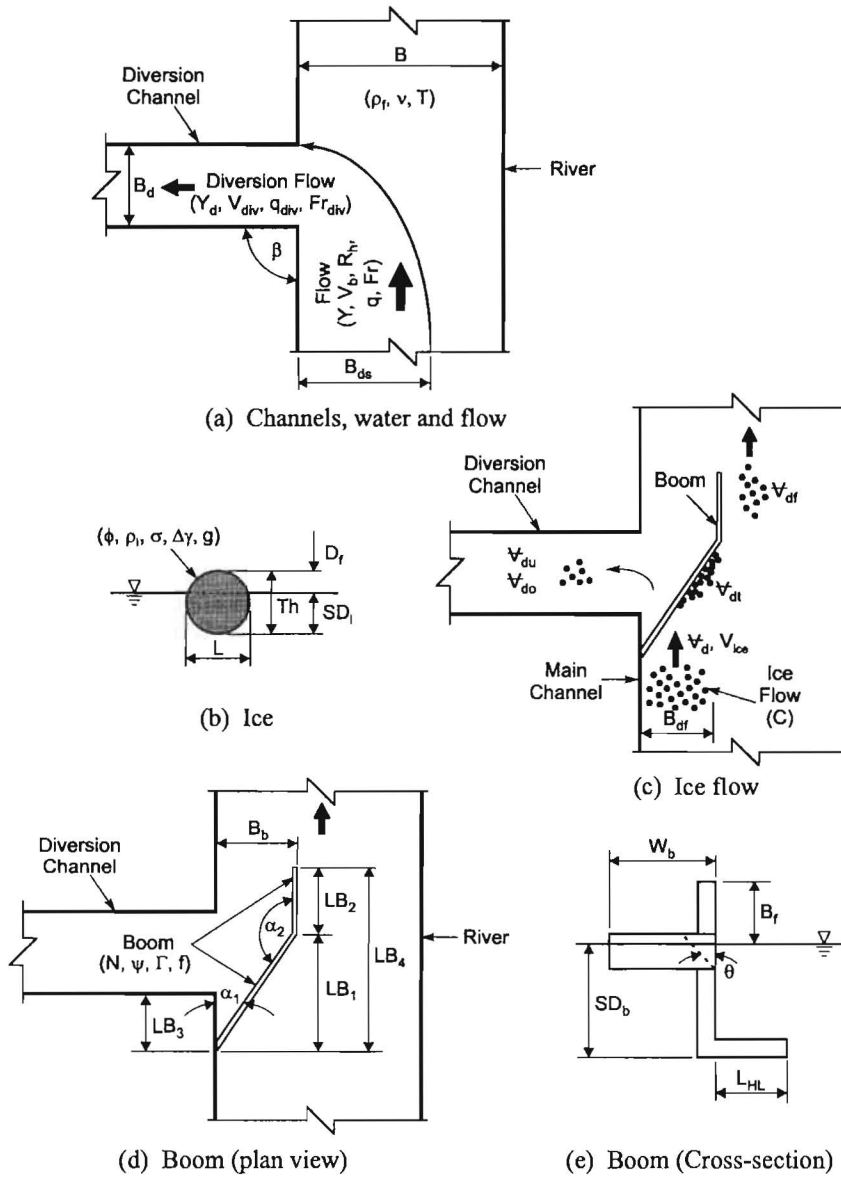


**Fig.1.** Variables associated with bent booms (straight boom,  $LB_2 = 0$ ); Kubit (2000) defines all variables.

## FLUME EXPERIMENTS

Experiments were conducted using a laboratory flume, with polypropylene pellets simulating drifting ice. Two boom shapes were tested: straight booms and bent booms. The straight boom is a simplified bent boom whose downstream boom segment,  $LB_2$ , is zero. Numerous tests were performed to investigate the influence of boom orientation, location, depth, and flow conditions on boom performance. Observations included location, size and mechanisms causing ice passage and accumulations along the boom. The range of Froude numbers tested covers values typically found in riverine and intake settings.

## PROCESSES

The four main hydraulic processes associated with boom performance include ice approach, ice accumulations along the boom, ice passing the boom, and ice flushing. These four processes are shown in Fig.2a.-f., which illustrate model-ice behavior at a bent boom. Essentially the same processes occurred at a straight boom. Each of these four processes is discussed briefly below.

Ice approach is strongly influenced by the dividing streamline geometry, which dictates the ice trajectory and volume impacting the boom. Generally, all ice within the dividing streamline impacts the boom. However, some ice outside the dividing streamline impacts the boom when the boom extends across the river (Fig.2a,b). Streamline contraction caused flow acceleration just upstream of the diversion, and was a primary cause of ice passage on the front of the boom.

### Ice Passage

Ice may enter the diversion channel by passing both under and over the boom. Mechanisms causing ice passage include hydrodynamic forces, waves, ice impact, and boom movements (tilt, sway, and submergence). Ice typically passed under the upstream boom segment as a result of flow contraction and acceleration at the intake entrance. At the downstream end, it only occurred during high Froude numbers in combination with a small boom distance out. Most ice enters the intake as it initially reached the boom. This observation reflects the importance of high velocities for ice passage to occur. In general, ice passage increases with an increase in  $V_r$ ,  $\alpha_1$ ,  $Fr$ ,  $Fr_{div}$ , and the presence of waves, boom tilt, and boom submergence. Ice passage decreases with an increase in  $SD_b/SD_d$ ,  $Lb_3/B_d$ , and  $LB_3/LB_1$ . Ice passage increases on the boom front, and decreases on the boom side, with an increase in  $B_b/B_d$ .

### Ice Flushing

Ice that does not accumulate along the boom or pass under/over the boom, is flushed downstream. Most of the ice that flushes does so immediately after impacting the boom. However, some ice s may accumulate along the boom, and be flushed downstream after remaining stationary for a period of time. Hydrodynamic forces, ice impact, and boom movement promoted ice flushing.

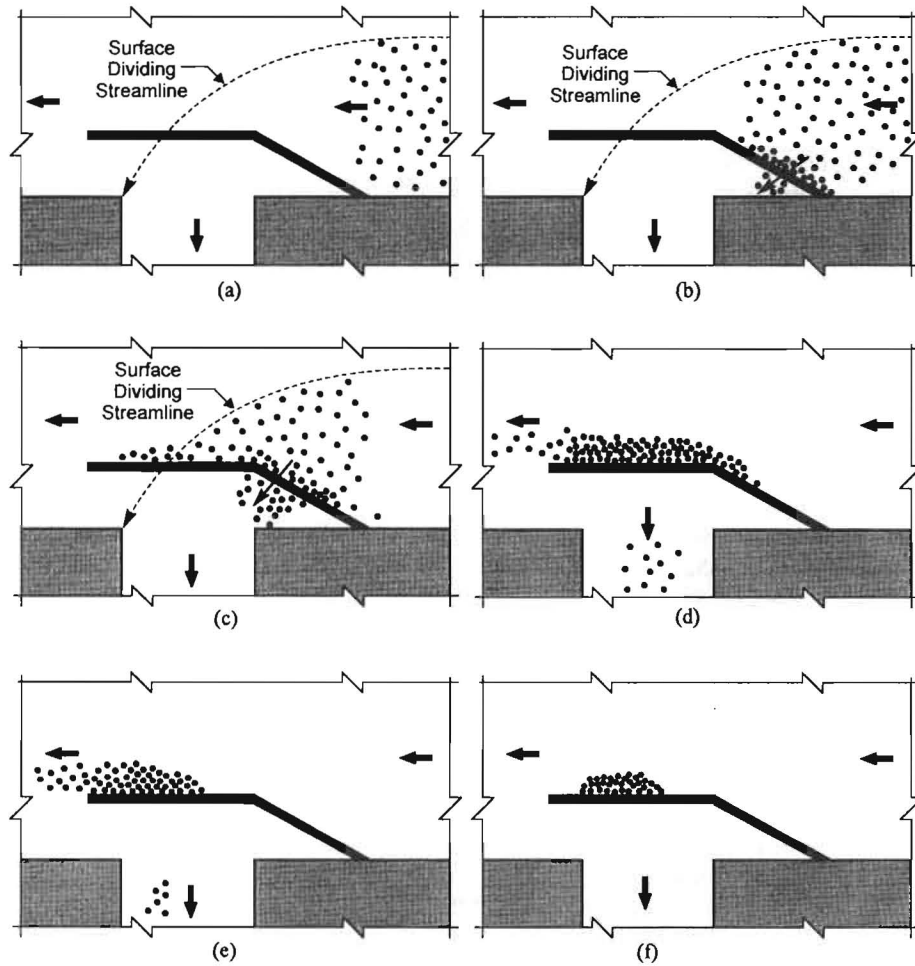


Fig.2. Schematic of ice skimming, passage and accumulation at a bent boom

## BOOM PERFORMANCE

### Straight Booms

The straight boom tests provide comparative performance data for a range of boom angles and velocity ratios. The test results are shown in Fig.3. A  $0^\circ$  boom provides good protection against ice passage, but the worst protection against accumulations. A  $0^\circ$  boom could be a viable alternative under low flow conditions ( $V_r < 0.8$ ), or during higher velocity ratios if artificial flushing methods, such as jet pulses or manual shoving, are employed. A  $30^\circ$  boom provides the best flushing performance over the entire range of flows tested. However, at low velocity ratios ( $V_r < 1.25$ ), smaller boom angles can provide equal flushing performance (Fig.3.). Smaller boom angles also experience lower ice passage. Hence, the smallest possible

angle should be used to minimize ice passage and interference with river traffic, while considering needs to minimize ice accumulations. Fig.3. is the primary product of the straight-boom tests. It provides boom angles that eliminate ice accumulations in the model environment as a function of velocity ratio. Fig.3. also shows flow regions where ice accumulations could not be prevented with straight booms. In these flow regions bent booms are recommended.

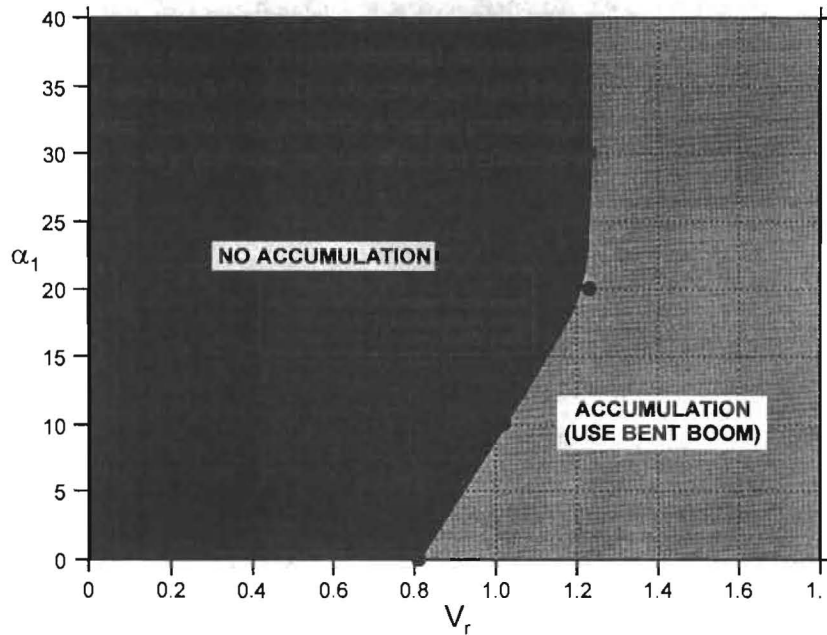


Fig.3. Optimum boom angle  $\alpha_1$  vs velocity ratio  $V_r$ ; straight boom

#### Bent Booms

Bent booms provide better overall performance than do straight booms. In particular, they deflect ice outward, and their distance out at their downstream end reduces ice accumulations. Ice passage increases with  $Fr$ ,  $Fr_{div}$ , and  $V_r$ , while ice accumulations vary only with  $V_r$ . The primary product of bent boom tests is Fig.4., which provides recommended boom distance out for a range of velocity ratios to prevent ice accumulations. A minimum boom distance out ( $B_b/B_d$ ) equal to 0.025 is recommended to account for horizontal boom sag, and ensure the boom is not recessed in the intake. The motive for this recommendation is the profusion of recessed and sagging booms trapping ice, as observed by the authors.

For the usual range of  $V_r$  values, at riverside diversions ( $V_r < 1.5$ ), bent booms only need extend at most 35 % of the dividing streamline width across the main channel to deflect all ice. This is considered a significant finding since a boom width equal to 100 % of the dividing streamline width was originally envisioned, and tested. The smaller boom width will reduce

impacts on river traffic. Flow acceleration just upstream of the diversion caused ice passage under the boom. However, ice passage was nominal when the upstream distance from diversion channel,  $LB_3/B_d$ , was 1.25.

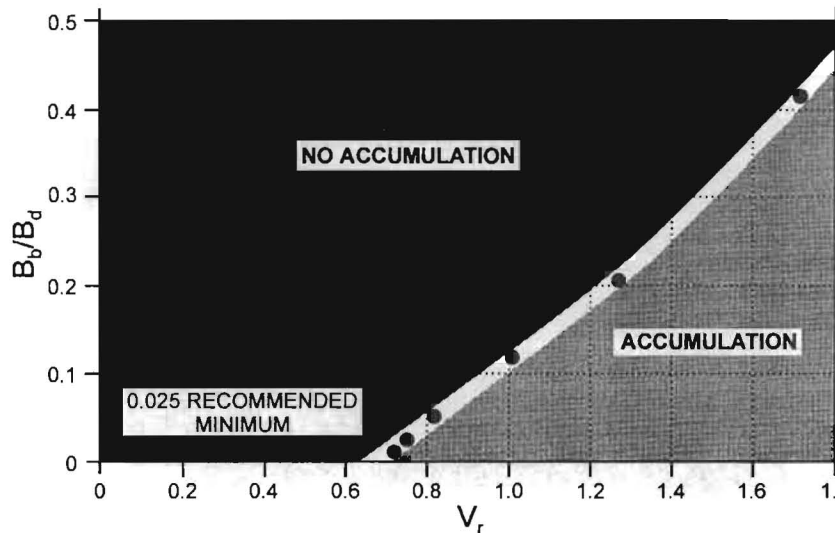


Fig.4. Boom distance out  $B_b/B_d$  vs velocity ratio  $V_r$ .

The boom angle,  $\alpha_b$ , was kept constant at  $30^\circ$  for all bent boom tests based on the results of tests with the straight booms, which showed  $20^\circ \sim 30^\circ$  provided optimal flushing. A boom angle as high as  $45^\circ$  may be possible if the boom has a smooth face, and is placed sufficiently upstream of the intake ( $LB_3/B_d > 1.25$ ).

#### CONCLUSIONS

Fig.5. summarizes the design criteria developed for bent boom deployment. The following additional recommendations should be made:

1. Enable booms to float freely with changes in water level.
2. Provide an anchoring system minimizing boom tilt, sway, and submergence, all of which decrease boom performance.
3. Eliminate horizontal boom sag, which promotes long-term retention of ice.

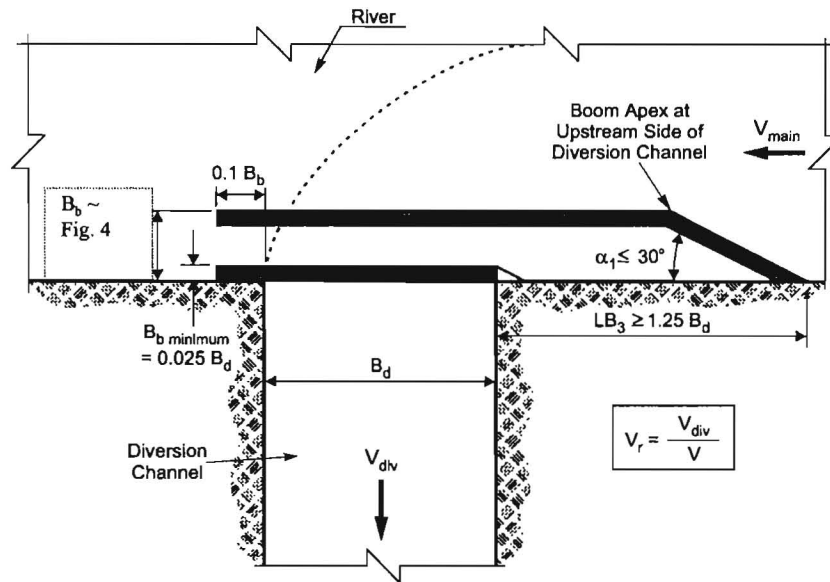
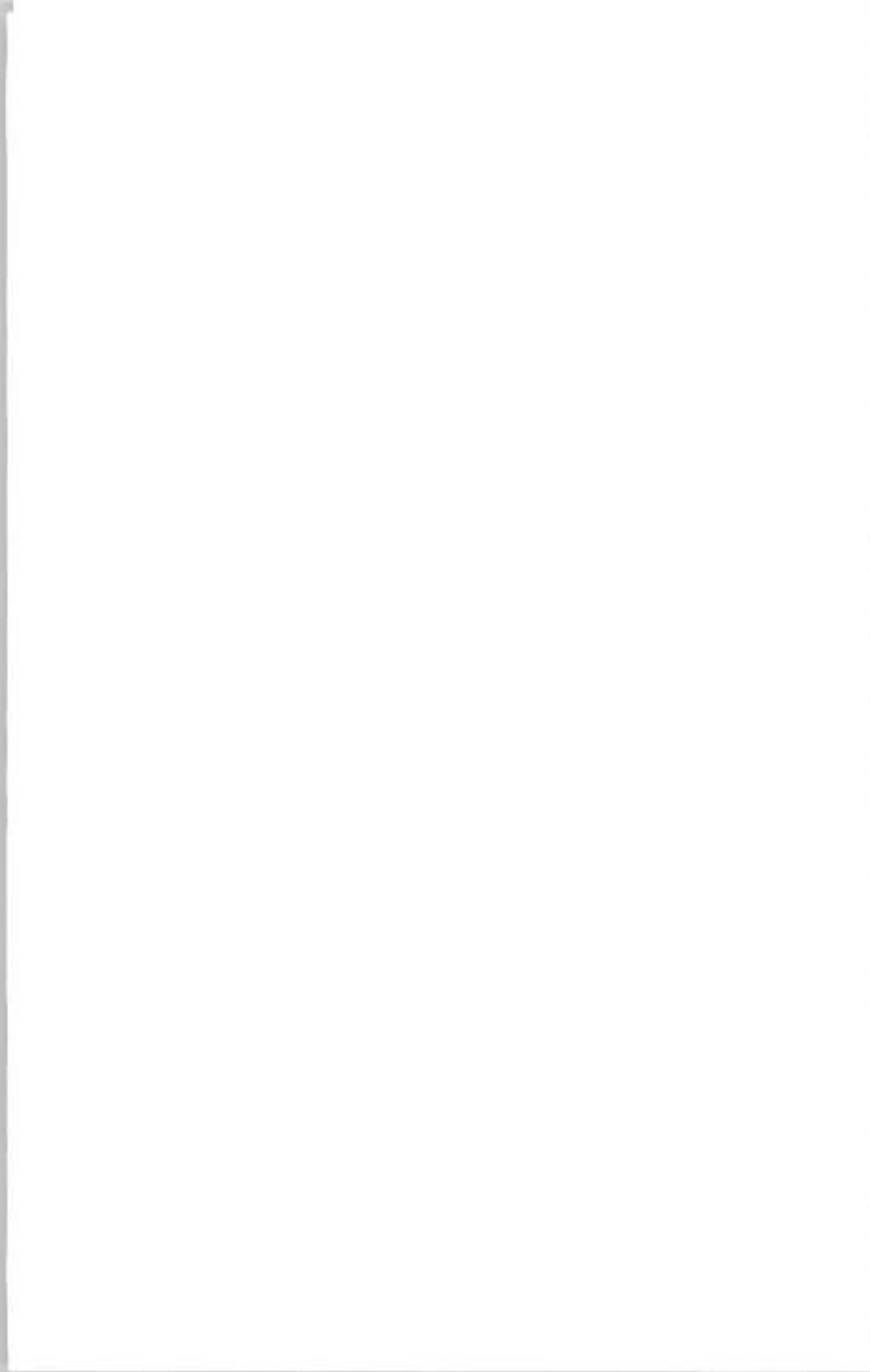


Fig.5. Recommended design parameters for bent boom deployment

#### REFERENCES

- ABDELNOUR R., NICHOLSON C., GONG Y. (1999): The Design, Fabrication, and Deployment of an Ice Boom to Protect Two Hydroelectric Power Plant Water Intakes from Ice Blockages During Winter. Proc. 14th International Symposium on Ice, Potsdam, NY, pp. 669-678.
- FOLTYN E. P., TUTHILL A. M. (1996): Design of Ice Booms. Cold Regions Technical Digest, 96(1), USACE Cold Regions Research and Engineering Laboratory, Hanover, N.H., pp. 1-31.
- KENNEDY R.J., LAZIER S.S. (1965): The Water Transportation of Pulpwood III. Structures. Pulp and Paper Research Institute of Canada, Montreal, Canada.
- KUBIT O.E. (2000): Ice-Skimming Booms for Riverside Water Intakes. Master's Thesis, Univ. of Iowa, Iowa City, IA.
- PERHAM R.E. (1988): Elements of Floating-Ice Control Systems. Technical Rep. REMR-HY-3, USACE Cold Regions Research and Engineering Laboratory, Hanover, NH.





## OBSERVATIONS ON THE WINTER PERFORMANCE OF CHANNEL-STABILIZATION STRUCTURES

R. Ettema<sup>1</sup>, L. Zabilansky<sup>2</sup>, J. Wuebben<sup>2</sup>

### ABSTRACT

Presented herein are winter observations of channel-stabilization structures at a site along the Fort Peck reach of the Missouri River. The observations were made in the course of conducting a survey that entailed extensive monitoring and detailed measurements of channel bathymetry, ice conditions, and flow-velocity distribution at sites along the Missouri River during the winter of 1998-1999. The survey of ice-cover influences on channel stability at one site provided a unique opportunity to monitor the wintertime performance of several methods for channel and riverbank stabilization implemented along the upstream half of the site.

### INTRODUCTION

The survey site is located at about river mile 1716 of the Fort Peck reach of the Missouri River. The reach, overall, stretches about 300 km from Fort Peck Dam, Montana, to Lake Sakakawea, North Dakota. The site itself is about 2 km long, and it comprises a channel of alluvial sinuous-braided morphology well known for its shifting thalweg and erosion-prone banks. The river forms a single-thalweg channel in most bends, which commonly occur where the river's course abuts against adjoining hills. Between bends, the river widens and usually flows in two sub-channels separated by low alluvial bars. At such locations, one sub-channel usually was larger and, thereby, formed the principal thalweg of the river. The river's banks largely comprise silty soils, typically layered with sand lenses, with clay zones. The banks commonly stand with a near vertical face, which flowing water quite readily may erode.

Fort Peck Dam regulates flow through the Fort Peck reach of the Missouri River. Flow-rate data from the Dam indicate that flow in the reach began at about 210 m<sup>3</sup>/s during October and November 1998, rose quite rapidly to about 300 m<sup>3</sup>/s throughout December, then rose again to about 341 m<sup>3</sup>/s during January and February. The flow rate dropped to about 255 m<sup>3</sup>/s during March, declining down to about 227 m<sup>3</sup>/s during April 1999.

---

<sup>1</sup> Iowa Institute of Hydraulic Research, Iowa City, IA 52242; e-mail: robert-ettema@uiowa.edu

<sup>2</sup> U.S. Army Cold Regions Research and Engineering Laboratory, Hanover, NH 03755

The winter of 1998-1999 was relatively warm for northeast Montana. The accumulated total of ( $^{\circ}\text{C}$ ) freezing-degree-days (afdd) for the period March 1998 through March 1999 winter was about 920 afdd. In contrast, the year running March 1996 through March 1997 was one of the coldest periods, having 1700 afdd. Ice-cover thickness ranged from about 0.20 to 1.00 m over the sites, being thicker at locations where the ice cover initially had formed as a thicker accumulation of juxtaposed frazil-ice pans. The initial formation of an ice cover typically elevated flow stage by about 1.0 m at the site.

#### **CHANNEL-STABILIZATION METHODS**

The observation site comprised two segments, one with channel-stabilization structures, and the other without structures. The locations of the structures are indicated in Fig.1. The following riverbank stabilization methods are implemented at the site: bendway weirs; log groins; log cribs; and, hay-bale revetment on riprap toe. The stabilization methods were implemented in 1997, and had undergone two winters prior to the survey. Fig.2., by way of example, shows the tall log groins frozen into the ice cover at the site. The methods were designed for openwater conditions. USCOE-Omaha (1997) and LaGrone and Remus (1998) document the design considerations associated with each stabilization method. The methods were implemented to address in part the specific severe bank erosion concerns at the site, and in part as a trial of several potentially cost-effective techniques for riverbank stabilization. Mellema (1997) describes the background to the stabilization methods and observations concerning the performance of each method under openwater conditions.

#### **PERFORMANCE OF CHANNEL-STABILIZATION METHODS**

Extensive bank erosion occurred along the unprotected half of the site's concave bank. The channel bed deepened (by about 2 m) along the toe of the bank. Consequently, the channel thalweg along this portion shifted slightly south toward the concave bank. The main bank erosion process observed was bankfast-ice loading and weakening of the bank. Freeze-thaw weakening of the bank material was a contributing factor, but it was not monitored, other than to observe that as a bank weakened by river-ice action, top-of-bank cracks widened, and thereby enabled deeper penetration of freezing of bank material.

##### **Bendway Weirs**

The two bendway weirs weathered the winter survey period apparently unscathed. Flows were of sufficiently large magnitude, and therefore flow stage sufficiently high, that the weirs lay submerged beneath the ice cover. The depth of submergence, though, was a matter of about 0.5 m. Additionally, the bendway weirs appear not to have been significantly damaged by ice during ice-cover breakup, as the ice cover weakened and disintegrated in place. Though the bendway weirs remained intact, the bank immediately upstream of bendway weir 2 suffered a local failure. A cusped segment of the bank collapsed (Fig.3.), most likely doing so immediately following ice-cover breakup.

Although no flow-velocity measurements were taken in the vicinity of the bendway weirs, it appears from observation of openwater-flow currents at the weirs that the weirs may have

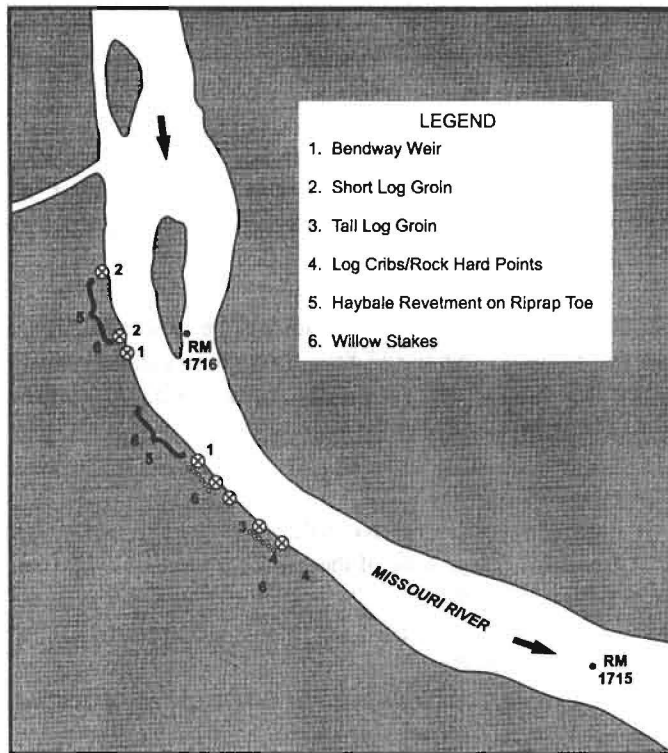


**Fig.1.** Locations of channel-stabilization methods



**Fig.2.** Tall log groins frozen into ice cover

partially blocked flow along the bank. The bendway weirs would have caused the flow to make a sharp turn at the weir, and thereby locally increased flow velocities and turbulence along the bank. This consequence may have led to localized scour of the bed at the bank toe, and thus contributed to the collapse of a portion of bank immediately upstream of bendway weir 2. This consequence is a prime concern associated with the use of upstream-oriented groins. The bendway weir, when not fully submerged or submerged to a shallow depth, essentially acts as an upstream-pointing groin.

Because the underside of the ice cover sat only about 0.5 m above the crest of the bendway weirs, flow over the bendway weir would have been constricted, thereby diminishing the desired effect of the weir turning flow away from a bank. Further investigation is needed of bendway weir performance in ice-covered flow.

#### **Hay-Bale Revetment on Riprap Toe**

A segment of the bank protected by the hay-bale revetment and its riprap toe failed. The segment is located immediately upstream of the bendway weir 2, which may have played a role in the bank's collapse. The elevation of the ice cover was such that the cover formed around and into the hay bales, which were wrapped in a geotextile fabric. The ice cover did not seem to have directly damaged the bales. It froze well into the bales, enveloping them. They, in turn, seem to provide a reasonably secure anchoring for the bankfast ice; the bales, themselves, are anchored to the bank top by means of steel cables. The crack delineating the outer extent of the bankfast ice was located outside the bales.

Flow conditions at the bank toe, however, seem to have undermined and removed the riprap protection placed beneath the bales, and thereby de-stabilized the bank. Once the ice cover broke up and no longer propped the bank, the bank failed in a more-or-less classic semi-circular failure surface. Fig.3. shows the collapsed segment of bank. Upstream, where the riverbank is parallel to the thalweg, the hay-bale revetment showed no sign of ice damage. There a wider riprap base provided adequate support for the bankfast ice as water receded following breakup. The wider beach uniformly supported the ice blocks, preventing block tipping and off-bank sliding, with commensurate damage to the riprap and the bank.

#### **Riprap**

The stone used to form the layer of riprap placed to protect the lower elevations and toe of the river bank is under-sized for ice conditions. Riprap stone could be plucked from the bank by bankfast ice as it rotated and collapsed from the bank immediately subsequent to ice cover breakup. As an approximate rule of thumb (e.g., Wuebben, 1995), riprap subject to ice plucking or ice impact should comprise stones of diameter equal to ice-sheet thickness. Large gravel stone, with diameters in the range of 0.05 to 0.15 m was used for control of upper-bank erosion, and cobbles with diameters in the range of 0.15 to 1.0 m were placed for controlling erosion of the bank toe (USCOE-Omaha, 1997). Additionally, as noted above, a wider riprap bench may reduce ice loading during collapse of bankfast ice.

### **Log Groins**

The log groins froze into, and were encompassed by, the bankfast ice that formed along the site's south bank. The groins, which are built from long log poles, withstood the ice loads associated with the ice cover, and appear to have experienced no damage when the cover broke up and departed the site. Fig.4. illustrates an inadvertent effect of the log groins that resulted in adverse consequences for the riverbank either side of the groin. The groins, by locally supporting the ice cover, enabled the bankfast ice to extend further out from the bank than would otherwise occur. In some circumstances the wider bankfast ice may help in fending drifting ice away from the bank. However, when the riverbank is steep, as at the site, a wider band of bankfast ice cantilevered from the bank exerts a larger load on the bank face; in approximate terms, the load increases proportionately with the square of the width of the bankfast ice. As can be seen from Fig.4., collapse of bankfast ice strips soil and vegetation from the face of the bank.

### **Log Hardpoints**

The log hardpoints, being short, stout, and submerged well below the ice cover appeared to function effectively. They suffered no damage attributable to ice. Also, they did not unduly increase the local width of bankfast ice. They did not extend bankfast ice width.

### **CONCLUSIONS**

Several tentative conclusions can be drawn regarding the performance of channel- and riverbank-stabilization structures during frigid winter conditions:

1. The length of such structures should not exceed the normal width of border ice at the bank they are required to protect. Compared to openwater conditions, shorter and closer spaced structures are preferable for use in ice-covered flow. Structures longer than the normal bankfast-ice width move the crack along the shoreline towards the channel, hence widen bankfast ice and, thereby, may excessively load banks. Bankfast ice between and near the timber groins at the site formed significantly wider than elsewhere at the site. When the river was ice covered, the bankfast ice formed a floating membrane attached to the groins and the bank. However, when the ice cover broke-up and flow stage subsided, large slabs of bankfast ice collapsed, damaging the banks and vegetation along the banks.
2. Ice formation may alter the flow field around long groins and bendway weirs so as to negate their intended action. Ice formation concentrated flow locally toward the bank rather than away from the bank. This adverse effect may have contributed to the collapse of a section of bank protected by riprap and hay bales.
3. Riprap stone must be sized, and riprap slope configured, for bankfast-ice conditions. At some locations along the protected bank, riprap stones had been plucked from the bank by collapsed bank ice. The upper elevation of riprap stone placement should take into account the probable elevation of the ice cover.



**Fig.3.** Bank failure consequent to ice-induced undermining of riprap



**Fig.4.** The log groins may have increased the width of bankfast ice

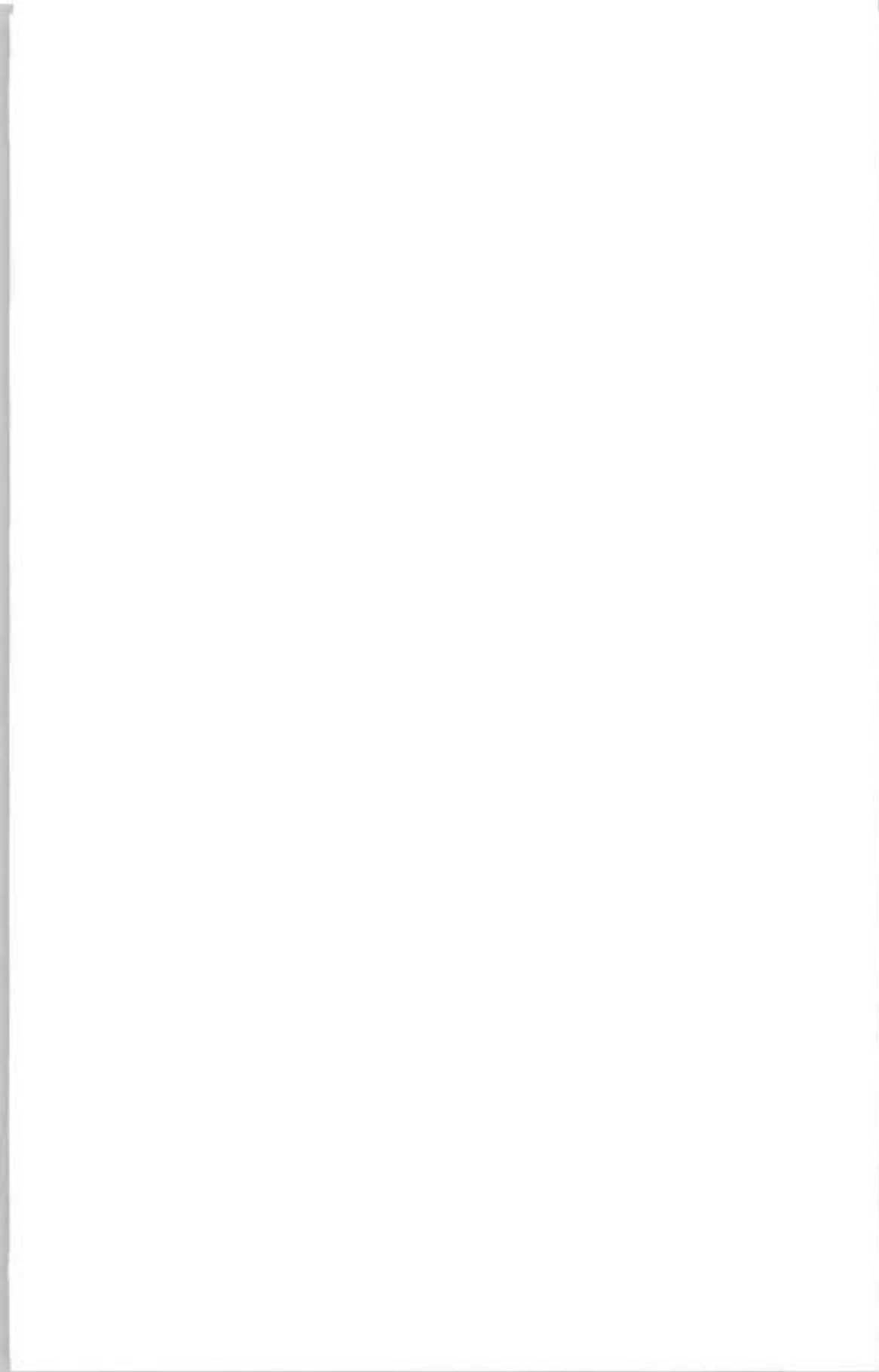
## REFERENCES

LAGRONE D.L., REMUS, J.I. (1998): Nontraditional Erosion Control Projects Constructed on the Missouri River. Proc. ASCE Conf. Water Resources Engineering, Memphis, pp 399-404.

MELLEMA W.J. (1997): An Evaluation of Streambank Erosion Control Projects Along the Upper Missouri River. Technical Report submitted to US Army Corps of Engineers, Omaha District.

USACOE-Omaha (1997): Section 33 Non-Traditional Bank Stabilization Projects, North Dakota and Montana: Design and Construction Lessons Learned. Technical Report, US Army Corps of Engineers, Omaha District.

WUEBBEN J.L. (1995): Ice Effects on Riprap. Chapter 31 in: River, Coastal and Shoreline Protection: Erosion Control Using Riprap and Armourstone, Ed. by Thorne, C.R., Abt, S., Barends, S.T. and Pilarczyk, K.W., pub. By John Wiley & Sons Ltd., New York.





## UNCONSOLIDATED RUBBLE FORCE OF FIRST YEAR RIDGE ACTING ON A VERTICAL SIDED STRUCTURE

Y. Yamauchi<sup>1</sup>, K. Kamesaki<sup>1</sup>, K. Kato<sup>2</sup>

### ABSTRACT

First year ridges or hummock fields will give a design global ice load acting on offshore structures placed in sub-arctic region like the sea of Okhotsk. The global loads are calculated by the sum of consolidated and unconsolidated layers. Although the force from unconsolidated layer is thought to be much smaller than one from consolidated layer, there exists unknown factors in terms of effects of grounding, velocity dependence and interaction with consolidated layer etc. Only unconsolidated rubble were built in ice tank and experimental studies were performed to clarify these points. The study shows that the force increases by grounding of the rubble on sea sediment.

### INTRODUCTION

It is believed that a first year ridge or hummock field governs a design global ice load acting on offshore structures placed in sub-arctic region like the sea of Okhotsk. Designers have to know the morphology and properties of first year ridges or hummock fields in order to estimate design ridges loads. Timco et al. (1997) made a comprehensive review of first year ridges including the Beaufort Sea and other temperate areas. Frederking et al.(1999) made extensive reviews on Russian publications and compared the data observed in the Beaufort Sea. A first year ridge contains three distinct parts, namely, a sail, a consolidated layer and a keel as schematically shown in Fig.1. During the interaction with a ridge, loads can be generated by the consolidated layer as well as the sail and keel of the ridge. There is no comprehensive approach to predict the loads due to the interaction of a first-year ridge with an offshore structure. To calculate the force of a ridge on an offshore structure, the usual approach is to predict the force for each of the three layers and sum these individual load

---

<sup>1</sup> NKK Engineering Research Center, NKK Corp., 1, Kumozukokan-cho, Tsu City, Mie Pref., 514-0393, Japan,  
fax: 81-59-246-2790, e-mail: kkamesak@lab.tsu.nkk.co.jp

<sup>2</sup> Department of Intelligent Mechanics, School of Biology-Oriented Science and Technology, Kinki University,  
930 Uchitacho, Naga-gun, Wakayama Pref., 649-6433, Japan, fax: 81-736-77-4754,  
e-mail: kazkato@mec.waka.kindai.ac.jp

components. It is intuitively trusted that sail and keel loads are much smaller than a load from consolidated layer. Timco et al. (1999) compared the sail and keel loads, or keel loads with the consolidated layer loads applying existing theoretical models by Dolgoplov et al. (1975), Prodanovic (1979), Mellor (1980), Hoikkanen (1984), etc. There exists considerable differences amongst these prediction methods, nevertheless, these results shows that keel loads are less than about 30 % of global loads even when applying Hoikkanen model that gives relatively higher keel loads. Although the results support engineers' intuitive judgements, following uncertainties shall be clarified to evaluate the force generated by the rubble rationally:

1. There have been no experience that an actual wide structure encounters a first year ridges over 20 m keel depth and how unconsolidated layer behaves and affects global loads.
2. Deep unconsolidated layer over 20 m may ground sea bottom if a structure is placed in relatively shallow sea of 30 to 40 m in depth. It is uncertain that the grounding mitigates or increases global ice loads. Generally, the ice cover in sub-arctic is more dynamic and it is more likely to have grounding than in the Beaufort Sea.
3. On the other hand, a consolidated layer prevents unconsolidated layer from moving upwards and how does it affect global loads.
4. How does ice drift velocity affect global loads?
5. Evaluate existing theoretical models to predict keel loads.

We conducted series of tests to confirm these uncertainties using ice tank. Only unconsolidated rubble was formed in ice tank to represent keels of first year ridges.

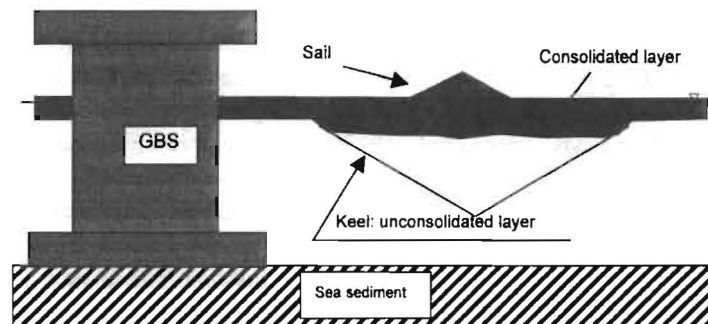


Fig.1. Schematics for the interaction between ridge and structure

## TEST ARRANGEMENT

### Assumed full scale conditions and their modeling

Bekker et al. (1997) suggested a first year ridge with 21 m keel depth for offshore Sakhalin island as 1 % annual exceedance level. In this test, the unconsolidated layer depth is assumed to be about 20 m at maximum and uniformly extended. This geometry will give larger and more conservative load than a corresponding first year ridge. The water depth, ice drift velocity and width of a structure in full scale were assumed to be 40 m, 2 knots and 80 m

respectively. Model scale was set to be 1/100 and the relations between model and full scale is summarized in Table 1.

**Table 1**

Comparison between full and model scales

Items	Full scale	Model scale
width of a structure	80m	800 mm
water depth	40m	400 mm
keel depth	20m	200 mm
maximum ice drift velocity	1.0 m/s	100 mm/s

**Test devices**

The test was performed at Ice and Snow Engineering Laboratory of NKK Corporation. The ice tank measures 20 m long, 6m wide and 1.8 m deep. Fig.2. shows a schematic view of the test arrangement prepared for the test. The model was mounted on an underwater carriage and towed against rubble ice instead the rubble ice moves towards the model. False bottom was attached to simulate an effect of rubble grounding and load cell was attached to 400 mm long portion of the false bottom. The consolidated layer of the hummock constrains upward movement of the rubble. We attached a rotary belt driven by motor to synchronize movement with the towing carriage. Consequently we successfully constrained the upward movement without giving any boundary changes and simulated the consolidated layer by the rotary belt. The rotary belt measures 1020 mm long and 800 mm wide.

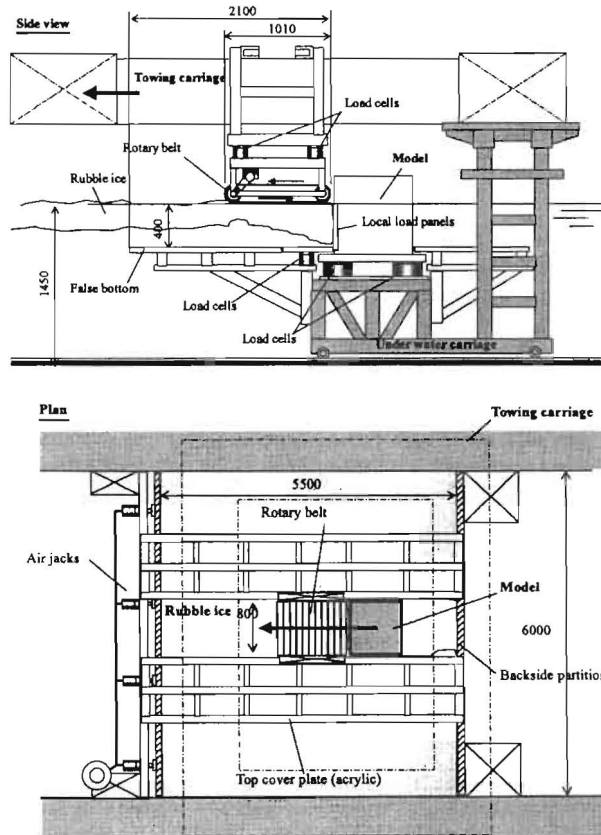


**Fig.2.** Test arrangements in view and plan

The rest of top of the rubble was covered with transparent plastic panels. The rubble was formed in the bay of 5.5 m long and 6 m wide, and air cylinders were attached to the end of the bay to apply pressure to the rubble.

The model was mounted on the underwater carriage through load cells and the front of the model was equipped with 14 segmented panels to measure ice pressure distributions as shown in Fig.3. Six smaller panels of 78.5 mm long were arrayed to measure pressure distribution in depth..

**Rubble preparation and test procedures**

The rubble was made from the relatively hard ice sheet of 15 mm thick to maintain the shape of ice blocks. We cut the ice sheet in 30 mm strips by cutters equally spaced at 30-mm attached to the carriage and then broke the strips with approximately 3 to 4 times of the width by hands. Then the ice blocks were put in the bay in specific depth. We apply pressure to the rubble by changing the force of the air cylinders in several steps to perform punching shear tests to determine Mohr-Column relations. The test device is depicted in Fig.4. After the physical property tests, the model was indented in 4 m length. After the test, we lifted the rubble in specific volume and determine the porosity of the rubble from the difference of bulk density and true ice density.

**Measured items**

Fig.5. shows the coordination system for force measurements and the following items were measured:

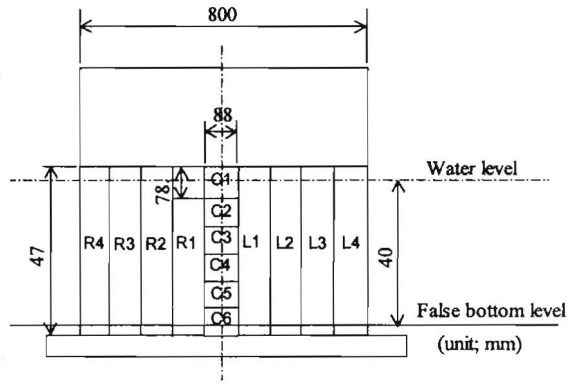


Fig.3. Model arrangement

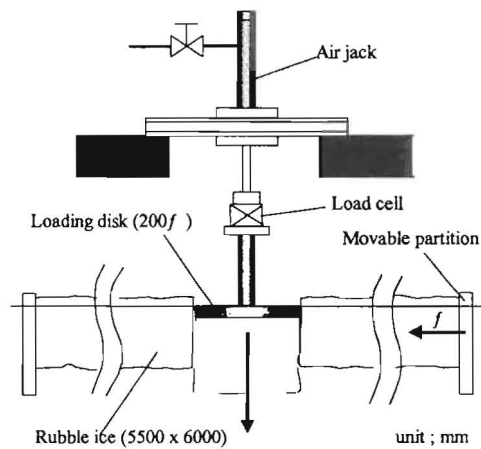


Fig.4. Device for punching shear test

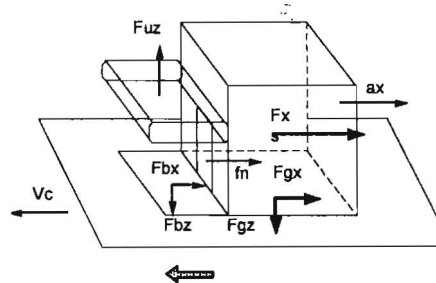


Fig.5. Coordination system for force measurements

- Indentation velocity:  $V_c$ , measured from the velocity of towing carriage;
- Acceleration of the model:  $ax$ , measured from the accelerometer mounted on the model;
- Global foundation loads:  $Fgx$ ,  $Fgz$ , measured from the load cells attached to the bottom of model;
- Local ice loads:  $fn-R1$  to  $fn-R4$ ,  $fn-L1$  to  $fn-L4$ ,  $fn-C$  (Sum of  $fn-C1$  to  $fn-C4$ ), measured from the segmented pressure panels;
- Global ice load:  $Fxs$ , calculated as sum of  $fn-R1$  to  $R4$ ,  $fn-L1$  to  $L4$ , and  $fn-C$ ;
- Bottom rubble load:  $Fbx$  (horizontal),  $Fbz$  (vertical), measured from the load cell attached to the false bottom;
- Upward rubble load:  $Fuz$  (vertical), measured from the load cell attached to the rotary belt that represents a consolidated layer.

## TEST RESULTS

### Test conditions

We prepared 100 and 200 mm deep rubbles and varied the indentation velocities in three steps. Test conditions are listed in together with the physical properties of the rubble. The measured internal friction angle and cohesion ranged from 10 to 20 degrees and 0.25 to 0.4 kPa respectively and for 100 and 200 mm deep rubbles.

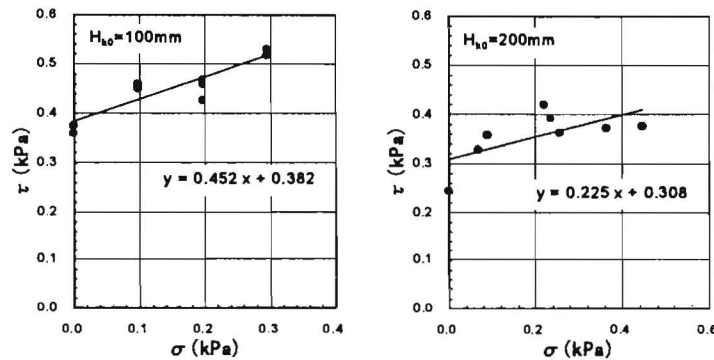


Fig.6. Mohr-Coulomb relation for the rubble

### Mode of failures and rubble accumulations

As the model indented, the rubble was gradually accumulated in front of the model and grounded on the false bottom. After the grounding, the accumulated area further grew and extended forward, sometimes beyond the rotary belt. The growth of accumulated area reached to steady state in 200 mm deep rubble tests and formed so called "pseudo bow". The shape of accumulations in view and plan was illustrated in Fig.7.  $Xu$ , upper length of the pseudo bow, tends to decrease as increasing indentation velocities. However,  $Xb$ , bottom length of the pseudo bow, did not show big differences between different indentation velocities. Fig.8. shows the relation for  $Xu$  and  $Xb$  as a function of indentation velocity. We sometimes observed slips between the top of rubbles and the rotary belts after the grounding and shear lines in front of the

pseudo bow. Although we found the grounding in the tests for 100 mm deep rubble, the pseudo bow did not reached to steady state. It is thought that 4 meter run was not adequate to form the steady state rubble accumulation and the tests were terminated before the steady state.

Table 2

Summary of the test results

Test No.	Rubble depth $H_{k0}$ (mm)	Velocity $V$ (mm/s)	Run Length $X$ (m)	Top cover plate	Porosity $n$	Cohesion $c$ (kPa)	Internal friction angle $\varphi$ (deg)	Horizontal load		
								$F_{xs1}$ (kPa)	$F_{xs2}$ (kPa)	$F_{xs3}$ (kPa)
RK06	100	10	4	ON	0.24	0.28	17.0	0.046	0.057	
RK07	100	50	4	ON	0.24	0.28	17.0	0.049	0.050	
RK08	100	100	4	ON	0.24	0.28	17.0	0.051	0.069	
RK10	100	50	4	ON	0.26	0.28	17.0	0.045	0.053	
RK11	100	100	4	ON	0.26	0.28	17.0	0.055	0.068	
RK12	100	100	4	ON	0.30	0.28	17.0	0.048	0.069	
RK14	200	50	4	ON	0.32	0.25	14.3	0.093	0.108	0.419
RK16	200	10	4	ON	0.30	0.25	14.3	0.115	0.119	0.349
RK17	200	50	4	ON	0.30	0.25	14.3	0.091	0.113	0.278
RK19	200	10	4	ON	0.30	0.25	14.3	0.092	0.094	0.205
RK20	200	50	4	ON	0.30	0.25	14.3	0.107	0.117	0.318
RK21	200	100	4	ON	0.30	0.25	14.3	0.111	0.126	0.223
RK22	200	10	4	ON	0.30	0.25	14.3	0.123	0.145	0.295
RK23	200	50	4	ON	0.30	0.25	14.3	0.084	0.089	0.253
RK24	200	100	4	ON	0.30	0.31	12.7	0.120	0.134	0.252
RK25	100	10	4	ON	0.31	0.28	17.0	0.053	0.061	0.122
RK26	100	50	4	ON	0.31	0.28	17.0	0.040	0.061	0.117
RK27	100	100	4	ON	0.31	0.31	12.7	0.040	0.060	
RK31	200	10	4	OFF	0.24	0.31	12.7	0.068	0.072	0.117
RK32	200	50	4	OFF	0.24	0.31	12.7	0.076	0.097	0.148
RK33	200	100	4	OFF	0.24	0.31	12.7	0.121	0.117	0.175
RK34	100	10	6.5	ON	0.30	0.28	17.0	0.046	0.061	0.161
RK35	100	50	8	ON	0.30	0.28	17.0	0.035	0.054	0.139
RK36	100	100	8	ON	0.30	0.28	17.0	0.037	0.050	0.140

$F_{xs1}$  : Load before grounding ( $H_{k0}=100\text{mm}\rightarrow H_k=250\text{mm}$ ,  $H_{k0}=200\text{mm}\rightarrow H_k=300\text{mm}$ )

$F_{xs2}$  : Load just after grounding

$F_{xs3}$  : Load at steady stage after grounding

#### Force trace curves and pressure distributions

Fig.9. shows the typical force time histories for 200 mm deep rubble tests. Shortly after the rubble grounded, both  $Fbz$  and  $Fuz$  increased and  $Fxs$  came to constant. On the other hand,  $Fxs$  continued to increase and did not reached to constant value in most tests for 100 mm deep rubble tests due to inadequate indentation distance. In the cases without the rotary belts,  $Fbz$  and  $Fbx$  are smaller than those with the rotary belts. We can see that the top constraint increased the horizontal load. Fig.10. shows the comparison of pressure distributions

measured at the center segmented pressure panels between without and with the top constraint. Generally the pressure decrease with increasing water depth and the higher pressure distribution was obtained in the cases with the top constraint, namely with the rotary belt.

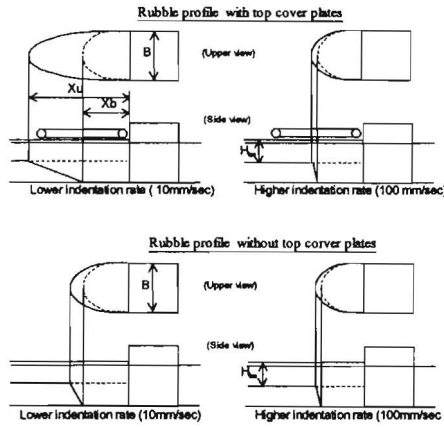


Fig. 7. Trends for the shapes of accumulated rubble in front of the model

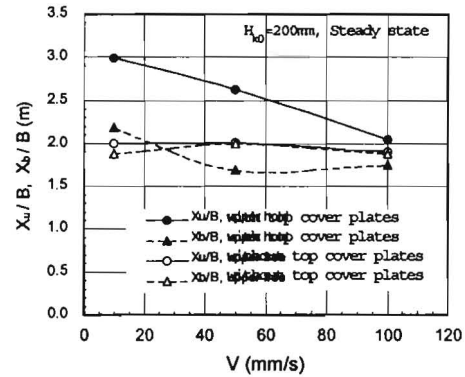


Fig. 8. Relation for  $X_u$  and  $X_b$  as a function of indentation velocity

### ANALYSIS

We analyzed the rubble loads as a function of the indentation velocities. Fig. 11. shows the relation between the indentation velocity and  $F_{xs1}$  (load before grounding).  $F_{xs1}$  defines the load when the rubble depth  $H_k$  reached 300 mm depth for 200 mm. When the top of the rubble was constrained, the effect of indentation velocity was not observed, however  $F_{xs1}$  slightly increased with increasing speeds for the tests without the top constraint. The difference of  $F_{xs1}$  was not so significant between the different top constraint.

$F_{xs1}$  values are compared with the calculated loads by Dolgoplov et al. (1975) and Prodanovic (1979). Both equations gave more than two times higher loads against the experimental results. Load  $F_{xs2}$  defines the load just after the grounding and  $F_{xs3}$

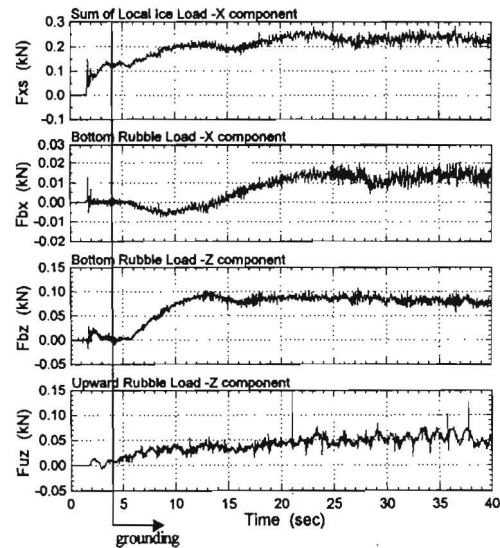


Fig. 9. An example of force traces for 200 mm rubble tests ( $F_{xs}$ ,  $F_{bx}$ ,  $F_{bz}$ ,  $F_{uz}$ ), test RK24

represents the load level when the load reaches to constant level as indicated in Fig.9. Fig.12. shows the relation between  $F_{xs3}$  and indentation velocities.  $F_{xs3}$  slightly increased with increasing the indentation velocity with top free conditions as well as  $F_{xs1}$ . However we could not observe obvious increase of  $F_{xs3}$  as the indentation velocity increased and the dependency on the speed is weak when the top of rubble prevent the upward movement. It is clear that  $F_{xs3}$  with the top constraint gave much higher loads than those with the top free conditions and the differences are almost double. Although the equations by Dolgoplov et al. (1975) and Prodanovic (1979) are not applicable when the rubble was grounded, the comparison was made. The calculated results represented the upper limit of the experimental results. Fig.3. represents the ratio of the vertical loads,  $F_{bz3}$ ,  $F_{uz3}$  to the horizontal load,  $F_{xs3}$  for the 200 mm rubble tests. The ratio approximately ranged 0.2 to 0.5 and the ratio of  $F_{bz}$  is slightly higher than that of  $F_{uz}$ .

### CONCLUSIONS

The following conclusions are drawn from the series of the rubble test against a vertical structure:

1. The vertical constraint, namely consolidated layers and sea sediments significantly increase horizontal loads. Therefore it is recommended to conduct a test with sea bottom when a structure is placed in shallow water depth and is probable to have grounding rubbles.
2. A horizontal load is not dependent on indentation speed when the rubble is grounded on sea sediment. However the horizontal load slightly increases as a indentation velocity increases when the rubble is not grounded.
3. Analytical models including sliding effects between a consolidated layer, sea sediment and the rubble when a structure is placed in shallow waters.

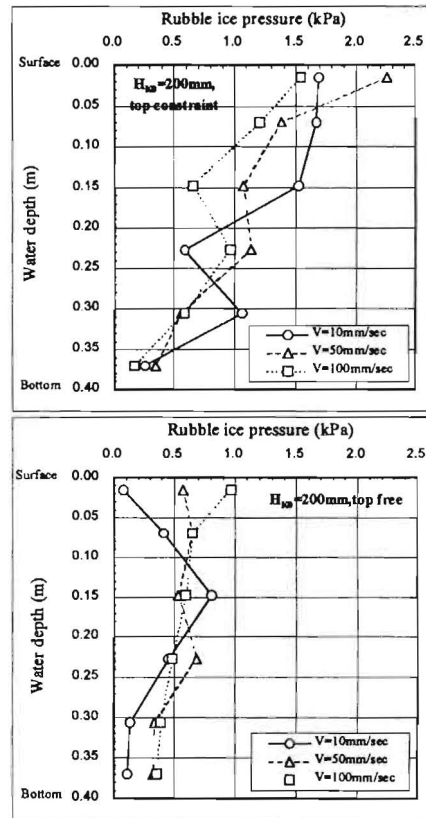


Fig.10. Pressure Distribution

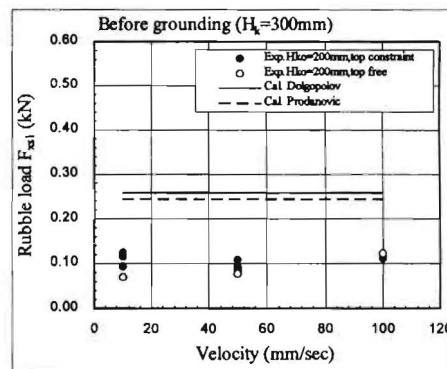


Fig.11.  $F_{xs1}$  vs. indentation velocity

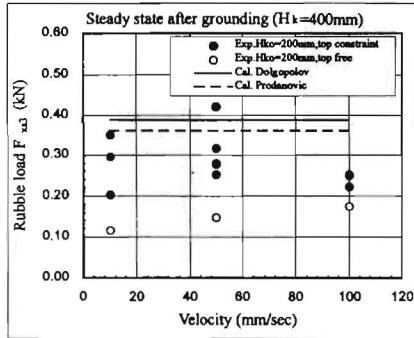


Fig.12.  $F_{xs3}$  vs. indentation velocity

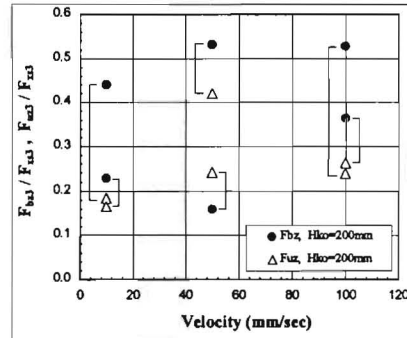


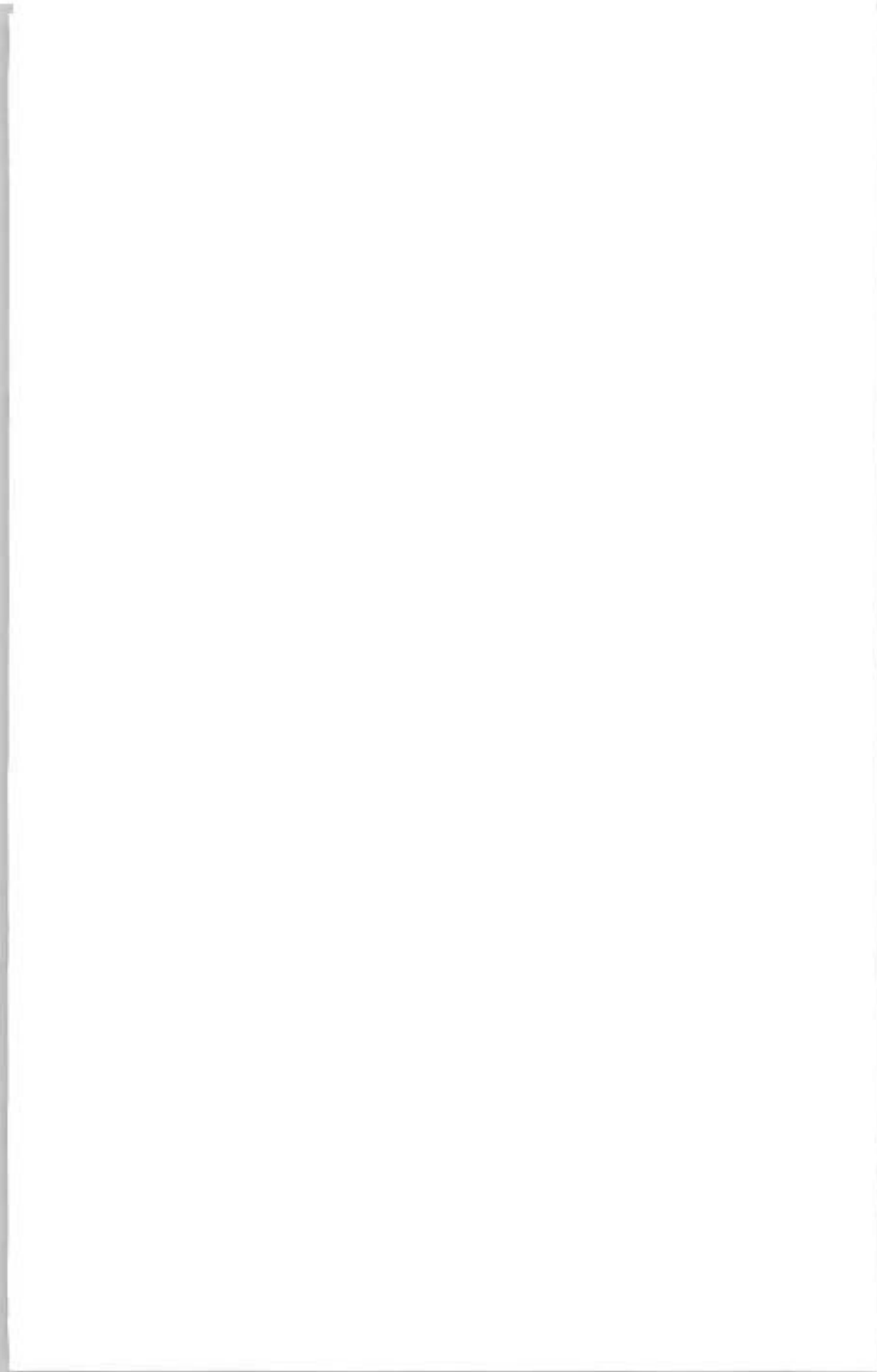
Fig.13.  $F_{bz3}/F_{xs3}$ ,  $F_{uz3}/F_{xs3}$  vs.  $V$

### ACKNOWLEDGMENTS

This test was conducted as a part of JOIA ice load project. The authors extend their sincere gratitude to JOIA for giving them an opportunity to present the result.

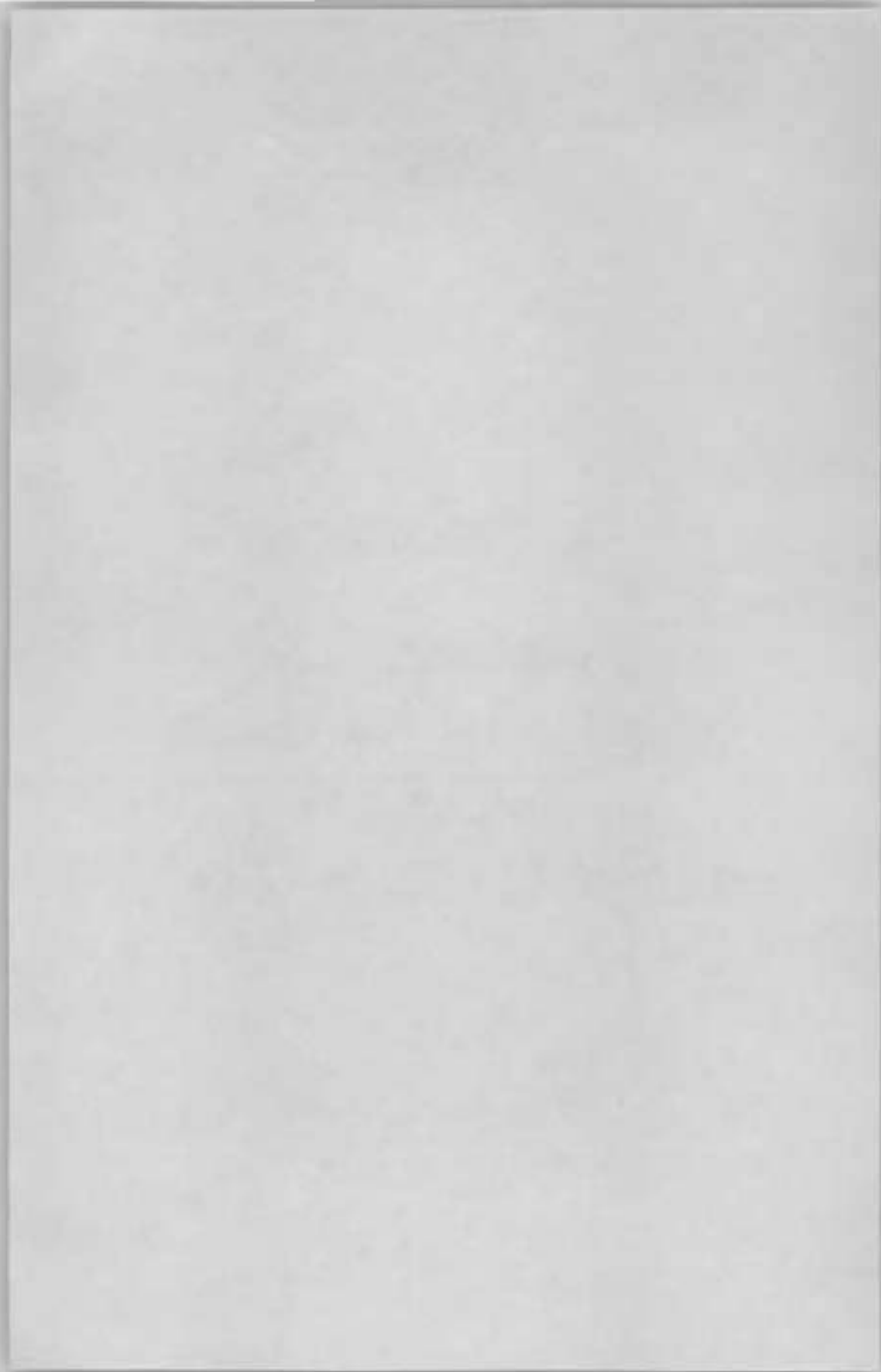
### REFERENCES

- DOLGPOLOV Y.V., AFANASEV V.A., KORENKO V.A., PANFILOV D.F. (1975): Effect of Hummocked Ice on Piers of Marine Hydraulic Structures. Proceedings IAHR Symposium on Ice, pp. 469-478, Hanover, NH, U.S.A.
- FREDERKING R., TIMCO G.W., KAMESAKI K., TADA H. (1999): Review of First-Year Ridge Geometries and Properties in Sakhalin Region. Proceedings of International Workshop on Rational Evaluation of Ice Forces on Structures, pp. 21-33, Mombetsu, Japan.
- HOIKKANEN J. (1984): Measurements and Analysis of Ice Pressure against a Structure in Level Ice and in Pressure Ridges. Proceedings of the 7th International IAHR Symposium on Ice, Vol. 3, pp. 151-160, Hamburg, Germany.
- MELLOR M. (1980): Ship Resistance in Thick Brash Ice. Cold Regions Science and Technology, Vol. 3, No. 4, pp. 305-321.
- PRODANOVIC A. (1979): Model Tests of Ice Rubble Strength. Proceedings POAC'79, pp. 89-105, Trondheim, Norway.
- TIMCO G.W., FREDERKING R., KAMESAKI K., TADA H. (1999): Comparison of Ice Load Calculation Algorithms for First-Year Ridge, Proceedings of International Workshop on Rational Evaluation of Ice Forces on Structures, pp. 88-102, Mombetsu, Japan.
- TIMCO G.W., BURDEN R.P. (1997): An Analysis of the Shapes of Sea Ice Ridges. Reprint From Cold Regions Science and Technology, Vol. 25, pp. 65-77.



**TOPIC C**

**HYDROLOGICAL  
AND METEOROLOGICAL  
INFLUENCES  
ON RIVER, LAKE, AND SEA ICE**





**SNOWMELT RUNOFF ANALYSIS FOR A BREAKUP ICE JAM  
IN THE SHOKOTSU RIVER BASIN**

**H. Baba<sup>1</sup>, K. Hoshi<sup>2</sup>, M. Yamazaki<sup>3</sup>, H.T. Shen<sup>4</sup>**

**ABSTRACT**

This paper presents hydrological analysis of the snowmelt runoff related to the Shokotsu River ice jam in March 1995. The actual contribution of snowmelt to the basin response was inversely calculated from the observed discharges at several gauging stations and compared with the snowmelt determined from heat budget analysis. Since only daily discharges were observed at most of gauging stations, hourly runoff hydrographs need to be determined for the ice jam analysis. In this study, hourly runoff hydrographs were obtained using a two-step storage function model based on inversely calculated effective snowmelt and observed rainfall with optimized model parameters.

**INTRODUCTION**

Breakup of river ice cover is usually caused by a rapid increase in river discharge. In regions with heavy snow accumulations, the snowmelt runoff could be the single most important factor in the initiation of ice cover breakup and ice jam formation. This study addresses hydrological analysis of snowmelt runoff, which caused the ice jam on the Shokotsu River in Hokkaido, Japan during the spring of 1995. It was the only ice jam occurred on the river in the recent history. An initial analysis of hydro-meteorological conditions showed that the rainfall during the period immediately before the breakup significantly increased the snowmelt runoff, which triggered the breakup and ice jamming (Shen et al., 2000). The record at Takinoue Station showed that the snow depth was reduced by 16 mm, and the rainfall was 10 mm, on March 17, 1995 (Hirai et al., 2000).

---

<sup>1</sup> River Management Division, Hokkaido Development Bureau, North 8 West 2, Kita-ku, Sapporo, Japan 060-8511, e-mail: h.baba@hda.go.jp

<sup>2</sup> Hokkaido River Disaster Prevention Research Center, Sapporo, Japan 060-0061

<sup>3</sup> Research & Develop. Dept., Hokkaido Electric Power Co., Inc., Ebetsu, Japan 067-0033

<sup>4</sup> Dept. Of Civil & Environ. Engrg., Clarkson University, Potsdam, NY 13699-5710 USA

In this study, the actual contribution of snowmelt to the flood runoff was inversely calculated from the observed discharge at several gauging stations and compared with the snowmelt determined from heat budget analysis. Due to the rapid variation of flow and ice conditions during the breakup and jamming period, hourly discharge hydrographs are needed in the analysis

and simulation of ice jam dynamics. Since only daily discharges were observed at most of gauging stations, hourly runoff hydrographs need to be determined from a hydrological model. In this study, hourly runoff hydrographs were obtained using a two-step storage function model (Saga et al., 1998), based on inversely calculated effective snowmelt and observed rainfall with optimized parameters of the storage-routing model (Saga and Hoshi, 1996). The simulated hourly hydrographs provided the needed information for simulating ice jam dynamics.

### HYDRO-METEOROLOGICAL CONDITIONS

Fig.1. summarizes the hourly data of air temperature, solar radiation, and snow depth in the Shokotsu River basin for March 1995. This figure shows that the peak air temperature and snowmelt were observed on March 17<sup>th</sup>. Rainfall and discharge were measured at Takinoue, Upper-Shokotsu, Utsutsu Bridge, and Shokotsu Bridge. Hourly discharge data are only available at Shokotsu Bridge for the entire March, and for the period after March 23<sup>rd</sup> at the gauging stations of Takinoue and Upper-Shokotsu. Only daily observations are available at Utsutsu Bridge and for the period before March 23<sup>rd</sup> at Takinoue and Upper-Shokotsu. Fig.2. and 3. show the records at Upper-Shokotsu and Shokotsu Bridge.

### INVERSE CALCULATION OF SNOWMELT AND EFFECTIVE OUTPUT RATIO OF SNOWMELT

Input water to the runoff system in the river basin was inversely calculated by the filter separation autoregressive method (Hino and Hasebe, 1984; Nakatsugawa et al., 1996) for all four discharge stations.

The potential unit snowmelt was calculated by the following heat loss model (Nakatsugawa et al., 1996):

$$m = a_1GI(1 - ref) + (a_2 + a_3V)T + \frac{rT}{L_m} + \frac{TSC_s}{2L_m}$$

$$ref = 0.85 \times 0.82^b \quad (1)$$

$$b = N^{0.46}$$

$$G = \sin(h)\cos(i) + \cos(h)\sin(i)\sin(d)$$

in which  $m$  = potential unit snow melt(mm/h);  $G$  = geological factor coefficient;  $I$  = solar radiation(MJ);  $ref$  = reflection ratio of snow surface;  $V$  = wind velocity(m/s);  $T$  = air temperature(°C);  $r$  = rainfall(mm/h);  $L_m$  = latent heat(80cal/g- °C);  $S$  = snow pack(mm);  $C_s$  = specific heat of snow(0.5 cal/g- °C);  $N$  = number of days after most recent snow fall;  $a_1$  = coefficient of snowmelt by solar radiation (= 0.03 mm/h/MJ);  $a_2$  = coefficient of snowmelt by

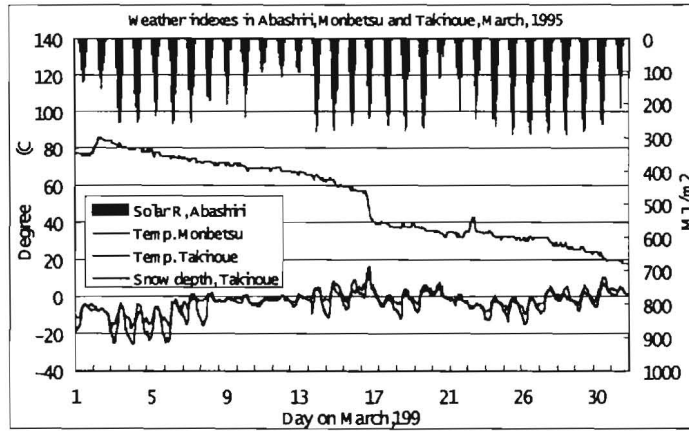


Fig.1. Hourly temperature, solar radiation and snow depth in March 1995 in the Shokotsu River

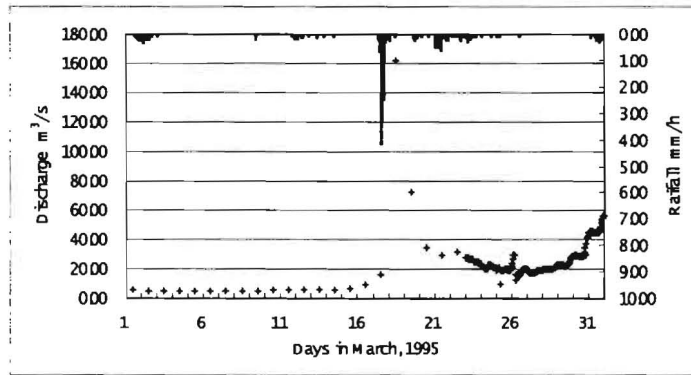


Fig.2. Rainfall and discharge records at Upper-Shokotsu,  $A=1198.2 \text{ km}^2$

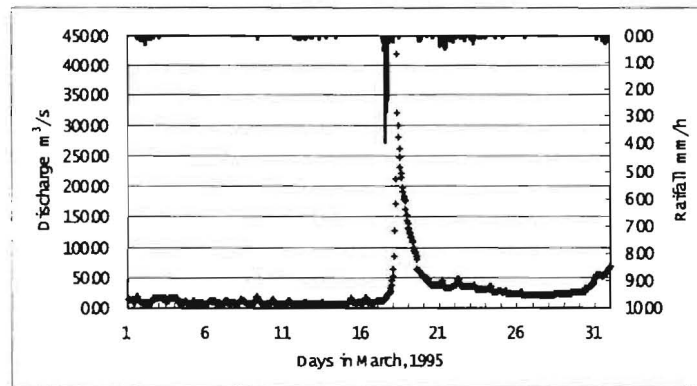


Fig.3. Rainfall and discharge records at Shokotsu Bridge,  $A=1225.6 \text{ km}^2$

air temperature ( $= 0.2 \text{ mm/h}^\circ\text{C}$ );  $a_3$  = coefficient of heat transit by air movement ( $= 0.002 \text{ mm/h}^\circ\text{C} /(\text{m/s})$ );  $h$  = horizontal solar height;  $i$  = inclination of ground surface;  $d$  = slope direction. In the above equation, the first term represents melting by solar radiation, the second term represents surface heat exchanges, the third term represents the effect of rainfall, and the fourth term represents re-freezing of water. The slope of ground surface was assumed to be flat in the calculation of  $G$ . The temperature record at Takinoue was used for the calculation of the second term and the effect of heat exchange by air movement was ignored.

**Table 1**

Effective output ratio of snowmelt

	Takinoue	Upper Shokotsu	Utsutsu Bridge	Shokotsu Bridge
1 <sup>st</sup> -10 <sup>th</sup> March	0.082	0.052	0.066	0.092
11 <sup>th</sup> -20 <sup>th</sup> March	0.155	0.111	0.129	0.120
21 <sup>st</sup> -31 <sup>st</sup> March	0.131	0.106	0.093	0.064
March	0.134	0.100	0.104	0.092

The effective output of snowmelt can be determined from the above calculations with the following definitions:

[Inversely calculated snowmelt] = [inversely calculated input water] - [observed rainfall]  
 [Effective output ratio of snowmelt] = [inversely calculated snowmelt] / [potential snowmelt]  
 Table 1 shows the larger effective output of snowmelt during the period of March 11 to 20.

#### RUNOFF ANALYSIS

Runoff analysis was conducted, using hourly data recorded for the period after 19<sup>th</sup> March. The runoff model is a two-step storage tank model coupled with loss mechanisms. The continuity equations and storage function for each tank are given as (Saga et al., 1998; Baba et al., 1999):

$$\begin{cases}
 s_1 = k_{11}q_1^{p_1} + k_{12} \frac{d}{dt}(q_1^{p_1}) \\
 \frac{ds_1}{dt} = r - q_1 - l \\
 l = \alpha_1 q_1
 \end{cases}
 \begin{cases}
 s_2 = k_2 q_2 \\
 \frac{ds_2}{dt} = l - q_2 - b \\
 b = \alpha_2 q_2
 \end{cases}
 \quad (2)$$

$$q = q_1 + q_2$$

in which  $s_i$  = storage(mm);  $r$  = observed rainfall intensity(mm/h);  $q_i$  = runoff depth(mm/h);  $l$  = input to the second tank(mm/h);  $b$  = loss component(mm/h);  $q$  = total discharge(mm/h). Storage coefficients  $k_{11}$ ,  $k_{12}$ ,  $k_2$ , and coefficients of permeable orifice,  $\alpha_1$  and  $\alpha_2$  are unknown parameters to be determined. The exponents are  $p_1 = 0.6$  and  $p_2 = 0.4648$ , assuming that the overland flow obeys Manning's law. After optimizing the model parameters, the runoff models at all four stations were determined.

Fig.4. and 5. show the comparisons of the optimized parameters  $k_{11}$  and  $k_{12}$  with previously synthesized ones in the Ishikari River, Japan. These comparisons showed that  $k_{11}$  values for the Shokotsu River basin are generally lower than those for the Ishikari River, while  $k_{12}$  values are higher. These differences, which could be caused by the basin characteristics and meteorological conditions, are considered to be reasonable.

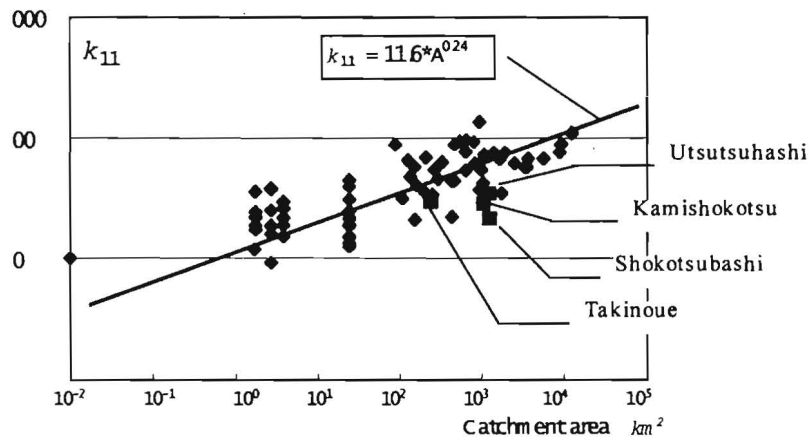


Fig.4. Optimized parameter  $k_{11}$  vs. catchment area

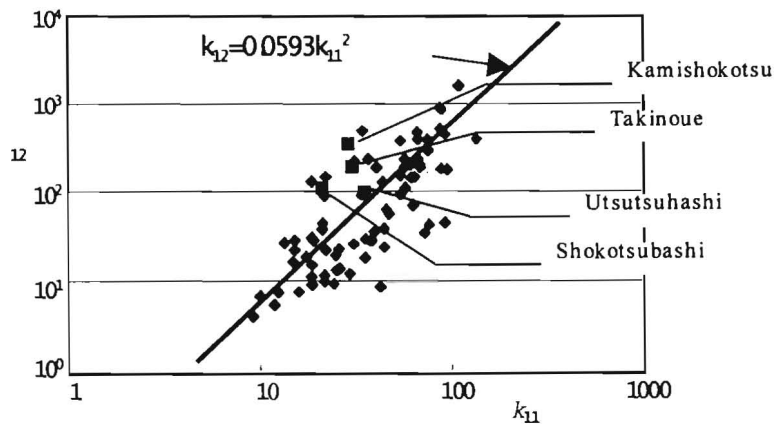
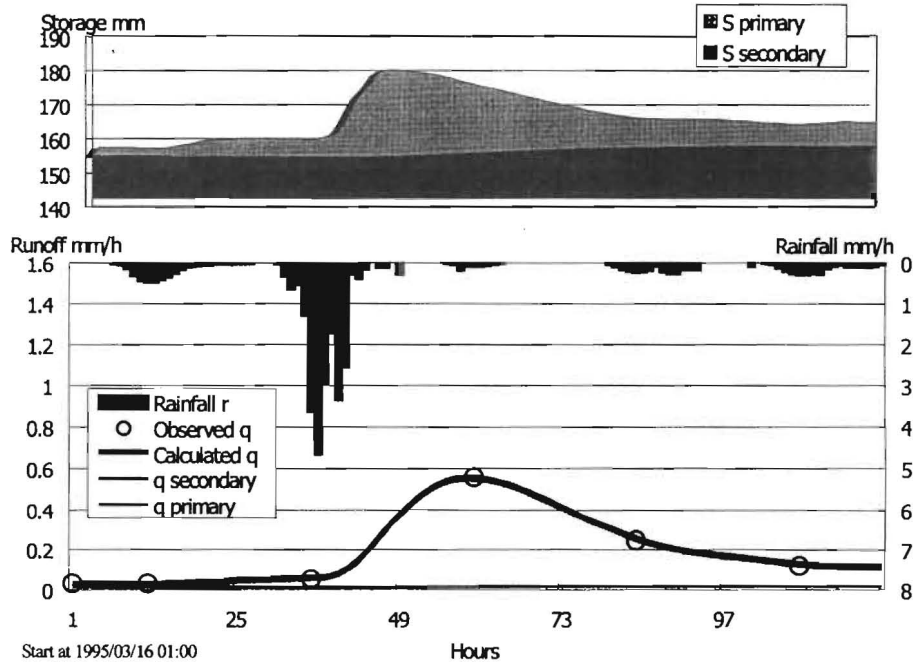


Fig.5. Optimized parameter  $k_{12}$  vs.  $k_{11}$

### SIMULATION OF HOURLY DISCHARGE

Hourly discharge hydrographs during the breakup/jamming period around 17<sup>th</sup> March at all four discharge stations are estimated with the calibrated parameters of runoff model. The calculated hydrographs showed that the discharge at all these stations is mainly contributed by the primary runoff (surface-subsurface component), which was produced by the rainfall and snowmelt over a short time period. Fig.6. shows a typical example of the calculated hydrograph and the observed daily discharge record at Upper-Shokotsu.



Time Lag of Runoff to Rainfall = 3 hours	Primary Storage Parameter k11 = 28.56
Initial Secondary flow proportion = 0.01	Primary Storage Parameter k12 = 350.47
Secondary flow lapse rate Ramda = 0.001429	Primary Storage Loss rate Alpha1 = 0.20
Secondary Storage Parameter k2 = 699.70	Primary Storage Parameter p1 = 0.60
Secondary Storage Loss rate Alpha2 = 0.00	Primary Storage Parameter p2 = 0.465

**Fig.6.** Simulated snowmelt runoff by storage-routing model coupled with loss mechanism at Upper Shokotsu from 16 March to 20 March, 1995

Specific peak discharges calculated from the observed and simulated hydrographs are compared in Table 2. The amount ranges from 0.15 to 0.22 m<sup>3</sup>/s/km<sup>2</sup> except for the observed specific peak discharge at Shokotsu Bridge where the shape of flash flood hydrograph was extremely peaked.

**Table 2**

Comparison of the simulated and observed specific peak discharges

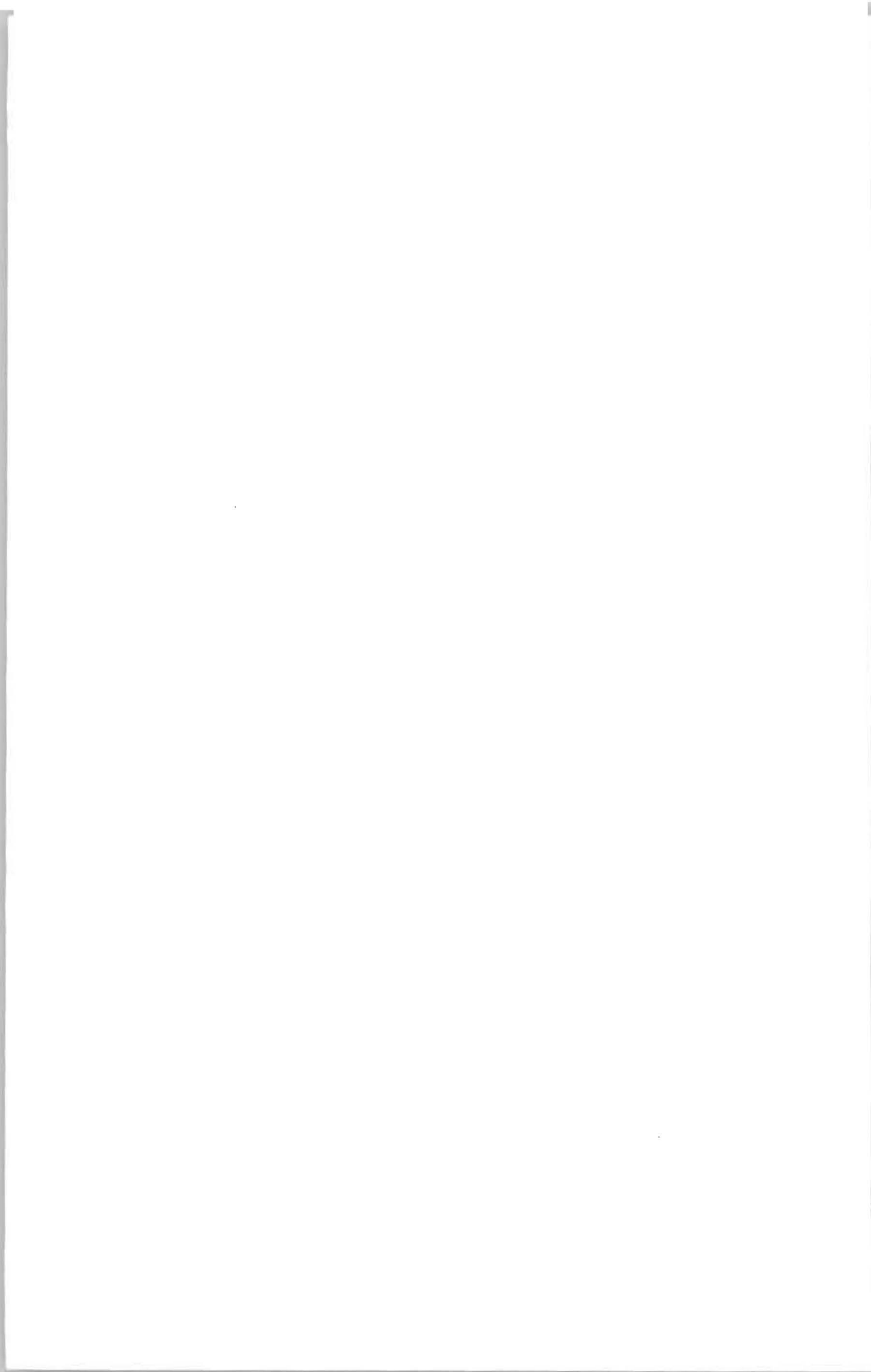
Specific Peak Discharge (m <sup>3</sup> /s/km <sup>2</sup> )	Takinoue	Upper-Shokotsu	Utsutsu Bridge	Shokotsu Bridge
Simulated	0.22	0.15	0.15	0.22
Observed	0.20	0.15	0.16	0.34

**ACKNOWLEDGEMENT**

H.T. Shen would like to acknowledge the support of the Hokkaido River Disaster Prevention Research Center, Japan, during the course of this study.

**REFERENCES**

- BABA H., HOSHI K., HASHIMOTO N. (1999): Synthetic storage routing model coupled with loss mechanisms. No. 550, Monthly Rep. of the Civil Engineering Research Inst., Sapporo, pp. 2-9.
- HINO M., HASEBE M. (1984): Identification and prediction of nonlinear hydrologic systems by the filter-separation autoregressive (AR) method. *J. of Hydrology*, 68, pp. 181-210.
- HIRAI Y., YAMAZAKI K., HIRAYAMA K., SHEN H.T. (2000): The March 1995 ice jamming in the Shokotsu River and Ashibetsu River. *Proc., 15th IAHR Ice Symp., Gdansk.*
- NAKATSUGAWA N., HOSHI K., YAMAGUCHI H. (1996): Analysis and prediction of snowmelt runoff based on heat balance. *Proc., Int'l Conf. on Water resources & Environmental Research: Towards 21st Century, Vol. 1, Kyoto*, pp. 245-253.
- SAGA H., HOSHI K., HASHIMOTO N. (1998): A new tank model coupled with the storage routing method, *XXth Nordic Hydrological Conf., Helsinki.*
- SAGA, H., HOSHI K. (1996): Optimization algorithm of parameters in the tank model. *Hydraulic Engineering Software VI, Blain, W.R. ed., Computational Mechanics Publications*, pp. 21-28.
- SHEN H.T., LIU, L., HOSHI K., WATANABE Y., AND HIRAYAMA K., 2000. Ice jam formation in the Shokotsu River, *Proc., 15th IAHR Ice Symp., Gdansk.*





## ICE JAMS ON THE LOWER ODRA

D. Dybkowska-Stefek<sup>1</sup>, M. Pluta<sup>1</sup>

### ABSTRACT

Ice conditions occurring on the lower Odra have been presented in the paper. Their differentiation caused both by hydrographic conditions and human activity has been pointed out. Ice jam spots on the lower Odra have been presented. For one of them – Bielinek cross-section (674,0 km of Odra) - characterisation of ice jams recorded during the period 1970-1999 has been presented. Exemplary ice jam cases for this cross-section have been discussed.

### ICE CONDITIONS ON LOWER ODRA

#### General characterisation of ice conditions on lower Odra

In the area of lower Odra - as a reason of different ice conditions - following characteristic areas are distinguished (Fig.1.):

1. upper section between Gozdowice and Widuchowa - the most susceptible to ice jams forming; ice is forming here both on site and comes from upper sections (especially after ice-breaking activities); influence of anthropogenic factors can be neglected,
2. lower section between Widuchowa and Szczecin - discharge of heated water from *Dolna Odra* power plant has big influence on ice conditions; after the plant was built in 1974, ice phenomena are much milder,
3. Szczecin Odra with harbour channels - ice conditions are influenced mainly by anthropogenic factors: big quantities of heat discharged with sewage, significant water pollution, city microclimate, movement of ships and continuous ice-breaking activity related to safety of the waterway,
4. Odra Lagoon - ice is formed mainly on site, and ice share coming with Odra waters is small; forming ice cover is being broken by waving process, change of water level and movement of ships on Szczecin-Świnoujście waterway; strong winds move groups of ice floats and pile them up within the shore zone,
5. Dąbie lake - ice phenomena are the longest here; first ice is formed in the south-western part of the lake, then in other bays and near the shore and at the end in Regalica inlet.

---

<sup>1</sup> Maritime Research Institute, Szczecin Branch Poland, Monte Cassino 18a, 70 - 467 Szczecin,  
Tel./fax: + 48 91 422 38 43, e-mail: dorota@estua.im.man.szczecin.pl



**Fig.1.** Situation scheme of lower Odra, characteristic water stages in Bielinek (1949-1999) and flows in Odra at Gozdowice cross-section (1952-1999)

For each of the mentioned areas, one representative ice-cover measurement station has been selected for which characterisation of ice conditions averaged for the long-term 1950-1985 has been made (Girjatowicz, 1990; Hydrodynamika ..., 1986; Roczniki ... 1950-1983). These characterisations indicate that:

1. ice cover occurs on Dąbie lake as the earliest (usually on 16.12), and then on Odra Lagoon (19.12); first ice on Odra river appears in Gozdowice (20.12), then in Bielinek, Widuchowa and in Szczecin (27.12) as the last place,
2. ice phenomena disappear on Odra in Gozdowice and Szczecin as the earliest (usually on 26.02), Gryfino (28.02), and on Odra Lagoon (13.03) and Dąbie lake (17.03) as the latest,
3. the most days with ice cover are observed on Dąbie lake (79 days a year on the average) and the least – in Szczecin (34 days) and Gryfino after 1974 (35 days); the longest period

with ice cover during analysed long-term was observed during winter 1969/1970 - 130 days on Dąbie lake, 128 on Odra Lagoon and about 100 days on Odra,

4. the thickness of steady ice cover is the biggest in Gozdowice (30 cm on the average) and Dąbie lake (27 cm), and the thinnest in Szczecin (11 cm); in Gryfino until 1974 the ice cover was 20 cm thick on the average and after building *Dolna Odra* power plant, ice conditions on the section downstream have been mitigated by about 40 % (Girjatowicz, 1984) and there is even no steady ice cover during moderate winters.

#### **Places of ice jams forming**

In the area of lower Odra, ice jams creating flood threat are formed on its upper section between Gozdowice and Widuchowa. These jams are formed mostly upstream bridges, in meanders, at places with natural contraction of a channel and sudden changes of its bottom slope. *Instruction for ice-breaking action on lower Odra* (Instrukcja ..., 1999) indicates four places on this section being the most threatened by ice jams occurrence (Fig.1.):

1. Gozdowice – Osinów - km 647,0
2. Bielinek - km 674,0
3. Krajnik Dolny - km 688,0
4. Widuchowa - km 699,0

Downstream Widuchowa, ice jams occur very seldom and do not cause dangerous floods. The reason for such situation is discharge of heated waters from *Dolna Odra* power plant, big depth of the river and numerous channels connecting Eastern Odra and Regalica with Western Odra and Dąbie lake.

#### **Ice-breaking on lower Odra**

*Instruction for ice-breaking action on lower Odra* (Instrukcja ..., 1999) predicts three - depending on ice conditions, temperatures and Odra flow - methods of ice-breaking on Odra river:

1. using Dąbie lake as an ice float reservoir - ice-breaking starts by breaking ice cover of Dąbie lake with 500 m wide stripe stretching from north to south. Then ice cover breaking is done on Odra upstream the river and created ice float is moved to Dąbie lake. This method is used only during plus air temperatures, because during minus ones, the ice float moved to Dąbie lake freezes very fast as a reason of small depths of the lake,
2. using discharge of heated waters from *Dolna Odra* power plant - ice-breaking starts from 717,3 km of Odra (discharge place) and is carried out upstream the river. Formed ice float flows downstream the discharge point and melts. The advantage of this method is the possibility of using it during minus air temperatures. However ice-breaking process has to be carried out in steps - after filling the section under influence of heated water with ice float, 2-4 days break is necessary for the ice-float to melt,
3. combination of two mentioned above - ice-breaking process starts at minus temperatures on Odra, starting from 717,0 km and proceeding upstream the river, and after thaw starting by breaking ice-cover on Dąbie lake and then proceeding upstream the river. Using this method allows for maximum reduction of ice breaking process time.

As a reason of border character of Odra river, ice-breaking action in its lower section is carried out together by Poland and Germany, while being technically supervised by the Polish side.

### ICE JAMS AT BIELINEK

There are favourable hydrographic conditions for ice jams forming in Bielinek area (km 674,0 of Odra): highly narrowed - by the upland on the eastern bank upstream Cedynia and by the embankment of Cedyński Polder - upstream river channel and big meander - along with local shoals and spurs - downstream.

Comparison of occurrence dates of maximum annual water stages at Bielinek (km 672,5) and maximum annual Odra flows in Gozdowice (km 645,3) during long-term 1952–1999, updated with analysis of ice and rainfall conditions indicates that in Bielinek area, only 2/3 of maximum annual water stages were related to maximum flows from upstream Odra catchment whereas 1/3 to ice jams. For 7 years, maximum annual stages in Bielinek - including long-term maximum stage – were caused by ice jam during the melting freshet.

Characterisation of ice jams on Odra in Bielinek area has been prepared on the basis of daily recordings of water stages at staff-gauge cross-section Bielinek (km 672,5) for the period 1970-1999 and data about ice conditions of Odra. Subjected to analysis were ice jams, during which an alarm stage equal to 460 cm for this cross-section had been exceeded.

### CHARACTERISATION OF ICE JAMS

Seventeen (17) ice jams falling into assumed criterion occurred during the discussed period. For selected ice jams following parameters have been analysed:

- $H_{max}$  - maximum water stage in Bielinek recorded during the ice jam (cm),
- $Q_G$  - Odra flow in Gozdowice on the occurrence day of  $H_{max}$  ( $m^3/s$ ),
- $\Delta H$  - total increment of water stages in Bielinek (cm),
- $\Delta t$  - time of total increment of water stages in Bielinek (days),
- $\Delta H_{max}$  - maximum daily increment of water stages in Bielinek (cm/day),
- $\Delta H_{av}$  - mean daily increment of water stages in Bielinek (cm/day).

Averaged characterisation of selected ice jams recorded in Bielinek cross-section during 1970 – 1999 has been presented in Table 1.

**Table 1**

Averaged characterisation of ice jams in Bielinek 1970 – 1999

parameter	$H_{max}$ (cm)	$Q_G$ ( $m^3/s$ )	$\Delta H$ (cm)	$\Delta t$ (days)	$\Delta H_{max}$ (cm/day)	$\Delta H_{av}$ (cm/day)
maximum	754	1430	260	13	124	114
mean	553	658	152	5	84	50
minimum	465	336	91	1	47	8

Analysis of this characterisation indicates, that during mean flows in Odra, ice jams cause water swelling in Bielinek, exceeding mean high level for this cross-section. Water stages observed during jam freshets are much higher, than it would result from relation  $H_B = f(Q_G)$  established for melting and rainfall freshets, namely these not disturbed by ice phenomena (Fig.2.).

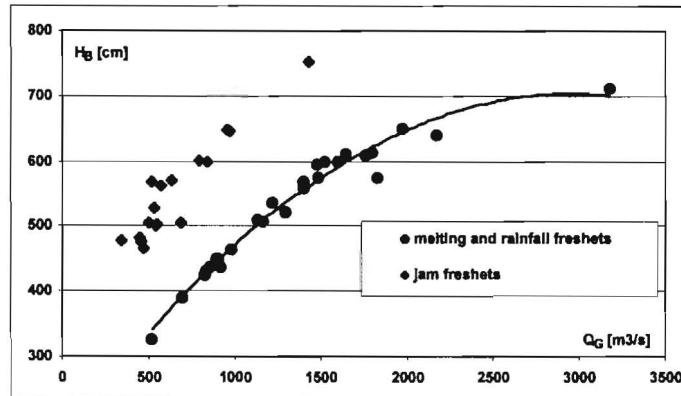


Fig.2. Relation  $H_B = f(Q_G)$  for melting, rainfall and jam freshets

### Description of selected ice jams

#### Ice jam during January 1982

During the discussed period the highest observed water stage in Bielinek equal to 754 cm occurred on 12 January 1982 (it exceeded an absolute maximum from 1892) and was the result of ice jam formation during the flow of melting ice water (Fig.3.). Culmination flow recorded at Gozdowice cross-section was equal to 1430 m<sup>3</sup>/s. During this ice jam the highest daily increment of water stages - 124 cm/day - was recorded as well.

During the winter of 1981/1982 first ice phenomena on lower Odra occurred on 11.12 and expanded on the whole river section and up to the Dąbie lake very fast. Formation of ice cover on Dąbie lake stopped the flow of slush ice and ice float on Odra and steady ice cover on the river reached km 640,5 on 27.12. As a reason of high water stages ice-breaking action started on 29.12, using free from ice section downstream the *Dolna Odra* power plant. On 5.01.82 I<sup>st</sup> stage of the action was finished. However already on 8.01, new ice cover started to form, which together with high water stages caused very serious flood threat for nearby areas. Despite minus temperatures and not-stabilised ice cover, II<sup>nd</sup> stage of ice-breaking action was started by crushing ice cover on the river downstream Gryfino. It was expected that by such action favourable conditions for continuation upstream the river would arise. However as a reason of lack of space for crushed ice float storage, it was directed via Klucz-Ustowo channel and further on via Western Odra to the harbour waters. On 26.01 the ice cover has reached km 551,0. Only after warming up at the beginning of February, ice-breakers were directed for ice-

breaking on Dąbie lake, making space for crushed ice coming from the upstream; it allowed to finish the action on 15<sup>th</sup> February.

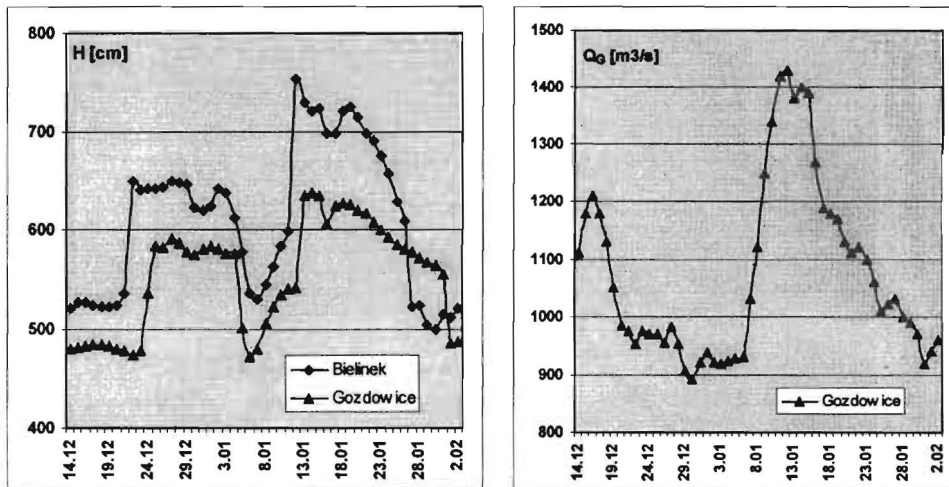


Fig.3. Hydrographs of water stages at Bielinek and Gozdowice, flows hydrograph at Gozdowice during: 14.12.1981 - 2.02.1982

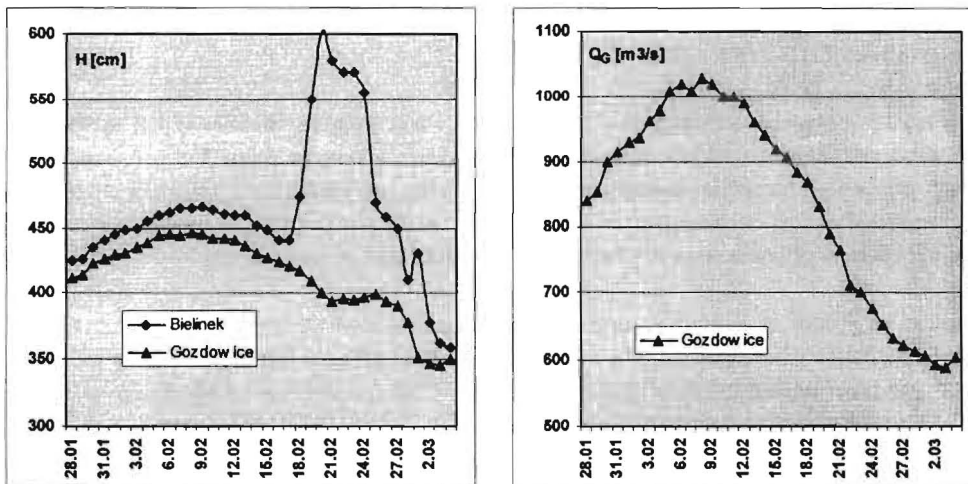


Fig.4. Hydrographs of water stages at Bielinek and Gozdowice, flows hydrograph at Gozdowice during: 28.01 - 5.03.1994

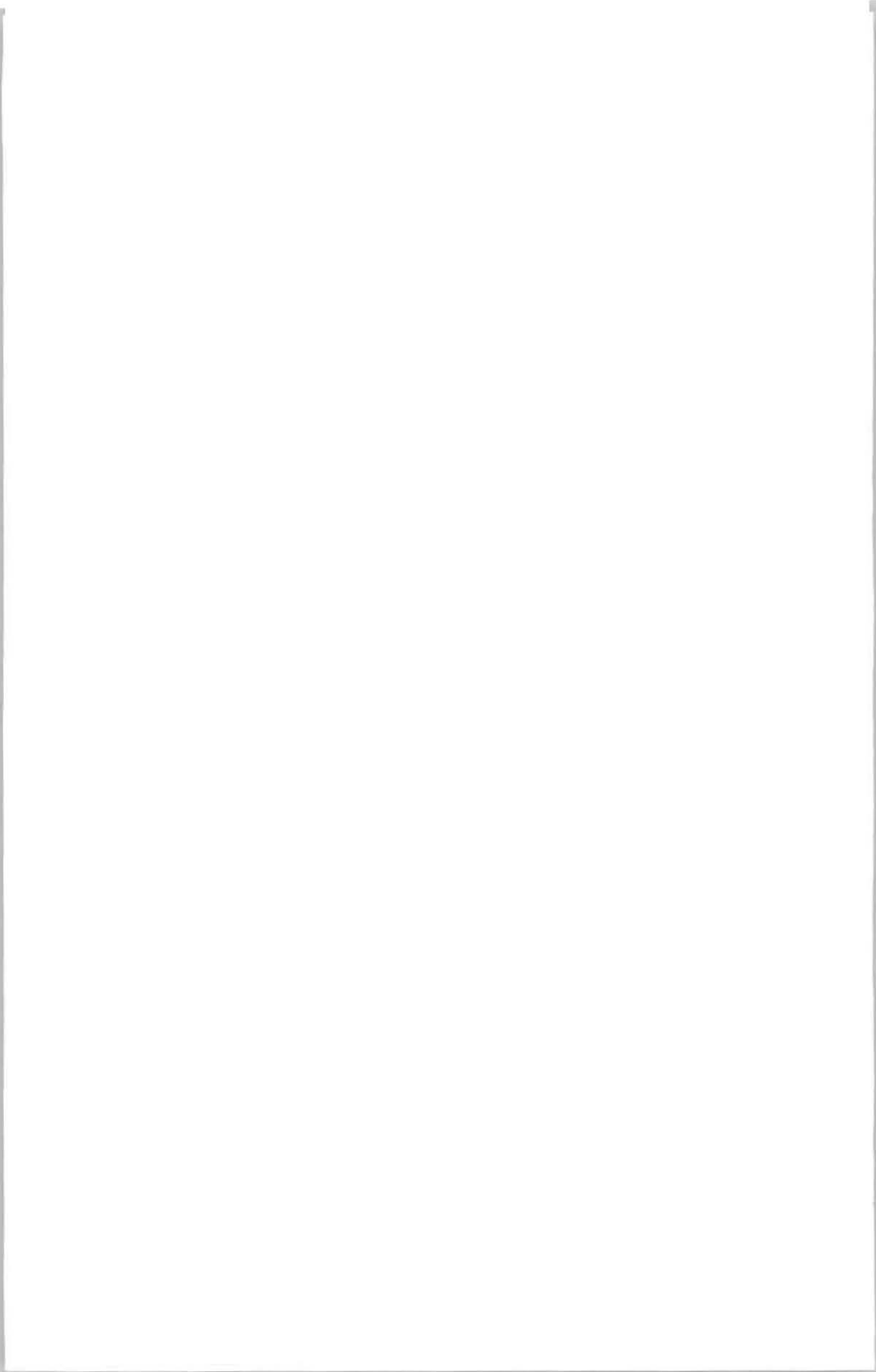
#### Ice jam during February 1994

During the discussed period the biggest (namely with the highest culmination stage) jam freshet on Odra in Bielinek area, not related to high flows, was the freshet during February 1994 (Fig.4.). During this freshet, water stage at Bielinek cross-section was equal to 602 cm on 20<sup>th</sup> February, while flow at Gozdowice cross-section was only 790 m<sup>3</sup>/s.

During 16 to 23 February, ice cover was formed on all water bodies of lower Odra starting from Osinów Dolny (km 661,0) up to Dąbie lake including it as well. As a reason of high water stages and numerous ice-slips, ice-breaking action started already on 17.02 despite unfavourable conditions. Six (6) Polish and three (3) German ice-breakers took part in this action. The main ice-breaking action was concentrated on Eastern Odra and Dąbie lake - the head consisting of two ice-breakers was crushing ice cover moving upstream, while the remaining ice-breakers controlled ice float flow on the section downstream. On 24<sup>th</sup> February ice-breakers crushed ice jam in Bielinek area and as a result, water level dropped almost 1 m during one day, decreasing flood threat in this region. On 28<sup>th</sup> February the head of ice-breakers reached km 665,0 removing the last section of ice cover. Further action was carried only to assure safe flow of ice float downstream to Dąbie lake.

#### **REFERENCES**

- GIRJATOWICZ J. (1984): Wpływ wód podgrzanych na zlodzenie dolnej Odry i jeziora Dąbie. Materiały z Konferencji: Wybrane problemy hydrotechniczne ujścia Odry do Bałtyku. Instytut Morski, Szczecin.
- GIRJATOWICZ P. (1990): Atlas zlodzenia wód polskiego wybrzeża Bałtyku. Szczecin.
- Hydrodynamika rejonu dolnej Odry (1986). Monografia. Wydawnictwo Instytutu Morskiego nr 3704, Szczecin.
- Instrukcja akcji lodołamania na dolnej Odrze (1999). ODGW Szczecin.
- Roczniki hydrologiczne wód powierzchniowych (1950–1983). Dorzecze Odry i rzeki Przymorza między Odrą i Wisłą. WKiŁ Warszawa.





## CALCULATIONS OF WATER TEMPERATURES IN A POWER PLANT RESERVOIR WITH FREE-CONVECTION MIXING CONSIDERED

I.N. Shatalina<sup>1</sup>, G.A. Tregub<sup>1</sup>, R.S. Frid<sup>1</sup>

### ABSTRACT

A new methodological approach to calculations of the temperature stratification in a reservoir is described. It is based on solving heat conductivity equations developed for a reservoir as a whole and for the so-called *thermics*, which form in water near its boundary with air. The approach enables the temperature stratification over a reservoir depth to be established. The results calculated are compared to field observation data, the comparison showing satisfactory agreement in cases when temperatures of surface water exceed those of ambient air. The processes take place in the autumn period of reservoir cooling as well as when hot water is discharged into the surface layer of a cooling pond.

Formation of thermal and ice regimes in a reservoir over an annual thermal cycle depends significantly upon mixing processes in water. Wherever density *jumps* are available we have the hydrodynamics of the motion of two layers of liquids characterized by different temperatures and densities.

The free-convection mixing processes are analysed by J. Turner (Turner, 1977).

The problems of free-convection mixing are important for calculating temperatures in a reservoir during water cooling in the autumn period from the maximum summer temperature down to the initial freeze-up and temperatures in cooling ponds where the processes of surface water cooling serve the basis for the power cycle formation. Existing methods of temperature calculations proceed from the methods of thermal balance or equations developed for shallow water under the assumption of the full mixing over the vertical. This leads to erroneous calculations of the date of ice freeze-up, ice cover thickness, cooling capacity of cooling pond et al. Under the conditions of free-convection mixing the mechanism of surface water layer cooling is discontinuous in nature.

---

<sup>1</sup> B.E. Vedenev VNIIG, 21 Gzhatskaya St., 195220 St. Petersburg, Russia, fax.: 535-67-20,  
e-mail: uugidro@gidro.odusz.electra.ru

When moving along the surface of a reservoir, liquid changes its temperature and density. Water of changed temperature and density accumulated near the surface, tears off as an unsteady convective jet (a *thermic*) and sinks by gravity down to the level of water of similar density. During the succeeding short time interval the conditions in the layer returns to the initial uniform state with the *thermic* displaced. Such a process and a number of external effects regulate both water temperatures and the thickness of water layers of different density. Calculation methods available enable mean parameters only to be determined, so they are not in line with the complex mechanism given above.

On the basis of the physics of the transfer processes described, a new methodological approach to calculations of the reservoir stratification is developed. It is designed for determining temperatures and densities of *thermics*, their motion towards the layer of similar density and returning the system to the uniform state.

The process of *thermic* generation in a flow of constrained motion is analogous to the formation of eddies near the free surface. These moving along the free surface gradually deepen in water as long as they exist. The criterion of the *thermic* tearing off is the condition  $Ra_{\delta}=10^3$ , that of the eddy tearing off is the condition  $Re_x = 3.2 \cdot 10^5$ , these being the Raley and Reynolds criterions, respectively:

$$Ra_{\delta} = g\beta \cdot \Delta t \frac{\delta^3}{\nu a}$$

$$Re_x = \frac{Vx}{\nu}$$

Here  $g$  is the gravitational acceleration,  $\beta$  is temperature coefficient of volume expansion,  $\Delta t$  is the difference between the temperatures of *thermion* and ambient water,  $\delta$  is the thickness of a water layer separating from the water mass, when *thermic* tears off,  $\nu$  is the kinematic viscosity of water,  $a$  is temperature conductivity of water,  $V$  is flow velocity,  $x$  is extension of the free surface over which an eddy is formed.

In both cases the quantity of heat in a *thermic* must be the same. It depends upon the thickness of a boundary layer formed in water close to its free surface and temperature variations occurring while an eddy exists.

Variation in temperature of a vortex during its existence is written as a non-stationary one-dimensional equation of heat conductivity.

$$\frac{\partial t}{\partial \tau} = a \frac{\partial^2 t}{\partial z^2} \quad (1)$$

Under the following boundary and initial conditions:

$$\begin{aligned}
\text{At } \tau = 0 & & t = t_0, \\
\text{At } \tau > 0 & & \\
z = 0 & & -\lambda_\delta \frac{\partial t}{\partial z} = S \\
z = \delta_{cr} & & t = t_0,
\end{aligned} \tag{2}$$

where:  $a$  - coefficient of water temperature conductivity;  
 $t_0$  - initial temperature of water surface;  
 $S$  - intensity of heat exchange between water and air;  
 $\delta_{cr}$  - critical thickness of laminar boundary layer.

According to Pekhovich and Zhidkikh, the solution of Eq. 1. takes the form:

$$t_{ed} = t_0 + \frac{S\bar{\delta}}{\lambda_\delta} \cdot \Theta \tag{3}$$

where

$$\Theta = 2\sqrt{\frac{Fo_\delta}{\pi}} \cdot \exp\left(-\frac{1}{4Fo_\delta}\right) - \operatorname{erfc} \frac{1}{2\sqrt{Fo_\delta}} \tag{4}$$

$$Fo_\delta = \frac{\lambda_\delta \cdot \tau_{ed}}{\bar{\delta}^2} \tag{5}$$

with  $\delta$  accepted as the mean thickness of laminar boundary layer over the length of  $x_\delta$  (Schlichting, 1969) :

$$\bar{\delta} = 3,33\sqrt{\frac{\nu x_\delta}{\nu}} = 1890 \frac{\nu}{\nu} ; \tag{6}$$

$\lambda_\delta$  is the heat conductivity of cold water in *thermic*, eddy sinking to the depth  $h_\rho$  where the condition is met:

$$\rho_{ed} \leq \rho_{h_\rho} \tag{7}$$

Here  $\rho_{ed}$  is water density in an eddy;  $\rho_{h_\rho}$  is water density at the depth  $h_\rho$ , free-convection mixing and homothermal conditions taking place in the layer  $h_\rho$ . Temperature in the water layer  $h_\rho$  is calculated by solving equation of conductivity 1 under the following initial and boundary conditions:

$$\begin{aligned}
\tau = 0 & & t = 0,5 \cdot (t_0 + t_{ed}), \\
\tau > 0 & & \\
z = 0 & & -\lambda_c \frac{\partial t}{\partial z} = 0, \\
z = h_\rho & & t = t_0, \frac{\partial t}{\partial z} = 0,
\end{aligned} \tag{8}$$

where  $\lambda_c$  is the heat conductivity of water in the layer of free-convection mixing. In accordance with (Mikheev & Mikheeva, 1977):

$$\lambda_c = 0,58\varepsilon_c, \text{ Wt/(mK)} \quad (9)$$

$$\varepsilon_c = 0,18 \frac{(g \cdot \beta \cdot Pr)^{0,25}}{\nu^{0,5}} \sqrt{h_p^2 |t_{ed} - \vartheta|} \quad (10)$$

where  $\beta$  is the coefficient of volume expansion ( $^{\circ}\text{C}^{-1}$ );  $Pr$  is the Prandtl's criterion of water:

$$Pr = \frac{\nu}{\alpha}; \vartheta \text{ is air temperature } (^{\circ}\text{C}).$$

Solution of Eq. 1 at 8 and 9 enables the water temperature averaged over the depth of the mixing layer to be established at  $z = h_p$ :

$$t_{h_p} = t + \Theta_1 \frac{Sh_p}{\lambda_c} \quad (11)$$

where

$$\Theta_1 = Fo_1 + \sqrt{\frac{Fo_1}{\pi}} \cdot \exp\left(-\frac{1}{4Fo_1}\right) - (Fo_1 + 0,5) \cdot \operatorname{erfc} \frac{1}{2\sqrt{Fo_1}} \quad (12a)$$

$$Fo_1 = \lambda_c \cdot \tau_1 / (c_v \cdot h_p^2) \quad (12b)$$

with  $c_v$  designating the volume specific heat of water and  $\tau_1$  the time of eddy sinking to the depth  $h_p$ :

$$\tau_1 = \frac{h_p}{v_g} \quad (13)$$

$$v_g = 2 \sqrt{\frac{0,5gh_p(\rho_{ed} - \rho_{t_0})}{\rho_{t_0} + \rho_{h_p}}} \quad (14)$$

where  $\rho_{ed}$ ,  $\rho_{t_0}$ ,  $\rho_{h_p}$  are water densities at temperature  $t_{ed}$ , surface water temperature  $t_0$  and water temperature at the depth  $h_p$ , respectively.

Water temperature distribution below the layer of free-convection mixing at  $h_p \ll z \leq H$  ( $H$  being the reservoir depth) is established by solving Eq. 1 at the boundary and initial conditions of:

$$\begin{aligned} \tau = 0 & & t = t_0(z), \\ z = h_p & & -\lambda_{\tau_1} \frac{\partial t}{\partial z} = \alpha(\vartheta - t), \\ z = H & & \frac{\partial t}{\partial z} = 0, \end{aligned} \quad (15)$$

where  $t_0(z)$  is the initial distribution of temperatures over the depth from  $z = h_\rho$  to  $z = H$ ;  $\alpha$  is the coefficient of heat exchange between water and air;  $\lambda_{Tl}$  is the coefficient of convective heat conductivity in the water layer limited by  $z = h_\rho$  and  $z = H$ .

Eq. 1 solved with account of 15 takes the form:

$$t = t_b + \Theta_2(\vartheta - t_b), \quad (16)$$

$$\Theta_2 = 1 - \sum_{n=1}^{\infty} A_n \cos[\mu_n(1-\eta)] \exp(-\mu_n^2 Fo_1^*). \quad (17)$$

The Fourier criterion  $Fo_1^*$  is calculated as

$$Fo_1^* = Fo_1' + \frac{\lambda_{Tl} \tau_1}{c_v (H - h_\rho)^2}, \quad (18)$$

where  $Fo_1'$  is used to take the curvilinearity of the initial distribution of water temperatures over the reservoir depth into account.

The block-diagram of the calculation program developed for water temperatures in a reservoir cooling from the surface downwards is shown in Fig.1. The results calculated by the program together with field observation data obtained at the Tolmachev lake (Kamchatka) which is to serve as the elevated storage of the Tolmachev power plant now under construction are given in Fig.2. Calculation results and field observation data are in satisfactory agreement.

In conclusion it should be noted that the calculation approach described above is based on more detailed analysis of the process of free-convection mixing. It enables temperature stratification of power plant reservoirs free of ice cover to be calculated irrespective of a phase of the annual thermal cycle. To use such an approach to calculating temperature distribution over the depth of transit flows in a cooling pond a number of verifying calculations should be performed for cooling ponds of thermal power plants in operation.

#### REFERENCES

- MIKHEEV M.A., MIKHEEVA I.M. (1977): Principles of heat transfer. - M.: Energia.
- PEKHOVICH A.I., ZHIDKIKH V.M. (1976): Calculation of thermal regimes of solids.-L.: Energia.
- SCHLICHTING H. (1969): The theory of boundary layer.- M.: Nauka.
- TURNER J. S. (1977): Buoyancy effects in fluids.- M.: Mir.

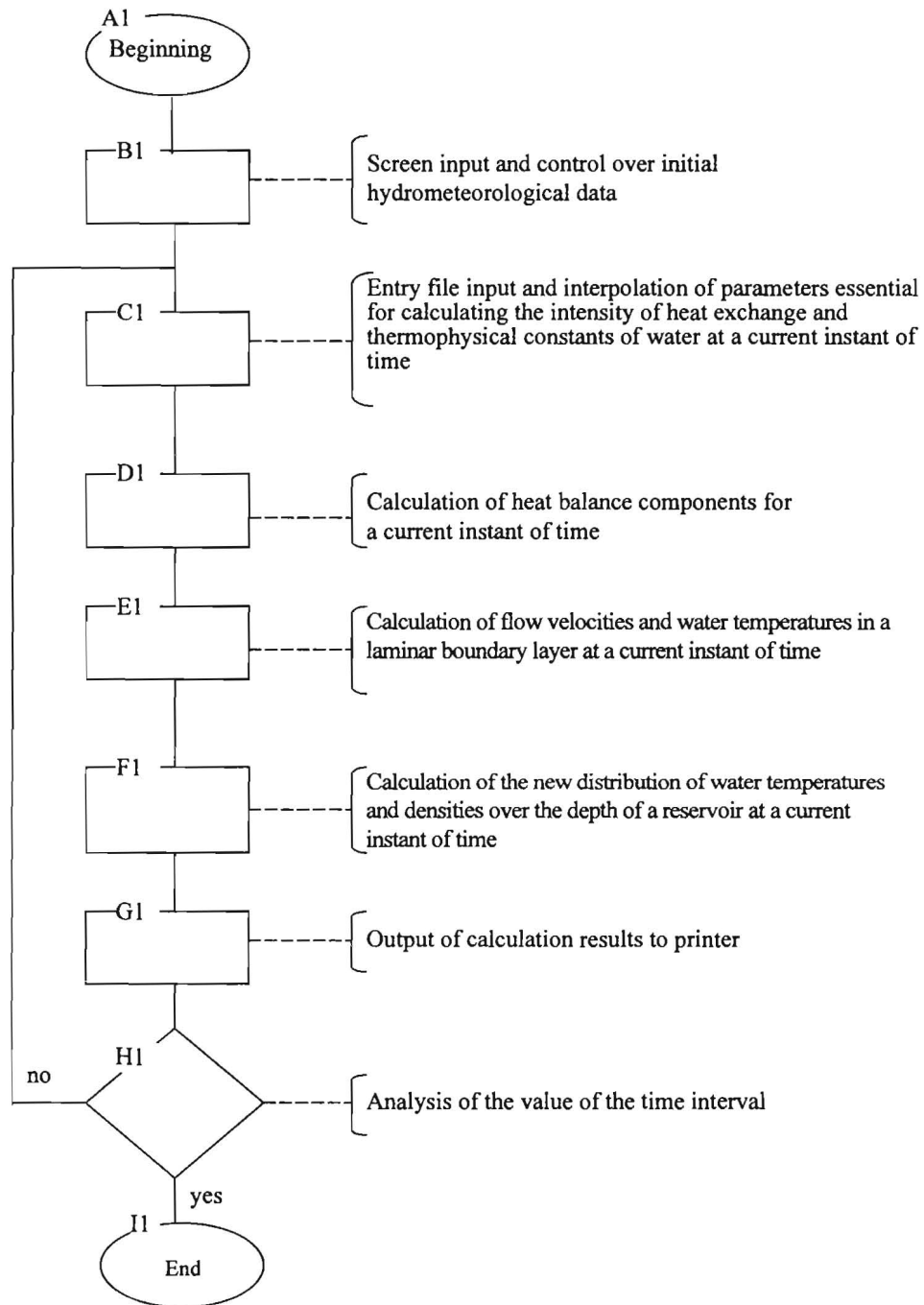
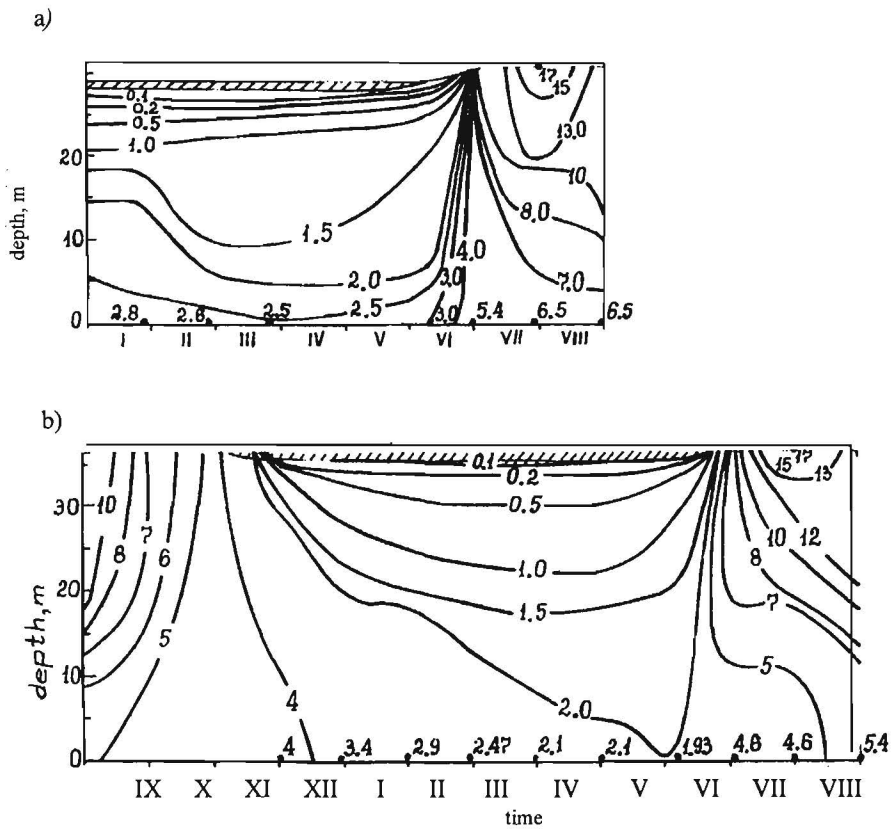
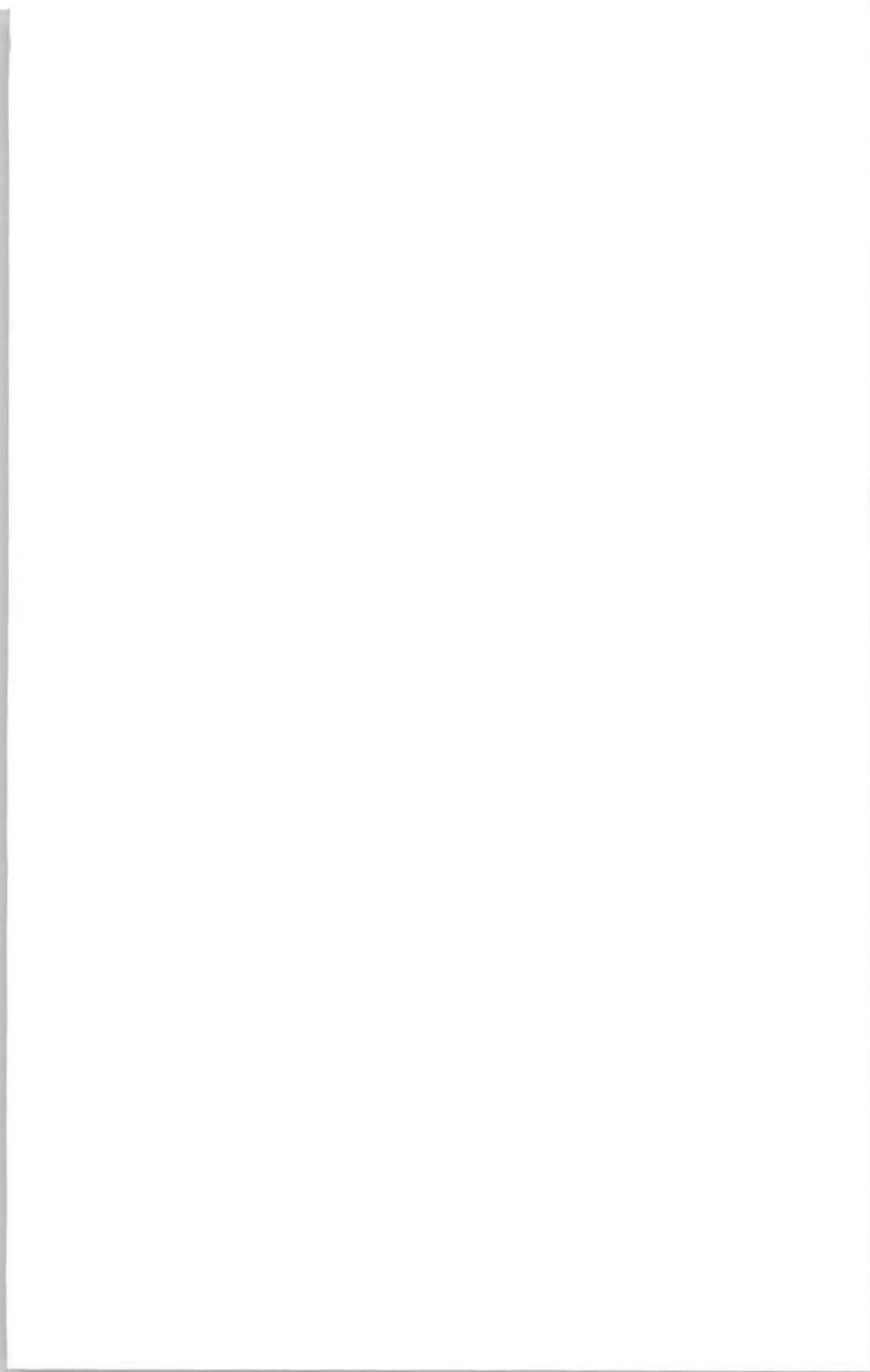


Fig.1. Block diagram of the calculation program



**Fig.2.** Comparison between calculated results and field observation data on water temperatures (the Tolmachev lake, Kamchatka)  
 a. Field observation data (1997 - 1998), b. Calculated results.





## NONLINEAR INTERACTION OF SHALLOW WATER WAVE WITH RIVER ICE COVERS

X. Xia<sup>1</sup>, H.T. Shen<sup>2</sup>

### ABSTRACT

The formation of closely spaced transverse cracks due to surge waves in river channels is a key mechanism in the formation of breakup ice runs. The existing linear theory indicated that transverse cracks spaced in the order of 10 m could form with waves of very small amplitude. Such a phenomenon has not been observed in the field. In this paper, a nonlinear analysis of interaction between the surge wave and a floating ice cover in river channels is presented. The analysis shown, that the nonlinear terms in the flow equation, which was neglected in the linear theory, is significant in highly unsteady flows such as surges caused by ice jam releases. An analytical solution of the nonlinear shallow water wave equation in the form of a KdV equation is obtained. Based on this solution the fracture of ice cover can be calculated. The calculated spacing between transverse cracks vary from 50m to a few hundred meters, which agrees with field observations.

### INTRODUCTION

The mechanical breakup of river ice is due to the fragmentation of a floating cover by hydraulic and mechanical forces associated with the changes in river discharge and water level. A mechanical breakup often leads to severe ice runs and ice jams. In the last ten years, significant progress has been made on the understanding of the dynamics of ice runs and ice jams (Shen et al., 1993; Liu et al., 1998; Lu et al., 1999). However, since a clear understanding on the mechanics of river ice breakup is not available, prediction of the occurrences of breakup ice runs and ice jams still can not be made. The lack of understanding of the mechanics of river ice breakup is mainly due to the lack of understanding of the fracture of ice cover under the action of surge waves, which is the key to the initiation of breakup ice runs. Daly (1995) used a linear analysis to study the interaction between river waves and ice

---

<sup>1</sup> Scientist, National Institute for Environmental Renewal, 1300 Old Plank Road, Mayfield, PA 18433, USA,  
e-mail: fxia@nier.org

<sup>2</sup> Department of Civil and Environmental Engineering, Clarkson University, Potsdam, NY 13699-5710 USA,  
e-mail: htshen@clarkson.edu

cover, and suggested the possibility of the formation of transverse cracks spaced at 10 m or less by waves in the gravity wave range with small wave amplitude. This phenomenon was not observed in the field. Parkinson (1982) observed cracks spaced at 50 to 200m apart formed across the ice cover during the passage of flood wave in the Liard-Mackenzie River. Gerard et al. (1984) and Prowse (1986) made similar observations. This paper presents a brief summary of a nonlinear analysis (Xia and Shen, 1999) on the interaction of a floating river ice cover with shallow water waves and the formation of transverse cracks.

### GOVERNING EQUATIONS

The linear analysis showed that friction and bed slopes contribute only to kinematic waves, and can be neglected in the analysis of transverse cracks. Based on this assumption, the mass and momentum conservation equations of the flow are:

$$\frac{\partial d}{\partial t} + \frac{\partial(ud)}{\partial x} = 0 \quad (1)$$

$$\frac{\partial u}{\partial t} + u \frac{\partial u}{\partial x} + g \frac{\partial d}{\partial x} + \frac{1}{\rho} \frac{\partial P'}{\partial x} = 0 \quad (2)$$

in which,  $x, t$  = space and time coordinates;  $u$  = flow velocity;  $d$  = flow depth under the cover;  $g$  = gravity;  $\rho$  = water density; and  $P'$  = pressure deviation from the hydrostatic pressure. The floating ice cover is assumed to be a homogeneous thin continuous elastic plate. The equation of motion of the cover can be written as:

$$\frac{EI}{1-\nu^2} \frac{\partial^4 d}{\partial x^4} + \rho_i \eta \frac{\partial^2 d}{\partial t^2} + N \frac{\partial^2 d}{\partial x^2} - P' = 0 \quad (3)$$

in which,  $E$  = elastic modulus of ice;  $I$  = moment of inertia of the ice cover cross section;  $\nu$  = Poisson's ratio;  $N$  = axial force along the cover;  $\rho_i$  = ice density; and  $\eta$  = ice cover thickness. Letting  $u = u_o + u'$ ;  $d = d_o + d'$ , where  $u_o$  and  $d_o$  are constants, representing the uniform flow, Eqs. 1 to 3 can be reduced to the following equations, after the coordinate transformation  $x' = x - u_o t$  and  $t' = t$ , and dropping the primes.

$$\frac{\partial d}{\partial t} + d_o \frac{\partial u}{\partial x} + \frac{\partial(ud)}{\partial x} = 0 \quad (4)$$

$$\frac{\partial u}{\partial t} + u \frac{\partial u}{\partial x} + g \frac{\partial d}{\partial x} + \frac{EI}{(1-\nu^2)\rho} \frac{\partial^5 d}{\partial x^5} + \frac{\rho_i \eta}{\rho} \left( \frac{\partial^3 d}{\partial t^2 \partial x} - 2u_o \frac{\partial^3 d}{\partial t \partial x^2} + u_o^2 \frac{\partial^3 d}{\partial x^3} \right) + \frac{N}{\rho} \frac{\partial^3 d}{\partial x^3} = 0 \quad (5)$$

Eqs. 4 and 5 can be reduced to the following dimensionless form.

$$\frac{\partial d^*}{\partial t^*} + \frac{\partial u^*}{\partial x^*} + \epsilon \frac{\partial(u^* d^*)}{\partial x^*} = 0 \quad (6)$$

$$\frac{\partial u^*}{\partial t^*} + \frac{\partial d^*}{\partial x^*} + \varepsilon u^* \frac{\partial u^*}{\partial x^*} + \delta \frac{\partial^3 d^*}{\partial x^{*3}} + N_o \frac{\partial^3 d^*}{\partial x^{*3}} + \gamma \left( \frac{\partial^3 d^*}{\partial t^{*2} \partial x^*} - 2F_r \frac{\partial^3 d^*}{\partial t^* \partial x^{*2}} + F_r^2 \frac{\partial^3 d^*}{\partial x^{*3}} \right) = 0 \quad (7)$$

in which, the dimensionless variables and parameters are scaled by a horizontal length scale  $L_o$ , a vertical scale  $d_o$ , and the wave amplitude  $a$  as:

$$F_r = \frac{u_o}{\sqrt{gd_o}}; \varepsilon = \frac{a}{d_o}; \delta = \frac{EI}{(1-\nu^2)\rho g L_o^4} = \frac{l^4}{L_o^4}; \gamma = \frac{\rho_i d_o \eta}{\rho L_o^2}; N_o = \frac{N}{\rho g L_o^2} \quad (8a)$$

and

$$x^* = \frac{x}{L_o}; d^* = \frac{d}{a}; t^* = \frac{ct}{L_o}; u^* = \frac{d_o u}{ac} \quad (8b)$$

in which, the characteristic length  $l = \left( \frac{EI}{\rho g (1-\nu^2)} \right)^{1/4} = \left( \frac{\eta^3 E}{12 \rho g (1-\nu^2)} \right)^{1/4}$ ; and  $c = \sqrt{gd_o}$ . Eqs.

6 and 7 are similar to the well-known Boussinesq equations (Debnath, 1994; Mei, 1983), albeit more complicated. Daly's (1995) linear analysis showed that waves with a wave length of  $2\pi l$  having amplitude of  $O(0.1 \text{ m})$  could cause transverse cracks to form. In such a case,

the order of the ice stiffness parameter  $\delta = \left( \frac{1}{2\pi} \right)^4$  is 0.001, and the order of the small amplitude parameter  $\varepsilon$  is 0.01 or larger. The nonlinear term in Eq. 7 is comparable to the ice stiffness term, and can not be neglected. The linear analysis is therefore not valid.

### NONLINEAR ANALYSIS

For a solution correct to the first order in  $\varepsilon$  and  $\delta$ , Eqs. 6 and 7 can be reduced to a modified Korteweg-de Vries (KdV) equation (Xia and Shen 1999). In dimensional form this equation is:

$$\frac{1}{c} d_t + d_x + \frac{3}{2d_o} dd_x + \frac{l^4}{2} d_{xxxx} + \frac{\rho_i}{2\rho} d_o \eta (1 + F_r)^2 d_{xxx} + \frac{N}{2\rho g} d_{xxx} = 0 \quad (9)$$

The first two terms describes the wave evolution at the shallow water wave speed. The third term represents a nonlinear wave steepening. These terms are the same as the KdV equation for free-surface shallow water waves. The rest of terms are dispersion terms due to ice cover bending, inertia of the ice cover, and the axial force. Thus, Eq. 9 is a balance between time evolution, nonlinearity, and dispersion.

We now seek a steady progressive wave solution of Eq. 9 traveling downstream. In the stationary reference frame  $\zeta$ ,  $d = d(\zeta)$ ,  $\zeta = x - Ut$ , Eq. 9 becomes:

$$\left( 1 - \frac{U}{c} \right) d' + \frac{3}{2d_o} dd' + \frac{l^4}{2} d'''' + \frac{\rho_i}{2\rho} d_o \eta (1 + F_r)^2 d''' + \frac{N}{2\rho g} d''' = 0 \quad (10)$$

The solution for Eq. 10 can be obtained (Xia and Shen, 1999). In the present paper, only solution for the case  $N=0$ , is given as the following:

$$d(x,t) = a \left[ \frac{1}{3} - cn^4 \left( \left( \frac{a}{140d_o} \right)^{\frac{1}{4}} \frac{(x-Ut)}{l}, \sqrt{\frac{1}{2}} \right) \right] \quad (11)$$

in which, the wave speed  $U$  and wavelength  $L_w$  are:

$$U = \left( 1 - \frac{1}{10} \frac{a}{d_o} \right) c \quad (12)$$

$$L_w = 2l \left( \frac{140d_o}{a} \right)^{\frac{1}{4}} K \left( \sqrt{\frac{1}{2}} \right) \quad (13)$$

where,  $cn$  is the elliptic function of the second kind, and  $K$  is the complete elliptic integral of the first kind. Eq. 12 shows that the wave speed is slightly reduced from the shallow water wave speed in open channels, as observed in the field (Parkinson, 1982). Figs. 1 to 5 show the plots of wave profile and wavelength in both dimensional and dimensionless forms, and the characteristic length of the ice cover.

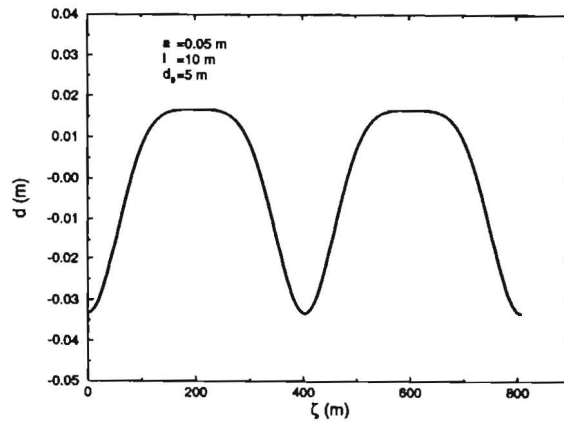


Fig.1. A typical wave profile under an ice cover

### ICE COVER FRACTURE

The maximum bending stress  $S_{X_{max}}$  in the ice cover is  $S_{X_{max}} = \frac{E}{1-\nu^2} \frac{\eta}{2} \frac{\partial^2 d}{\partial x^2}$ . Hence, Eq. 11 gives the maximum bending stress as:

$$S_{X_{max}} = \frac{E}{1-\nu^2} \frac{\eta}{l^2} \frac{a^{\frac{3}{2}}}{\sqrt{35d_o}} \quad (14)$$

For an ice cover with a maximum flexural strength  $S_{XB}$ , the minimum wave amplitude that can cause ice cover fracture is:

$$a_{min} = \left( \frac{S_{xb}(1-\nu^2)}{E\eta} l^2 \sqrt{35d_o} \right)^{\frac{2}{3}} \quad (15)$$

Eqs. 15, 12, and 13, can be used to determine  $a_{min}$  and corresponding values of  $U$  and  $L_w$ , which is the maximum wavelength corresponding to the minimum amplitude. Table 1 gives sample values for different ice cover conditions.

**Table 1**

Values for  $a_{min}$  and corresponding wave characteristics

$d_o(m)$	$E(Gpa)$	$\eta(m)$	$l(m)$	$a_{min}(m)$	$U(m/s)$	$LW_{max}(m)$
5	1	0.2	2.87	0.475	6.934	65.98
5	1	0.5	5.71	0.645	6.910	121.54
5	1	1.0	9.60	0.812	6.886	192.93
5	10	0.2	5.11	0.220	6.969	142.15
5	10	0.5	10.15	0.299	6.958	261.85
5	10	1.0	17.08	0.377	6.947	415.65
3	1	0.2	2.87	0.401	5.350	60.60
3	1	0.5	5.71	0.544	5.324	111.62
3	1	1.0	9.60	0.685	5.298	177.19
3	10	0.2	5.11	0.186	5.388	130.55
3	10	0.5	10.15	0.252	5.376	240.48
3	10	1.0	17.08	0.318	5.365	381.73

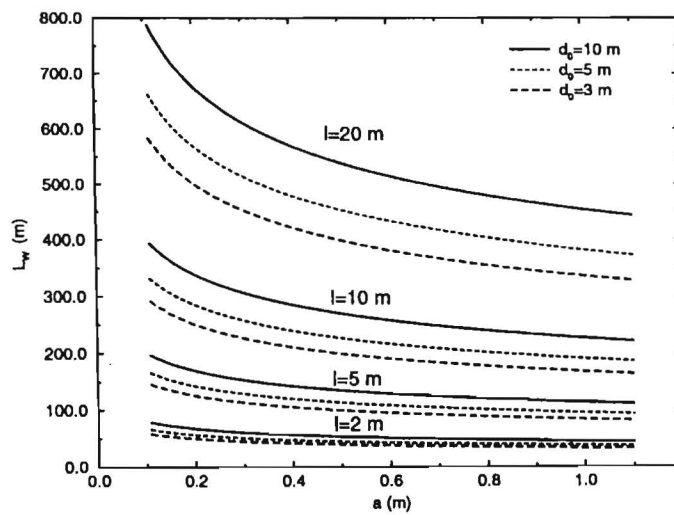


**Fig.2.** Wave length and amplitude relationship

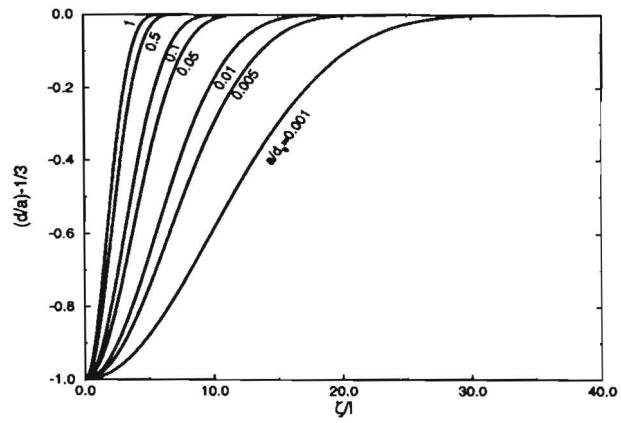


Fig.3. Dimensionless wave profile under ice cover

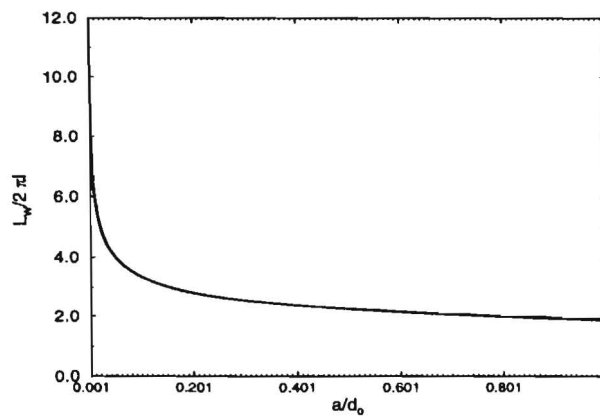


Fig.4. Relationship between wave length and amplitude in dimensionless form

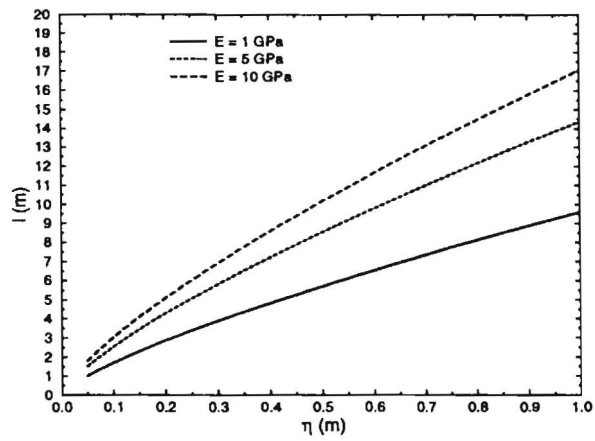


Fig.5. Characteristic length of ice cover

## SUMMARY

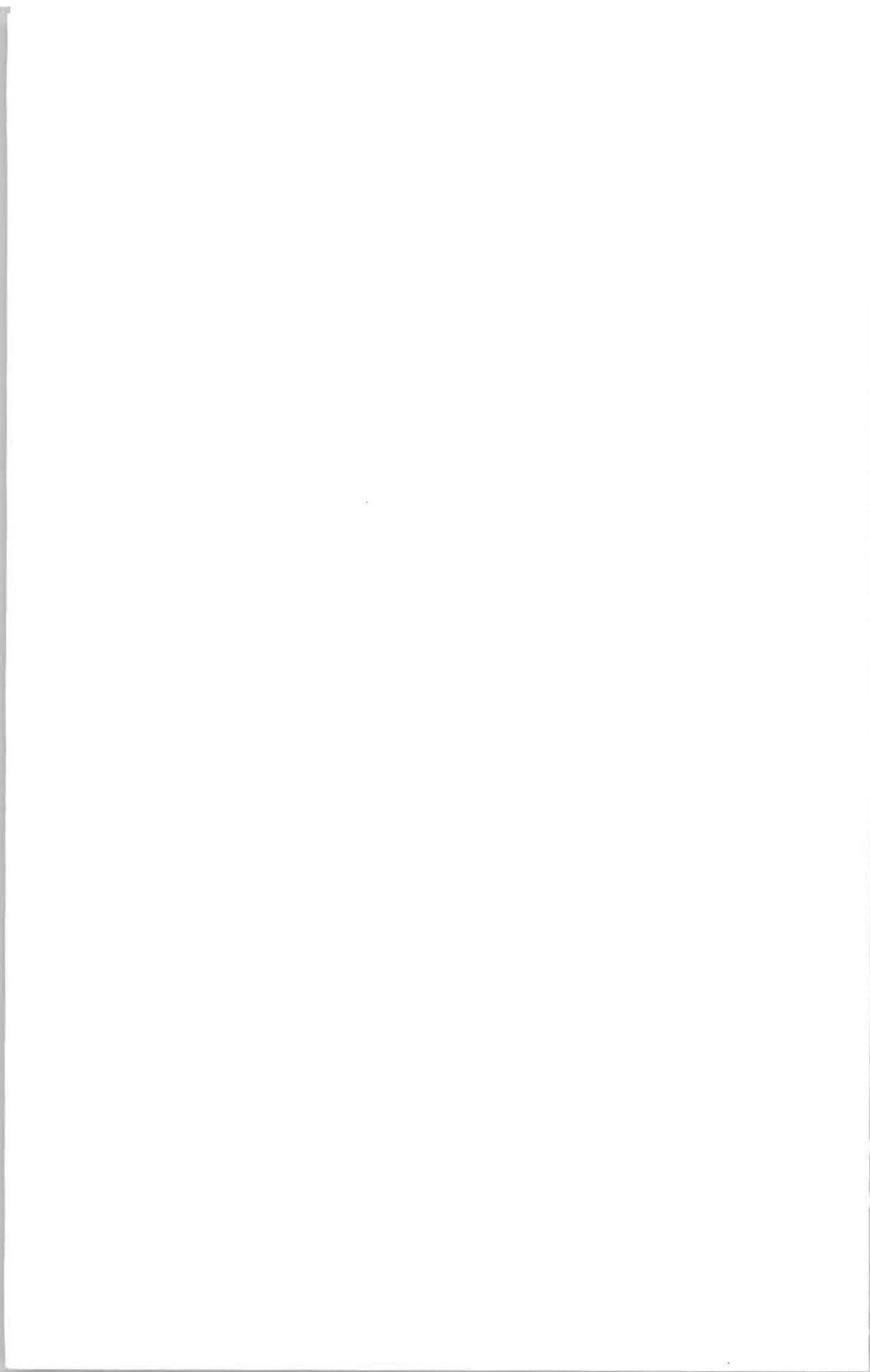
A nonlinear analysis on the interaction of shallow waves with a floating ice cover in a uniform channel is presented. An analytical solution for the nonlinear equation, which is in the general form of the KdV equation, is obtained. This solution is used to determine the conditions for the formation of transverse cracks in the river ice cover. The result shows that the celerity of the shallow water wave is slightly reduced by the floating ice cover. The minimum wave height that is required to fracture the ice cover is typically in the range of 0.2 to 0.8 m, depending on the ice cover thickness and strength. The corresponding wave length, i.e. the distance between the transverse cracks that formed by the propagating wave, varies between 50 to 400 m. For typical ice cover conditions during the spring breakup, the range is in the order of 50 to 150 m. These results agree closely with existing field observations.

## ACKNOWLEDGEMENTS

This study was partially supported by the U.S. Army Research Office through Grant No. DAAG55-98-1-0520, and the U.S. Army Cold Regions Research and Engineering Laboratory through Contract No. DACA89-94-K-0017.

## REFERENCES

- DALY S.F. (1995): Fracture of river ice covers by river waves. *Journal of Hydraulic Engineering, ASCE*, 119(8), pp. 41-52.
- DEBNATH L. (1994): *Nonlinear Water Waves*. Academic Press, San Diego.
- GERARD R., KENT T.D., JANOWICZ R., LYONS, R.O. (1984): Ice regime reconnaissance, Yukon River, Yukon, Cold Regions Engineering Specialty Conference, Edmonton, pp. 1059-1073.
- LIU L., SHEN H.T., TUTHILL A. (1998): A numerical model for river ice jam evolution. *Proceedings, 14th IAHR Symposium on Ice, Potsdam, NY.*, pp. 739-746.
- LU S., SHEN H.T., CRISSMAN R.D. (1999): Numerical study of ice jam dynamics in upper Niagara River. *Journal of Cold Regions Engineering, ASCE*, 13(2), pp. 78-102.
- MEI C.C. (1983): *The Applied Dynamics of Ocean Surface Waves*. Wiley, New York.
- PARKINSON F.E. (1982): Water temperature observations during breakup on the Liard-Mackenzie River system. *Proceedings, Workshop on Hydraulics of Ice-Covered-Rivers, Edmonton*, pp. 261-290.
- PROWSE T.D. (1986): Ice jam characteristics, Liard-Mackenzie River confluence. *Canadian Journal of Civil Engineering*, 13(6), pp. 653-665.
- SHEN H.T., CHEN Y.C., CRISSMAN R.D., WAKE A. (1993): Lagrangian discrete parcel simulation of river ice dynamics. *International Journal of Offshore and Polar Engineering*, 3(4), pp. 328-332.
- XIA X., SHEN H.T. (1999): Interaction of shallow water waves with ice cover. Report No. 99-3, Department of Civil and Environ. Engrg., Clarkson University, Potsdam, NY.





## ICE FLOOD IN NORTHEAST REGION

Liu Cuijie<sup>1</sup>, Yu Hong<sup>1</sup>, Ma Xuemei<sup>1</sup>

### ABSTRACT

This paper discusses the classification, cause and character of ice flood. The damaged flood mainly caused by ice dam in Northeast Region China. Ice flood often happens on the upper reaches of Heilong River, the upper reaches of Nen River and lower reaches of Songhua River. The probability of the annual maximum water level appearing in ice flood period is 20 to 60 %, and the annual maximum water level can reach to 10 year or 50 year flood in main flood period, and in some region it even reaches to 100 year flood. Ice flood prevention and method of reducing damage are presented.

### CLASSIFICATION, CAUSE AND CHARACTER OF ICE FLOOD

#### Classification and causes of ice flood

Ice flood is the flood caused by ice that can produce jam in the ice channel, which is the typical flood of the river in North China. Northeast region is located in 40°-53°N, where winter is long and the climate is cold. In the long period of winter, with the climate changing the different condition can be made. Under certain climate, river channel topography and hydraulic condition, river can produce a series of complex and severe ice condition, and even produce ice flood to cause damage. According to the cause and time, river ice flood can be divided into two classes: ice flood caused by ice jam during freeze-up period and the ice flood caused by the ice dam in thawing period.

#### Ice flood caused by ice jam

When it is winter the temperature is below 0°C and it is continue descending in Northeast region, the water body of the river is losing heat at the same time, and the temperature descends to the over cooling status which is 0°C or below 0°C, and then the ice flush appears in the river. Due to the turbulence of the river channel stream, the body losing heat happens in the whole section. Hence, not only the ice needle, silver frost and shore ice appears on the surface of water but also the underwater ice appears in water and the bottom of the river. Which floats to the surface of river, and the ice needle, silver frost, underwater ice and the

---

<sup>1</sup>Engineers, Changchun, PRC., Northeast China Investigation Design and Research Institute, MWR,  
No.10 Gongnong Road, Changchun, Jinlin, China, Tel.: 431-5607316, fax: 0431-5607318

broken shore ice are called frazil flush. Among these the underwater ice is the main body of frazil flush. As the temperature dropping, the number of frazil flush is more and more large. When the concentrated flowing ice is jammed at the abrupt bend, shallow and constricted section of river, the fixed ice cover is formed. The following flowing ice stops in front of the ice cover, which made the border of the ice developed toward upstream.

When the ice cover developing toward upstream, if it meets abrupt bend and shallow the border of the ice stops developing, because the flow velocity is very fast, the flowing ice reach the border of ice and then drop into the ice cover. Which stacked under the ice cover and blocked the wetted cross-section, then the ice jam formed. As the body of ice jam developed, water level of the upstream becomes high, to some extent the damage would be made, for instance, on the upper Yellow River, at the end of Yanguoxia reservoir 35 km long big ice jam was formed in 1961 winter. Volume of that was more than 4000 cubic meter, that made the water level of Liujiaxia dam site grew 11 m. When it exceeds 1000 year flood water level, the whole holes will be blocked by frazil flush for over two months, which made the severe damages such as flooded living- region and traffic blocked.

In Northeast region the river can form the ice jam at certain topographic condition, but it is not too big. The reason is the climate of Northeast region is cold and the autumn flowing ice period is not long, 15 days or so. When the river freezes, water flow looses the over cooling condition, thus the underwater ice stops forming, then the supply of raw materials which constitute the ice jam body is stopped, underwater ice is limited which produced in several leads. So the ice jam in Northeast region is not large. According to observation, ice jam backwater level does not exceed 3 m in the natural channel. The ice jam at the end of reservoir is not severe either. For example, Fengman hydropower Station on the Second Songhua River has been operated for over fifty years, but the ice flood caused by the ice jam has not happened at the end of reservoir.

#### Ice flood caused by ice dam

Ice dam is the special ice condition in the river thawing period. In Northeast region the river often thaw in March and April, to the North of 50°N region it is delayed to the last ten-day of April or the beginning of May.

To form ice dam, at first concentrated and enough flowing ice is needed, which is the material condition to constitute ice dam, at same time the suitable channel topography condition is needed, such as continual bend channel, narrow section, shallow and freezing section without thawing etc. Once the ice dam is formed, water level of the upstream raises suddenly, with the ice dam developing, water level of the upstream raises continually, which can form ice flood to damage both banks. When the ice dam grows to some extent and under the effects of integrating thermodynamic and hydraulic factors, because that it can not bear the pressure of upstream ice and water, ice dam collapse and the ice and water outburst which can damage the region of the downstream.

The ice flood caused by ice dam is the most popular flood type in Northeast region. In some river reaches, it often happens, the possibility of the annual maximum water level happening in ice flood period is 20 % to 60 %, and the water volume is large, in fact the maximum ice flood is 10 %~2 % of that in flood period. In several river reaches, it even can reach to 100 year flood water level.

#### **Characters of ice flood**

Comparing ice flood with normal flood, it has following characters:

1. Fluctuation of the ice flood caused by ice jam is slow, and the fluctuation of the water level corresponds to temperature variation. With the temperature descending backwater level is lifted gradually, after cold winter the temperature begin to raise, then the backwater level descends slowly. But the high water level of flood lasts all freeze-up period near two months, and the discharge is low that changes little.
2. The ice flood caused by ice dam of which fluctuation is obvious. Once the ice dam formed the water level of upstream raises immediately. The maximum observed velocity of rising is 22 cm/min, it costs 7 or 8 hours to rise up to peak. In the period of ice dam lasting, for floes sometime block and sometime break-up, the variation of the water level is zigzag: the ice dam lasts for over ten hours or 4~5 days, several can last for over ten days. Once ice dam collapses, water level of the upstream descends immediately, and concentrated ice and water burst downstream, which often cause new damages, especially for bridges, bank protection and hydraulic structure. That is the most destructive. Additionally, the new ice dam probably formed in the proper region of the downstream, which can cause new flood.
3. The affected range of single ice dam is limited, which is 7~8km or 30~40 km. Hence, the ice flood caused by ice dam only affects local reach. In some years and in some rivers it dropped moderate rain in drainage basin prior to break-up period, then the violent break-up took place in the whole basin, and thus many ice dams can be formed upstream and downstream at same time. For instance, in 1981 break-up period, from Yilan to Fujin almost 365 km reach on the lower Songhua River, there were 16 ice dams with 6~13 m high. In a word, ice flood affects local reach, and on the head of ice dam, the backwater is the most high, and the effect is the biggest. The more far from the head the effect is the more little.
4. Though to form ice dam has certain regulation, it still occurs occasionally. It can be judged which reach can form ice dam, but the site is variable. The climate condition of forming ice dam does not clear, and it is not as obvious as storm rainfall. Thus the ice flood caused by ice dam occurs suddenly not only on the site but also on the time, which is hard to prevent. In Yellow River basin there were sayings such as: "If ice flood outbursts the governor is off duty." and "It is easy to prevent flood in summer, but it is difficult for ice flood." which proves that ice flood prevention is complex and difficult.
5. The ice flood is destructive, and the region damaged by ice flood is devastated. Because except the shock and soak of flow, there is impact of ice pack. A piece of that are  $4 \times 4 \text{ m}^2$ , 0.8 m thick and 11.5 T weight, so it is destructive to the building along the river. Additionally, because of the flood with ice floes, it is difficult to save things and properties and to transfer people.

## TIME AND SPACE DISTRIBUTION OF ICE FLOOD

### Region distribution of ice flood

The rivers of Liaoning Province thaw in the first or second ten days of March. Because the temperature in winter is relatively high and short of snow and precipitation, the discharge is low when the rivers break-up. The thickness of ice cover is 0.5 m or so and the ice is friable at that time, thus most rivers in Liaoning Province are steady tranquil break-up without ice flood problem. In the middle and small basins in middle region of Jilin Province and Heilongjiang Province, because volume of water is low, ice condition is very simple. In northeast region, the places where ice flood occurs, mainly concentrates in the region north to 46°N on upper Heilong River, downstream from Yilan on Songhua River and upper reaches of Nen River where the ice flood most probably occurs.

### Upper reaches of Heilong River

The main river of Heilong River is the Boundary River of China and Russia. There are two sources on upper Heilong River. The east slope of Xiangtixin Mountain at the border of Russia and Mongolia is the source of north source, Shile River, and the upstream of that is called Emin River with 1592 km long. West slope of Daxing'an Mountain is the source of south source Erguna River, the upstream of that is called Hailar River with 1520 km long. Two sources merge to Heilong River of which main stream is 2824 km long. The upper reach is the upstream of Hei River (Jieya River junction) with 900 km long; From Hei River to Wusuli River is the middle reach, 994 km long; Downstream from river junction is the lower reach, 930 km (out of Chinese border).

Erguna River flows from south to north, from Hailar of Hailar River (49°15') to Luogu River on the junction of Shile River (53°27'), across 4°12'N. That is similar to Inner Mongolia reach from Lanzhou to Baotou on Yellow River across 4°37'. That is also same as Shile River flowing from southeast to northwest, across 5 longitudes. Thus, when river break-up in spring, the two rivers are earlier than main stream of Heilong River, which result in upper reach of main stream of Heilong River producing upper reach break-up at first that is the necessary condition to form ice dam.

The upper reach of Heilong River is located in high longitude region (49°~54°), where the climate in winter is cold, and the mean temperature of January is about -27°C, and the minimum temperature is -40°C~-52°C. The freeze-up period is almost 170 days, and the maximum ice thickness is over 1.2 m. Before break-up the thickness of ice is still 1 m, and the ice is hard, which offer enough conditions to form ice dam.

The upper Heilong River flows across the North Slope of Da and Xiao xing'an Mountains, the river channel is bend. Most of them flow across valleys, and both banks are high mountains, so some reaches absorb little heat, and ice cover break-up much later. Some reaches have the characters of the river in plain, which appear in island, shallow, torrent and series ditches alternately. Some reaches are bend, and among these the famous 80 km Big Bend is 4 km straight distance from here. These are the channel characters, which are easy to form ice dam.

In local reach of upper Heilong River there are ice run jam every year. Every 3 years certain scale ice dam can be formed, and the range of the reach to form ice dam is 200~400 km, in some years it even can reach to 600~1000 km. Backwater level of ice dam (from the original water level to the maximum water level) normally is 6~8meter and the maximum is 14m. Length of ice dam is 10~30 km and it can last for 3~5 days, some can last for 14 days. Since 1958, there appear 14 ice dams on the upper Heilong River, and among these the scale of 1960 and 1985 was the largest.

#### The downstream reach of Songhua River

The downstream of Yilan on Songhua River is located in 46°~48°N, where the climate in winter is cold, the mean temperature of January is -19.8°C and freeze-up period is 146 days, the annual maximum ice thickness is 1.13 m.

The downstream Tong River on Songhua River it flows from southwest to northeast, in upper reach the break-up is earlier than downstream reach. From statistics, the break-up date of Jiamusi is later than Yilan 3 days and later than Harbin 8 days. Others, on the south branch Mudan River and Suiken River, of which the break-up date is earlier than mainstream 2~6 days. The characters of the upper reach break-up earlier and branch break-up earlier than main stream provide the conditions to produce ice dam on downstream Yilan of Songhua River.

70 km downstream from Tonghe County on main stream of Songhua River is the famous Shallow Region with 3 Names. The shallow reach is 27 km long and 1500~2000 m width. In the river, there are islands, sandbars and hidden rocks, additionally there are many rocks out of water surface which are called *Stars in Sky* and *Iron Gate Sill* with less than 1 m water deep in dry season. That is the famous Obstacle Reach in main stream of Songhua River. Passing by the Shallow Region with 3 Names, the Mudan River and Weiken River join in. The channel changes from wide and flat to deep and narrow, and on the reach near Yilan the width of water surface does not exceed 300m in dry season. And more there are over 100 m high mountains close to river bank, thus on the reach the ice cover is thick and break-up is late, which is easy to form ice dams. Passing by Tongyuan County, the channel gradually becomes wide and the river is bend. In center of river there are many sandbars. The ice dams are often occurred in famous *Five Flows* and *S Shape Bend in Aoji*. The lower channel of Jiamusi City runs across the Sanjiang Plain. In river there are many shallows and distorted channels. These characters are easy to cause ice dam.

From Yilan to Fujin reach with 365 km long, the ice dam is most probably occurring. The five big ice floods have occurred since New China built 1957, 1960, 1964, 1973 and 1981, among these that in 1981 is the most severe. The reach from Yilan to Fujin, 16 ice dams have occurred. The ice dam is 3~8 m width and 2~4 km long. It can last for 1~2 days and the maximum is 4 days. The maximum water level of Jiamusi in ice flood period is 78.89 m, which is equal to 14 year flood water level in flood period.

### The upper Nen River

The South Slope of Yilehuli Mountain in Daxing'an Mountain is the source of Nen River. The upstream of Nenjiang County is the upper reach with 66 km total long. The upper reach of Nen River flows across the rock massifs made by Da and Xiao xing'an Mountain branch vein. The valleys are wide. There are many marshes on both banks and the river is bend. On the lower Gugu River, it flows into gorge region, of which the mountains on both banks are 100~300 m high. Passing by Lapao the valley is wide again, and there are many braided courses and distorted flows. The river network of Nen River is well developed and there are many branches in that. Naduli River and Duobukur River are right branches on upper reach; The rivers on the left branch are Wodu River, Gugu River, Menlu River and Keluo River. The basin of the upstream of Nenjiang County is fan-shaped basin. The water volume increases immediately caused by many branches merging. Thus the confluence is fast and concentrated.

The upper basin of Nen River is located in 49°~52°N. The climate in winter is cold. The mean temperature of January is -25.6°C. The minimum temperature is -47.3°C. The freeze-up period of river is 160 days, and the maximum ice thickness is 1.3 m. The temperature rises up fast in spring. Prior to break-up the thickness of ice cover is 1m and it is hard. If the hydraulic condition is enough, it is easy to produce violent break-up and lead to ice dam.

Every spring with cold high pressure from Siberia goes northward, frontal surface of cool and warm air goes northward. Then the precipitation raises especially on the upper Nen River. Because the basin of Da and Xiao Xing'an Mountain are splay and the topography is lifted, which cause the precipitation on the upper Nen River is larger than that of middle and lower reaches, see Table 1.

**Table 1**

Precipitation of stations on upper and middle reach of Nen River (mm)

Stations	Shihuiyao	Xiecaigou	Kumetun	Nenjiang	Ayanqian	Tongmeng
Longitude	50°04'	49°42'	49°27'	49°11'	48°46'	48°04'
Precipitation	April	33.7	30.2	22.9	19.1	12.7
	Total year	496	470	461	445	409

Note: based on data collected form 1971 to 1980.

In break-up period, there is some snow in the basin and the surface of ground does not break-up, so runoff coefficient is big. Thus, if there are concentrated precipitation before break-up, the runoff yield is large. There are many branches in the basin, which is fan-shaped, so the confluence is fast and concentrated. That is easy to form violent break-up and form ice dam to cause ice flood in reach of suitable topography. According to statistics from 51 years data of Kumotun station, there are 11 years when the dangerous ice dam occurred, among these 1957, 1973 and 1984 are the most severe.

**Table 2**

Ice flood condition of the reaches in northeast region where ice flood often occurs

Reaches	Stations	Statistics number of years( $n_1$ )	The number of years the annual maximum water level appearing in ice flood period( $n_2$ )	$(n_2/n_1) \times 100\%$	The maximum water level of ice flood period(m)	Equal to the flood frequency in open-river period(%)
The upper Heilong River	Bokeluofuka	90	48	53.3	312.50	1.25
	Luoguhe	13	8	61.5	101.91	2.59
	Mohe	32	14	43.8	97.61	6.1
	Kaikukang	29	12	41.4	96.04	13.3
	Huma	37	10	27.0	101.06	10.5
	Sandaoka	37	11	29.7	100.58	7.9
	Heihe	38	9	23.7	97.48	7.7
The downstream of Yilan on Songhua River	Yilan	35	11	31	97.1	15
	Jiamusi	39	9	23	79.43	14
	Fujin	39	9	23	60.75	14-15
The upper Nen River	Shihuiyao	26	11	42.3	251.03	74
	Kumotun	48	20	41.7	234.71	5
	Nenjiang	30	5	16.7	221.15	12.5

**Frequency and severe degree of ice flood occurring**

To sum up, the upper Heilong River, the lower Songhua River and the upper nen River are the places where the ice flood most probably occurs. Based on the data of the upstream of Kukang on upper Heilong River, the possibility of the maximum water level appearing in the ice flood period is 40 %~60 %, and that of reach from Huma to Heihe is 20 %~30 %. In 1960 the maximum water level of Bokekaluo in ice period is near 100-year flood water level, and that of Luogu River in 1994 is near 50 year flood water level, and that of the stations on the upstream of Heihe is 10 year flood water level.

On the downstream reaches of Yilan of Songhua River, based on the 35 years data of Yilan station, the possibility is 31 % that the annual maximum water level appears in ice period. That of the downstream Jamusi and Fujin is 23 %. The maximum water level of ice flood period can reach to 5 year to 10 year flood water level.

On the reach from Shihuiyao to Kumotun on the upper En River, the possibility of the annual maximum water level taking place in ice period is over 40 %, and that of En River is 20 %. In 1957 the water level of ice flood period is equal to 20 year flood water level, see Table 2.

## **THE ICE FLOOD PREVENTION AND METHOD TO REDUCE DAMAGE**

The possibility of ice flood taking place in some northeast region is high, and the volume of flood is not low. Thus it is harm in industry and agriculture of cities and villages and people's lives and property. At present, ice flood takes place in the region where there are few people and the damage does not obvious. But with the development of economy in these regions, the damages will be more severe than before. Thus it is very necessary to strengthen the prevention. From the active prevention of ice flood, it can be classified into non-engineering method and engineering method.

### **Non-engineering method**

#### Observation and forecast of ice condition

Proved by practice, ice flood is affected by temperature, precipitation and shapes of channel. It has auspice and principle. It is important to strengthen the observation of ice condition and to grasp the variation of ice condition of river channel. That's foundation of preventing and fighting for ice flood. Based on the characters of northeast region, the emphases should be placed on the break-up period, namely March and April. The hydrological station of the important reaches should report ice condition to the leadership form 1st March. Additionally, based on the data of ice dam investigation, the number of the ice condition observing station should be increased in suitable reach. The hydrological station nearby should take the touring observation or entrusting observation.

The ice condition forecast is the important foundation of decision for each preventing ice flood organization to command fighting for ice flood. If it is forecasted correctly, the battle of preventing ice can take place in forecast period. The emphasis of ice flood forecast should be placed on break-up period. The forecasting contents are: features of break-up, date of break-up, the maximum water level of break-up, the maximum discharge, the possible site of forming ice dam and the maximum backwater level of ice dam.

#### Build up all levels of preventing ice organization and information sending system

In every ice flood period, the ice prevention headquarters work from 1st March in some regions. The duties of those are to know and grasp variation of the hydrology, meteorology, ice condition, engineering condition in dominating reaches, to forecast ice condition, to establish ice prevention scheme and direct fighting for ice prevention. The basic ice prevention organization should organize the troops of ice prevention to deal with emergency and block leak, so that ensures the security of flood protection dike.

Not only to gather the information of hydrology, meteorology and ice condition and to make and send forecast, but also to direct fighting for ice, are all need advanced and credible information sending system.

## **Engineering method**

### Flood prevention dike

The most basic method of engineering ice prevention is to build the flood prevention dike. The flood prevention dike of the large rivers in northeast region should prevent ice flood besides to prevent storm and flood. Because of the limitation of all features and the low standard in some reaches, once the ice flood occurs, the overtopping dike and breaking dike possibly occurs. Thus, it should be planned to reinforce dike and increase the standard of prevention. In addition, troop of dealing with emergency should be organized and the goods and property for emergency should be prepared. When ice comes to dike, perambulation dike should be enforced, so that ensures the dike passing ice flood period safely.

### Ice breaking

Ice breaking is the normal method for ice prevention. The affections are good or not are based on choosing of site and date of ice breaking. The site of ice breaking should be support point of ice dam. It can be confirmed by site investigation. Choosing the time of ice breaking can be classified: one is prebreaking, namely ice breaking for ice dam controlled reaches before break-up period; the other is emergency ice breaking when the ice dam developed to danger for security of both banks.

It's much better to use manual explosion for prebreaking. Based on the design of site of hole, drive in the ice cover and put the explosive under the ice cover. The way of all holes exploding at same time can give out the power of explosive completely, at same time using the power of water wave oscillation to get good explosion affection. Lianhua power station on Mudan River the ice prevention method is manual explosion. Prebreaking should not start too early, or it will be frozen again when cold wave comes. It should be in the last ten-days of march based on the climate condition of north region in Heilongjiang Province.

When ice dam forms and will damage the villages of both banks, the organizations can use thawing explosive by air, all exploding or putting explosive by man to bomb out the dam. Because it only can explode on the surface of the ice cover, the effect is not too good. Under the emergency, that is a good method to meet an emergency. The affection can be increased obviously if the explosive explodes under the ice cover.

### Regulating discharge of reservoir

After the large reservoir constructed on the river, because of the reservoir action, the undershot discharge of dry season is larger than normal station. Thus the water level of the downstream river of reservoir is increased and the volume of overflowing under the ice cover is increased in freezing period or freeze-up period. In April, the break-up period, the water level of annual storage reservoir is near dead water level. Use the discharge of reservoir regulation in break-up period to prevent the violent break-up. A series of reservoirs on Yellow River have accumulated many experiences. For instance, there are 12 years that violent break-up or semi-violent break-up had happened within 17 years before Liujiaxia reservoir on inner Mongolia reach of yellow river constructed. In 9 years after Liujiaxia reservoir began to

storage and to operate, there were no violent break-up and only 2 years semi-violent break-up. Thus, if the condition exists, it is an effective method to use reservoir regulating the discharge of break-up period.

Practice proved that integration of the engineering method and non-engineering method of ice prevention is much effective. Thus, continually completing the engineering serves of ice prevention, at same time the non-engineering serves should be enforced, so that it can reduce the damage of ice flood to the maximum degree.

This paper expresses our thanks to prof. Chen Chujun for the selfless help from him.

#### **REFERENCES**

Heihe hydrological survey team, Heilongjiang Province, collection of ice dam investigation data over the years on the upper reaches of the Heilong River (in Chinese), unpublished, July (1988).

Heihe hydrological survey team, Heilongjiang Province, report of ice dam investigation on Heilong River and Nen River in 1971 and 1973 (in Chinese), unpublished, July (1988).

LIU GUIJUN ETC. (1983): Analysis and forecast of ice dam forming condition on the upper Songhua River. Hydrology, 2.

Songliao Water Resources Commission, Ministry of Water Resources, Brief report of water resources comprehensive utilization and planing on China and Russia Erguna River and Heilong River boundary river (1994).

XIAO DIFANG ETC. (1997): The method of ice dam sources and forecast on upper Nen River, Water resources & hydropower of northeast China, 1.



## THE CAUSES OF ICE DAM FORMATION AND ITS MAJOR CONTRIBUTING FACTORS

Duan Yuansheng<sup>1</sup>, Liu Shubao<sup>1</sup>, Li Yingshi<sup>1</sup>

### ABSTRACT

This paper analyzed the forming process of the three serious ice dam that happened on upper reaches of Heilongjiang River, lower reaches of Songhuajiang River and upper reaches of Nenjiang River. This paper sums up and puts forward the major factors that affect the scale of ice dam.

### INTRODUCTION

Ice dam is a special ice condition in terms of ice breakup. Rivers in Northeast area generally breakup in March and April. In areas north to the 50°N, the term of ice breakup will be postponed till the last ten days of April or the beginning of May. Ice breakup has three stages according to the situation and the intensity extent: they are tranquil breakup, violent breakup and semi-violent break-up. The type of violent breakup and semi-violent breakup are easy to form ice dam and cause to ice flood.

To form ice dam, first there should be concentrated and enough ice run. This is the material condition. Besides, there also should be suitable river course topography, such as continuous sinuous channel, narrow section, river shoal, none thawing freezing up river reach, etc. Once the ice dam forms, the water level rises sharply on Upper River and the scale of ice dam growing fast. Then the ice flood will be formed and bring disaster. Because of the comprehensive effect of thermodynamic and waterpower, the ice dam will collapse if it cannot bear the pressure of ice water from upper reach. The ice and water will flow down together. The discharge of the downstream increases sharply and the water level rises steeply. So the local reach of the downstream will suffer from flood disaster.

Ice flood caused by ice dam is a common flood type in northeast area. In some reaches, the probability that the highest water level occurs in term of ice flood period comes to 20~60 %.

---

<sup>1</sup> Engineer, Changchun, China

Northeast Investigation, Design and Research Institute, MWR., NO.10 Gongnong Road Changchun, Jilin, China, Tel.: 0431-5607315, fax: 0431-5607318

In fact the biggest ice flood that had happened amounts to 10~20 % of major flood volume. In some exceptional reaches the water level of ice flood even approach the 100-year flood water level. So it's very important to analyze and study the cause of ice dam formation and its contributing factors. The paper analyses and studies these several aspects based on the gathering relevant data of the three extraordinary ice dams occurred on upper Heilongjiang River, lower Songhuajiang River and upper Nenjiang River.

## **ANALYSIS OF INDIVIDUAL ICE DAM**

### **Ice dam on upper Heilong River 1960**

#### Introduction Of Ice Condition

The air temperature from last winter to this spring is much lower than usual in upper Heilongjiang River area, especially in the first and middle ten days of April. The temperature is 2~4°C lower than normal year and it keeps below 0°C till the middle ten days of April. On April 19 the temperature returned to normal and became stable. In the last ten days of April the temperature grew up sharply and there was a 15mm-rainfall around April 20. All these factors forced the rain and snow runoff on upper reach increasing rapidly. Aaoluoqia Hydrological Station on Ergunahe River and Qiasuowaya Hydrological Station on Shikekahe River were both break-up on April 24. The discharge steeply increased each from 100 m<sup>3</sup>/s to 1220 m<sup>3</sup>/s and 10 m<sup>3</sup>/s to 1140 m<sup>3</sup>/s. The discharge continue increasing to 1890 m<sup>3</sup>/s at Qiasuowaya Station. Ice flood of these two big branch rivers converged into the main river of Heilongjiang River. This helped violent break-up take places on Luoguhe River reach on April 25 and then the ice dam formed. At Bokeluofuka Hydrological Station (former the Soviet Union), the water level had risen from 2.05 m (April 20) to 10.32 m (April 26) ( $Q=112$  m<sup>3</sup>/s), 8.27 m in total. The discharge was 1620 m<sup>3</sup>/s. The ice dam last for two days and then collapsed naturally at deep night April 26. It pushed towards downstream with a water head of 7~8 m. Four o'clock early next morning, water level of Mohe River Hydrological Station, which is located 60 km far away, had risen to 97.26 m. The ice flood pushed towards downstream and converged into ice flood of some other branch rivers such as Ermuerhe River, Panguhe River and Humahe River, etc. Thirteen ice dams were formed differently at Lianyin, Guchengdaodao Island, Malun, Kaikukang, Yiciken, Sanhezhan, Xinjieji, Dalazi, Baishilazi, Zhangdiyingzi, Hoerxin, Dayinshan and Huoermojin, etc. The biggest ice dam occurred at Guchengdao Island and 20 km around that there were more than 20 islands with different size. Guchengdao Island stood in the middle of the river, which made the main river have to make two sharp 90 degree turning continuously. So ice dams were easy to form there. On April 27 about 30km length reach around Guocheng Island, ice dam occurred. At Jialinda Hydrological Station (former the Soviet Union) which located at end of the ice dam, the highest backwater level has reached 13.56 m, rising extent was 12.56 m, 2.16 m higher than the water level of extraordinary flood in 1958 (11.36 m).

In 1960 there were fourteen ice dams occurred in overall 980km-length river reach of upper Heilongjiang River, from Luoguhe River to Huoermojin reach which below Jieyahe River confluence. It is rare in history, for its quantity, its scale, the time it went on and its intensity.

### Factors analysis of Ice Dam forming

1. The weather was cold in winter and the air temperature of last ten days in April recovered too sharply. In January the air temperature was 3~7°C lower than normal year on upper reach of Heilongjiang River. In the middle ten days of April air temperature was 2~4°C lower than usual and kept below 0°C. In the last ten days of April the air temperature rose steeply and reached to 9.4°C on April 24, then 14.1°C on April 29. The same thing happened on upper Ergunahe River, and even more seriously. On April 24 ice breakup occurred on the two upstream and soon formed ice flood, converging into the main river of Heilongjiang River.
2. There is excessive precipitation in winter. The precipitation amount was twice the size of normal year (see Table 1). In addition to the concentrated rainfall before ice break-up, the precipitation amount reached to 15 mm from April 18 to April 22, which made ice break-up be possible. Ice and water pushed towards downstream steadily and formed many ice dams in different reaches. From the end of April to the beginning of May there was another precipitation. The scale of ice dam was increased, and finally ice of allover river was breakup. Ice dam on Guchengdao Island lasted till May 10.
3. The freezing level was much high in last year. In 1959, freezing level of the reach between Mohe River on upper Heilongjiang River and Heihe River was 0.50 m higher than normal year.

**Table 1**

Statistics of precipitation amount of different hydrological stations on Ergunahe River and Heilongjiang River in 1959 (mm)

Date	item	Hailaer	Heishantou	Taipingchun	Mohe	the 25th Station	the 23th Station	Huma	Sandaka
Nov.~Mar.	1960	29.5	30.9	31.8	43.3	36.6	65.4	37.0	26.2
	average	20.2	18.6	26.0	29.8	30.0	35.3	31.0	24.6
Oct.~Mar.	1960	64.7	114.2	71.8	76.8	63.6	96.3	126.4	114.8
	average	32.1	31.5	37.5	47.8	50.0	49.9	50.6	49.7
April 18~1960	1960	0	2.0	3.7	18.0	10.8	8.9	1.6	15.1
April 1~April 25	1960	7.1	3.5	14.0	22.3	14.5	12.7	3.9	15.8
April 25~April 28	1960	0	0	0	1.1	8.6	22.2	4.5	0.2
April 30~May 4	1960	8.8	3.2	8.3	12.3	17.9	34.9	31.3	31.2

### **Ice dam on lower Songhua River 1981**

#### Introduction of Ice Condition

On April 5 to April 19, 1981, there had formed sixteen ice dams in succession in allover 365 km-long reach between Yilan and Fujin on lower Songhuajiang River. It was rare in history on the quantity and scale.

In this year the snowfall of Mar. was clearly on the high side between Yilan and Jiamusi basin interval. Around Mar. 25 there was a 10mm-snowfall. In addition to the steep rising of air temperature in the middle ten-days of Mar. the maximum temperature reached to 10.7°C. This sped the melting of the snow accumulation in the basin. The time of Violent breakup of some branch river in this region such as Songmuhe River, Wokenhe River and Mudanjiang River had moved up to the end of Mar. Water and ice in these branch rivers converged into main river of Songhuajiang River. At Yilan Hydrological Station below Mudanjiang River confluence the time of ice breakup had been seven days moved up to April 6 and come to Violent breakup. The concentrated ice and water pushed towards downstream and ice dams formed at Hasu and Sule of Yilan County. The ice dam was 3~5 m high. On April 9 another big ice dams about 7~8 m high was formed at Hongkeli. This ice dam lasted three days. During this period there was another 10~15 mm rainfall. The ice dam collapsed on April 12. On April 13 ice dams of 3~5 m high were formed at Yongan, Sihe and Rileway Bridge separately. These ice dams were manual broken at 14 o'clock on April 14. The concentrated water and ice formed ice dams again at 9 spots at Xinmin reach 14 km lower than Jiamusi City, Xinghuo Commue, Wendenggang, Makulixiao, Lufucui, Duitong, Miantong, Yaotong and Sibotong in Huachuan County. These ice dams were 3~6 m high, and lasted 1~2 days. The ice flood successfully flew through Fujin Hydrological Station cross section on April 20.

The water level rose sharply because of the formation of ice dam. At 14 o'clock April 14 the highest water level reach 78.89 m, only 1.74 m lower than the maximum water level 80.63 m (Aug. 27, 1960) since there was records.

#### Factors Analysis of Ice Dam Forming

1. Air temperature recovered steeply in the last twenty-days of Mar. and the first ten-days of April. This impelled the moving up of ice breakup, and formed typical violent break-up and inverse break-up. Air temperature in the first ten days of March was 3°C lower than normal year. The air temperature rose suddenly in the middle ten-days of Mar., the diurnal maximum temperature was over 0°C and reached 10.7°C on March 18. The extent of rising air temperature increased even more in April. The average temperature of ten days period was 6.1°C, 4.2°C higher than normal. In the first ten days of April the diurnal maximum temperature kept over 10°C and reach to 16.0°C on April 5 and 20.4°C on April 8. This sped the melting of snow accumulation in the basin. The discharge of channel increased speedily and formed a typical violent break-up. The date of break-up was 1~7 days earlier than normal.
2. Excessive precipitation amount in winter and gathering precipitation during ice breakup period was another important factor of this ice flood forming. According to the data shown on table 2, the winter precipitation amount is obviously high in region between Yilan and Jiamusi, especially in March, the precipitation amount is 2~3 times of the average value of many years. And most of the precipitation gathered in south branch rivers, such as Modanjiang River, the snowfall amount was over 20 mm in March. Air temperature has risen up after the snow. The melting snow runoff gathered and led to intense violent break-up on some branch river. For example, at Changjiantun Hydrological Station on

lower Mudanjiang River, the water discharge increased from 70 m<sup>3</sup>/s of the middle ten days to 200 m<sup>3</sup>/s of the last ten days in Mar., and it reach 476 m<sup>3</sup>/s on April 5. This forced the ice break-up of Yilan reach happened on April 6, 7 days in advance. And then from April 8 to April 11, a 15mm rainfall further developed the ice dam. It pushed towards downstream gradually and brings to typical reverse ice break-up.

3. The freezing level was high. In early winter of 1980, the freezing level of Jiamusi Hydrological Station was 76.53 m, about 1.2 m higher than normal year. At Fujin Hydrological Station the freezing level was 57.24 m, 0.41 m higher than the over years. So the water storage and ice storage in river channel was quite large before ice break-up. This increased the effect of flow dynamic and forced the formation of violent break-up and ice dam.

**Table 2**

Statistics of precipitation amount of different hydrological stations on river reach from Yilan to Fujin in 1981 (mm)

month and date	Item	Songhuajiang River			Modanjiang River	Wusihunhe River	Wuokenhe River	Songmuhe River
		Yilan	Jiamosi	Fujin	Taiping	Linkou	Tuanzishan	Yugong
Nov. ~ Mar.	1981	57.6	40.0	45.3	65.7	53.7	55.3	43.0
	Average	32.3	38.5	44.9	40.8	34.3	36.8	37.0
Mar.	1981	31.8	18.2	18.6	25.8	22.8	22.4	20.4
	Average	9.1	10.1	12.1	9.0	7.0	9.1	9.8
April	1981	30.8	19.4	25.8	29.5	13.3	22.4	16.7
	Average	24.5	24.7	29.5	24.6	19.6	19.1	17.8
The first ten days of Mar.	1981	5.0	0.2	0.4	5.6	2.5	2.1	3.5
Mar.13~Mar.16	1981	7.3	10.4	15.0	8.6	1.9	9.4	8.0
Mar.24~Mar.26	1981	19.4	6.5	2.3	11.6	16.5	10.3	6.1
April 8~April 11	1981	15.8	18.1	14.6	15.0	9.2	14.5	11.6

#### **Ice dam on upper Nen River 1984**

##### Introduction of Ice Condition

In the middle ten days of April in 1984, there appeared five huge ice dams in the allover 127km-long river reach between Shihuiyao and Kumotun after the violent breakup. These ice dams were 6~7 meter high and brought a serious ice flood.

Air temperature went up early this spring on upper Nenjiang River region. On April 7, the diurnal average temperature recovered to steady 4 days earlier than average year. Subsequently the air temperature steep rose. The diurnal maximum average temperature of on April 13 to April 16 was higher than 5°C, the highest temperature kept over 10°C; the highest temperature even reached to 15.9°C. At the same time there were three rainfalls over 10 mm

during April 5~6, April 8~10, April 16~7. The rainfall increased the rain and snow runoff amount of river channel. At Shihuiyao Hydrological Station the discharge on April 10 was about  $0 \text{ m}^3/\text{s}$  and steeply increased to  $230 \text{ m}^3/\text{s}$  on April 15. Violent break-up occurred at 15 o'clock on April 15. At the Duobukuer River Hydrological Station on the right branch, ice breakup occurred on April 13, the discharge on April 15 was  $139 \text{ m}^3/\text{s}$ . On April 16 to April 17 there was another 10mm-rainfall on upper region. At 15 o'clock of April 16 violent break-up occurred at Kumotun Hydrological station. Drifting ice flowed together and soon formed ice dams at a bend reach on upstream 2 km away. At Kumotun Hydrological Station the water level rose continuously. On April 16, the highest water level reach to 233.58 m. At 16 o'clock of April 17 the lower ice dam began to slide. During this period the water level once fall for a short time, but it still kept around 233 m. On April 18 concentrated drifting ice from upper reach flowed down again and forced the further development of ice dam. The water level of Kumotun rose again and reached to 234.28 m at 5 o'clock of April 19. This water level was on the third place in the Hydrological Station of its 51-year's records. It was only 0.72 m lower than the highest flood water level (235.00 m, on Jul. 6, 1955) and 0.43 m lower than the highest water level of ice flood (234.71 m, on April 11, 1957). The ice dam on lower reach didn't breached until 20 o'clock of April 19. Then the water level fell rapidly.

#### Factors analysis of Ice Dam forming

1. Air temperature in the middle ten days of April raised sharply and it kept high for many days. Melting snow runoff increased speedily. These were the important causes that the violent breakup occurred. Air temperature in last winter and this spring were as usual as before, but in the middle and last ten days of April the air temperature rose fast. The highest air temperature kept over  $0^\circ\text{C}$ , the diurnal average air temperature kept over  $5^\circ\text{C}$  since April 14, and got to  $15.9^\circ\text{C}$  on April 16. Snow accumulation in the basin melting speedy because of the high air temperature. Meanwhile the steep gradient and the fan-shape basin the concentrated rain and snow runoff increased. The stream flow increased speedily and came to a favorable condition for violent break-up.
2. The snowfall was high in last winter and this spring. The excessive precipitation amount of April was a direct reason of violent break-up and the formation of those ice dams on upper Nenjiang River. On upper Nenjiang River, especially on the right side of the basin the rainfall amount reach to 40 mm around, 30~40 % much than normal year; meanwhile precipitation of April was twice to third times of normal year and reach to 50 mm around.

#### **THE MAJOR AFFECTED FACTORS OF THE ICE DAM**

According to the analysis of ice dam examples the above mentioned we could see the major factors that affect the formation of ice dam as follow:

##### **The river's geographic position its strike**

All serious ice dams occurred in northeast area were on the reaches located on the high latitude area north to  $50^\circ\text{N}$ . Weather is cold there in winter. The maximum ice cover thickness of river channel was over 1.0 m. The ice cover is still hard just before ice breakup. It provides enough ice quantity to form ice dams.

Table 3

Statistics of Rainfall Amount in Different Hydrological Stations  
on Upper Nenjiang River (mm)

Month and year	Item	Nenjiang River					Menluhe River	Keluohe River
		Woduhe	Shihuiyao	Xiecaizhan	Kumotun	Nenjiang	Menluhe	Kehou
Nov. ~Mar.	1981~1984	37.9	42.2	42.2	31.9	21.1	41.6	27.2
	years average	27.3	32.0	27.3	27.4	26.2	26.5	27.2
April	1984	30.0	53.7	64.8	55.5	37.2	51.1	27.5
	years average	27.3	24.3	30.2	17.3	17.3	20.5	20.8
1984	April 5~April 6	2.7	11.1	9.9	3.7	1.6	8.7	1.7
	April 8~April 9	8.5	9.9	10.6	11.7	5.9	8.5	7.0
	April 16~April 17	5.3	8.2	8.1	8.2	5.2	5.2	7.1
	April 19~April 20	8.0	12.4	11.9	12.9	13.5	11.5	6.6
	April 25~April 26	1.7	9.8	19.1	18.1	10.3	17.0	4.4

River strike is another important factor affect the formation of ice dams. Rivers flowing from low latitude area to high latitude area are easy to form ice dams. Because in these rivers ice break-up usually first occurs on upper reach instead of lower reach. Drifting ice from upper reach cannot flow through smoothly, so it is easy to form a blockage and then form ice dam. Between Luoguhe River reach to Humahe river reach on upper Heilongjiang River lie on the north area. The two sources of Heilongjiang River and the major branch rivers such as Ermuhe River, Panguhe River and Humahe River lie on the south section of Luoguhe River reach to Humahe River reach. Ice break-up occurred early on south reach. So in this river reach ice dam occurred the most frequently in allover Main River of Heilongjiang River. The strike of Yilan reach to Jiamusi reach of Songhuajiang River is from southwest to northeast. There is a major branch river Mudanjiang River converges into it in this period. And the river strike is from south to north. Usually in this kind of river reach ice breakup term is earlier than the main river of Songhuajiang River. So it is easy to form ice dam in the Yilan reach to Jiamusi reach.

#### River feature

The factors of ice dam forming can be briefly account to the ice inflow account exceeding the ice conveying capacity. River feature is the important factors that affect the ice conveying capacity of river.

Upper reach of Heilongjiang River flows through hilly region, plain and forges alternately. Each river is quite different in feature there. Some reaches flow through mountains and

gorges, ice cover is thick because of the less heating of ice surface. In these river reaches ice break-up lag occurs; The channels of some reaches are meandering and narrow, the surface of the river is only 1/3 to 1/2 wide of upstream. On some river reach there are many small islands and series gully in it. The complex river feature provided favorable boundary conditions for the formation of ice dam.

Under similar circumstances Yilan to Jiamusi river reach of Songhuajiang River also has complex river feature, such as the Sanxing river shoal near Yilan, the narrow river reach on lower Yilan, Wuguliu in Tangyuan County and Aoqi S-shape bend near Jiamusi City. Ice dam is frequently occurred in these places.

#### **Thermodynamic factors**

Air temperature affect ice dam major on the following two sections:

1. Low air temperature is propitious to the increasing of ice cover thickness, especially in the last ten days of March. The lower air temperature is good for keeping the thickness and quality of ice cover. It provides enough quantity hard ice for the formation of ice dam.
2. The rate of air temperature grows up obviously affects the collection of snowmelt runoff and the quantity of drifting ice. The gathering procession of snowmelt runoff would be long and infirm if the air temperature grows up slowly, and there would be enough time for the ablation of the ice cover. Whereas if the air temperature grows up speedily, the snowmelt runoff would gathers together, the drifting ice flow was excessive and the ice was hard. This makes it possible to come to violent breakup and form ice dam. Based on the above mentioned lower air temperature in prophase and the steep rising of the air temperature before ice break-up are the necessary condition for forming ice dam.

#### **Flow dynamic conditions**

The contributing flow dynamic conditions of ice dam are reflected through the following three factors:

- The freezing level - as we all know the necessary condition of violent breakup is that the discharge must exceed the over flowing capacity. Only under this condition the ice cover could be break up and come to "ice breakup". So the more freezing level higher, the more ice breakup discharge and water and ice storage larger in river channel; meanwhile the effect of flow dynamic is increased also. So this factor is closely connected with the size of the ice dam and the height of the water level.
- Snowfall amount in winter - snowfall amount in winter is an indirect index. It is reflected through the recover of air temperature and the collection of snowmelt runoff. Especially in the prophase of ice breakup such as the middle and last ten-days of march, the effect is more remarkable.
- Rainfall on the eve of ice breakup - the rainfall on the eve of ice breakup is the most directly and most important factor to the formation of ice dam and its size. On the eve of ice breakup, the runoff coefficient in basin is quite large, meanwhile it can also speed the melting of the snow accumulation and bring to rain and snow runoff. The flow dynamic of the river channel is increased and finally impels violent breakup and forms ice dam.

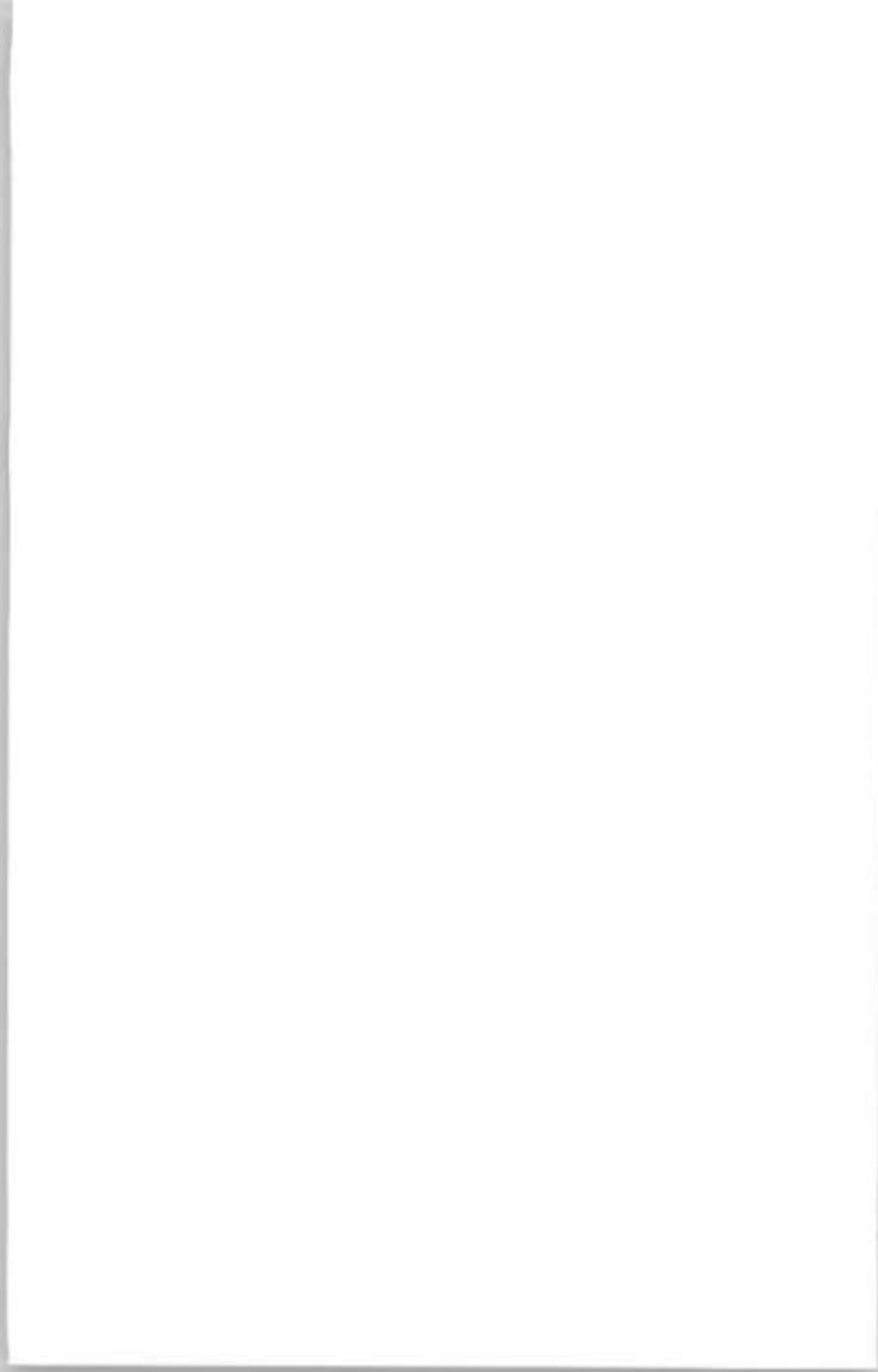
According to the above mentioned we know that in all those years when the huge ice dam occurred there was rainfall process over 10 mm on the eve of ice breakup.

#### **REFERENCES**

LIU GUIJUN ETC. (1983): Analysis of the Conditions for Forming Ice Dam and the Forecast Method on Lower Songhuajiang River. Hydrology, 2.

Hei River Hydrological Exploration Crew, Investigation Data Compilation of Ice Dam for Over the Years on Upper and Middle Heilongjiang River, 7 (1988).

XIAO DIFANG ETC. (1997): Contributing Factors and Forecast Method of Ice Dam on Lower Nenjiang River, Water Resources & Hydropower of Northeast China, 1.





## MODELLING OF WET ICE ACCRETIONS THAT RESULT FROM SPRAY

K. Szilder<sup>1</sup>, E.P. Lozowski<sup>1</sup>, T. Forest<sup>2</sup>, G. Reuter<sup>1</sup>, R. Gagnon<sup>3</sup>

### ABSTRACT

A morphogenetic model has been developed to predict the ice accretion on an ice sensor resulting from water spray. In the numerical model, the spray is divided into an ensemble of fluid elements and their motion and freezing are considered simultaneously. The stochastic model predicts both the ice accretion on the vertical cylindrical surface of the sensor and the accretion below the sensor, including icicle formation. The model also allows the simulation and investigation of the stochastic variability of the accretion shape, something that cannot be achieved with conventional continuous, deterministic models. The model predictions of ice accretion shape and mass have been analyzed as functions of water spray mass flux and heat transfer conditions. The prediction of the overall ice structure agrees with a simple heat-balance model and our experimental data.

### INTRODUCTION

Offshore structures in the marine winter environment are likely to be subjected to ice accretion when the wind and waves interacting with the structure are sufficient to generate significant amounts of spray. To measure this icing, we have developed a novel marine icing sensor, which was designed to operate automatically on board a rig, and to provide continuous quantitative ice thickness measurement (Chung et al., 1998). The principle of the sensor is to measure the equilibrium forces acting on a vertical plate on which spray ice has accreted. From the measured weight of the ice and its moment, it is possible to infer the average ice thickness on the plate. Cold room tests were conducted to simulate marine spray ice accretion on the instrument and to verify the procedures for estimating ice thickness.

---

<sup>1</sup> Department of Earth and Atmospheric Sciences, University of Alberta, Edmonton, Alberta, T6G 2E3, Canada, Tel.: 1-780-492-5406, fax: 1-780-492-2030, e-mail: kszilder@ualberta.ca

<sup>2</sup> Department of Mechanical Engineering, University of Alberta, Edmonton, Alberta, T6G 2E3, Canada

<sup>3</sup> Institute for Marine Dynamics, National Research Council of Canada

The objective of the present work is to model numerically the ice accretion on the sensor. The numerical model was developed to simulate cold room conditions rather than actual conditions at the sea. Two main simplifying assumptions are made in the model. Due to the complexity of the brine freezing process, we have considered fresh water. In addition, as a result of computational constraints, we have modelled ice formation on a sensor that has been scaled down by a factor of ten.

### MODEL DESCRIPTION

The morphogenetic model presented in this paper is an improved version of the model described by Szilder and Lozowski (1995a and 1995b). In the old version, the behaviour of every fluid element was considered separately, and once motion of the fluid element was terminated, the conduct of the next fluid element was analysed. In the new version of the model presented here, the behaviour of many fluid elements is considered simultaneously. The fluid elements are fired towards the sensor axis along straight horizontal trajectories from a random location within a specified range of azimuthal impingement angle. The time interval between two consecutive releases of fluid elements is determined by the spray mass flux, spray surface area and the fluid element size and density. From the impact location, the fluid elements begin their random walk along the ice structure and the model traces the motion of all fluid elements simultaneously. When a critical number of unfrozen fluid elements reach the lowest accretion level, all these elements drip. The ability of the new model to track simultaneously the positions of all fluid elements eliminates the need for the previously used shedding parameter. The highlights of the model and the derivation of the relations between microscopic model parameters and macroscopic atmospheric conditions are given below.

We start with the derivation of an expression for the average velocity of water film flow on a vertical surface exposed to homogeneous water spray. The difference between the directly impinging water spray mass flux and the rate of mass freezing at this level determines the change of the water mass flux flowing on the surface:

$$d\Gamma = \left(m - \frac{q}{L_f}\right) dz \quad (1)$$

where:  $\Gamma$  is the film mass flow rate per unit width,  $\text{kg m}^{-1} \text{s}^{-1}$ ;  $m$  is the water spray mass flux,  $\text{kg m}^{-2} \text{s}^{-1}$ ;  $q$  is the external heat flux,  $\text{W m}^{-2}$ ;  $L_f$  is the latent heat of fusion,  $334 \times 10^3 \text{ J kg}^{-1}$ ;  $z$  is the vertical coordinate, m. In general, the heat flux between the ice surface and the cold air stream consists of convective, evaporative and radiative terms. For convenience, however, we will simply refer to the sum of these as the heat flux. The average speed of a water film flowing on a vertical surface is given by Szilder et al. (2000):

$$u = \left(\frac{g}{3\mu_w\rho_w}\right)^{1/3} \Gamma^{2/3} \quad (2)$$

where:  $g$  is the acceleration of gravity,  $9.8 \text{ m s}^{-2}$ ;  $\mu_w$  is the viscosity of water,  $1.79 \times 10^{-3} \text{ kg m}^{-1} \text{ s}^{-1}$ ;  $\rho_w$  is the density of water,  $10^3 \text{ kg m}^{-3}$ . After integrating Eq. 1 and inserting the expression

for  $\Gamma$  into Eq. 2, we may integrate Eq. 2 with respect to height to obtain the average vertical water speed:

$$u_{av} = \frac{3}{5} \left( \frac{g}{3\mu_w \rho_w} \right)^{1/3} \left[ \left( m - \frac{q}{L_f} \right) z_o \right]^{2/3} \quad (3)$$

where:  $z_o$  is the height of the sensor, m.

The random walk of a fluid element consists of a series of moves through a three-dimensional lattice. At each time step there are seven possibilities: the fluid element may move one cell in any of six perpendicular directions, or it may freeze *in situ*. It is assumed that the probabilities of moving horizontally, in any of four perpendicular directions, and the probability of moving upward, are the same. The ratio of the probability of moving downward to the probability of motion in any other direction is assumed to be three (Szilder and Lozowski, 1995b). In order to correlate macroscopic conditions with model parameters, the following relation for average vertical velocity may be written:

$$u_{av} = V \frac{\Delta l}{\Delta T} \quad (4)$$

where:  $\Delta l$  is the grid size, 1 mm;  $\Delta T$  is the motion time step, s;  $V$  is the model's dimensionless velocity. Based on numerical results (Szilder et al., 2000) the value of  $V$  is taken to be 0.15. The motion time step, which is the time required for all fluid elements currently on the surface to complete a single move, may be written as:

$$\Delta T = \frac{5V \Delta l}{3} \left( \frac{3\mu_w \rho_w}{g} \right)^{1/3} \left[ \left( m - \frac{q}{L_f} \right) z_o \right]^{-2/3} \quad (5)$$

The motion of each fluid element on the ice surface ends either by dripping or freezing. Dripping from the ice structure occurs when a critical number of fluid elements has accumulated at the lowest level of the accretion. The critical number of fluid elements is 65, this value being based on the diameter of a typical pendant drop namely 5 mm. Freezing *in situ*, like motion, has a specified probability of occurrence. When a number corresponding to the freezing probability is randomly chosen, the fluid element does not necessarily freeze in its present location. Rather a *cradle* location is sought for the fluid element in the neighbourhood of its current location (Szilder and Lozowski, 1995a).

The freezing probability may be expressed as a function of the freezing fraction,  $f$ , defined as the ratio of the external heat flux to the product of spray mass flux and the latent heat of fusion. This may be shown as follows. Let us consider level  $n$  below the upper surface of the sensor. The incoming mass of water flowing downward from level  $n-1$  is given by  $(1-f)(n-1)m\Delta l$ . The spray mass directly impinging at level  $n$  is  $m\Delta l$  and the mass that freezes at this level is  $fm\Delta l$ . The probability of freezing,  $P$ , at level  $n$  is the product of the dimensionless velocity and the ratio of the freezing mass to the total water mass entering level  $n$ . The

dimensionless velocity is included in the definition, since on average it takes  $V^{-1}$  time steps for a fluid element to move one level down. After transformation we could write:

$$P = \frac{V}{n(f^{-1} - 1) + 1} \times 100\% \quad \text{where} \quad f = \frac{q}{mL_f} \quad (6)$$

When  $q > mL_f$ , the freezing fraction is equal to one.

### MODEL RESULTS AND DISCUSSION

The morphogenetic model predictions have been compared quantitatively with a simple analytical heat-balance model. This model assumes that the total external heat flux balances the latent heat of freezing. If the heat flux is not sufficient to freeze instantaneously all the impinging spray, the remaining water will drip from the base of the cylinder.

$$m_i = \frac{qAt}{L_f} \quad \text{when} \quad q \leq mL_f \quad \text{and} \quad m_i = mAt \quad \text{when} \quad q > mL_f \quad (7)$$

Where  $m_i$  is the ice mass, kg;  $A$  is the sprayed surface area,  $m^2$ ;  $t$  is the time, s.

The numerical simulations are performed on a three-dimensional lattice, consisting of  $60 \times 60$  cells (horizontal) by 170 cells (vertical). The cylinder height,  $z_0$ , is 0.1 m (the vertical coordinate of the cylinder base is  $z=0$ , see Fig.1a.), the cylinder radius is 0.02 m and the spray angle is 90 degrees (see Fig.1b.). The fluid elements are fired towards the cylinder surface between levels  $z=0$  and  $z=100$  mm. In the results shown below, the total simulation time of 1 h is kept constant and the heat flux and spray mass flux are allowed to vary.

Examples of the simulated ice accretion shape for different values of the heat flux are shown in Figs.1. and 2. For the conditions of Fig.1., the ice grows mainly on the cylinder surface exposed to spray. Ice also forms below the cylinder base as a pendant. Approximately 80 % of spray mass drips from the accretion. For greater values of the heat flux, Fig.2., more ice grows on the cylinder surface and well-developed pendant ice forms. The influence of the heat flux on the ice accretion process is summarized in Fig.3. For a value of the spray mass flux of  $3.0 \times 10^{-3} \text{ kg m}^{-2} \text{ s}^{-1}$ , the critical value of the heat flux for which all impinging water freezes on impact (freezing fraction equal to one, see Eq. 6) is  $1002 \text{ Wm}^{-2}$ . However, the gradual increase of the accretion mass as a function of the heat flux reaches its maximum value, equal to the total impinging mass, at a heat flux value almost 20 % smaller. This occurs because the freezing takes place not only on the cylinder's vertical surface but also below the cylinder base. This is clearly seen in Fig.3b. where the pendular accretion length reaches a maximum (plotted negatively) when the dripping from the accretion diminishes. For a heat flux greater than the critical value, the pendular ice vanishes. As the pendular accretion length grows, the centre of mass of the ice accretion descends to lower values of  $z$ . Initially, when the heat flux increases, the centre of accretion mass moves downward from the cylinder centre. At very high values of the external heat flux, a gradual disappearance of pendular accretion leads to a rise of the centre of mass of the ice. In order to show the model's stochastic variability, results are displayed for five different values of the numerical seed, which is used to generate pseudo

random number sequence used by the model. These results are shown for external heat fluxes of 400 and 800 W m<sup>-2</sup>.

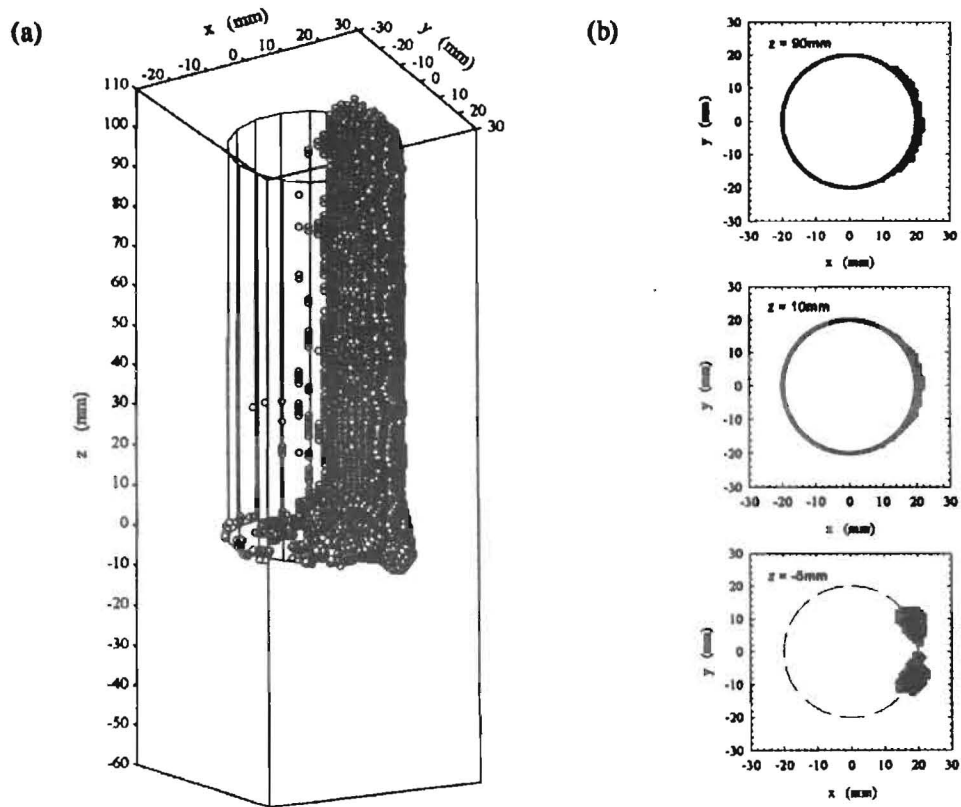


**Fig.1.** Simulated ice accretion on the marine icing sensor. The spray mass flux is  $3.0 \times 10^{-3}$  kg m<sup>-2</sup> s<sup>-1</sup>, the external heat flux is 200 W m<sup>-2</sup> and the simulation time is 1 h.

- a) Three-dimensional view of the accretion.
- b) Horizontal accretion cross-sections at different levels.

The influence of the spray mass flux on the ice accretion growth has been examined while maintaining a constant value of the external heat flux of 200 W m<sup>-2</sup> (corresponding to a critical spray mass flux of  $0.6 \times 10^{-3}$  kg m<sup>-2</sup> s<sup>-1</sup>), Fig.4. At low values of the spray mass flux, the heat flux is large enough to freeze immediately all the impinging liquid. For a spray flux somewhat greater than the critical value, the pendant accretion lengthens considerably and the centre of mass moves downwards. However, further increases of the spray flux increase the drip rate. This leads to a gradual decrease of the accretion mass, a lifting of the centre of mass, and the gradual shortening of pendular accretion.

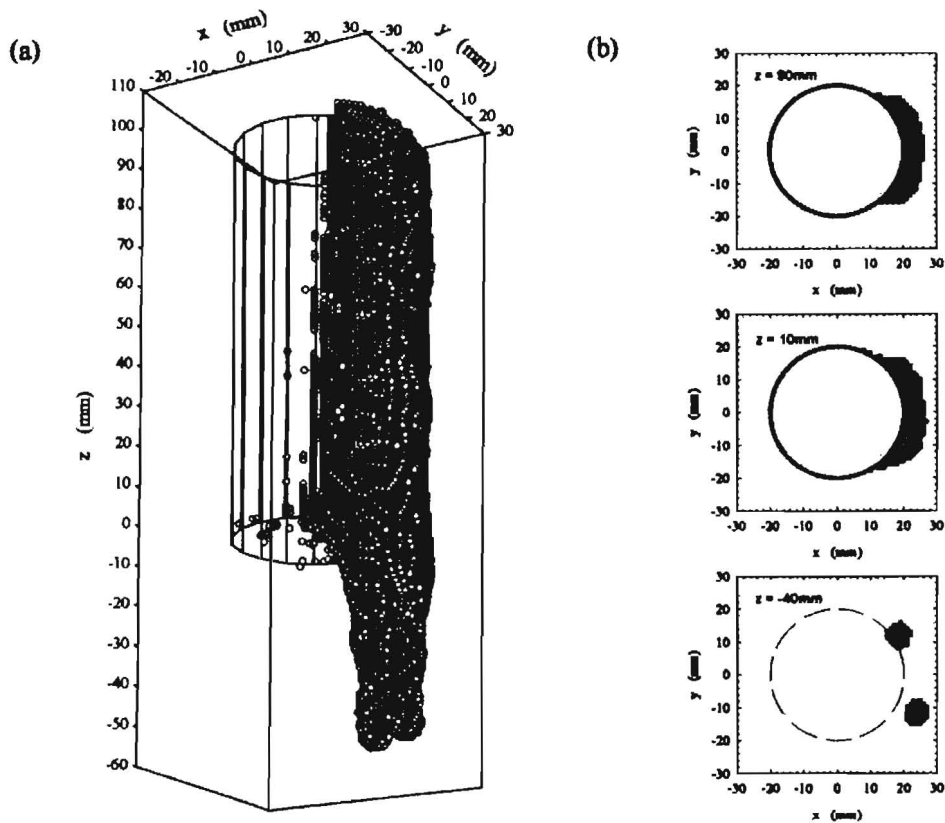
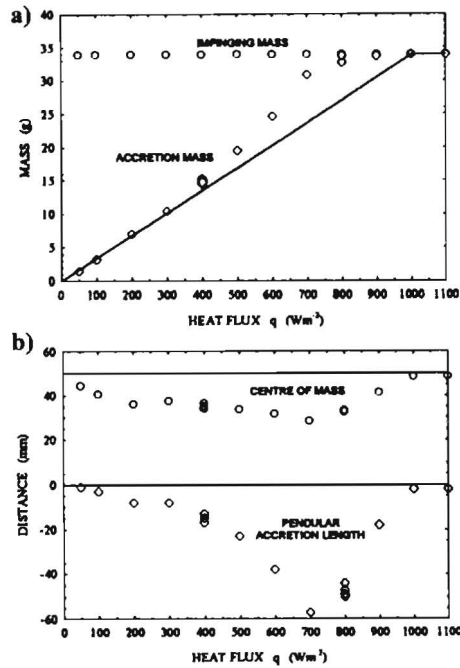


Fig.2. The same as Fig. 1 but for a heat flux of  $700 \text{ Wm}^{-2}$

### CONCLUSIONS

A three-dimensional morphogenetic model with a probabilistic random walk component has been used successfully to simulate at a 1:10 scale the accretion on a marine icing sensor. The model predicts ice accretion formation as a function of the spray mass flux and the external heat flux between the accretion and the cold air stream. The model predicts the formation of ice on the ice sensor surface and also the creation of a pendular accretion below the sensor base. This could be especially significant under conditions when water dripping from the ice structure diminishes. The formation of pendular ice cannot be handled easily by conventional ice accretion models. In the future, we plan to perform further numerical experiments at larger scale. A comparison with experimental data is also planned. While used here to simulate ice accretion on an icing sensor, the morphogenetic model may be used to simulate ice accretion on any element of offshore structures, power transmission lines or telecommunication masts.



**Fig.3.** The influence of the external heat flux on the accretion process for a spray mass flux of  $3.0 \times 10^{-3} \text{ kg m}^{-2} \text{ s}^{-1}$  and a simulation time of 1 h. The solid lines correspond to the analytical model given by Eq. 7.

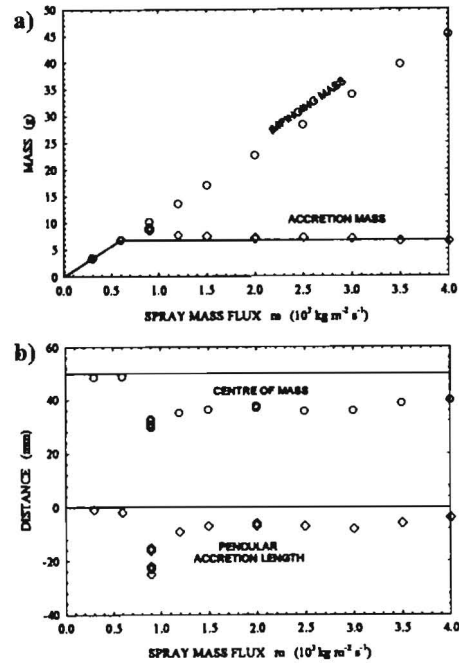


**Fig.4.** The influence of the spray mass flux on the accretion process for an external heat flux of  $200 \text{ W m}^{-2}$  and a simulation time of 1 h. The solid lines correspond to the analytical model given by Eq. 7.

#### ACKNOWLEDGEMENT

This research has been sponsored through funding from PERD and NSERC, which we gratefully acknowledge.

#### REFERENCES

- CHUNG K.K., FOREST T.W., LOZOWSKI E.P., GAGNON R., FAULKNER B., CHEKHAR M. (1998): Application of New Measurement and Simulation Methods to Marine Icing on Offshore Structures. ISOPE-98-RF-009.
- SZILDER K., LOZOWSKI, E.P. (1995a): A New Method of Modelling Ice Accretion on Objects of Complex Geometry. *Int J Offshore Polar Engng*, Vol 5, No 1, pp. 37-42.

SZILDER K., LOZOWSKI E.P. (1995b): Simulation of Icicle Growth Using a Three-Dimensional Random Walk Model. *Atmospheric Research*, Vol 36, pp. 243-249.

SZILDER K., FARZANEH M., LOZOWSKI E.P. (2000): Analysis of Water Film Flow on an Icing Surface. *Proc. The Ninth Int. Workshop on Atmospheric Icing of Structures* (in press).



## THE MARCH 1995 ICE JAMMING IN THE SHOKOTSU RIVER AND ASHIBETSU RIVER

Y. Hirai<sup>1</sup>, M. Yamazaki<sup>1</sup>, K. Hirayama<sup>2</sup>, H.T. Shen<sup>3</sup>

### ABSTRACT

Ice jamming and ice run occurred in the Shokotsu River and Ashibetsu River on March 17 and 18, 1995. It was the first time that ice jamming was observed at Ashibetsu Dam, owned by Hokkaido Electric Power Co., Inc. In the Shokotsu River, a similar event was observed on March 18, 1955. Although geometric and hydraulic characteristics of Hokkaido rivers are ideal for ice jam formation, ice jamming does not occur very often. Hokkaido rivers generally run through mountainous areas. The slopes are usually very steep, and lengths are relatively short. These basins typically accumulate deep snow packs through the winter that melt slowly in the spring, minimizing the possibility of abrupt flow increase and ice jamming at breakup.

This report examines meteorological and hydrological data on March 17 and 18, 1995, when ice jamming and ice run occurred in the Shokotsu River and Ashibetsu River.

### INTRODUCTION

An observation record shows that on March 17, 1995, a huge amount of fragmented ice pieces resulted from the breakup flowed into the Ashibetsu Reservoir which was constructed in 1953 along the Sorachi River. In the Shokotsu River, ice jamming and ice run occurred on the same day. Fig.1. shows comparison of river bed profiles in Japan and World famous rivers. In Japan, the slopes are usually very steep, and lengths are relatively short. River basins in Hokkaido typically accumulate deep snow packs through the winter. Different from those in North America and Europe, the rivers in Hokkaido seldom produce dynamic ice jamming and ice run, which makes the event of the breakup ice jam detected in March 1995 a valuable observation record in this field. In the Shokotsu River, a similar ice jam flooding was

---

<sup>1</sup>Hokkaido Electric Power Co., Inc., Sapporo, Japan, 2-1, Tsuishikari, Ebetsu, Hokkaido, 067-0033,  
Tel.: +81-11-385-6553, fax: +81-11-385-7553, e-mail : y-hirai@epmail.hepco.co.jp

<sup>2</sup>Department of Civil Engineering, University of Iwate, Japan

<sup>3</sup>Clarkson University, Potsdam, New York, USA



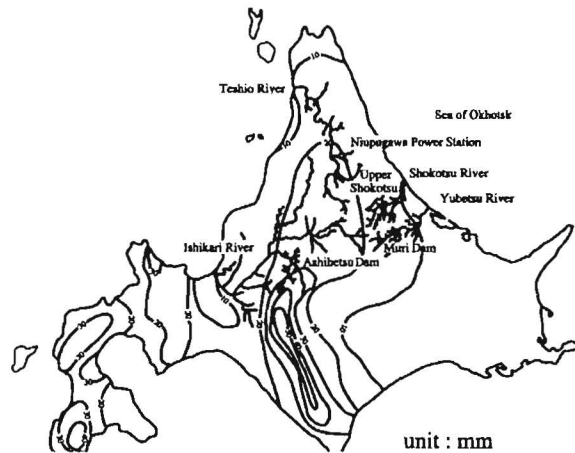
(HEPCO). These records show that the raining area of a cold front crossed Hokkaido from the southwest to the northeast.

Fig.4. shows location maps observed hydro-meteorological data in the Shokotsu River and Ashibetsu River. Observation data at Takinoue Gauging Station (catchment area = 251 km<sup>2</sup>) show that in the winter season, the river discharge goes down to the minimum in late March and goes up again in late April, following the melting of snow and ice in the districts along the river. Fig.5. shows the transitional changes in the snow depth, air temperature and snow precipitation measured at Takinoue Meteorological Station. All these meteorological records point it out that the climate of March 17 was exceptional. However, Takinoue Gauging Station in the upstream of the Shokotsu River showed no substantial change in discharge.

Takinoue Gauging Station stops taking measurements of water level in the winter because of the formation of ice covers in its area. When the gauging station is not in service, field measurement of river discharge has been practiced every 10 days to directly supplement the observation data. Fig.6. shows the cross-sectional profiles of the river at the time of the

**Table 1**  
Weather data of a spring storm in 1955 and 1995

	Mar-1955	Mar-1995
Duration of a spring storm	17th 9PM - 18th 9PM	17th 9AM - 18th 9AM
Low Pressure	990 - 984hpa	992 - 970hpa
Velocity of the Wind	14.5m/s (Abashiri)	14.6m/s (Abashiri)
Direction of the Wind	South (Abashiri)	South (Abashiri)
Precipitation	22mm (Takinoue)	14mm (Takinoue)
Maximum Air Temperature	14°C (Takinoue)	13.2°C (Takinoue)



**Fig.3.** Distribution of rain precipitation in Hokkaido on March 17, 1995, in the unit of daily amount of rainfall (millimeters)

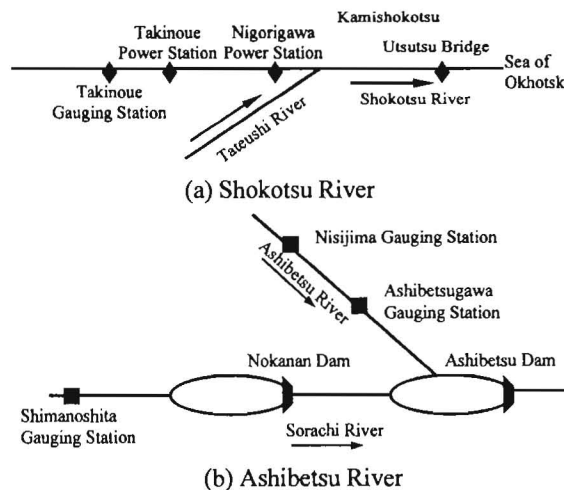


**Fig.4.** Location maps of observation points

discharge measurement on March 9, 19 and 29, 1995. These profiles show that the upstream of the Shokotsu River was totally closed with ice covers on March 17 when the ice jamming and ice run occurred. Besides, it may be concluded that ice clearing or breakup started at Hour 06:00 on March 24 in the area of the gauging station, which restarted the measurement of water level with a level gauge on the same day.

For the areas adjacent to the Shokotsu River, at its hydraulic power stations operated along the Penke-Niupu River, a tributary of the Teshio River, as well as the Yubetsu River and Sorachi River, HEPCO has taken the data of these rivers, including inflow into dam. Fig.7. shows the river discharges measured at the 3 points in the period from March 16 to 21. On the upstream of the Yubetsu River, located on the eastern side of the Shokotsu River, HEPCO has Muri Dam for its Setose Power Station. The river discharge is calculated from the change in the reservoir amount based on the difference in water level.

At Niupugawa Power Station along the Penke-Niupu River, a tributary of the Teshio River, the change in river discharge ( $Q_{max} = 7.13 \text{ m}^3/\text{s}$ , calculated from the water consumption for power generation) was almost identical to that measured at Muri Dam on March 17, 1995. Niupugawa Power Station has a catchment area of  $184 \text{ km}^2$ .

At Ashibetsu Dam of the Sorachi River, as the measurements taken every 10 minutes show in Fig.8., the river discharge increased on the two stages from the evening toward the night of March 17. According to the report of the dam watchman assigned to the dam, slush ice run flowed twice into the reservoir of Ashibetsu Dam from the upper Ashibetsu River, a tributary of the Sorachi River. In the next morning, they took pictures (see Fig.9.), which show the reservoir filled up with a huge amount of fragmented ice pieces. Ashibetsu

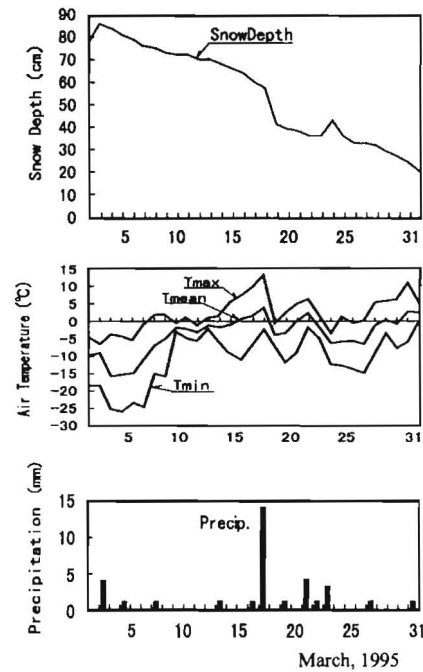


Fig.5. Transitional changes in the snow depth, air temperature and snow precipitation measured at Takinoue Meteorological Station on March, 1995

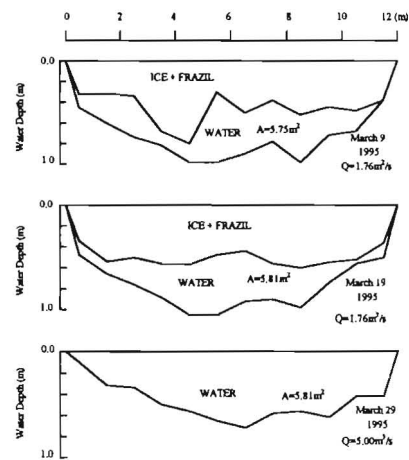
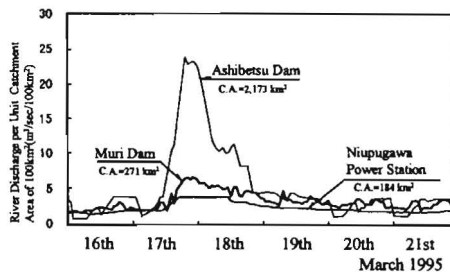


Fig.6. Cross-sectional profiles of Takinoue Gauging Station at the time of the discharge measurement on March 9, 19 and 29, 1995



**Fig.7.** River discharges measured at the 3 points in the period from March 16 to 21 in 1995

Dam has a catchment area of 2,173 km<sup>2</sup> and the catchment area of Ashibetsu River is 393 km<sup>2</sup>.

The Ashibetsu River showed the first peak of its discharge around Hour 17:00 on March 17 while the Shokotsu River reached the peak discharge at Upper Shokotsu Gauging Station around Hour 00:00 in the midnight. Start of ice jamming in the Shokotsu River was 6 or 7 hours behind that in the Ashibetsu River. This means that besides the difference in the amount of rainfall, there might be some difference in the breakup process of ice covers between the two rivers.

#### FORMATION OF ICE JAMMING

Although there are no data available on the water temperature in the Shokotsu River, water temperatures of the Penke-Niupu River need examination. As shown in Fig.10., the water temperature sharply went up on March 16 and 17 after reaching the lowest 0°C at Hour 06:00 on March 15. Unfortunately the water temperature gauge was removed from the river at Hour 12:00 on March 17. The highest water temperature before the removal of the gauge was 4.6°C, which was recorded at Hour 14:00 on March 16. Those unusually warm water temperatures melted the border ice along the river banks, which may have allowed the departure of ice covers and the floatation of the frazil slush accumulated in the river.

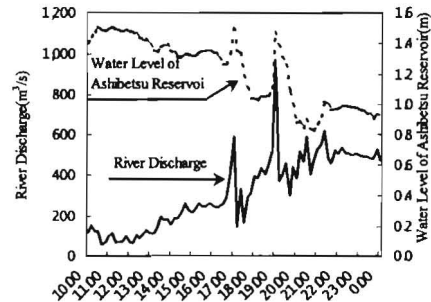


**Fig.8.** Inflow discharge to Ashibetsu Dam on March 17, every 10 minute record in 1995

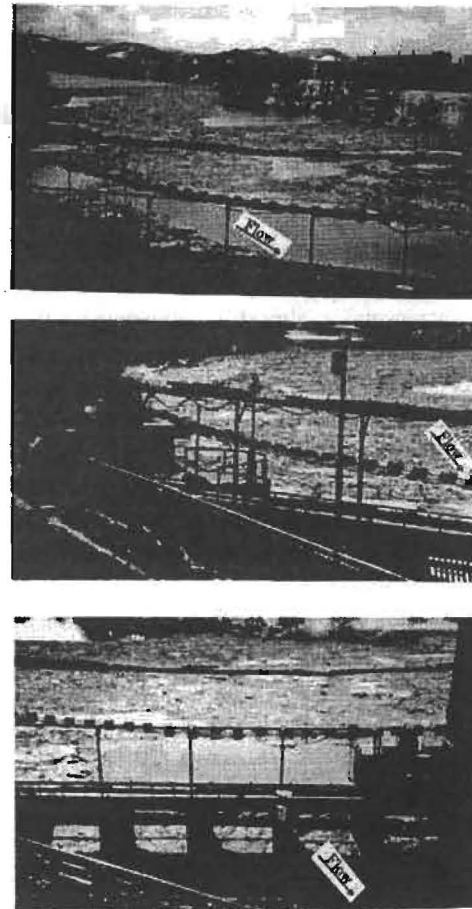


**Fig.9.** Slush Ice Run occurred in the Ashibetsu River, in the morning on March 18, 1995

Rapid thawing resulted in the saturation of the snow accumulated on the ice covers in the period of mid March. At warm water temperatures, rainfall may have easily created desirable conditions for both ice breakup and ice jamming.

### RUNOFF ANALYSIS

Fig.11. shows the water levels measured on March 17 at 3 gauging stations; Shimanoshita Station along the Sorachi River, a main stream flowing into Ashibetsu Dam, Ashibetsugawa and Nishijima Stations along the Ashibetsu River, a tributary of the Sorachi River (see Fig.4b.). On this particular day, rain started drizzly around Hour 10:00 and developed into real rain in the period from Hour 13:00 to Hour 17:00. The peak rainfall occurred at Hour 13:00 at rate of 8 mm/h.

Comparison among the records taken at those 3 gauging stations shows that water level started increasing almost simultaneously at Shimanoshita and Nishijima Stations. At Ashibetsugawa Gauging Station, water level suddenly increased around Hour 11:00 just before raining in earnest. This leads to an assumption that increase in river water temperature may have generated cracks on the ice covers at the midstream and downstream of the Ashibetsu River. Fractured ice covers settled on the river bed, which impeded the water flow and generated small-scale ice jamming on early stages.

Ice covers were all broken up in both dam reservoirs and the river sections between them on March 17. However, in the Ashibetsu River, a tributary of the Sorachi River, ice covers and accumulated frazil slush remained as they were. To examine the abrupt changes in river discharge taking place twice at Hour 17:00 and Hour 19:00, which are shown in Fig.8., the authors tried a runoff analysis with a basic equation of snow melting runoff, which uses a two-layers model as shown in the formula below.

$$\gamma \frac{\partial H}{\partial t} = -k \sin \theta \frac{\partial H}{\partial x} + r_e \quad (1)$$

in which,  $\gamma$  = percentage of effective void (snow or soil);  $H$  = water depth in an active layer or an accumulated snow layer;  $K$  = coefficient of permeability (snow or soil);  $\sin \theta$  = slope of

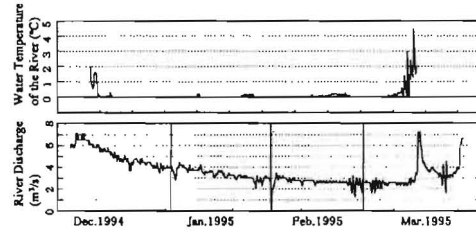


Fig.10. Observation records with the river water temperature and the discharge in the Penke-Niupu River

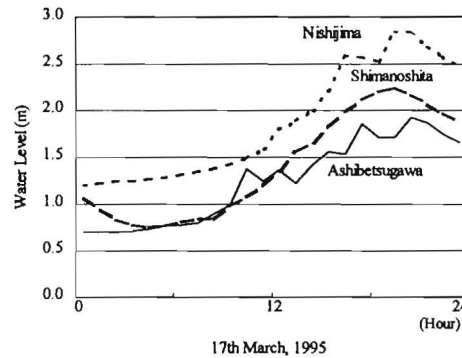


Fig.11. Water levels measured on March 17 at 3 gauging stations, Shimanoshita, Ashibetsugawa and Nishijima

mountain flank;  $x$  = distance from the sloped upstream end, and  $r_e$  = rainfall intensity + snow melting amount.

Calculation was made to obtain the inflow into Nokanan Reservoir (catchment area =  $1,780 \text{ km}^2$ ) and the discharge of Ashibetsu River (catchment area =  $393 \text{ km}^2$ ). The sum of their calculation results was compared with the river flow into Ashibetsu Reservoir (catchment area of  $2,173 \text{ km}^2$ ).

Fig.12. shows the result of a calculation made on an assumption that the amount of rainfall throughout the reaches of the Ashibetsu River was equivalent to the measurement at Nishijima Gauging Station. In this calculation, total inflow for 3 days from March 17 to 19 was equalized to the measured river flow by setting the runoff coefficient at 0.7 and the base flow at  $15 \text{ m}^3/\text{s}$ .

With Fig.11., only the amount of rainfall was enough to reproduce almost the measured inflow into Ashibetsu Reservoir, indicating that the snow melting amount scarcely contributed to the runoff.

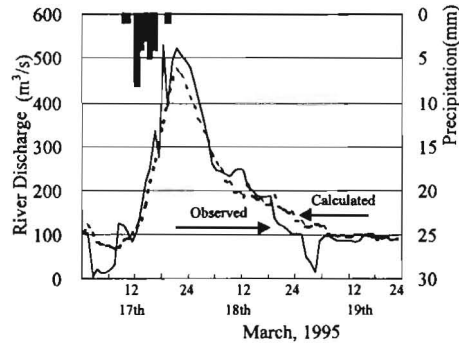


**Fig.12.** Comparison of the calculated and the observed river discharge at Ashibetsu Dam in 1995

## CONCLUSIONS

Ice jamming seldom happens in Hokkaido. Because of a large amount of snowfall, increase in river water temperature at the beginning of the thawing season melts ice covers along the thalweg of the river, resulting in ice clearing. In the Shokotsu River, two events of ice jam were observed in 1955 and 1995. Ice breakup accompanied with ice run takes place in the winter only when several conditions happen concurrently, summarized below:

1. Ice cover and accumulated frazil slush raised up from the river bed due to increasing water temperature over  $0^\circ\text{C}$  at the beginning of March.
2. Spring storm with high air temperature and warm rain accelerated melting snow and ice.
3. Melting water with high temperature weakened adhesive force of the snow pack. Boundary resistance to ice motion along banks decreased.
4. Melting snow and rain added the mass of snow pack on the ice cover.
5. Both snow pack and surface soil were fully saturated with water supplied melting snow. Almost amount of precipitation directly contributed to run off.

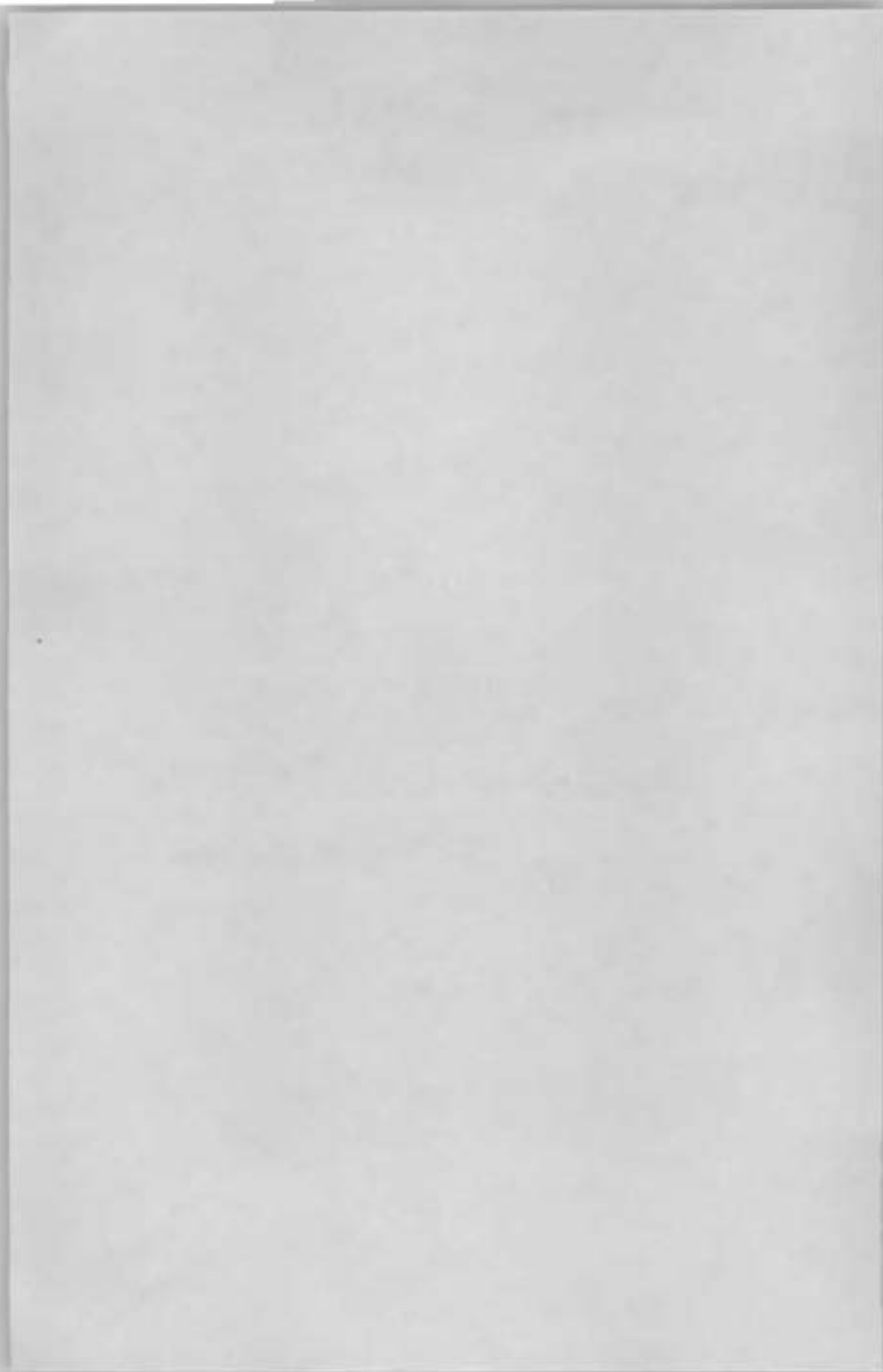
## REFERENCES

HIRAYAMA K., YAMAZAKI M., SHEN H.T. (1999): Aspects of River Ice Hydrology in Japan, IAHS99 Symposium, Birmingham UK.

SAKAGUCHI Y., TAKAHASHI H., OMORI H. (1986): Rivers in Japan. Iwanami Publications, Co., (in Japanese).

**TOPIC D**

**NAVIGATION  
AND OFFSHORE ACTIVITIES  
IN ICE CONDITIONS**



**MODEL TESTS OF AN ARCTIC TANKER CONCEPT  
FOR LOADING OIL  
PART I: MANOEUVRING INTO LOADING POSITION**

**A. Jensen<sup>1,2</sup>, S. Løset<sup>1</sup>, J. Hellmann<sup>3</sup>, O.T. Gudmestad<sup>4</sup>, O. Ravndal<sup>5</sup>**

**ABSTRACT**

One of the keys to an efficient loading of oil in the Arctic offshore is probably a subsea solution where the interference with ice is at a minimum. Therefore an attempt to assess the performance of an Arctic Shuttle Barge System including a subsea mooring and loading terminal was done in model-scale in the Hamburg Ship Model Basin (HSVA) ice tank in 1999. The operational performance and forces exerted on the barge, the pusher and the mooring system, including a riser, were investigated. The system was pushed by the pusher through level ice or towed through level ice and pressure ridges by the mooring system. The latter simulated the moored condition in drifting ice. This paper describes the test set-up, procedures and performance of the concept when manoeuvring into the loading position in level ice.

**INTRODUCTION**

On a larger scale there is no proper experience with production and export of oil and gas from the Arctic offshore using icebreakers and tankers. However, recently several efforts have been made to demonstrate that new techniques such as the Submerged Turret Loading (STL) can be utilised for this purpose (Løset et al., 1998). In open water this concept proves an excellent performance (Fig.1.). In Arctic waters, such as the Eastern Barents Sea, the presence of drifting ice implies additional challenges such as loads from level ice and pressure ridges.

The use of the barge concept for export of oil includes the following four major phases: initial approach to the loading facility, final approach and hook-up, loading and departure. The physical environment and its rate of change will have impact on each of these operations and

---

<sup>1</sup> Department of Structural Engineering, Norwegian University of Science and Technology

<sup>2</sup> Barlindhaug Consult AS, Norway

<sup>3</sup> Hamburg Ship Model Basin, Germany

<sup>4</sup> Statoil, Norway

<sup>5</sup> Navion, Norway

especially affect the feasibility, time consumption, and thus the regularity. The initial approach includes the last part of the transit where the tanker is in a more or less straight transit mode heading against or with the ice drift. In this phase we believe that the shuttle tanker typically will run at 1 to 2 knots in 1.2 m thick level ice, i.e. 2 to 4 nautical miles in 2 hours without icebreaker support. The concerns are then the ice breaking performance of the tanker and the manoeuvrability. The final approach and hook-up include sailing from the end of the initial phase to the loading position. This phase also includes manoeuvring time and hook-up time. Based on Jolles et al. (1997) we believe that the time consumption will be maximum four hours when unescorted and about one hour when escorted. In this phase the major concerns are the horizontal positioning (becoming increasingly important in shallow waters due to less horizontal flexibility of the buoy), ice breaking performance of the tanker and loads on the tanker.

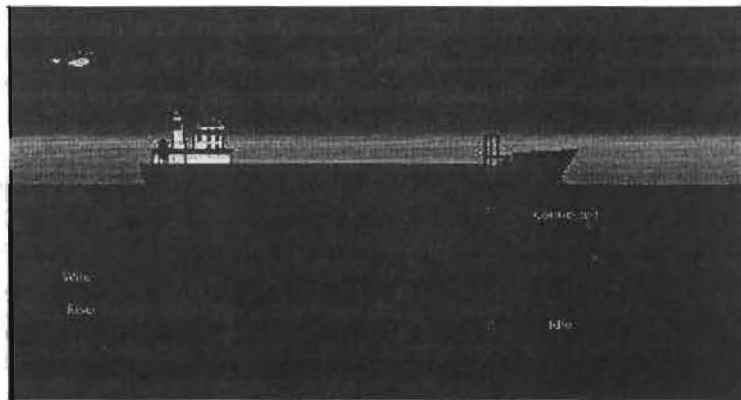


**Fig.1.** Sketch of the STL in use, open water.

During loading the major concerns are related to ice loads on the tanker from pressure ridges and mooring/riser interference with ice when ridges are passing. In case of shifts in the ice drift direction, concerns are also connected to the ice vaning ability of the tanker with the possibility of having ridges that move into the side of the ship.

Departure is the process of unhooking from the loading facility and leaving the loading position. The departure ends when the ship has disconnected from the buoy and is ready to continue in the transit mode. There are no major concerns connected to this latter phase.

## **EXPERIMENTAL SET-UP AND PROCEDURES**

### **The Arctic Shuttle Barge System**

The system is based on a barge of about 120 000 tons loaded displacement and 80 000 tons ballast displacement (90 000 DWT). The main dimensions are as follows: length overall  $L_{oa} = 265.5$  m, length between perpendiculars  $L_{pp} = 255.0$  m, breadth  $B = 38.0$  m. The scantling (maximum) draft of the barge is 16 m while the ballast draft is 11.5 m. Further, a

pusher/icebreaker serves as the main propulsion and connects/disconnects to a notch in the aft of the barge. The pusher of about 8000 tons displacement (2000 DWT) has the following characteristics:  $L_{oa} = 86$  m,  $L_{pp} = 80$  m and  $B = 23$  m. The maximum draft is 8.5 m. The pusher is equipped with two azimuth propellers and the barge has two retractable azimuthing bow propellers for ice milling and manoeuvring, and one tunnel thruster each at bow and stern. Fig.2. depicts a side view of the barge/pusher while a plan view is given in Fig.3. With a model scale of 1:25, the total model length (barge with pusher in the notch) is about 13 m.

For this concept we foresee a loading site of minimum 30 m water depth unless some excavation of the sea floor is done at the buoy. In the Eastern Barents Sea (Pechora Sea) pressure ridges may extend 20-22 m below the sea surface and their presence may therefore exceed the draft of the barge (Løset et al., 1999). Although the ridges are unconsolidated at these depths (loose ice blocks in the lower part of the keels), their possible keel-interference with the mooring lines and riser is a concern.

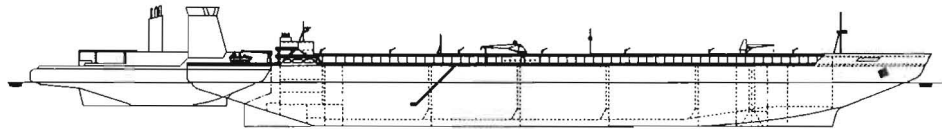


Fig.2. Sketch of the barge and the pusher, side view.

#### Test Set-up

The experiments were conducted in the large ice tank at HSVA during the autumn of 1999. The tank is 78 m long, 10 m wide and 2.5 m deep. The basin is equipped with a motor driven towing carriage and a movable underwater platform 1.20 m below the water surface. The model-scale was 1:25. In this way the underwater platform served to model a water depth of 30 m. The wheels of the underwater platform ('sea bed') were hooked on rails mounted on the tank wall about 0.5 m below the water surface. The underwater platform could either stay fixed at a certain position in the tank or be connected to the main carriage and follow its motion. In this way two principle different modes could be run. The fixed position mode is shown in Fig.3. Sketches of the mooring system are shown in Figs.4. and 5.

Froude scaling is used for scaling the model results (see Ashton, 1986; Løset et al., 1998). The forces are scaled by  $\lambda^3$  ( $\lambda=25$ ). Speeds and time are scaled by  $\lambda^{1/2}$ . The scaled results are used when evaluating the feasibility of the tanker concept.

The testing was conducted in level ice. A full-scale ice thickness of 1.2 m ( $h_{fs} = 1.20$  m) corresponds to  $h_{ms} = 48$  mm in model-scale. The model ice was of fine-grained columnar type and grown from a sodium chloride solution (about 0.65 % concentration). The

procedures and preparation of the HSVA model ice are thoroughly described by Evers and Jochmann (1993).

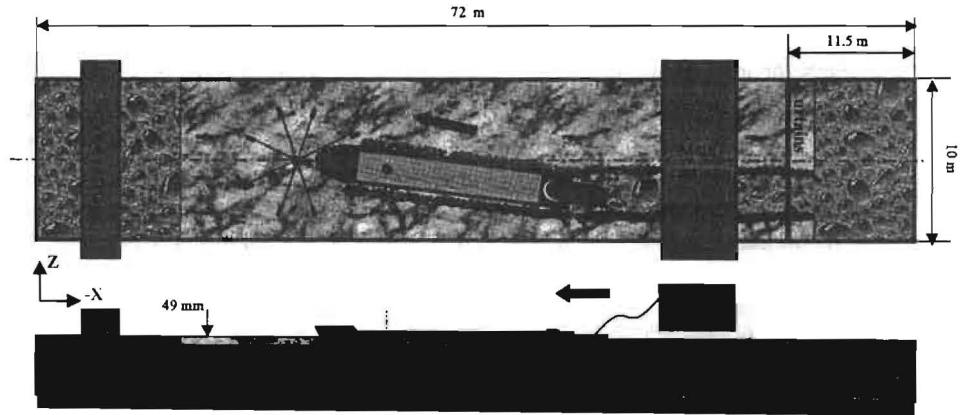


Fig. 3. Sketch of the test set-up with fixed position of the false bottom.

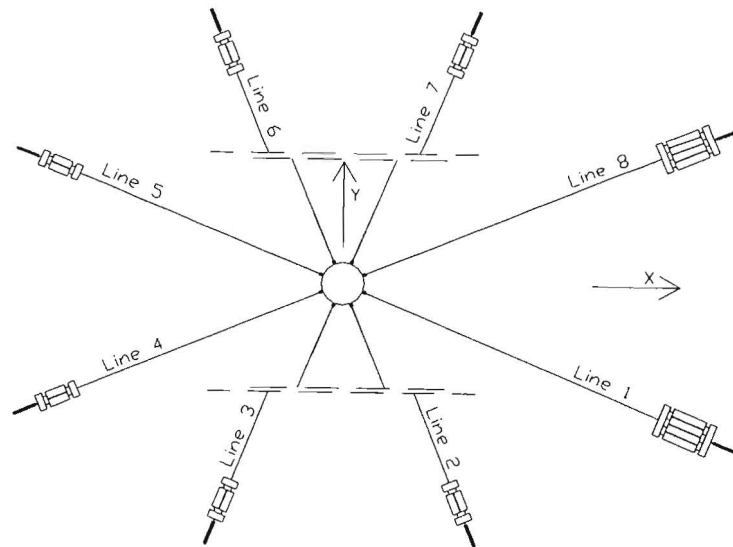


Fig. 4. Sketch of the mooring system, plan view (x-dir. is forward).

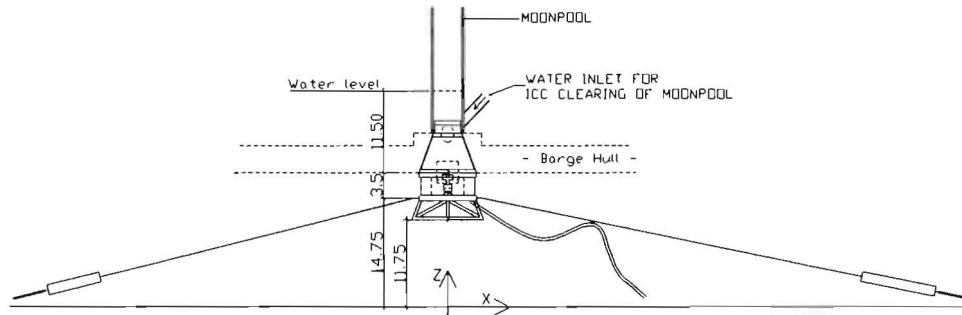


Fig.5. Illustration of the mooring lines, side view (full-scale). All units in metres.

### TEST MATRIX

The test matrix for Part I is shown in Table 1.

Table 1

Test matrix for Part I (all numbers in model-scale)

Test #	Test set-up	Description
1000	Level ice $h = 48 \text{ mm}$ , $\sigma_f = 30 \text{ kPa}$	Barge in ballast with reamers, pusher. Connecting/disconnecting under load. The turret was located at the 50 m tank mark. Initial position: the barge bow at 25 m (pushed just into the ice sheet) and 1.8 m off the centre-line of the tank. Ice was placed into the notch. The pusher was manoeuvred into the notch and pushed the barge towards and finally above the buoy. The buoy was manually connected to the barge. The false bottom was connected to the main carriage. Then the main carriage moved forward at 0.1 m/s speed and the buoy was dropped at full load after 3-4 m forward movement.
2000	Level ice $h = 48 \text{ mm}$ , $\sigma_f = 30 \text{ kPa}$	Barge in ballast without reamers, pusher. Connecting/disconnecting under load. The procedure was equal to Test 1000.

### FINAL APPROACH, HOOK-UP AND EMERGENCY SHUT DOWN

#### Power and thrust in level ice

Power and propeller thrust during the final approach through level ice were analysed for Tests 1000 and 2000 within a time window after the first acceleration of the model until the first backing. In both tests the model had to perform a curved track (turning circle) i.e., the azimuth thrusters were operated with significant steering angles (about  $30^\circ$ ). Additional steering forces were applied by one of the azimuth bow thrusters on the barge. The approach was performed with the barge in ballast draft.

The average speed and the maximum thruster azimuth angle as well as the actual ice properties in the actual time window are shown in Table 2. The time-traces of the speed are shown in Fig 6.

**Table 2**

Speed and thruster azimuth angle of the model together with the actual ice thickness, flexural strength and friction coefficient (full-scale values are given)

Test number	Average speed, $v$ (m/s)	Max. thruster azimuth angle, $\delta r$ ( $^{\circ}$ )	Ice thickness, $h_i$ (m)	Flex. strength, $\sigma_f$ (kPa)	Friction coeff., $f_{id}$ (-)
1000	0.42	30	1.17	950	0.11
2000	0.60	30	1.20	950	0.11

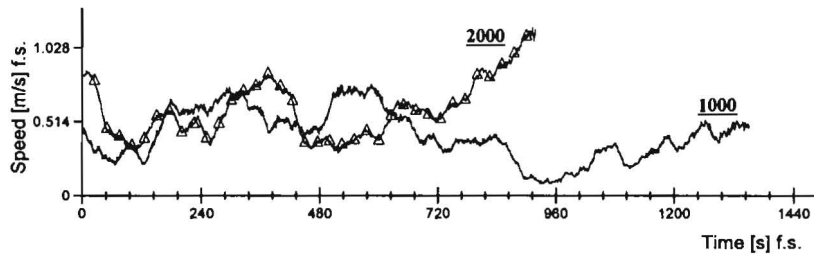


**Fig.6.** Time-trace for speed during Tests 1000 and 2000.

The average thrust developed by the azimuth thrusters of the pusher was measured by the load cells in the azimuth thrusters on the port and starboard side. The power was calculated from the propeller torque and angular speed. The measured values are corrected for a target ice thickness of 1.20 m, a target flexural strength of 750 kPa and a target skin friction factor of 0.10.

The target flexural strength was 750 kPa. Since this is a rather high value, the power and thrust are also estimated for a value of 500 kPa (for correction procedure, see Elvebakk and Lindberg, 1998). The total developed thrust  $T_{total}$  and the total delivered power  $P_{d total}$  is reported in Table 3.

#### Manoeuvring in ice

The manoeuvrability of the barge in level ice was demonstrated in Tests 1000 and 2000 and is reported in three different ways:

- A general impression of the manoeuvrability was obtained from visual observations (and video records).

- The trace of the barge (Fig.7.) moving from the initial position to the hook-up point at the 50 m tank mark was estimated from the speed and the yaw angle.
- The turning circle (tactical circle) in undisturbed level ice is calculated and reported in Table 4 (for the same time window as reported in Table 2).

**Table 3**

Power and thrust (in full-scale)

Test #	Measured in turning motion ( $\sigma_f = 950$ kPa)		Corrected for target ice properties in turning motion ( $\sigma_f = 750$ kPa)		Corrected for target ice properties in turning motion ( $\sigma_f = 500$ kPa)		Corrected for target ice properties and straight motion ( $\sigma_f = 500$ kPa)	
	$T_{total}$ (kN)	$Pd_{total}$ (MW)	$T_{total}$ (kN)	$Pd_{total}$ (MW)	$T_{total}$ (kN)	$Pd_{total}$ (MW)	$T_{total}$ (kN)	$Pd_{total}$ (MW)
1000	3922	47.2	3403	38.5	2910	30.4	2134	25.9
2000	3891	47.5	3422	39.2	3050	33.0	1881	23.1

Heideman et al. (1996) report from full-scale trials that azimuth thrusters provide a very good manoeuvrability in ice. This is also the impression from the present model-scale tests. The manoeuvring into the hook-up position was easily done both with and without reamers on the barge. However, the operation worked somewhat better with reamers. It was found that the optimum procedure to get into the hook-up position was: first to overrun the buoy, then to back 1-2  $L_{pp}$  and simultaneously widen the broken channel by the propeller wash and finally to manoeuvre into position. In the ice tank the lateral deviation from the target position above the buoy was in the range of 1 to 3 m, full-scale. This is a very good positioning but we should bear in mind that the coupling and manoeuvring into position was done without any lateral ice pressure present.

The general impression from the manoeuvring is that the pusher/barge system is able to turn provided that a working mode is chosen where the system is oscillated about 1-2  $L_{pp}$  forward and backwards, and at the same time widening the broken channel with the propeller wash of the azimuth thrusters. The calculated barge trace for Test 1000 (with reamers) and Test 2000 without reamers, is shown in Fig. 7. The calculation is based on the measured speed and yaw angle.

The minimum turning circle (tactical circle) is calculated from the speed and acceleration in the x- and y-directions via the measured yaw angle and speed. The calculation is done for a time window starting after the first acceleration of the model and ending at the first backing of the system i.e. for undisturbed level ice. The calculations show a relatively large difference between Test 1000 (barge with reamers) and the other tests without reamers. The minimum

turning circle is calculated in areas where the barge is performing with maximum possible steering capacity (30° rudder angle, both azimuth propellers active and side-way use of one front propeller) without stalling. The average circle is calculated in the full time window. The turning circle is reported as multiplicands of the  $L_{pp}$  of the barge (255 m).

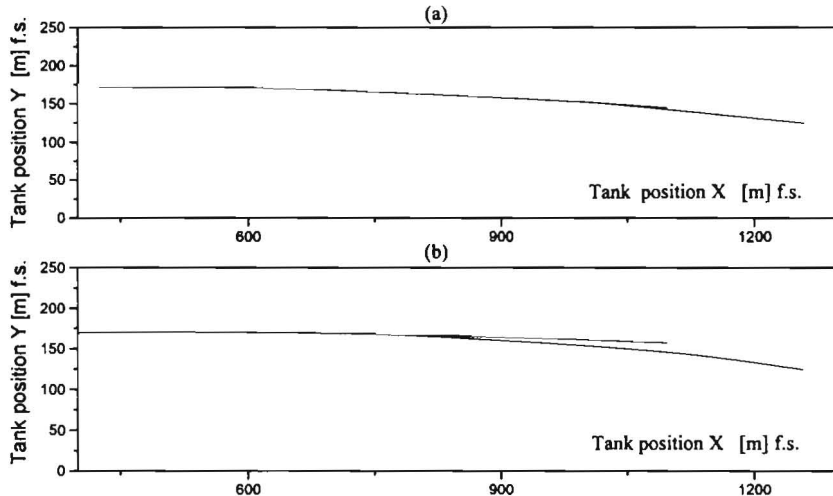


Fig.7. Trace of the model movement in the tank: a. Test 1000 and b. Test 2000.

Table 4

Turning circle in level ice

Test number	Min. turning circle $D_{min}$	Average turning circle $D_{mean}$
1000 (with reamers)	$30 \times L_{pp} = 7.5 \text{ km}$	$60 \times L_{pp} = 15 \text{ km}$
2000 (without reamers)	$80 \times L_{pp} = 20 \text{ km}$	$125 \times L_{pp} = 30 \text{ km}$

**Loads on pins**

Each of the pin connections between the pusher and the barge have a triaxial load cell. From these measurements the maximum, minimum and average loads are reported for each test run. A typical time-trace for the total pin loads and the x-dir. loads during Test 1000 is shown in Fig.8.

The pin loads are not corrected for the target value in flexural strength. The statistics is made during test run (see Fig.7.) in both the starboard (st) and port side (ps) load cell, and the pretensioning force in the pins in y-direction is subtracted.

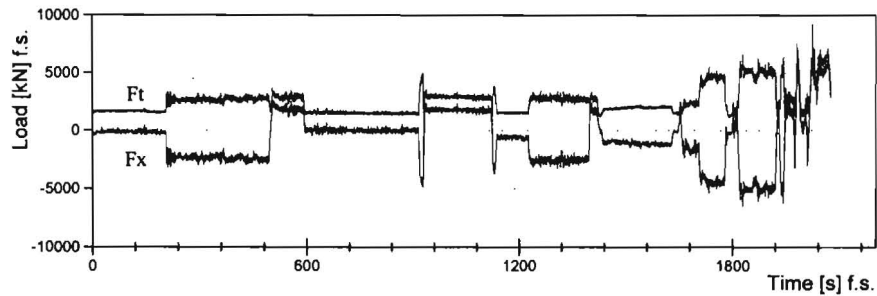


Fig.8. Full-scale load in the starboard pin connection in Test 1000

Table 5

Pin forces during Test 1000

Action	Minimum	Maximum	Average	Std. Dev
$F_{xps}$ (kN)	-9307	6180	-3037	2628
$F_{y ps}$ (kN)	-931	3265	927	631
$F_{z ps}$ (kN)	-2289	1068	-797	701
$F_{i ps}$ (kN)		10 068	3748	2114
$F_{x st}$ (kN)	-6485	8240	-741	2122
$F_{y st}$ (kN)	-1160	2349	73	456
$F_{z st}$ (kN)	-1220	1678	41	485
$F_{i st}$ (kN)		8731	1824	1476

#### Hook-up, emergency shut down of the buoy

The hook-up procedure was the following: manoeuvring into position, clearing of ice from the moon pool, release of the pop-up buoy and connecting of the buoy. During transit and manoeuvring ice may accumulate in the moon pool. This requires an ice clearing system in the moon pool. In these tests a system for pumping water into the moon pool was installed (see Fig.5.). The system performed well.

As previously reported, the manoeuvring into position was easily done. In general the barge was located 0.05-0.10 m (1-3 m in full-scale) off the target position above the buoy. A small pop-up buoy was installed on the top of the buoy. The small buoy was released by a remote line and appeared in the moon pool where the buoy was connected to the barge manually.

The conditions for this operation in the tank is favourable compared to a real situation where ice drift and wind will be present. For the ice drift situation an area around the target position of about one ship length should be cleared.

An emergency shut-down situation with ice pressure present was tested by moving the barge at 0.5 m/s speed (full-scale) forward in level ice. Then a rapid disconnection of the buoy was

undertaken. In these tests the buoy left the moon pool nicely and went into its idle position in  $\pm 0.01$  m (0.25 m in full-scale). The performance of the buoy in this situation will very much depend on the stiffness of the mooring system and the submerged weight of the buoy.

#### **Connecting of pusher and barge in ice**

An important part of the performance of this concept is the ability of connecting and disconnecting the pusher in various situations. The testing of a connecting situation with ice accumulated in the barge notch was done during Tests 1000 and 2000. These tests showed that ice was easily removed from the notch by just entering the pusher bow into the notch. Some power had to be added for this situation and the barge had a slight movement forward. The power/thrust to move the pusher into the notch was rather low, but to adjust the pins (after putting pressure on the pins) when they were not immediately on the correct position, required some steering forces and power.

#### **CONCLUSIONS**

The Arctic Shuttle Barge System typically consists of a barge of approximately 120 000 tons loaded displacement and 80 000 tons ballast displacement (90 000 DWT). A number of model tests have been performed in the HSVA ice tank in Hamburg at a scale of 1:25. The purpose of the testing was to identify and demonstrate the potential of the concept as well as suggesting modifications that can lead to an optimum design of the concept. The most important results are as follows:

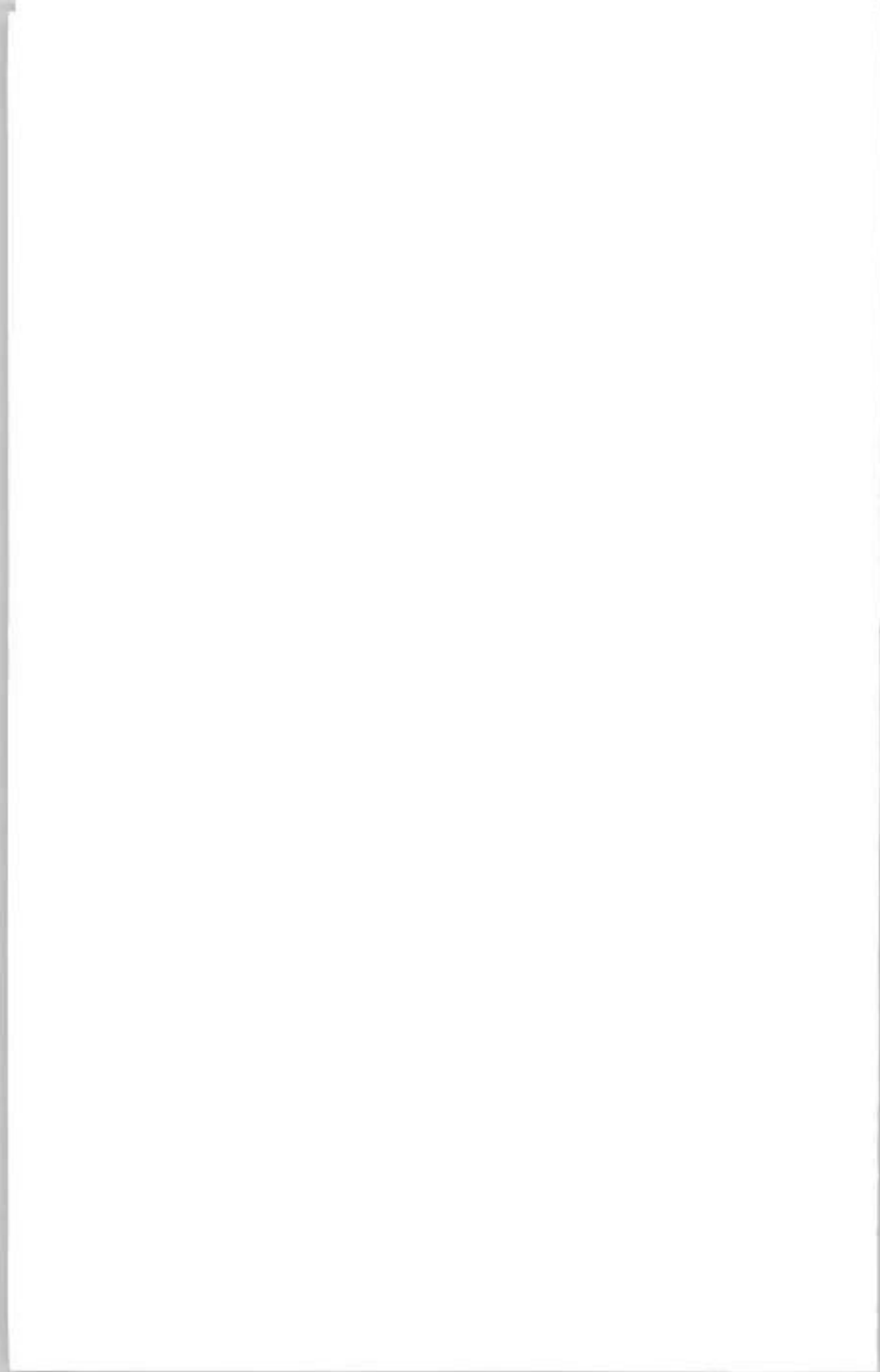
- The testing showed that the manoeuvring into the hook-up position was easily done both with and without reamers. The operation worked better with reamers on the barge.
- The general impression of manoeuvring in ice is that the barge is able to turn when the pusher is connected.
- The minimum turning circle when moving forward in level ice was estimated to:  $30 \times L_{pp} = 7.5$  km (with reamers) and  $80 \times L_{pp} = 20$  km (without reamers).
- During transit and manoeuvring ice may accumulate in the moon pool. A system for pumping water into the moon pool was installed and cleared ice from the moon pool effectively.
- A rapid disconnecting of the buoy under stress was undertaken. In these tests the buoy left the moon pool nicely and went into its idle position in  $\pm 0.01$  m (0.25 m in full-scale).
- The total thrust used in 1.2 m thick level ice was about 1900 kN without reamers and 2100 kN with reamers.

#### **ACKNOWLEDGEMENT**

The authors would like to thank APL for technical assistance in the test set-up and Navion for financial support to the project. We highly appreciate the graphical work done on some of the figures by dr. student Dennis Tazov. Further we would like to thank the Hamburg Ship Model Basin (HSVA), especially the ice tank crew, for the hospitality, technical support and professional execution of the test programme in the ARCTECLAB. The research activities carried out at the Large Scale Facility ARCTECLAB were granted by the TMR Programme from the European Commission through contract N°ERBFMGECT950081.

## REFERENCES

- ASHTON G.D., Ed. (1986): River and Lake Ice Engineering. Water Resources Publications, Book Crafters Inc., Chelsea, Michigan, USA, 485 p.
- ELVEBAKK T., LINDBERG E. (1998): Ice model testing of coast guard patrol vessel KBV201. M.Sc. Thesis Chalmers University of Technology Report no: X-98/96, 68 p.
- EVERS K.U., JOCHMAN P. (1993): An advanced Technique to Improve the Mechanical Properties of Model Ice Developed at the HSVA Ice Tank. Proceedings of the 12th International Conference on Port and Ocean Engineering under Arctic Conditions (POAC), 17-20 August, 1993, Hamburg, pp. 877- 888.
- HEIDEMAN T., SALMI P., UUSKALLIO A., WILKMAN G. (1996): Full-scale trials in ridges with the Azipod Tanker Lunni in the Bay of Bothnia in 1996. Polartech'96, 24-26 September, 1996, St. Petersburg, Russia, 2 p.
- ITTC (1981): Report of Committee on Ships in Ice-Covered Waters. Proc. of the 16th International Towing Tank Conference, Leningrad, USSR, Vol. 1, pp. 363-376.
- JOLLES W., BROWNE R., KEINONEN A. (1997): Model development of vessel approach and mooring operations at arctic loading terminals. Proceedings of the 16th International Conference on Offshore Mechanics and Arctic Engineering, Yokohama, 13-18 April 1997, Vol. IV, pp. 393-400.
- LØSET S., KANESTRØM Ø., PYTTE T. (1998): Model Tests of a Submerged Turret Loading Concept in Level Ice, Broken Ice and Pressure Ridges. Cold Regions Science and Technology, Vol. 27, pp. 57-73.
- LØSET S., SHKHINEK K., GUDMESTAD O.T., STRASS P., MICHALENKO E., FREDERKING R., KÄRNÄ T. (1999): Comparison of the physical environment of some Arctic seas. Cold Regions Science and Technology (29)3, pp. 201-214.
- SCHWARZ J. (1977): New Developments in Modeling Ice Problems. Proceedings of the 4th International Conference on Port and Ocean Engineering under Arctic Conditions (POAC), St. Johns, Canada, 1977, pp. 45-61.





**MODEL TESTS OF AN ARCTIC TANKER CONCEPT  
FOR LOADING OIL  
PART II: BARGE IN A MOORED LOADING POSITION**

**A. Jensen<sup>1,2</sup>, S. Løset<sup>1</sup>, K. V. Høyland<sup>1</sup>, J. Hellmann<sup>3</sup>, B. P. Vodahl<sup>1</sup>**

**ABSTRACT**

Model testing of a concept with Submerged Turret Loading of oil by an Arctic Shuttle Barge in ice covered water has been done. The tests were performed in the large ice tank at the Hamburg Ship Model Basin (HSVA), Hamburg, at a model-scale of 1:25. This paper describes part two of this testing with the barge in a loading situation. The barge was connected to a false bottom via a submerged turret and mooring system. This system was towed through level ice with embedded ridges simulating a loading situation in drift ice. The maximum ice breaking force was about 23000 kN during a ridge event. The present paper also elaborates on the use of a wedged plough and ice milling propellers to avoid ice from interfering with the mooring lines and riser.

**INTRODUCTION**

In 1999 an attempt to assess the performance of an Arctic Shuttle Barge System was done in model-scale in the HSVA ice tank, Hamburg. The system consists of a barge and a pusher/icebreaker that serves as the main propulsion and connects/disconnects to a notch in the aft of the barge. During loading, the major concerns are connected to ice loads on the tanker from pressure ridges and mooring/riser interference with ice especially when breaking ridges. In case of shifts in the ice drift direction, concerns are also connected to the ice vaning ability of the tanker. The operational performance and forces exerted on the barge and the mooring system, including a riser, were explored both in level ice and pressure ridges. The test set-up, procedures and performance of the concept when manoeuvring into the loading position is described in a separate paper (Jensen et al., 2000a). The barge had a state-of-the-art icebreaking bow with high icebreaking capability. The bow form is important for the concept and can be characterised as a spoon bow with 22° stem angle and highly flared frames in the

---

<sup>1</sup> Department of Structural Engineering, Norwegian University of Science and Technology

<sup>2</sup> Barlindhaug Consult AS, Norway

<sup>3</sup> Hamburg Ship Model Basin, Germany

icebreaking zone. A wedge plough is provided in the lower part of the bow for ice clearing of the turret/moon pool area. Further, the barge was equipped with two retractable front propellers with 360° azimuth angle. In the tests described in the present paper, the system was driven by the pusher or towed by the mooring system. No reamers were attached to the bow of the barge in these tests. The paper elaborates on the forces measured on the turret and mooring lines as well as interference of ice with the mooring lines when breaking ridges.

### TEST MATRIX AND TESTING PROCEDURES

The test matrix for the barge in loading condition is shown in Table 1. The tests were performed with the barge towed by the mooring system through level ice and ridges (see Fig.1.). During the tests forces in the mooring lines and the total forces in a triaxial load cell in the buoy were recorded. We measured also the rate of revolution and azimuth angle of the front propellers, and surge movement of the barge. On the false bottom three underwater video cameras were recording the ice situation in the turret and moon pool area.

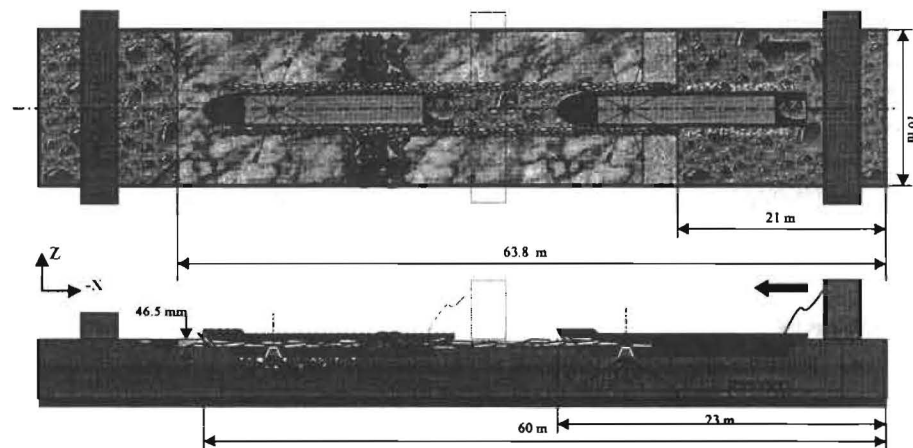


Fig.1. Sketch of the test set-up

### PREPARATION OF ICE RIDGES

The testing was conducted in level ice with ridges embedded. A full-scale ( $fs$ ) ice thickness of  $h_{ifs} = 1.20$  m corresponds to  $h_{ims} = 48$  mm in model-scale ( $ms$ ) with a scale of 1:25. Table 2 reports the actual level ice thickness for Tests 3000 and 4000 and the actual flexural strength ( $\sigma_f$ ).

**Table 1**

Test matrix for Part II (model-scale values in brackets)

Test #	Test set-up	Description
3000	Level ice $h_i = 1.2$ m (48 mm) $\sigma_f = 750$ kPa (30 kPa) $v = 0.5$ m/s (0.1 m/s)	Barge moored on location, in ballast condition and no pusher. The bow moved from the 27 m to the 46 m tank mark. Bow thrusters active, washing backwards (45°) in pulling mode.
3100	Ridge $v = 0.5$ m/s (0.1 m/s)	Consolidated ridge at the 48 m tank mark. Continuation of Test 3000. Bow: 46 m - 60 m. Bow thrusters active, washing backward (45°) in pulling mode.
4000	Level ice $h_i = 1.2$ m (48 mm) $\sigma_f = 750$ kPa (30 kPa) $v = 0.5$ m/s (0.1 m/s)	Barge moored on location, in loaded condition and no pusher. Bow: 27 m - 46 m. Bow thrusters active, washing backward (45°) in pulling mode.
4100	Ridge $v = 0.5$ m/s (0.1 m/s)	Consolidated ridge at 48 m. Continuation of Test 4000. Bow: 46 m - 60 m. Bow thrusters active, washing backward (45°) in pulling mode.
5000	Ridge $v = 0.5$ m/s (0.1 m/s)	Consolidated ridge at 48 m. Barge in ballast condition and no pusher. Bow: 41 m - 54 m. Bow thrusters active, washing backward in the pulling mode.
5100	Ridge $v = 0.5$ m/s (0.1 m/s)	Consolidated ridge at 56 m. Barge moored on location, ballast condition and no pusher. Bow: 54 m - 62 m. Bow thrusters active, washing forward (-45°) in the pulling mode.

**Table 2**

Level ice thickness and bending strength in full-scale.

$h_{ifs}$ (m)			$\sigma_{fs}$ (kPa)		
Test 3000	Test 4000	Test 5000	Test 3000	Test 4000	Test 5000
1.11	1.20	1.25	750	775	1375

The ridges in the tank were prepared by pushing level ice against a transverse beam as shown in Fig.2. The boom was successively moved forward, each time 0.6 m, until a complete ridge with the desired width and keel was formed (Jensen et al., 2000b).

A typical ridge profile is shown in Fig.3. Table 3 reports the ridge dimensions i.e., keel depth  $h_k$ , sail height  $h_s$  and the keel width  $w_k$ .

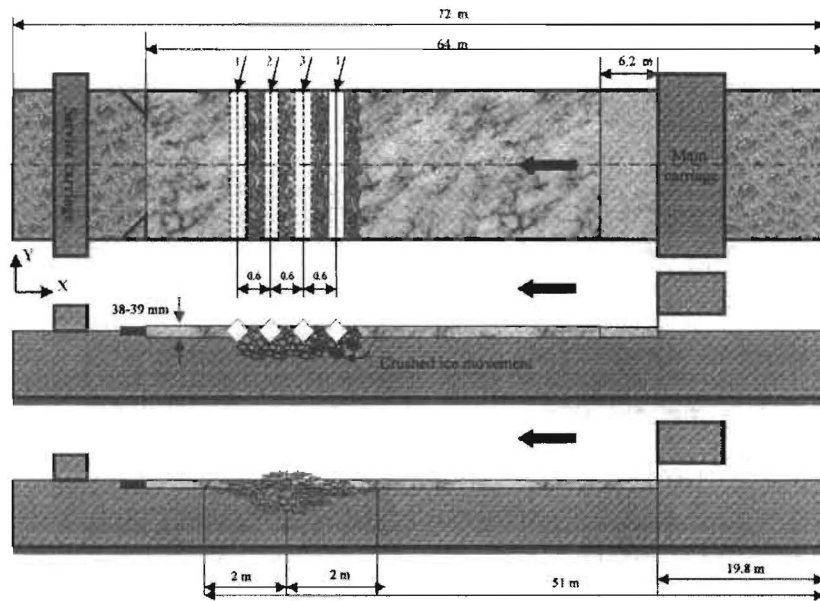


Fig.2. Principle for preparation of ice ridges

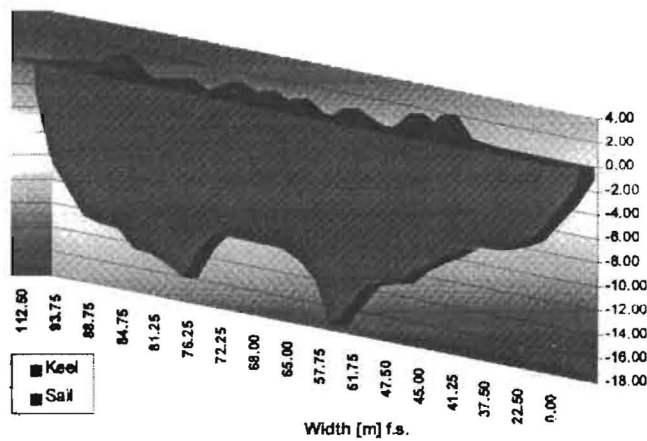


Fig.3. Sketch of the profile of Ridge 1, Test 5000. All units in metres

Table 3

Summary of ridge parameters in full-scale and model-scale

Test #	Model-scale			Full-scale		
	$h_k$ (mm)	$h_s$ (mm)	$w_k$ (m)	$h_k$ (m)	$h_s$ (m)	$w_k$ (m)
3000	580	70	7	14.5	1.75	175
4000	600	47	3.5	15.0	1.18	88
5000 R1	680	98	3.25	17.0	2.45	81
5000 R2	695	81	4.0	17.4	2.03	100

## BARGE IN LOADING CONDITION

### Level ice

Moving the barge, the mooring system and the false bottom altogether through the stationary model ice formations in the tank simulated drifting ice. Figs.4. and 5. show a sketch of the mooring system. Two tests in level ice were conducted with the barge moving straight forward. In this situation no ice interaction with the buoy and riser was seen and the wedge shaped plough effectively cleared ice from the riser and mooring system. Table 4 reports the loads on the mooring lines. Table 5 comprises the loads recorded by the triaxial load cell together with maximum displacement in the  $x$ - $y$  plane.

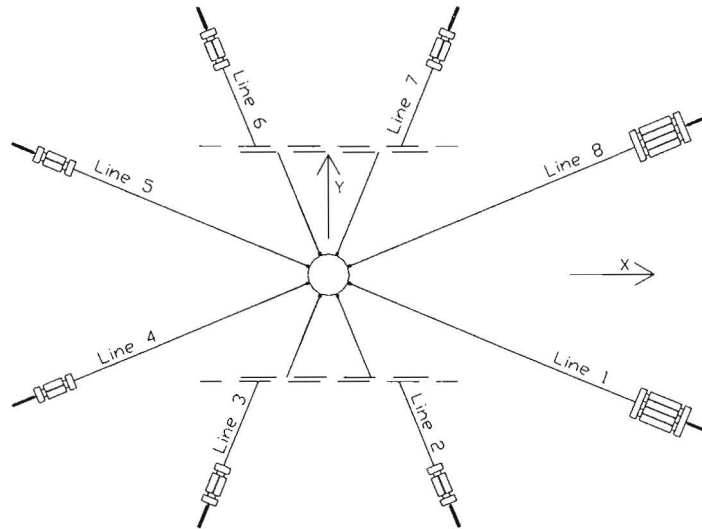


Fig. 4. Sketch of the mooring system, plan view (x-dir. is forward).

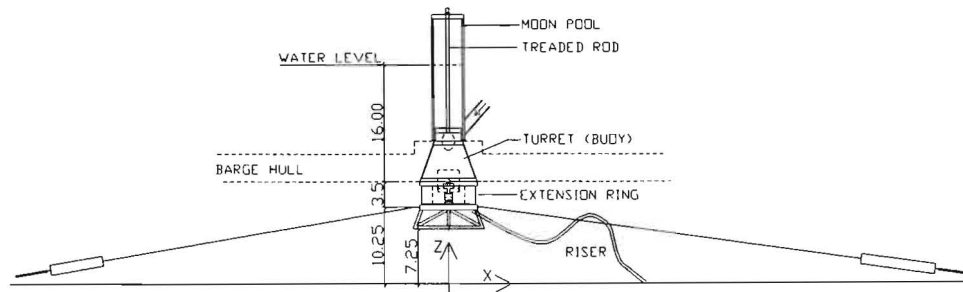


Fig.5. Illustration of the mooring lines and buoys hook-up, side view.

**Table 4**

Mooring line forces in Tests 3000 and 4000 (full-scale values in kN)

		Line 1	Line 2	Line 3	Line 4	Line 5	Line 6	Line 8
Test 3000	Avg	1386	1336	993	836	1197	875	1784
	Stdev	192	201	184	110	175	145	163
	Max	1840	1756	1337	1190	1844	1346	2270
Test 4000	Avg	383	389	255	50	176	869	1590
	Stdev	514	676	467	79	223	728	859
	Max	2195	2754	2073	654	1082	2076	2863

**Table 5**

Forces in the triaxial load cell and maximum displacement of the turret (full-scale values, forces in kN and displacements in m)

		$F_x$	$F_y$	$F_z$	$F_t$	$D_x$	$D_y$
Test 3000	Avg	-1309	-133	2415	2909	-1.38	-0.11
	Stdev	710	717	54	351	0.11	0.10
	Max	-3015	-1848	2633	3990	-1.74	-0.29
Test 4000	Avg	-2120	-2640	2391	5109	-0.80	-0.60
	Stdev	1176	3215	322	1705	0.28	0.73
	Max	-4825	-6286	2888	7749	-1.45	-1.42

**Ridge**

Fig.6. shows a typical time-trace of the total forces in the triaxial load cell during a ridge event.

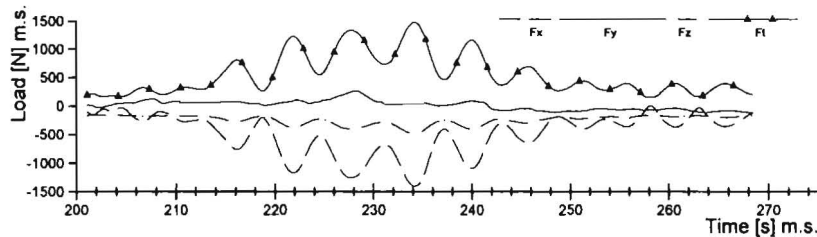
**Fig.6.** Time-trace of the forces in the triaxial load cell during Test 5000

Table 6 reports the maximum forces in the triaxial load cell and the three front mooring lines as well as the maximum surge and sway displacement.

Table 6

Maximum forces and horizontal displacements during ridge events  
(full-scale values: forces in kN and displacements in m)

	$F_x$	$F_y$	$F_z$	$F_t$	Line 1	Line 2	Line 8	$D_x$	$D_y$
Test 3100	-18596	1198	7656	19546	7623	5148	8003	-5.07	0.25
Test 4100	-19896	-4673	5878	20777	7455	2505	8724	-4.90	-1.06
Test 5000	-22516	4271	7675	23797	9416	5555	9193	-5.11	0.73
Test 5100	-18768	1524	6458	19768	7901	5166	7819	-4.34	0.32

#### Ice in the turret area

To reduce the ice interaction with the turret, mooring lines and riser, a wedge-shaped plough at the bow of the barge was introduced. Further, the barge was equipped with two retractable azimuthing bow propellers for ice milling. One of the major conclusions from the tests was that both devices are efficient for clearing of ice from the buoy area. However, with ridges present it is not possible to fully avoid ice interaction in the turret area, especially for ridges with keels that exceed the draft of the barge. This is clearly seen from the video spot shown in Fig.7.

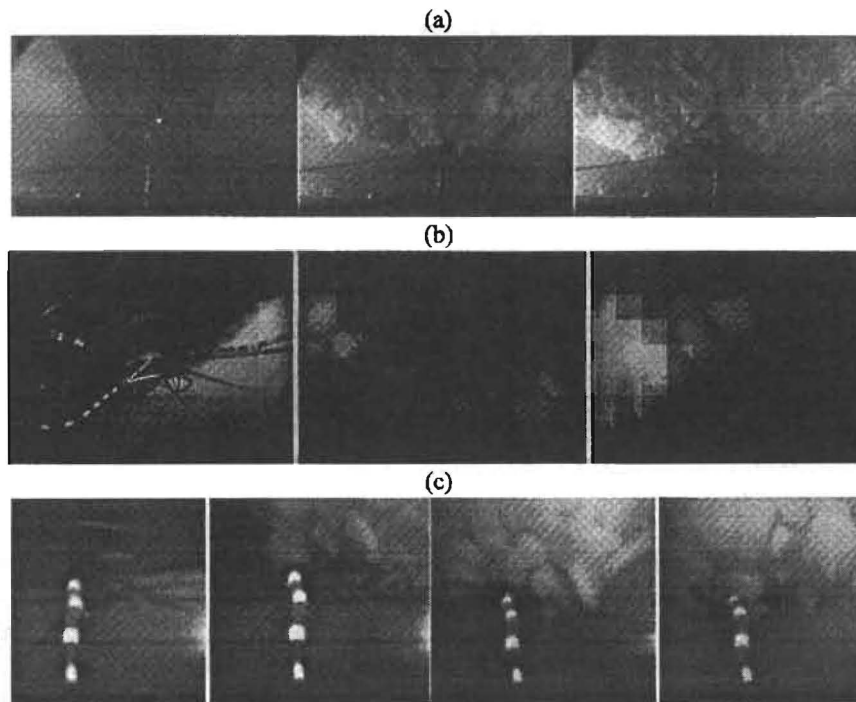


Fig.7. Pictures from UW-video in Test 5000:  
a) Front camera, b) near camera and c) side camera.

During the ridge testing a variation of three parameters have been done during the four tests:

- The draught of the barge in Test 4000 was 16 m and in the other tests 11.5 m.
- The extension between the barge and the mooring hook-up on the buoy in Test 5000 and Test 5100 was 5.75 m while it was 3.5 m in Tests 3000 and 4000.
- The front propellers washed backwards at a 45° angle in Tests 3000, 4000 and 5000 while in Test 5100 the propeller washed forward.

All these parameters have impact on the ice situation in the buoy area. From the underwater videos the interaction between the mooring lines and ice blocks are observed. It is obvious that mooring Line 2 has significantly more impact than Line 1. Fig.8. shows a time-trace of the mooring forces in Test 5000. Areas marked with circles are typical areas where ice interacts with the mooring lines. It appears as ripples on the smooth graph. Only a few spots of ice interaction with mooring Line 1 are seen.

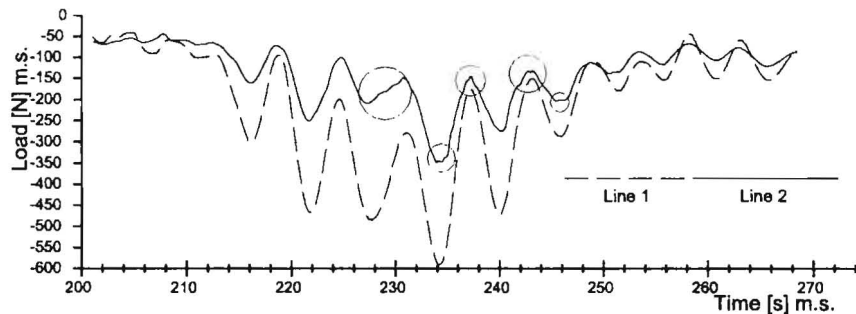
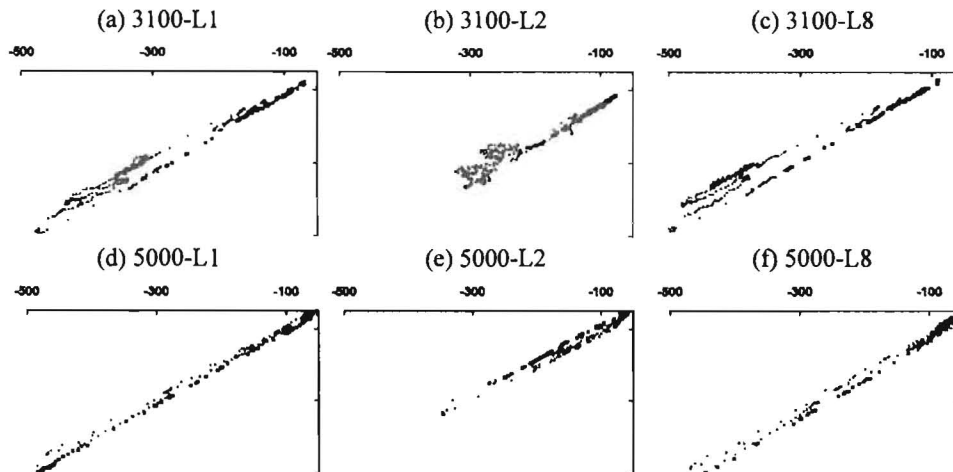


Fig.8. Time-trace of forces in mooring Lines 1 and 2 in Test 5000

To identify the mooring line forces we developed a numerical model of the mooring line system. With input from the global forces measured by the triaxial load cell to this model, we were able to compare the calculated and the measured line loads. Fig.9. shows six examples of such scatter plots where the measured line forces versus the calculated forces are displayed. Bold marks show the first part of the ridge interaction where no ice is present near the mooring system and light marks for the latter part of the tests where ice clearly interacts with the mooring lines.

No ice interaction with the mooring lines gives a linear dependence while a scatter originates from ice that directly interacts with the lines. These figures also demonstrate the effect of the buoy extension. For instance, Test 5000 shows a significant less scatter and thereby less ice interaction with the mooring lines than Test 3100. Similar curves can be made for all tests and would give an impression of the ice interaction with the mooring lines during the ridge tests.



**Fig. 9.** Scatter plot of calculated forces (vertical) and measured forces (hor.) for Test 3100 in a)-c), and for Test 5000 in d)-f)

Both the video records and the scatter plots show that the extended mooring line hook-up and the barge draft are important parameters for the ice/mooring line interference. At present the effect of the propeller wash and its direction is not properly quantified.

#### CONCLUSIONS

The present paper deals with the results from two level ice tests and four ridge tests of the Arctic Shuttle Barge System in an oil loading situation. The test set-up simulates shallow ice covered waters in the Eastern Barents Sea. The major conclusions are as follows:

- The maximum ice breaking force was about 23000 kN during a ridge event.
- The average ice breaking force in 1.2 m level ice was about 1400 kN in ballast condition and 2100 kN in loaded condition.
- Ice interaction with the riser/mooring lines is an important parameter for this concept. The wedged plough and the ice milling propellers are efficient for clearing of ice from the buoy area. However, with ridges present it is not possible to fully avoid ice in the turret area, especially for ridges with keels that exceed the draft of the barge.
- Video records and load calculations show that an extension of the mooring line hook-up from the barge hull and the barge draft are important parameters for the ice/mooring line interference.

#### ACKNOWLEDGEMENT

The authors would like to thank APL for technical assistance in the test set-up and Navion for financial support to the project. We highly appreciate the graphical work done on some of the figures by dr. student Dennis Tazov. Further we would like to thank the Hamburg Ship Model

Basin (HSVA), especially the ice tank crew, for the hospitality, technical support and professional execution of the test programme in the ARCTECLAB. The research activities carried out at the Large Scale Facility ARCTECLAB were granted by the TMR Programme from the European Commission through contract N°ERBFMGECT950081.

## REFERENCES

JENSEN A., LØSET S., HELLMANN J., GUDMESTAD O.T., RAVNDAL O. (2000a): Model tests of an Arctic Tanker Concept for loading oil. Part I: Manoeuvring into loading position. Proceedings of the 15th International Symposium on Ice (IAHR), Gdansk, Poland, Aug. 28-Sep. 01, 2000 (submitted).

JENSEN A., HØYLAND K. V., EVERS K.-U. (2000b): Scaling and measurement of ice rubble properties in laboratory tests. Proceedings of the 15th International Symposium on Ice (IAHR), Gdansk, Poland, Aug. 28-Sep. 01, 2000 (submitted).

LØSET S. (1995): Ice Loads on the STL Tanker. The Norwegian Institute of Technology, Department of Structural Engineering, Report No. R-9-95, Trondheim, 26 p.

LØSET S., KANESTRØM Ø., PYTTE T. (1998): Model Tests of a Submerged Turret Loading Concept in Level Ice, Broken Ice and Pressure Ridges. Cold Regions Science and Technology, Vol. 27, pp. 57-73.

LØSET S., SHKHINEK K., GUDMESTAD O.T., STRASS P., MICHALENKO E., FREDERKING R., KÄRNÄ T. (1999): Comparison of the physical environment of some Arctic seas, Cold Regions Science and Technology (29)3, pp. 201-214.

SCHWARZ J. (1977): New Developments in Modeling Ice Problems. Proceedings of the 4th International Conference on Port and Ocean Engineering under Arctic Conditions (POAC), St. Johns, Canada, 1977, pp. 45-61.



## ICE MODEL TESTS WITH AN OIL EXPLORATION BARGE IN THE NORTH CASPIAN SEA

K.-U. Evers<sup>1</sup>, P. Jochmann<sup>2</sup>, W. Kuehnlein<sup>3</sup>

### ABSTRACT

The Offshore Kazakhstan International Operating Company (OKIOC) has started exploration wells in the North Caspian Sea. These first wells target the ultra-shallow water Kashagan formation. The drilling operation is being performed by Rig 257, a modified swamp barge. The rig is 84.5 m long, 52.7 m wide with a draft of about 2.15 m. The barge will be installed on a pre-fabricated underwater berm made of limestone. The largest horizontal loads will be caused by sea ice, which occurs in the North Caspian Sea between November and April. In order to reduce the ice loads on the barge, inclined outer-walls have been designed to cause an initial failure of the ice by downward bending. Ice deflectors have been installed around the barge in order to prevent overriding of the barge by rubble ice. Ice model tests, with two differently scaled models have been carried out in the Large Ice Model Basin of HSVA in order to measure the vertical and horizontal ice loads acting on the ice deflector, barge, berm, and on the breasting piles in front of the barge. In addition to the load measurements the rubble pile-up process in front of the barge was investigated. The results of the model tests have been used to determine the design ice loads for the full-scale structure.

### INTRODUCTION

The drilling barge *Sunkar* (Rig 257), owned and operated by Parker Drilling under contract to the Offshore Kazakhstan Operating Company (OKIOC), has been especially designed to meet the unique conditions in the North Caspian Sea. OKIOC is a consortium consisting of Phillips Petroleum (USA), Inpex (Japan), Agip (Italy), British Gas (UK), BP Amoco (UK), Statoil (Norway), ExxonMobil (USA), Shell (The Netherlands), and TotalFina (France). The rig has been designed to withstand extreme ice forces and may be operated in a mean temperature ranging from -40° to 35° Celsius. The world's biggest posted barge has been adapted from a standard swamp barge, equipped with new-built sponsons, accommodation, mast, drilling

---

<sup>1</sup> Hamburgische Schiffbau-Versuchsanstalt GmbH (HSVA), Germany, Bramfelderstraße 164, D-22305 Hamburg, Tel.:+49 40 69203426, fax +49 40 69203345, e-mail: Evers@hsva.de

<sup>2</sup> Hamburgische Schiffbau-Versuchsanstalt GmbH (HSVA), Germany, e-mail: Jochmann@hsva.de

<sup>3</sup> IMPaC Offshore Engineering, Germany, e-mail: Kuehnlein@impac.de

equipment, and state of the art environmental equipment. *Sunkar* has been designed to withstand expected reservoir high pressures and to deal with corrosive hydrogen sulfide gas. As the barge is drilling in a nature preserve zone, the highest standards of care have been used. No drilling waste will be dumped into the Caspian Sea. Drilling mud will be recycled and the cuttings will be transported to an onshore state of the art treatment plant. All other wastes will be also recycled or treated to meet the highest standards.

Satellite imagery data for the period 1988 to 1997 have been analysed to obtain additional information on the ice concentration, stages of development, and forms of ice in the relevant area. Ice model tests were carried out in the Large Ice Model Basin of the Hamburg Ship Model Basin (HSVA) in order to determine the global ice loads acting on barge, ice deflector, breasting piles, and of the berm (dike) in shallow water conditions. The ice rubble pile processes around the barge was investigated in comprehensive ice model tests.

### ICE CONDITIONS IN THE NORTH CASPIAN SEA

In winter the area north of 45° latitude in the Caspian Sea is normally covered by ice of various conditions, i.e. level ice, land fast ice, ice floes, rafted ice and pressure ice ridges.

SSM/I and AVHRR satellite images have been processed to establish ice charts based on observations during a period of ten years. An example of an AVHRR image from February 18<sup>th</sup>, 1995 including corresponding ice chart is shown in Fig.1. The average ice concentration was larger than 7/10 and land fast ice was observed along the shoreline. For this particular case the ice thickness was in the range 0.10 m to 0.30 m. The northeastern part of the Caspian Sea was predominantly governed by land fast ice. In Tab. 1 information from the AVHRR study of ice formation and duration of ice coverage is summarised for three different sites. During the ten years observation period the ice formation at the 3 sites started in the period November, 29<sup>th</sup> to December, 5<sup>th</sup> and ended in the period March, 23<sup>rd</sup> to March, 24<sup>th</sup>. The duration of ice coverage was 112 days in average.

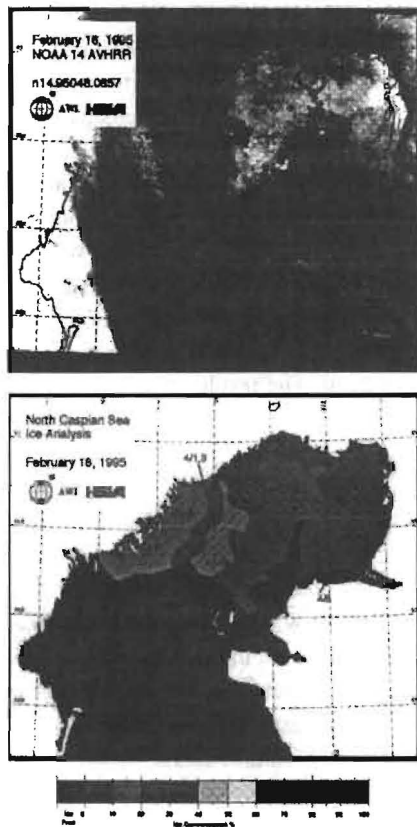


Fig.1. Example of AVHRR image and corresponding ice chart

During the North Caspian Ice Field Programme in February-March 1997 ice rubble piles were investigated at various locations of grounded vessels. One rubble pile of 14 m height in 3.5 m water depth was found in front of one of the grounded vessels. It had been formed during several ice movement events. Ice blocks were also found on deck of the grounded vessel which had a free board elevation of 6 m. The 0.90 m thick sheet ice was composed of several rafts of 0.10 m thick ice (Spring, 1997). The flexural ice strength of 750 kPa was determined as the average value of a large number of Soviet Union field data tests. The data sets for the North Caspian Sea were mainly obtained in the 1960s to 1970s by „ring or disc“ tests and have been corrected to western testing methods (personal communication with W. Spring, 1997).

**Table 1**

**Summary of Start/End of Ice Formation and Duration of Ice Coverage  
at Sites #A - #C**

Years	Site # A			Site # B			Site # C		
	Start	End	Duration	Start	End	Duration	Start	End	Duration
-	day	Day	days	Day	day	days	day	day	days
1996 / 97	341	79	104	347	89	108	338	85	113
1995 / 96	331	81	115	331	79	113	329	77	113
1994 / 95	343	82	104	347	81	99	342	84	107
1993 / 94	316	103	152	317	101	150	314	100	151
1992 / 93	340	96	122	345	94	115	338	85	113
1991 / 92	353	93	105	352	91	104	354	92	103
1990 / 91	345	86	106	348	85	102	343	92	114
1989 / 90	342	80	103	342	82	105	337	78	106
1988 / 89	328	75	113	338	74	102	318	76	124
Average	338±11	85±9	114±16	341±11	85±8	111±16	335±12	84±8	111±16

#### EXPERIMENTAL TEST SET-UP

The investigated drilling barge has the main dimensions of about 85 m length and 53 m width (full scale). The barge has 45° inclined sidewalls and the main deck is about 2.5 m above the design water level. A special concave shaped ice deflector of 4 m height, designed by IMPaC Offshore Engineering, Germany, was fixed on the main deck to avoid ice over-riding. At the drilling site the barge is located on a previously built gravel berm, which was designed by Witteveen and Bos, The Netherlands. Along the long sides of the barge, cylindrical piles of 1.6 m diameter (full scale) were installed in order to reduce the ice loads, which are acting on the barge, by pre-cutting the ice sheet and by creating an ice rubble formation process. For the ice model tests, to obtain the global ice loads on barge, ice deflector, berm (dike) and piles, a model scale of  $\lambda=25$ , was used, while for the ice rubble formation tests without load measurements the model scale was,  $\lambda=15$ . An artist impression of the drilling rig is given in Fig 2. The model test set-up and main dimensions are shown in Fig.3. and Fig.4.

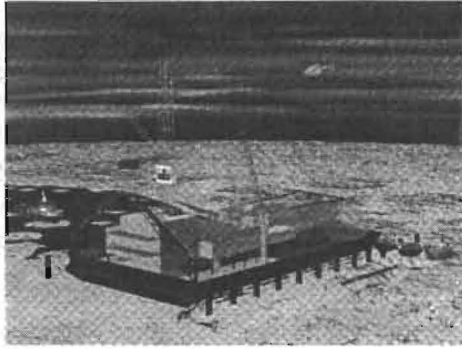


**Fig.2.** Artist impression of the drilling barge (courtesy IMPaC)

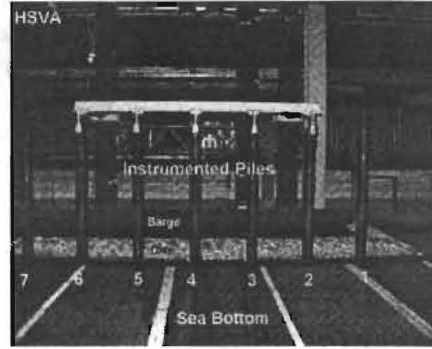


**Fig.3.** Model test set-up arrangement

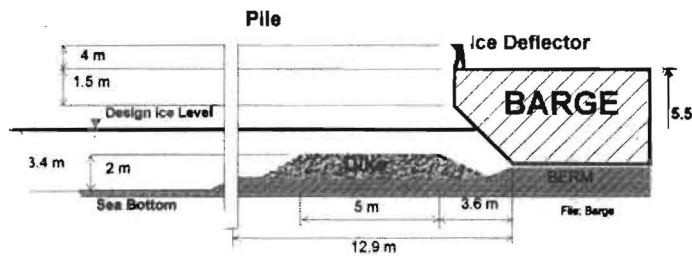


**Fig.4.** Main dimensions of the test set-up (full-scale values)

## ICE MODEL TESTS

### Model Test Procedure (Global Load Tests)

As mentioned before the tests were carried out in the Large Ice Model Basin at HSVA. The entire test set-up was installed on a shallow water bottom, which was rigidly connected to the towing carriage. The model was pushed at three different velocities through ice sheets of 20 mm and 45 mm thickness, when the target flexural ice strength was about 30 kPa. Each ice sheet was divided into three sections, in order to perform three different tests with each ice sheet.

Before starting each test run the ice rubble in front of the barge as well as in front of the piles was cleared. In open water the model/carriage was accelerated to the target velocity, which was reached before the model encountered the ice. During each test, the model velocity, vertical ( $F_z$ ) and horizontal ( $F_x$ ) ice loads acting on piles, barge, ice deflector and berm (dike) were measured. After the ice rubble formation in front of the barge had been stabilised the test run was stopped. The height and the horizontal extent of the ice rubble were measured

after each test run. The test matrix is given in Table 2. All indicated values are full scale values.

**Table 2**

**Test Matrix of the Global Load Test Series  
and Design Ice Loads on the Barge + Ice Deflector (full-scale values)**

Ice Loads on Barge + Ice Deflector					Gumbel-Distribution			
Run No.	Ice Thickness	Velocity	Piles	Ice Defl.	$F_x$ (90%) 1.4688	$F_x$ (95%) 1.7049	$F_z$ (90%) 1.4688	$F_z$ (95%) 1.7049
	m	knots			kN	kN	kN	kN
1000	1.10	0.25	no	no				
1100	1.10	0.50	no	no	15636	18149	9852	11435
1200	1.10	1.00	no	no				
2000	0.50	0.25	no	no				
2100	0.50	0.50	no	no	9670	11224	9224	10707
2200	0.50	1.00	no	no				
8000	1.10	0.25	$L=16m$	no				
8100	1.10	0.50	$L=16m$	no	12663	14699	11293	13108
8200	1.10	1.00	$L=16m$	no				
11000	1.10	0.25	$L=8m$	yes				
11100	1.10	0.50	$L=8m$	yes	15334	17799	3753	4357
11200	1.10	1.00	$L=8m$	yes				
12000	0.50	0.25	$L=8m$	yes				
12200	0.50	1.00	$L=8m$	yes	3741	4342	3286	4335
14100	0.50	0.50	$L=8m$	yes				
13000	0.50	0.25	no	yes				
13200	0.50	1.00	no	yes	11829	13730	11650	13522
17000	1.10	0.25	$L=8m$	yes				
17100	1.10	0.50	$L=8m$	yes	17398	20195	8926	10361
17200	1.10	1.00	$L=8m$	yes				
18000	0.50	0.25	no	yes				
18100	0.50	0.50	no	yes	14960	17365	8852	10275
18200	0.50	1.00	no	yes				

**Model Test Procedure (Ice Rubble Formation)**

For the ice rubble formation tests, water depth, barge and berm dimensions were scaled by  $\lambda=15$ . The model test set-up was installed and fixed on a shallow water bottom at the far end of the ice tank. After freezing the ice sheet, the ice was cut along the tank walls. The free floating ice sheet was then pushed by the towing carriage against the shorter side of the barge. These tests were conducted without any load measurements, as only the ice rubble formation processes were of interest in these test series.

## TEST RESULTS

### Global Load Tests

The maximum measured ice load values are much more scattered than the mean values of these tests. To establish the design loads a Gumbel-probability-distribution (GPD) on the ice loads has been applied. The individual maximum values of a test series have been normalised by the mean value of these series. The normalised values have been used in order to calculate the parameters of the GPD. Finally the design ice load has been obtained by multiplying the mean value of the series with the corresponding factors of the possibility of exceedance or underrun (e.g. 90 %, 95 %, 97.5 %).

Only the results of the design ice loads acting on barge and ice deflector are given (as full scale values) in Tab.2, where  $L$  is the distance between the piles. The probability distribution of the ice loads on barge and ice deflector are given in Fig.5. The design ice loads have been evaluated in cooperation with IMPaC Offshore Engineering, Hamburg.

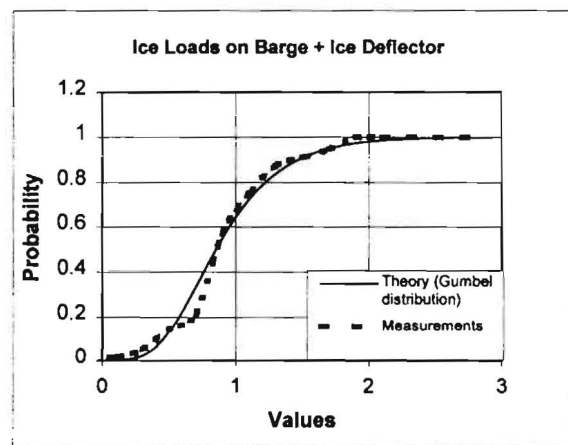


Fig. 5. Probability distribution of ice loads on the barge and ice deflector (Gumbel-Probability-Distribution)

## DISCUSSION

At first, the barge was tested for 0.5 m and 1.1 m thick ice without ice deflector and without piles in front of the long side of the barge. When the barge encountered the ice, the ice failed by downward bending, which was induced by the inclined sidewalls ( $\alpha = 45^\circ$ ). Due to the low water depth of 2 m (full scale) above the berm (dike) the ice rubble formation occurred very early in front of the barge. After a short time the ice rubble had the same elevation as the main deck and ice over-riding was observed. To avoid severe ice over-riding a concave shaped ice deflector (4 m height, full scale) was mounted. The installation of the ice deflector caused an increase of horizontal ice load of about 54 % compared to the horizontal ice loads on the barge without ice deflector, because the hull area of the barge is now about 1.7 times larger.

A reduction of horizontal ice loads on the barge was achieved by the installation of cylindrical piles. The reduction of vertical ice loads on the barge in the thick ice was significant, i.e. in the order 65 %. For the 0.5 m (full scale) thick ice the horizontal ice loads on the barge were 4.1 to 4.7 times smaller than with 1.1 m (full scale) thick ice. It is assumed that rafting of the thick ice in front of the barge is more efficient due to low water depth as the ice loads are acting directly on the barge. Contrary to this behaviour, the thin ice built an ice rubble of larger horizontal extent, thus the ice sheet failed along the slope of the ice rubble and the horizontal ice loads were more directed to the sea bottom berm (dike).

Fig.6. shows the ice rubble of the 0.5 m thick ice sheet and Fig.7. shows the ice rubble of the 1.1 m thick ice, where a little amount of broken ice was partly on top of the ice deflector.

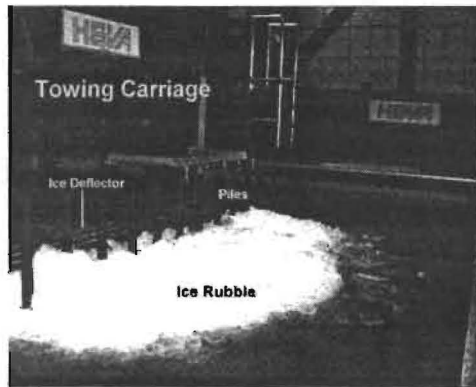


Fig.6. Ice rubble formation in front of the barge with piles ice thickness 0.5 m (full-scale)

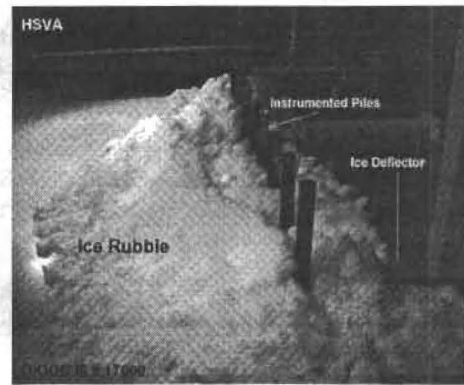


Fig. 7. Ice rubble in front of the formation barge with piles, ice thickness 1.1 m (full-scale)

#### SUMMARY AND CONCLUSIONS

Satellite imagery data for the period 1988 to 1997 were analysed to obtain additional information of ice concentration, stages of development and forms of ice in the North Caspian Sea. Ice model tests were carried out in the Large Ice Model Basin of HSVA in order to determine global design ice loads acting on the barge, ice deflector, berm (dike) and piles. In addition ice rubble formation processes around the barge were investigated with respect to ice over-riding problems. The most important results can be summarised :

- Ice formation on the three relevant sites is expected to start in the period 29<sup>th</sup> November to 5<sup>th</sup> December and end in the period of 23<sup>rd</sup> March to 24<sup>th</sup> March. Landfast ice, level ice, rafted ice and ridges, partly grounded are typical ice features.
- It is essential to install ice deflectors on the main deck of the barge due to avoid ice over-riding.
- Due to the inclined sidewalls of the barge the ice forces are lower than they would be on a vertical structure.

- The piles in front of the barge promote the ice rubble formation especially in thinner ice conditions. The ice rubble acts as a natural barrier, that leads to a reduction of horizontal ice loads on the barge.

#### **ACKNOWLEDGEMENT**

The authors gratefully acknowledge the support of the Offshore Kazakhstan International Operating Company (OKIOC) for this publication and the advice of Walt Spring as representative of OKIOC during the ice model test programme.

#### **REFERENCES**

EVERS K.-U., WESSELS E. (1986): Model test study of level ice forces on cylindrical multi-legged structures. Proceedings POLARTECH'86, Volume 3, VTT Symposium 73, Espoo, Finland.

EVERS K.-U., JOCHMANN P. (1993): An advanced technique to improve the mechanical properties of model ice developed at the HSVA ice tank. Proceedings of 12th International Conference on Port and Ocean Engineering under Arctic Conditions (POAC'93), Volume 2, Hamburg, Germany.

EVERS K.-U., KOLATSCHEK J.: (1997): Analysis of the ice conditions in the North Caspian Sea (Period 1988 - 1997 / Part I and II). Report to The North Caspian Project Team / OKIOC, October, (unpublished).

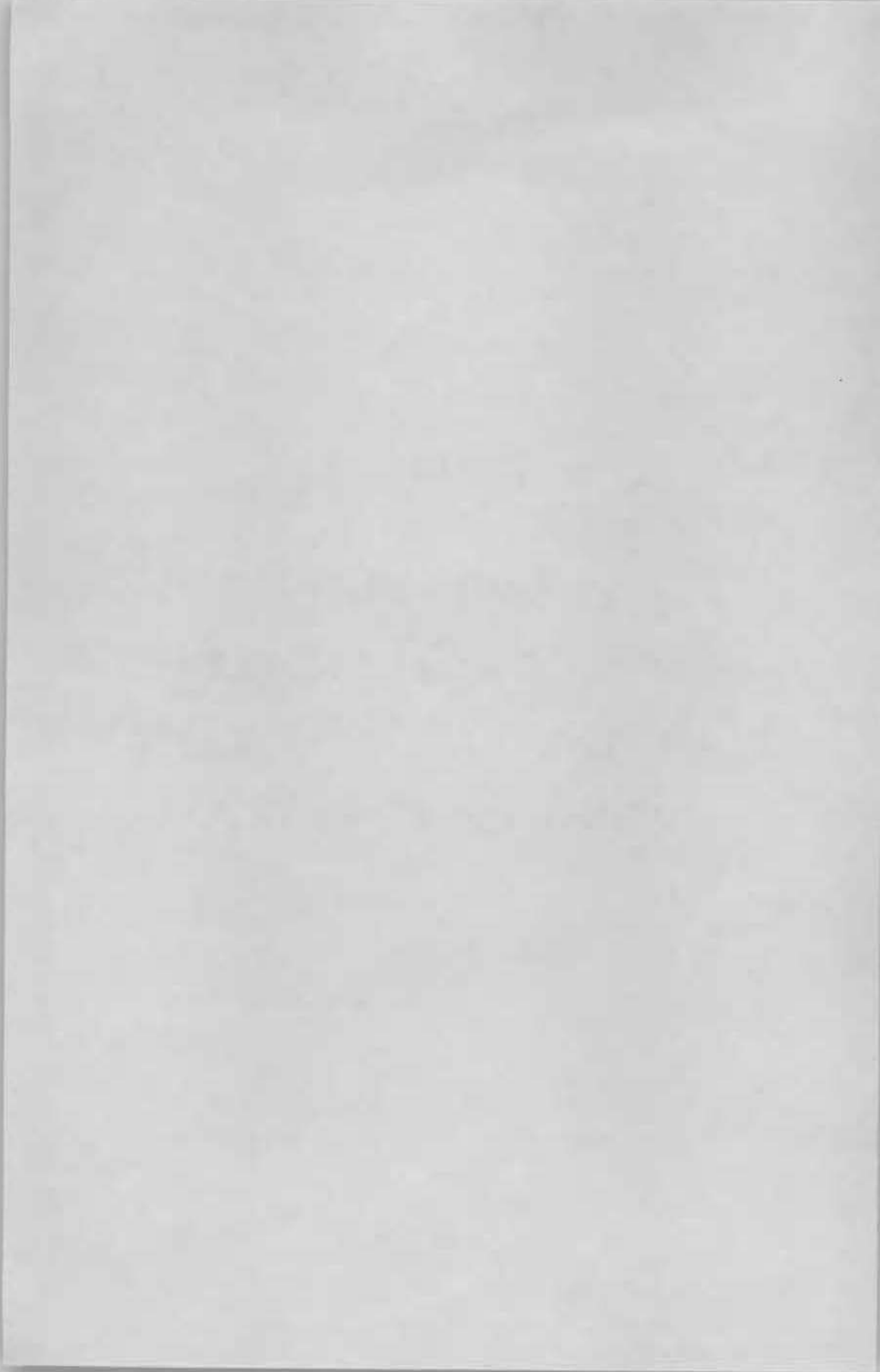
KATO K., SODHI D. (1983): Ice action on pairs of cylindrical and conical structures. CRREL Report 83-25 / US Army Corps of Engineers, Cold Regions Research and Engineering Laboratory, September.

SODHI D., MORRIS C.E. (1984): Ice forces on rigid, vertical cylindrical structures. CRREL Report 84-33 / US Army Corps of Engineers, Cold Regions Research and Engineering Laboratory, December.

SPRING W. (1997): 1997 North Caspian Ice Field Program. Mobil Technology Company, Report to The North Caspian Project Team /OKIOC, June (unpublished).

**TOPIC E**

**ENVIRONMENTAL  
AND ECOLOGICAL PROBLEMS  
IN LAKES, RIVERS, AND COASTAL  
ZONES IN ICE CONDITIONS**





## EFFECTS OF ICE COVER ON THE VOLATILE PHENOL BEHAVIOR AND ECOLOGY IN THE NORTHEAST RIVERS OF CHINA

Shen Xianchen<sup>1</sup>

### ABSTRACT

In the northeast rivers of China the length of freeze period is 3-6 months. The concentrations of volatile phenols in these rivers are much different in freeze and unfreeze. In general, the regularity was found, that is, average concentration of volatile phenols in freeze is larger than in cold period, which is much larger than in warm period at same station. In warm period it is 2% - 5% of freeze period only. The load reduction rate of them came to 97% over after flowing of 98 km. The difference of these rates between warm and freeze periods can go 10 times. Ecological effects of volatile phenols are very serious in freeze period. In some stations a lot of dead fish was found when pollution accident of phenols appeared. In the fish bodies the content of them can come to 2.25 mg/kg. The phenol toxicosis by drinking was found in special area. The cause analysis of phenol pollution in freeze was completed

### INTRODUCTION

Phenol is public name of all of aromatic compounds with oxyhydrate. It almost comes from coke plant. Some of them which with one oxyhydrate and boiling point < 230°C is called as volatile phenols. This kind of phenols is dangers for life of biont and human beings. In water quality monitoring the amount of volatile phenols is calculated by benzene phenol amount. The major properties of volatile phenols are volatility and biological decay. The effects of low temperature and ice cover on environmental kinetic property of them in water body are significant. In the winter of cold area its capacities of volatilization and biological decay are largely reduce due to the low temperature and ice cover. This period is very danger for biota in the volatile phenol pollution rivers. The northeast rivers of China are located in the north latitude 38°45' to 53°31' and east longitude 115°30' to 132°20', the average air temperature of January in this area range from -5°C to -23°C. The length of freeze period is 3-6 months. In this period some rivers of this region appeared serious volatile phenol pollution, this was a significant factor for fish killed and human being toxicosis. So, the behavior of volatile phenols in winter special in freeze period should be vigilant by government and people.

---

<sup>1</sup> Water Quality Research Center, China, P.O.Box 366 Beijing, Tel.: 010-68415522-3204, fax: 68425954,  
e-mail: shenxc@iwhr.com

## EFFECTS OF LOW TEMPERATURE AND FREEZE ON CONCENTRATION OF VOLATILE PHENOLES IN THE RIVERS

The Chinese northeast rivers have large different concentrations of volatile phenols in winter and summer, because of effects of water temperature and freeze. The general regular is that median concentration in freeze period is larger than in cold (water temperature < 10°C) which is much larger than in warm (water temperature > 10°C). In Benxi where there are big iron and steel plants, the load of volatile phenols discharged into the Tize River was higher 180 tons per year from coke plant effluent (according to the data of 1991). The concentrations of them are viewable in this river in four seasons of a year. The concentrations of volatile phenols, simultaneously sampling dates and discharges and its statistical values in freeze, cold, and warm periods in Tize River at Benxi station from 1991 to 1997 are shown in Table 1. At Benxi station the time of water temperature larger than 10°C from May to October was called warm period. From November to April of next year which water temperature less than 10°C was called cold period, of them from December to February of next year is freeze period. The statistical distributions of its concentrations in freeze, cold, and warm at Benxi station are shown in Fig.1. According to the analysis of the medium in the three periods indicate that the concentration of them in warm is 2 % - 5 % of freeze period only. The Liaoyang station is located in the downstream of Benxi station about 89 km. In the distance from Benxi to Liaoyang the major pollution sources of volatile phenols do not be found. At this station the concentrations of them were less than detection limit (< 0.002 mg/l) in warm period, but in freeze period most of them is obviously higher than detection limit. The regular of content of them is that in freeze it is larger than in warm period. At Liaoyang station although the regular is similar in Benxi station, but special statistical values of concentrations are much less than at Benxi. In freeze, median of them =0.023 mg/l, for

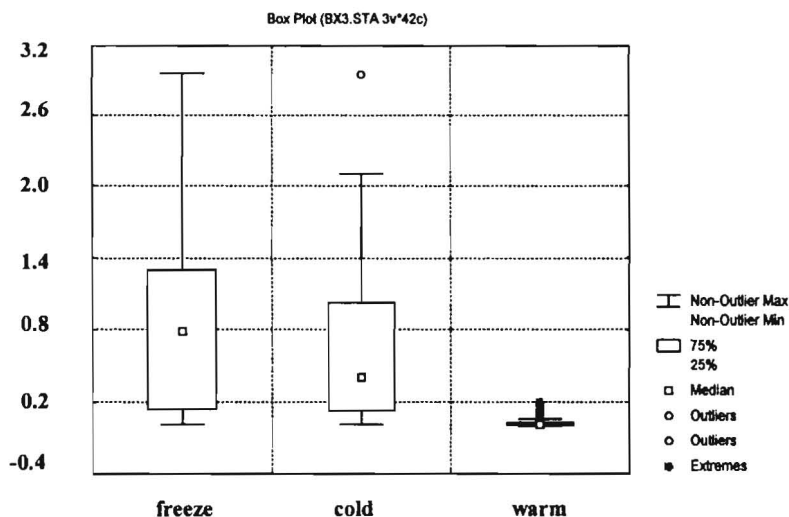


Fig 1. Statistical box for concentration of volatile phenols in three periods at Benxi station

**Table 1**  
 Concentrations of volatile phenols, sampling dates and discharges and its statistical values at Benxi station. ( C is concentration mg/l, Q is discharge m<sup>3</sup>/s, -- is no data)

FREEZE			COLD			WARM		
C	Q	date	C	Q	date	C	Q	date
2.10	4.60	91.01	2.10	4.60	91.01	.011	31.60	91.05
1.31	4.40	91.02	1.31	4.40	91.02	.016	14.90	91.06
1.00	6.30	91.12	.977	6.80	91.03	.009	29.00	91.07
1.28	3.78	92.01	.729	6.80	91.04	.013	140.00	91.08
.706	5.00	92.02	.084	16.50	91.11	.033	21.10	91.09
.016	20.709	92.12	1.00	6.30	91.12	.174	7.80	91.10
.196	9.60	93.01	1.28	3.78	92.01	.023	21.50	92.05
.884	8.00	93.02	.70	5.00	92.02	.005	15.00	92.06
.631	5.95	93.12	.413	7.31	92.03	.011	23.10	92.07
1.19	5.21	94.01	1.260	3.78	92.04	.009	30.40	92.08
.996	8.17	94.02	.017	12.90	92.11	.012	36.50	92.09
2.96	4.50	94.12	.016	20.70	92.12	.027	17.00	92.10
1.92	3.30	95.01	.196	9.60	93.01	.009	71.00	93.05
1.54	6.00	95.02	.884	8.00	93.02	.090	11.20	93.06
.123	40.00	95.12	1.02	7.90	93.03	.021	14.30	93.07
.133	33.80	96.01	.331	11.0	93.04	.010	125.0	93.08
.060	50.00	96.02	.853	6.75	93.11	.010	27.90	93.09
.250	9.50	96.12	.631	5.95	93.12	.032	12.00	93.10
.161	12.00	97.01	1.19	5.21	94.01	.008	33.00	94.05
--	--	97.02	.996	8.17	94.02	.119	13.20	94.06
.018	23.00	97.12	1.02	4.60	94.03	<0.002	320.00	94.07
			.041	42.60	94.04	.011	270.00	94.08
			.167	5.40	94.11	.006	60.00	94.09
			2.96	4.50	94.12	.125	11.00	94.10
			1.92	3.30	95.01	.197	6.35	95.05
			1.54	6.00	95.02	.008	17.00	95.06
			--	--	95.03	.019	67.00	95.07
			.405	6.15	95.04	.011	76.00	95.08
			.370	--	95.11	.012	43.00	95.09
			.123	40.00	95.12	.027	--	95.10
			.133	33.80	96.01	.107	22.00	96.05
			.060	50.00	96.02	.013	--	96.06
			.028	47.00	96.03	.017	14.00	96.07
			--	--	96.04	<0.002	115.00	96.08
			.143	--	96.11	.061	50.00	96.09
			.250	9.50	96.12	.141	15.00	96.10
			.161	12.00	97.01	.074	52.00	97.05
			--	--	97.02	.003	80.00	97.06
			--	--	97.03	--	--	97.07
			.024	52.00	97.04	.009	60.00	97.08
			.018	20.00	97.11	.003	--	97.09
			.018	23.00	97.12	.003	14.50	97.10

Item	C	Q	Case	C	Q	Case	C	Q
MEAN (21)	.874	13.19	case 42	.668	14.48	case 42	.036	52.32
MEDIAN (21)	.795	7.15	case 42	.409	7.60	case 42	.012	28.45
MIN (21)	.016	3.30	case 42	.016	3.30	case 42	<0.002	6.35
MAX (21)	2.960	50.00	case 42	2.960	52.00	case 42	.197	320.00
25th%(21)	.147	4.80	case 42	.123	5.30	case 42	.009	14.90
75th%(21)	1.295	16.35	case 42	1.020	18.25	case 42	.032	60.00

25th % = 0.007 mg/l, for 75th % = 0.053 mg/l; in warm period all of above three statistical values is less than 0.002 mg/l. Because the concentrations of volatile phenols were very low at this station, a lot of values were lower than 0.002 mg/l, the true concentrations of them can not been found. So, the statistical values of them can not be compared like at Benxi station. The determinations of < 0.002 mg/l appeared are in warm > in cold > in freeze. The percentage of them is 9 % of total in freeze, 19 % for cold and 79 % for warm. Compared the volatile phenol concentrations in freeze period at above two stations indicate that they are much different (medium values are 0.795 and 0.023 respectively), which is shown in Fig.2. Comparisons of volatile phenol concentrations at above two stations show that the concentration changes of them have large different in different periods also.

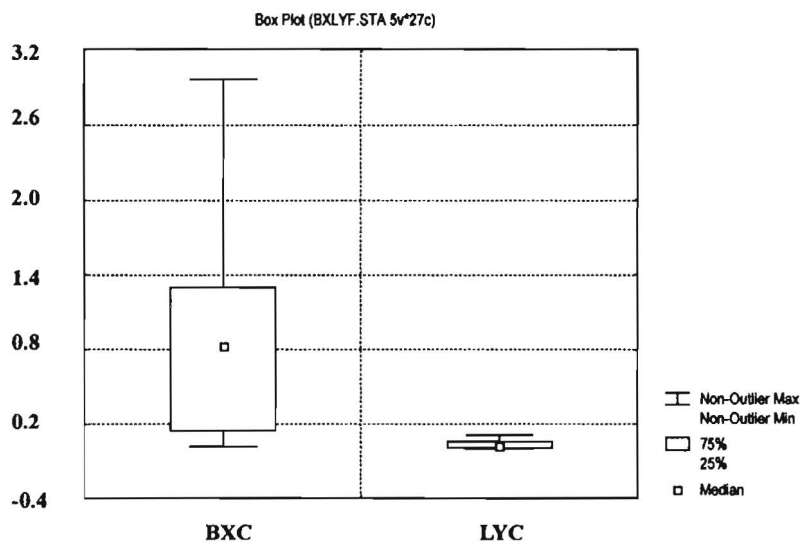


Fig.2. Statistical box for concentration of volatile phenols in freeze period at Benxi and Liaoyang station. ( *BXC*= concentration, mg/l in Benxi station, *LYC* is for Liaoyang )

In order to reduce the effect of discharge on concentration analysis of volatile phenols in different periods the analysis of loading changes and decay rate of them from Benxi to Liaoyang station under similar flow in different periods was completed. The result is similar with above concentration analysis. This result is given in Table 2. The table shows that the rates of decay in freeze are 97-99 % only, but in warm period they can go 99.7-99.9 %. The proportion of them can be up to 10 times.

**Table 2**

Load changes of volatile phenols from Benxi to Laioyang in freeze and unfreeze periods  
(unf. = unfreeze, f. = freeze, C and Q are same to Table 1)

Benxi station					Laioyang station					rate of decay
date	period	Q	C	load	date	period	Q	C	load	
91.04	unf.	6.8	0.729	4.95	91.4	unf.	5.8	<0.002	0.0058	0.0012
92.02	f.	5.0	0.706	3.53	92.2	f.	4.3	0.009	0.018	0.011
93.11	unf.	6.75	0.853	5.75	93.11	unf.	1.25	0.015	0.018	0.0030
94.02	f.	8.17	0.996	8.13	94.02	f.	2.5	0.100	0.25	0.031

### EFFECT OF HIGH CONTENT VOLATILE PHENOLS ON ECOLOGY

Because the decay and volatilization velocities of volatile phenols are reduced by low temperature and ice cover so that rivers continuously keep high concentration of them, which results in dangers for biota and human live. Several accidents of dead fish and human toxication were appeared due to phenol pollution in the northeast rivers of China. For example, the fish coma or dead situation continually took place at Fularji reach of Nanjing River in January 30 and February 5 and 14 1973. Of them the young fish, baby and larva are very much. According to a incomplete statistics in six stations, Tilan, Shirengo, Maty, Moxinhu etc, the weight of coma and dead fish taken from this reach come up to two hundred tons. There are 20 kinds of fishes in them, such as carp, big head, young whitefish, flathead. The analysis of content of volatile phenols in the fish bodies was made using the coma carp taken at Shirengo station of Nanjing River in February 21 1973. The results show that the content of volatile phenols in gill of carp was 2.25 mg/kg. In the body of the carp was 0.7 mg/kg. Other analysis result is that the content of gill and body of live fish was 0.8 mg/kg, which was taken in March 8 1973 in pollution water from Flarji electric plant.

The water with high concentration volatile phenols can make trouble for people too. According to water quality investigations of 88 times in Jijihar reach of Nanjing River during 1968-1969, the situation is that volatile phenols were found in every times. Some time the concentration of them was 60 times higher than its effluent standard value. After people drink this water the symptoms of headache, coma, insomnia, hearing loss and red blood cell reduction were found. At one time in this river reach the volatile phenol concentration come up to 2000 mg/l which caused by effluent accident. It made water color changed to yellow in its downstream of 15 km, as result the concentration of volatile phenols rose up to 0.5 mg/l in drinking water supply in Jijihar city which exceeded for drinking water standard of 250 times. After drinking this water the residents of this city took place some toxicosis symptoms of vomit and uncomfortable in all of body. A lot of volatile phenols in rivers can not only cause surface water pollution but make ground water pollution also. An investigation for wells near the river shows that the content of them in some wells was exceeded national water quality standard value of 2850 times. They can not be used for drinking.

## CAUSE ANALYSIS OF VOLATILE PHENOL POLLUTION IN THE COLD AND FREEZE PERIODS

The major causes of volatile phenol pollution aggravation in rivers come from reduction of decay velocity under low temperature and ice cover.

### Effect of low temperature on biological decay of volatile phenols

The decay of volatile phenols in water basically is a process of biochemistry. The biological decay of phenols with one oxyhydrate is easier than others. They can be decayed up to 99 % over during 3 hours under 25°C when starting concentration of 1 mg/l. The reaction velocity of them is controlled by temperature. The studies show that relationship between reaction velocity and temperature for this kind of process has following equation consuming that there are enough nutrition, such nitrogen and phosphorus and suitable pH as well as oxygen supply:

$$K_2 = K_1 \theta^{(T_2 - T_1)} \quad (1)$$

Where:  $K_2$  = reaction velocity coefficient under  $T_2$  temperature 1/day

$K_1$  = reaction velocity coefficient under  $T_1$  temperature 1/day

$\theta$  = temperature coefficient of reaction 1.03-1.15

$T_1, T_2$  = temperature, °K 273+ °C

The effect of temperature is significant under low temperature and higher starting concentration of pollutant. The decay velocity of them generally is growing with temperature increasing. In order to confirm the effect by temperature on volatile phenol purification from water body scientists have completed a set experiment in temperature region from 0°C to 40°C. The results indicate that when temperature is increase 10°C each the reaction velocity can be increase 1 times.

### Effect of freeze on volatilization of volatile phenols

The effect of ice cover on volatilization of volatile phenols is very obvious. The volatilization experiment was done used water contenting volatile phenols with and no bacteria respectively. The water aired then volatile phenols volatilized from water and into an absorbent tube with base and they were determined. The test results show that volatile phenols volatilized from no bacteria water by air-blowing were 100 % of purification amount of them, but one from water with bacteria is 40 % of purification amount of them. These experiments indicate that volatilization is an important factor for purification of volatile phenols. The reaeration of rivers under unfreeze generally is good, purification of them not only is contribution of biological decay but is volatilization also. So, the decay of them in unfreeze is quicker than in freeze. Under the effects by two factors of low temperature and ice cover the purification of volatile phenols in freeze is much slower then unfreeze. The concentration of volatile phenols in freeze should be about 2 times higher than in open river of water temperature > 10°C if considering above two factors only. In fact, its different in freeze and unfreeze is much higher than 2 times because of comprehensive effects by several factors in the natural rivers such as

the oxygen supply not enough and so on. Sometimes the concentration of them in freeze rivers is 10 times higher than in open.

### **CONCLUSIONS**

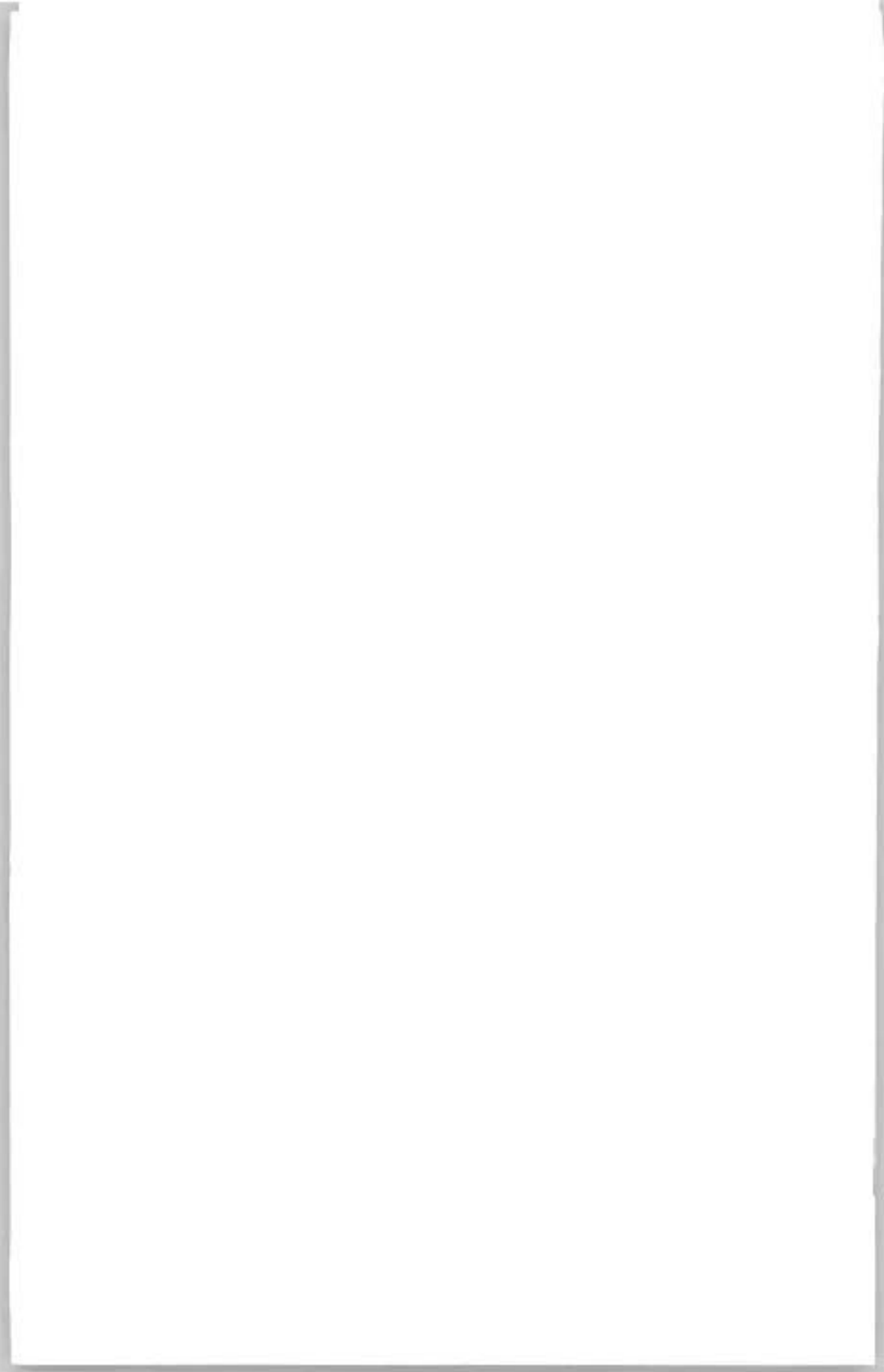
According to above analysis we can get following conclusions:

In volatile phenol pollution rivers its concentration in freeze is larger than in cold and much larger than in warm. In contrast, its purification rate is that in freeze it is less than in cold and much less than in warm. According to theory analysis the volatilization is about 40% of its purification in warm water: The biochemical reaction velocity of them increase with temperature growing up. It generally is increase of 1 times when the temperature growing 10°C each. So, the concentration of them in freeze can be 2 times larger than in warm if just considering above two factor effects. In fact, the monitoring data show that different of concentration or decay rate of them in above periods can go to 10 times in the natural rivers because of comprehensive factor effects such as reaeration, biological activity and flowing state etc. In winter special in freeze period some ecological problems may be found in volatile phenol pollution rivers, it has to be given attention by government and people.

### **REFERENCE**

Water Quality Assessment in China (1995). Department of Hydrology, MWR of China.

WANG JUN ET AL. (1993): Ecological effects of chemical pollutants, China Environmental Science Press.





## TURBULENT STRUCTURE OF ICE-COVERED FLOW AND ICE IMPACT UPON HABITAT IN RIVERS

E.N. Dolgoplova<sup>1</sup>, E. Tesaker<sup>2</sup>

### ABSTRACT

The influence of a stable surface ice cover on the habitat conditions of a river as compared to open surface flow has been approached by analysis of the turbulent structure in the bulk of the stream and near the bottom. Provisional estimates are presented. Velocity data from rivers under both free surface and ice conditions are compared and discussed. Changes in the flow structure under winter conditions are presented in terms of mean velocity distribution and observed fluctuations of the longitudinal velocity components in the river. It is concluded that the ice cover may have significant effects on the local habitat, but further research is needed.

### INTRODUCTION

Habitat hydraulics has become a fronted research topic in recent years, but most of the research has been concentrated on open surface flow conditions. Systematic investigation of under ice habitat is hampered by difficult conditions for fieldwork, and by complicated flow patterns in the often shallow and shifting space between ice and river bed. It has been measured in field and laboratory that the turbulent structure of flow under ice is significantly different from open surface flow. Some of the results are presented here and possible implications on habitat parameters are discussed.

### BASIC COMPONENTS OF HABITAT IN RIVERS

To analyse impacts of ice cover on the river ecosystem it is necessary to consider the main characteristics of habitat conditions. Important characteristics are related to water quality, velocity, depth, and bottom sediments (Tesaker, 1998). As noted by Shen (1998), the ice cover induces considerable effects on water quality related to fish life. The concentration of dissolved oxygen is one important parameter. Oxygen depressions in rivers under winter conditions have been attributed to lack of re-aeration due to the ice cover, oxidation of organic material, and input of oxygen-depleted groundwater (White, 1998). High metal concentrations

---

<sup>1</sup> Water Problems Inst., Russ. Ac. of Sc, ul. Gubkina 3, 117735 Moscow, Russia, e-mail: endol@iwapr.msk.su

<sup>2</sup> SINTEF Civil & Environm. Eng., N-7465 Trondheim, Norway, e-mail: Einar.Tesaker@civil.sintef.no

during ice break-up is another source of deterioration of water quality (Beltaos, 1998). As will be shown below, the ice cover may increase both turbulence and riverbed erosion, and concentrations of metals largely adsorbed by sediment particles may increase locally under a stable ice cover.

Light is necessary for the photosynthesis of water plants providing food for the invertebrates. The deeper and less transparent the river, the less amount of light will penetrate. Surface ice will influence on the light conditions by its filtering effect on the light, and also by its effects on suspended particle concentration and depth. It has also been observed that some species prefer night-time for migration etc and hide at daytime (Johnson & Covich, 2000). Ice cover effects may affect this attitude.

Velocity is important for the life of invertebrate fauna inhabiting the boundary layer between the substratum and the bulk of water. The flow velocity in this layer is small; at the same time turbulence is the main source of oxygen exchange to this layer. Many researchers show clear dependence of bed sediment size on the number of invertebrates near the bottom, decreasing in the row: shingle, coarse gravel, fine gravel, sand, and mud (Gore, 1989). Generally speaking, in free surface streams the higher the velocity, the larger the median diameter of the bed sediments. Shear stress and turbulence, the more precise parameters, depend on the velocity distribution as well. As will be shown below, both bed shear stress and turbulence are enhanced by the presence of ice cover, which therefore will influence on the near bed flow and the substrate composition.

Different authors summarised by Gore (1989) show that optimum velocities for invertebrates lie in the range: 0.15-0.9 m/s. Important river habitats may therefore be rapids with velocities higher than the mean velocity and depths less than the mean depth, and with bottom sediments consisting of shingle and gravel.

## **ICE IMPACT ON CHARACTERISTICS OF THE RIVER FLOW**

### **Morphology of the River Bed**

The morphology of the riverbed plays an important role for the survival of larvae and fry, especially in winter. Formation of ice cover is often connected with production of frazil and bottom ice, which may occupy considerable parts of the river cross-section. Sometimes an ice-covered flow transforms into several small streams, the velocities of each of them being more than that of the initial flow at the same places in summer (Majewski, 1994; Brown et al., 1998). The velocities of these streams can exceed the critical magnitude, in which case erosion may start at areas stable in summer. Though such phenomena often occur in rivers in winter and their influence on survival of bottom plants and fauna is considerable, the research in this field is still in its infancy.

### **Sediment Transport**

Milburn & Prowse (1998) mention that transport and settling of fine-grained sediments plays the most important role in secondary pollution of water. The authors show that changes of

hydraulic characteristics caused by ice-cover induce a decrease of transport capacity of the stream, resulting in deposition of fine-grained sediments.

Sediment transport has been investigated in some ice-covered tidal mouths of Russian rivers (Zyryanov, 1995). The outlet jets of rivers flowing into the Arctic Ocean decline to the right. Studying the motion of fine-grained sediments in the mouth of Western Dvina, it has been found experimentally and explained theoretically that suspended fractions of sediments which have no time to settle during the period between tide and ebb, tend to decline to the left relative to the outflowing river jet. Under winter conditions, when the velocity at the river mouth decreases, this fine-grained fraction of sediments containing all pollutants from the upstream towns, will settle out in the left area of the river mouth.

Ettema & Braileanu (1998) reported investigations of sediment transport velocity, presenting expressions for the rate of bed-load and suspended-load transport in the ice-covered flow. To estimate the bed-load discharge it is necessary to know the relation between velocities of water and solid particles. This competent velocity has a specific value for a given stream; the accuracy of its definition depends on the homogeneity of the granular composition of the bottom sediments. Knowing the granular composition of the bed-load and the hydraulic characteristics of an ice-covered flow, one can predict areas of washout and deposition, and as a result define dangerous places of possible secondary pollution of water.

#### Mean Velocity

The ice-covered flow structure is formed under the influence of both bottom and ice roughness. If we consider the ice-covered flow as consisting of two layers influenced by the bottom and the underneath of ice respectively, each can be described by the power law for velocity distribution (Dolgopolova, 1996):

$$u = u_{sb} y_b^{n_b} \quad u = u_{si} y_i^{n_i} \quad (1)$$

Here  $y_b = y/h_b$ ,  $y_i = (h-y)/(h-h_b)$ ,  $y$  = vertical coordinate,  $h$  = depth of flow,  $h_b$  = depth of the near-bed flow,  $y_b$ ,  $y_i$ ,  $n_b$ ,  $n_i$ ,  $u_{sb}$ ,  $u_{si}$  = dimensionless distances from the boundaries, power exponents and "conditional surface velocities" for near-bottom and near-ice flows correspondingly. Using the power law, parameters of mean velocity distributions for some open and ice-covered flows were calculated and presented in Tables 1, 2, and 3.

#### Shear Stress

The shear stress  $\tau$  can be described by:

$$\tau = u_*^2 \rho \quad (2)$$

where  $u_*$  = shear velocity,  $\rho$  = fluid density. The shear velocity can also be defined by using the depth averaged velocity  $\langle u \rangle$ , the power exponent  $n$  in the velocity distribution, and von Karman's constant  $\kappa$  (Dolgopolova, 1993):

$$u_* = \kappa n \langle u \rangle \quad (3)$$

**Table 1**

Power coefficient  $n$  and bottom shear stress for River Missouri (McQuivey, 1973)

Vertical number	$z$ , m	$h$ , m	Bottom character	$n$	$\langle u \rangle$ m/s	$u_*$ m/s	$\bar{\tau}$ kg/m $\cdot$ s $^2$
1	176.8	4.4	dunes	0.105	1.29	0.054	2.91
2	164.6	4.97	flat	0.194	1.84	0.142	10.13
3	155.5	4.75	dunes	0.143	1.77	0.101	10.18
4	146.6	4.36	flat	0.141	2.08	0.119	14.14
5	134.1	4.15	dunes	0.113	1.93	0.087	7.56
6	113.7	3.44	dunes	0.126	1.83	0.092	8.45
7	103.6	3.29	flat	0.155	1.88	0.117	13.66
8	68.9	1.95	dunes	0.084	1.51	0.051	2.60
Mean cross-sectional shear stress for the River Missouri is $\bar{\tau} = 9.04 \text{ kg} \cdot \text{m} / \text{s}^2$							

Legend for Tables 1, 2 and 3:

$B$  = width of the river,  $z$  = distance from left bank,  $h$  = depth,  $n$  = power coefficient in the velocity distribution,  $u_*$  = shear velocity,  $\tau$  = bottom shear stress,  $\bar{\tau}$  = mean cross-sectional shear stress, subscript  $b$  is used for flow related to the bottom.

**Table 2**

Calculation of exponent  $n$  and bottom shear stress for the River Kirhzach

Section Width $B$	No. Vert.	$z$ , m	$h$ , m	$n$	$\langle u \rangle$ m/s	$u_b$ m/s	$u_*$ m/s	$\tau$ kg/m $\cdot$ s $^2$	$\bar{\tau}$ kg/m $\cdot$ s $^2$
I 18.5 m	1	6.0	0.47	0.185	0.37	0.230	0.027	0.728	0.342
	2	9.5	0.40	0.221	0.36	0.235	0.032	1.023	
	3	14.0	0.42	0.120	0.36	0.204	0.017	0.289	
II 17.5 m	1	4.0	0.52	0.183	0.35	0.207	0.026	0.675	0.440
	2	7.5	0.43	0.167	0.35	0.210	0.023	0.528	
	3	11.0	0.37	0.190	0.37	0.238	0.028	0.783	
	4	14.5	0.42	0.311	0.35	0.254	0.044	1.933	
III 17.3 m	1	4.0	0.55	0.233	0.37	0.253	0.035	1.223	0.259
	2	8.0	0.40	0.088	0.38	0.215	0.013	0.169	
	3	11.0	0.39	0.084	0.36	0.185	0.012	0.144	
	4	13.5	0.38	0.122	0.38	0.233	0.019	0.361	
IV 16.5 m	1	3.0	0.56	0.200	0.36	0.236	0.029	0.840	0.783
	2	6.0	0.44	0.148	0.39	0.245	0.023	0.528	
	3	9.3	0.43	0.306	0.34	0.238	0.042	1.762	
	4	12.3	0.45	0.350	0.31	0.214	0.043	1.846	
	5	14.5	0.39	0.231	0.29	0.139	0.027	0.728	

Table 3

Calculation of shear stress for the Moskva River in winter

<i>B</i> , m	No. Vert	<i>z</i> , m	<i>H</i> , m	<i>h<sub>b</sub></i> , m	<i>n<sub>b</sub></i>	$\langle u \rangle_b$ , m/s	<i>u<sub>ob</sub></i> , m/s	$\tau_b$ , kg/m s <sup>2</sup>	$\bar{\tau}$ , kg/m s <sup>2</sup>
I <i>B</i> =64.8	1	9.6	1.68	0.77	0.266	0.40	0.043	1.81	1.403
	2	18.8	1.50	0.80	0.263	0.47	0.049	2.44	
	3	31.8	1.55	0.64	0.231	0.45	0.042	1.73	
	4	42.4	1.72	0.81	0.199	0.52	0.041	1.71	
	5	53.6	1.73	0.69	0.160	0.41	0.026	0.69	
II <i>B</i> =56.6	1	9.0	1.47	0.65	0.335	0.39	0.052	2.73	6.66
	2	17.6	1.79	1.00	0.614	0.34	0.084	6.96	
	3	27.6	1.82	1.04	0.698	0.41	0.114	13.09	
	4	37.6	2.0	0.80	0.230	0.45	0.041	1.71	
	5	45.5	1.58	0.75	0.612	0.50	0.122	14.96	
III <i>B</i> =52.7	1	8.0	1.47	0.59	0.451	0.35	0.063	3.98	2.66
	2	16.8	1.73	0.88	0.302	0.38	0.046	2.10	
	3	26.0	1.99	0.77	0.306	0.38	0.047	2.16	
	4	34.0	2.10	0.93	0.361	0.47	0.068	4.60	
	5	42.0	2.03	0.98	0.289	0.51	0.059	3.47	
IV <i>B</i> =64.1	1	11.6	1.56	0.75	0.225	0.48	0.043	1.85	1.86
	2	23.0	1.55	0.78	0.230	0.46	0.042	1.76	
	3	35.0	1.79	1.10	0.289	0.44	0.051	2.60	
	4	46.4	1.58	1.00	0.256	0.40	0.041	1.68	
	5	58.4	1.66	1.00	0.237	0.30	0.028	0.78	
V <i>B</i> =71.1	1	20.0	1.25			0.24			
	2	28.0	1.30	0.69	0.435	0.25	0.044	1.89	
	3	37.2	1.34	0.74	0.207	0.21	0.017	0.30	
	4	54.0	1.51		0.089	0.33	0.012	0.14	
	5	67.6	1.62		0.216	0.32	0.028	0.76	

Substituting Eq. 3 into 2 one can estimate the bottom shear stress of the flow under both summer and winter conditions as follows:

$$\tau = \rho \kappa^2 n^2 \langle u \rangle^2 \quad (4)$$

This expression shows that shear stress depends on the mean velocity and the shape of the mean velocity distribution along the depth. Results of calculations of the shear stress near the bottom using Eq. 4 for a number of rivers are shown in Tables 1, 2, and 3.

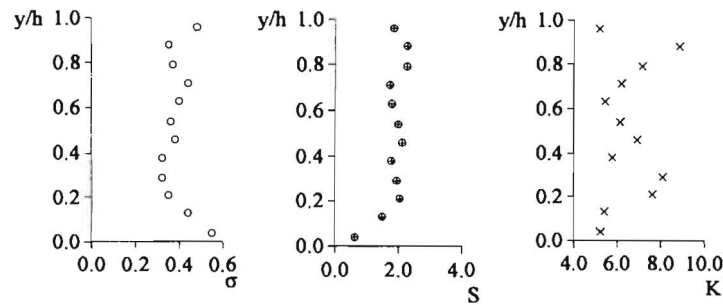


Fig.1. Depth distribution of turbulence intensity,  $\sigma = \sigma_y / \langle u \rangle$ , skewness  $S$  and kurtosis  $K$  for Moskva River in winter.

### Turbulent Characteristics of Ice-Covered Flow

Measured fluctuations in the stream-wise component of velocity have been used to obtain depth distributions of the second, third, and fourth statistical moments, shown in Fig.1. (Dolgoplova, 1994). The turbulence intensity  $\sigma$  increases towards the flow boundaries, and has a maximum at dimensionless depth 0.7. The depth-averaged turbulence intensity is equal to 0.4, approximately five times larger than that for open channels (Orlov et al., 1985).

Skewness  $S$  and kurtosis  $K$  of fluctuations of the streamwise velocity in an ice-covered flow are very different from those for an open channel. Near the bottom and the ice cover, coefficients of skewness and kurtosis become close to those of the Gaussian distribution, 0 and 3 correspondingly. Thus, one can expect considerable change of the structure of an ice-covered flow as compared to ice-free conditions.

## DISCUSSION

### Shear Stress

Tables 1 and 2 show how the mean velocity of a river influences on the interaction between flow and riverbed and the bottom shear stress. The values of power  $n$  in Eq. 4 for Missouri and Kirzhach depend on the depth of the river, confirming the dependence  $n(Re)$  found earlier (Dolgoplova, 1993). The average cross-sectional shear stress for Missouri is more than one order greater than for Kirzhach. Thus, to estimate the change of the bottom shear stress under winter conditions one needs mean velocity profiles measured in the same river in summer or in a river (or flume) with scales ( $B/h$ ,  $Re$ ) near to that under investigation.

Comparison of Tables 2 and 3 shows that the power exponent of the velocity distribution in the near-bottom flow increases under winter conditions. The mean velocities of the river Kirzhach and of the near-bottom flow of the river Moskva are numerically close, what enables us to compare the power exponents and the shear stresses for these flows. One can note considerable increase of  $\overline{\tau_b}$  under winter conditions. (At cross-section II warm wastewaters were discharged. Although we could not find the influence of this warm inflow on the depth

averaged velocity, it resulted in noticeable change of the shape of the velocity profile and hence in considerable increases of the power exponent  $n_b$ .) In conclusion, the bottom shear stress increases under ice, disturbing the life conditions of bottom-dwelling organisms.

**Turbulent Structure of Ice-Covered Flow**

The distribution of turbulence intensity  $\sigma_u = \sqrt{u'^2}$  in open channels is investigated by many researchers, e.g.: Sukhodolov & Tile (1999), Knight & Shiano (1990), Orlov et al.(1985). As a result, the depth distribution with a maximum near the bottom and decreasing to the surface of an open channel is presently accepted. Our investigations show that the distribution of turbulence intensity in an ice-covered flow has three maxima (Fig.1.), two near the solid boundaries of the flow and a third one at the dynamic axes of the flow  $y/h \approx 0.7$ , where  $\tau = 0$ . The fact that for plane rivers of aspect ratio  $B/h \gg 1$  the depth-averaged turbulence intensity in ice-covered flow is several times larger than that for the open stream, indicates high turbulisation of the flow. The increase of turbulence and the emergence of the turbulence intensity maximum in the bulk of an ice-covered river can be explained as a result of interaction of two boundary layers, formed near the bottom and the ice cover.

Comparing the distributions of skewness and kurtosis presented in Fig.1. with those obtained for an open channel by Dolgopolova & Orlov (1985), Fig.2., one can see the discrepancy. If the distribution of stream-wise velocity fluctuations can be described by the first four statistic moments, then the Pearson's method of analysis can be used (Dolgopolova, 1994). The depth averaged magnitudes  $\bar{S} = 2$  and  $\bar{K} = 6$  obtained from the measurements show, that in an ice-covered flow, fluctuations of velocity above the mean occur with higher probability than for the Gaussian distribution, and they are concentrated in a more narrow interval than for the normal law  $\pm 3\sigma$ . This fact can be considered an origin for production of coherent structures in an ice-covered flow. Thus, the changes of flow structure and turbulence in an ice-covered stream increase the intensity of transfer processes.

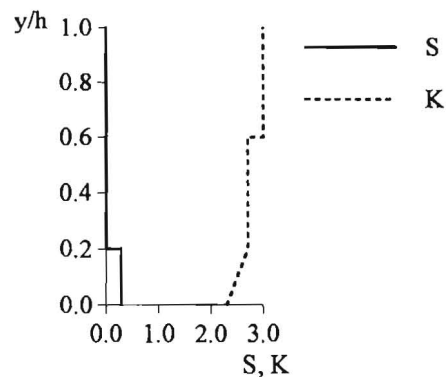


**Fig.2.** Division of an open stream into layers as a function of skewness  $S$  and kurtosis  $K$

### Estimate of eddy viscosity

The eddy viscosity  $\varepsilon$  can be estimated by the mixing length hypothesis (Schlichting, 1968). The depth distribution of the mixing length  $l$  was obtained in a laboratory flume by Cardoso et al. (1989), but there are some difficulties in developing the same procedure for an ice-covered flow in nature. It seems reasonable to define  $\varepsilon$  with the help of the Lagrangian time scale of turbulence  $T$ , being a measure of the time during which the individual character of motion of a chosen particle is conserved.

$$\varepsilon = T \overline{(u'^2)} \quad (5)$$

where  $\overline{(u'^2)}$  is the variance of velocity fluctuations,  $T = \int_0^{\infty} R(t) dt$ , and  $R(t)$  is the normalised correlation function of the actual velocity of the same fluid particle at different moments. (Fischer, 1973; Fidman, 1991). Information about the Lagrangian correlation functions is of great interest in studies of transfer processes in rivers. The Lagrangian characteristics of a velocity field can only be investigated with the help of visualisation methods, which can be used only in laboratory flumes.

The Eulerian time scale  $\theta$  can be obtained from raw data of velocity fluctuations measured in flumes as well as in rivers. Based on extensive studies in flumes, rivers and channels by our laboratory and published by other authors, the following connection between  $T$  and  $\theta$  has been proposed (Dolgoplova, 1995):

$$T = \theta / 1.4n \quad (6)$$

Inserting Eq. 6 into 5, one obtain:

$$\varepsilon = \sigma_y^2 \theta / 1.4n \quad (7)$$

valid for both near-bottom and near-ice flows under ice-cover. The dependence  $\varepsilon = f(\sigma_y^2)$ , and hence the increase of eddy viscosity in an ice-covered flow in comparison with free-surface stream is confirmed by results of authors developing mathematical simulations of ice-covered flow, but we lack sufficient data e.g. from the Moskva River to verify relation 7.

### CONCLUSION

Considerable distinction between the turbulent structures of ice-covered and free surface flows, increasing the bottom shear stress in winter, has been detected, and seems to have great influence on life conditions in rivers under ice cover. The study of effects of ice cover on the habitat conditions in rivers is in the initial stage. Monitoring and control of ice related habitat conditions demand further experimental research.

### ACKNOWLEDGEMENT

This work was partially supported by RFBR grant No. 97-05-64592.

## REFERENCES

- BELTAOS S., BURRELL B.C. (1998): Proc. of the 14th Symp. on Ice, Potsdam, NY, USA, V. 2, pp. 793-800.
- BROWN R.S., POWER G., MCKINLEY R.S. (1998): Effects of hanging dams, surface ice break-up, and flooding on fish. Proc. of the 14th Symp. on Ice, Potsdam, NY, USA, V. 1, pp. 175-181.
- CARDOSO A.H., GRAF W.H., GUST G. (1989): J. Hydr. Research, V. 27, No.5, pp. 603-616.
- DOLGOPOLOVA E.N., ORLOV A.S. (1989): J. Water Resources, No.2, pp. 85-89.
- DOLGOPOLOVA E.N. (1993): Proc. Symp. Runoff and sediment yield modelling. Warsaw, pp. 285-290.
- DOLGOPOLOVA E.N. (1994): Proc. 12th Int. Symp. on Ice, IAHR, Trondheim,; pp. 79-83.
- DOLGOPOLOVA E.N. (1995): Scales of river flow turbulence. J. Hydr. and Met., No.12, pp. 106-112.
- DOLGOPOLOVA E.N. (1996): Proc. 13th Int. Symp. on Ice, IAHR, Beijing, 27-31 August: pp. 497- 504.
- ETTEMA R., BRAILENAU F. (1998): Proc. of the 14th Symp. on Ice, Potsdam, NY, USA, V. 2, pp. 717-723.
- FIDMAN B.A. (1991): Turbulence in water flows. Hidrometeoizdat, Leningrad.
- FISCHER H.B. (1973): J. Fluid Mech., V. 56, pp. 59-78.
- GORE A. (1985): The restoration of rivers and streams. Theories and experience. Butterworth.
- JOHNSON S.L., COVICH A.P. (2000): Regulated Rivers: Res. Mgmt. 16: 1, pp. 91-99.
- KNIGHT D.W., SHIONO K. (1990): J. Hydr. Research, V. 28, No.2, pp. 175-196.
- MAJEWSKI W. (1994): Proc. of the 12th Symp. on Ice, Trondheim, Norway, V. 1, pp. 22-30.
- MILBURN D., PROWSE T.D. (1998): Proc. of the 14th Symp. on Ice, Potsdam, NY, USA, V.1, pp. 189-196.
- MCQUIVEY R.S. (1973): Prof. Paper 802B, Geol. Survey, U.S.
- ORLOV A.S., DOLGOPOLOVA E.N., DEBOLSKY V.K. (1985): J. Water Resources, No.1, pp. 92-99.
- SHEN X. (1998): Proc. of the 14th Symp. on Ice, Potsdam, New York, USA, V. 1, pp. 169-174.
- SCHLICHTING H. (1968): Boundary-layer theory. Sixth ed., McGraw-hill, New York.
- SUKHODOLOV A.N., TILE M. (1999): J. Water Resources, V. 26, No.1, pp. 14-22.

TESAKER E. (1998): Proc. of the 14th Symp. on Ice, Potsdam, New York, USA, V.1, pp. 161-167.

WHITE K.D. (1998): Proc. of the 14th Symp. on Ice, Potsdam, New York, USA, V. 2, pp. 801-807

ZYRYANOV V.N. (1995): Topographic eddies in sea current dynamics. Moscow, Russ. Acad. of Sci.



## EVALUATION OF DOMINANT PARAMETERS ABOUT THE ICE SCOUR EVENTS

S. Kioka<sup>1</sup>, Y. Yasunaga<sup>1</sup>, H. Saeki<sup>1</sup>, H. Nishimaki<sup>2</sup>

### ABSTRACT

Ice scouring is a phenomenon which occurs when sea ice moves in contact with seabed. It has been reported to have caused damage to communication cables and water intake pipelines. Therefore, it will be very important to understand its mechanisms in order to design the safety buried structures against "ice scouring".

In our previous researches, we concluded that local fluctuations in ice forces in the horizontal direction depended on the slope at the corresponding point on the scour curve, and in many cases, ice was tend to move upward. We have developed the rational experimental device system as compared to previous device system. Under the renewal conditions, we conducted a lot of test series, and we revealed relationships between ice forces and behavior of ice, variations of its behavior due to varies condition (attack angle, travelling velocity). And we also revealed the probability distribution of some random variable under the same experimental condition.

### INTRODUCTION

Ice scour is a phenomenon in which ice (pressure ridge, hummock or iceberg) pushed by wind or sea currents from an offshore ice field scrapes the sea bottom, and the sea ice exerts a great force on the sea bottom. This phenomenon has been reported to have caused damage to communication cables and to water intake pipelines e.g. (Duval, 1975; Green et al., 1983; Noble et al., 1980; Grass, 1984). Thus, if there are buried structures such as oil, natural gas or water intake pipelines in an area where there is a possibility that ice scour will occur, serious damage such as deformation, rupture of pipelines, or leakage of oil or gas may occur due to the dynamic or static forces of sea ice. Of particular concern is the increasing number of offshore oil exploration projects in ocean areas where ice forms in winter. Therefore, it will be very important to understand its mechanisms in order to design the safety buried structures

---

<sup>1</sup> Dept. of Engineering, Hokkaido University, Sapporo, Japan, N-13, W-8, Sapporo 060-8628, Japan ,  
Tel.: +81-11-706-6183, fax: +81-11-726-2296, e-mail: kioka@kowanws1.hyd.eng.hokudai.ac.jp

<sup>2</sup> Shimada Kensestu, Co., Ltd., Japan

against "ice scouring". In this study, we conducted a lot of test series, and we revealed some dominant parameters of behavioral characteristics of ice at a time of ice scouring.

## EXPERIMENTS

### Experimental equipment and method

Fig.1. shows the equipment used in the experiment, which was developed not merely to improve the experiments of Kioka and Saeki (1999), but also to make up for their shortcomings. First, sand was placed on a 60 cm-wide water channel for a slope of a constant gradient of  $1/50 i$ . A

steel model keel with three attack angles  $\theta$  was pushed horizontally at constant velocities  $V_0$  by a carriage

travelling on a pinion rack of maximum length  $L$  of 5 m. In addition, the results of the experiments by Kioka and Saeki (1999) proved that local changes of ice forces (bulldozing forces) occur in response to the changes in shapes of excavated ice surfaces. Thus, the model keel was not allowed to rotate, but rollers were placed between the model and the traveling carriage for free vertical movements to measure the relative vertical displacement at the center of gravity of the model using a displacement gauge. A load cell was placed between the model keel and the plate in contact with the rollers to measure the horizontal ice force. This horizontal ice force is the pushing force of the carriage, which is the horizontal drag force applied to the model keel. The horizontal displacement of the model keel was calculated from the relationship between the four travelling velocities of the carriage and the elapsed times measured by software to process measured data, or by making some corrections through monitoring.

### Experimental conditions

The model keel used in the experiment was made of steel and was 30 cm wide and had three attack angles  $\theta$  of 30, 45, and 90 degrees (see Fig.2.). The weights of the three model types (300 N, the main part, the load cell, and the roller plate) and their initial draft depths (20 cm  $\pm$  1 cm) were all designed to be identical as much as possible and to be adjusted by the weight and float. next the travelling velocity of model keel  $V_0$  was maintained at a constant range of 1-20 cm/s for each ice model. The travelling carriage (motor 200 W / AC 200V) was driven horizontally on the rack by the pinion gear. the sand used was sandy soil available on the market (siliceous sand). For

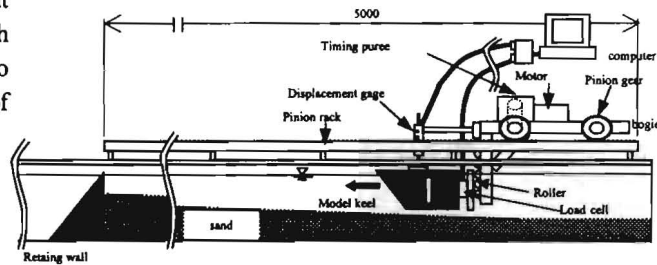


Fig.1. General view of the experimental equipment

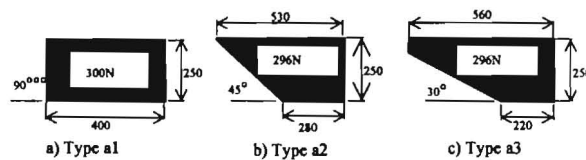


Fig.2. Type of model keel

the soil conditions to be as uniform as possible, after completing of every experimental situation, sand maintenance was carefully performed, and sufficient time was taken to prepare for the next set of the experiment. Table 1 shows the characteristics of the sand used.

**Table 1**  
Characteristic values of the sand used

Mean grain diameter	0.147 mm
Angle of internal friction $\phi$	37°
Submerged angle of repose	32°
Saturated unit weight	15.68 kN/m <sup>3</sup>

The maximum scour length of the model keel was 5 m (the maximum length of the rack). However, the actual range of measurement was set at 3 m to include the possibility that excavated sand appears on the water surface and that the stability of behavior of the model keel deteriorates. Table 2 shows the major and shows that the conditions of this experiment were nearer to reality than those of previous experiments.

**Table 2**  
Comparison with past experimental conditions

	The previous study	This study
Travelling velocity	0.4 -1.4 cm/s	1-20 cm/s
Attack angle	60, 75, and 90 (deg)	30, 45, and 90 (deg)
Scour length	50 cm	300 cm
Seabed slope	1/10 and 1/5	1/50
Driving device system	Oil jack system	Pinion rack system

#### MECHANICAL MODEL OF ICE SCOUR

The fundamental concept of mechanical model follows the our previous method (Kioka et al., 1999). Its concept is follows. Various external and resistant forces act on the ice. These forces include ice forces(bulldozing force, driving force) in the horizontal direction that occur between drifting ices due to environmental forces such as wind and sea currents, buoyancy, reaction force of the seabed (contact pressure), dynamic friction, continuous shear failure of the sand that occurs at the front part of the ice, and weight of the sand assuming there is a slip surface. If the scour depth (scour curve) is known, the approximate ice force  $F$  (bulldozing force) can be calculated by using equations of motion in the horizontal and vertical directions. By comparing calculated values  $F$  with measurement value, we will verify the mechanical model indirectly and will grasp the mechanisms of Ice scour.

#### EXPERIMENTAL AND ANALYSIS RESULTS

As measured values are expected to show some deviations, each set of the experiment was performed many times. Table 3 summarizes the experimental sets and the number of measurements  $n$ . The differences between  $\zeta$  and  $F$  were arose by omitting unusable results due to some kind of trouble, etc., in advance. One experimental set, (a1v2), was repeated much more than the others to analyze the degree of deviations, which is to be discussed later.

**Probability distribution characteristics of the measurements**

Many measurements were performed for one of the experimental sets (alv2) to study the probability distribution characteristics of the measured values:  $F_{max}$ ,  $F_{mean}$ ,  $Z_{max}/h_0$ , and  $\Omega$  (the range of measurement:  $0 < X < L$ ,  $L = 300$  cm), where:

- $F_{max}$ : the maximum value of  $F$  ( $L = 300$  cm)
- $F_{mean}$ : the time average value of  $F$
- $Z_{max}/h_0$ : the maximum scour depth made dimensionless by the initial draft depth
- $\Omega$ : the amount of sand excavated by the model keel divided by the amount of sand excavated when the model keel is assumed to travel horizontally in the range of  $0 < X < L$  is made dimensionless (conceptually, the time average value of  $F$ ).

For example, we consider the probability distribution of  $F_{mean}$ . Here, provided a random variable,  $F_{mean}$ , conforms to the behavior of either normal distribution or log-normal distribution. Next, the measured values of this random variable were plotted on the probability papers (normal and log-normal papers). For example, Fig.4b. show log-normal papers with an R-square value ( $R^2=0.974$  (log-norm.dist),  $R^2=0.919$  (norm.dist)). As a results,  $F_{mean}$  can be said to behave as a log-normal distribution rather than as a normal distribution. Similarly random variable ( $F_{mean}$ ,  $Z_{max}/h_0$ , and  $\Omega$ ) were examined by plotting on the probability papers. These four random values can be said to behave as log-normal distribution than as normal distribution. In view these results, measured values of the other experimental sets are assumed to behave as log-normal distribution. So, we adopted the mean value  $\mu$  and the median  $X_m$  as representative values.

As a results,  $F_{mean}$  can be said to behave as a log-normal distribution rather than as a normal distribution. Similarly random variable ( $F_{mean}$ ,  $Z_{max}/h_0$ , and  $\Omega$ ) were examined by plotting on the probability papers. These four random values can be said to behave as log-normal distribution than as normal distribution. In view these results, measured values of the other experimental sets are assumed to behave as log-normal distribution. So, we adopted the mean value  $\mu$  and the median  $X_m$  as representative values.

**Dependence of the ice force (bulldozing force) and the scour depth on the velocity**

First, the dependence of  $F_{max}/W$  and  $F_{mean}/W$ , which represent values of  $F_{max}$  and  $F_{mean}$  made dimensionless by the dead weight of the ice, respectively, on the velocity of the model keel was studied. However, the attack angle was constant at 90 degrees. Fig.4. shows the ice force increase with increase in the velocity. When  $V_0$  was below 5 cm/s, the ice force was almost constant irrespective of the value of  $V_0$ . This propensity was similar to the results of the traditional experiments of Kioka and Saeki (1999), which were conducted in the range of  $0.4 \text{ cm/s} < V_0 < 1.4 \text{ cm/s}$ . Also,  $F_{max}/W$  and  $F_{mean}/W$  started to increase after  $V_0$  exceeded 5 cm/s and markedly increased between 5 cm/s and 10 cm/s. When  $V_0$  was larger than

**Table .3**

Experimental sets and the number of measurements

Test set	Item		n	
	$\theta$ (deg)	$V_0$ (cm/s)	$\zeta$ (Z)	F
alv1	90	1	5	5
alv2	90	5	29	22
alv3	90	10	6	6
alv4	90	20	7	6
a2v2	45	5	5	4
a3v2	30	5	5	4

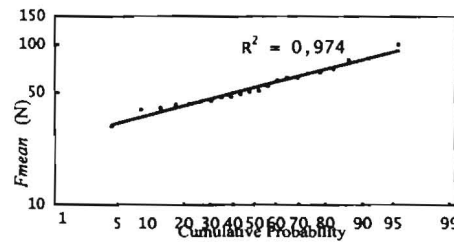


**Fig.3. Probability Paper (Log-normal)**

10 cm/s, the rate of increase was negative. The following factors are considered to be responsible for increasing the ice force with an increase in the velocity:

1. Increase in the vertical force of inertia of the ice
2. Increase in fluid resistance
3. When the travelling velocity of the model keel is larger than the rate of the sand excavated by the model flowing out to the sides of the model or the rate of forming the angle at rest in the sand, the apparent angle at rest of the sand accumulated in front of the model increases, and the amount of the sand flowing out to the sides of the model decreases. As a result, the drag force of the sand increases (the amount of the sand in front of the model increases).
4. Exposure of sand on the water surface, which made measurement difficult (increase in consistency and the unit weight of the sand exposed, as well as generating a meniscus and an apparent cohesiveness (because of 3) above)).
5. Generation of pore water pressure.

Unfortunately, dominant factors among these six factor could not be confirmed, but the effects of Factors 1 and 2 are presumed to be numerically small.

Fig.5. shows the relations of  $Z_{max}/h_0$  and  $\Omega$  both of which are defined above, to the travelling velocity. According to this figure,  $Z_{max}/h_0$  and  $\Omega$  depend very little on the velocity, which agrees with the results of the experiments of Kioka and Saeki (1999). Also, the transitions of the COV(coefficients of variation) of the measured values ( $F_{max}/W$ ,  $F_{mean}/W$ ,  $Z_{max}/h_0$ , and  $\Omega$ ) with respect to the velocity, did not depend on the velocity.

#### Dependence of the ice force (bulldozing force) and scour depth on the attack angle

Fig.6. shows the relations of  $F_{max}/W$  and  $F_{mean}/W$  to the attack angle when  $V_0$  was constant at 5 cm/s. When the attack angle increased,  $F_{max}/W$  increased slightly, but  $F_{mean}/W$  decreased slightly. Changes in the values with respect to the attack angle were minimal. It is possible that their dependence on the attack angle is not great.

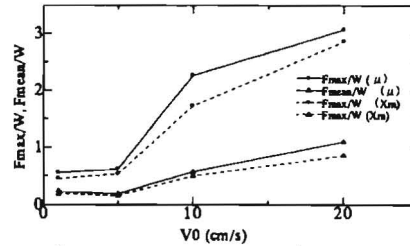


Fig.4. Dependence of the ice force on the velocity

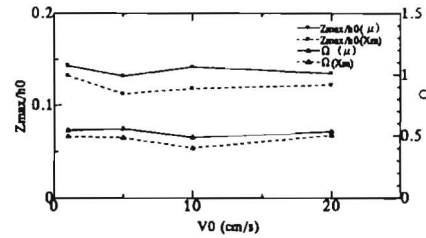


Fig.5. Dependence of the scour depth on the velocity

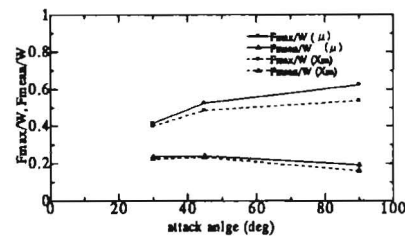


Fig 6. Dependence of the ice force on the attack angle

Fig.7. shows the relationship between  $Z_{max}/h0.\Omega$  and its attack angle. The relationship is a systematic relationship, that is, a smaller attack angle causes less sand digging, verifying previous research. When the sand shear resistance increases because of keel movement, slickness tends to occur on the boundaries of the surface of the keel front and the sand, increasing the upward movement.

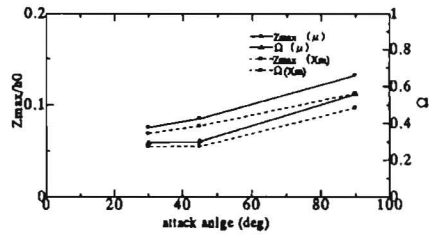


Fig 7. Dependence of the scour depth on the attack angle

Next we consider the change in the COV of each measurement ( $F_{max}/W$ ,  $F_{mean}/W$ ,  $Z_{max}/h0$ ,  $\Omega$ ). This relationship was also systematic, indicating that the larger the attack angle, the larger the coefficient of variation. This means that a complicated and uncertain sand resistance caused by an increase in the attack angle increases accordingly. In other words, when the attack angle decreases, it can be freed from these complicated factors (fracture mechanism). That is, rough ice scouring shows indirectly that the friction movement between ice and sand is in an excellent and stable condition .

### Behavioral characteristics of a model keel in ice scouring

#### Scour curve and scour depth

As the quantity of scraped sand does not depend on the speed of movement of the keel at the same attack angle as shown above, the behavioral characteristics of the keel in conjunction with the attack angle change at the same speed of movement. Fig.8a. to c show the relationship between the scour curve and scour length (dimensionless at  $h0$ ). For the scour curve, ice basically displacing upward in all cases. This vertical displacement mechanism seems to be caused by 1) occurrence of sand sliding at the surface at the front of the keel (Soil clumps are instantaneously pulverized and ice also is displaced in the same direction), 2) sliding between the front of the keel and sand becomes marked when the shear resistance of sand increases. After all, measurements vary even in identical situations. The smaller the attack angle, the smaller the variation index, decreasing the degree of difference. Also, when the attack angle becomes smaller, the rate of upward displacement of ice increases. Next the scour depth generally

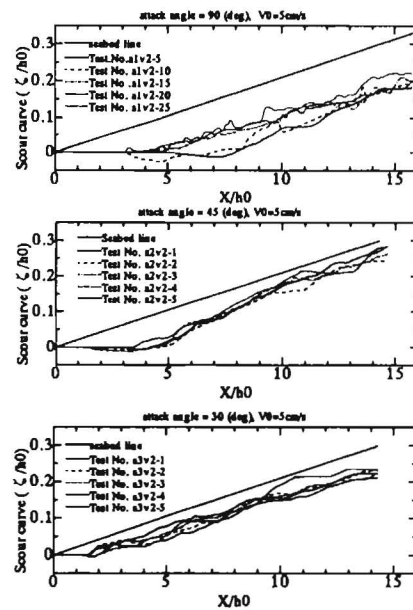


Fig.8a.-c. Behavioral characteristics of a model keel in ice scouring

reaches a ceiling instead of increasing continuously if the scour length increases. In other words, an extreme value or a maximum and the scour-curve cannot be linear (straight line). When closely observing a group of figures and carrying logic to extremes, ice can be said to basically have a periodic motion based on the subseabed, and that the cycle becomes small when the attack angle decreases. As a dynamic mechanism, when the keel penetrates the ground and the sand resistance increases, the ice is displaced vertically (See the previous section) and will be restored to the initial state when freed from the large sand resistance, repeating this movement. The amplitude is also expected to decrease accordingly, indicating that observing the amplitude at the initial cycle is sufficient. However, this experiment was conducted under simple and ideal conditions. In reality, because of such factors as 1) the complicated shapes of keel parts, 2) the keel part contacting with an unconsolidated (floating) part of the sub-sea bed separation occurs (especially a first-year pressure ridge) and 3) the rotation of ice (iceberg), 4) ice stays at the limit of environmental forces, the above mentioned items are impossible to be concluded. In fact in 2), separation occurs at the unconsolidated (floating) part and the ice block that is formed is stuck in the sub-sea bed (Woodworth-Lynas, 1998). In addition, some researchers analyze ice scouring as horizontal or linear (Chari, 1979; Yoon, 1997). However, in many cases the attack angle is within 20-45 degrees, and by its behavior all the ice is presumed to displace upward non-linearly when considering the separation of unconsolidated parts at the bottom.

Local variation response characteristics of the scour curves and the ice force

Fig.9. provides an example of local variations in the scour curves and  $F/W$  associated with the scour length. Although slight variations in the phase angles still remain, both curves are quite similar and are consistent in their peaking patterns, which is primarily due to variations in the horizontal constraining force proportional to the derivative of the scour curves in so far as the constrained movement of the ice along the scour curves is considered. Local variations in the ice force (bulldozing force) might therefore be understood as responses to local variations in the scour curves.

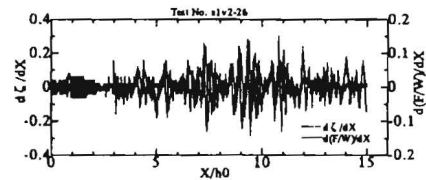


Fig 9. Local variation response characteristics of the scour curve and the ice force

**Assessment of the dynamic model**

Comparison of the observed values and the calculated values

Given the scope of our discussion, a typical case from each experiment is shown as an example, while the results from the simulation experiments are omitted. Fig.10a.-c. represent the attack angle at 90, 45 and 30 degrees, with  $V0$  held constant at 5 cm/s. Fig.11a.-d. represent  $V0$  at 1, 5, 10, 20cm, with the attack angle held constant at 90 degrees. The horizontal axis represents the quotient of the scour length divided by the initial water level (the actual time line). The thick line indicates observed values and the thin line indicates values from the simulation.

Fig.10a.-c. suggest a tendency in the variability of  $F$  to decrease as the attack angle diminishes, as discussed above. Moreover, the absolute value of  $F$  does not vary markedly with the attack angle, as discussed above. While the observed values are slightly greater, in absolute terms, than the values from the simulation, the phase angles of the curves and the peaks match once again, indicating that the simulation usually replicated the behavior of the actual experiment, which indirectly indicates a constrained motion along the curvature with the ice. These findings show that our model is appropriate under the experimental conditions.

Fig.11a.-d. show an increase in  $F$  as the speed of the keel increases. Comparing the observed values and the values from the simulation, the absolute value of the movement speed below 5cm/s corresponds to the curves, but above 10cm/s, the observed values are greater, indicating that the behavior is not replicated accurately, which is attributable to the following possible reasons that were excluded from our calculations:

1. As the speed of movement of the keel surpasses that of the sand displaced by the keel towards the keel, or surpasses the speed at which the resting angle of the sand is formed, the apparent resting angle of the sand depositing on the frontal side of the keel increases, the amount of erosion to the side decreases, and the resistance of the sand increases (i.e. the amount of sand on the frontal side of the keel increases).
2. Because of 1), the sand at the surface of the water caused calculation errors (viscosity, meniscus, an increase in consistency, unit volume weight of the exposed sand).
3. Increases in the unit weight attributable to 1), the angle of the internal friction, and the shear strength, due to dilatancy effect.
4. Pore water pressure.

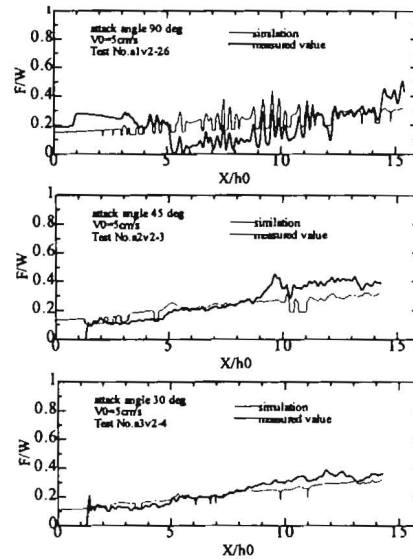


Fig.10a.-c. Experimental and analytical result ( $V_0 = 5\text{cm/s}$ )

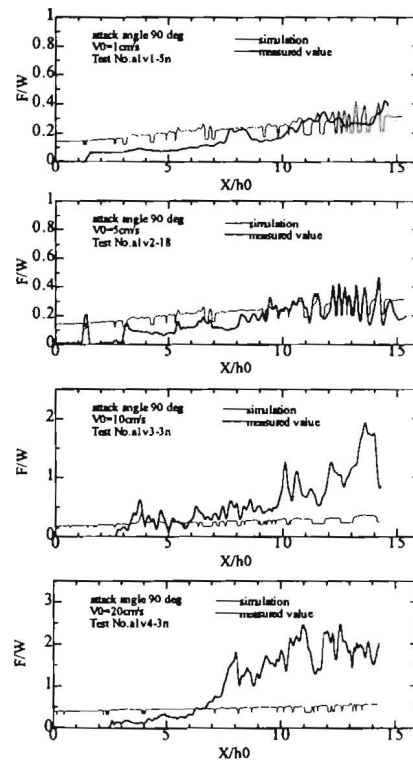
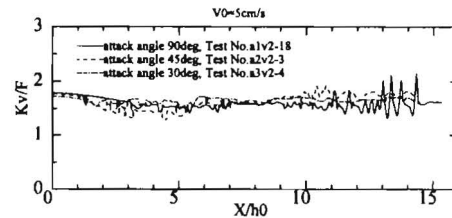


Fig.11a.-d. Experimental and analytical result (attack angle = 90 deg)

The scour curve must be considered, for even at the same scour depth the ice load on the ground at a point varies depending on the course of flow. When protecting a buried structure from ice, installing the structure below the maximum scour depth does not necessarily ensure safety. Estimating  $K$  acting upon the ground is important, because of stress transmission and deformation in the sand below the keel.

Relationship between ice force (bulldozing force) and subgrade reaction

Fig.12. shows an example of the relationship between  $F$  and the load  $K_v$  that acts upon the ground surface. The results of simulation show a fairly strong consistency with the observed value  $F$ . Accordingly,  $K_v$  is greater than  $F$ , which indicates a constant of approximately 1.6 regardless of the attack angle or the scour length. In view of other studies, the results from our simulation are, despite slight differences in the definition of force, similar to the test results showing that the vertical ice load is 1 to 1.5 times the horizontal ice load (Poulin, 1992) and to the results from simulations based on the finite element method (approximately three times) (Yang, 1991). Therefore, once  $F$  is estimated, the load of the ice on the ground can also be obtained.



**Fig.12.** Relationship between ice force  $F$  and subgrade reaction  $K_v$  (the load that acts upon the ground surface)

Simulating the dependence of variability in the internal frictional angle on  $F$

Our simulation does not include changes in mechanical characteristics, such as the internal frictional angle of the sand due to a movement of the keel, variations in the weight of sand (compression, expansion), the dilatancy effect, pore water pressure, etc (they have been indirectly included to a certain degree as the observed values of the scour curve have been considered). The contribution rate of change in the internal frictional angle to change (absolute term) in  $F$  was mathematically analyzed. Here, we provide as an example of experimental data that is comparatively inconsistent with the experimental values. Fig.13a. and Fig.13b. describe the results. The horizontal axis represents the ratio of change in the internal frictional angle, the vertical axis represents the ration of change in  $F$ , and  $F_{\varnothing 0}$  represents the value of the normal internal frictional angle at  $\varphi_0 = 37^\circ$ .  $F_\varphi$  represents the value at the internal fractional angle  $\varphi$ . The experimental range of  $\varphi$  is  $31^\circ$  to  $41^\circ$ .  $F$  increases as the internal frictional angle increases and the growth rate of the internal frictional angle is less than the growth rate of  $F$ , both being less than 2 % against 5 %.

In Fig.13b., the  $F^*_{mean}$  and  $F^*_{max}$  divide the scour length into several blocks and represent the mean value and the maximum value when the observed value  $F$  is within the range of the blocks.  $F_{max\varnothing}$  and  $F_{mean\varnothing}$  indicate the calculated values of  $F$  at the calculated value  $\varphi$ . The figure suggests that, generally speaking, the increase in the observed value  $F$  cannot be explained simply by the increase in the internal frictional angle. Therefore, the effect of changes in the internal frictional angle is small.

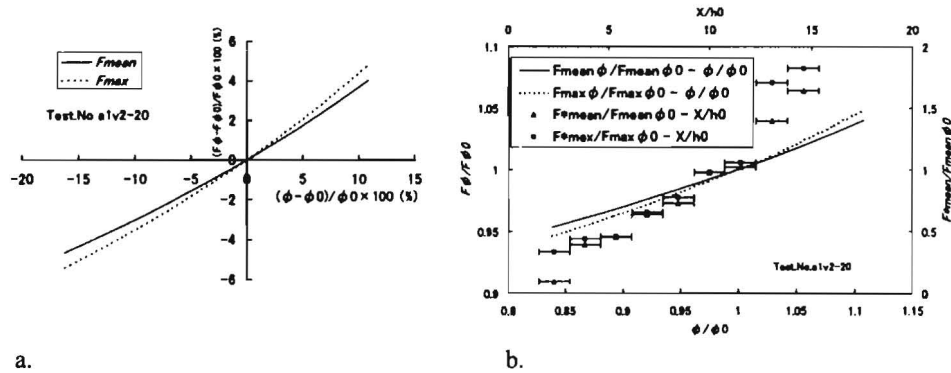


Fig.13. The contribution rate of change in the internal frictional angle to change (absolute term) in  $F$  according to mathematical analysis

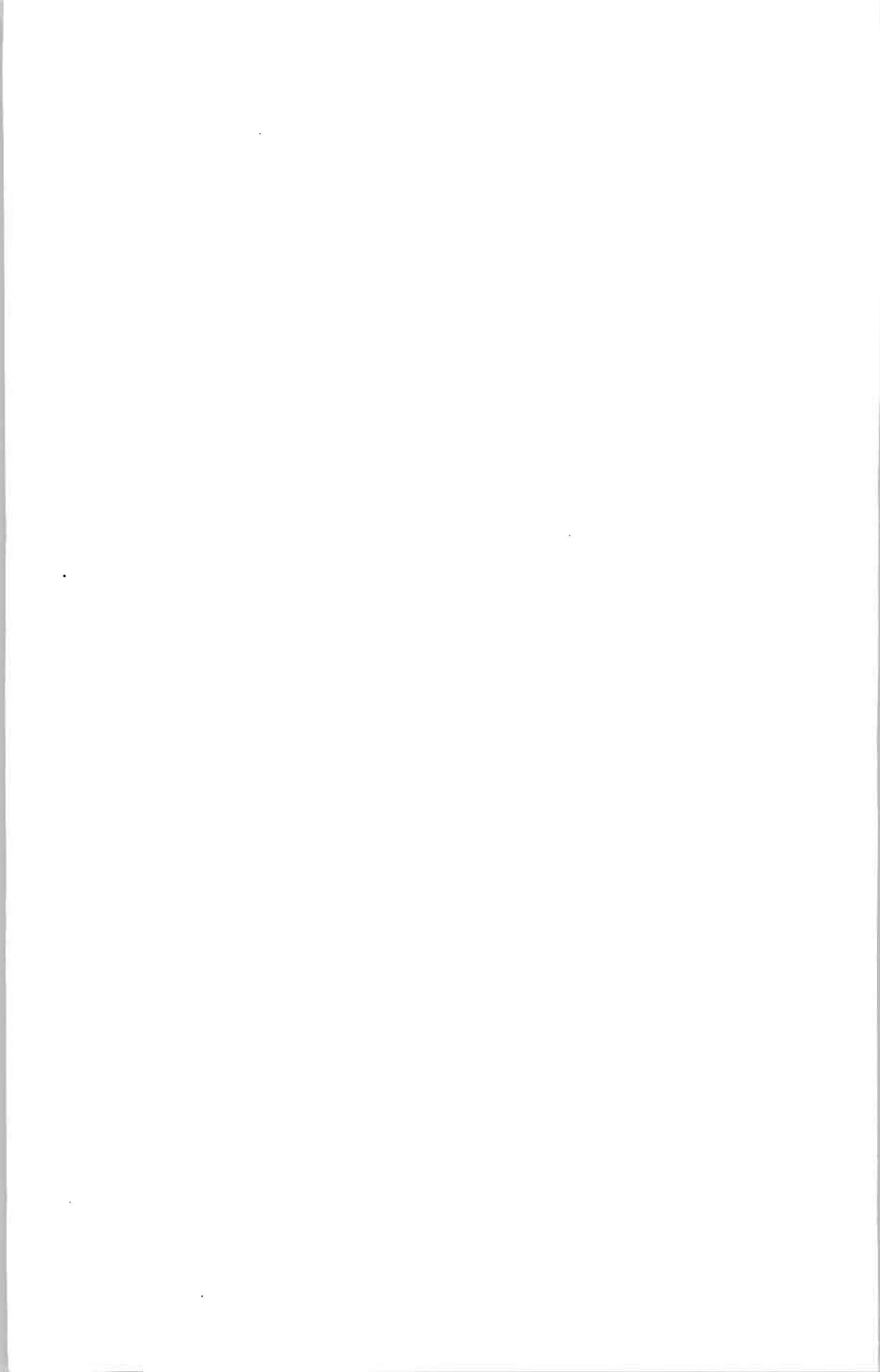
## CONCLUSIONS

1. Under the same conditions, the observed variables ( $F_{max}$ ,  $F_{mean}$ ,  $Z_{max}$ ,  $\Omega(Z_{mean})$ ) follow a log-normal distribution.
2. Generally, the ice force  $F$  (bulldozing force) increases as the speed  $V_0$  of the keel increases and its growth rate stays constant at  $V_0 < 5$  cm/s, increases rapidly at  $5 < V_0 < 10$  and decreases at  $10$  cm/s  $< V_0$ . The geometric mean of the scour depth  $Z$  and the maximum scour depth  $Z_{max}$  remain constant, regardless of the speed of movement of the keel. No systematic relationship is found between the COV in each experimental case and the moving speed of movement of the keel.
3. No apparent change in  $F$  due to the ice force (bulldozing force) at the attack angle is found. However, a systematic relationship exists with the scour depth: the smaller the attack angle, the less erosion tends to occur. Also, as the attack angle diminishes, the COV of the measured variables decreases.
4. In all experimental cases the model keel is generally displaced upward and as the attack angle diminishes the rate of climb increases. Scour depth does not increase with the scour length at a constant rate, but extreme and maximum values exist and the scour curve is not necessarily linear. The ice shows a periodic motion in reference to the sub-sea bed, and as the attack angle diminishes the cycle is expected to shorten and the amplitude decrease.
5. Local variations in the ice force (bulldozing force) or subgrade reaction  $K$  are responses to local variations in the scour-curve. Hence, even at the same point (scour depth), the load of the ice varies depending on its course (scour-curve).
6. Comparing observed values and calculated values, the absolute values and the variability (curve and peak phases) of the changes over a particular time frame seem fairly consistent. However, at  $10$  cm/s  $< V_0$ , the observed values were clearly greater, indicating the need to include the speed-dependent changes in the dynamics of the sand.
7. The ratio of  $F$  and the vertical subgrade reaction  $K_v$ ,  $K_v/F$  from the simulation remained constant at approximately 1.6 independent of the attack angle and the scour length.

8. The increase in the observed value  $F$  cannot be explained simply by the increase in the internal frictional angle. The effect of changes in the internal frictional angle is smaller than the other parameters.

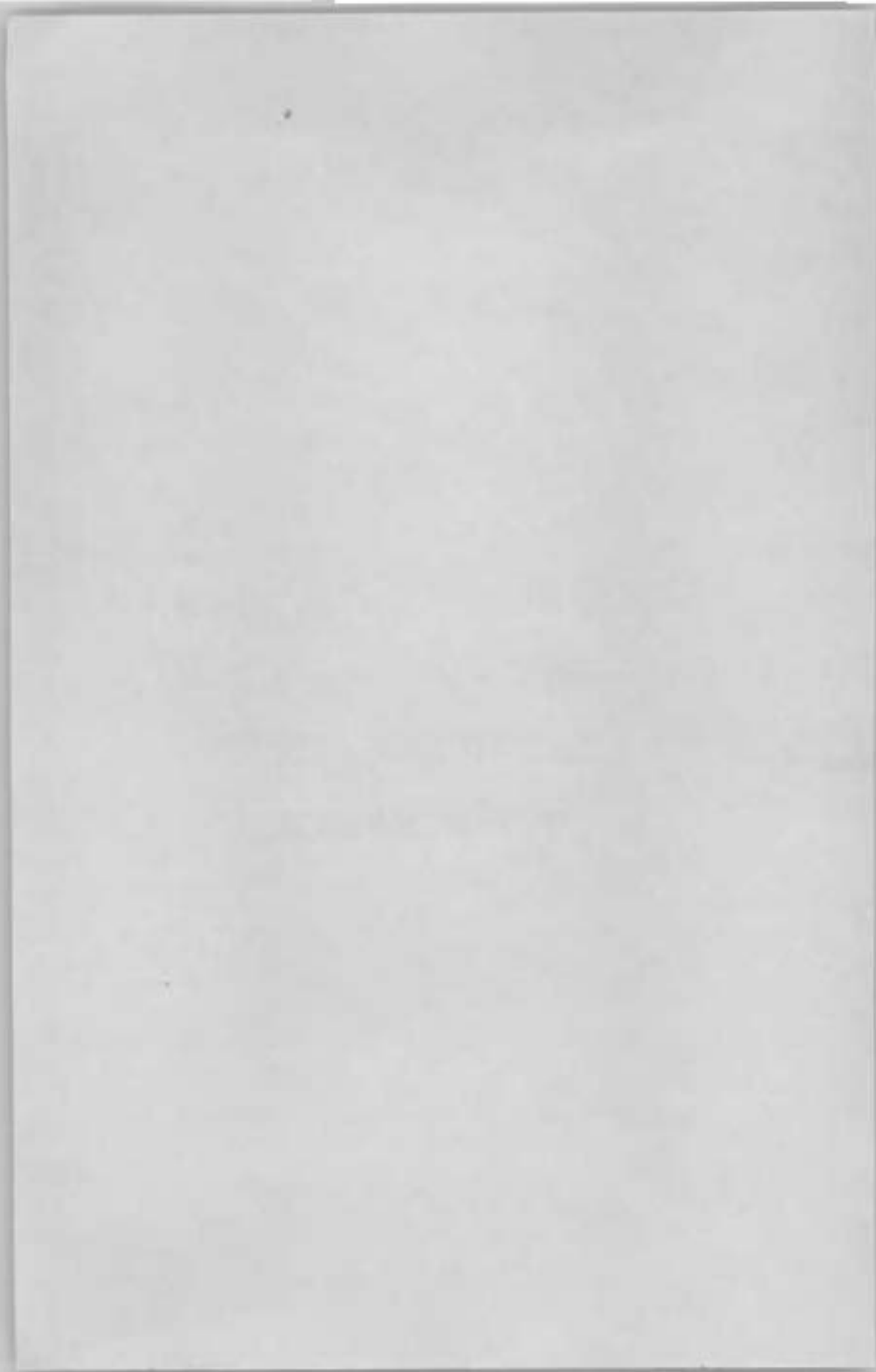
#### REFERENCES

- CHARI T.R. (1979): Geotechnical aspects of iceberg scours on oceanfloors. Canadian Geotechnical Journal, Vol.16, no.2, pp. 379-390.
- DUVAL B.C. (1975): Exploratory drilling on the Canadian continental shelf, Labrador Sea. Offshore Technology Conference, Paper No.2155, pp. 59-67.
- GRASS J.D. (1984): Ice Scour and ice ridging studies in lake Erie. Proc. of Int. Symp. on Ice, Hamburg, Vol. 2, pp. 33-43.
- GREEN H.P., REDDY A.S., CHARI T.R. (1983): Iceberg scouring and Pipeline burial depth. Proc. of 7th International Conference on Port and Ocean Eng. Under Arctic Conditions (POAC-83), Vol. 1, pp. 280-288.
- KIOKA S., ABE S., SASAKI H., SAEKI H. (1999): Mechanical model of Ice Scour. Proc. of 15th International Conference on Port and Ocean Eng. Under Arctic Conditions (POAC-99), Helsinki, Vol. II, pp. 537-544.
- NOBLE P.A., COMFORT G. (1980): Damage to an underwater pipeline by ice ridges. Proc. of Workshop on Sea Ice Ridgeing and Pile up, Alberta, pp. 43-47.
- PAULIN M.J. (1992): Physical model analysis of iceberg scour in dry and submerged sand. M.Eng. Thesis, Memorial University of Newfoundland, St. John's Newfoundland.
- WOODWORTH-LYNAS C.M.T. (1998): Sub-Scour Deformation and the development of Ideas from Field Work in the Last Decade. Proc. of Ice Scour and Arctic Marine Pipelines Workshop Published by C-CORE (ISAMP), Hokkaido, Japan. pp. 33-38.
- YANG Q.S., POOROOSHASB F., PROOROOSHASB H.B. (1993): Analysis of Subscour Deformation by Finite Element Method. Proc. of 4th Canadian Conference on Marine Geotechnical Engineering, St. John's, Newfoundland, Canada, pp. 739-754.
- YOON Y. (1997): A numerical Simulation to Determine Ice Scour and Pipeline Burial Depth. Proceedings of the 7th International Offshore and Polar Engineering Conference (ISOPE-97) Honolulu, USA, pp. 212-219.



**TOPIC F**

**ICE FORECASTING AND  
MANAGEMENT OF HYDRAULIC  
AND HYDROPOWER  
INSTALLATIONS**





## STUDY ON WINTER ICE DAMAGE OF TANGHE HYDROPOWER STATION OF TIBET

Shu-You Cao<sup>1</sup>, Ran Li,<sup>1</sup> Banjiuciren<sup>1</sup>

### ABSTRACT

The winter ice damage of Tanghe hydropower station of Tibet is analyzed. Preliminary suggestions in designs for diversion water power station of Rikaze, a prefecture of Tibet, are proposed. It is of great importance not just to the winter operation of diversion water power station of Rikaze, but to that of Tibet as well.

### INTRODUCTION

The Tibet Autonomous Region is situated in Qing-Zang plateau, where the average sea level is more than 4000 meters. Because the winter is very cold and long, all minor hydropower stations in the region have problems of ice damage in different degrees. The ice period of some stations is as long as 3 to 5 months.

Tanghe hydropower station belongs to Rikaze prefecture of Tibet. It is located in the up reaches of Tanghe river, the first level tributary of Yaluzangbu River. As the only prefectural level station, Tanghe power station takes on the main industrial and agricultural power supply of Rikaze. It was built in 1980. The station is a diversion water power station, with 6400 kW installed capacity. The operation for many years shows that the ice in headrace and pressure head pond always prevents the normal operating of the power station, sometimes power generation is even forced to stopped. Whereas the severe cold winter is the peak period of life power consumption for Rikaza residents, this aggravates the existed serious lack of power for many years and influences the people's normal life order and economic development seriously. From 1993 to 1995, completely technological transformation of Tanghe power station was done, with nearly one-billion-yuan investment. The station was put into operation again in the beginning of 1996. Many successful ice-control measures outside Tibet were used during the transformation. A series of ice-control structures, such as ice storage and ice sluice in head system, ice-deflecting boom in upstream position of the dam, pontoon-type ice raft

---

<sup>1</sup>The State Key Hydraulics Laboratory of High Speed Flows, Sichuan University, Chengdu, China,  
24, South Section No.1, Yihuan Road, Chengdu 610065, China. Tel: 86-028-5405644, fax: 86-028-5405148,  
e-mail: caosy@mail.sc.cninfo.net

before intake sluice of headrace, ice sluices in headrace and pressure head pond, etc., were built. Although these measures play an important part in the operation, the ice damage problems are still serious after the transformation due to the bad weather of the region. The author gives detailed analysis of ice damage problems of Tanghe power station in winter. With the combination of international research progress and operating experience in ice damage control, preliminary suggestions for designing diversion water power station of Rikaze are proposed.

### **ANALYSIS OF THE ICE DAMAGE OF TANGHE POWER STATION**

The ice damage of Tanghe power station exists mainly in head system, headrace and pressure head pond, where the ice consists of ice flowers, border ice, anchor ice, ice floe and ice cover mainly.

#### **Ice damage in head system**

An ice storage with a capacity of 147,000 cubic meters in head system and an ice-deflecting boom in 85 m upstream the dam are set up during technological transformation. The ice-deflecting boom is arranged in arch type with steel wire rope and the dimension of the logs is 0.6×0.4×0.6 cubic meters. The straight-line distance between the anchor logs on the opposite banks is 160 m. These projects not only basically assure the diversion in winter, but also retain the upstream incoming ice to form ice cover. But most of the upstream incoming ice flowers were transported into headrace through the trash rack at intake. There is a big freshet ditch at the right side 1 km up from the storage dam. Debris flow is often occurred here, resulting the departure of the main current to the loose accumulation horizon of sand and gravel on the opposite side and causing the slide of the accumulation horizon. As a result of the process and incomplete deposit clearance in construction stage, a great amount of sand and gravel deposits in the storage and forms overbank. The main current then becomes unsteady and ice-deflecting boom cannot take the effect of ice retaining. The ice then strikes against obstructions directly.

#### **Ice damage in headrace**

Completely transformation of the headrace was made in the technological transformation. The channel is 16.63 km long and the concrete lining along the whole channel was adopted, improving the headrace operating condition greatly. In spite of this, there are still many problems during winter operation of the headrace, which are ice flowers, border ice and anchor ice.

Ice flowers are loose ice pieces formed in channels or rivers. The ice flowers of Tanghe power station mainly include the upstream incoming ice flowers and the ice flowers formed in channel. The sand and stones held in ice flowers can abrade turbine blades if they enter the turbine.

Border ice is the narrow long ice block attached to riverbank (Wasantha Lal & Shen, 1991). The border ice of Tanghe power station forms from November to February and its thickness is

from 2 to 40 cm. In the daytime, with the air temperature rising some border ice breaks and forms ice jam in cross constructions, causing overbanking of ice slush and destroying the channel. A large number of labor forces have to break and drain off ice along the whole channel. From November to January each year, the border ice can grow into ice cover. But due to big diurnal temperature difference and daily load fluctuation, the water level in channel change sharply and the ice cover is not steady.

Anchor ice appears mainly in channel and pressure pond during winter operation period. It develops when the bottom water temperature drops below the freezing point as the air temperature drops. The process is related with air temperature, channel section, water depth and velocity.

According to the opinion of Zhao Yuncheng, the anchor ice damage is not occurred suddenly and its elimination can be done easily. But it is not same for Tanghe power station. Due to big diurnal temperature difference, the water temperature in headrace drops with the sharp drop of the air temperature in the evening. At the same time the power consumption is small in the evening. A large quantity of ice is then accumulated in the pressure pond and the discharge is resisted, resulting in the decrease of velocity and the formation of anchor ice. In the daytime, as air temperature increases, the freezing force between anchor ice and channel bottom becomes small. When the buoyancy force is bigger than the freezing force, the anchor ice will departure from the bottom, run downstream with water and form ice jam at the intake of cross constructions. This kind of ice jam of Tanghe power station comes suddenly. Workers along the channel have to observe ice regime all the time and break ice according to the situation.

There is another kind of anchor ice damage. When the anchor ice left channel bottom, sand, stones and broken concrete in the bottom will be taken up. Some of them go into the turbine and lead to the turbine blades to be destroyed. For the reason, the turbine blade needs to be repaired at least twice once a year and the turbine runner has to be changed every four years. The price of one turbine runner is 80,000 yuan, so we can imagine how great the anchor damage is.

#### **Ice damage in pressure head pond**

The ice damage in pressure pond origins in upstream incoming ice floe and the ice formed in the pressure pond. The ice accumulated in the pressure pond is as thick as 30 to 80 cm. Its main damage is blocking the trash rack and outlet. It is not only influence the inflow of pressure conduit, but also lead to channel blockage and over-banking of ice slush. In order to assure normal operation of the power station, manual or dynamite means must be taken to break ice in the evening when the load is small. It is about 80 days in each winter when the ice needs to be broken, 10 to 40 labor forces needed one day.

#### **Ice damage in gates**

All the gates of Tanghe power station have serious attached ice, which is frozen or attached by ice slush on the faces of hydraulic structures, gates and trash racks. The electric warming

method is adopted in the ice sluice in pressure pond and has received good effects. But as there is no electric warming in ice sluices of intake and channel, the injection of hot water into the gate grooves needs to be done when lifting up and down the gates. An ice sluice in the headrace was also setup after the technological transformation and is arranged together with the sand basin. Due to the arrangement, circulating current prevails and the effect is not satisfied. Besides, as there is no warming measures taken for the ice sluice, its operation is not quick.

### **ICE CONTROL SUGGESTIONS FOR RIKAZE PREFECTURE**

Up to the present, eighty-percent townships and villages in Rikaze including some places where the county governments located have no power. Among the 18 counties belonging to Rikaze, there are 8 county government sites where lighting by small diesel generators in winter. There are many rivers in Rikaze, such as Yaluzangbu river, Nianchu river, Pengqu river, Xiabuqu river, Duoxongzangbu river, Xiangqu river, Chaiqu river, Laiwuzangbu river and Jiazhezangbu river, etc., containing abundant water energy resources. With the small population distributed in vast areas, it is unrealistic and uneconomical to build large water power station and power network for Rikaze. The only way is to setup minor power station and supply power by means of sole network or minor network. The biggest difficulties of the minor power station are how to assure its operation in winter and what ice control suggestions suitable for the local region should be proposed. It is an important subject in the face of us. With the combination of the international ice control research progress and operating experience of Tanghe station, some suggestions are proposed based on the natural conditions of Rikaze.

#### **Ice control measures of head systems**

Under normal natural conditions, ice storage in head constructions is a good measure for ice control. There is almost no vegetation cover in drainage area of most rivers and there are many freshet ditches in Rikaze. After a heavy rain, a small freshet ditch can even cause debris, whose damage on projects is difficult to imagine. One suggestion made here is that firstly we should have a full knowledge of the freshet ditches in the upstream of the dam when choosing the site of the intake or the axes of the dam. Measures, such as prolonging the headrace and minimizing the capacity of the storage, can be adopted to avoid the influence of freshet ditches as far as possible. Otherwise, ice control actions must be taken.

#### **Ice control measures of headrace**

Most diversion water power stations of Rikaze need headraces of several miles. Its main reason is to gain certain head and choose suitable topography for the arrangement of workshops. For the lack of the knowledge about ice damage, there is no fully consideration to the operation in winter. Especially in the design of the minor village water power stations, no actions on ice control is taken, because of the opinion that the headrace's frozen is a natural law. For the reason, most water power stations cannot operate normally, sometimes even to be obliged to stop generating. In recent years, with the projects-Project of 'Yi Jiang Liang He' of Tibet and Project of Eliminating Counties Without Power of Water Conservancy Ministry

putting into practice, successful ice control technology in other provinces has been introduced into Tibet. It has been shown that the completely sealing with armored concrete plates from intake to pressure pond is an effective measure. It can not only control ice damage, but also prevent debris into channel. Its disadvantages are high cost and difficult silt clearing. Besides, it is difficult to achieve completely sealing for big diversion runoff in daily regulation pressure pond.

Although the ice storage of Tanghe power station plays a good part in ice control, the overlong headrace brings extra serious ice damage. So we should harmonize the dam height and headrace length according to natural conditions in the design of ice control for head constructions and avoid overlong headrace.

#### **Ice control measures in pressure pond**

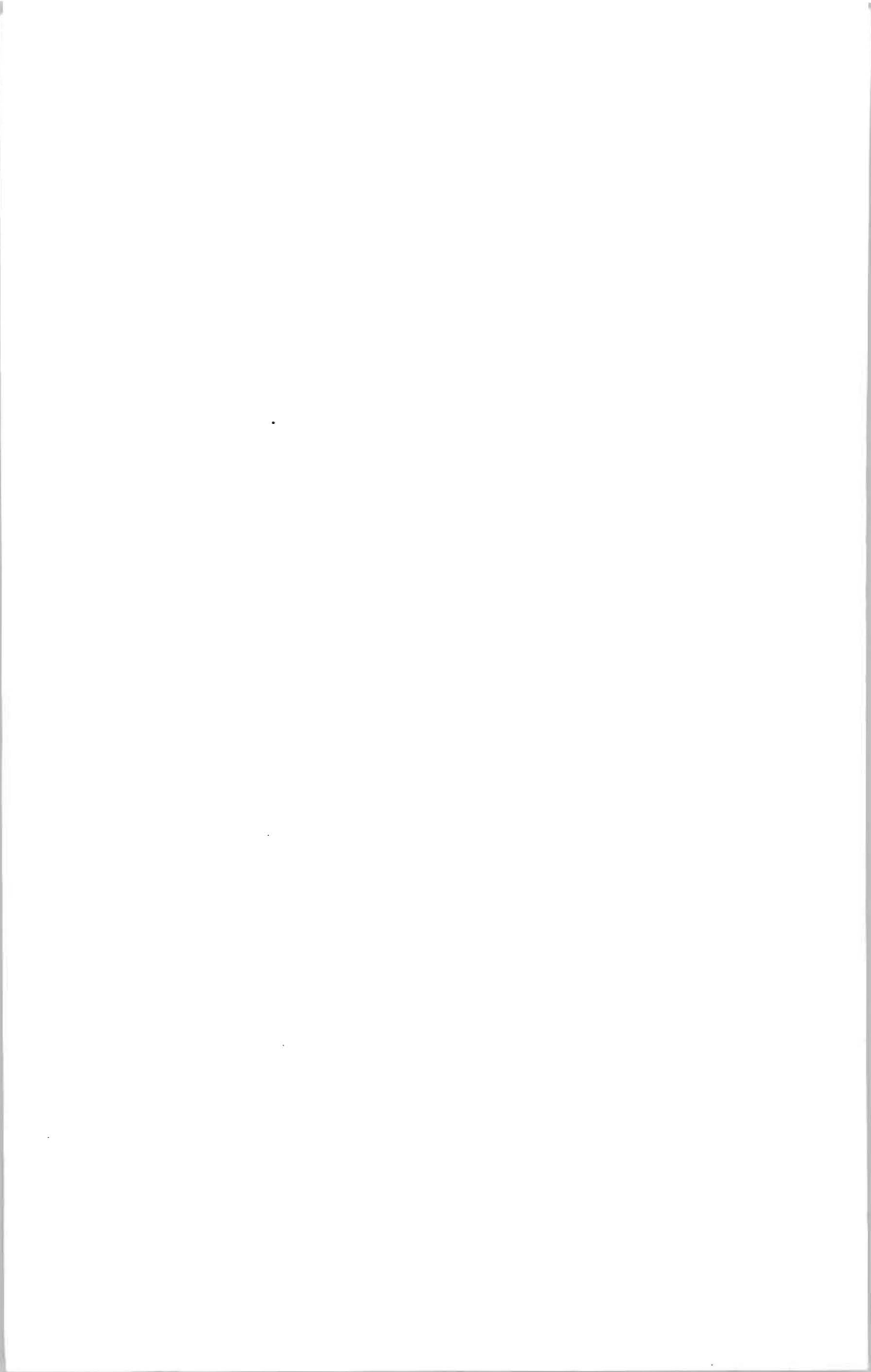
Pressure pond is the last defense line for ice control of the power station. Although ice drainage constructions can be setup here, it is suggested that the ice control measures be taken in the intake and headrace mainly. This is because that due to the little incoming runoff of most rivers in winter in Rikaze, the water quantity for generation is difficult to be satisfied, and so there is no much water for ice drainage. In order to minimise the ice damages as far as possible, the water surface area of pressure pond section should not be designed too large.

In a word, four taches, including storing, preventing, conveying and drainage, should be paid attention to in the ice control for diversion power station and comprehensive measures combing the four taches should be taken according to local natural condition. At the same time, it has 1500~34000 sunshine hours and exceptionally rich solar energy resource in Tibet. Controlling ice by means of solar energy seems to have a bright prospect.

#### **REFERENCES**

WASANTHA LAL A. M., SHEN H. T. (1991): Mathematical model for river ice processes. *Journal of Hydraulic Engineering*, July, , Vol. 117, No.7, pp. 851-867.

ZHAO YUNCHENG: The winter operation of diversion water power station. *Qinghai Water Resource and power*.





## A STUDY OF OPERATION AND CONTROL OF XIGOU HYDROPOWER PLANT DURING ICE PERIOD

Guifen Li<sup>1</sup>, Difang Xiao<sup>2</sup>

### ABSTRACT

An optimized regulation scheme for operation of Xigou Hydropower Plant during ice period is discussed in this paper. The scheme presented herein can not only keep the economic benefits, but also resolve the problem of downstream ice flood.

### INTRODUCTION

Xigou Hydropower Plant located in Xigou River, Heilongjiang province, China. Its catchment area is 1777 km<sup>2</sup> and the mean annual runoff is  $3.13 \times 10^8$  m<sup>3</sup>. The installed capacity of the plant is  $3.6 \times 10^4$  kW and its generation is 99.14 MWh per year. Good economic benefits has been obtained since its operation. Because the plant situates in cold region, the flow discharge downstream is not continuous and unstable during winter operation. And moreover, the downstream ice slush has been more intensively since the daily regulation has been taken into practice. During January and February, ice jam occurs in the downstream each year, which causes flow overtopping the river bank and then a flood disaster. For example, more than 200 hectare fertile farmland and 12000 hectare wild and plough were flooded in 1994. In order to solve the contradictory between power generation and ice flood, field prototype observation has been put up by China Institute Of Water Resources and Hydropower Research (IWHR) and Heihe Hydrology Survey Team for three years. On the basis of observed data, analyses and research were carried out. Then a reasonable relation was established among the reservoir storage, hydropower generation and flow discharge downstream, in order to obtain the maximum generation benefit, keep the reservoir storage at a corresponding volume for aquaculture and minimize the ice flood disaster. Experiences showed that the expected result was obtained very well.

### MAJOR PROBLEMS SINCE OPERATION DURING ICE PERIOD

It was found out through field observation in the winter from November to the next March, 1991 through 1994 that the reservoir inflow volume was  $0.295 \times 10^8$  m<sup>3</sup>, the water volume

---

<sup>1</sup> China Institute of Water Resources and Hydropower Research

<sup>2</sup> China Heihe Hydrology Survey Team

regulated through reservoir was  $3.02 \times 10^8 \text{ m}^3$ . The water volume discharged downstream was  $0.14 \times 10^8 \text{ m}^3$  and the hydropower generation was  $1.17 \times 10^8 \text{ kWh}$ . The basic conditions of operation are shown in the following Table. The daily variations of hydropower generation and flow discharge downstream are shown in Fig.1.

**Table 1**

Basic conditions of winter operation of the reservoir

Date	Reservoir Level (m)	Storage Volume ( $10^8 \text{ m}^3$ )	Inflow Volume ( $10^8 \text{ m}^3$ )	Available Outflow Volume ( $10^8 \text{ m}^3$ )	Monthly Generation ( $10^4 \text{ kWh}$ )	Monthly Distribution of Generation (%)	Monthly Operation Hour Ratio ( $h_{max}/h_{min}$ )	Monthly Distribution of Discharge (%)	Daily discharge Ratio ( $Q_{max}/Q_{min}$ )
91.11	43.55	1.628	500.5	1129	458.6	13.1		13.9	
12	43.18	1.194	135.5	1537	633.9	18.2	1.59	18.9	2.43
92.01	42.3	1.012	0	1777	742.3	21.3	1.49	21.9	1.47
02	41.06	0.843	0	1788	811.9	23.2	4.18	22.0	2.75
03	39.37	0.637	107.4	1900	843.4	24.2	1.35	23.3	2.62
92.11	43.62	1.276	620.6	2380	973.9	18.7	1.21	19.5	2.32
12	42.60	1.093	39.3	3030	1253.2	24.1	2.33	24.8	4.21
93.01	40.47	0.768	0	3424	1506.4	29.0	3.00	28.0	3.13
02	36.67	0.384	0	2718	1203.3	23.2	1.21	22.2	1.49
03	28.45	0.061	101.5	669	258.3	5.0	7.20	5.5	4.87
93.11	42.86	1.136	1231.8	1205	488.7	13.4	6.01	14.0	9.24
12	42.53	1.181	0	1645	682.5	18.7	3.11	19.1	4.87
94.01	41.41	0.898	0	2631	1145.7	31.4	1.24	30.4	1.75
02	39.02	0.595	0	1358	602.7	16.5	5.61	15.7	11.06
03	37.27	0.432	229.3	1795	728.6	20.2	6.86	20.8	12.48
Total			2947	28990	12333		3.09		

On the basis of analyses, it was concluded that the water volume regulated by the reservoir and the economic benefit of the power plant are reasonable, while the ice flood disaster occurred downstream the reservoir. The three major problems are as follows: The first, the characteristics during ice period for small and middle size river are not considered in design. For these rivers, the runoff in winter is little, the discharge capacity through flow section is low and ice slush develops rapidly during January and February, which may sometimes cause flow to be zero; The second, water discharged downstream and water utilized in power generation are not reasonably distributed according to seasons. The hydrographs of water discharged and utilized in power generation are shown in Fig.2. It can be seen from Fig.2. that in January and February, both peaks coincide with the minimum air temperature and the ice-up peak, which likely cause ice jam and reduce the discharge capacity; The third, the operation of turbine sets and the flow discharge downstream are all not stable. When two sets operate alternately, the maximum discharge is  $27.1 \text{ m}^3/\text{s}$ , while, the minimum is zero, which may be considered the major reason for downstream disaster.

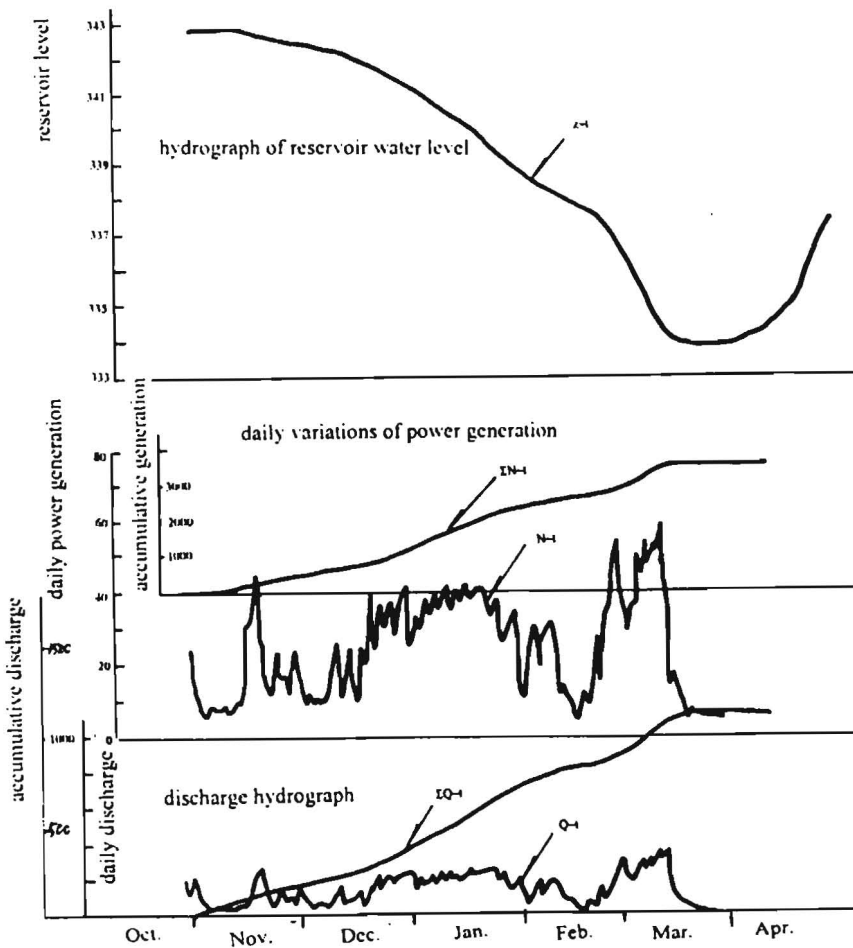


Fig.1. The daily variations of reservoir water level, flow discharge and power generation

In addition, the width of riverbed downstream the hydropower station in winter is only 35~40 m whereas more and further downstream the width becomes 2500~3000 m, where is a plain. In data of 1994, the width of ice field was 1720~2300 m; total water storage in the reach 23km long was 7.834 million  $m^3$  and the total area covered by ice is 15.293 million  $m^2$ , which was 11.2 times more than usual year. At that time, daily mean temperature is  $-19^{\circ}C \sim -22^{\circ}C$  and the maximum thickness of ice in the river 1.5~2.5 m, for some part 3.5 m. Under operation of the hydropower station, special regime such as laminating of water and ice, subsiding of ice mound and ice layer, as well as ice cavern, may be seen everywhere in the river. Therefore significant ice flood disaster occurred in February, 1994.

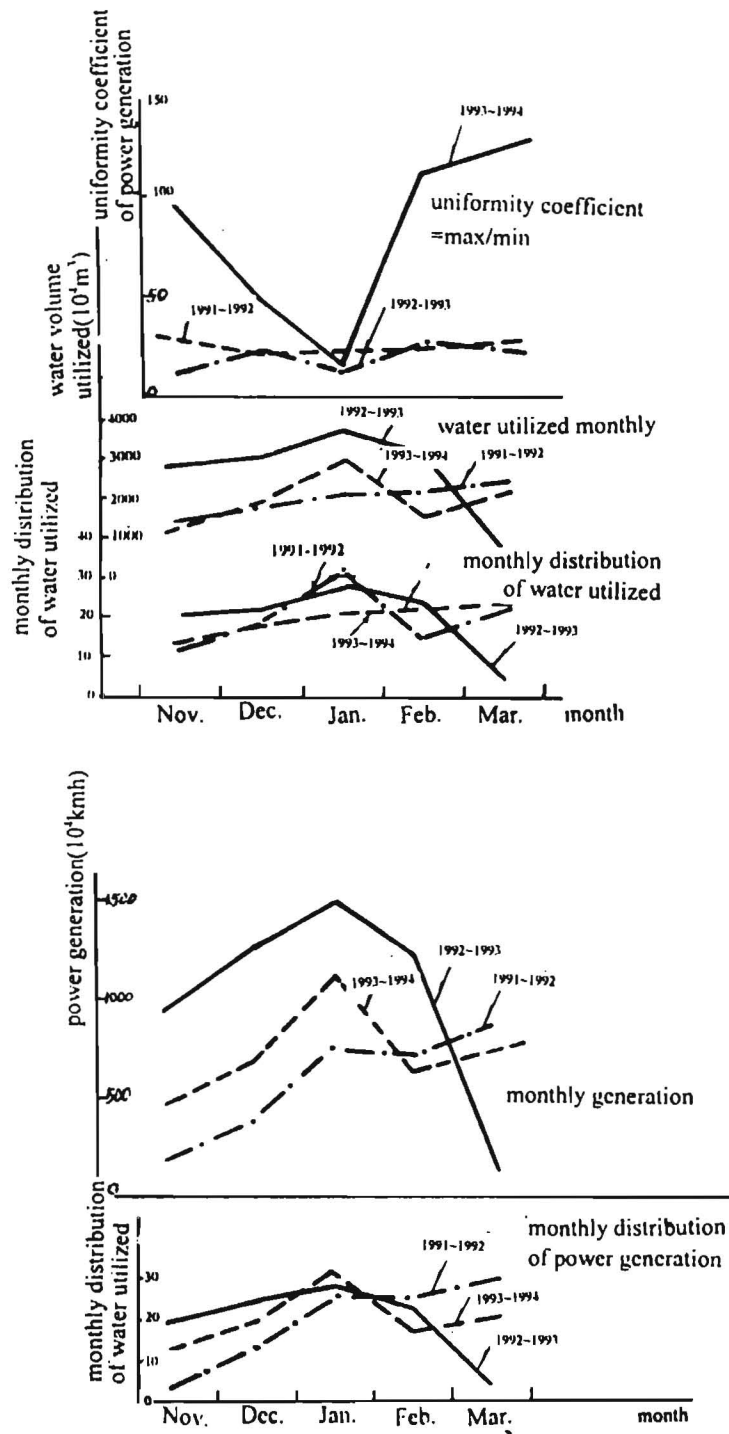


Fig.2. The variation of water volume utilized for power generation and power generation

## RESEARCH IN OPTIMIZATION OF OPERATION AND REGULATION OF THE HYDROPOWER STATION

Ice is inevitable in downstream reach when small and middle size hydropower station in high cold region are put in service, however, it is possible to reduce the ice flood if a relation among water storage, power generation and flow discharge is well arranged through reasonable regulation and operation. The aim of Xigou Hydropower Station is to gain maximum power generation, keep the correspond storage for the aquiculture and minimize the ice flood disaster. The following aspects are optimized.

1. Regulating the volume of water reasonably to keep the operation under high head. The hydropower output is defined as the following formula:

$$N=9.81\eta QH \quad (1)$$

Where:  $\eta$  is efficiency coefficient of turbine set;  $Q$  is flow;  $H$  is water head. The output is mainly determined by  $H$  when  $\eta$  and  $Q$  are given. To keep  $H$  be maximum, the key point for Xigou hydropower station is to regulate reasonably in autumn.

2. Arranging operation reasonably

From Eq. 1, it may be seen that the power station load and head loss are related to the load distribution among turbine sets and the sequence of switching when water reservoir water level and turbine efficiency are given. Therefore, the economic operation should put the loss of head to minimum. Computation of head and output loss may be expressed as follows:

$$\left. \begin{aligned} H &= Z_1 - Z_2 - H_s \\ H_s &= \eta_s Q^2 \\ \Delta N &= k Q^3 \end{aligned} \right\} \quad (2)$$

where:  $H_s$  is head loss;  $\eta_s$  is coefficient of head loss;  $\Delta N$  is output loss;  $k$  is coefficient of overall efficiency. From Eq. 2, it can be seen that  $H_s$  varies with  $Q^2$  and  $\Delta N$  varies with  $Q^3$ . It is found through computations that the value of  $H_s$  for one set operation and two sets operation is 4.82 and 19.28 respectively and then the ratio of them is nearly 4, whereas, their generation load differs to only 8.5%. Therefore, when the reservoir storage and power generation are both given in winter, the total output for one set is greater than that for two sets.

3. Accordingly, generating with one set in winter is an important measure for increasing economic benefits. Determining a reasonable amount of power generation and controlling the flow discharge downstream. as discussed above, after putting into service of the hydropower station in cold region, the key point for reducing ice flood is the degree of stability between power generation and flow discharge, if the peak of flow discharge and the peak of head loss of ice freeze-up could be staggered in time. Ice-up, freezing-up and thawing process of the river ice is sketched in Fig.3. Generally, for the downstream reach of the river the beginning of freezing is the last ten-days of October, freezing-up occurs in the middle ten-days of November, freezing-up to the river bed occurs in the last ten-days of April and flowing with ice occurs at the beginning of May. After the reservoir put into

service, the flow discharge becomes unstable and the minimum discharge capacity occurs within January to March. To keep the flow discharge relatively stable, the following methods should be carried out.

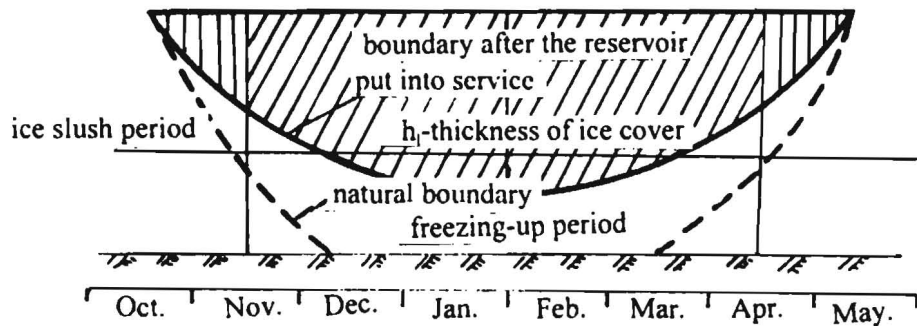


Fig.3. A sketch of river freezing-up process

The first, during initial of freezing-up period within November to December, increasing the power generation and flow discharge to delay the time of freezing-up, raise the elevation of ice cover, and increasing the discharge capacity of the river. Moreover, the peak of power generation should be arranged so that it occurs before the formation of maximum ice thickness. The monthly distribution percentage of power generation may be as follows: November, 20 %; December, 3 %; the next January, 16 %; February, 16 %; March, 14 %.

The second, adjusting stability coefficient of power generation and flow discharge. Stability coefficient is expressed by the ratio of the daily maximum to the daily minimum of power generation and flow discharge. It is appropriate to adjust the daily variation of the coefficient from 3~12 within 1991~1994 to 1~1.5, and the maximum to be about 2.0.

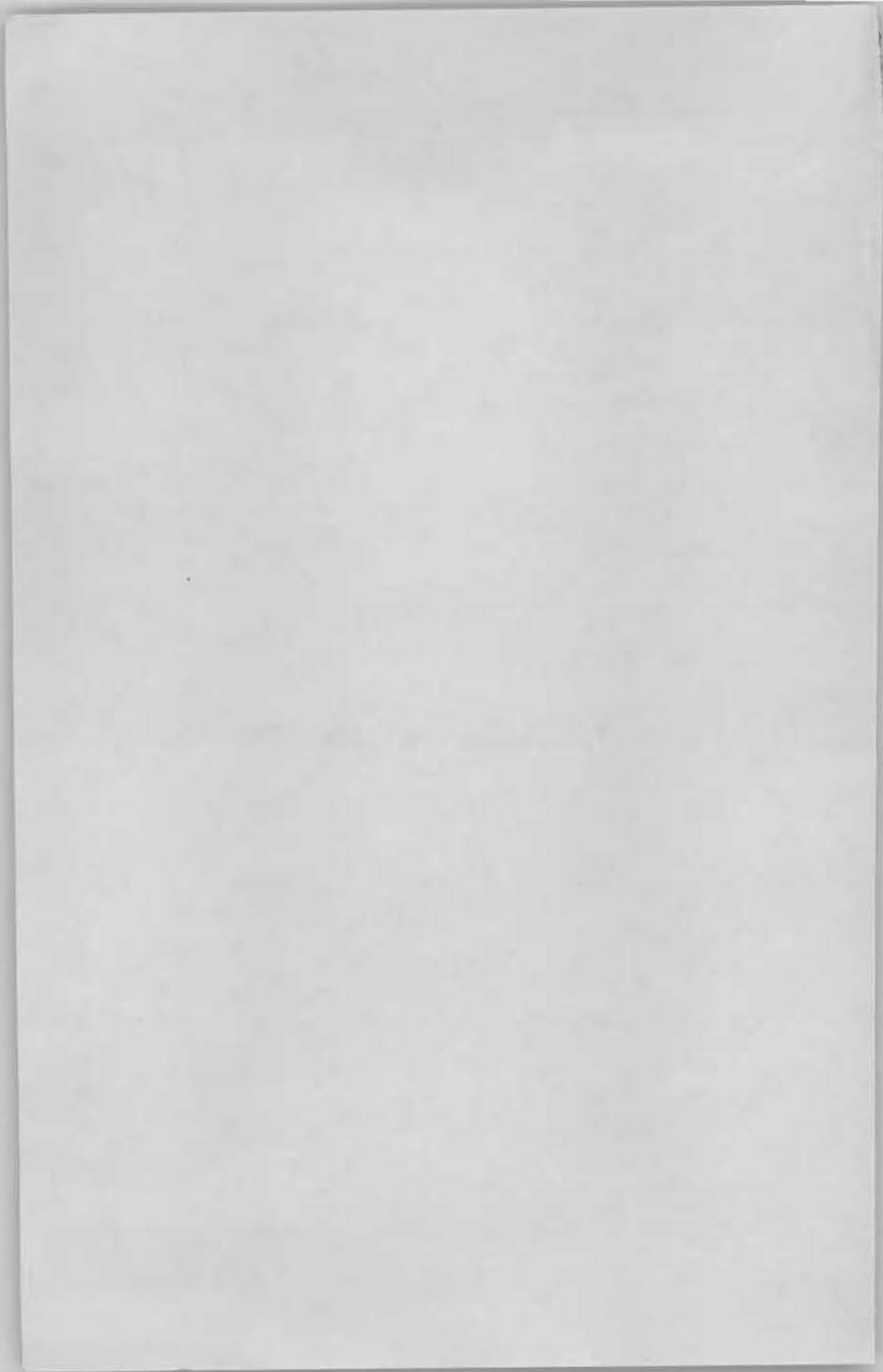
The third, adjusting the daily operation time of turbine sets. Prolonging the daily operation for power generation in winter is favorable to keep the continuity of flow discharge. Keeping the daily operation time uniform and steady can avoid the ice cover floating up and down as well as keep the discharge capacity of the river relatively stable. Generally speaking, it is specified that only one turbine set operation should be taken in winter and the time for power generation should be prolonged from 11.4 h to 17 h. Thus ice flood downstream may be alleviated correspondingly.

### CONCLUSION

In this paper, the ice flood effect at downstream river reach of reservoir after the reservoir put into service was studied with emphasis and some problems in the operation and regulation of the hydropower station were analysed. Furthermore, the preliminary results of reasonable optimization of reservoir regulation to reduce the ice flood damage are presented. These results have brought a lot of economic benefits when they were putting into practice.

**TOPIC G**

**MISCELLANEOUS**





## FROZEN GROUND FROM ARTIFICIAL GROUND FREEZING METHOD FOR THE ICE STORAGE AIR CONDITIONING SYSTEM

Jiang Du Hsin<sup>1</sup>, Chen Hao Hua<sup>1</sup>

### ABSTRACT

This project is a concept. Due to the large increasing of using ice storage air conditioning system it is able to save energy and exert the economical efficiency. But this system needs extra space for ice tank. Thus we propose to use artificial ground freezing method to freeze the underground soil for substituting ice tank. The frozen soil can also stop the leakage in the basement and increasing the bearing capacity. Because the frozen soil is icy and hard like a rock. It will stop the groundwater flow or change its direction. Another possibility is to stop the contaminated groundwater pollution and thus collecting them from an artificial underground reservoir formed by frozen soil. Although it is high power energy consumption. The air conditioning system will use only the off peak hour power to lower down the temperature of the frozen soil. So we can win the cost of the difference from the off peak power. The economic efficiency analysis will be study to show its feasibility.

### INTRODUCTION

Electrical power resources in Taiwan are nearly all imported. Recently the economic growth and natural disaster like earthquake and typhoon have caused power broken and shortage. But the environmental protection agencies place the highest conditions for the construction of new power plant. Thus the situation is even worse now. Further more, increasing power capacity is not an economic way of power operation. The equal consumption of power in the day and night can be a solution to cover the shortage of power and reduce the investment of power plant. The different cost of peak hour power consumption encourage the consumer to invest their facility to use off peak hour. Ice storage air conditioning system is one of the methods for saving cost. Its basic idea is using off peak hour power in the nighttime to freeze water into ice and melting the ice in the day time thus release cold energy to cool the air in the building. Because of the lower temperature in the night power consumption will be lesser than in the day time. So surplus energy have more in the night than the day time. Reducing hot air from the air conditioning system in the day time can low down the green house effect in the

---

<sup>1</sup> Feng Chia University, Taichung, Taiwan, No. 100 Wen Hwa Road, Taichung 407, Taiwan

city environment. The different price of power for day and night make an advantage for ice storage air conditioning system.

Ice storage system needs a place for ice tank. This paper present an idea using frozen ground to replace ice tank. It is not only saving a lot of space in the basement but also stop the leakage of groundwater to the cellar and strengthen the bearing capacity of the ground to the foundation. The way we do is just keeping frozen soil in frozen condition but fluctuating the frozen ground temperature to release the cold energy to cool down the building environment. All this process will use off peak hour power, which is in the night, to save the cost and solving the unequal power consumption problem for the power company.

#### **TYPE OF ICE STORAGE AIR CONDITIONING SYSTEM**

According to the method of cold storage form there are following way to do it:

1. Ice-on-coil: Direct freeze ice on coil. The advantage is quick release cold energy.
2. Total-freeze-up: Put the freeze tube in the freeze tank to freeze water. The advantage is simple piping system, easy operation and maintain cost.
3. Dynamic ice-maker: Sprinkling water on the refrigerant evaporator to form ice. Extract ice by sudden input warm refrigerant to drop the ice.
4. Ice ball: Pour water into plastic ball to form ice.
5. Crystal ice or Ice slurry: Freeze compound solvent to form ice slurry or crystal ice.
6. Eutectic salt: freeze at 8°C thus can be operated at existing chiller.

There is full and partial storage system for cooling load transfer. Full storage system will stop chiller operation during the daytime. The cool air is thus supplied by ice. This type is good for those big differences of cooling load transfer between the day and night.

#### **APPLICATION OF GROUND FREEZING METHOD TO ICE STORAGE AIR CONDITIONING SYSTEM**

Since ice storage air conditioning system needs an ice storage tank in the building to store cool energy for day time we can use frozen soil from the artificial ground freezing method to substitute ice tank. It has the following advantages:

1. The space in the building for ice tank can be reduced.
2. The foundation soil, after freezing, is hard like a rock thus increases its bearing capacity.
3. The groundwater will be frozen thus no leakage problem in the basement.

The disadvantage is the electrical consumption, ice heaving, isolation and the maintenance of the freeze tube. Thank to the ice storage system of air condition we use the same off peak hour electricity. Power cost are then reduced. It is even good for power company to have less investment on power plant. The capacity of chiller is also reduced and then equipment cost and basic electrical price are low down, too. Chiller working at off peak hour so the noise will be reduced during the working time. Quality of in door air condition will be better because the relative humidity is lower.

The solution of ice heaving and isolation for the building and maintenance of freeze tube can be shown in the Fig.1. As we know most of the high rise building needs slurry wall to retain soil. The deep foundation are piling or raft foundation inside the wall. Pile foundation are under footing. The freeze tube can be placed between the footing and nothing to disturb pile. For raft foundation the freeze pipe can be placed underneath. The freeze tube are placed in vertical direction. It can be easily hoist up to repair on the floor of basement and put it back. The height of basement is enough for the length of freeze tube. Around the frozen soil there is a layer of thermal isolation. It is used to isolate cool energy but also absorbing ice heaving force to protect the building. Depending on the material it used, the isolation layer can also considering as a absorption for damping earthquake force. The heaving force of ice will seal the leakage of groundwater into the cellar. The layer of soil for freezing can be removed and graded by sand to form a best frozen ground for cool storage. The frozen layer is thus a homogenous saturated water content sand layer.

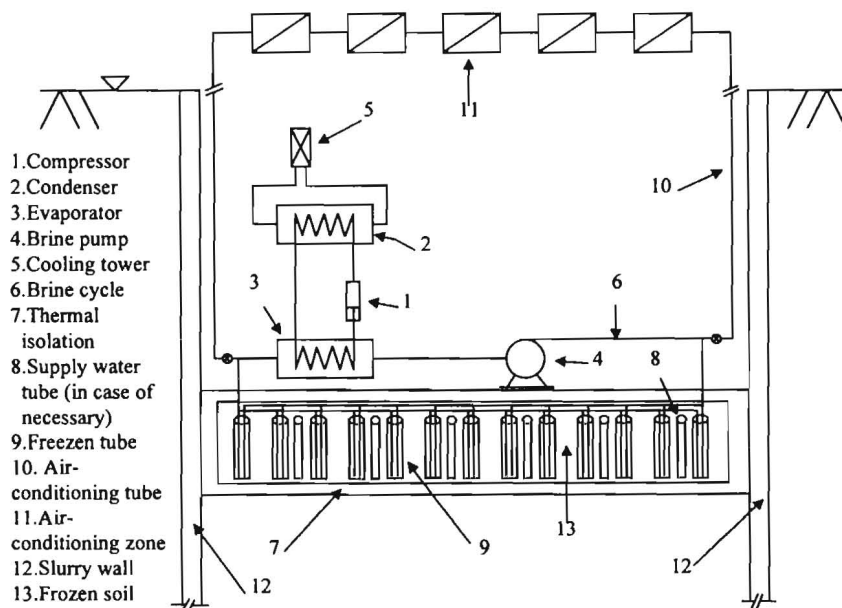


**Fig.1. Outline of an Artificial Ground Freezing Scheme for Ice Storage Air Conditioning System**

**CALCULATION OF FROZEN SOIL**

For the calculation of forming frozen soil the following formulas are used:

1. Time to form frozen layer:

$$t_f = \frac{L_0 E^2}{16K_f |T_0|} \left( 2 \ln \frac{E}{2r_0} - 1 + \frac{C_f |T_0|}{L_0} \right) \quad (1)$$

and

$$L_0 = L + 3.64 T_u C_u$$

where:  $L$ : Thermal consumption of  $1\text{m}^3$  soil from  $0^\circ\text{C}$  phase change

$C_u$ : Unit volume of thermal capacity of unfrozen soil

$C_f$ : Unit volume of thermal capacity of frozen soil

$E$ : Spacing of freeze pipe

$K_f$ : Thermal conductivity of frozen soil

$r_0$ : Radius of freeze tube

$T_0$ : Average temperature of freezing tube

$T_u$ : Temperature of unfrozen soil

2. Cool energy of ice layer of each time per m:

$$P = 2K_f |T_0'| \frac{1}{R} \quad (2)$$

and

$$T_0' = \frac{1}{2}(T_0 + T_0'')$$

where:  $R$ : Distance between  $0^\circ\text{C}$  frozen line and freeze tube after time  $t$

$T_0''$ : Temperature at line of freeze tube after frozen time  $t$

3. Released cool energy

$$H = V \cdot C_{vf} \cdot \Delta T \quad (3)$$

and

$$c_{vf} = \gamma_d \left( c_{ms} + \frac{c_{mi} \cdot w}{100} \right)$$

where:  $V$ : Volume of frozen soil

$\Delta T$ : Difference of Temperature

$c_{vf}$ : Mass heat capacity of frozen soil

$c_{ms}$ : Mass heat capacity of dry soil

$c_{mi}$ : Mass heat capacity of ice

$\gamma_d$ : Dry weight of soil

$w$ : Water content

### CASE STUDY

Let us take an office building in Taiwan as an example: The building has 10 floors above ground and two floors underneath. Each floor has  $1200\text{m}^2$  ( $30\text{m} \times 40\text{m}$ ). The total cooling load is 1480RT-hr. The electrical consumption is shown in Table 1.

**Table 1**

Electrical consumption of a Taiwanese Office Building

Classification				Summer season	Off summer
Electricity price in US \$	Basic charge	Demand charge	Each kW month	6.66	4.97
		Off hour charge	Each kW month	1.33	0.99
	Energy charge	Peak hour	Each kWh	0.061	0.059
		Off peak hour	Each kWh	0.024	0.022

Notes: 1: Time of off peak time: Monday to Friday 10:30 PM to 7:30 AM and weekend

2: Summer time: 1<sup>st</sup> of June to 30<sup>th</sup> of September

3: 25% more discount for off peak hour use of ice storage system

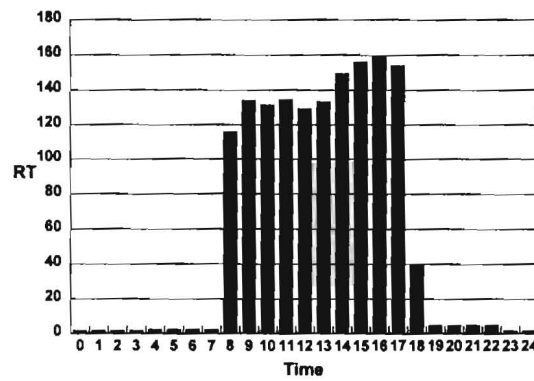


**Fig.2.** Histogram of Cool Energy Consumption per day for a Taiwanese Office Building

Following the formulas before we take the freeze tube diameter of 8.8 cm ( $3\frac{1}{2}$  ") and spacing of 1 m. The thickness of frozen soil layer is  $1\text{ m} \times \frac{\pi}{4} \cong 0.8\text{ m}$  take 1 m. The freeze time is 280hrs to form ice layer of -25°C. The cool energy of ice layer are 34 372 800 kcal. Released cool energy from -25°C to -10°C will be 7 351 327 kcal. For daily air condition requirement is in total 1480RT-hr = 4 913 600 kcal < 7 351 327 kcal. Which is sufficient.

To decide the volume of the ice storage tank for each required 1000 RT-hr of ice storage the necessary volume and its cost are listed in Table 2 & 3:

Comparison of establishing and total costs for different method of air conditioning system are listed in Table 4.

Further comparison for the rate of return with the method of pay back year is listed in Table 5.

**Table 2**  
Required Volume of Each 1000 RT-hr for Different Storage System

Type of system	Ice-on-Coil	Dynamic Ice-Maker	Crystal Ice	Ice Ball	Total-Freeze-UP	Eutectic Salt
Volume for each 1000RT-hr (m <sup>3</sup> )	85	85	70	50	50	120

Note: Actual quantity needs to multiple by 1.3~1.5

**Table 3**  
Initial cost for chiller and ice tank

Type of system	Unit	Tradition	Ice-on-Coil	Dynamic Ice-Maker	Total-Freeze-Up	Eutectic Salt	Artificial ground freezing method
Cost of chiller	\$/RT	312.5	343.8	1,121.5	312.5	312.5	375
Cost of ice tank	\$/RT-hr	0	68.8		87.5	118.8	0

**Table 4**  
Comparison of Total Initial Cost for Different Method of Air Condition

Method	Traditional Method	Ice Storage	Artificial ground freezing
Item of cost US\$			
1. Chiller	57,150	61,884	67,500
2. Electricity cost per year	79,197	23,039	23,039
3. Ice tank and rental cost of space	0	239,500	0
4. Freeze tube isolation and frozen soil	0	0	92,000

**Table 5**  
Comparison of rate of return

	Ice Storage	Artificial ground freezing
Initial cost(\$)	301,384	159,500
Operation cost(\$)	23,039	23,039
Saving cost of energy(\$)	56,158	56,158
Rate of return (year)	5.4	2.8

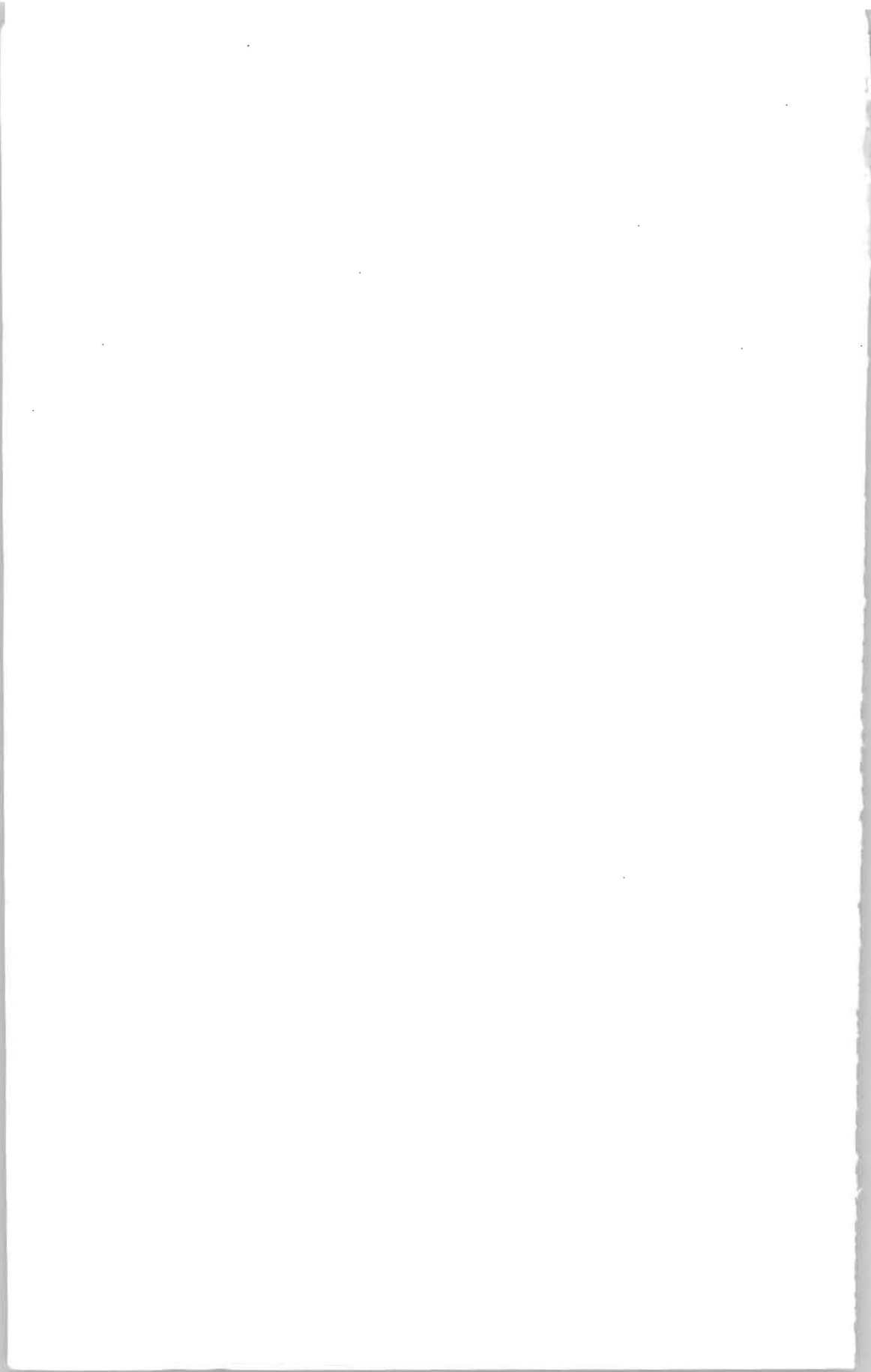
## **CONCLUSION**

Modern civil technology has no problem to build a frozen soil cold chamber underground for ice storage air condition system. The economic analysis shows that the rate of return is only 2.8 years. This is far more economic than other energy saving method.

Energy consumption is a weak point for artificial ground freezing method. In this case frozen soil not only solving the engineering problem during the foundation construction but also serve as an energy saving facility to cool the building. It can be another way to apply cold region technology. For instance, high toxic solid waste and radio active wastes can be saved to collect in this place without any further ground water pollution and disturbance.

## **REFERENCES**

- DINTER F., GEYER M., TAMME R.. (1991): Thermal Energy Storage for Commercial Applications. Springer-Verlag.
- JIANG D.H. (1988): Ground Freezing Method-Feasibility study for applying to the South Link Railway tunneling projects in Taiwan R.O.C.
- JUMIKIS A.R. (1977): Thermal Geotechnics. Rutgers University.
- LADANYI A. (1994): An Introduction to Frozen Ground Engineering. Chapman & Hall.
- YANG K. H. (1998): The Analysis of Thermal Energy Storage Air-Conditioning System. Chang-nien publishing company.
- YU XIANG, WANG CHANGSHENG (1992): Ground Freezing 91. A. A. Balkema.



56000 823-56000 830  
MP 5754 MP 5755

# 15th INTERNATIONAL SYMPOSIUM ON ICE

August 28 – September 1, 2000  
Gdańsk, Poland

## PROCEEDINGS

Volume II



Editor: W. Majewski



INSTITUTE OF HYDROENGINEERING  
POLISH ACADEMY OF SCIENCES  
GDAŃSK, POLAND

INTERNATIONAL ASSOCIATION  
OF HYDRAULIC ENGINEERING AND RESEARCH



Gdańsk, 2000

551.345  
IN 8 15<sup>th</sup>  
2000 v.2

**Published by The Institute of Hydroengineering,  
Polish Academy of Sciences (IBW PAN), Gdańsk, Poland**

Technical Editor: T. Jarzębińska

**This publication (Vol. I and II) has been prepared and printed  
with kind financial support  
of the Polish Committee for Scientific Research (KBN).**

**ISBN 83-85708-42-1**

Copyright © by the Authors unless otherwise stated, 2000.

The materials and information contained herein are published in the exact form submitted by authors. No attempt has been made to alter the material except where obvious errors or discrepancies were detected. Any statements or view presented are totally those of the authors and should not necessarily be taken as having the support of the Symposium Organizing or Scientific Committee.

This book is published on the understanding that the authors are solely responsible for the statement made and opinions expressed in it and that its publication does not necessarily imply that such statements and/or opinions are or reflect the views or opinions of the organizers or publishers.

Copies of the proceedings may be obtained from:  
Institute of Hydroengineering, Polish Academy of Sciences (IBW PAN)  
P.O.Box 61, 80-953 Gdańsk, Poland  
tel. +48 58 552 39 03  
fax: +48 58 552 42 11  
e-mail: [sekr@ibwpan.gda.pl](mailto:sekr@ibwpan.gda.pl)

Front cover designed by T. Jarzębińska  
Photo on the cover: Icebreakers on Włocławek reservoir (Lower Vistula River). Author: B. Pawłowski

Printed and bound in Poland by GRAFIX, Piastowska 70, 80-363 Gdańsk.

S-40074  
6/3/08

## PREFACE

15th International Symposium on Ice was held in Gdańsk from 28 August to 1 September 2000. This Symposium closed the period of 30 years of these important scientific and engineering events. First Symposium was organized in 1970 in Reykjavik, Iceland. 15th Symposium was organized by the Institute of Hydroengineering of the Polish Academy of Sciences in Gdańsk. The venue of the Symposium was the Center of Technical Society in Gdańsk (Dom Technika NOT), very close to the old city of Gdańsk.

Symposium was authorized by the Section of Ice Research and Engineering of the International Association of Hydraulic Engineering and Research (IAHR). Close collaboration was maintained with the Section during preparation and the organization of Symposium. Patronage of the Symposium was kindly accepted by Paweł Adamowicz, the Mayor of Gdańsk.

During Symposium broad social program was organized for participants and accompanying persons. It started with the visit to famous Artus Court where the Mayor of Gdańsk gave the reception. Visit to the old city of Gdańsk and walk along beautiful old streets was very much appreciated by the participants. The history of the development of Gdańsk Harbor was presented during boat excursion, which was terminated with the visit of Westerplatte, where the Second World War began. Visit to the famous Oliwa Cathedral together with organ concert and the walk through the famous Oliwa Park was an enjoyable event for Symposium participants. Accompanying persons had the opportunity to visit famous, for its natural beauty, Cashubian Lake District often called Cashubian Switzerland. Good weather accompanied all these events. Symposium dinner terminated the social program of the Symposium.

57 participants from 12 countries attended the Symposium. 52 papers were accepted for the presentation. 50 papers were published in Vol. I of the Proceedings, which was distributed to Symposium participants.

During Symposium the Third Ice Research and Engineering Award was handed to Prof. Mauri Määttänen from Helsinki University of Technology for his outstanding activity in Ice Research. Prof. Määttänen was the member of the Section on Ice Research and Engineering and previous chairman of the Section. He was also organizer of the 10th International Symposium on Ice in Espoo, Finland.

The Award for the best student paper received Knut V. Høyland from Trondheim Institute of Technology, Norway for the paper: *Measurements of consolidation in three first first-year ridges.*

Four invited lectures were presented during Symposium. Report of the Working Group: Under Ice Habitat was presented and discussed. They are included in Vol. II of the Proceedings. Vol. II includes also two late papers.

At the end of Symposium a panel discussion was organized to discuss the topic: Research needs in Ice Engineering. Elections of new members of the Section were completed. Prof. H.T. Shen from Clarkson University, USA has been elected as new Chairman of the Section. The activity of Working Groups has been also discussed.

On behalf of Organizing and Scientific Committees I would like to express thanks and appreciation to all participants for attending the Symposium. I would like also to thank all authors for preparation and presentation of the papers and invited lectures. Thanks are also to all those who actively participated in discussions.

As the chairman of the Organizing Committee I wish to express my appreciation to all members of the Organizing and Scientific Committees for their efforts in preparing and conducting of this Symposium.

Gdańsk, November 2000.

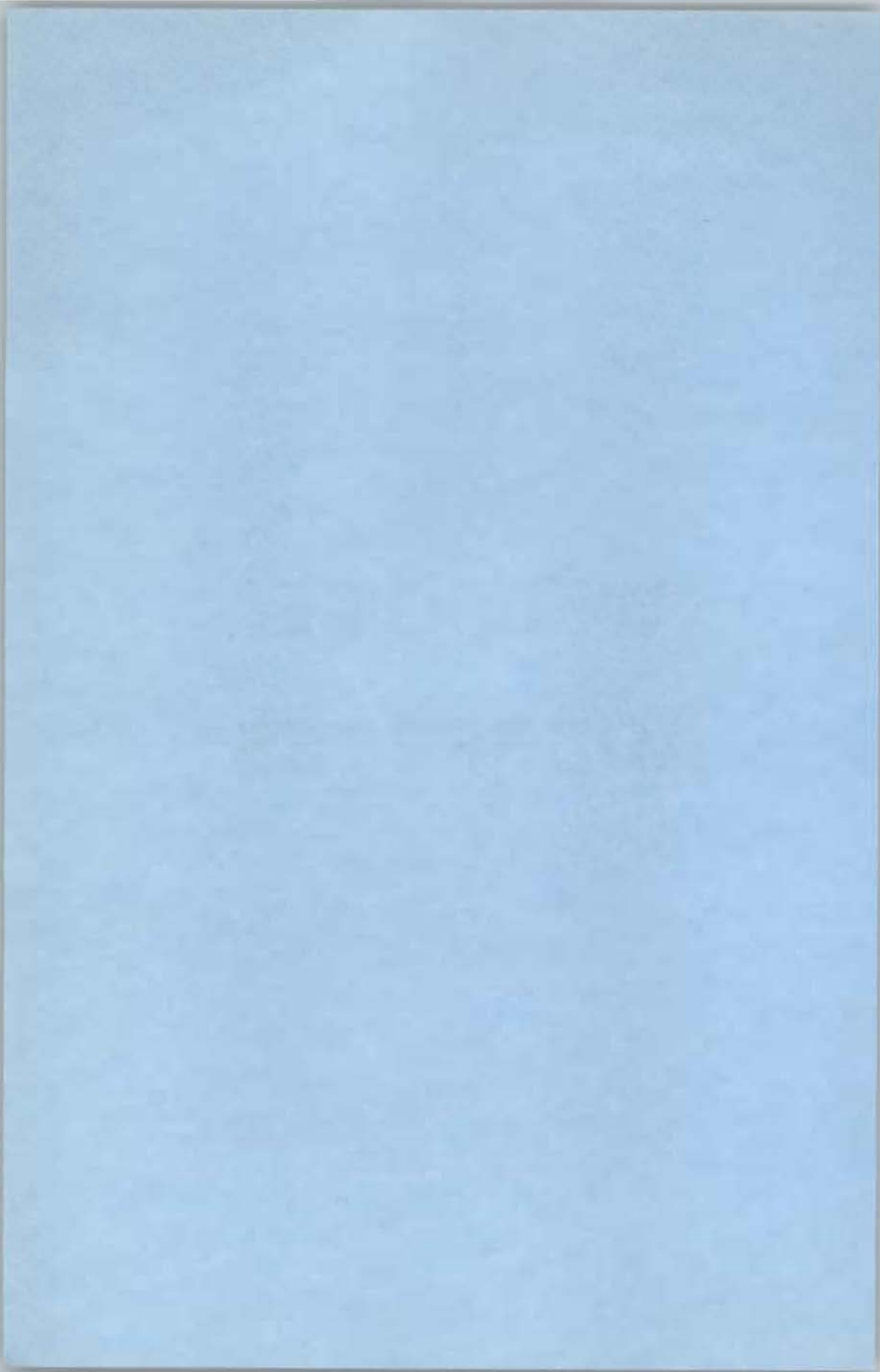
Prof. Wojciech Majewski  
Chairman of the Organizing Committee

## TABLE OF CONTENTS

<b><u>WELCOME ADDRESSES</u></b>	7
<b><u>INVITED LECTURES</u></b>	15
Wojciech Majewski <b>Poland, Gdańsk, Vistula River and Ice Problems</b>	17
Hung Tao Shen <b>River ice transport theories: past, present, and future</b>	29
Guenther E. Frankenstein <b>Thirty years of Ice Symposia</b>	41
Einar Tesaker <b>Some hydraulic aspects of fish life under ice</b>	57
<b><u>LATE PAPERS</u></b>	69
C. McKenzie, P.J. Langhorne, T.G. Haskell <b>Acoustic emission location and cracking in sea ice</b>	71
Andrew M. Tuthill <b>Managing ice at Corps of Engineers locks and dams; current solutions and future needs</b>	81
<b><u>WORKING GROUP REPORT</u></b>	91
<b><u>SUPPLEMENT</u></b>	105
Ice Research and Engineering Award	107
Student Paper Award	109
New Composition of the Committee of the Section on Ice Research and Engineering	111
Next International Symposia on Ice	111
Working Groups activity	112
Panel discussion: Research needs in Ice Research and Engineering	112
Statistics of previous 14 Ice Symposia	112
<i>List of participants of 15th International Symposium on Ice</i>	117



# **WELCOME ADDRESSES**



**Opening Address  
of the Chairman  
of the Organizing Committee**

**WOJCIECH MAJEWSKI**



**Mr. Paweł Adamowicz – Mayor of Gdańsk,  
Prof. Piotr Wilde - President of Gdańsk Branch of the Polish Academy of Sciences,  
Prof. Kenichi Hirayama - Chairman of the Section on Ice Research and Engineering,  
International Association of Hydraulic Engineering and Research,  
Distinguished Guests,  
Symposium Participants,  
Ladies and Gentlemen,**

It is my great pleasure and honor to welcome all of you in Gdańsk on behalf of the Organizing and Scientific Committees of the 15th International Symposium on Ice.

International Symposium on Ice is being organized for the first time in Poland. It is organized by the Institute of Hydroengineering of the Polish Academy of Sciences in Gdańsk. We are very proud that the Section of Ice Research and Engineering has chosen Gdańsk and our Institute for the organization of this Symposium.

Ice Symposia are organized since 1970 every two years. This Symposium is a kind of jubilee Symposium because it closes 30 years of this important scientific and engineering activity. Special invited lecture will give a review of past 14 Symposia, their achievements and also future research and engineering needs.

Participants of this Symposium come from 13 countries. Fifty papers and 4 invited lectures were prepared. Papers are published in Vol. I of the Proceedings. Invited lectures and some additional papers will appear after Symposium in Vol. II.

Organizing Committee has done all necessary preparations. We would like this Symposium to be an important scientific and engineering achievement, however, apart from scientific and engineering program we would like also to show you our beautiful city Gdańsk and picturesque Cashubian Lake District. We hope to have nice weather. We would like to acquaint you with the past history of Gdańsk. Important political, economical and social transformations began here in Gdańsk. There is a lot of information in booklets and brochures we provided you.

I wish all participants scientific and engineering successes and a very pleasant stay in Gdańsk. 15th International Symposium on Ice I declare opened.

Now I would like to ask Mr. Paweł Adamowicz – the Mayor of Gdańsk, who kindly accepted the patronage on this Symposium, to present opening address to Symposium Participants.

**Opening Address  
of the Mayor of the City of Gdańsk**

**PAWEŁ ADAMOWICZ**



**Ladies and Gentlemen,**

First of all I would like to welcome you most cordially in Gdańsk – the stronghold on Motława River.

It is a great honor and privilege for us to host the **15th International Symposium on Ice**. All the more so as Gdańsk has been chosen as the only city in Poland to hold such an important event.

Gdańsk is a city of rich Hanseatic tradition where the past and present smoothly combine and create its unique atmosphere so appreciated both by the citizens and all those coming to visit. Tolerant and open, it created the particular atmosphere of a western European civilization, in which a variety of economic factors and different customs and cultural trends of many nationalities and religions all played their part. Here Germans, Dutch, English, Scandinavian and French met and made their home.

The 1000-years old Gdańsk has always been a proud city ready to stand up for itself. It is here that the paths of history cross, where the World War II began and where communism was overthrown, where Solidarity Movement was launched giving birth to important social, political and economic changes thus introducing democracy in this part of Europe.

Gdańsk today is a forum for meeting of politicians and business people, for people associated with learning, science, culture and sport. Numerous international organizations choose our

city as the venue for their meetings thus strengthening its position not only on the map of Europe but also world-wide.

Ladies and Gentlemen, thank you for choosing Gdańsk as the venue for the conference. I do hope that the meeting will provide a great opportunity for you to exchange experience and challenges in ice research and engineering and the particular atmosphere of the city will let you enjoy your stay even more.

Thank you for your attention.

**Opening Address  
of the Chairman of the Section  
on Ice Research and Engineering  
of the International Association  
of Hydraulic Engineering  
and Research**

**KENICHI HIRAYAMA**



**Mr. Paweł Adamowicz, Mayor of Gdańsk,  
Prof. Piotr Wilde, President of the Gdańsk Branch of the Polish Academy of Sciences,  
Prof. Wojciech Majewski, Chairman of the Organizing Committee,  
Distinguished Guests,  
Ladies and Gentlemen,**

On behalf of the Committee of the Section of Ice Research and Engineering, International Association of Hydraulic Engineering and Research, it is a great honor to welcome you all to this Ice Symposium in Gdańsk.

The IAHR Section of Ice Problems was established in 1959 at Montreal Congress, and the third Symposium was held in Budapest, Hungary in 1974. Therefore the Symposium returned to the Central European country after 27 years absence. And this is the last Symposium in 20<sup>th</sup> century.

First of all, on behalf of Section Committee members and all participants, I would like to express sincere thanks to the host, Institute of Hydroengineering, Polish Academy of Sciences and the City of Gdańsk for inviting us to this beautiful city with more than 1000 year history.

Especially I would like to thank Prof. Majewski and his colleagues, who spent hard time to prepare the Symposium. When I visited Gdańsk last summer, Prof. Majewski was sitting on a wheel chair. It was soon after his serious medical operation. I celebrate his perfect recovery at

present and it is truly his strong sense of responsibility that made this opening ceremony possible with perfect preparations.

Our Section of Ice Research and Engineering has come a long way to achieve tremendous works in the field of ice research and engineering. We have published 1238 papers from 23 countries in the past 14 symposia. We started our big concerns to prevent hazardous ice jamming, to increase the efficiency of ice control structures, and to attain the safety of winter navigation. And in the seventies, with finding of huge oil reserves in the arctic, the emphasis of the research moved to the ice force on structures, which are constructed in the ice infested water. Research on the basic properties of ice itself and ice processes have been remaining as the basic problems, which have to be clarified before we start thinking about ice problems caused by human activities.

Recently environmental and ecological effects of ice become new attractive field of research. Important topics are effects of global climate change on ice regime of rivers, lakes and reservoirs. Diffusion and dispersion of pollutants under ice covered streams, oil spill in ice infested water, impact of ice on stream ecology and habitat become significant issues.

These are all important topics for human activities to accommodate with existing nature, which is very sensitive and has to be maintained as long, and as much possible.

In Sapporo Symposium in 1988, Dr Frankenstein mentioned in the opening ceremony that field experience never be replaced by computer modeling. It is also my experience from the University of Iowa and CRREL test basin. Though our field of research now became broader, it is still our basic research attitude to join field experiments and to repeat the experiments to understand the phenomena well. Theory and computer modeling alone will not produce a good solution to our problems.

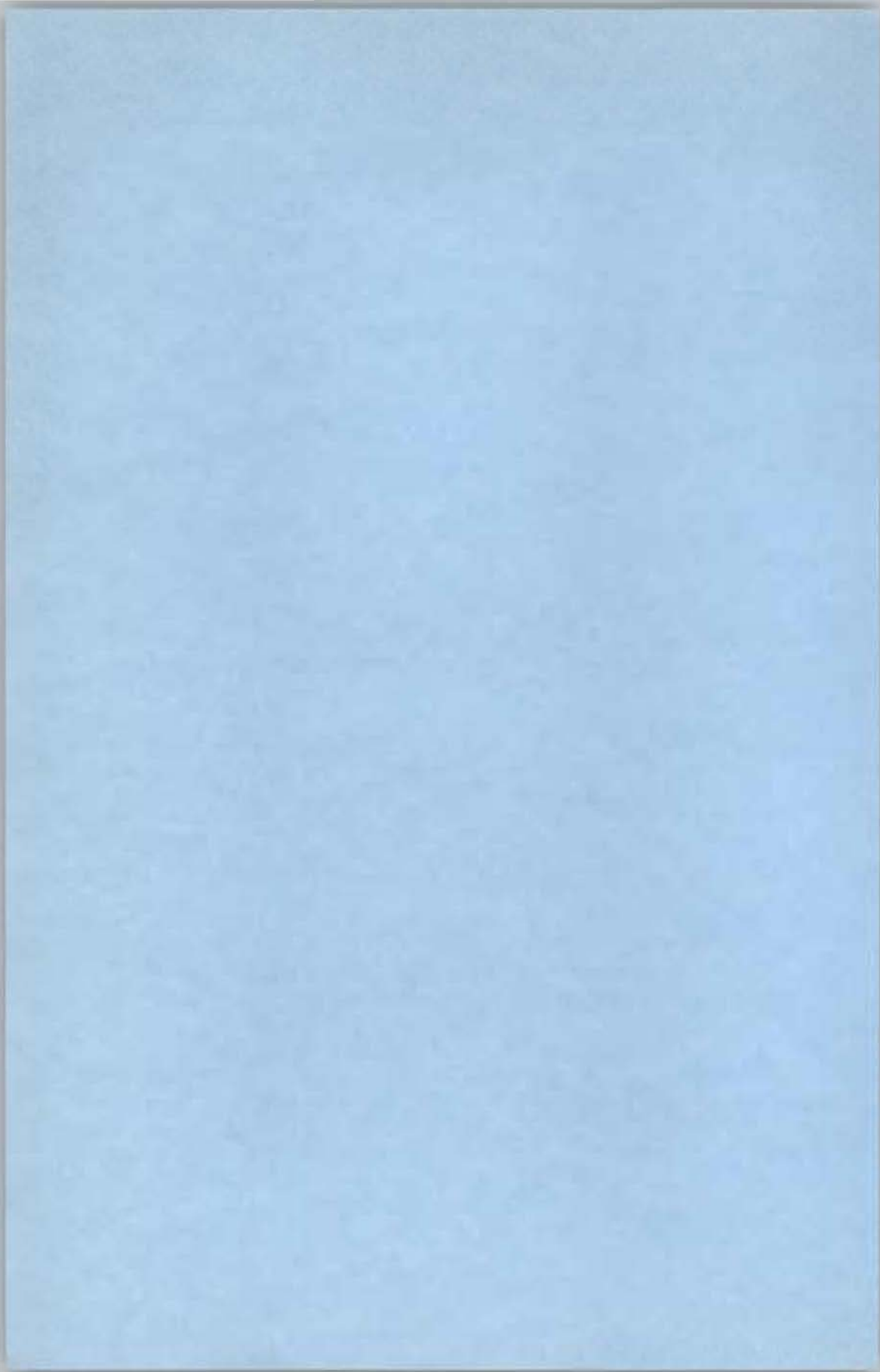
Today financial support for our research in many countries is very much restricted, and therefore we have to choose the cheapest approach to the solution. It is really a time to collaborate with other international scientific societies and to work together among industry, university, and government institution beyond the barrier of countries. This cooperation is so important if you want to make the maximum progress. In this sense, workshop on River Ice organized by Canadian people is a good example of worldwide cooperation.

Among many other meetings on ice, it is our duty to maintain the high scientific quality and close international communication of this Symposium. I hope participants will have much success in their contributions during this Symposium.

Let us start the Symposium, so that you leave Gdańsk having gained more intelligence and having deepened friendship.

Thank you.

# **INVITED LECTURES**





## POLAND, GDAŃSK, VISTULA RIVER AND ICE PROBLEMS

Wojciech Majewski<sup>1</sup>

### ABSTRACT

The paper presents general information about Poland and the city of Gdańsk, which is the venue of the International Symposium on Ice. Gdańsk, is a very important industrial, cultural, economic and scientific center in the northern Poland. It has been always closely connected with Vistula River, which discharges here to the Baltic Sea. There have been numerous benefits resulting from this situation, but also very often the city was flooded thus bringing significant economic losses. Vistula is the largest Polish River. Its catchment occupies more than 50% of the country territory and its length exceeds one thousand kilometers. Various forms of ice predominantly caused floods on the Lower Vistula.

### POLAND

Poland - full name: Republic of Poland, is situated in Central Europe. The neighboring countries are: Germany, Czech Republic, Slovak Republic, Ukraine, Belarus, Lithuania, and Russian Federation. Poland has more than 400 km long access to the Baltic Sea with important harbors Gdańsk-Gdynia and Szczecin-Świnoujście. Location of Poland on the European continent, which extends from Atlantic Ocean and Portugal in the west to the range of Ural Mountains in the East, is shown in Fig.1.

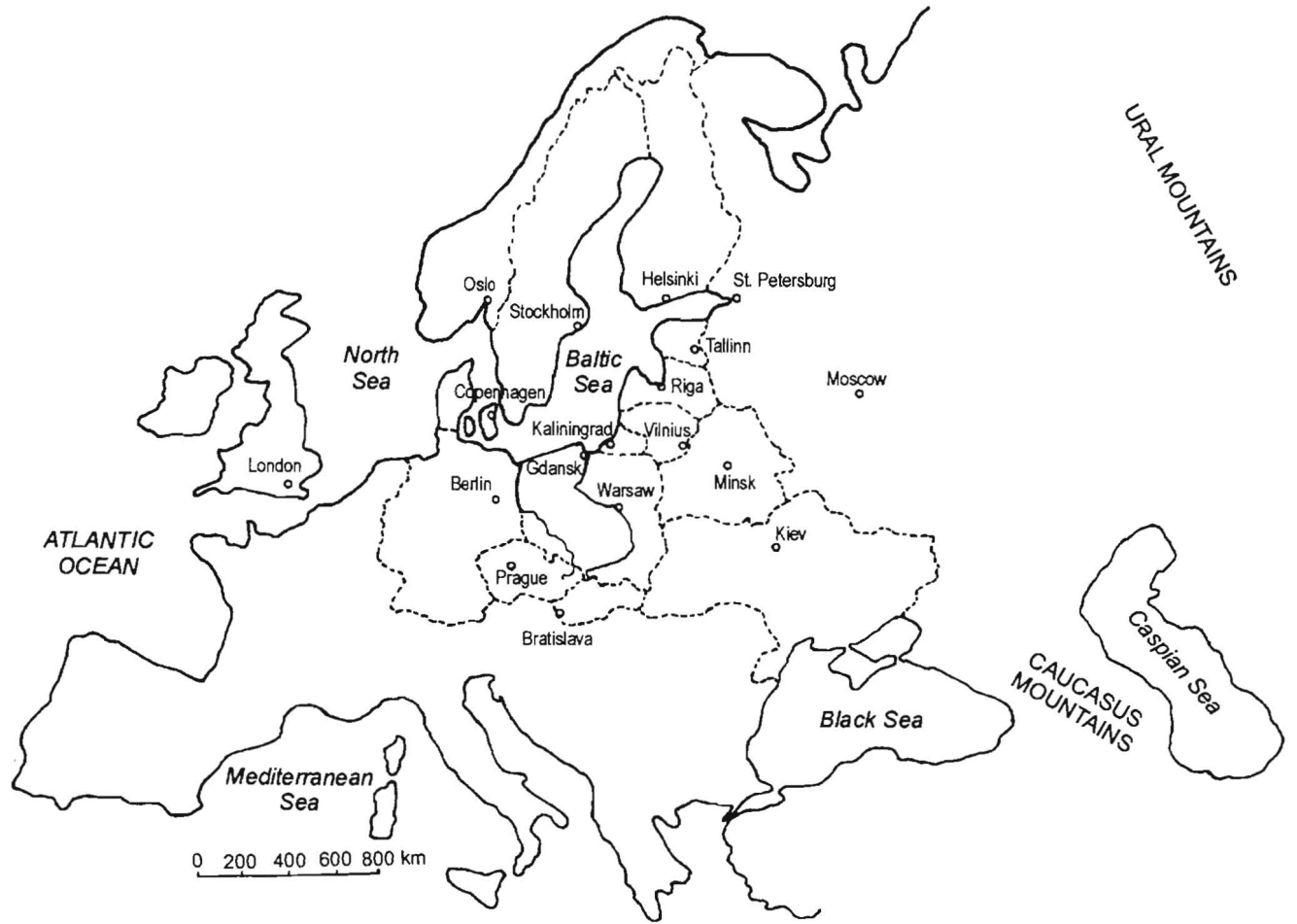
Population of Poland amounts to 38.6 mln people and the surface area of the country is 312.7 thousands square kilometers. This gives the population density of 123 inhabitants per square kilometer.

Because of important excess of Poland to the Baltic Sea there is significant collaboration with other Baltic countries: Germany, Denmark, Sweden, Finland, Estonia, Latvia, Lithuania, and the Russian Federation. The predominant problem of the collaboration is the quality of water in the Baltic Sea and the reduction of wastes discharged to the Baltic through the rivers. Several agreements and conventions have been signed in the past aiming in the achievement of the main goal - good quality of sea water.

---

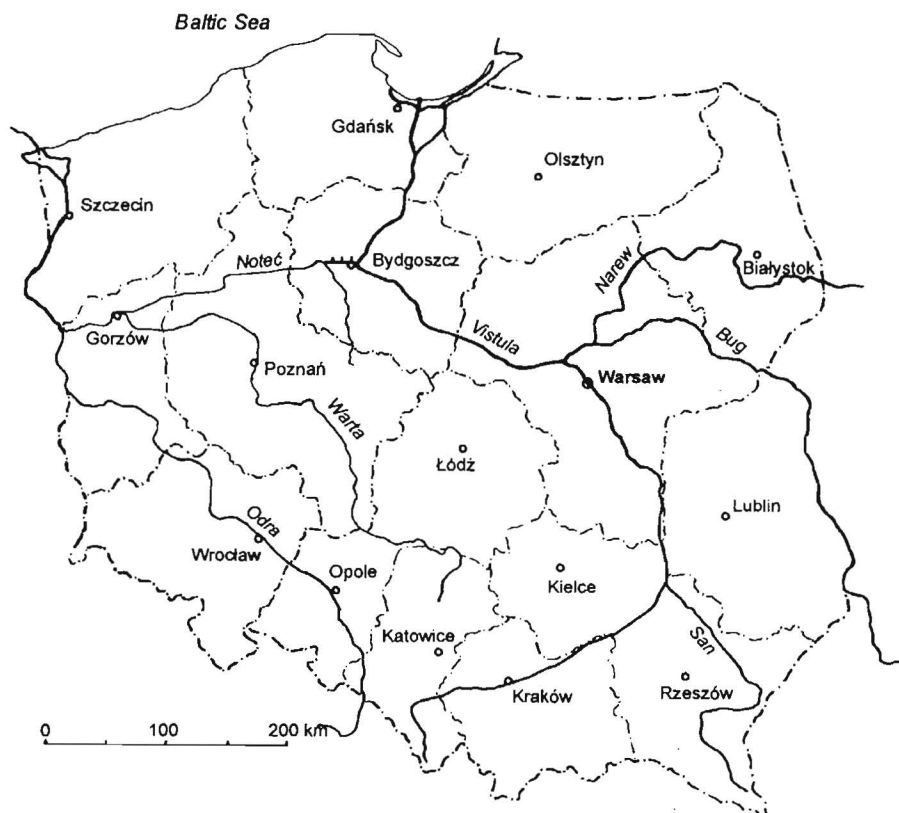
<sup>1</sup> Institute of Hydroengineering of the Polish Academy of Sciences, Gdańsk, Poland, Kościarska 7,  
80-953 Gdańsk, Poland, Tel.+48-58-552 3903, fax: +48-58-552 4211 e-mail: [wmaj@ibwpan.gda.pl](mailto:wmaj@ibwpan.gda.pl)

Fig.1. Europe and the location of Poland



Poland has a very long history and tradition. In this century we celebrated the millennium of the existence. Some important recent events concerning the whole country started in Gdańsk. In 1980 the Solidarity movement which had its beginning in Gdańsk shipyard started important social, political and economical changes. In 1990 these changes became a reality. In Gdańsk and in fact on a small piece of land, called Westerplatte where Polish military depot was situated, in 1939 the Second World War broke out.

Poland is a democratic country, which recently became the member of **NATO** and now continues its efforts to become the member of European Union. Administrative system in Poland, recently introduced, divides the whole country into 16 provinces (voivodeships), 373 districts, and 2498 communes.



**Fig.2.** Administrative division of Poland

Administration of water resources in Poland is based on the river basin system. The country has four hydrographic systems: Vistula, Odra, Rivers discharging directly to the Baltic Sea, and rivers contributing to large European Rivers - Elbe, Danube, Dniestr and Niemen. The territory of Poland is divided into 7 Regional Boards of Water Resources. Three of them (Kraków, Warsaw and Gdańsk) include the Vistula catchment, and other three (Wrocław, Poznań and Szczecin) the catchment of Odra. The seventh Board (Gliwice) occupies rather small system of industrial and urbanized area, but very important from water resources management point of view, part of the country - Silesia. This board includes part of the upper Vistula and upper Odra catchments. Poland has very limited water resources per capita, one of the smallest in Europe. They amount to 1600 m<sup>3</sup> per capita in hydrologically average year. This amount is nearly three times smaller than European average, and four times smaller than the world average. Water resources management is one of the most important sectors of national economy. It is within the Ministry of Environment. Present economic situation of Poland may be defined by the gross domestic product per capita (**GDP**), which for 1997 was 3590 USD. Administrative division of Poland into 16 provinces is shown in Fig.2.

### **GDAŃSK**

Gdańsk is a very old city with a very rich historical background. In 1997 Gdańsk celebrated its millennium. For many centuries Gdańsk played a very important economical, social, political and cultural role. It was one of famous hanseatic cities. Through the harbor of Gdańsk the export of goods from Poland was transferred to the whole Europe. These were mainly agricultural products but also timber, salt and sulfur. One of the luxury goods was amber. During 20 years between World Wars Gdańsk was a Free City, however, with strong influence of Germany. In the morning of 1 September the Second World War started here.

Now it is not possible to consider Gdańsk as a separate unit. It forms so-called Three-City together with Gdynia (250 thousands inhabitants) - important harbor with shipyard, and Sopot - famous summer resort (70 thousands inhabitants) situated between these two larger cities.

Gdańsk with 460 thousands of inhabitants is a very important industrial, scientific, cultural and economic center of Poland and the capital of Pomeranian Province. Forty thousands students study in Gdańsk at the Technical University of Gdańsk, University, Medical University, Academy of Fine Arts, Academy of Music, and Academy of Physical Education. There are also Research Institutes of the Polish Academy of Sciences and Institutes belonging to various ministries. Gdańsk has very good theatre, Philharmonic Orchestra, Opera and several museums.

Gdańsk was in the past and is now very well-known for its harbor and many shipyards. Nowadays, however, Gdańsk changes its main strategy from industry into trade and services. The city has very important and well-developed collaboration with many other harbors located at the Baltic Sea in various Baltic countries. Gdańsk is a very important crossing of the roads between east and west as well as between north and south.

A very important role in the development of Gdańsk played the harbor where goods from the whole Poland coming to Gdańsk by Vistula River were exported abroad, and where the imported goods were unloaded. The first harbor was situated on the banks of Motława, the tributary of Vistula. This first harbor together with most important buildings and hotels in the main city of Gdańsk is shown in Fig.3.

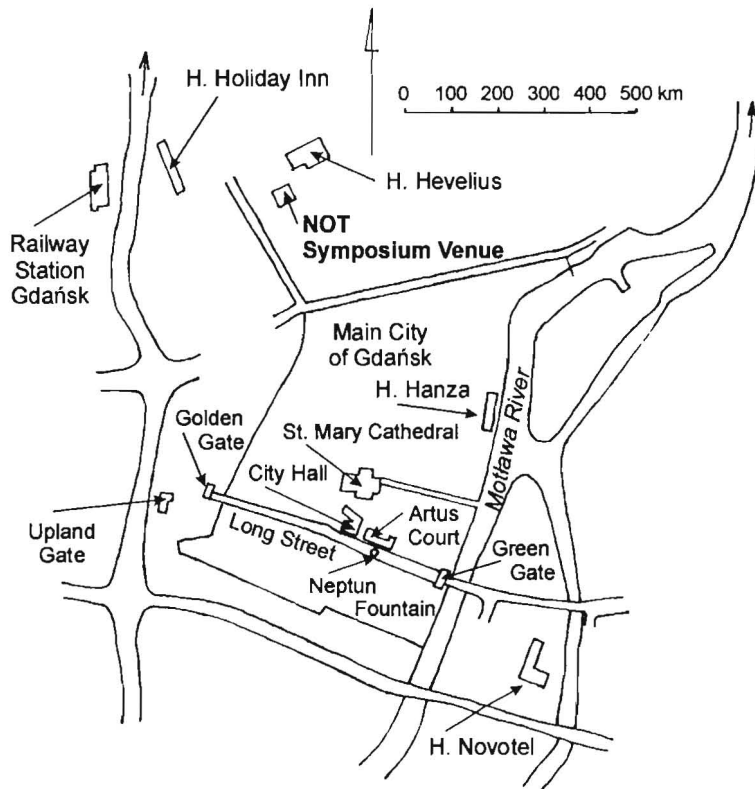


**Fig.3.** Main city of Gdańsk and the old harbor

When with time the ships grew larger and larger the water depths on the Motława River were not sufficient and the harbor moved gradually to Vistula River. Large shipyards developed on the branch of Vistula. This part of the main channel of Vistula became in 1895 Dead Vistula when the new channel of Vistula River was formed discharging its waters directly to the sea. This situation is shown in Fig.4.

This situation lasted until the sixties of the present century. For large ships transporting coal and oil the entrance to Gdańsk harbor through the winding channel of Vistula became unacceptable and it has been decided to build completely new harbor with direct access from

the sea. This way the North Harbor was constructed. Hydraulic model tests of this harbor layout were carried out in the Institute of Hydroengineering on specially constructed new open-air hydraulic laboratory in Oliwa. The layout of the North Harbor together with Westerplatte and the old Fortress Wisłoujście is shown in Fig.5. Now the main function of North Harbor is export of coal and import of oil. The area of Westerplatte, with the monument commemorating the Polish soldiers who were fighting on many fronts during the Second World War, is now place where many tourists visiting Gdańsk come every year.

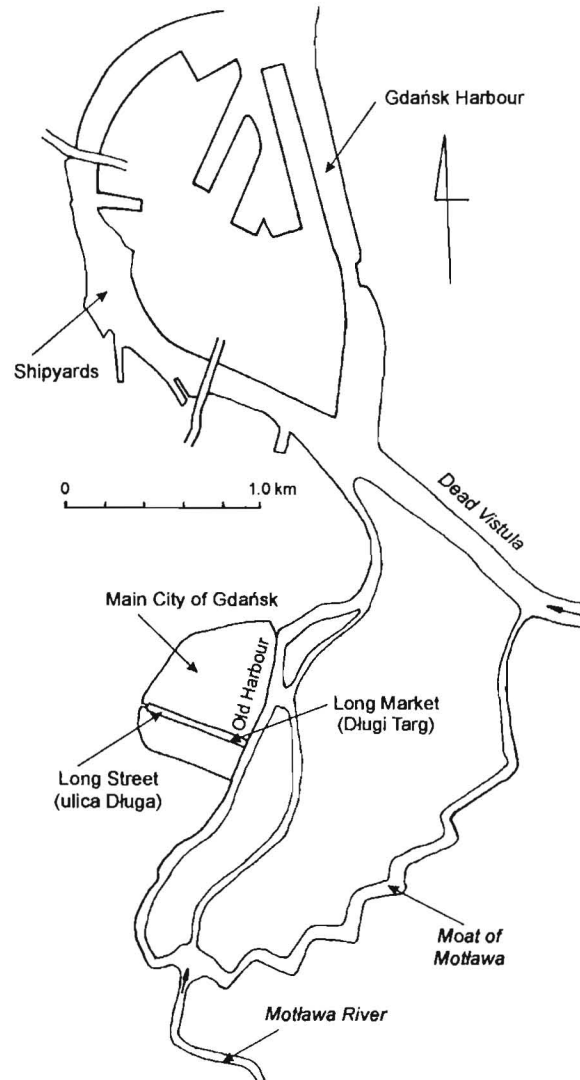


Fig.4. Harbor of Gdańsk and shipyards along Dead Vistula

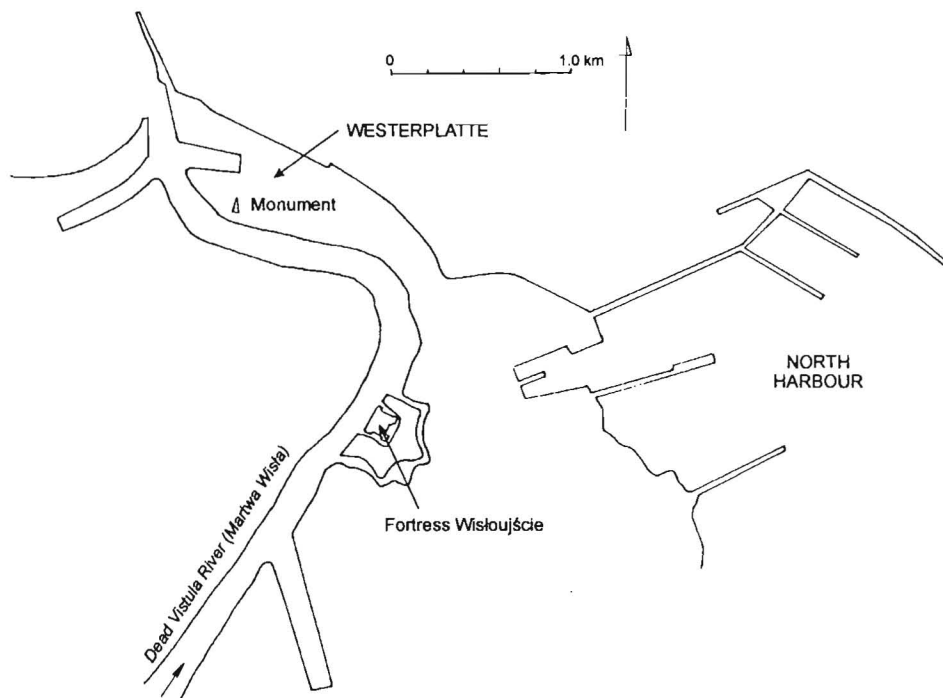


Fig.5. The layout of North Harbor

#### VISTULA RIVER

Vistula is the largest Polish river flowing from south in the northern direction. The total length of the river is 1068 km. 941 km of the river (from Przemsza tributary to the sea) is considered as navigable. The first 127 km of the river is called Small Vistula. Vistula discharges to the Baltic Sea and is the second largest river (after Neva) of the Baltic Sea basin. Vistula supplies about 6% of fresh water to the Baltic. Total river catchment is 193 911 km<sup>2</sup> of which 87% (168 700 km<sup>2</sup>) is within Polish boundaries. The catchment of Vistula River occupies 54% of the Polish territory. Annual outflow of Vistula in an average hydrological year amounts to 34.0 km<sup>3</sup>, while minimum and maximum annual outflows are 20.5 (in 1954) and 50.8 km<sup>3</sup> (in 1981) respectively. These data are from 1951-90 observations of the Institute for Meteorology and Water Resources Management. The average discharge of Vistula to the Baltic amounts to 1080 m<sup>3</sup>/s, while minimum and maximum discharges are 253 m<sup>3</sup>/s (December 1962) and 7840 m<sup>3</sup>/s (June 1962) respectively. Calculated Q<sub>1%</sub> discharge is 9190 m<sup>3</sup>/s.

In the XVII century Vistula was one of the most developed for navigation rivers in Europe. Partition of Poland in XVIII an XIX century and in consequence division of the river into 3 parts caused the decline of river importance, while other European rivers were developing

rapidly for navigation, hydroenergy and water supply. Now the main functions of Vistula are water supply and sewage discharges.

From hydrographic point of view Vistula is divided into three parts. Upper Vistula 280 km long from Przemsza tributary to San tributary. This part includes all mountain tributaries having high flood potential. It results from high precipitation rates and high surface runoff. Middle Vistula 270 km long extends from the San tributary to Narew tributary. This river section has the largest catchment area. The main water inflow comes from rivers Bug and Narew. The longest Vistula section is Lower Vistula 391 km long. It has the smallest catchment, which has no significant influence on Vistula discharges. Lower Vistula has very high hydroenergy potential - approximately 1/3 of the total hydroenergy potential of Poland. Lower Vistula hydroenergy potential, technically feasible is estimated for 4200 GWh in an average hydrological year. Most of the Lower Vistula can be utilized for navigation. Division of the Vistula catchment is shown in Fig.6.

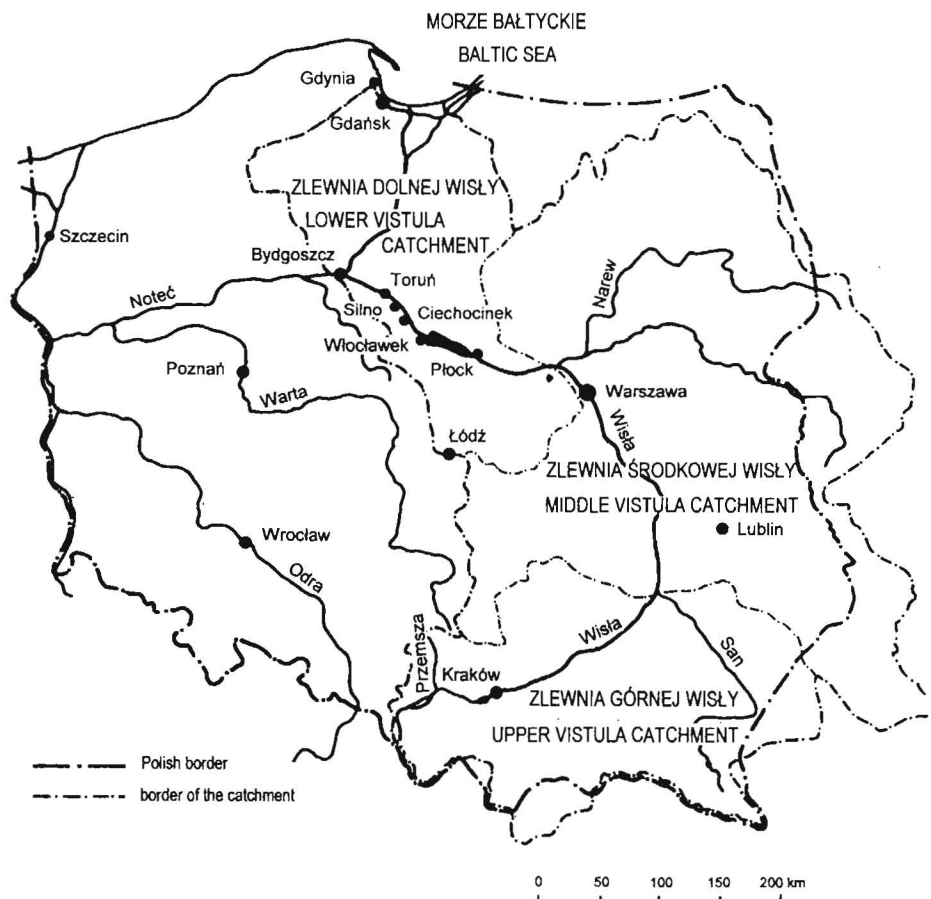


Fig.6. Catchment of Vistula River

The final section of the Lower Vistula 54 km long has been completely changed when in 1895 the new river channel of Vistula River directing its water straight to the Baltic has been developed. The side arms of Vistula (Nogat, Szkarpa, and Gdańsk Vistula) have been cut off by means of navigation locks. This important engineering project was carried out to decrease numerous floods caused by ice jams, which resulted in severe inundation every two to three years. Since the construction of new Vistula channel to the sea, that is more than 100 years, no flood appeared in this area. Certain disadvantages appeared, when as the result of river channel shortening and thus increased erosion and sediment transport, in the form of sedimentation cone at the end of river channel. Now this sedimentation cone has the length of more than 2 km extending into the Bay of Gdańsk. This area represents lowland and about 30% of it is below sea level. In case of flood this will cause very dangerous situation. This area is called Żuławy. The whole river system is shown in Fig.7.

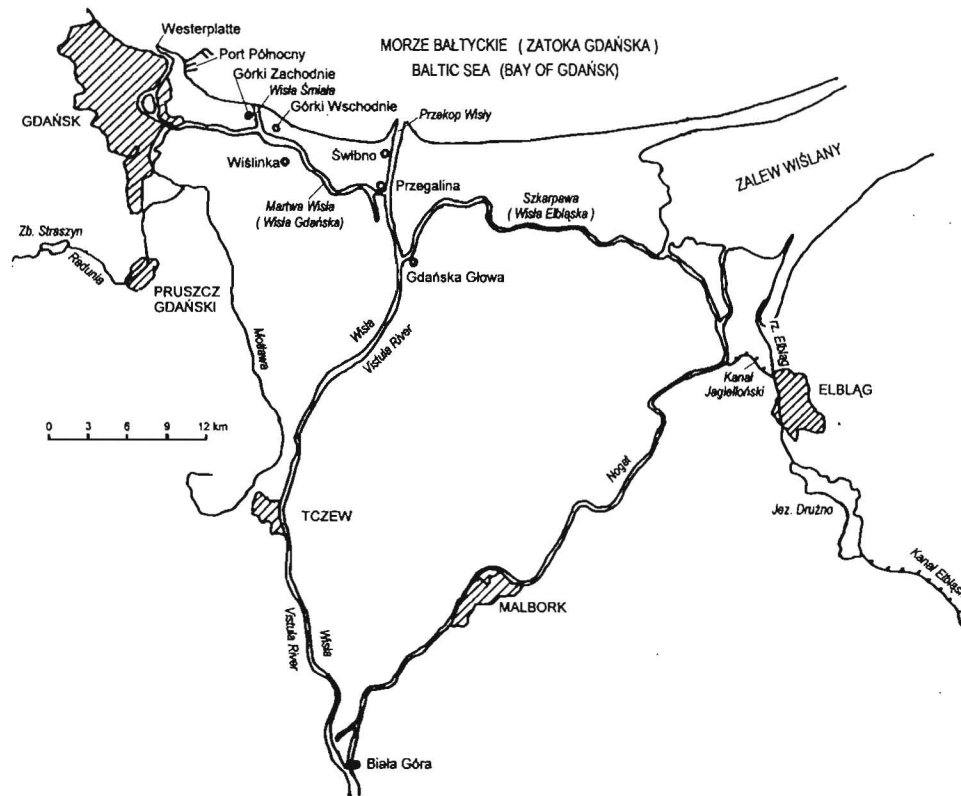


Fig.7. Final section of Vistula River

### ICE PROBLEMS ON THE LOWER VISTULA

Vistula River and especially its lower section always presented many problem connected with ice cover formation and ice run. The first and very important feature of Vistula is that it flows from south to north. When in the south ice breaks up and should be transported downstream, the northern part is still frozen. Artificial channel in the river for discharging ice can be formed by means of icebreakers. There is, however, problem of sufficient water depth for the operation of icebreakers, which in natural river is usually too small. Very often icebreaking could not be completed because of this reason. The problem of ice jams forming in spring during ice run was very severe in the estuarine part of Vistula. Complicated layout of river channels together with increased water elevations in Baltic Sea resulted in many severe ice jams which caused inundation of large areas of Żuławy and also bringing threat to the city of Gdańsk. In 1840 large ice jam on the Gdańsk Vistula resulted in the breach of sand dunes along the sea coast and formed new outlet for Vistula called Bold Vistula (Wisła Śmiała) - Fig.7. Construction of the new artificial outlet for Vistula River radically solved the problem of ice jams in this area. In many cities along the Lower Vistula the marks of high flood water indicate that these water stages appeared during winter months, not necessarily during high discharges, but they were caused by blocking of river channel cross-section with frazil ice, floats, frazil pans or frazil slush. It has been found that good solution is the use of icebreakers, but they require sufficient water depth for operation.

The most severe winter flood was in 1982 on the Włocławek reservoir which was caused by the coincidence of very unfavorable hydrological and meteorological conditions. This reservoir extends over about 40 km between two large cities on the Lower Vistula - Włocławek and Płock. Flood occurred during relatively low discharge for this river section i.e. 3900 m<sup>3</sup>/s. Details of this flood which caused inundation of large terrains on the left Vistula bank in the region of Płock will be presented in the paper RIVER ICE PROBLEMS ON THE LOWER VISTULA. During this flood due to breaching of side dams in 7 places 10 000 ha of land were inundated and 2230 farms were flooded. Considerable economic losses were caused by the flood. Fortunately there were no human losses.

### REFERENCES

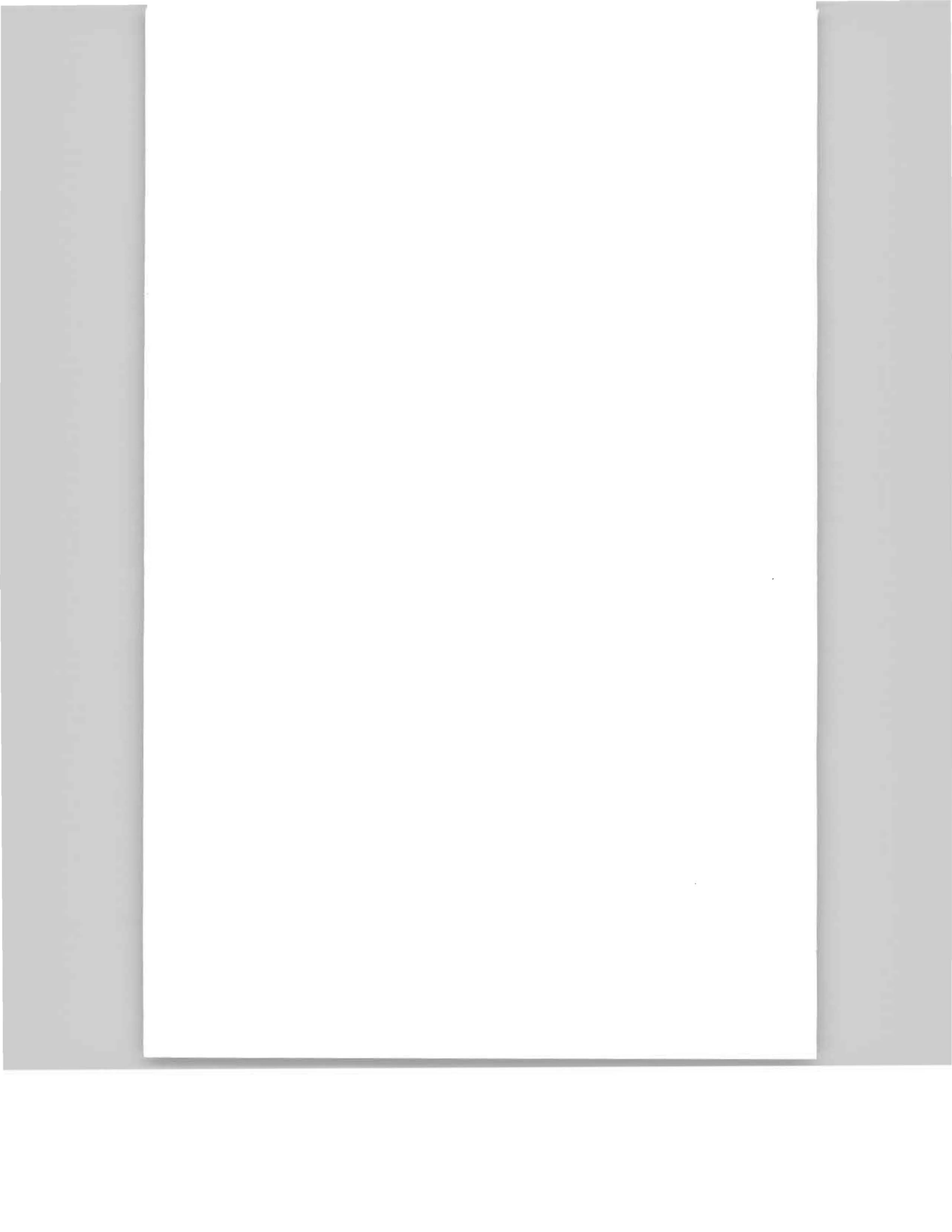
- GRZEŚ M., MAJEWSKI W. (2000): River ice problems on the Lower Vistula. Proceedings: 15th International Symposium on Ice, Gdańsk, Vol. I. pp. 97-104.
- JARZĘBIŃSKA T., MAJEWSKI W. (1996): Water Resources and the Management of Vistula River. In: Inland and Maritime Navigation and Coastal Problems in Poland - Selected Contributions. Technical University of Gdańsk, Marine Civil Engineering Department, Gdańsk, Poland, pp. 11-24.
- MAJEWSKI W. (1984): Backwater profiles on hydroelectric reservoir with ice cover. Proceedings: 7th International Symposium on Ice, Hamburg, Vol. I.
- MAJEWSKI W. (1990): River ice hydraulics (invited lecture). Proceedings: 10th International Symposium on Ice, Espoo, Finland, Vol. 3.

## WOJCIECH MAJEWSKI



Dr Hab. Wojciech Majewski is a Professor of Hydraulic and Environmental Engineering and Water Resources Management. At present he is the director of the Institute of Hydroengineering of the Polish Academy of Sciences in Gdańsk. For many years he has been employed at the Gdańsk Technical University, teaching river hydraulics, environmental engineering and water resources management. He has been active for several years in river ice hydraulics presenting many papers and actively participating in the organization of the Section on Ice Research and Engineering of IAHR. Prof. Majewski published more than 200 scientific and technical papers in various realms of river hydraulics and water resources management. He was supervisor of many diploma (Master Engineer) and doctor of technical sciences

thesis. He received many scientific and engineering awards from the Polish Academy of Sciences and Technical Universities. Prof. Majewski served on several national and international scientific and engineering committees. He is the Chief Editor of the Hydroengineering Proceedings of the Institute of Hydroengineering in Gdańsk. He was Chairman of the Section on Ice Research and Engineering in 1988 – 92.





**RIVER ICE TRANSPORT THEORIES:  
PAST, PRESENT, AND FUTURE**

**Hung Tao Shen<sup>1</sup>**

**ABSTRACT**

Understanding the river ice transport phenomena is one of the most important aspects of river ice engineering. River ice transport processes, such as the transport of thermal energy, formation and evolution of frazil ice, undercover transport of frazil granules, and surface ice transport and jam formation, affect ice conditions through out the entire winter. In this paper, theories on river ice transport will be reviewed. Future research needs to improve the current state of knowledge will be discussed.

**INTRODUCTION**

Many river ice phenomena are governed by transport processes. These phenomena occur during different stages of the river ice evolution, encompassing the entire winter ice season from freeze up to breakup, as shown in Fig.1. They play important roles in the changing river ice condition in relation to engineering, environmental, and ecological problems. The river ice transport phenomena, which involve mechanical and thermal processes, and phase changes, are much more complicated than other river transport phenomena, such as sediment or pollutant transport. Significant advances have been made in the last couple decades on river ice transport theories along with the development of the analytical framework for mathematical modeling of river ice processes (Shen, 1996). In this paper, theories on major river ice transport processes, including the transport and evolution of thermal energy and frazil ice, the formation of anchor ice on channel bed, the transport and accumulation of frazil granules on the underside of the ice cover and the associated frazil jam (hanging dam) formation, and the transport of surface ice and the associated surface ice jams formation will be discussed. Lal and Shen (1989, 1991) introduced a two-layer analytical framework for modeling river ice processes. The refined formulation by Shen et al. (1995) will be used here to facilitate the discussion. This one-dimensional formulation, which include all the major ice transport processes and can easily be extended into two- or three-dimensional forms, is used here for the convenience of presentation.

---

<sup>1</sup> Professor, Department of Civil and Environmental Engineering, Clarkson University, Potsdam, NY,  
13699-5710, USA, e-mail: htshen@clarkson.edu

In the two-layer formulation, the ice discharge in the river is considered to consist of surface ice and suspended ice discharges:

$$Q_d^i = AUC_s \quad (1)$$

$$Q_s^i = B_o U_s C_a [h_i + (1 - e_f) h_f] \quad (2)$$

in which,

$Q_d^i, Q_s^i$  = volumetric suspended and surface ice discharge rates, respectively;

$A$  = flow cross sectional area;

$B_o$  = width of the water surface between the border ice;

$C_v$  = ice concentration in the suspended layer;

$C_a$  = area concentration of the surface ice;

$h_i$  = thickness of the solid portion of the surface ice elements;

$h_f$  = thickness of the frazil accumulation on the underside of surface ice elements;

$e_f$  = porosity of the frazil ice portion of surface ice elements;

$U$  = cross-section-averaged flow velocity;

$U_s$  = cross-section averaged surface ice velocity.

Thermal and ice transport processes that govern variations of surface and suspended concentrations, velocity, and thickness of ice in Eqs. (1) and (2) are closely inter-related. These processes and the associated mathematical formulation and theories will be discussed in the following sections.

#### **WATER TEMPERATURE VARIATION AND SUSPENDED ICE TRANSPORT**

The change in water temperature, and the evolution and transport of frazil ice, anchor ice, and surface ice, could occur simultaneously. These phenomena are intricately related to each other. Frazil ice production occurs over the depth of the turbulent river flow when the water temperature is supercooled. In open water reaches, with continuous surface heat exchanges, frazil will grow or decay in size and number. Part of the frazil ice will rise to the surface to contribute to the surface ice discharge. Another part may accumulate to the channel bottom to form anchor ice. The surface ice discharge contributes to the ice cover formation or to the undercover transport or accumulation in an ice-covered reach. Partial coverage of the water surface by surface ice elements reduces the net ice production due to their insulating effect. Concomitantly, the latent heat release from the frazil growth will balance with the surface heat loss and reduce the degree of supercooling. This recovery of water temperature is further enhanced by the insulating effect of the surface ice and the latent heat released from the thermal growth of anchor ice.

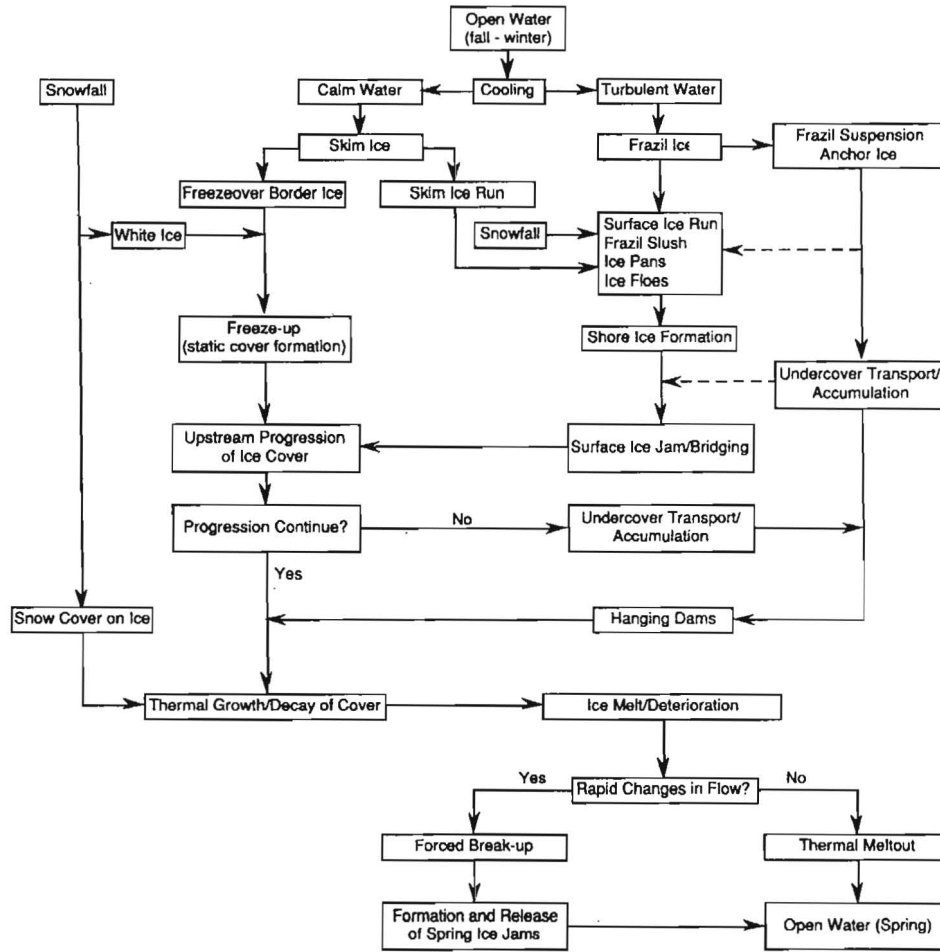


Fig.1. River ice processes

The distributions of water temperature and the suspended ice concentration can be described by the conservation of thermal energy,  $e_T$ , for the ice-water mixture:

$$\frac{De_T}{Dt} = \frac{1}{A}(\phi_{ss} + \phi_{sk}) + \rho_i L_i E \quad (3)$$

in which,

$$\text{the material derivative } \frac{D}{Dt} = \frac{\partial}{\partial t} + \vec{U} \cdot \nabla;$$

$$e_T = C_p \rho (1 - C_v) T_w - \rho_i C_v L_i;$$

$\phi_{st}, \phi_{sk}$  = heat gain and loss through top and bottom boundaries, respectively;

$$E = \frac{1}{d_w} (\alpha V_b C_v - \beta h C_a + \gamma C_v) = \text{net volumetric rate of loss of frazil ice to surface layer}$$

and anchor ice;

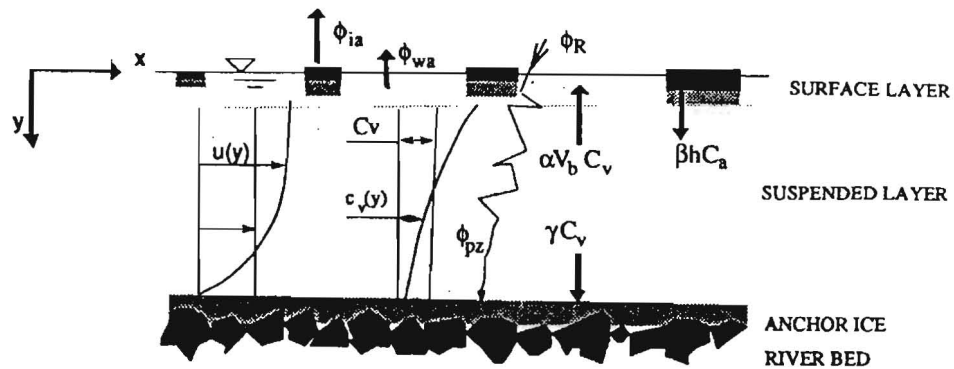
$\rho, \rho_i$  = mass density of water and ice, respectively;

$C_p$  and  $L_i$  = specific heat of water and latent heat of fusion, respectively;

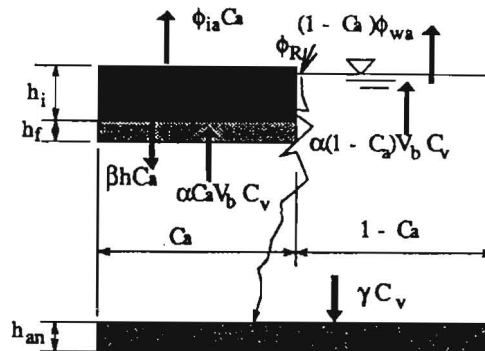
$d_w$  = flow depth;

$V_b$  = average rising velocity of suspended ice;

$\alpha, \beta,$  and  $\gamma$  = mass exchange coefficients at the interfaces between the suspended layer and the surface ice layer and anchor ice, as shown in Fig.2.



a. Definition sketch



b. Mass and heat exchanges in a water column of unit surface area

Fig.2. Two-layer ice transport in an open water reach (Shen et al., 1995)

In Fig.2.,  $\phi_{ia}$ ,  $\phi_{wa}$ , and  $\phi_R$  are surface heat exchanges over the ice and water surfaces, and the solar radiation, respectively. The exchange coefficients  $\alpha$ ,  $\beta$ , and  $\gamma$ , are governed by the turbulent intensity and the characteristics of ice particles. Since complete theories on the exchanges at interfaces are not yet available, these coefficients need to be selected empirically.

The suspended ice concentration changes with the thermal growth and decay of frazil and the mass exchanges with the surface and anchor ice. Hence,

$$\frac{DC_v}{Dt} = \frac{DC_v^g}{Dt} - E \quad (4)$$

in which,  $\frac{DC_v^g}{Dt}$  = rate of change of frazil concentration due to thermal growth. The formation and evolution of frazil have been studied extensively (Daly, 1994). Hammar and Shen (1995) formulated a model for formation and evolution of frazil ice and the corresponding water temperature change in turbulent channel flows. The model was validated with observed water temperature during frazil formation in a laboratory flume (Carsterns, 1966). In this model, the frazil formation is initiated by the mass exchange of seeding crystals at the water surface. The frazil size and concentration distributions in the flow are produced by turbulent heat transfer between the frazil particles and the ambient water, the secondary nucleation, and flocculation. The disaggregation of particles, which controls the limiting size of frazil flocs are not well understood and needs to be studied. In a much simplified formulation, assuming a well-mixed, uniform particle size frazil suspension, the rate of change of frazil concentration in a one-dimensional model can be formulated as  $\frac{DC_v^g}{Dt} = \frac{1}{\rho_i L_i} q a_o N_f$  (Shen et al., 1995), in which,  $q$  = heat transfer between water and a frazil particle per unit frazil surface area;  $a_o$  = surface area of a frazil particle; and  $N_f$  = number of frazil particles per unit volume.

Frazil and anchor ice growths require the supercooling condition. The supercooling condition can be simulated by including the heat exchange between water and ice in the conservation of thermal energy in water, as described in the following water temperature equation:

$$\frac{D(C_p \rho (1 - C_v) T_w)}{Dt} = \frac{1}{A} (\phi_{ss} - \phi_{sk}) + \rho_i L_i \frac{DC_v^g}{Dt} \quad (5)$$

in which,  $\phi_{ss}$  and  $\phi_{sk}$  = rates of heat gain and loss through the top and bottom boundaries.

#### **Anchor ice evolution**

Theoretical understanding on anchor ice evolution is very limited, although it is generally accepted that the anchor ice growth is produced by the adhesion of frazil present at the channel bottom and the thermal growth due to the heat exchange with the supercooled river water. A few analytical and experimental investigations have been conducted on the growth and release of anchor ice (Hammar et al., 1996; Terada et al., 1998; Kerr et al., 1998; and

Doering et al., 1999). These studies provided some preliminary information. Much more research is needed. In the one-dimensional formulation of Shen et al. (1995), the rate of change of anchor ice thickness  $h_{an}$  on its top surface can be calculated by considering the deposition of frazil and heat exchange with the river water:

$$\frac{dh_{an}}{dt} = \frac{1}{1-e_a} \left( \gamma C_v + \frac{\phi_{wi}}{\rho_i L_i} \right) \quad (6)$$

in which,  $e_a$  = porosity of anchor ice. Since the anchor ice does not completely fill the space between the bed particles, a channel of substrate flow will form beneath the anchor ice. Anchor ice could grow or melt from underneath depending on the water temperature. Anchor ice release can occur when the thermal erosion from its underside reduced the binding contact between the anchor ice and the bed particles. Anchor ice can also detach from the bed when the buoyant force of the anchor ice overcomes the resistance due to the weight and inter-particle resistance of the bed particles, or when the hydrodynamic force acting on the anchor ice exceeds a critical condition.

The preceding discussion on water temperature and suspended ice concentration was based on the condition that turbulence intensity in the river is large enough for frazil ice to form below the water surface. It is well known that various type of ice can form in the river during freeze up. In slow flow areas skim ice can form even before the cross-section averaged water temperature drops to the freezing point. Svensson et al. (1989) developed a two-dimensional model for the formation of static border ice. Matousek (1984) provided a semi-empirical method for determining the occurrence of different types of ice. Andreasson et al. (1998) attempted to establish the theoretical understanding on the conditions for different types of freeze up ice runs. Further investigations are needed in order to establish a clear understanding on this subject.

#### SURFACE ICE TRANSPORT AND ICE JAM FORMATION

The conservation of surface ice mass gives the following equation for surface ice concentration:

$$\frac{DC_a}{Dt} = \frac{(1-C_a)}{h} \left[ \alpha V_b C_v - \beta h C_a + \frac{R_{an}}{B_o} \right] - \frac{C_a}{B_o} \frac{DB_o}{Dt} - C_a \frac{\partial U_x}{\partial x} \quad (7)$$

in which,

$$\text{the material derivative } \frac{D}{Dt} = \frac{\partial}{\partial t} + \vec{U}_s \cdot \nabla ;$$

$$h = h_i + h_f(1-e_f) = \text{equivalent thickness of surface ice floes};$$

$$B_o = (1-f_B)B = \text{open water width},$$

$$R_{an} = \text{contribution from anchor ice release}.$$

The rates of change in the solid and frazil ice thickness portions of surface ice floes are:

$$\frac{Dh_i}{Dt} = \frac{\phi_{ia}}{e_f \rho_i L_i} \quad (8)$$

and

$$\frac{Dh_f}{Dt} = \frac{(\alpha V_b C_v - \beta h C_a)}{(1 - e_f)} - \frac{Dh_i}{Dt} - \frac{h_w (T_w - T_m)}{(1 - e_f) \rho_i L_i} \quad (9)$$

There are two types of surface ice transport exist. They are the transport of surface ice floes on the open water surface, and the transport of frazil slush on the underside of ice covers. Both of these are of significant importance in river ice engineering, and will be discussed here.

#### **Dynamic transport on water surface**

Phenomena such as the lateral growth of border ice and ice jam or ice cover initiation are governed by the dynamics of surface ice transport. The border ice growth due to the lateral accumulation of surface ice is a result of the balance of the drag and gravity forces and the boundary friction acting on the ice floes along the edge of the border ice. The initiation of ice jam or ice cover due to the congestion of surface ice runs is a result of the dynamic balance between the internal ice resistance produced by the interaction between ice floes, and external forces including the gravity force, current and wind drags, and the bank friction (Shen et al., 1990). Matousek (1990) and Shen and Van De Valk (1984) suggested that the border ice growth would cease when the local depth-averaged velocity exceeds a critical value of 0.4 m/s based on limited field data. One-dimensional empirical criteria have been proposed for the ice cover or jam initiation (Ackermann and Shen, 1983; Matousek, 1988). However, surface ice transport phenomena, especially those of border ice growth and surface ice jamming, are two-dimensional processes, which can not be adequately described by a one-dimensional formulation. Two-dimensional dynamic surface ice transport theory has been established during the last decade (Shen et al., 1993, 1994). Numerical models have been developed and successfully applied to study ice runs and ice jams, as well as river ice control structures in different rivers (Liu and Shen, 2000; Liu et al., 1998; Lu et al., 1999; Shen et al., 1997, 2000). Further extension of the model to include the thermal ice processes will be useful for engineering applications.

#### **Undercover slush ice transport**

An open water reach upstream of an ice cover will produce frazil ice through out the winter. Upon entering the ice-covered reach, this discharge of frazil slush will transport and accumulate along the underside of the ice cover (Grześ, 1989). A large undercover accumulation, or a frazil jam, could cause significant head loss and rise in water level due to the blockage effects. Localized frazil jams are often called hanging dams by hydraulic engineers. For several decades, critical shear stress or critical velocity concepts (Kivislid, 1959; Tesaker, 1975; Michel and Drouin, 1974) were used to determine the location and thickness of frazil jams. However, these concepts were not able to explain the field data and no method was established to determine the critical shear stress or critical velocity. Shen and

Wang (1995) developed the concept of ice transport capacity for the undercover transport of slush ice. They also developed a formula relating the ice transport capacity to the flow strength and ice particle characteristics based on field and laboratory data. According to the transport capacity concept, the ice discharge in the river adjusts itself towards the ice transport capacity of the river flow through erosion and deposition. Deposition will occur when the incoming ice discharge exceeds the transport capacity. Erosion will occur when the incoming ice discharge is less than the transport capacity.

### CONCLUSIONS

The transport process is the main physical process of river ice. The understanding on the transport of river ice is the basis for the understanding of river ice phenomena during the entire winter. Theories on river ice transport will allow the development of models to simulate river ice and hydraulic conditions, the analysis of ice control schemes, and the assessment of environmental and ecological impacts of river ice. This paper briefly reviewed the past knowledge, present understanding, and future research needs on theories of river ice transport.

### REFERENCES

- ACKERMANN N.L., SHEN H.T. (1983): Mechanics of ice jam formation in rivers. CRREL Report, 83-31, US Army CRREL, Hanover, NH.
- ANDREASSON P., HAMMAR L., SHEN H.T. (1998): The influence of surface turbulence on the formation of ice pans. Vol. 1, Ice in Surface Waters, H.T. Shen ed., A.A. Balkema, pp. 69-76.
- CARSTERN S T. (1966): Experiments with supercooling and ice formation in flowing water. *Geofysiske Publikasjoner*, 26(9), pp. 3-18.
- DALY S.F., ed. (1994): Report on frazil ice (Report of IAHR Working Group on Thermal Regimes). CRREL Special Report 94-32, US Army CRREL, Hanover, NH, 43p.
- DOREING J.C., MORRIS M.P., GIRLING W.C., DOW K. (1999): Laboratory studies of anchor ice growth using a digital image processing system. Proceedings, 10th Workshop on River Ice, Winnipeg, pp. 377-387.
- GRZEŚ M. (1989): Inner structures and surface morphology of ice jams. Proceedings, Ice Seminar, Polish Academy of Sciences, Warsaw, pp. 66-75.
- HAMMAR L., SHEN H.T. (1995): Frazil evolution in channels. *Journal of Hydraulic Research*, 33(3), pp. 291-306.
- HAMMAR L., KERR D.J., SHEN H.T., LIU L. (1996): Anchor ice formation in gravel-bedded channels. 13th IAHR Symposium on Ice, Vol. 3, Beijing, pp. 843-850.
- KERR D.J., SHEN H.T., DALY S.F. (1998): Evolution and hydraulic resistance of anchor ice on gravel beds. Vol. 2, Ice in Surface Waters, H.T. Shen ed., A.A. Balkema, pp. 703-710.
- KIVISLID H.R. (1959): Hanging ice dams. Proceedings, 8th IAHR Congress, Montreal, 23F, pp. 1-30.

- LAL A.M.W., SHEN H.T. (1991): A mathematical model for river ice processes. *Journal of Hydraulic Engineering*, ASCE, 117(7), pp.851-867 (Also, CRREL Report 93-4).
- LIU L., SHEN H.T. (2000): Numerical simulation of river ice control with booms. CRREL Report TR-00-10, US Army CRREL, Hanover, NH, 28p.
- LIU L., SHEN H.T., TUTHILL A.M. (1998): A numerical model for river ice jam evolution. Vol. 2, *Ice in Surface Waters*, H.T. Shen ed., A.A. Balkema, pp.739-746.
- LU S., SHEN H.T., CRISSMAN R.D. (1999): Numerical study of ice jam dynamics in upper Niagara River. *Journal of Cold Regions Engineering*, ASCE, 13(2), pp. 78-102.
- MATOUSEK V. (1984): Types of ice run and conditions for their formation. IAHR Ice Symposium, Hamburg, pp. 315-327.
- MATOUSEK V. (1988): Hypothesis of dynamic ice bridge formation. IAHR Ice Symposium, V. 2, Sapporo, pp. 249-260.
- MATOUSEK V. (1990): Thermal processes and ice formation in rivers. *Papers and Studies No. 180*, Water Resources Institute, Prague, 146p.
- MICHEL B., DROUIN M. (1975): Equilibrium of an underhanging dam at the La Grande River. Report GCS-75-03-01, Laval University, Quebec.
- SHEN H.T. (1996): River ice processes - state of research. 13th IAHR Ice Symposium, Vol. 3, Beijing, pp. 825-833.
- SHEN H.T., VAN DE VALK W.A. (1984): Field investigation of St. Lawrence River hanging ice dams. IAHR Ice Symposium, Hamburg, pp. 214-249.
- SHEN H.T., WANG D.S. (1995): Under cover transport and accumulation of frazil granules. *Journal of Hydraulic Engineering*, ASCE, 121(2), pp. 184-195.
- SHEN H.T., SHEN H.H., TSAI S.M. (1990): Dynamic transport of river ice. *Journal of Hydraulic Research*, 28(6), pp. 659-671.
- SHEN H.T., CHEN Y.C., WAKE A., CRISSMAN R.D. (1993): Lagrangian discrete parcel simulation of river ice dynamics. *International Journal of Offshore and Polar Engineering*, 3(4), pp. 328-332.
- SHEN H.T., SU J., LU S., WAKE A. (1994): A two-dimensional model for dynamic ice transport and jamming in the upper Niagara River. 12th IAHR Ice Symposium, Trondheim, pp. 724-733.
- SHEN H.T., LU S., CRISSMAN R.D. (1997): Numerical simulation of ice transport over the Lake Erie-Niagara River ice boom. *Cold Regions Science and Technology*, V. 26, pp. 17-33.
- SHEN H.T., LIU L., HOSHI K., WATANABE Y., HIRAYAMA K. (2000): Ice jam formation in the Shokotsu River, 15th IAHR Ice Symposium, Gdansk, pp. 81-88.
- SHEN H.T., WANG D.S., WASANTHA LAL A.M. (1995): Numerical simulation of river ice processes. *Journal of Cold Regions Engineering*, ASCE, 9(3), pp.107-118.
- SVENSSON U., BILLFALK L., HAMMAR L. (1989): A mathematical model for border ice formation in rivers. *Cold Regions Science and Technology*, V. 16, pp. 179-189.

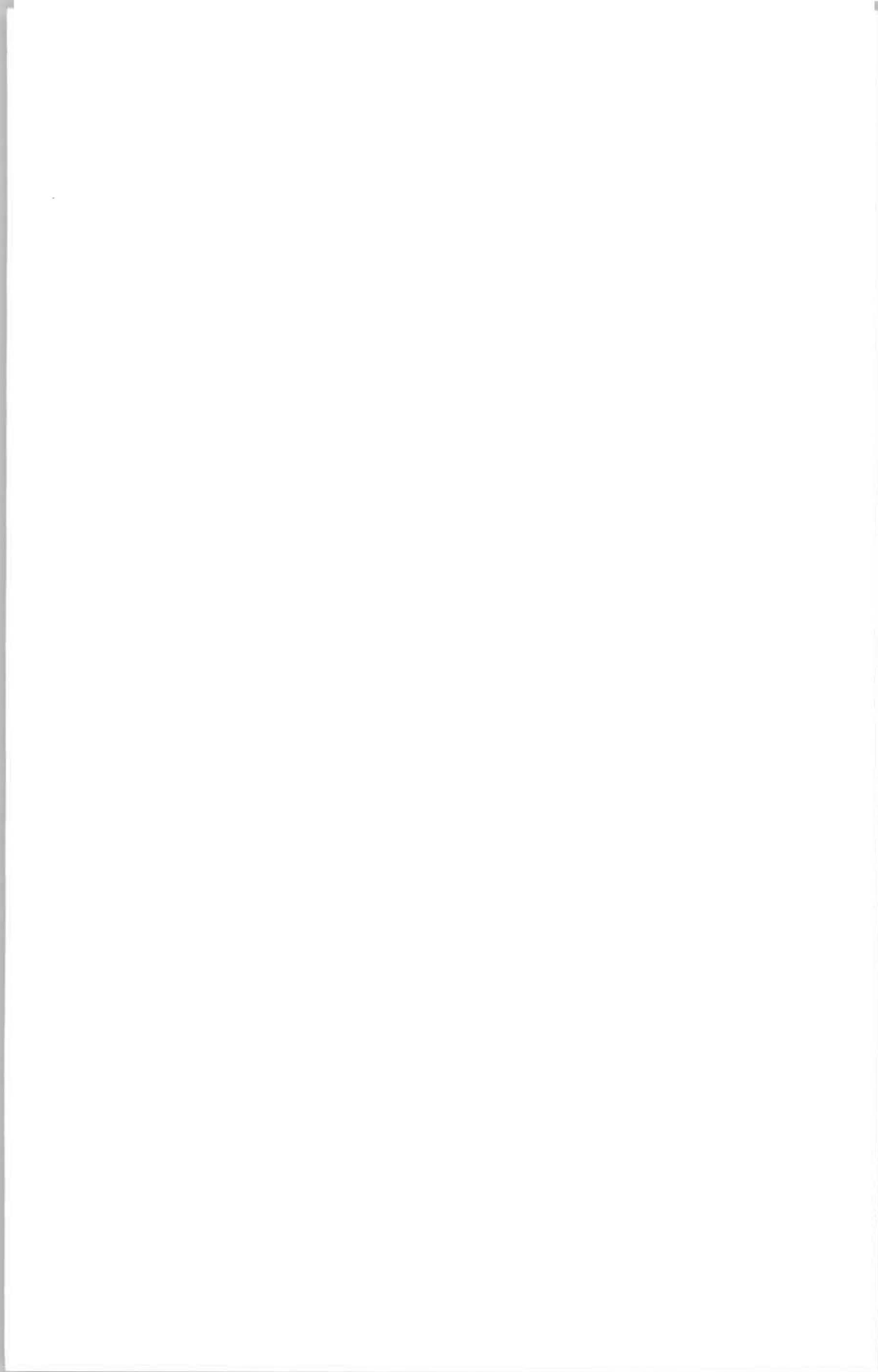
TERADA K., HIRAYAMA K., SASAMOTO M. (1998): Field measurement of anchor and frazil ice. Vol. 2, Ice in Surface Waters, H.T. Shen ed., A.A. Balkema, 697-702.

TESAKER E. (1975): Accumulation of frazil ice in an intake reservoir. IAHR 3rd International Symposium on Ice Problems, Hanover, NH, pp. 25-35.

## HUNG TAO SHEN



Dr. Hung Tao Shen is a Professor of Civil and Environmental Engineering, Clarkson University. He has been active in cold regions engineering research for many years. He has conducted research on various aspects of river and sea ice, including thermal ice regimes, frazil and anchor ice evolution, dynamic ice jam theories, breakup dynamics, and sea ice dynamics. Dr. Shen has published over 150 technical papers, developed state-of-the-art ice simulation models, and taught courses on river ice internationally. He is a recipient of the Harold R. Peyton Cold Regions Engineering Award, and the CAN-AM Civil Engineering Award, of the American Society of Civil Engineers (ASCE). Dr. Shen serves on several national and international committees. He is the Editor of the Journal of Cold Regions Engineering.





## **THIRTY YEARS OF ICE SYMPOSIA**

**Guenther E. Frankenstein<sup>1</sup>**

This paper is an updated version of the „Twenty Years of Ice Symposia,” which was published in the 1990 ESPOO, Finland Proceedings and included as an appendix to this paper. Those who would like a copy should contact Professor M. Maattanen at the Helsinki University of Technology. Summaries of the last five symposia will be included or added to get to our thirty years.

If one looks back thirty years they will observe that the Ice Committee or those interested in ice problems were largely those who represented hydropower companies. They were responsible for emphasizing the problems associated with river ice and how it impacted on power production. It was through their efforts that the IAHR Council established a committee, or originally a work group, to join forces in solving these problems. The hydro engineers are still active in the Ice Research and Engineering Section, but not to the same level as thirty or more years ago.

At the Ice Section’s first symposium it became obvious that there existed other groups that were experiencing problems related to ice interaction. These included offshore oil, navigation, and flood control, etc. Our group became the world’s number one association for the discussion of ice problems and research results. One can not disagree with the above statement when a review is made of all of our conference proceedings, work group reports, and books. One can not guess as to how many ice problems have been solved through the interaction of engineers and researchers during the ice symposium. We can all be proud of these accomplishments.

Attendance and participation in our section’s activities has always been high. Is this support going to continue? I would like to suggest that the participants at this symposium develop a long-range plan for the section. The Kennedy report suggested that each section be reviewed every six years. The IAHR Council doesn’t have time or interest to do this review. I feel that

---

<sup>1</sup>Chief, Ice Engineering (Ret.), U. S. Army Cold Regions Research and Engineering Laboratory,  
72 Lyme Rd., Hanover, NH 03755, USA

this is something that our section should do periodically, say during each symposium. We don't want to become unproductive.

Since this will be my last IAHR associated paper, I would like to clarify, or try to, why there was a change in the numbering of the symposium. At the Second Symposium in Leningrad the members of the Section on Ice recommended that the third symposium be organized in Hanover, New Hampshire, USA, in 1975. The committee further recommended that the section would take part in the Hungary meeting with a limited agenda and not convene as an Ice Section Symposium. These recommendations were agreed upon by the delegates.

The council however approved the Hungarian request and forgot to inform the chairman of the Section on Ice. This created political problems, which hopefully will never be repeated.

In my opinion the relationship between the IAHR council and sections is not a strong one. The section's representative to the council is a council appointed division chairman who has no voting rights. This means then that the sections are background members of IAHR. The Kennedy report recommended that the division chairman be a voting member of the council, which I strongly agree with, but this was never adopted.

At the 1990 Symposium in Espoo, Finland, the secretary general of IAHR, Dr. J.E. Prins, attended. Dr. Prins addressed both the committee and delegates on the workings of IAHR in general. He was well received and the symposium attendees were pleased that he attended. It would be impossible for the secretary general to attend every IAHR section symposium, but an effort should be made by the council to send an official delegate to as many meetings as possible.

The IAHR Section on Ice Research can be proud of our accomplishments. The quality of our proceedings, work group reports, and books are outstanding. Political differences never interfered with our technical progress. We should continue to be productive and work together to solve the many problems that remain in our field of ice research and engineering.

I for one have a lot to thank our section for. On top of the list are the many friends that I have met through our section. The sad part of reaching the age of retirement is that you lose some of these friends as well as contact with others. This has been very sad for me. I don't worry about the section's future however because I know that the younger researchers and engineers with their enthusiasm will continue the work and achieve ever better results. It has been a real pleasure for me to be part of this great group.

**Espoo, Finland (19-23 August 1990)**

Dr. M. Maattanen was the chairman of the organizing committee. Dr. Prins, secretary general of IAHR attended the symposium and briefed the attendees on IAHR in general, and their activities worldwide.

An ice Research and Engineering Section award, proposed by L. Gerard, was established. The award would be announced at the closing of a symposium and then awarded at the next one. The award would be given by the section to recognize significant achievements in ice research and engineering.

At the suggestion of Chairman Majewski the committee established co-opted members. They would serve for a two-year term and could extend for an additional two years. The committee then proposed that L. Gerard and G. Frankenstein be elected to membership in this new category.

The committee recommended to the Banff organizing committee that they considered setting up a student paper competition.

**Banff, Alberta, Canada (15-19 June 1992)**

The organizer of this symposium was Larry Gerard. Unfortunately Larry passed away in November 1991. K. Croasdale took over as the chairman with strong help from his strong committee.

The first Ice Research and Engineering Award was presented. The recipient of this first award was Dr. Bernard Michel. During the symposium Dr. Michel has a heart attach and stroke, so was unable to receive the award in person. One of his sons received the award for him.

A student paper award was established and will be awarded at each future symposium.

Professor M. Mauri Maattanen was elected as chairman of the section.

**Trondheim, Norway (23-26 August 1994)**

S. Loset was chairman of the organizing committee and E. Tesaker was chairman of the scientific committees.

The first Student Paper Award will be presented at the symposium's closing session. The winner was Melanie Schacter of the University of Manitoba. The title of her paper was „Parameters influencing ice arch formation”.

G. Frankenstein was selected to receive the Ice Research and Engineering Award. It will be presented at the next symposium in Beijing.

E. Tesaker announced that there were 112 participants from 14 countries who registered.

**Beijing, China (27-30 August 1996)**

Yang, Xiaoqing was the secretary general of the symposium and Li Guifen was the chairman of the organizing committee. She reported that there were 145 delegates and 126 papers accepted for presentation.

Fumihito Hara from Hokkaido University received the Student Paper Award for his paper titled „A field survey of an ice jam in the Hassamo River and a comparison with the results of model tests”.

G. Frankenstein was awarded the Ice Research and Engineering Award, Professor Hirayama was elected chairman of the section and K. Kato the secretary.

**Potsdam, NY, (26-31 July 1998)**

Clarkson University hosted the Symposium, with Hung Tao Shen and John Dempsey acting as co-chairmen. Over 170 engineers and scientists from 15 countries attended.

The second student paper award was presented to Daniel Iliescu (Dartmouth College) and David Kerr (Clarkson University). The committee agreed to develop guidelines for future such awards.

Prof. Mauri Maattanen was proposed by the committee to receive the Ice Research and Engineering Award, to be presented at Gdansk Symposium in 2000.

New committee members elected were Ian Jordan (Canada) and Pat Langhorne (New Zealand). Hung Tao Shen was proposed and nominated as the new co-opted member.

**Gdansk, Poland (28- August-1 September 2000)**

So that brings us up to the present where we are assembled for the 15th International Ice Symposium here in Gdansk.

## **APPENDIX**

Text of talk delivered at the 10th International Ice Symposium in Espoo, Finland on 20 August 1990.

### **Twenty Years of Ice Symposia**

Guenther E. Frankenstein

USACRREL USA

Executive Assistant, Hanover, New Hampshire

#### **Part 1: 1959-1970**

The title of this paper suggests that the Section for Ice Research and Engineering of IAHR is celebrating its 20th birthday. In actuality the section was established 31 years ago, while this year marks 20 years of separate ice symposia. Both birthdays are something that ice researchers and engineers can be proud of. It's appropriate, therefore, to discuss the early years of our section before the symposium years.

The Section on Ice Problems was established at the Montreal (8th) congress in 1959. This was the first IAHR Congress that included a seminar on ice. The title of the seminar was „Ice Problems on Hydraulic Structures” and was chaired by Mr. J. B. Bryce. There were 29 papers contributed, which caused a problem regarding presentations. The papers were separated into four groups and each was summarized by a reporter. The seminar attendees then discussed the individual papers with the authors.

It was during the seminar, and because of the great international interest in ice problems, that the council formed a „Subcommittee on Ice”. The congress chairman, Mr. R. Dupuis, announced this and stated that, „it was a privilege granted to the few countries that have ice problems to be placed in the orbit of the association to benefit of their own research or of time”. He wanted a committee formed that would meet frequently to discuss ice problems. He was appointed the first chairman of the Subcommittee on Ice by the council and planned to form a full committee as soon as possible. He recommended that the first item on the ice committee's agenda be the publication of a list of definitions and terminology for ice phenomena.

There was a lot of enthusiasm at the time of its formation but the subcommittee remained inactive. In 1961 Mr. Dubuis resigned as chairman but agreed to continue as a member of the committee. In 1962, Prof. A. T. Ippen, President of IAHR, nominated a new committee under the chairmanship of H. L. Rundgren of Sweden.

The first meeting of the new Section on Ice Problems was in September 1963 during the 10th congress in London. The first item of business was to develop bylaws, which were completed and submitted to the IAHR Council for approval. The bylaws stated that the purpose of the section was to foster a bond between those concerned with ice phenomena in general and with

ice problems in connection with hydraulic structures. This statement of purpose is still applicable today.

The Section on Ice Problems had no secretary, so the chairman proposed that Mr. F. Gerritsen, of the Netherlands, be elected to the committee and be the first secretary. The committee approved and Mr. F. Gerritsen accepted. Mr. H.L. Rundgren presented a classification of ice problems which was discussed by the members present. The members also provided information on ice research that was being conducted in their respective countries and agreed to develop a bibliography on ice. Lectures by members L. Lliboutry and O. Devik were presented to the Congress. The next meeting of the committee was at the IAHR Congress in Leningrad in 1965. The Leningrad Congress had a seminar on ice problems with the theme of „Low Temperature Effects on the Flow in Rivers and Reservoirs Including Ice Problems”. Fourteen individual papers were presented. In addition, each member of the Section on Ice Problems that attended discussed his country's ice research program.

The members agreed, as they did at their London meeting, that a bibliography be compiled and made available to those working in ice. Dr. Oudshoorn, of the Netherlands, agreed to compile the bibliography from the lists furnished by the section committee members and then distribute it to those requesting the list. The classification of ice problems proposed and accepted at the London Congress would be the basis for the bibliography. The members present also generally agreed that travel costs made it more favorable to combine the ice seminars with each Congress.

The subject for the ice seminar as part of the 12th Congress, Fort Collins, Colorado, 1967, was „Ice Effects on the Flow in Rivers and Reservoirs Including Pressure on Structures”. There were sixteen technical and five discussion papers presented. The Section on Ice Problems had a new chairman in Prof. B. Michel (elected at the Leningrad Congress, 1965) and a new secretary, Dr. H.N. Oudshoorn. A number of committee member changes were made, which are listed in the appendix.

A number of minor changes to the bylaws, relating to the election of new members, quorum, majority vote, and the conduct of business meetings, were presented and approved by the members present and the council. In addition, the chairman proposed that the section name be changed from „Section on Ice Problems” to „Ice Section”. The council decided to keep the title as is, but agreed to add a French title, „Section des glaces”.

The chairman proposed the creation of a subcommittee on „terminology and graphical representation for river and lake ice” to standardize them. He recommended that the terminology be established in three languages: English, French, and Russian. The committee accepted the proposal and Dr. H. Kivisild agreed to being the sub-committee chairman. This was the beginning of the working groups, as they are now titled. As we all know, the working groups within our-section have produced some excellent work. They are the strength of our section.

The Section on Ice Problems had no scheduled seminar at the 13th Congress, Kyoto, Japan. However, it was at this Congress that the section chairman, Prof. B. Michel, made the announcement that the first IAHR Symposium on Ice would be held in Reykjavik, Iceland, 7-10 September 1970. This would be the first of many successful symposiums.

In addition to the announcement of the first „Ice Symposium,” a general meeting was held with those members that attended the Congress. The first item discussed was the section's bibliography. There had been so few requests for copies that the committee had to decide if the service should be continued. This would be a priority item at the next section meeting.

The subcommittee on ice terminology had been active and would have a final report completed and ready for distribution at the Reykjavik Symposium. The subcommittee chairman, Dr. H. Kivisild, had contacted the World Meteorological Organization, which had compiled a nomenclature for sea ice. He decided that the best approach would be to use their nomenclature as a guide.

#### **Part 2: 1970-1990**

The first Symposium on Ice was held at **Reykjavik, Iceland, 7-10 September 1970**, with Mr. S. Freysteinnsson as chairman of the organizing committee. The chairman of the Section on Ice Problems, Prof. B. Michel, was responsible for this event. He conceived of the idea to have separate symposiums and contacted Mr. Freysteinnsson requesting that Iceland be the first organizer of an ice symposium. He even had the IAHR Council contribute to publishing of the proceedings. We all owe Prof. Michel a big thank you for this outstanding accomplishment.

The title of the first symposium was „Ice and its Action on Hydraulic Structures”, which attracted engineers and scientists from Europe, Canada, Japan, USA, USSR, and from each of the Scandinavian countries. There were 61 technical and four summary papers presented.

Dr. Kivisild presented the first subcommittee report, „River and Lake Ice Terminology”. During the preparation of the report the committee found that the Office of Hydrology of the United Nations Education, Scientific, and Cultural Organization (UNESCO) had done substantial studies on ice nomenclature. The committee reviewed the UNESCO report and decided to prepare a submission to them to be a representative ice terminology. The attendees were to review the list and recommend changes where needed. The final report would then be submitted to UNESCO. This first list of terms and definitions would be in English but would be translated into Russian and French by the next symposium.

This being the first of many IAHR ice symposia, the association agreed to publish the proceedings. The first volume contained the accepted abstracts and the second the reviewed papers, discussions, ice committee minutes, and general addresses. The papers were presented in English but four were published in French.

The second chairman of our Section on Ice Problems, H. L. Rundgren, gave the banquet address. His address was both serious and humorous. He presented his now famous two laws of ice. Ice Law No. 1, „Do not fight against the ice -avoid it”, and Ice Law No. 2, „Do not fight against the ice make use of it”.

The secretary of the committee, Dr. Oudshoorn, reported that there had been fewer than requests for the bibliography. The chairman recommended, and the committee agreed, that further activities on the bibliography be suspended.

The committee recommended that the ice symposia should be held every two years. The next one would be held in Leningrad in September 1972.

In closing, the chairman stated that Iceland, being half way between America and Europe and at the Arctic Circle, was the ideal location for the First Symposium on Ice.

#### **Leningrad, USSR (26-29 September 1972)**

The Second Ice Symposium was also titled „Ice and its Action on Hydraulic Structures”. The chairman of the organizing committee was M. F. Skladnev, who was President of the IAHR Soviet National Committee. Prof. Balanin was nominated to be the acting committee secretary because Mr. Oudshoorn was not able to attend.

A total of 170 people attended the symposium, with 60 coming from outside the USSR. There were 47 papers published in Volume I of the proceedings, while Volume II contained the four lectures, late papers, and discussions. The lectures were presented by B. Michel, A. Assur, T. Carstens, and K. Korzhavin. All the USSR papers and discussions were presented in Russian, but simultaneous translation was provided for those attending.

The symposium program included tours of laboratories in the Leningrad area and a scientific tour to Novosibirsk, Irkutsk, and Bratsk to visit hydro projects and the Academic City. The latter tour was outstanding according to those who participated.

The committee of the Section on Ice Problems met on two occasions during the days of the symposium. They discussed the nominations of new committee members, the report on ice terminology, and the location of the next ice symposium. The chairman proposed a list of individuals to be future chairmen and secretaries for the symposium sessions, which was adopted.

The ice terminology report had been translated into French and Russian but had not yet been published. The chairman recommended that the translations be published in Vol. II of the proceedings, but for some reason they were omitted.

The chairman stated that he had received three requests as to the location and date for the next ice symposium. The Hungarian National Committee was co-sponsoring a meeting in January

1974 with the Fluvial Hydraulics Section and the Section on Ice Problems of IAHR and the Section of Inland Navigation of the Permanent International Association of Navigation Congresses (PIANC). The other requests came from Hanover, New Hampshire, for either 1974 or 1975 and the University of Alaska for 1974. The chairman proposed that the third ice symposium be held in 1975 in the USA-to begin in Hanover, New Hampshire and finish in Fairbanks, Alaska. In addition, he proposed to take part in the Budapest, Hungary, Symposium and that the organizing committee limit it to the hydraulic and ice phenomena associated with navigation in both regulated and non-regulated rivers. This proposal was accepted.

Soon after the Leningrad Symposium the University of Alaska decided not to sponsor the proposed 1975 meeting because of its commitment to host the POAC Conference. The chairman contacted the organizing committee in Hanover and requested that they sponsor a full ice symposium.

**Budapest, Hungary (14-18 January 1974)**

The IAHR Sections for Fluvial Hydraulics and for Ice Problems, in cooperation with the Section for Inland Navigation of PIANC, sponsored the Symposium on Hydraulic Research on Rivers and Ice, with special regard to navigation. The symposium was held under the auspices of the Hungarian Academy of Sciences and the National Water Authority of Hungary.

Mr. Vincze, Vice-President of the National Water Authority was the chairman of the local organizing committee. There were 38 papers submitted and 15 were presented by the authors or co-authors. In addition, representatives from different countries and laboratories discussed their research programs and laboratory capabilities. A simultaneous translation was provided for all speakers from Hungarian to English or the reverse.

Tours of local research laboratories were provided for the attendees. An ice breaking demonstration aboard a Hungarian vessel was scheduled, but due to warm weather there was no ice on the river. However, the attendees enjoyed the scenery along the Danube.

Three members of the Section on Ice Problems Committee were in attendance and held a meeting. The items discussed were the Russian and French versions of the ice terminology list and the formation of a new working group.

The Russian and French versions were to be completed and available by the next ice symposium. A request was made to those attending to provide versions of the ice terminology in their country's language.

A new work group, proposed by Dr. J. Schwarz of Germany, would study the mechanical properties of ice, including testing techniques, sample preparation and test equipment. The section committee okayed the request and a group was formed with Schwarz as chairman.

**Hanover, New Hampshire, USA (18-21 August 1975)**

This symposium was sponsored by the Cold Regions Research and Engineering Laboratory (CRREL) and held on the campus of Dartmouth College. The chairman of the organizing committee was G. Frankenstein, assisted by S. DenHartog and R. McMillen. Approximately 150 engineers and scientists attended.

Dr. O. Starosolszky, the new section chairman, opened the symposium by reviewing the history and bylaws of the Section on Ice Problems. One statement that he made is worthy of a quote, „International cooperation is based on the fact that ice, just as water, does not respect political borders and its properties and basic behavior are identical all over the globe. There is no American and no European ice, only plain ice”. The technical exchanges and cooperation that have taken place at this and all-of the ice symposium have proven Dr. Starosolszky correct.

The symposium was divided into three themes: extended season navigation, ice jam control, and effects of ice on marine structures. Approximately 15 papers were presented under each theme. An invited lecturer presented a review for each of the themes.

The highlight of this, the 3rd Ice Symposium, was the establishment of formal working groups. Our first working group was the one covering ice terminology which presented its final report at our first symposium. Schwarz, in January 1974 while he was a visiting researcher at the University of Iowa, requested that a working group be established to standardize ice testing methods. Their first report was included in the Hanover proceedings.

In addition, two new working groups were established: Ice Jams, headed by G. Frankenstein, and Ice Forces on Structures, headed by T. Carstens. Both working groups held their first meetings during the symposium.

The Committee on Ice Problems had a meeting on the day before the symposium. The new members of the committee were G. Ashton (USA), J. Schwarz (Germany) and T. Rekonen (Finland). The new chairman was O. Starosolszky (Hungary) and G. Ashton was elected secretary. Also in attendance were J. Kennedy, Vice President of IAHR, and B. Michel. Much discussion was given to the formation of work groups, cooperation with other organizations with related interests, publication of the ice terminology, and, future meetings. It was decided to publish the Russian and French versions of the ice terminology in the Hanover proceedings. The committee accepted Sweden's kind invitation to hold the 1978 Symposium in Lulea under the direction of Professor Lars Bengtsson.

Following the symposium a tour was made to observe the ice control techniques of the lower St. Lawrence Seaway, near Montreal.

### **Lulea, Sweden (7-9 August 1978)**

This symposium on Ice Problems was sponsored by the town of Lulea with assistance from the University. The symposium was held at the University of Lulea under the chairmanship of Professor L. Bengtsson. Over 200 (including spouses) engineers and scientists attended and presented 70 technical papers.

The section committee held meetings on 5-6 August that included representatives from the following organizations: WHO, ICSI, UNESCO, IUTAM, and IGS. By inviting the other organizations our chairman was attempting to establish better working relationships between them. The three new committee members, L. Bengtsson, Sweden; G. Frankenstein, USA; and P. Tryde, Denmark; were also present.

Dr. Starosolszky distributed copies of the multilingual ice terminology, which is now in 14 languages, to the members. This was published by the Hungarian Research Center for Water Resources. This report has turned out to be a valuable resource to those working in ice engineering research.

The committee meetings held during the Lulea Symposium were very successful and, one could say, a turning point for future success. It was at this meeting that cooperation was established with other research organizations that would benefit the world. Dr. Michel, a former chairman of our committee, volunteered to host the next symposium in 1981 in Quebec. He would also host a Port and Ocean Engineering Under Arctic Conditions Symposium at the same time. This had been discussed for many years but never undertaken because of the work involved.

One of the highlights of the Lulea meeting was the decision to publish a treatise on „River and Lake Ice Engineering”. Dr. G. Ashton, CRREL, was asked to become the editor of this book and he accepted. The book was divided into eight chapters, each having an editor. It was hoped that the book would be available by the 1981 Quebec Symposium. That date became unrealistic and it was not published until 1986.

The Working Group on Ice Forces produced a report that contained a number of individual state-of-the-art papers. CRREL was requested to publish these papers, which they did as Special Report 80-26. After six years of effort, it was at this meeting that an ice jam was defined: „An ice jam is an accumulation of fragmented ice or frazil that restricts flow”.

As usual, the individual papers presented were excellent, as was the support given by the organizing committee. At the closing ceremony it was announced that Prof. T. Carstens was nominated to become the next Ice Committee Chairman and R. Gerard (Canada), V.E. Lyapin (USSR), M. Drouin (Canada), H. Saeki (Japan), M. Maattanen (Finland), and E. Zsilak (Hungary) members. Prof. Michel invited all participants to attend the next symposium in Quebec in 1981.

**Quebec City, Quebec, Canada, (26-31 July 1981)**

Prof. Bernard Michel was the chairman of the organizing committee for both the IAHR Ice Symposium and the POAC Conference. This was a tremendous undertaking but, as expected, both meetings were a huge success. Attendance at our IAHR Symposium was approximately 200 and for POAC over 300. In addition, representatives of six other international organizations were in attendance.

The working group chairmen reported on their progress since the Lulea symposium. These working groups have been very successful and a very important part of the Section on Ice Problems. The working groups provide a means for researchers from different countries to discuss their ideas and document recent work that has not been published. This relationship should be encouraged to continue.

A newly published addendum to the multilingual terminology was presented that contained eight new languages. This has been a very popular publication throughout the world.

An invitation to hold the next symposium in Hamburg, Germany, August 1984 was presented by J. Schwarz and accepted by the committee. F. Hausler, W. Germany, and J.-C. Tatinclaux, United States, were nominated as the new committee members.

The committee thanked Prof. B. Michel for his efforts in organizing the two conferences. It was agreed that having the two organizations meeting together created a problem that affected paper presentation and working group meetings. Therefore, it was decided that such a schedule would not be proposed in the future.

A special meeting of the Committee on Ice Problems was held at Hanover, New Hampshire, on 22 August 1982. This meeting was called by T. Carstens, chairman, to discuss the progress of the working groups and the book. The meeting was held in Hanover because many on the committee were planning to attend the IGS Symposium on Applied Glaciology.

Each chapter of „River and Ice Engineering” was discussed for content and progress. Following the discussion it was planned to complete the chapters and have the book ready for distribution by the August 1984 Hamburg Ice Meeting.

The committee discussed the subjects-of-the Hamburg meeting. J. Schwarz stated that plans for the meeting were on schedule and informed the committee that each working group chairman was asked to make a presentation at the 1983 POAC Conference to be held at Helsinki.

**Hamburg, Germany (27-30 August 1984)**

The Hamburg Symposium was chaired by J. Schwarz from Hamburgische Schiffbau-Versuchsanstalt. A number of important items were discussed by the Section on Ice Problems and some were adopted.

It was decided by the committee that since the IAHR was a research society, the ice committee would hold a symposium every two years, on even numbered years. This would eliminate any conflict with POAC, which met on every other odd year. This will also help maintain the quality of papers at both conferences.

The committee, through R. Gerard, suggested that a newsletter be published two times every year. Gerard volunteered to be the editor, and it was announced that members should submit news items to him to include especially publications that were unavailable in the open literature.

J. Schwarz reported that approximately 200 individuals attended and that 85 papers were presented. In summary, the Hamburg Symposium was a huge success. The technical papers and the social program were both outstanding. The symposium included a tour and celebration at the new HSVA Ice Laboratory. It was so new that it had not yet been dedicated.

G. Ashton reported that the progress of the book was such that it should be available at the 1986 Iowa Symposium.

The new committee members elected were L. Billfalk (Sweden), K. Davar (Canada), K. Hirayama (Japan), W. Majewski (Poland), I. Meyer (Hungary) and E. Tesaker (Norway). The committee secretary, J.-C. Tatinclaux, reported that hereafter three new members would be elected at each symposium. G. Frankenstein was nominated as the Ice Committee chairman. J.-C. Tatinclaux was re-elected as secretary.

The individual working groups reported on their progress. Each report was included in Volume IV of the proceedings.

#### **Iowa City, Iowa (18-22 August 1986)**

When J. Kennedy and R. Ettema invited the Ice Committee to Iowa City many members thought that fewer than usual would attend. To everyone's surprise, approximately 200 attended and 80 technical papers were presented. The social program was again outstanding and all attendees received a baseball cap to remind them of the great time and hospitality received at Iowa City.

The big news at the Symposium was that the book, „River and Lake Ice Engineering”, was available. The book was a great accomplishment for the IAHR Committee on Ice Problems and all of its active members. A special thanks was given to G. Ashton, Editor, for all his efforts in preparing the book.

The committee recommended that all future working group reports be published separately from the proceedings so that they would be available to students at reduced or no cost. The newsletter was discussed and the first addition was scheduled for distribution in January 1987. It was at the Iowa Symposium that the committee proposed a name change. The

recommended name was the Section for Ice Research and Engineering, which was adopted by the attendees.

The three new committee members elected were G. Timco (Canada), M. Lapparanta (Finland), and V. Ivanov (USSR).

J.-C. Tatinclaux, secretary, campaigned to members to sponsor future symposiums. His efforts were successful in that a schedule for future meetings was completed through 1996. The next, 1988, meeting would be held in Sapporo, Japan; 1990 Finland; 1992 Canada; 1994 Norway and 1996 China. In addition, there would be an ice seminar held during the XXIII Congress in Ottawa in August 1989.

#### **Sapporo, Japan (22-26 August 1988)**

The Sapporo meeting was similar to the Iowa City event in that the organizers had no idea on the number of researchers who would travel that distance to attend. Like Iowa City, approximately 200 individuals attended this outstanding symposium. Prof. H. Saeki and Prof. K. Hirayama performed an outstanding effort in organizing both the technical and social programs.

The newsletter was again discussed and J.-C. Tatinclaux and G. Frankenstein volunteered to act as editors if they received cooperation from the membership. Two publications have been distributed and the third is on its way.

Four new committee members were elected at Sapporo: H.T. Shen (USA), J. Wuebben (USA), E. Wessels (Germany) and J.C. Sun (China).

Each working group reported on its progress and included a report in Volume III of the proceedings. The group on ice forces completed its fourth state-of-the-art report, which was published as Special Report 89-5 by CRREL. These are available for anyone and have been welcomed by students.

In April 1989 Prof. W. Majewski, chairman of the ice committee, sponsored a European meeting. Technical papers were presented and proceedings were published. Eight present and former committee members attended, along with many of those who were interested in ice problems.

W. Majewski (Poland) was elected chairman of the ice committee and J. Wuebben (USA) as secretary. The next symposium will be held in Helsinki, Finland, with Prof. Mauri Maattinen as the chairman of the organizing committee. This will mark our 20th year of IAHR Ice Conferences.

**Summary**

Today we are celebrating our 20th year of ice symposiums or our 9th or 10th meeting. We have seen a large increase in the number of ice conferences; in fact, there were three other international ones this year. In spite of this, the interest and participation in our IAHR Section on Ice Research and Engineering Conferences has not declined but increased. This was proven by the 176 abstracts submitted to Prof. Maattanen for this meeting.

During the past 20 years some of our countries have had political differences. These differences have not affected the cooperation that we have had as ice researchers. We never could have had so many accomplishments if these political differences had affected our desire to collectively increase our knowledge of ice.

Twenty years ago our section was a lot younger in age as well as in our knowledge of ice problems. The number of us that attended the first symposium was small but eager. It's obvious that one of our major successes was to convince others to study ice problems. We did that by our contributions and not by advertising. A positive side of our increase in membership is that we now have our children presenting papers and for the first time a joint family paper included in these proceedings.

I want to thank Prof. Maattanen for the opportunity to write this paper. It has taken a long time but was very interesting. I have learned a lot and hope that you will also. I recommend that this report be updated at the end of each ice conference.

## **GUENTHER E. FRANKENSTEIN**



Mr. Guenther E. Frankenstein obtained his MSc in Civil Engineering from Michigan Technological University. His professional affiliations include American Society of Civil Engineers, the International Association for Hydraulic Research, and the International Towing Tank Congress. He is a member of the International Society of Who's Who, and registered professional engineer in the State of New Hampshire. He is the past chairman of the IAHR International Committee on Ice Problems, and was responsible for convening international symposia and producing working reports on many aspects of ice engineering phenomena. He has travelled to the Arctic and Antarctic in support of his ice engineering studies. In 1996 he received the second IAHR Ice Research and Engineering

Award. G. Frankenstein is a past president of the New Hampshire section of ASCE. He received Harold R. Payton Award for the Cold Regions Engineering in 1992. He is a past member of the Engineering Advisory Council of Clarkson University. Mr. Frankenstein has published numerous papers on ice engineering problems including ice jam flooding, ice control, ice mechanics, infrastructure rehabilitation in cold regions, etc.

Mr. G. Frankenstein retired from CRREL as Chief of the Ice Engineering Research Branch and Director of the Ice Engineering Laboratory in November 1990. He now serves as expert and consultant to government and private organizations on ice problems.



## SOME HYDRAULIC ASPECTS OF FISH LIFE UNDER ICE

Einar Tesaker<sup>1</sup>

### ABSTRACT

The fish habitat in a river usually undergoes large changes as a result of the formation and presence of ice cover. The ice period frequently coincides with shallow flows, causing increased potential for local blocking of the flow profile and redistribution of the flow. Changes in the vertical flow and turbulence profiles, reduced oxygen exchange, erosion and relocation of the substrate, restrictions to fish migration, and damage to roe pits are other effects.

While research on habitat hydraulics in open surface flows is well in progress, the study of under ice habitat is in the starting phase. The interest so far seems to concentrate on regulated river conditions, where problems are most easily discovered, demands for mitigating measures and actions are in force, and funding of research seems to be easier.

This presentation reviews some important effects on fish life caused by the ice. Needs and possibilities for research, including improved methods, instrumentation and facilities for field and laboratory simulations, are finally discussed.

### PRESENTATION OF THE TOPIC

#### Factors affecting fish life

Fish, like humans, prefer the good life rather than just survival. It is therefore possible to list aspects of fish life in different levels of priority:

Level No 1. Absolute short time needs:

- suitable water ambient
- oxygen
- acceptable temperature

Level No 2. Absolute long time needs:

- food

---

<sup>1</sup> SINTEF Civil & Environmental. Eng., N-7465 Trondheim, Norway, e-mail: Einar.Tesaker@civil.sintef.no

- acceptable levels of contamination and diseases
- mating possibilities
- roe survival

Level No 3. Comfort and activity factors:

- temperature level
- type of food
- flow structure: velocity/ depth/ turbulence / pressure fluctuations
- stress level: sound / predators / research activities
- level and type of water pollution
- convenient light conditions
- conditions for migration
- substrate and bed morphology
- shelter.

### **Ice cover effects related to the thriving or survival of fish under ice**

Level No 1:

The ice cover will reduce the exchange of oxygen and heat between atmosphere and water. Water bodies containing fish may be cut off and finally suffer from shortage of oxygen. In extreme situations pools containing trapped fish may freeze to the bottom. Temperatures will usually be more stable than without ice, but at a low activity level for fish.

Level No 2:

Detection of available food will suffer from restrictions imposed to migration. Reduced light, oxygen content and temperature under ice will affect the food production.

Harmful contaminants and diseases, e.g. from industrial and domestic effluents, may have stronger impact, mainly due to generally low winter discharge, but also as a result of oxygen deficiency and reduced light.

Spawning is usually not a winter activity, but the survival of hard roe is a crucial factor. Local erosion caused by various ice processes may damage roe pits, and diversion of flow channels may in certain cases expose roe pits to drying or freezing. Frequent shifting of the bed morphology from year to year due to erosion or accretion caused by ice may have long time effects on the suitability of a reach for spawning.

Level No 3:

The comfort aspects of under-ice fish life include a large variety of processes and factors. Fish, like most living beings, are capable of selecting between various available habitat conditions, and capable to adjust to and survive under conditions far from optimal when needed. As soon as basic needs are covered, however, comfort factors will be increasingly important for choice of habitat, and in the long run determine the quality and population of fish in a river.

Ice cover effects that may affect comfort topics are e.g.:

- The vertical and horizontal distribution of velocity and turbulence will change.
- Velocity and pressure effects may occur during ice formation and break-up.
- Conditions for migration of fish may change, or even be blocked.
- The penetration of light will be reduced, changing the day/night balance.
- Temperature and light effects may inflict on velocity and depth priorities (activity level).
- New situations with respect to shelter and predators may alter the stress level.
- Food may be scarce or less varied.
- Decomposition of water pollution may be retarded by scarcity of light and oxygen.

#### **Other effects of the ice season**

Frazil ice accumulations and anchor ice are commonly observed in the beginning of the ice season, and also after a temporary break-up of the ice cover.

Anchor ice tends to accumulate on protruding objects or directly on the substrate. Roe pits and vegetation may first be sealed off from the fresh water, and later be lifted off the bed, together with important elements of the substrate. Underwater pictures of fish in anchor ice have recently been published by CRREL (White, 2000).

Anchor ice dams may create temporary 2-3 m deep pools, and similar high barriers to migration in streams with slopes typically in the range 0.005-0.05. Drifting frazil may create temporary jams, constricting channels or the whole stream.

Drainage or collapse of anchor ice dams result in violent flash floods. Ice runs are the result when a series of ice dams collapse - often causing serious damage to bed and banks, changes of the channel system, and new jams at a downstream site of lesser slope.

#### **UNDER-ICE HYDRAULICS AND THE WINTER FLOW REGIME**

The flow structure and turbulence under the ice cover will differ from free surface flow both due to the friction caused by the new ceiling, and increased average flow velocities due to reduced available cross sections. This will have secondary effects on the bed morphology, and affect benthos life and algae growth. It is also assumed that fish in situations of rest will prefer positions closer to the bed (or near the ice boundary) due to reduced boundary layer thickness. Fig. 1a.-1b. show simulated velocity fields without and with ice cover (Alfredsen & Tesaker, 1999). Fig. 2. show turbulence intensity distribution under ice measured in Moskva River (Dolgopolova & Tesaker, 2000).

The ice cover will increase the wetted periphery of the flow, causing added total friction and increasing the energy slope. Fig. 1.-2. demonstrate how the vertical flow and turbulence patterns will differ from the open surface situation. The ice cover will occupy part of the cross section, and affect the flow velocities. Starting from a downstream level unaffected by ice, e.g. at a lake or waterfall, in a case of steady discharge, the combination of increased friction and velocities will cause a gradual increase of the flow depth in the upstream direction until a

new energy balance is obtained. Reduced flow depth due to ice cover is therefore a problem mainly in the downstream part of long river reaches with stable flow.

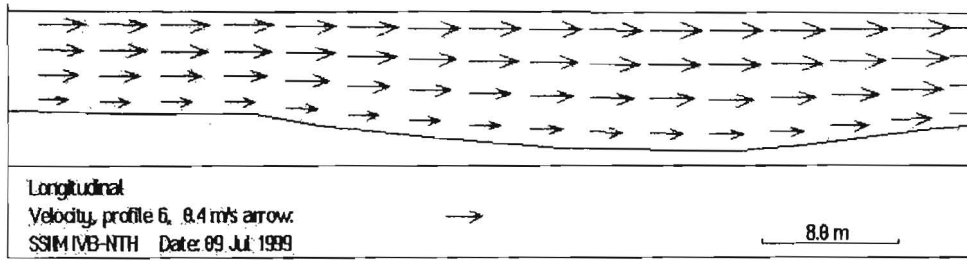


Fig.1a. Simulated velocity field without ice cover

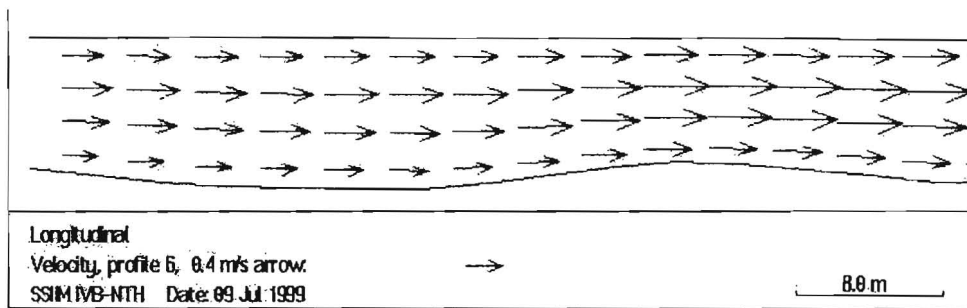


Fig.1b. Simulated velocity field under ice cover

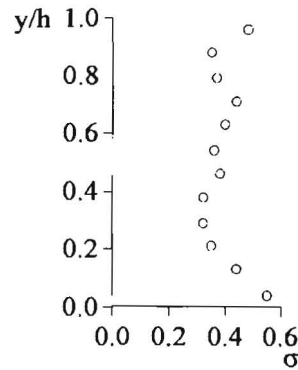


Fig.2. Depth distribution of turbulence intensity under ice in Moskva River

In natural rivers the winter run-off and discharge will normally decline, however. Ice formed while the discharge is still sufficient to cover the full river width may end up resting on boulders or shallow parts of the bed as the water level declines. An ice cover on a shallow stream will therefore soon tend to constrict or divert the flow, and generally reduce the possibilities for migration of fish. Parts of the fish habitat, including pools and migration channels, may even be secluded from the main stream. Despite decreasing total discharge, the constricted and divided flow area may cause locally increased velocities, eroding banks and riverbed and causing temporary or permanent changes of the channel system.

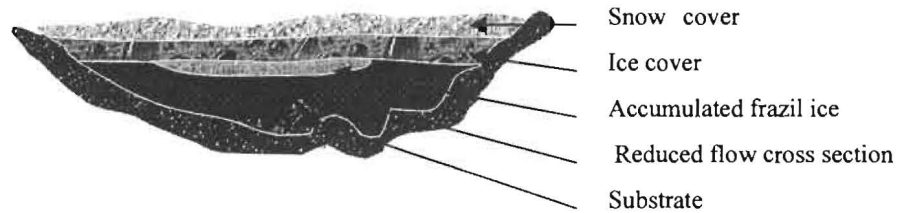


Fig.3. Elements of an under-ice cross section

### EXAMPLES OF FISH LIFE IN THE ICE ENVIRONMENT

#### Velocity and depth preferences vs. temperature in open surface flow

The fish activity is lower in cold water than in warm. This is reflected in the preferred velocities found by observing positions of fish in a known velocity field. Fig.4. shows velocity preferences for Atlantic salmon observed in a Norwegian river for winter and summer respectively. It is seen that preferred velocities drop from 10-20 cm/s in "warm" water (9-12 °C) to 0-10 cm/s in cold water (3-7 °C). Velocities above 40-50 cm/s are avoided in cold water.

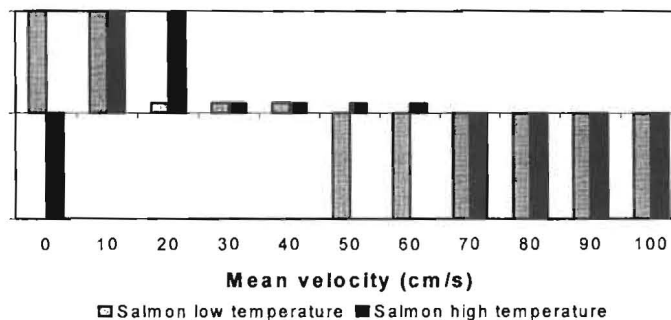


Fig.4. Preference velocities for juvenile Atlantic salmon from a Norwegian river (Heggenes & Dokk, 1995). Under the line: avoid; over the line: prefer.

Depth preferences have been registered in a similar way. By combining the preferences with actual depth and velocity data for a particular reach, it has been possible to map areas of joint preferences for a variety of discharges, as shown on Fig.5. (Fjeldstad & Heggenes, 1999). It is seen that the sum of indifferent and preferred areas in this location is almost the same for 15 m<sup>3</sup>/s and 40 m<sup>3</sup>/s discharge, while notably less for the smallest discharge.

Similar mapping has so far not been made for under-ice conditions. On the other hand it is known that the limiting condition for deposition of frazil ice under an ice cover occur when the maximum velocity in the channel reaches 40-50 cm/s (Majewski, 1994; Tesaker, 1975). These are higher values than preferred by juvenile Atlantic salmon in the cold season, see Fig.4. Where and when deposition of frazil occur, therefore, the habitat is not generally favourable for salmon. Velocities are less near the bed or the frazil deposit, but these boundary layers are usually thinner in ice covered flow than without ice.

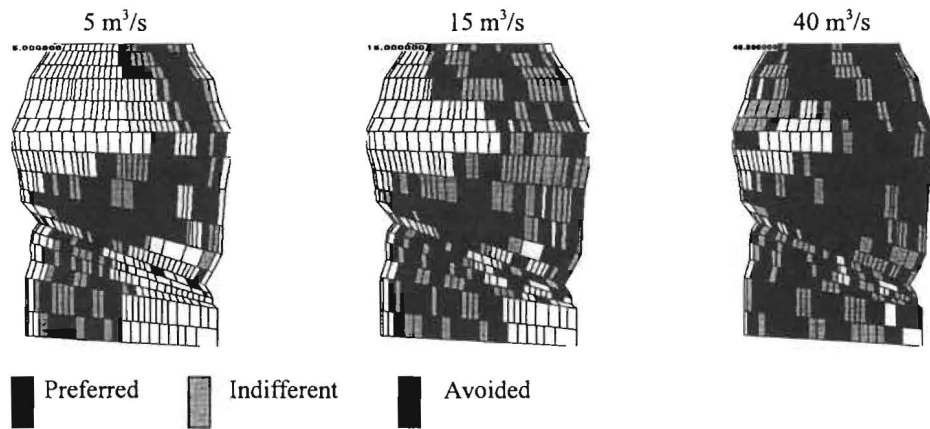


Fig.5. Mapping of preferred fish locations for 5, 15 and 40 m<sup>3</sup>/s (white: no water)

#### Survival of spawn during extreme conditions

The survival of spawn through the winter is a vulnerable process. During mating the spawn is deposited in pits and covered by substrate well under water. The pits are vulnerable to damage from anchor ice, which may hinder oxygen, or to erosion by local strong currents in constricted channels caused by ice. In natural rivers the location of the pits are chosen by instinct to avoid such problems.

Frequent water level variations are common mainly in regulated rivers. Low (winter) discharges may bring the pits above the water level for some period without harming the spawn, as long as the substrate remains moist and unfrozen. A snow-covered ice layer will usually be enough for protection of the pits over short periods. On the other hand, low water levels without ice or snow cover pose threats of both drying and freezing.

A special situation was reported from river Vossa in Norway (Harby, 1998). It is not uncommon in this river that water levels sink below the spawn pits for some periods during normal winters. This will usually not harm the spawn, because of sufficient insulation from the snow cover. Fig.6a. shows a common winter situation. A layer of ice and snow protects the river banks. The ground temperature will remain above zero. Sufficient moisture and oxygen remain in the spawning pits, preventing the roe from drying.

The special situation occurred during a repair period for an upstream dam. A cofferdam was used to reduce the discharge during daytime, while the dam was emptied every night for capacity reasons. The night discharge during emptying of the cofferdam removed the ice and snow cover, Fig.6b. Low discharge during the construction period at daytime dried out the pits, Fig.6c, and the spawn was finally killed when some extremely cold days appeared. The result was a significant reduction of the young fish population next year.

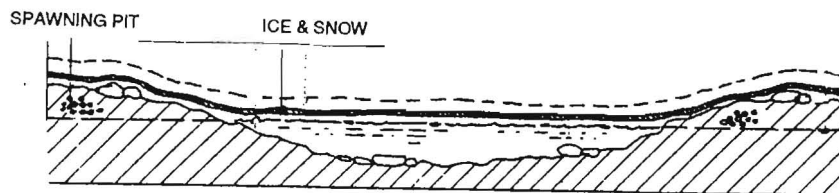


**Fig.6a.** The normal winter situation with minimum discharge.  
Spawn pits covered by ice and snow



**Fig.6b.** Civil works situation 1: full flow at night, removing the ice and snow cover.



**Fig.6c.** Civil works situation 2: reduced daytime discharge,  
causing the roe to dry out and freeze in cold days.

### Effects of ice events on the fish population

The effect of the winter season on the fish population may vary from year to year, depending on climatic and hydraulic conditions. Certain ice events, e.g. severe anchor ice production or violent ice runs may be detrimental to the local fish population. Particularly the young fish is vulnerable. An example is shown on Fig.7.: the entire Age 0 population has disappeared during the winter, while the adult fish population has survived.

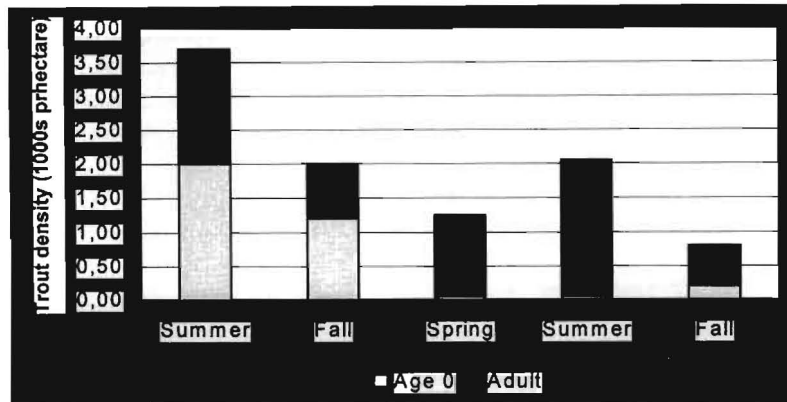


Fig.7. Density variation of trout over two seasons in Tye River (La Roche, 1991)

### Migration of fish under ice. Shelter preferences.

It is known from open surface investigations that young *salmo salar* is most active at night and hide in the substrate or underneath overhanging banks at daylight. It has been anticipated that threats from predators may be one reason for this.

Studies of fish movement under ice are still few. It has been observed that fish tend to prefer the sheltered habitat under the border ice when the river is partly ice covered. Some observations indicate more active use of the daytime for migration under ice. This may be due to the fact that winter daylight is weaker and further dimmed by ice and snow, but may also be influenced by safer "feelings" due to the shelter effect under ice cover from dangers from above.

In Canadian study of fall and winter movement and behaviour of *Oncorhynchus clarki* (cutthroat trout), using radiotelemetry, Brown (1999) found that as water temperatures decreased, the trout moved from more solitary positions to aggregations. With few exceptions, radio-tagged fish aggregated in groups varying from 5 to approximately 70 fish. Both the percentage of fish aggregating and the mean size of aggregation correlated negatively with water temperature.

Still according to the same source, the mean distance moved by radio-tagged trout from 1 September to 12 January was 1.0 km. After forming aggregations, fish tended to stay within only 120 m length of stream until the end of tracking in mid-January. Fish that were less sedentary tended to move when their habitat was occluded by anchor ice. These fish moved thirty times farther and six times more often than fish in stable overwintering areas. In Dutch Creek multiple freezing events caused several ice related habitat exclusions and movements associated with large decreases in air temperature.

## **ARTIFICIAL MODIFICATIONS OF THE HABITAT**

### **Modification of natural rivers**

In natural rivers, remedial action for improving the habitat is usually limited to moderate modification of the local geometry. Various measures to improve local conditions for shelter and spawning have been proposed, and in a few cases tried. Construction works in a river otherwise protected against regulation will always be disputed, however. Hydraulic and sedimentary effects of remedial measures (or research activities) may be difficult to predict and should be carefully investigated and monitored.

Some experience from river Gaula in Norway may serve as examples. Gaula is an important salmon river protected against hydropower development, but has until recently been severely affected by uncontrolled gravel mining. It was finally discovered that bed erosion due to removal of the natural armour layer and sediment supply during about 50 year had caused about 2 m degradation of the bed. Reproduction conditions for fish was badly reduced in the lower reach of the river. Gravel mining is now almost concluded.

The first mitigation attempt comprised placing small mounds of cobbles on the bed, in an attempt to provide shelter for fry in their risky first year (Hvidsten, 1993). Observations of fish population showed great increase the first season, but soon the mounds became filled with finer sediments and the effect declined.

The next idea was to improve habitat and shelter conditions in a reach by placing large size quarry rocks in shallow areas of the river. Various patterns were suggested: regular rows of rocks normal to the bank or parallel to the bank, as well as singular rocks or mounds of rocks. The final installation comprised mounds and singular rocks in an irregular pattern over the rather shallow area in the wake downstream of a moderate bend in the river. This installation is still under evaluation. It was suspected that the installations would promote sedimentation in the area, but so far local erosion around the installations prevail and tend to influence on the general development of the reach.

Regarding the under-ice habitat, the natural reduction of winter discharge and water level caused the ice cover to rest on the installed rocks, partly spanning free from rock to rock. Parts of the underlying bed became dry, which combined with locally eroded channels created a very confusing habitat situation, still to be investigated.

### **Regulation of discharge and stage**

In regulated rivers the regulation itself usually imposes disputed effects. But regulation also represents a possibility for improvement of the winter habitat, e.g. by control of discharge, reduction of ice runs, arrangement of artificial pools or under-ice passages, or even temperature control.

Short term manipulation of the discharge will cause the ice cover to crack and partly rest on the bed during low discharge periods and be lifted again and possibly drift away or jam when the discharge increases. Restrictions are therefore commonly imposed on the winter flow in regulated streams in order to avoid ice runs and flooding.

Effects of rapid discharge reductions on stranding of young salmon in open surface flow is the topic of a research project "Environmental effects of hydropeaking" at SINTEF (Saltveit et al., 1999). Experiments in field and laboratory shows that only a smaller part of the fry population actually get stranded, most of the fry hide in the substrate or escape to deep water when their habitat dries out temporarily. Added stress to fish living under such conditions, is now under investigation.

So far under-ice conditions have not been included, but it should be obvious that escape conditions will be much more complex under ice.

### **Engineering works for habitat improvement**

Engineering works of larger consequences for the flow of the river are e.g. thresholds, jetties and channel deepening. Such methods are rarely applied because of very complicated effects during varying discharges and seasons, and little experience with respect to under-ice habitat exist.

Thresholds may be thought of as a means to improve the under-ice habitat. It will increase the under-ice depth, reduce velocities and promote ice cover formation. Negative side effects for the under-ice habitat are reduced or hindered migration possibilities and risk of floods and jamming in connection with ice break-up. Other adverse effects in general are obstruction of the natural sediment transport, and risk of increased flood levels and downstream scour.

### **SUMMING UP**

- The ice covered season is a period of rest for the fish due to low temperatures, reduced suitable ambient and restrictions to migration.
- The period represent hazards as choking in deadlocked ambient, increased concentration of contaminants, and violent ice processes. On the positive side is less risk from external predators. The spawn and young fish are threatened by anchor ice, erosion of spawn pits, and drying out during reduced discharge.
- Few feasible means have been established for improving the under ice habitat, but investigations continue.

## REFERENCES

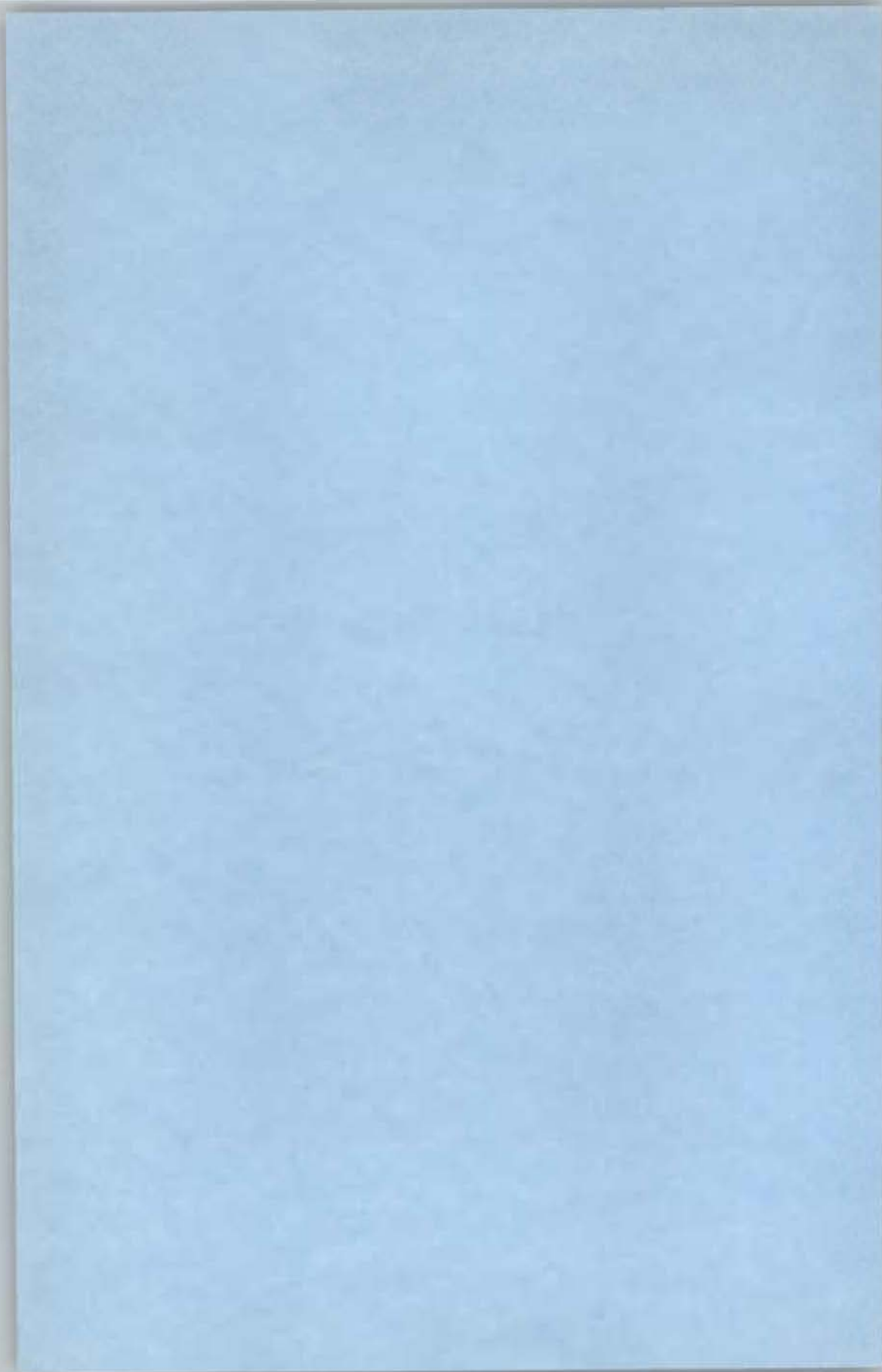
- ALFREDSSEN, TESAHER E. (1999): Incorporating ice and effects of ice into the Norwegian habitat assessment strategies and the HABITAT program system. IAHS Workshop, Birmingham, UK.
- BROWN R.S., POWER G., MCKINLEY R.S. (1998): Effects of hanging dams, surface ice break-up, and flooding on fish. Proc. 14th Symposium on Ice, Potsdam, NY, USA, v.1, pp. 175-181.
- BROWN R.S. (1999): Fall and early winter movements of cutthroat trout, *Oncorhynchus clarki*, in relation to water temperature and ice conditions in Dutch Creek, Alberta. *Environmental Biology of Fishes*, 55: pp. 359-368.
- DOLGOPOLOVA E.N., TESAHER E. (2000): Turbulent Structure of Ice-Covered Flow and Ice Impact upon Habitat in Rivers. 15th International Symposium on Ice, Gdansk, Poland.
- FJELDSTAD, HEGGENES (1999): Fiskehabitatforhold i Stjørdalselva ved Gudå: fiskepreferanser (Fish habitat conditions.....: fish preferences). SINTEF rep STF22 A99409.
- HARBY A. (1998): Effects of civil works in Vossa river. Personal communication.
- HEGGENES, DOKK (1995): Habitatvalg til laks og orretunger i Suldalslaagen. (Choice of habitation areas in Suldalslaagen by young salmon and trout). Project report No 9, Statkraft Engineering, Høvik, Norway.
- HVIDSTEN N.A. (1993): Forbedring av oppvekstområder for laksefisk i Gaula. (Improving habitation areas for salmon in Gaula). F. rapport nr 41, NINA, Trondheim, Norway.
- MAJEWSKI W. (1994): Flow characteristics in open channels with floating ice cover. 12th Symposium on Ice, Trondheim, Norway, v.1, pp. 22-30.
- SALTVEIT S.J., ARNEKLEIV J.V., HALLERAKER J.H., HARBY A. (1999): Experimental studies on the effect of rapid flow decreases on juvenile Atlantic salmon (*salmo salar*) and Brown trout (*salmo trutta*). 3rd International Symposium on Ecohydraulics, Salt Lake City.
- TESAKER E. (1975): Accumulation of frazil ice in an intake reservoir. 3rd International Symposium on Ice, Hanover, NH, pp. 25-38.
- TESAKER E. (1998): Mitigation of ice effects on the habitat in regulated and natural rivers. 14th International Symposium on Ice, Potsdam, NY, v1, pp. 161-168.
- WHITE K. (2000): Rainbow trout in flume pictures.doc. Personal communication.

**EINAR TESAKER**



Dr. Einar Tesaker obtained his Master of Science in Civil Engineering at the Norwegian Institute of Technology in Trondheim in 1958. Dr. Ing. (Ph.D.) was awarded to him in 1969 also by the Norwegian Institute of Technology in Trondheim. At present he is employed as Senior Research Engineer at SINTEF Civil and Environmental Engineering, Water Resources. Dr. Tesaker has been very active in ice research and engineering presenting more than 20 papers on various topics. He also actively participated in most International Ice Symposia beginning from 1970 in Reykjavik where he presented the paper. Dr. Tesaker was also very active in many Norwegian and international scientific and engineering societies and committees. He was very active in the Section of Ice Research and Engineering (IAHR) as the member of the Section and member of the Working Group.

**LATE  
PAPERS**





## ACOUSTIC EMISSION LOCATION AND CRACKING IN SEA ICE

C. McKenzie<sup>1</sup>, P.J. Langhorne<sup>2</sup>, T.G. Haskell<sup>3</sup>

### ABSTRACT

Analysis of acoustic emissions is an important tool in the non-destructive testing of materials. Experiments are described in which a four transducer array was used to locate the sources of acoustic emissions during the fracture of cantilever beams of Antarctic land-fast sea ice. Crack propagation was examined when the beam failed in tension at the upper ice surface (ie "push down" to failure), and this was compared with results for compression at the upper ice surface (ie "pull up" to failure). Significant differences were found between the two situations, implying that the acoustic emissions observed were the result of tensile fractures in both cases. The errors inherent in source location are discussed.

### INTRODUCTION

Acoustic emission techniques have proved useful in the study of cracking in freshwater ice. However our attention here will be confined to the radiation of acoustic waves as a result of damage in sea ice. In the laboratory, acoustic emissions have provided supplementary information in compression tests on multiyear sea ice (Sinha, 1985), and in creep deformation measurements on first year sea ice (Cole, 1993; Sinha, 1994). But it is to *in situ* testing that acoustic emission techniques are ideally suited. Here they have been used to determine cracking rate and propagation velocities in a large-scale tensile fracture test in first year ice (Adamson and others, 1995). Emissions also occur during cyclic experiments where the acoustic event rate is highest during initial cycles and just prior to fracture (Cole and Dempsey, 2000), and where they have highest density close to the position of eventual fracture (Langhorne and Haskell, 1996a). The sources have frequency spectra consistent with the growth of microcracks in which the rupture is terminated slowly, having undergone rapid nucleation. Further results suggest that the acoustic source is the incremental growth of a microcrack (Langhorne and Haskell, 1995), with behaviour reminiscent of the stable, brittle, stick-slip crack growth described for cold, saline ice (DeFranco and Dempsey, 1994). The

---

<sup>1</sup> Department of Physics, University of Otago, P.O. Box 56, Dunedin

<sup>2</sup> Department of Physics, University of Otago, P.O. Box 56, Dunedin, New Zealand, Tel.: +643 479 7787,  
fax: +643 479 0964, e-mail: [pjl@physics.otago.ac.nz](mailto:pjl@physics.otago.ac.nz)

<sup>3</sup> Industrial Research Ltd, P.O. Box 31-310, Lower Hutt, New Zealand

emissions from sea ice cantilever beams that were pulled up to failure have been found to differ from those generated when the beam is pushed down to failure (Langhorne and Haskell, 1996b), and it is the reason for this phenomenon that is described in this paper.

In the experiments analysed here, cantilever beams of first year, landfast sea ice are loaded in one direction until they fracture in either "push down" or "pull up" mode. The acoustic emissions from the fracturing processes were recorded by a four transducer array. We describe some of the considerations involved in locating the source of the emissions from this signal array.

### EXPERIMENTAL CONSIDERATIONS

Due to its structure and imposed temperature and salinity profiles, sea ice is both inhomogeneous and anisotropic. To make the problem of source location tractable we must make some observations concerning the propagation of acoustic waves in the ice. Dealing with an anisotropic solid is notoriously difficult since mode conversion occurs causing simple methods, like ray tracing, to fail. However, provided the frequency of the waves is greater than 4 Hz, McKenzie (1996) has shown that coupling of modes does not occur in sea ice. The frequencies of interest here are in the 5 kHz to 167 kHz range.

The modelling of a horizontally stratified solid is most easily achieved via numerical solutions of the wave equation with the velocity varying with height. Fig.1a. shows characteristic profiles for shear, compressional, Rayleigh and plate wave velocities through the first year, landfast sea ice sheet of McMurdo Sound, Antarctica, derived from density, salinity and temperature profiles (Langhorne and Haskell, 1996a). The transducers used in this experiment will respond only to the Rayleigh and to the shear waves at the surface (Langhorne and Haskell, 1996a). Using the profiles of Fig.1. we examine possible propagation paths for the waves, following the formulation of the ray propagation equations used in seismology texts like Bullen and Bolt (1985). Since the velocity increases towards the centre of the ice sheet (see Fig.1a.), waves that approach the central layers of the ice from the outer layers at shallow angles will be reflected. In other words a critical angle,  $\theta$ , exists and total internal reflection may occur (see Fig.1b.). This critical angle splits the rays into two classes; those greater than  $\theta$  return to the layer of the ice from which they originated where they can be detected, while those at angles less than  $\theta$  never do (Straight Through Rays in Fig.1b.).

Raytracing experiments were also used to investigate the error arising from the assumption of straight line propagation. This was found to be lower than the errors from other sources (e.g. sound speed profile, sensor location and time difference calculation), particularly where the rays are nearly vertical or where the rays are shallow (nearly horizontal). It was concluded that most curved rays have a travel time within 1% of the corresponding surface wave, which is smaller than the envelope of an acoustic event. Also for sources close to the surface, shear waves will have a very similar travel time to surface Rayleigh waves (see Fig.1a.).

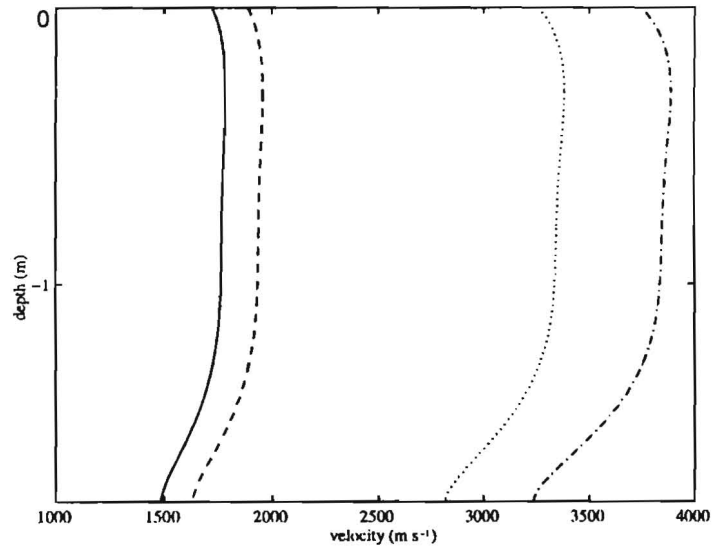


**Fig.1a.** Depth profiles of Rayleigh (solid), shear (dash), compressional (dotted) and plate waves through sea ice.

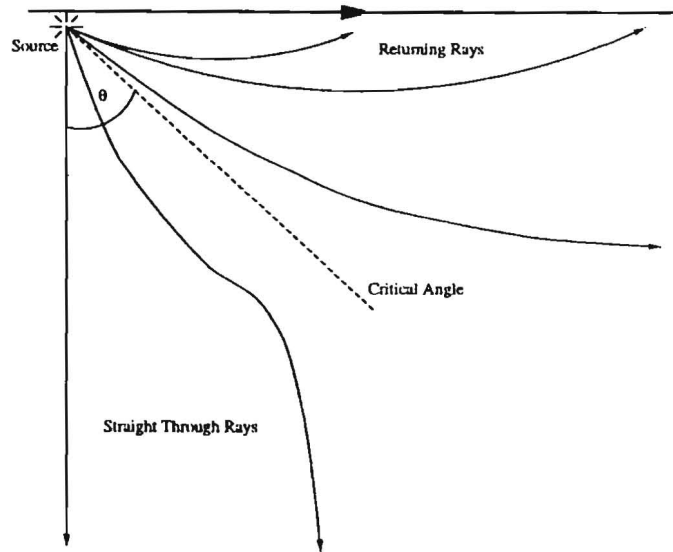


**Fig.1b.** Typical wave paths.

For a system of  $n$  transducers,  $n-1$  independent time differences can be found. So in an 3 dimensional system, 4 transducers are required to locate the source. If the timing differences are completely accurate, it is possible to derive an analytical solution to translate timing differences into a location. This is not the case here and an iterative approximation method must be used (Thurber, 1985). It involves using Newton's method to minimise the time differences of the predicted location with respect to the observed time differences. We define the difference between the observed  $t_i^{obs}$  and predicted  $t_i^{pre}$  arrival times at the  $i$ th transducer as

$$r_i = t_i^{obs} - t_i^{pre}$$

Assuming straight line propagation we minimise the  $r_i$  (McKenzie, 1996), which gives good results provided the initial guess for the location is close to the solution.

The uncertainty in the positioning of the transducers was the largest source of error. To estimate this error we take a lattice of imaginary sources and calculate, for each source and the chosen transducer layout, the time delays to each transducer. These are then assembled into an error volume (of dimensions  $10^{-4}$  s) in the time domain. This time delay error ( $10^{-4}$  s) was based on expected accuracies in the cross-correlation methods used in the processing of the time delay data. The errors were then converted from the time domain to an error in source location which ranged from the order of 3 cm in the accurate regions to 0.5 m or more in the inaccurate regions (see Table 1). The error volumes for the transducer layout in beam 15 is presented in Fig.2. using the coordinate system of Fig.3. The error volume is vertically elongated in most cases, meaning that the vertical resolution is less than the horizontal.

As well as using sea ice physical properties to determine wave speeds (as in Fig.1a.), wave velocities can be estimated by creating an event at a known location. Either the breaking of a pencil lead (probably creating surface Rayleigh waves) or the tap of a metal bar on the ice surface (probably generating shear waves) is used. All the artificial events were generated close to the origin. A Rayleigh wave velocity of  $1000 \pm 300 \text{ ms}^{-1}$  was estimated. Fortunately the location algorithm is insensitive to the inaccuracy in this measurement. The shear velocity at the surface was determined to be  $1290 \text{ ms}^{-1}$  which is within error of the prediction from Rayleigh wave velocities ( $c_R = 0.911 c_S$ ), and within error of the results of the core sample close to the surface (see Fig.1a.). For the purposes of locating the deep events, it was assumed that the physical properties data were reliable and the shear wave velocity was taken to be constant at  $c_S = 1740 \text{ ms}^{-1}$ .

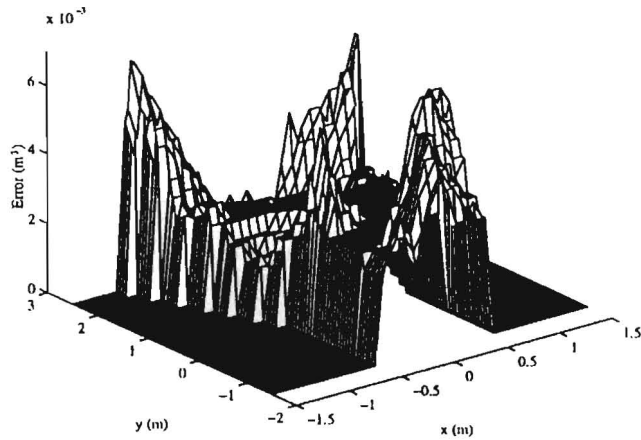


Fig.2. Error volumes for beam 15

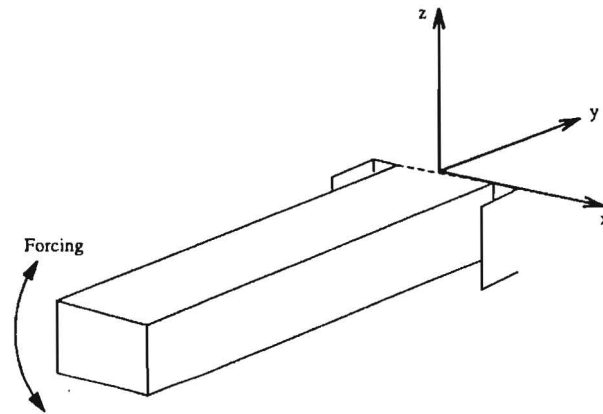


Fig.3. Cantilever beam with coordinate system

The experiment was performed on the land-fast, first year sea ice of McMurdo Sound, Antarctica. A computer-controlled load was applied close to the free end of cantilever beams of sea ice. These beams were nominally 1m wide ( $x$ -direction in Fig.3.) and 10m long ( $y$ -direction in Fig.3.) and cut through the 2m thickness of the ice ( $z$ -direction in Fig.3.). A displacement transducer measured the change in length of a surface filament at the hinge of the beam (along the  $y$ -axis in Fig.3.), from which hinge strain is derived. This provides an external measurement of the time at which the beam fails. Three of the four acoustic emission transducers were frozen onto the sea ice surface, while the fourth was placed about 30 cm below the surface. In all experiments the acoustic emission data in the range 5 kHz to 167 kHz were sampled at 500 kHz for 1.05 s.

## EXPERIMENTAL RESULTS

Table 1 lists the acoustic source locations found for both the “pull up” and the “push down” experiments. One of two velocity models have been used in the calculation: the first assumes shear wave propagation from the source to all four channels and is labeled the deep model (labeled D in Table 1), while the second, which assumes Rayleigh wave propagation to the surface mounted transducers and shear wave propagation to the buried transducer, is labeled the surface model (S in Table 1). Ice thickness was  $1.97 \pm 0.02$  m. The flexural strength of the sea ice did not depend on the direction of loading (see Table 1).

**Table 1**

Source locations and times for “pull up” and “push down” experiments

Event	Type	Location (m)	Time (s)	Velocity model	Flexural strength (kPa)
13	up	$(0.27, -0.08, -1.78) \pm (0.3, 0.07, 0.25)$	$0.496 \pm 0.003$	D	362
14a	up	$(0.34, 0.39, -1.78) \pm (0.06, 0.05, 0.15)$	$0.5184 \pm 0.0001$	D	399
14b	up	$(-0.23, 0.13, -1.19) \pm (0.25, 0.2, 0.25)$	$0.6687 \pm 0.0001$	D	
14c	up	$(0.30, 0.17, -1.19) \pm (0.08, 0.15, 0.1)$	$0.5684 \pm 0.0001$	D	
14d	up	$(0.48, 0.24, -1.55) \pm (0.03, 0.03, 0.1)$	$0.6077 \pm 0.0003$	D	
7a	dn	$(0.45, -0.61, 0) \pm (0.3, 0.07, 0.22)$	$0.4974 \pm 0.0005$	S	360
7b	dn	$(-0.18, -0.35, -0.01) \pm (0.2, 0.07, 0.22)$	$0.71 \pm 0.02$	S	
15a	dn	$(0.07, -0.35, 0) \pm (0.1, 0.03, 0.13)$	$0.488 \pm 0.001$	S	367
15b	dn	$(0.25, -0.18, 0) \pm (0.25, 0.15, 0.13)$	$0.541 \pm 0.002$	S	

For both “pull up” experiments the use of a Rayleigh surface wave model predicts a source at depth, which is clearly in violation of our assumption of a surface source. It therefore appears that the source locations for these experiments were close to the ice-water interface, and the D model was appropriate. For beam 13 the source listed on Table 1 is the first of the high amplitude events in the data and has an  $x$ - $y$  location within error of the hinge of the beam where failure occurs. The associated emissions appear to be from the early stages of this failure. Four events can be obtained from the data of “pull up” beam 14, of which the final one (event 14b) occurs at about mid-depth in the ice, approximately 0.05 seconds before total failure of the beam. This suggests it might emanate from the end of a well developed crack. Note that the  $x$ - $y$  locations of the four events are all 10-30 cm away from the butt of the beam on the supporting ice, an unlikely location since the host ice experiences lower stresses than the beam. Fig.4. shows the vertical location of these events as a function of time. If the events were the result of a single crack, this would indicate slow crack propagation, of the order of  $5 \text{ ms}^{-1}$  (see Fig.4.). It appears that the crack either developed discontinuously or that the fracturing consisted of a series of individual cracks which finally connected with each other. What is clear is that the crack is growing from the bottom of the ice, if somewhat unevenly.

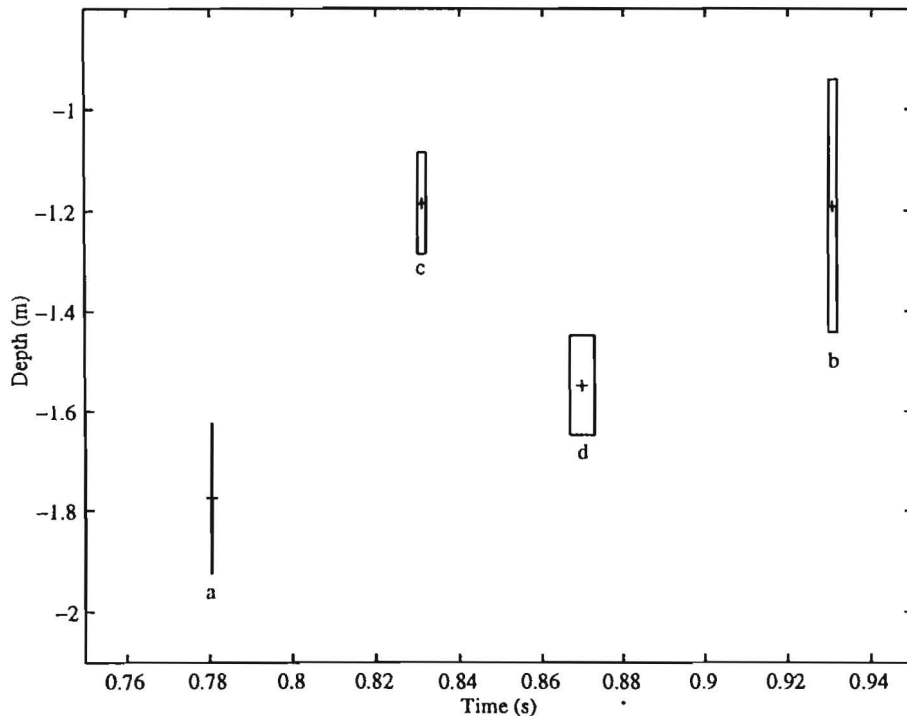


Fig.4. Vertical location of the events of "pull up" experiment beam 14 as a function of time

The other two experiments examined were of the "push down" type which have a characteristic form (Langhorne and Haskell, 1996b) involving a long quiet period and then a strong event about 0.02 s before the beam fails. The results of these experiments are also listed on Table 1. Note that it is physically impossible for a source to have a location above the ice. Consequently source locations above the beam are "rounded" to the surface of the beam. The data from the acoustic emission channels and the hinge strain of beam 15 are displayed in Fig.5. Two events were isolated for this beam, event 15a just before failure, and event 15b which is identified with the onset of emissions at the point of beam fracture.

#### DISCUSSION AND CONCLUSIONS

For the "push down" experiments, most of the events appear to occur near to or at the surface, and in the period immediately before the failure of the beam. This is consistent with a model where the warmer deeper sections of the ice are sustaining the compressive load without cracking, and the colder, more brittle upper layers of the ice are failing catastrophically. Any noise from deep crushing does not register at the transducers, suggesting either that no compressive cracking takes place at the imposed stress levels, or that compressive cracking is of low amplitude compared to the tensile cracking events. This is supported by the fact that

the "pull up" experiments did not record compressive events either, even though these events should have been close to the transducers at the surface. Consequently our ability to locate the emissions in 3-dimensions has allowed us to identify tensile cracking as the dominant acoustic emission source during this type of *in situ* testing. For the present experiments the upward crack velocity in the lower half of the sea ice sheet was  $5 \text{ ms}^{-1}$  in the range of values quoted by Parsons and others (1987) and Petrenko and Gluschenkov (1996).

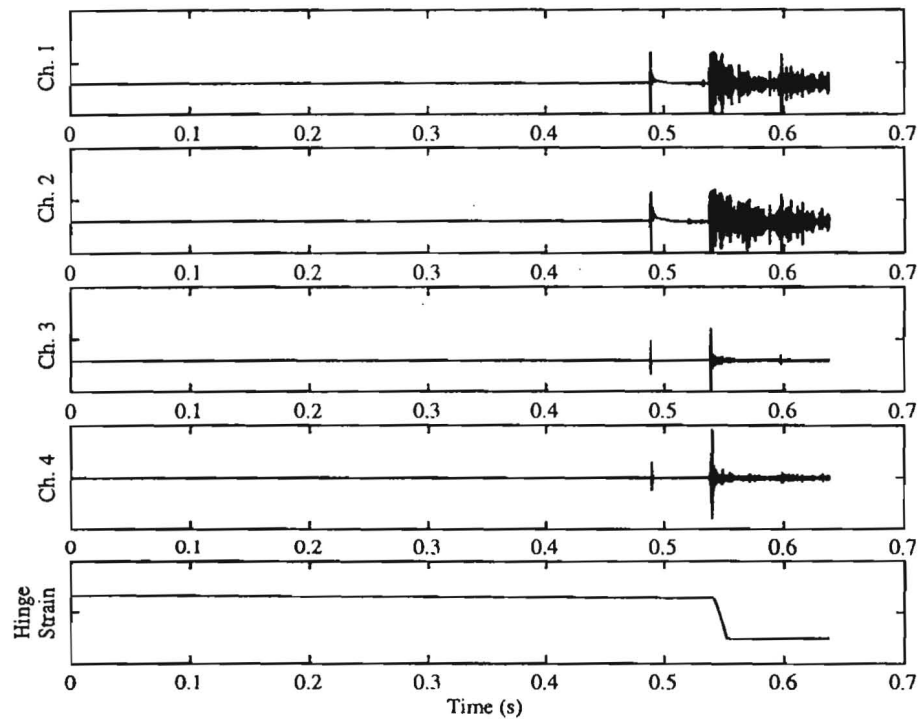


Fig.5. Acoustic emission data channels and hinge strain for beam 15

#### REFERENCES

- ADAMSON R.M., DEMPSEY J.P., DEFRANCO S.J., XIE Y. (1995): Large-scale in-situ fracture experiments Part 1: Experimental aspects. In AMD-Vol. 207, Ice Mechanics, eds J.P. Dempsey and Y.D.S. Rajapakse, American Society of Mechanical Engineers, pp. 107-128.
- BULLEN K.E., BOLT B.A. (1985): An Introduction to the Theory of Seismology. Cambridge University Press, 4th edition.
- COLE D.M. (1993): The effect of creep on the constitutive behaviour of saline ice at low strains. In AMD-Vol. 163, Ice Mechanics, Amer. Soc. of Mechanical Engineers, pp. 261-271.

COLE D.M., DEMPSEY J.P. (2000): Modelling the in situ constitutive behaviour of sea ice. In Proc. IUTAM Conference on Scaling Laws in Ice Mechanics and Ice Dynamics, Fairbanks, USA, June 13-16, 2000.

DEFRANCO S.J., DEMPSEY J.P. (1994): Crack propagation and fracture resistance in saline ice. *J. Glaciol.*, 40, pp. 451-462.

LANGHORNE P.J., HASKELL T.G. (1995): High frequency acoustic response of sea ice to single load cycles: a preliminary analysis. In Proc. 14th International Conference on Offshore Mechanics and Arctic Engineering, 4, pp. 29-34.

LANGHORNE P.J., HASKELL T.G. (1996a): Acoustic emission during fatigue experiments on first year sea ice. *Cold Regions Science and Technology*, 24, pp. 237-250.

LANGHORNE P.J., HASKELL T.G. (1996b): Stress-induced acoustic emissions in sea ice. International Association for Hydraulic Research 13th International Ice Symposium, Vol. 1, Beijing, China, 27-30 August 1996, pp. 131-141

MCKENZIE C. (1996): Location and Analysis of Acoustic Emissions in Sea Ice. MSc Thesis, University of Otago, Dunedin, New Zealand.

PARSONS B.L., SNELLEN J.B., HILL B. (1987): Preliminary measurements of terminal crack velocity in ice. *Cold Regions Science and Technology*, 13, pp. 233-238.

PETRENKO V.F., GLUSCHENKOV O. (1996): Crack velocities in freshwater and saline ice. *J. Geophys. Res.*, 101(B5), pp. 11541-11551.

SINHA N.K. (1985): Acoustic emission study on multi-year sea ice in an Arctic field laboratory. *J. Acoust. Emission*, 4(2/3), S290-293.

SINHA N.K. (1994): Characteristics of acoustic emissions from different types of polycrystalline ice. Proc. Int'l. Symposium on Snow and Related Manifestations, Manali, India, 26-28 Sept. 1994.

THURBER C.H. (1985): Nonlinear earthquake location: Theory and examples. *Bull. Seis. Soc. Am.*, 75(3), pp. 779-790.





**MANAGING ICE AT CORPS OF ENGINEERS LOCKS AND DAMS;  
CURRENT SOLUTIONS AND FUTURE NEEDS**

**Andrew M. Tuthill<sup>1</sup>**

**ABSTRACT**

This paper overviews common ice problems encountered at U. S. Army Corps of Engineers locks and describes current solutions. In spite of major advances in ice control methods during the last several decades, a number of the most serious ice problems still lack practical solutions at many of the projects, such as passing brash ice that accumulates in the upper lock approach and removing ice from and lock walls and gate recesses. Research directions and possible strategies for addressing these problems are discussed.

**INTRODUCTION**

The United States has a total of 17 000 km of inland waterways on which about 11 billion metric tons move annually. About half of this water-borne commerce takes place on ice-affected portions of the Mississippi River System, which include the Ohio and Illinois Rivers (Fig.1.). The U. S. Army Corps of Engineers operates a total 76 locks and dams on these waterways, all of which experience ice to some extent. Most of these projects were built between 1930 and 1970 and, due in part to their age, operation and maintenance consumes a major portion of the Corps of Engineers annual budget. In addition to the Mississippi River System, there is a limited amount of navigation in ice on the Great Lakes and connecting channels. Table 1 shows reach lengths, annual tonnages and the number of navigation projects on the important waterways in the U. S. where ice is present.

Winter-long navigation on the mainstem Mississippi extends 260 river km and seven lock and dam projects above St. Louis, Missouri. The 19 navigation projects above this point are closed to navigation from about 1 January to 1 March of each year, but can still face serious ice before and after the closed period. The Corps takes advantage of the closure to scheduling structural rehabilitation and major maintenance of the locks.

---

<sup>1</sup>U. S. Army Cold Regions Research and Engineering Laboratory, Hanover, NH, USA, Tel.: 603-646-4225,  
fax: 603-646-44477, e-mail: atuthill@crrel.usace.army.mil



Fig.1. Navigation projects on the Mississippi River System with winter navigation :

Table 1

Major Ice-Affected Inland Waterways in the United States

River or Reach	River Kilometers	Millions of Metric Tons	Locks and Dams
Mississippi River			
Ohio mouth to Missouri mouth	314	107	1
Missouri mouth St. Paul, MN	1067	77	27
Illinois River	575	43	8
Missouri River	1180	6	0
Ohio River	1580	212	23
Monongahela River	207	34	8
Allegheny River	116	3	8
St. Marys River (Soo Locks)		77	1
Totals	5039	559	76

Navigation continues all winter in the Illinois Waterway, which connects Lake Michigan to the Mississippi via a series of eight locks and dams. Much of the Midwest grain harvest moves down the Illinois in winter, and at times, severe ice can bring this barge traffic to a standstill. The ice problems occur both at these navigation projects and at reach locations in between, and, as a result, it is sometimes necessary to limit tow size so that the barges can enter the ice-filled locks or push through ice-congested channels.

The Ohio River and its tributaries, where the Corps operates 39 locks and dams, are navigated all winter. Due to its more southerly location, the ice on the Ohio is typically less severe than on the upper Mississippi or Illinois, but extreme ice is possible, the winters of 1978 and 1979 being examples. In addition to the milder climate, many of the newer Ohio River locks and dams are better equipped to deal with ice than their counterparts on the upper Mississippi and Illinois Rivers.

Although the Soo Locks in northern Michigan closes for about 2 ½ months each winter, it still faces some of the worst ice problems in the nation, particularly following the reopening to navigation in late March.

#### **COMMON ICE PROBLEMS AT LOCKS AND DAMS**

Based on surveys by Zufelt and Calkins (1985), Haynes et al. (1993), and discussions with lock personnel, the most important ice problems at locks include;

- a.) ice in congestion in the upper approach,
- b.) ice in the miter gate recesses,
- c.) ice buildup on lock walls,
- d.) ice on miter gates, and
- e.) brash ice in the lock chamber.

#### **Ice in the upper approach**

Brash ice in the upper approach is the most serious problem in winter operations and it leads to many of the other ice problems faced at locks (Fig.2.). Also, because the supply of ice is often nearly continuous, solutions are difficult. The severity of the problem depends on factors such as air and water temperature, river discharge, wind and the location of the lock with respect to upstream channel configuration. The worst problems arise when, during prolonged cold periods, the channel upstream of a lock and dam freezes over completely, except for the navigation track where the ice is continually rebroken by tow traffic and moved downstream by the current and barges. Brash ice pushed ahead of downbound tows is pushed into the lock, and at least one ice lockage is usually needed to pass the tow. Under extreme circumstances it can take up to eight hours to get a single tow through the lock. In some cases, frazil or brash ice in the upper approach can be so thick that it is drawn into the culvert intakes clogging the lock filling valves. This problem is particularly severe at Lock 19 on the Mississippi where the intakes are located in the upper gate sill.



**Fig.2. Ice in the upper approach of Lock 27 on the Mississippi River**

If air temperature is above freezing, and the ice accumulation is loose, it may be possible to draw ice out of the upper approach and pass it through adjacent dam gates, either around the end of the river guardwall or through openings in the wall or "drift passes". Most existing drift passes are too narrow to be effective though, a problem that is being corrected at several projects on the upper Mississippi.

High flow air curtains across the upper gate sill or aligned diagonally help deflect the ice pushed ahead of barges, reducing the amount of ice that enters the lock. Ice deflection is most effective when the deflected ice is continuously passed through an adjacent dam gate or a parallel lock chamber. Free towboats often position themselves across the upper approach to the lock, or use their propeller wash to move brash towards dam gates. If an adjacent lock is equipped with submergible lift gates or special overflow bulkheads at its upstream end, ice may be skimmed through the lock chamber (Fig.3.). This practice is very effective at some of the newer projects on the Ohio River and at the new Mel Price Lock on the Mississippi River, completed in 1989.

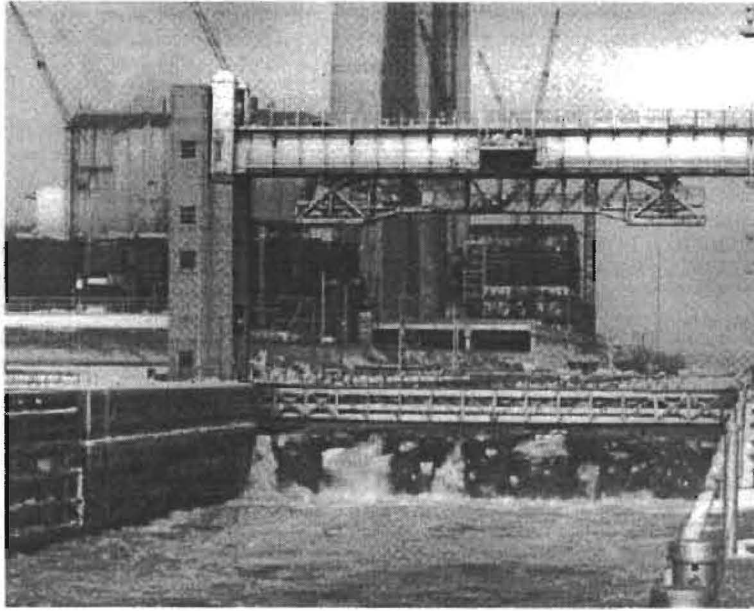


**Fig.3.** Skimming ice over bulkheads at New Cumberland Lock and Dam on the Ohio River

#### **Brash ice in the miter gate recesses**

Brash in the miter gate recesses greatly hinders winter operation and can prevent the gates from fully opening. Once this situation occurs, the Corps may require the barge industry to limit the length and width of their tows, a measure that greatly reduces the cargo capacity of the waterway system. Ice caught between the back of the miter gate and the recess wall can damage gate and put dangerously high stresses on the gate hinge mechanisms. In the past, operators manually cleared ice from the recesses using pike poles and ice rakes, methods that were slow and labor-intensive. They would also swing the miter gates back and forth or "fan the gates" in an effort to force the ice out of the recess.

The development of high flow bubbler systems during the last two decades has done much to solve this problem. This relatively low cost solution is now widely accepted within the Corps, and high flow systems are now installed during most major lock rehabilitation projects on ice-affected rivers. The typical system, developed by Hanamoto (1981) and Rand (1988), consists of air curtains in the four gate recesses and two lateral air curtains upstream of the miter gates (Fig.4.). Electric or diesel powered compressors in the 230 to 300 m<sup>3</sup>/m range supply the diffusers via valve manifolds that permit the entire airflow be switched to one diffuser at a time. Even with these high flow air systems, some gate fanning is usually needed to force brash ice out of the gate recesses.

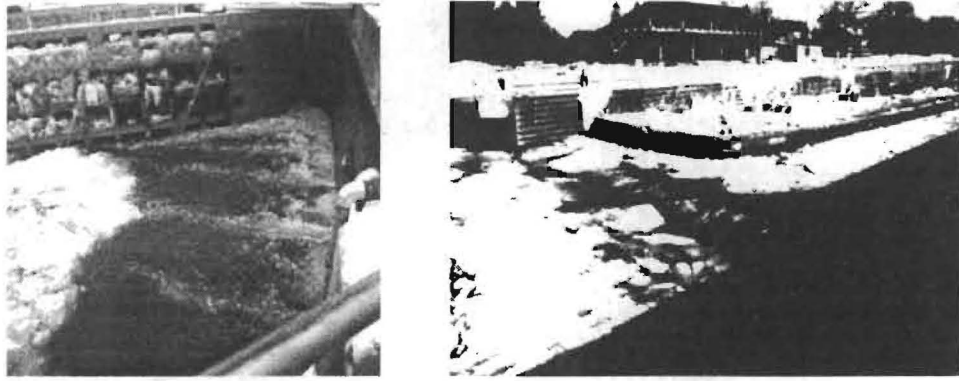


**Fig.4.** High-flow air curtains; in the miter gate recess (left), and across the upper sill (right).

#### **Icing of gate recess walls and lock walls**

The icing of gate recess and lock walls still lacks a widespread practical solution. Ice buildups or "collars" typically form at the high pool level and can achieve widths of greater than 1 m, preventing barges from entering the lock (Fig.5). Ice formation on the gate recess wall can prevent the gates from fully opening and cause structural damage to the gate, particularly in the hinge or "quoin" area.



**Fig.5.** Ice collars in the gate recess and lock wall

The most common method for removing ice from the lock walls is still chipping, which is extremely slow and labor-intensive. If a portable boiler is available, steaming is more effective but still time consuming. Some Corps facilities rent "Hotsy" brand, high-pressure hot water washers, which have the advantages of being portable and easily available, but are slow especially if a large area is to be deiced.

Haynes et al. (1997) installed a 1.22 x 2.44 m, 1920 W electric heater panel that successfully shed ice collars from lower gate recess at Starved Rock Lock on the Illinois River. The authors proposed installing panels along the entire 22 m length of the gate recess and cycling power from one panel to the next every 30 minutes to conserve power. The plan, though feasible, has not been carried out to date, perhaps due to a recent string of mild winters on the Illinois River. High density polyethylene panels were installed in the gate recess at Starved Rock Lock to help shed ice, but performance declined as the plastic became more and more abraded.

Probably the most effective solution for deicing large areas was the copolymer coating tested at the Soo locks in 1979, during the Winter Navigation Program (Frankenstein and Hanamoto, 1983) (Fig.6.). The coating was relatively costly to apply though, requiring steam cleaning of the lock wall and an epoxy undercoat. Some steaming was required, but the ice came off the coated lockwall much more easily than from bare concrete. Within a few years, vessels had scraped off most of the coating, and it was not re-applied due to cost and the fact that winter-long operation of the Soo Locks had been discontinued.

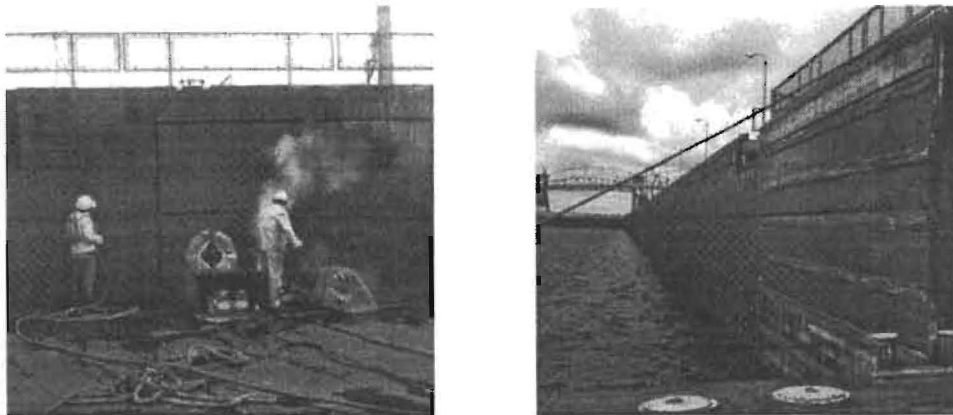


Fig.6. Steam cleaning the lock wall (left), and the newly-applied copolymer coating (right)

#### **Icing of miter gates**

Brush and slush ice packed into the trusswork of miter gates by vessels increases the total weight of the gate leaf, stressing supports and gate operating equipment. These ice accretions impinge against the recess wall preventing full gate opening. At many locks on the upper

Mississippi, low flow bubbler lines along the bases of the gates are used to circulate warmer water from below to suppress surface ice formation on the upstream sides of the gates. At the Soo Locks, plywood panels enclose the trusswork on the upstream side of the miter gates, and steam diffusers inside the gate provide heat to melt ice off the gate exterior. Ultra high molecular weight (UHMW) polyethylene panels are now replacing the plywood due to their improved durability and lower coefficient of friction.

On the Illinois Waterway, replacement miter gates have the steel skinplates on the upstream rather than the downstream side. The new gates are also less thick, which allows more clearance between the gate and the recess wall for ice. Both these design features improve gate performance in ice.

#### **Brash ice in the lock chamber**

Brash ice congestion in the lock chamber is the direct result of ice in the upper approach. The common solution is to lock this ice through, at the expense of delaying navigation. One problem common to ice lockages is the difficulty of flushing ice from the upper end of the lock when the chamber is at low pool. At the Soo Locks, four 60 cm diameter manifolds, installed in the upper miter gates at the low pool water level, create horizontal surface jets to move this ice as far downstream as the filling ports. Opening the filling valves then creates sufficient current through the ports to flush the ice out of the lock.

Brash ice beneath barges presents a serious problem during winter lockages. This ice accumulates as the tows negotiate the ice-filled approaches and makes it difficult for the tow to enter the lock. Damage can result as the tow passes over and the ice scrapes off on the lock sill. When locking down, the barges and ice may come to rest on directly on the lock floor, and, because there is more ice beneath the center barges, the barges settle unevenly, snapping the cables. Depending on the design of the port system, structural damage is possible. When this occurs, operators respond by refilling the lock in an effort to redistribute the ice more evenly.

#### **CONCLUSIONS AND FUTURE NEEDS**

Brash ice management at Corps locks has greatly improved over the last two decades as a result of developments in high-flow bubbler systems. Bubblers have the advantage of being relatively low cost and simple to implement at existing structures. The relationship between airflow from the compressor and ice-moving performance of the bubbler system is not well understood at this point. Research in this area would help designers size compressors and improve accuracy in scaling airflow from bubblers tested in physical models to prototype values.

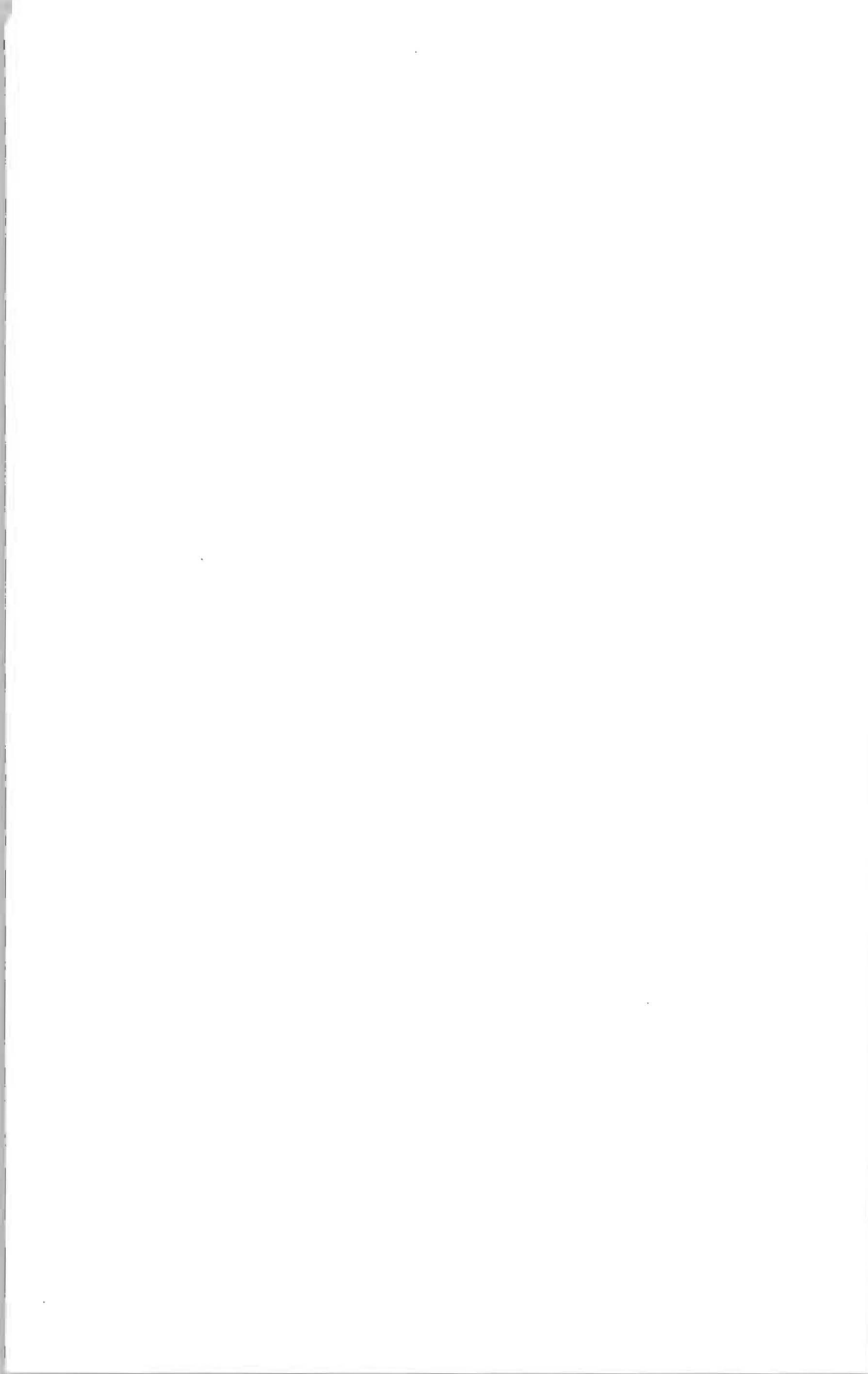
Better methods are needed to prevent brash ice in the upper approach from entering the lock chamber. Possibilities include "super" high-flow deflector bubblers and specially designed openings in the river guardwall to allow the ice to move to adjacent dam gates.

Although these measures may not be economical as retrofits to existing projects, they should be seriously considered in the design of new structures or major rehabilitation projects. Efforts are now underway at CRREL to develop and adapt ice-hydraulic numerical models to evaluate ice passage at locks and dams.

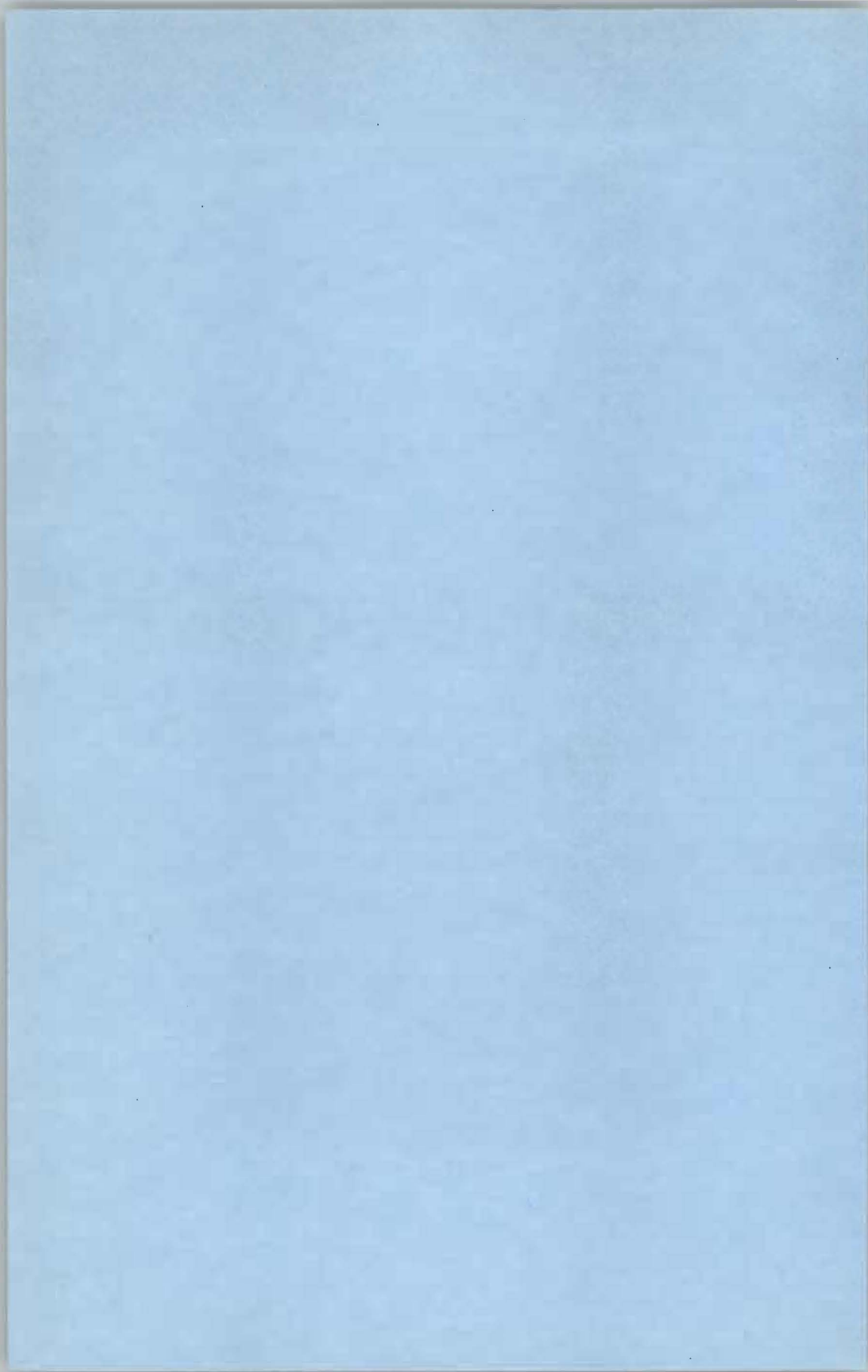
Practical solutions to lock wall and miter gate recess deicing are still lacking. Although electric resistance heating is an efficient method of deicing on a small scale, it is not economical for large areas. The low-adhesion coating tested at the Soo Locks in the late 1970's was good start, and further work in this area is needed. Methods that take advantage of solar radiation need to be explored such as painting south-facing lock walls black, or using parabolic reflectors to melt ice in shady areas. Flexible rubber membranes, similar in concept to airplane wing de-icing boots might be an effective, low-energy method for removing ice from gate recess walls. Rubber dams shed ice effectively, and this technology might be adapted to ice remove ice from lock walls. Mechanical means such as impact chisels or ice scrapers mounted to towboat bows are also possibilities.

#### REFERENCES

- FRANKENSTEIN G.E., HANAMOTO B. (1983): ASCE State of Practice Report; Design for Ice Forces, Chapter; Methods of Ice Control, pp. 205-215, ©1983 American Society of Civil, New York, NY.
- HAEHNEL R.B. (1998): Nonstructural Ice Control. CRREL Special Report 98-14, U.S. Army Cold Regions Research and Engineering Laboratory, Hanover NH, USA.
- HANAMOTO B. (1981): Ice Control at Navigation Locks. Proceedings: Water Forum '81, pp. 1088-1095, American Society of Civil Engineers, August 10-14, 1981, San Francisco, CA.
- HAYNES D.F., HAEHNEL R.B., ZABILANSKY L. (1993): Ice Control Techniques at Corps Projects. REMR Technical Report HY-14, Repair, Evaluation, Maintenance, and Rehabilitation Research Program, U.S. Army Corps of Engineers, Washington, D. C., USA.
- HAYNES D.F., HAEHNEL R.B., CLARK C., ZABILANSKY L. (1997): Icing Problems at Corps Projects. REMR Technical Report HY-10, Repair, Evaluation, Maintenance, and Rehabilitation Research Program, U.S. Army Corps of Engineers, Washington, D. C., USA.
- RAND J.H. (1988): High Flow Air Screens Reduce Ice-Related Problems at Navigation Locks. Proceedings, 9th International IAHR Ice Symposium on Ice, pp. 34-43, August 23-27, Sapporo, Japan.
- ZUFELT J.E., CALKINS D. (1985): Survey of Ice Problem Areas in Navigable Waterways. CRREL Special Report 85-2, U.S. Army Cold Regions Research and Engineering Laboratory, Hanover NH, USA.



# **WORKING GROUP REPORT**





## **UNDER ICE HABITAT**

### **Report of the Working Group, edited by Einar Tesaker**

#### **INTRODUCTION**

A working group named "Under Ice Habitat" was established during the meeting of the IAHR Ice Engineering Section at the 14th International Symposium on Ice in Hanover, NH 1998. The group shall report to the Ice Symposium in Poland in 2000.

The ambitious scope of the working group was understood to include:

- Review and describe state-of-the-art, including synthesis of presentations in international periodica and conferences on Ice Related Hydraulics and Habitat Hydraulics, (IAHR Ice Symposia, Nordic Research Basin Workshops, Int. Symposia on Habitat hydraulics, Engineering and Environmental literature related to ice, etc.)
- Identify research needs, and if possible initiate research on selected topics, e.g.:
  - Velocities, current distribution and geometry under ice and during ice formation
  - Preferred velocities by fish under winter conditions
  - Effects of ice cover on temperature, light and water quality
  - Ice formation and break up effects on vegetation, survival of roe etc
- Include winter effects in habitat models. The present HABITAT model has been based on data from field research under ice-free conditions. In order to incorporate ice conditions in the model scope, adjustment and new routines are needed, with reference to research on winter habitat.
- Evaluate practical methods for improvement of the winter habitat

#### **WORKING GROUP ACTIVITY AND MEMBERS**

A call for interest was initially sent to a large number of e-mail addresses, quoted from participants lists, literature references etc. Two groups of respondents emerged from this call, viz.: those interested in participation in the group, and those interested in remaining on the mailing list. A list of names and addresses is presented below.

Relevant information and comments were presented in a web page: "Under Ice Habitat": [http://www.sintef.no/units/civil/water/habitat/under\\_ice\\_habitat.html](http://www.sintef.no/units/civil/water/habitat/under_ice_habitat.html). This page has been updated from time to time with new information and comments from working group members and others.

**Contacts and Working Group Members:**

	Mailing list:	Members:
" Annear Tom "	<tannea@missc.state.wy.us>;	Yes
" Beltaos, Spyros "	<spyros.beltaos@cciw.ca>;	
" Bergeron Normand "	<ess-inrs-nbergeron@S0-OTT-XBH1.NRCan.gc.ca>;	Yes
" Brown, Richard "	<rs3brown@sciborg.uwaterloo.ca>;	
" Clarke, Keith "	<clarke@athena.nwafc.nf.ca>;	
" Daly, Steven F CRL "	<sfdaly@crl02.crrel.usace.army.mil>;	
" Dolgoplova, Elena "	<endol@iwapr.msk.su>;	
" Doyle, Paul "	<pdoyle@kamloops.env.gov.bc.ca>;	
" Hamilton, Stuart "	<stuart.hamilton@ec.gc.ca>;	
" Helwig Trevor "	<thelwi@po-box.mcgill.ca>	
" Ikaevalko, Johanna "	<jikavalko@ipoe.de>;	
" Kempema, Ed "	<kempema@uwyo.edu>;	
" Lavender, Tom "	<TLavender@Acres.com>;	
" Reid, Bruce "	<bareid@rideauvalley.on.ca>;	
" Richter, Susan "	<srichter@acres.com>;	
" Threader, Ron, dr "	<ron.threader@ontariopowergeneration.com>;	Yes
" Wang, Dapei "	<dapei.wang@ec.gc.ca>;	Yes
" White, Kathleen D. CRL "	<kwhite@crl02.crrel.usace.army.mil>;	Yes
" Yamazaki, Makoto "	<makoto@epmail.hepco.co.jp>;	

	Relevant web pages	
" Brown, Richard "	<a href="http://sciborg.uwaterloo.ca/~rs3brown/">http://sciborg.uwaterloo.ca/~rs3brown/</a>	
" Daly, Steven F CRL "	<a href="http://www.mesc.nbs.gov/Default.htm">http://www.mesc.nbs.gov/Default.htm</a> <a href="http://www.crrel.usace.army.mil/">http://www.crrel.usace.army.mil/</a>	
" Tesaker, Einar "	<a href="http://www.sintef.no/units/civil/water/">http://www.sintef.no/units/civil/water/</a>	
" White, Kathleen D. CRL "	<a href="http://www.crrel.usace.army.mil/ierd/">http://www.crrel.usace.army.mil/ierd/</a>	

**RELEVANT TOPICS FOR RESEARCH**

Habitat conditions in watercourses depend on many variables, e.g.: geometry, flow distribution, temperature, water quality, etc. The formation and presence of ice influence strongly on many of these factors. It follows that modification of e.g. geometry or flow may change the winter habitat to the better or worse.

So far research on the winter habitat and its relations to ice has been limited, probably due to difficult field access and lack of suitable instrumentation. There is obviously a need for studies both on the general relations between habitat and winter conditions, and on possible measures for the control and improvement of the winter habitat.

Important topics related to the thriving or survival of fish etc under ice are e.g.:

- Effects of ice on the food chain, temperature, contamination and air contents.
- Conditions for migration of fish under ice.
- Variation of velocity and pressure during ice formation and break-up.
- Ice effects on roe and fry.
- Long term influence of ice on local fish population and type of fish.
- Effects caused by regulation of flow and stage.
- Possible measures to improve/influence on the winter habitat.
- Hydraulic and sedimentary effects of such measures or other structures.
- Restrictions to impose on the winter flow in regulated streams.

In natural rivers, remedial action for improving the habitat is usually limited to moderate modification of the local geometry.

In regulated rivers the regulation itself usually imposes disputed effects. But regulation also represents a possibility for improvement of the winter habitat, e.g. by control of discharge, reduction of ice runs, arrangement of artificial pools or under-ice passages, or even temperature control.

#### **PUBLICATIONS**

A search for publications related to the Working Group subject has so far resulted in more than fifty references, tentatively grouped under the following headings:

- General ice related topics.
- Ice-cover effects on bed morphology.
- Under-ice effects on ecology and habitat in general.
- Under-ice effects on ecology and habitat (fish-related).
- Frazil ice effects etc on fish and benthic substrate.
- Stress and fish.
- Water quality.
- The IAHS Workshop W3: The Hydrology of Ice-Covered Rivers and Lakes, Birmingham, UK, 1999: Five relevant references, some to be published in Hydrological Processes during 2000.

The full reference list is given at the end of the report.

#### **RESEARCH IN PROGRESS OR PLANNED**

By surveying the listed publications the following notes on current research seem to cover most of the ongoing activities, and some possibilities for further activity:

### Field research

Field investigation of habitat-related factors under ice conditions is generally difficult because of short daylight, ever-changing and unsuitable weather conditions and difficult access to relevant parameters. Few systematic field studies have therefore been completed and published. Many attempts to approach the topic have been made in recent years, however, but observations are so far scattered and difficult to analyse. Instrumentation and methods are rapidly improving, however.

The following list refers status for a few methods and ideas for measurements and research:

- Time lapse video recordings of e.g. ice formation and break up has been tried, and should be further encouraged. Under-ice video recordings from the field have so far not been reported, probably due to lack of suitable equipment.
- Sonar, echo sounder or telemetry for registration of fish behaviour under ice is in the beginning stage (Brown et al. several items)
- Systematic collection of water quality data is needed for comparison of under-ice and ice-free situations (e.g. temperature, oxygen, sediment distribution).
- Horizontal and vertical current and turbulence patterns under ice have been measured and analysed, but there is lack of data from important habitat-related locations, e.g. pools, rapids, boulder beds.
- Studies of fish behaviour under ice cover, e.g. depth and velocity preferences by various types of fish, are in progress, but need further investigation.
- The study of local velocity and turbulence peaks under ice cover as the cause of damage to roe pits and changing of migration routes should be further investigated. The method of "standard hemispheres" (Stazner et al., 1989) as indicators of local shear stresses on uneven (boulder) beds has so far been used only without ice, but might be adapted to under-ice conditions with suitable methodology.
- Effects from short-term discharge variations (hydro-peaking) on fish related parameters may be more serious under ice cover than in open surface flow. (Open surface study of fish escape conditions is in progress at [SINTEF](http://www.sintef.no/units/civil/water/effekt/hydpeak.htm), see <<http://www.sintef.no/units/civil/water/effekt/hydpeak.htm>>)
- Some observations of fish mortality associated with ice blasting have been collected and analysed (Schaap et al., 1998)
- Some installations for improving the habitat in shallow rivers have been reported, but few results are known, and none for ice covered conditions. Structures placed in the river may cause grounding and free spans of ice, with interesting effects on the habitat.

### Model development

- The [HABITAT](http://www.sintef.no/units/civil/water/habitat.htm) model (<<http://www.sintef.no/units/civil/water/habitat.htm>>) does not presently include surface ice effects
- Flow simulations including solid ice covers have been reported using the models [RICE](http://www.clarkson.edu/~htshen/ice.htm) (see <<http://www.clarkson.edu/~htshen/ice.htm>>) and [SSIIM](http://www.sintef.no/units/civil/nhl/vass/ssiim.html) (see <<http://www.sintef.no/units/civil/nhl/vass/ssiim.html>>)

- Modelling of near bed hydraulics for rough beds has been approached, e.g. by use of the model SSIIM. Similar approach may be tried for under-ice roughness.
- Other model developments, including calibration of HEC-2 for under-ice flow have been reported (Calkins et al., 1986; White, 1998; Yoon & Patel, 1993).

#### **Laboratory studies**

- In November, 1998, CRREL and University of Waterloo researchers performed tests on the effects of frazil ice on rainbow trout in CRREL's refrigerated hydraulic flume, and reported these at the Workshop on River Ice in Winnipeg June 1999 (White) (see <<http://www.crrel.usace.army.mil/welcome/facilities/flume.html>> and <[http://www.sintef.no/units/civil/water/habitat/Rainbow\\_trout\\_in\\_flume\\_pictures.htm](http://www.sintef.no/units/civil/water/habitat/Rainbow_trout_in_flume_pictures.htm)>).
- A shallow flume study of escape conditions for small fry during rapid stage variations in open flow is in progress at SINTEF. This study is a continuation of the open surface field study mentioned above. The study does not so far include ice cover effects.
- A study of fish behaviour under various shelter arrangements has been carried out at the Finnish Game and Fisheries Research Institute (Vehanen et al., 1999).

### **THE WAY AHEAD**

#### **Field and laboratory studies**

Field observations and systematic field research will be needed also in the future, in order to reveal and sort out general principles of fish behaviour under ice. Regulated rivers pose special challenges to the research, because it is easy to relate most adverse conditions to the regulation effects. It is therefore important to perform parallel studies in regulated and natural rivers.

Testing and evaluation of large-scale methods for habitat improvement will also require field observations of actual installations.

As soon as the research ventures from general phenomena towards more detailed studies of parameters, systematic variation of parameters is usually too difficult or impossible in the field. In regulated streams some controlled variation of discharge and stage may be possible, but usually at great expenses due to loss of water or energy production. Field research is also time consuming and costly for the researcher. Future field research should therefore mainly provide calibration data and serve as a means to keep organised laboratory/flume studies at the right track.

In order to serve this purpose development and use of sophisticated field instrumentation will still have high priority.

Possible approaches for further laboratory studies of life processes under ice might include:

- Cold room studies in a glass walled flume for observations of behaviour and choice of living conditions by fish under ice at various water temperatures.

- Study of migration patterns etc of fish in a wide, shallow flume, where ice cover effects may be simulated by a cover of transparent plastics. The habitat flume at SINTEF, might be suitable for such tests. See also Vehanen et al. (1999).
- Fish behaviour under ice may be studied in permanent ice laboratory flumes, like the one at CRREL. Observations by submerged instruments or video-cameras, laboratory sonar etc. are in progress. Some underwater PICTURES are found on the web. Visual observations from above through real (opaque) ice covers are difficult even in a laboratory (Web-references under Laboratory studies above).

#### **Artificial habitat improving field measures**

Habitat improving installations that have been attempted recently include:

- large singular rock elements or rock mounds placed on the river bed;
- short jetties from the river bank;
- artificial gravel bed layers;
- protection / re-installation of bank vegetation.

It seems likely that new types of artificial installations for habitat "improvement" will be proposed and installed.

Such installations should be carefully planned and monitored in order to avoid adverse effects, e.g.:

- bank erosion due to shifted flow distribution;
- reshaping of bed topography, e.g. (fishing) pools and spawning grounds;
- unwanted shifting of stream bed channels;
- local erosion around the installations;
- ice jams;
- increased flood water levels during natural flood events;
- secondary under-ice cooling/ice formation due to "chimney effects".

Their actual effect on the habitat may be of short duration or at least greatly reduced by rapid modification of the stream bed or flow distribution following as a result of the installations.

#### **Winter discharges in regulated rivers**

Regulated river management may produce both rather steady or typical on-off type discharges, but usually far from the natural winter flow regime.

Modern management of regulated rivers may include prescribed maximum and minimum discharges or other discharge restrictions. Effects of regulated discharges on the ice formation, ice jams and ice runs are fairly well known, while effects on flora and fauna life and reproduction are much less known.

The economical aspects of regulated river management, mainly energy production, have traditionally been given high priority. More recently also ecological values have been given

some attention. Because river fishery as food source and recreation also has a notable economical value, it is the habitat conditions for fish life and reproduction that has been easiest to promote in negotiations about regulated river management as well as research funding. In many contexts so far, "habitat" is still more or less synonymous with fish related habitat.

It seems natural to increase our knowledge and understanding of the relations between river management and all aspects of habitat in the future. Since the winter habitat is particularly sensible and crucial for the survival and thriving of many life forms, the under ice conditions in regulated rivers should be given increased attention in the near future.

#### **Numerical modelling and data analysis**

The complex aspects of under-ice flow are assumed to be a challenge for further numerical model developers. It is still a long way to go before numerical models can describe details of flow, ice, river life and habitat in a manner that can be used for detail analysis of practical local problems. The models HABITAT and RICE are so far prepared for free surface flow. Models for analysis and classification of river bed relations between hydraulics and fish preferences are presented, but need further refinement.

3-dimensional models like SSIIM have for some time been able to describe the near-bed flow in cobble bed rivers. By use of object-oriented modelling techniques, various habitat aspects are now being approached for numerical treatment. This development is only in the initial stage, and will be continued.

The following recent summary of the under-ice modelling status was presented at the IAHS Workshop W3 in Birmingham, UK (Alfredsen & Tesaker, 1999):

- Examples of severe ice effects on under ice habitat exist;
- Some data exist both for fish and ice in rivers, but they are not collected with modelling in mind;
- Modelling methods seem to be promising, but little validation data is currently available;
- Further method development is needed together with collection of more fish and ice data;
- Bioenergetic modelling may be a useful tool for handling effects on fish from changes in temperature and discharge.

## LITERATURE

The following list of literature has been collected from various sources, including items supplied by working group members. The list includes many more items than referred to in the text above.

### General ice related topics

CALKINS J.D., BROCKETT B.E. (1988): Ice-cover distribution in Vermont and New Hampshire atlantic salmon rearing streams. 5th Workshop on Hydraulics of River Ice.

FERRICK M.G., PROWSE T.D. (2000): Hydrology of Ice-Covered Rivers and Lakes. Manuscript accepted for EOS.

HAMILTON, MOORE, WIEBE (1996): Winter-flow characteristics in cold regions. 2nd Int. Symp. on Habitat Hydraulics, A459-470.

KERR D.J., SHEN H.T., DALY S.F. (1998): Evolution and hydraulic resistance of anchor ice on gravel bed. 14th IAHR Ice Symposium, 2, pp. 703-709.

MARTINS, GOY, BERGERON (1996): Structure of turbulent flow in an ice-covered tidal environment. 2nd Int. Symp. on Habitat Hydraulics, A435-446.

TEAL M.J. (1993): Estimation of mean velocity for flow under ice cover. M.S. Thesis, University of Iowa, US.

TESAKER E. (1970): Measurements of ice roughness and the effect if ice cover on water levels in three Norwegian rivers. IAHR Symposium, Reykjavik, paper 3.4.

### Ice cover effects on bed morphology

BERGERON, GOY, CHAUMONT (1996): Winter geomorphological processes in the Sainte-Anne River and their impact on the migratory behaviour of the Atlantic Tomcod. 2nd Int. Symp. on Habitat Hydraulics, A379-388.

BRENNAN T.S., ETTEMA R. (1995): Ice-cover influence on flow and bed-load transport in dune-bed channels. IIHR Report No. 374. Univ. of Iowa.

LAU L.L., KRISHNAPPAN B.G. (1995): Sediment transport under ice cover. J. Hydr. Engr. 119(6) pp. 934-950.

MILBURN D., PROWSE T. (1998): Observations on the role of an ice cover in sediment deposition in a northern delta. 14th IAHR Ice Symp, 1, pp. 189-196.

SAYRE W.W., SONG G.B. (1973): Effects of ice covers on alluvial channel flow and sediment transport processes. IIHR Report No. 218: U. of Iowa, US.

TSAI W.F., ETTEMA R. (1994): Ice cover influence on transverse bed slopes in a curved alluvial channel. J. Hydr. Res. 32(4) pp. 561-581.

WUEBBEN J.L. (1988): Effects of an ice cover on flow in a movable bed channel. 9th IAHR Ice Symposium, 1, pp. 137-146.

### **Under-ice effects on ecology and habitat in general**

DOLGOPOLOVA L.N., TESAKER E. (2000): Turbulent structure of ice-covered flow and ice impact upon habitat in rivers. Accepted for 15th IAHR Ice Symposium.

NISLOW K.H., LEVER J.H. (1998): Assessing the ecological impact of an ice control structure. 14th IAHR Ice Symposium, 2, pp. 787-792.

POWER G., BROWN R.S., IMHOF J.G. (1998): Groundwater and fish - insight from North America. *Hydrological Processes*, 13, pp. 401-422.

PROWSE T.D., GRIDLEY N.C., ed. (1993): *Environmental Aspect of River Ice*, NHRI Science. Rep. No 5, ISBN 0-662-20820-X.

PROWSE T.D. (1996): Significance of River Ice to Environmental Processes and Aquatic Systems. 13th IAHR Ice Symposium, III, pp. 865-872.

SHEN XIANCHEN (1998): Impacts of ice cover on water quality and fish life in the Songhuajiang Basin. 14th IAHR Ice Symposium, 1, pp. 169-174.

TESAKER E. (1998): Mitigation of ice effects in the habitat in regulated and natural rivers. 14th IAHR Ice Symposium, 1, pp. 161-167.

VEHANEN T., BJERKE P.L., HEGGENES J., HUUSKO A., MÄKI-PETÄS A. (2000): Effect of fluctuating flow and temperature on cover type selection and behaviour by juvenile brown trout in artificial flumes. *J. Fish Biology* (2000) 56, pp. 923-937.

WHALEN, PARRISH (1996): Effect of ice formation on the physical stream environment and the overwinter distribution of pre-smolt Atlantic salmon parr. *Proc. 2nd Int. Symp. on Habitat Hydraulics*, A 471-484.

### **Under-ice effects on ecology and habitat (fish-related)**

BALTZ D.M., VONDRACEK, BROWN, MOYLE (1991): Seasonal changes in microhabitat selection by rainbow trout in a small stream. *Trans. Am. Fish. Soc.* 120: pp. 166-176.

BROWN R.S. (1999): Fall and early winter movements of cutthroat trout, *Oncorhynchus clarki*, in relation to water temperature and ice conditions in Dutch Creek, Alberta. *Environmental Biology of Fishes*, 55 pp. 359-368.

BROWN R.S., POWER, MCKINLEY, BELTAOS (1998): Effects of hanging ice dams, surface ice break-up, and flooding on fish. *Proc., 14th IAHR Ice Symp., Potsdam, NY, Volume 1*, pp. 175-181.

BROWN R.S., MACKAY W.C.. (1995): Fall and winter movements of and habitat use by cutthroat trout in the Ram River, Alberta. *Trans. Amer. Fish. Soc.*, 124 pp. 873-885.

CHISHOLM I.M., HUBERT, WESCHE (1987): Winter stream conditions and use of habitat by brook trout in high-elevation Wyoming streams. *Trans. Amer. Fish. Soc.* 116 pp. 176-184.

CUNJAK R.A., CURRY, POWER (1987): Seasonal energy budget of brook trout in streams: Implications of a possible deficit in early winter. *Trans. Am. Fish. Soc.* 116 pp. 817-828.

JAKOBER M.J., MCMAHON, THUROW, CLANCY (1998): Role of stream ice on fall and winter movements and habitat use by bull trout and cutthroat trout in Montana headwater streams. *Trans. Amer. Fish. Soc.* 127: 223-235.

Johnson B.L. AND AL. (1998): Estimating flow rates to optimise winter habitat for centrarchid fish in Mississippi river backwaters. *Regulated Rivers: Res. Mgmt.* 14: 499-510.

MACIOLEK J.A., NEEDHAM (1952): Ecological effects of winter conditions on trout and trout foods in Convict Creek, California, 1951. *Trans. Am. Fish. Soc.*, Vol. 81, pp. 202-217.

WHALEN K.G., PARRISH, MATHER (1999): Effect of ice formation on selection of habitats and winter distribution of post-young-of-the-year Atlantic salmon parr. *Can. J. Fish. Aquat. Sci.* 56 pp. 87-96.

#### **Frazil ice effects etc on fish and substrate**

BENSON N.G. (1955): Observations of anchor ice in a Michigan trout stream. *Ecology*, v.36, pp. 529-530.

BROWN R.S., BRODEUR, POWER, DALY, WHITE, MCKINLEY (1999): Blood chemistry and swimming activity of rainbow trout exposed to supercooling and frazil ice. *Proc. 10th Workshop on River Ice, Winnipeg, Manitoba*, pp. 97-110.

BROWN R.S., STANISLAWSKI, MACKAY (1994): Effects of frazil ice on fish. In T.D. Prowse (ed.): *Proc. Workshop on Environmental Aspects of River Ice*, pp. 261-278. NHRI Symp. No. 12, Environment Canada, Saskatoon, Sask.

CUNJAK R.A., CAISSIE (1994): Frazil ice accumulation in a large salmon pool in the Miramichi River, New Brunswick: Ecological implications for overwintering fishes. In T.D. Prowse (ed): *Proc. Workshop on Environmental Aspects of River Ice*, pp. 279-295. NHRI Symp. No. 12, Environment Canada, Saskatoon, Sask.

CURTSINGER B. (1986): Under Antarctic ice. *National Geographic*, v. 169, no.4, April 1986, pp. 497-511. (Popular, but contains some fine photos of sponges lifted off the sea bed by anchor ice, and of starfish and fish trapped in anchor ice masses on the sea bed.)

DAYTON P.K. (1989): Interdecadal variation in an Antarctic sponge and its predators from oceanographic climate shifts: *Science*, v.245, pp. 1484-1486.

DAYTON P.K., ROBILLIARD G.A., DEVRIES A.L. (1969): Anchor ice formation in McMurdo Sound, Antarctica, and its biological effects: *Science*, v.163, pp. 273-274.

POWER G., CUNJACK, FLANNAGAN, KATAPODIS (1993): Biological effects of river ice. In: *Environmental Aspects of River Ice* In T.D. Prowse and N.C. Gridley (eds.) *National Hydrology Res. Inst.: Saskatoon, Sask.*, pp. 97-120.

SIMPKINS D.G., HUBERT, WESCHE (2000): Effects of Fall-to-Winter Changes in Habitat and Frazil Ice on the Movements and Habitat Use of Juvenile Rainbow Trout in a Wyoming Tailwater. *Trans. Amer. Fish. Soc.*, 129(1) pp. 101-118.

TESAKER E. (1975): Accumulation of frazil ice in an intake reservoir. *IAHR 3rd Int. Symp. on Ice, Hanover, NH*, pp. 15-24.

### **Stress and fish**

POWER G. (1997): A review of fish ecology in Arctic North America. American Fisheries Society Symposium, Volume 19, pp. 13-39.

SCHRECK C.B. (1981): Stress and compensation in teleostean fishes: Response to social and physical factors. In: Stress and Fish. A. D. Pickering, ed.. Academic Press, NY.

SCHAAP P.R., THOMAS C.J., REID B.A. (1998): Observations of Fish Mortality Associated with Ice Blasting on the Lower Rideau River, Ottawa, Ontario. The Canadian Field-Naturalist, Volume 112(2), pp. 241-244.

### **Water quality**

BELTAOS S., BURRELL B.C. (1998): Transport of metals on sediment during the spring breakup of ice. 14th IAHR Ice Symposium, 2, pp. 793-800.

CALKINS D.J., ASHTON G.D. (1988): Winter water quality in lakes and streams. US Corps of Eng., 7th Seminar on Water Quality.

MESSIER, ANCTIL (1996): Under ice river plumes in James and Hudson Bays. 2nd Int. Symp. on Habitat Hydraulics, A447-458.

WHITE K.D., MELLOH R.A. (1999): Diurnal variation in dissolved oxygen measurements during late winter ice-covered period, Sleeper's River. 10th Int. Conf. on Cold Regions Engineering, Lincoln, NH. US, pp. 550-560.

### **Methods, models and instruments**

CAI L. AND AL. (1998): Method for calculating flow resistance and discharge capacity under ice cover. Proc. 14th IAHR Ice Symposium, 2, pp. 711-715.

CALKINS J.D., ADLEY M.D. (1986): Calibrating HEC-2 in a shallow, ice-covered river. CRREL, Spes rep 86-34.

ETTEMA R., BRAILEANU F. (1998): A method for estimating sediment-transport rates in ice-covered channels. 14th IAHR Ice Symposium, 2, pp. 717-723.

STATZNER B., MULLER R. (1989): Standard hemispheres as indicators of flow characteristics in lotic benthos research. Freshwater Bio, 21, pp. 445-459.

WHITE K.D., DALY, GAGNON (1999): Use of CRREL refrigerated flume facility in simulating winter environments for aquatic life. 10th Workshop on River Ice, Winnipeg, Manitoba, June 9-11, pp. 85-96.

WHITE K.D. (1998): 1-D streamwise finite element model of dissolved oxygen under river ice. 14th IAHR Ice Symposium, 2, pp. 801-807.

YOON J.Y., PATEL V.C. (1993): A numerical model of flow in channels with sand dune beds and ice covers. IIHR Report No.362. University of Iowa, US.

**Contributions IAHS Workshop W3: The Hydrology of Ice-Covered Rivers and Lakes.**  
Session II: Ecological aspects of ice-covered rivers. Birmingham, UK, 1999:

CHAMBERS P.A., PIETRONIRO A.: Dissolved oxygen declines in ice-covered rivers: causes and environmental consequences.

ALFREDSSEN K., TESAKER E.: Incorporating ice and effects of ice into the Norwegian habitat assessment strategies and the HABITAT program system.

MARSH P., LESACK L.: The role of river ice covers in the hydrology and ecology of the Mackenzie Delta.

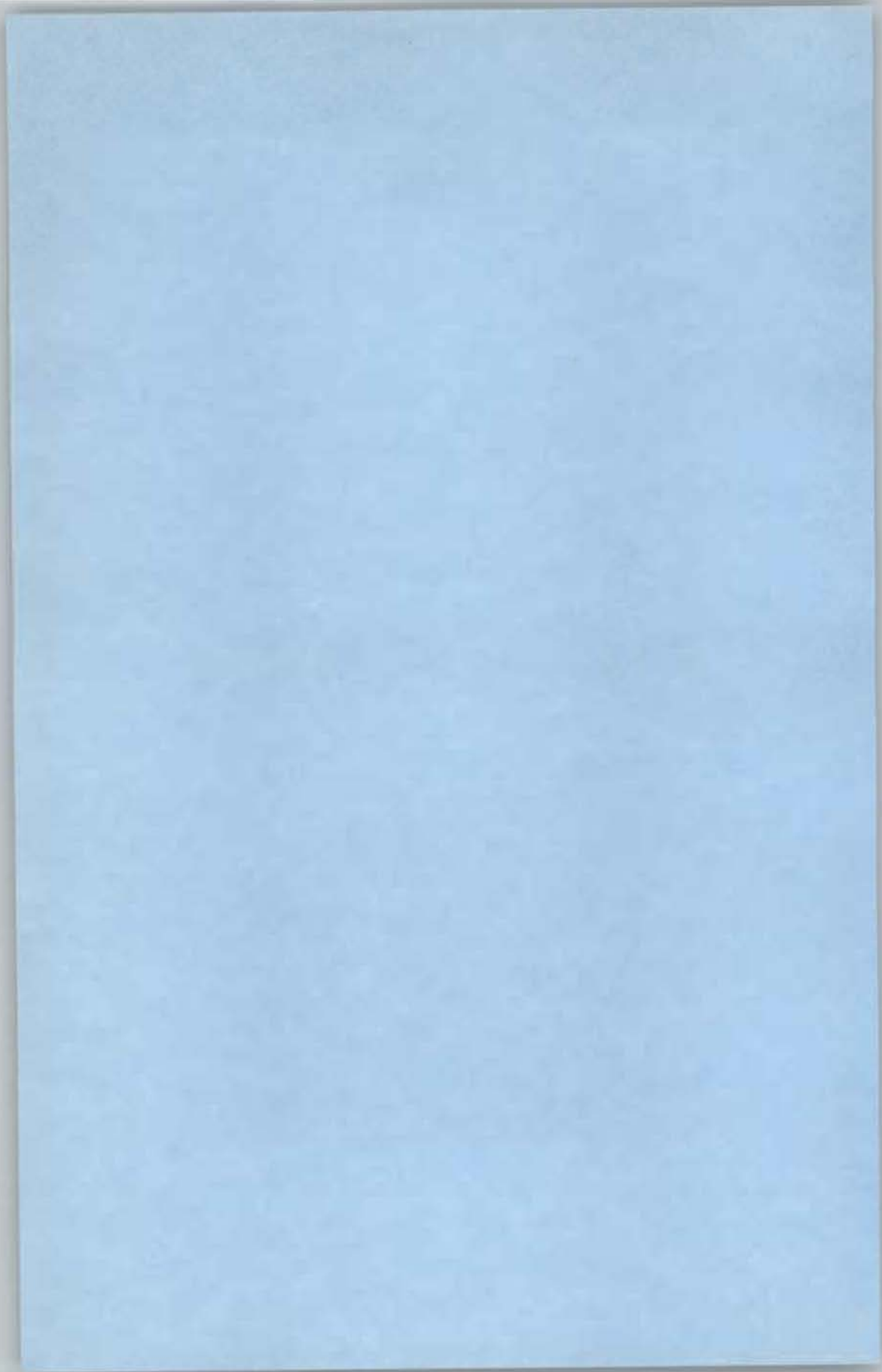
ANNEAR T.C. AND AL.: Behavioural and physiological response of trout to winter habitats in Wyoming, USA.

Round Table Discussion: "Research directions in climate change and ecological aspects of ice-covered rivers and lakes."

Some of these contributions will be published in Hydrological Processes during 2000.

In November, 1998, CRREL and University of Waterloo researchers performed tests on the effects of frazil ice on rainbow trout in CRREL's refrigerated hydraulic flume, and reported these at the Workshop on River Ice in Winnipeg June 1999 (Ref: Kathleen D. White).

# **SUPPLEMENT**



## ICE RESEARCH AND ENGINEERING AWARD

During 15th International Symposium on Ice Committee of the Section Ice Research and Engineering decided to award third **Ice research and Engineering Award** to Prof. Mauri Määttänen from Helsinki University of Technology, Finland for his outstanding contributions to ice research and engineering. Prof. M. Määttänen was member and Chairman of the Committee of the Section Ice Research and Engineering. He was the organizer of 10th International Symposium on Ice held in Espoo, Finland. Two previous Awards received Prof. Bernard Michel from Canada and Guenther Frankenstein from USA.

### MAURI PELLERVO MÄÄTTÄNEN



Mauri P. Määttänen obtained MSc in Aeronautical Engineering from Helsinki University of Technology in 1968, and Dr. Techn. (PhD), (Ice induced structural vibrations) from Helsinki University of Technology (HUT) in 1978. He was Teaching Assistant in Strength of Materials (Solid Mechanics) at HUT during 1965-68, and Researcher 1968 – 70. He became Associate Professor in Strength of Materials at the University of Oulu in 1970 and worked there at this position till 1977. From 1978 to 1987 was Professor of Technical Mechanics at the University of Oulu. During 1978 – 1980 was on sabbatical leave at US Army Cold Regions Research and Engineering Laboratory. Since 1988 he is Professor of Strength of Materials at HUT. His main research interest is ice mechanics,

especially dynamic ice-structure interaction and ice forces. He is member of IAHR and SAE. M. P. Määttänen was Chairman of the Section on Ice Research and Engineering from 1992-96. He published more than 100 papers mostly in ice engineering.



International Association  
of Hydraulic Engineering  
and Research

In recognition of his many outstanding technical contributions  
in the field of ice engineering and research, as well as his  
long term support of the activities of the IAHR,  
the Section on Ice Research and Engineering proudly  
presents the third

ICE RESEARCH AND  
ENGINEERING AWARD

To

*Mauri Määtänen*

With the deepest appreciation

A handwritten signature in cursive script, appearing to read 'K. HIRAYAMA'.

K. HIRAYAMA  
CHAIRMAN OF IAHR COMMITTEE  
ON ICE RESEARCH AND ENGINEERING

GDANSK, AUGUST 30, 2000

## AWARD FOR THE BEST STUDENT PAPER

Committee of the Section Ice Research and Engineering decided to give Award for the best student paper of 15th International Symposium on Ice to Knut V. Høyland from Trondheim University of Technology, Norway for the paper: **Measurements of consolidation in three first – year ridges.**

### KNUT V. HØYLAND



Knut V. Høyland obtained M.Sc. in Engineering from the Faculty of Marine Technology of NTNU Trondheim. In 1994-1997 he was assistant in applied mechanics at the Faculty of Mechanical Engineering of NTNU. In 1997 he began doctorate studies in arctic technology on the Faculty of Civil and Environmental Engineering, Department of Structural Engineering of NTNU Trondheim. The subject of his studies is the consolidation process in first-year sea ice ridges and the examination of their physical and mechanical properties. His supervisor is Professor S. Løset.



International Association  
of Hydraulic Engineering  
and Research  
Section on Ice Research  
and Engineering

This is to certify that

*Knut V. Høyland*

is the recipient of the best student paper  
award of the 15th International Symposium  
on Ice held in Gdańsk for his paper

Measurements of Consolidation in the  
Three First-Year Ridges

With the deepest appreciation

A handwritten signature in cursive script, appearing to read 'K. HIRAYAMA'.

K. HIRAYAMA  
CHAIRMAN OF IAHR COMMITTEE  
ON ICE RESEARCH AND ENGINEERING

GDAŃSK, AUGUST 30, 2000

## **NEW COMPOSITION OF THE COMMITTEE OF THE SECTION ON ICE RESEARCH AND ENGINEERING**

During organizational session Prof. Hung Tao SHEN from Clarkson University, USA has been elected new chairman for two years term (2001-2003). He replaced Prof. Ken Ichi Hirayama from Iwate University, Japan who acted as chairman for 4 —year term 1997-2000.

New composition of the Committee of the Section on Ice Research and Engineering is as follows:

H.T. Shen	USA	Chairman
J. Dempsey	USA	Secretary

### Members:

R. Aswall	Norway
S. Daly	USA
K.-U. Evers	Germany
M.G. Gladkov	Russia
L. Hammar	Sweden
K. Hirayama	Japan (coopted)
H. Jordan	Canada
K. Kato	Japan
P. Langhorne	New Zealand
T. Prowse	Canada
J. Tuhkuri	Finland
H. Wu	China

## **NEXT INTERNATIONAL SYMPOSIA ON ICE**

It has been decided that next 16th International Symposium on Ice in 2002 will be organized by the University of Otago, Dunedin, New Zealand. P.J. Langhorne will be chairman of the Organizing Committee. Topics for 16th Symposium were tentatively presented.

17th Symposium will take place in 2004 in St. Petersburg, Russia. It will be organized by the Research Institute VNIIG and dr. I. Shatalina will be chairman of the Organizing Committee.

## WORKING GROUPS ACTIVITY

The activity of working groups was discussed during special session. The following working groups are active in the Section on Ice Research and Engineering:

- River ice hydraulics
- Ice crushing processes
- Under ice habitat
- River ice ecology
- Symbols and definitions
- Scale effects
- Climate change effects on river ice regimes

E. Tesaker (chairman) presented the report of Working Group Under Ice Habitat.

## PANEL DISCUSSION: RESEARCH NEEDS IN ICE ENGINEERING

Panel discussion was lead by K.-E Evers (Germany), G. Timco (Canada) and M. Määttänen (Finland). It has been emphasized that all important problems of ice research are included in topics of Working Groups which exist in the Section. It would be very good to increase their activity. Problem of global climate change and its effect on ice regime has been regarded as very important in future.

## STATISTICS ABOUT PAST 14 ICE SYMPOSIA

Prof. K. Hirayama prepared some statistical data concerning previous 14 Ice Symposia. Symposia were organized by 12 countries. Twice Symposia were organized by USA (1975 – Hanover, 1998 – Potsdam), and Canada (1981 – Quebec, 1992 – Banff). Other countries organized Ice Symposium once: 1970- Iceland, 1972 – USSR, 1974 – Hungary, 1978 – Sweden, 1984 – Germany, 1988 – Japan, 1990 – Finland, 1994 – Norway, 1996 – China.

The amount of papers presented during Ice Symposia varied considerably from 41 (Budapest, Hungary in 1974) to 161 (Potsdam, USA in 1998). Altogether 1238 papers were presented during 14 Symposia which makes the average of 88 papers. 24 countries presented papers during previous 14 Symposia. Minimum of 1 paper was submitted by Korea and Yugoslavia. The highest amount of papers was presented by USA – 302 papers, Canada – 252 papers, China – 160, and 152 – (USSR) Russia. The topics presented during these Symposia included: ice properties, ice processes, ice hydraulics, instrumentation, ice forces, navigation in ice, and ice ecology. The most popular topics were: ice hydraulics – 342 papers, ice forces – 294 papers, and ice processes – 220 papers.

1986 - Iowa City



Participants of 15th International Symposium on Ice

*fol. Teresa Jarzębińska*



Committee of the Section on Ice Research and Engineering at work

*fol. Grzegorz Zastawny*



Participants of 15th International Symposium on Ice on board of the ship

*fol. Grzegorz Zastawny*



Participants of 15th International Symposium on Ice on Westerplatte

*fot. Grzegorz Zastawny*

## LIST OF PARTICIPANTS OF 15TH INTERNATIONAL SYMPOSIUM ON ICE

No.	First Name	Last Name	Country	e-mail
1	Randi	Pytte	Norway	rpa@nve.no
2	George	Comfort	Canada	gcomfort@fleetech.com
3	Andrzej	Dobrowolski	Poland	andrzej_dobrowolski@imgw.pl
4	Elena	Dolgoplova	Russia	endol@iwapr.msk.su / endol@agua.laser.ru
5	Dorota	Dybkowska-Stefek	Poland	dorota@estua.im.man.szczecin.pl
6	Robert	Ettema	USA	robert-ettema@uiowa.edu
7	Karl-Ulrich	Evers	Germany	evers@hsva.de
8	Mariusz	Gajda	Poland	office@rzgw.gda.pl
9	Kjell Inge	Gausland	Norway	kjell-inge.gausland@tietoenator.com
10	Barbara	Głowacka	Poland	andrzej_dobrowolski@imgw.pl
11	Jaakko	Heinonen	Finland	Jaakko.Heinonen@hut.fi
12	Yujiro	Hirai	Japan	y-hirai@epmail.hepco.co.jp
13	Ken-Ichi	Hirayama	Japan	tbucho@iwate-u.ac.jp
14	Kiyoshi	Hoshi	Japan	k.hoshi@bousai.or.jp
15	Knut V.	Høyland	Norway	knut.hoyland@bygg.ntnu.no
16	Koh	Izumiyama	Japan	koh@srimot.go.jp
17	Arnor	Jensen	Norway	arnor.jensen@bygg.ntnu.no
18	Teresa	Jarzębińska	Poland	tjarz@pg.gda.pl
19	Ewa	Jasińska	Poland	ewaj@ibwpan.gda.pl
20	Kazuhiro	Kamesaki	Japan	kkamesak@lab.tsu.nkk.co.jp
21	Tuomo	Kärnä	Finland	tuomo.karna@vtt.fi
22	Kazuyuki	Kato	Japan	kazkato@mec.waka.kindai.ac.jp
23	Masaya	Kato	Japan	mkatoh@kowanws1.hyd.eng.hokudai.ac.jp
24	Hiroyasu	Kawaguchi	Japan	kawaguti@mjoia.ot.jp
25	Mueno	Kawamura	Japan	kawamura@sit.shimz.co.jp
26	Ånund Sigurd	Kvambekk	Norway	aask@nve.no
27	Patricia	Langhorne	New Zealand	pjl@physics.otago.ac.nz
28	Pavel	Liferov	Russia / Norway	pavel.liferov@barlindhaug.no
29	Ingo	Lux	Germany	ingolux@bwbrs1.bau.tu-dresden.de
30	Kalle	Lyytinen	Finland	kalle.lyytinen@fma.fi
31	Mauri	Määttänen	Finland	Mauri.Maattanen@hut.fi
32	Wojciech	Majewski	Poland	wmaj@ibwpan.gda.pl
33	Shunsuke	Makita	Japan	makita@eng.hokudai.ac.jp
34	Stanisław R.	Massel	Poland	smas@iopan.gda.pl
35	Dmitri	Matskevitch	USA	dgmatsk@upstream.xomcorp.com
36	Bolesław	Mazurkiewicz	Poland	bmazur@pg.gda.pl
37	Jacques	Meysonnier	France	jacques@glaciog.ujf-grenoble.fr
38	Makoto	Nakatsugawa	Japan	makoto@hda.go.jp
39	Małgorzata	Pluta	Poland	gosia@marea.im.man.szczecin.pl
40	Hiroshi	Saeki	Japan	h-saeki@eng.hokudai.ac.jp
41	Iren	Shatalina	Russia	prokklm@hydro.vniig.ru / vniig@vniig.ru
42	Hung Tao	Shen	USA	htshen@clarkson.edu
43	Orson P.	Smith	USA	afops@uaa.alaska.edu
44	Devinder S.	Sodhi	USA	dsodhi@crrel.usace.army.mil
45	Gennady	Surkov	Russia	ice@smng.com
46	Krzysztof	Szilder	Canada	kszilder@ualberta.ca
47	Marzenna	Sztobryn	Poland	pga@stratus.imgw.gdynia.pl
48	Romuald	Szymkiewicz	Poland	rszym@pg.gda.pl
49	Takahiro	Takeuchi	Japan	take@hi-tech.ac.jp
50	Einar	Tesaker	Norway	einar.tesaker@civil.sintef.no
51	Garry	Timco	Canada	garry.timco@nrc.ca
52	Jukka	Tuhkuri	Finland	jukka.tuhkuri@hut.fi
53	Andrew	Tuthill	USA	atuthill@crrel.usace.army.mil
54	Yasuharu	Watanabe	Japan	y-watanb@ceri.go.jp
55	Piotr	Wilde	Poland	pwilde@ibwpan.gda.pl
56	Shen	Xianchen	China	shenxc@iwhr.com
57	Yoshikatu	Yasunaga	Japan	yasunaga@eng.hokudai.ac.jp

